UNIVERSITAT DE BARCELONA

Assessing metabolic plasticity in diet-induced obese mice upon lifestyle intervention. An integrative approach.

Alba González Franquesa

Universitat de Barcelona
Doctoral Programme in Biomedicine

ASSESSING METABOLIC PLASTICITY IN DIET-INDUCED OBESE MICE UPON LIFESTYLE INTERVENTION. AN INTEGRATIVE APPROACH.

Alba Gonzalez Franquesa
2015

DOCTORAL PROGRAMME IN BIOMEDICINE

ASSESSING METABOLIC PLASTICITY IN DIET-INDUCED OBESE MICE UPON LIFESTYLE INTERVENTION.

AN INTEGRATIVE APPROACH.

PhD Student

Alba Gonzalez Franquesa

Supervisor

Pablo M. Garcia-Roves

Diabetes and Obesity Laboratory

Institut d'Investigacions Biomèdiques August Pi i Sunyer (IDIBAPS)

Faculty of Medicine

Universitat de Barcelona

2015

Cover by Georgina Gonzàlez Puig.

DOCTORAL PROGRAMME IN BIOMEDICINE

ASSESSING METABOLIC PLASTICITY IN DIET-INDUCED OBESE MICE UPON LIFESTYLE INTERVENTION.

AN INTEGRATIVE APPROACH.

A dissertation submitted to the Faculty of Medicine of the University of Barcelona

for the degree of Doctor of Philosophy in Biomedicine.

by

Alba Gonzalez Franquesa

This PhD Thesis has been conducted under the supervision of Dr. Pablo M. Garcia-Roves mainly at Diabetes and Obesity Laboratory of Institut d'Investigacions Biomèdiques August Pi i Sunyer (IDIBAPS) at University of Barcelona; in collaboration with other departments within IDIBAPS, the Department of Physiological Sciences II (Faculty of Medicine, University of Barcelona), the Metabolomics Platform (COS, Centre for Omics Sciences, Universitat Rovira i Virgili, Reus), and the Department of Biochemistry and Molecular Biology (Faculty of Pharmacy, University of Barcelona). PhD experimental stays and collaborations have been conduced at NeurObesity group (CiMUS, Center for Research in Molecular Medicine and Chronic Diseases, Universidade de Santiago de Compostela), at SEES:lab (Science and Engineering of Emerging Systems, Chemical Engineering Department, Universitat Rovira i Virgili, Tarragona), at Integrative Systems Biology group (CBS, Center for Biological Sequence Analysis, Technical University of Denmark, Lyngby); and at the Disease Systems Biology group (CPR, The Novo Nordisk Foundation Center for Protein Research, Faculty of Health and Medical Sciences, University of Copenhagen).

ABSTRACT

Type 2 Diabetes Mellitus (T2DM) is the metabolic disorder that accounts for the presence of hyperglycemia within insulin resistance (IR). The International Diabetes Federation estimated in 2013 that 382 million people (8.3% of world society) had diabetes and that this number is set to rise beyond 592 million people in the next 22 years. T2DM accounts for 90% of people with diabetes (WHO 1999). Obesity is considered a major risk factor for developing T2DM over time. The World Health Organization (WHO) stated in 2014 that more than 1.9 billion adults were overweight and of these, over 600 million were obese (body mass index (BMI) > 30 kg/m^2). Besides healthcare costs, WHO projects that diabetes will be the 7th leading cause of death in 2030 (Mathers & Loncar 2006). Once T2DM is diagnosed, the first therapeutic approach is by lifestyle counselling consisting of an increase in physical activity and changes in the patient dietary habits.

The aim of this project is to study and integrate the metabolic responses that regulate systemic glucose homeostasis. We are not aware of other works describing in a holistic way the different metabolic processes regulating glucose homeostasis in different tissues that play an important role during the development and onset of diet-induced T2DM. With this approach, we will gain more insight and a better knowledge of the metabolic alterations taking place during an obese state induced by high-fat diet, as well as assess the degree of reversibility that can be reached by undergoing a lifestyle intervention, known as "metabolic plasticity".

For this purpose a diet-induced obese animal model of T2DM is used. To achieve the presented aims, a phenotypical and funcional study is performed at systemic level in order to complete a more experimental and detailed approach afterwards in each of the studied tissues: pancreas, white adipose tissue, liver, oxidative and glycolytic skeletal muscle, and hypothalamus. This experimental approach encompasses tissue-specific-functional analysis, gene expression studies, protein content determination and signalling, metabolomics and RNAseq. Likewise, systems biology tools have been developed and have allowed to measure several correlations as well as perform different types of multivariant analysis with the studied parameters.

Three experimental groups are defined representing the metabolic stages of interest: control group (Ctrl); pathologic group (HFD, that mimic diet-induced T2DM after 16 wks on HFD; and in which animals showed overweight, and fasting hyperglycemia and hyperinsulinemia); and a third group (Int) that follows a lifestyle intervention consisting of caloric restriction, modification of the fatty acid source and carbohydrates in the diet, and the performance of an exercise training programme.

The diet-induced obese experimental group (HFD group) reported the typical physiological features of the pathological state: overweight, fasting hyperglycemia, hyperinsulinemia and hyperleptinemia, increase in fat mass and volume, increase of white adipose tissue, liver and pancreas weight, increase of liver and oxidative skeletal muscle triglycerice levels, glucose intolerance, insulin resistance, increase in beta-cell mass along with hypertrophic enlarged islets and dysfunction in glucose-stimulated insulin secretion *in vivo* and *in vitro*, and a diminishment in oxygen consumption, heat production and scapular temperature.

Lifestyle intervention was enough to revert most of the disruptions reported in the pathological group. However, certain irreversibility degree was still observed in particular studied parameters: (1) alteration in fasting glucose and glucose-stimulated insulin secretion *in vivo*, (2) increment in pancreatic beta-cell area, (3) affectation in the epididymal white adipose tissue with inflammation

and immune cell infiltration, as well as (4) mitochondria dysfunction, already observed in the pathological state. Taken all this together, we can conclude that the pathological state left a certain degree of metabolic irreversibility does not allow a total recovery of the phenotype across the different tissues studied, at least with this type of intervention and timings.

The development and application of systems biology tools have allowed the study the irreversibility degree in an integrative mode, the correlations among certain parameters at a multiorganic level, the gene expression patterns of complexes described from a protein-protein interaction (PPI) network. These strategies and computational approaches have led to the identification of most of the altered tissues and metabòlic pathways in the different states under study.

La Diabetes Mellitus del tipo 2 (DM2) es una enfermedad que se caracteriza por unos niveles anómalamente elevados de glucosa e insulina circulante ocasionados por un estado de resistencia a la insulina. Según la International Diabetes Federation, en 2013 382 millones de personas estaban diagnosticadas de diabetes (8.3% de la población mundial), y acorde con las predicciones esta cifra aumentará hasta los 592 millones en los próximos 22 años. La DM2 explica el 90% de los casos de diabetes (WHO 1999). La obesidad es un factor de riesgo para DM2 y hoy en día supone una epidemia: en 2014 la OMS cifró en 1.9 billones la población adulta con sobrepeso y 600 millones con obesidad. Aparte del coste económico que supone para la sociedad, la OMS proyectó que en 2030 la DM2 será la séptima causa de muerte en el mundo (Mathers & Loncar 2006). La primera aproximación en el asesoramiento al paciente con DM2 o en estado de riesgo consiste en una intervención sobre el estilo de vida: incrementando la actividad física y llevando a cabo una dieta equilibrada y saludable.

Este proyecto tiene como objetivo el estudio e integración de las respuestas metabólicas responsables de regular la homeostasis de la glucosa a nivel sistémico. No existe hasta la fecha ningún trabajo que describa de forma holística los distintos procesos metabólicos que regulan la homeostasis de la glucosa en todos los tejidos que juegan un papel determinante durante el desarrollo de la DM2 asociada a obesidad.

De esta forma, se pretende ganar conocimiento sobre las alteraciones metabólicas que tienen lugar en un estado de obesidad inducido por la dieta grasa, y así mismo valorar el grado de reversibilidad que se puede alcanzar mediante una intervención en el estilo de vida, a lo que nos referimos como "plasticidad metabólica". Empleamos un modelo animal de obesidad y DM2 inducida por una dieta alta en grasas. Para alcanzar los objetivos planteados inicialmente se realiza un estudio fenotípico y funcional a nivel sistémico para luego realizar una aproximación experimental más exhaustiva en cada uno de los tejidos de interés: páncreas, tejido adiposo blanco, hígado, músculo esquelético oxidativo y glucolítico, e hipotálamo. Dicha aproximación experimental engloba análisis funcionales-tejido específico, estudios de expresión génica, determinación del contenido proteico y señalización, metabolómica y RNAseq. Así mismo, se han desarrollado herramientas de biología de sistemas que han permitido calcular distintas correlaciones y hacer diferentes tipos de análisis multivariante con todos los parámetros estudiados.

Se definen tres grupos experimentales de animales que concretan los estados metabólicos de interés: grupo control (Ctrl); grupo patológico (HFD) (que simula DM2 inducida por dieta grasa durante 16 semanas, y en que los animales muestran sobrepeso y la glucosa e insulina circulante elevadas en ayuno); y un tercer grupo que sigue una intervención en el estilo de vida (Int) que

consiste en restricción calórica, una modificación en la fuente de ácidos grasos e hidratos de carbono de la dieta, junto con la realización de un programa de ejercicio.

El grupo experimental de obesidad inducida por la dieta (grupo HFD) presenta las características fisiológicas propias del estado patológico: sobrepeso, hiperglucemia, hiperinsulinemia e hiperleptinemia en ayuno, aumento de masa y volumen de grasa, aumento del peso del tejido adiposo blanco, hígado y páncreas, aumento de triglicéridos en hígado y músculo oxidativo, intolerancia a la glucosa, resistencia a la insulina, aumento de la masa de célula beta en el páncreas juntamente con islotes hipertróficos agrandados y disfunción de la secreción de insulina estimulada por glucosa *in vivo* e *in vitro*, y disminución del consumo de oxígeno, generación de calor y temperatura escapular.

La intervención fue suficiente para revertir gran parte de las alteraciones observadas en el grupo patológico. No obstante, aún se observa cierto grado de irreversibilidad en determinados parámetros estudiados: (1) alteración de la glucosa en ayunas y la respuesta insulínica ante un estímulo de glucosa *in vivo*, (2) incremento en área de célula beta pancreática, (3) afectación en el tejido adiposo blanco epididimal con la presencia de inflamación e infiltración de células inmune, así como (4) disfunción mitocondrial, ya observados en el estado patológico. Con todo, podemos concluir que el estado patológico deja un cierto grado de irreversibilidad metabólica no permitiendo una recuperación total del fenotipo en todos los tejidos estudiados, al menos, con este tipo de intervención y estos periodos de tiempo.

El desarrollo y aplicación de herramientas de biología de sistemas ha permitido estudiar el grado de reversibilidad de un modo integrado, las correlaciones entre parámetros concretos a nivel multiorgánico, el patrón de expresión génica de complejos descritos en una red de protein-protein-interaction (PPI). Estas estrategias computacionales han permitido identificar aquellos tejidos y vías metabólicas más alteradas en los distintos estados estudiados.

La Diabetes Mellitus del tipus 2 (DM2) és una malaltia que es caracteritza per uns nivells elevats de glucosa i insulina circulants ocasionats per un estat de resistència a la insulina. Segons la International Diabetes Federation, el 2013 382 milions de persones van ser diagnosticades de diabetes (8.3% de la població mundial), i d'acord amb les prediccions aquesta xifra augmentarà fins els 592 milions en els pròxims 22 anys. La DM2 explica el 90% dels casos de diabetes (WHO 1999). L'obesitat és un factor de risc per la DM2 i avui en dia suposa una epidèmia: el 2014 la OMS va xifrar en 1.9 bilions la població adulta amb sobrepès i 600 milions amb obesitat. A part del cost econòmic que suposa per a la societat, la OMS va projectar que el 2013 la DM2 serà la setena causa de mort al món (Mathers & Loncar 2006). Un cop diagnosticada, la primera aproximació en l'assessorament al pacient amb DM2 o en un estat de risc consisteix en una intervenció en l'estil de vida: incrementant l'activitat física i portant a terme una dieta equilibrada i saludable.

Aquest projecte té com a objectiu l'estudi i la integració de les respostes metabòliques responsables de regular l'homeostasi de la glucosa a nivell sistèmic. Avui en dia, no existeix cap treball que descrigui de forma holística els diferents processos metabòlics que regulen l'homeostasi de la glucosa en tots els teixits que juguen un paper determinant durant el desenvolupament de la DM2 associada a l'obesitat.

D'aquesta manera, es pretén guanyar coneixement sobre les alteracions metabòliques que tenen lloc en un estat d'obesitat induït per una dieta rica en greixos, i així mateix valorar el grau de reversibilitat que es pot assolir mitjançant una intervenció en l'estil de vida, al que ens referim com a "plasticitat metabòlica". Utilitzem un model animal d'obesitat i DM2 induïda per una dieta alta en greixos. Per aconseguir els objectius plantejats inicialment es realitza un estudi fenotípic i funcional a nivell sistèmic per més tard realizar una aproximació experimental més exhaustiva en cadascun dels teixits d'interès: pàncrees, teixit adipós blanc, fetge, múscul esquelètic oxidatiu i glicolític, i hipotàlem. Aquesta aproximació experimental engloba anàlisis funcionals-teixit específic, estudis d'expressió gènica, determinació del contingut proteic i les vies de senyalització, metabolòmica i RNAseq. Així mateix, s'han desenvolupat eines de biologia de sistemes que han permès calcular diferents correlacions i fer diferents tipus d'anàlisis multivariant amb tots els paràmetres estudiats.

Es defineixen tres grups experimentals d'animals que concreten els estats metabòlics d'interès: grup control (Ctrl); grup patològic (HFD) (que simula la DM2 induïda per la dieta grassa durant 16 setmanes, i en què els animals tenen sobrepès i la glucosa i insulina circulants elevades en dejú); i un tercer grup que segueix una intervenció en l'estil de vida (Int) que consisteix en restricció calòrica, una modificació de la font d'àcids grassos i hidrats de carboni de la dieta, juntament amb la realització d'un programa d'exercici.

El grup experimental d'obesitat induïda per una dieta grassa (grup HFD) presenta les característiques fisiològiques pròpies de l'estat patològic: sobrepès, hiperglucèmia, hiperinsulinèmia i hiperleptinèmia en dejú, augment de la massa i el volum de greix, augment del pes del teixit adipós blanc, el fetge i el pàncrees, augment dels nivells de triglicèrids en fetge i múscul oxidatiu, intolerància a la glucosa, resistència a la insulina, augment de la massa de cèl·lula beta en el pàncrees juntament amb illots hipertròfics engrandits i disfunció de la secreció d'insulina estimulada per glucosa *in vivo* i *in vitro*, i disfunció del consum d'oxigen, generació de calor i temperatura escapular.

La intervenció va ser suficient per revertir gran part de les alteracions observades en el grup patològic. No obstant, encara s'observa cert grau d'irreversibilitat en determinats paràmetres estudiats: (1) alteració de la glucosa en dejú i la resposta insulínica davant d'un estímul de glucosa *in vivo*, (2) increment en l'àrea de cèl·lula beta pancreàtica, (3) afectació en el teixit adipós blanc epididimal amb la presència d'inflamació i infiltració de cèl·lules immunes, així com (4) disfunció mitocondrial, ja observats en l'estat patològic. Amb tot, podem concloure que l'estat patològic deixa un cert grau d'irreversibilitat metabòlica no permetent així una recuperació total del fenotip en tots els teixits estudiats, almenys, amb aquest tipus d'intervenció i aquests períodes de temps.

El desenvolupament i l'aplicació d'eines de biologia de sistemes han permès estudiar el grau de reversibilitat d'una manera integrada, les correlacions entre paràmetres concrets a nivel multiorgànic, el patró d'expressió gènica de complexes descrits en una xarxa de protein-protein-interaction (PPI). Aquestes estratègies computacionals han permès identificar aquells teixits i vies metabòliques més alterades en els diferents estats estudiats.

"If we break up a living organism by isolating its different parts it is only for the sake of ease in analysis and by no means in order to consider them separately. Indeed when we wish to ascribe to a physiological quality its value and true significance we must always refer it to this whole and draw our final conclusions only in relation to the effects in the whole."

Claude Bernard, *Introduction à l'étude de la medicine expérimentale* (1865)

"Energy and life go hand in hand. If you stop breathing, you will not be able to generate the energy you need for staying alive and you'll be dead in a few minutes. Keep breathing. You are a fantastically energetic machine. Gram per gram, even when sitting comfortably, you are converting 10.000 times more energy than the sun every second."

Nick Lane, *Power, Sex, Suicide: Mitochondria and the meaning of life* (2005)

ACKNOWLEDGEMENTS

Aún recuerdo entrar en la salita de reuniones de la quinta planta, asustada y curiosa por saber de tu proyecto, por saber cómo era el tipo de estudiante que buscabas, por saber si mi interés por empezar un proyecto nuevo y el tuyo para compartirlo se juntarían… y míranos. ¡No me negarás que lo de "esto no es piramidal" lo he llevado a la perfección! Bueno, también te recuerdo insistiéndole a la gente sobre cómo te habías olvidado el test psicotécnico a la hora de entrevistarme… pero ahora nada, parece que es demasiado tarde. No podría escribir todas las palabras que me harían falta para agradecerte TODO, Pablo. Gracias por todos los momentos llenos de ciencia que me has regalado, gracias por haberme hecho espabilarme yo solita, gracias por haberme ayudado en tantísimos experimentos, gracias por, aparte de jefe, haber sido un maravilloso compañero con quien compartir momentos buenos y malos, y mirar siempre el lado bueno de las cosas. Paul! La tesis me ha cambiado: ahora palabras como "oxygraph", "holistic", "proyecto ambicioso" hasta me parecen tiernas… no sé si esto es bueno del todo, eh. Muchísimas gracias por la guía, por la enseñanza, por las broncas, por leerte "uno de esos emails" a menudo, por las risas, y por haber hecho de estos años un maravilloso rincón de tiempo que quedará para siempre en mi memoria. ¡Te voy a echar de menos! Ya ta. ¡Munches gracies!

I ara arribes tu, d'entre arrels tiroleses, però català de cap a peus. Saps que gràcies a tu he fet el projecte on l'he fet, envoltat de persones tan capacitades científicament com fantàstiques. I és a tu a qui haig de donar les gràcies per tot també, Marc. Dins i fora del laboratori, un suport constant a totes hores, per riure o per plorar. Per ser el millor xef de menjars meravellosos mentre salvàvem el món tots plegats. Gràcies per ser-hi. Vielen Dank für dieses schöne und "hetzig" Erfahrung Schatz!

Valeria, Vale… tu sai più di chiunque altro quanto fantastico e meraviglioso ha stato questo viaggio con te. Abbiamo viaggiato insieme in un mondo pieno di scienza, felicità, frustrazione, amore... ma soprattutto: la speranza. Te ringrazio molto per essere lì nel bene e brutti momenti. Grazie mille beneventana!

Rebe-quois! ¿Y cómo me pongo ahora seria e intento agradecerte todo lo que has hecho por mí y todo con lo que me has ayudado? Si eso te lo cuento con unas cervezas a la

salida… munches gracies! También a ti, por las risas y por siempre encontrar lo positivo en lo (que parecía) malo, en reír y disfrutar dentro y fuera la ciencia como modo de vida, gracias por la ternura y el amor, muchas gracias. I ara és quan diviso la resta de l'escamot de donasses: la Mercè, l'Aliceeee i l'Alba. Moltíssimes gràcies per tot, sobretot per les hores convertides dins i fora del CEK, per comentar tots els merders en què ens embrolla la vida, i els "afternoon snacks" que tant ens han distret… Joel (Joey!) gràcies per haver-hi estat I haver-nos bàsicament suportat a la resta. Gràcies per les estones divertides, pels congressos (amb reclamacions incloses!) i per la disponibilitat d'ajudar en tot moment a l'hora de fer els experiments. Pau (Paul 2.0)! Ha estat un camí difícil però ara et deixo sense la pressió d'organitzar la vida al lab amb un codi de colors, tot i que ha quedat demostrat que és més fàcil, ehem. Ah, i recorda tenir paciència amb en Paul 1.0, i bé, recorda-li de tant en tant que és d'Avilés… per si algun dia se li oblidés, haha! Moltes gràcies! Laura, cuca, moltíssimes gràcies per suportar-me sempre amb les meves bogeries i els meus moments d'histèria! Gemma, ara per Canadà! Moltíssimes gràcies per tot, per riure i estar plena de bondat. Marta i Edu, ja d'aventura per terres alemanyes, moltíssimes gràcies pel suport, per haver-hi estat tan lluny com a prop, en tot tipus de moments! Moltíssimes gràcies Lourdes per tota l'ajuda durant la teva estada al CEK amb nosaltres, i per totes les vegades que vam riure entre ratolins i pel laboratori!

I no podia oblidar-me la resta de persones del Laboratori de Diabetis i Obesitat que han estat allà sempre que he necessitat un cop de mà: Gema, Lisa, Montse, Paola i Maud, moltíssimes gràcies per tolerar els meus moments de caos i fer que les hores passin al laboratori amb tant de gust! Yaiza, Ainhoa i Carlos, ha estat un plaer haver treballat amb vosaltres, però sobretot haver-vos conegut i haver compartit estones ben divertides, sovint més a fora que dins del CEK! Moltes gràcies! Joan, Hugo i Analu: moltíssimes gràcies (obrigado! ¡gracias!) per les bones estones que hem compartit, per ensenyar-me que McGyver segueix viu i entre nosaltres… Elena, Mariona, Liz, Elaine, Rosa, Marc (sènior), Carles, Marce, Sara, Joan Marc, Anna i Ramon moltíssimes gràcies per haver-me permés parlar de ciència i comentar les jugades quan ha calgut. Kim i Marta "juli", a vosaltres què dir-vos? Sempre allà, disposades a riure mentre poseu ordre en aquesta olla de grills… us estic molt agraïda de tot cor per haver estat allà durant el meu pas pel CEK. I no em vull oblidar de l'altra banda: moltes gràcies al Xavi, la Vane, la Meritxell, la Mar… i tota la troupe que habiteu el "dark side" de la cinquena planta! Moltes gràcies! No me olvido de Oihana, por las horitas compartidas en el lab, y por demostrarme que siempre es más importante el lado humano que cualquier otro: eskerrik asko! I em deixo molta gent del laboratori que ha arribat més tard, però que no per això no es mereixen un GRÀCIES

gegant per haver fet d'un lloc de treball un lloc on estar a gust fent allò que t'agrada. Així doncs, moltíssimes gràcies a l'IDIBAPS pel suport econòmic durant la major part d'aquest doctorat, i per haver estat una petita gran família!

De Barrios, no podia tampoc oblidar-me de tu, després d'haver fet gran part del camí plegats! Moltíssimes gràcies, tak! Tak pels bons moments a Barcelona i a Copenhagen. Gràcies també al José Carlos, a la Sònia, al Xevi, a la Petra, a l'Anna, i al Juan que m'han acollit en les meves visites a Bellvitge com si fos una més del laboratori!

Gràcies a la Laura Herrero per l'ajuda en els estudis de morfometria i en la discussió dels resultats de la tesi, així com pels inputs a l'hora de fer passos en el teixit adipós. Gràcies també a la Lupe per ajudar-nos a "fotografiar" el greix dels animalons!

Gracias a Ruben y a la gente de su grupo del CIMUS, por la acogida esas semanas en Santiago de Compostela y por enseñarme la magia de la "caña más tapa". En especial gracias a Estrella, por tu ayuda incondicional durante mis días allí. Moitas grazas pola axuda e por todo.

Gràcies al Roger i a la Marta per la increíble oportunitat que em vau donar per endinsar-me en el món dels codis, dels scripts, del descobrir com de fàcil pot ser manejar una immensitat de dades sense trepitjar l'Excel! Moltes gràcies per fer dels meus dies a Tarragona uns dies plens d'aprenentatge i de suport per part vostra. Gràcies al Toni i al Manu, per respondre a tots els "pots ajudar-me un momentet?" que mai eren només un momentet... I gràcies a l'altre Toni, a l'Oriol, al Francesco, a la Toñi i al Marc, per haver-me ajudat i, sobretot, per haver-me fet disfrutar els dies al SEESlab! Sense marxar de la provincia, moltíssimes gràcies a l'Oscar, la Sara i al seu equip de metabolòmica del COS, per la col·laboració i la realització dels experiments, així com per l'input científic rebut.

Thanks to Kirstine and Søren, and to the rest of the faculty team at Center for Biological Sequencing Analysis at DTU, and at The Novo Nordisk Foundation Center for Protein Research at KU. Thanks for the advices, help and support during my stay in Copenhagen. Thanks to Isa for helping me through my scripts. And a very big thanks to the "A-Team": Anders, Alberto and Annelaura... for the help and advices for my scripts and for solving some problems, and being a team altogether. Tak, fordi du har gjort det sjovt at komme på arbejde, even though I was having my personal-intimate war against computing and programming... somehow working became "hyggeligt" and I am really grateful for all the

hours we spent together inside and outside of work. Muchas gracias Alberto por las risas, y también gracias a Rebeca, que en el fondo siempre quiso ser del "A-team" haha! Thanks also to "la otra" Rebeca, Mette, Jessica, Cecilia, Poppi, Helen, David, Jan, Atul, Nanna… and the rest of the team at CPR, for making my stay enjoyable. Jeg nød det meget, og det skal i alle have en stor tak for. Tusind tak til jer alle! Jeg håber snart at se jer igen.
Sense marxar de Copenhagen, em quedo curta en paraules per agrair-vos el recolzament rebut per vosaltres durant la meva estada: Irene, Elena, Cristina, Laia i Rosa. Res hagués estat tan màgic ni fantàstic sense vosaltres. Copenhagen i nosaltres ha estat una etapa molt dolça durant aquesta tesi així que em toca dir-vos: mange tak min danske seje piger! Gràcies per pintar de colors el cel gris danès! Mona, mange tak for at være den bedste roommate, man kan få. Tak for alle månederne og alle de gode stunder, som vi havde sammen. Tak fordi du hjalp mig med at forbedre mit dansk... Og Sofie og Rasmus: mange tak til jer også, for de gode øjeblikke som vi havde sammen! Moltíssimes gràcies a la Fundació Universitària Agustí Pedro i Pons pel suport econòmic rebut durant la meva estada a Dinamarca.

Buscant l'origen del viatge científic que he fet… a les farmacèutiques… us estic molt agraïda Fleck, Xio, Annablancototjunt, Anna, Júlia, Marta, Anna Prat i Meri. Gràcies per les estones convertides mentre rèiem i fèiem que el temps passes més dolçament. Gràcies per aquest viatge científic que vaig començar amb vosaltres ara fa més de 10 anys! Us estimo graw-graws. I tu Rufus, una persona molt important en la meva vida, com deus saber, moltíssimes gràcies per trobar-te amb mi i posar-me els peus a terra quan toca. þakka þér kærlega, ég elska þig. Vull agraïr també a la Dolors, al Jose, a la Núria, la Maria, la Majo, el Bernat i tota la troupe del Departament de Química Terapèutica perquè allà vaig començar a estimar la ciència. Thanks to Lennart and Tri, who allowed me to do a project in Copenhagen years ago, and helped me fighting troublesome chemistry! Thanks to all the members of the Medicinal Chemistry building. Mange tak! No em puc oblidar tampoc de l'Analu, la Mariona, l'Anna, la Joana i l'Albert i el Departament de Bioquímica i Biologia Molecular per acollir-me durant el Màster… moltíssimes gràcies.

I penso en els amics i amigues que han fet amb mi aquest viatge els útims anys… Gràcies Agnès. Aix… moltíssimes gràcies per haver-hi estat des que tinc ús de raó (i fins i tot abans!). Per haver suportat que t'expliqués les meves mogudes de la recerca i de la tesi sense importar-te que fos un rotllo i recolzar-me en tot moment. Panda, és imposible imaginar-me una vida paral·lela a algú que no siguis tu. T'estimo moltíssim. Ona i Ferran, a vosaltres també us he d'agraïr l'haver estat allà sempre que m'han agafat moments de caos

per culpa del projecte o bé, per culpa de moltíssimes altres coses. #somiseremgdc, moltíssimes gràcies, us estimo moltíssim. Crajes, moltíssimes gràcies per ser-hi i per ensenyar-me racons de la vida artística que desconexia, gràcies per posar colors als llenços blancs, i també en la meva vida amb hores convertides. Zuma i Nina, us veig amb comptagotes últimament, però heu estat sempre en els pilars de la meva vida, us estimo i us vull donar mil gràcies per donar-me de la mà en aquest viatge tan dolç. Espero que compartim moltes estones més plegades. Petros, Bernat, Maria, Anna, Dani, Sergi, Roger, Alba, Mon, Ferran, Cris, Berta… hartelijk dank voor u ook, Jeroen! I la resta d'amics i amigues a Badalona, Barcelona i pel món que heu compartit alguna estona o moltes amb mi durant aquests anys. Per l'amor dipositat en entendre la meva dèria de fer ciència i descobrir coses noves, pel suport sentit de que hi sou passi el que passi. Per les hores convertides, moltíssimes gràcies.

I ara tornem a les arrels… moltíssimes gràcies a tots els meus tiets i tietes, i especialment a tots els meus cosins i cosines. Gràcies família! La vida és més maca quan es comparteix, i per descomptat que som uns i unes quantes per compartir-la. Gràcies per moments concrets i no tan concrets, per trobades, per ser d'on vinc i on pertanyo. Us estimo molt a tots i a totes. #perquètenimtantescosesencomú. I en especial, moltes gràcies a la Georgi per posar un toc d'art a tanta ciència i tantes xifres!

Enric i Ferran, no m'imagino ni haver fet aquesta tesi, ni una vida sense vosaltres. No la puc concebre. Us estimo amb bogeria, i us vull donar les gràcies per suportar-me i acompanyar-me sempre. Per fer de l'equip "germanístic" un equip unit, un equip amb ganes de tot i amb la força per fer-ho. Un equip amb un recolzament constant, un equip amb crits i bronques que després se solucionen amb abraçades plenes de contingut. Gràcies, de tot cor. Em prenc la llibertat d'incorporar la Tona a l'equip, que ha jugat molts partits amb nosaltres. I durant l'escriptura de la tesi a Nevà ha estat un element clau.

Diuen que els agraïments més importants van al final… Albert i Eulàlia, no m'hi cabria espai en mil tesis per donar-vos les gràcies com us mereixeu. Quan veig on sóc, el que he fet, el que he aconseguit, tots els somnis que he complert… i la gent que em diu "enhorabona", i jo em trobo més tard pensant que tots aquests "enhorabona" són per vosaltres. Cadascun dels nostres èxits és un èxit vostre. Per l'educació, els valors, l'esperança i, sobretot, per l'amor en què hem crescut.

Així doncs, em veig molt incapacitada per agraïr-vos tot el que em cal agraïr en aquest petit paràgraf... Els poemes que tan m'agraden, diuen que condensen molt més del que es llegeix, així que us he escrit unes paraules:

Gràcies pare i mare
I en un instant acluco els ulls
diviso allò que seria l'espai i el temps
ja no tinc por, la que potser tenia
ja no temo estimar, ni viure
ja no temo aprendre i equivocar-me
no tinc por a perdre,
ja no em dol el fracàs,
si sé que hi sou.
I en un instant acuclo els ulls
i m'adono que tot té un sentit
tinc el millor regal del món:
una vida,
una vida on hi sou.

Gràcies.

"Have I dared wrongly, ah well, then life will help me with the punishment.
But have I not dared at all, who will help me then?"
Søren Kierkegaard, *Sygdommen til Døden* (1849)

Som-hi!

A la tieta Marta,

TABLE OF CONTENTS

ABBREVIATIONS

(Gene names that are not in the list are indicated in Materials and Methods part 6.4 section)

ABCA1/Abca1	ATP-binding cassette transporter
ACADM/Acadm	acyl-CoA dehydrogenase C-4 to C-12 straight chain or MCAD
ADA	American Diabetes Association
ADP	adenosine diphosphate
AGRP/Agrp	agouti-related protein
AHEAD	Action for Health in Diabetes study
AIF	apoptosis-inducing factor
AIM	apoptosis inhibitor of macrophages
AKT/PKB/Akt	Protein Kinase B
AMP	adenosine monophosphate
AMPK	AMP-activated kinase
ANT1	protein encoded by solute carrier family 25 (Slc25a4) gene also known as mitochondrial carrier: adenine nucleotide translocator (ANT)
AP1	protein encoded by Jun Proto-Oncogene (Jun) gene also known as activator protein 1
ApoC3	apolipoprotein CIII
ARA	arachidonic acid
ARC	arcuate nucleus
ASC	protein encoded by PYD and CARD Domain Containing (Pycard) gene also known as apoptosis-associated speck-like protein containing CARD
ASPN/Aspn	asporin
ATF/Atf	activating transcription factor (different factors)
ATGL	protein encoded by patatin-like phospholipase domain containing 2 (Pnpla2) gene also known as adipose triglyceride lipase
ATM	adipose tissue macrophages
ATP	adenosine triphosphate
BAT	brown adipose tissue
BIP/Bip	binding immunoglobulin protein (=heat shock 70KDa Protein 5 (HSPA5) and GRP78)
BMI	body mass index
BW	body weight
C	cytosine
C/EBP	protein encoded by CCAAT/enhancer binding proteins (Cebp) gene
CaMKII	calcium/calmodulin kinase II (Camk2a encodes KCC2A protein)
CART/Cartpt	cocaine and amphetamine-related transcript
CCL2/Ccl2/MCP1/Mcp1	monocyte chemotactic protein 1(=CCL2)
CD/Cd	cluster of differentiation (markers)

CDA	content delivery application
CH	carbohydrates
CHOP/Chop	C/EBP homologous protein or DNA-Damage-Inducible Transcript 3
ChREBP	carboxylate-responsive element-binding protein
CI/CI+II/ETS CI+II/ETS CII	respiratory states
CI/II/III/IV/V	OxPhos complexes
CLS	crown-like structures
CMA	content management application
CMS	content management system
CNS	central nervous system
Cnts	counts (movement units)
CoA	coenzyme A
COL1a1/Col1a1	collagen, type I, alpha 1
COX/Cox	cytochrome C oxidase (different subunits)
CPT1/Cpt1	carnitil palmitoyltransferase 1
CR	caloric restriction
CREB/Creb	cAMP response element-binding
CS/Cs	citrate synthase
Ctrl	control experimental group
CV	cardiovascular
D	diet intervention group
DAG	diacylglycerol
DB	database (created for this project)
DDIT3/Ddit3	C/EBP homologous protein or DNA-Damage-Inducible Transcript 3
DEX	diet+exercise intervention group
DGAT/Dgat	diglyceride acyltransferase
DHA	docosahexaenoic acid
DI	disposition index
DIAMAP	Road MAP for DIAbetes Research in Europe
DIO	diet-induced obesity
DIRECT	Diabetes REsearCh on patient straTification study
DNL	de novo lipogenesis
DNM1L/Dnm1l	dynamin-1-like protein or DRP1
DPP	Diabetes Prevention Program
DPP-4	dipeptidyl peptidase 4
DPPOS	Diabetes Prevention Program Outcomes Study
DR	dietary restriction (=CR)
DSE	Diabetes Support and Education
DSME and DSMS	Diabetes Self-Management Education And Support
EASD	European Association for the Study of Diabetes
EDL	extensor digitorum longus
ELISA	enzyme-linked immunosorbent assay
EMEA	European Medecine Agency
eNOS	endothelial nitric oxide synthase

EPA	eicosapentaenoic acid
ER	endoplasmic reticulum
ERR/Err	estrogen-related receptor
ETS	electron transport system
eWAT	epididymal adipose tissue
EX	exercise intervention group
FA	fatty acids
FADH	flavin adenine dinucleotide
FADH2	reduced FADH
FATP/Fatp	fatty acid transport proteins
FCCP	carbonyl cyanide-4-(trifluoromethoxy)phenylhydrazone
FCR	flux control ratio
FDA	Food and Drug Administration
FFA	free fatty acids
FGF21/Fgf21	fibroblast growth factor 21
FIRKO	fat-specific insulin receptor KO
FO	fish oils
FSP27/Fsp27/CIDEC/Cidec	fat-specific protein 27
G	guanosine
G6P	glucose-6-phosphate
GDM	gestational diabetes mellitus
GDR	glucose disposal rate
GIP	gastic inhibitory polypeptide
GK	glucokinase
GLP1	glucagon-like peptide-1
GLUT2/GLUT4	glucose transporter isoform 2/4
GPR78/Gpr78	binding immunoglobulin protein (BIP) (=heat shock 70KDa Protein 5 (HSPA5) and GRP78)
GSIS	glucose-stimulated insulin secretion
HADH	β-hydroxyacyl coenzyme A dehydrogenase
HbA1c	glycated hemoglobin
HBSS	Hank's Balanced Salt Solution
HFD	high fat diet
HFD	pathological experimental group
HGP	hepatic glucose production
HIF1α/Hif1α	hypoxia inducible factor 1 α
HK	hexokinase
HOMA	homeostatic model assessment
HSPA5/Hspa5	binding immunoglobulin protein (BIP) (=heat shock 70KDa Protein 5 (HSPA5) and GRP78)
HYOU1/Hyou1	hypoxia up-regulated 1
IAPP	islet amyloid polypeptide
ICV	intracerebroventricular
IDF	International Diabetes Federation

IFG	impaired fasting glucose
IGT	impaired glucose tolerance
IHC	immunohistochemistry
IKK/Ikk	inhibitor of κB kinase
IL/Il	interleukin
ILI	intensive lifestyle intervention
IMAT	intramuscular adipose tissue
IMF	intramyofibrillar
iNOS	inducible nitric oxide synthase
Int	intervention experimental group
IGTT	intraperitoneal glucose tolerance test
IR	insulin resistance
IRE1/Ire1	inositol-requiring protein-1
IRS1/2	insulin receptor substrate 1 or 2
ITT	insulin tolerance test
JNK1/Jnk1	Jun-N terminal kinase
kcal	kilocalories
LCAD	long-chain acyl-CoA dehydrogenase
LCFA	long-chain fatty acid
LDF	low fat diet
LI	lifestyle intervention
LPL/Lpl	lipoprotein lipase
LPS	lipopolysaccharide
LTB4	leukotriene B4
M1/M2	polarized macrophage
MAP	mitogen-activated protein
MAPK	mitogen-activated protein kinases
MCFA	medium-chain fatty acid
MCP1/Mcp1/CCL2/Ccl2	monocyte chemotactic protein 1(=CCL2)
MFN/Mfn	mitofusin
MKP1	mitogen-activated kinase phosphatase 1
MMe	metabolic activated macrophage
MnSOD	manganese superoxide dismutase
MODY	Maturity Onset Diabetes of the Young
MRS	magnetic resonance spectroscopy
mtDNA	mitochondrial DNA
mTORC1	mammalian target of rapamycin complex 1
MUFA	monounsaturated fatty acid
MYOC1C/Myo1c	myosin-1c
NAD^+	Nicotinamide adenine dinucleotide
NADH	reduced NAD^+
NAFLD	non-alcoholic fatty liver disease
NASH	non-alcoholic steatohepatitis
NDUF/Nduf	NADH Dehydrogenase (Ubiquinone) (different subunits)

NEFA	non-sterified fatty-acids
NGT	normal glucose tolerance
NLRP3/Nlrp3	NOD-like receptor family, pyrin domain containing 3 that encodes human protein NACHT, LRR and PYD domains-containing protein 3(NALP3) or cryopyrin
NO	nitric oxygen
NOS	nitric oxide synthase
NPY/Npy	neuropeptide Y
NRF/Nrf	nuclear respiratory factor
ObRb/Obrb	leptin receptor
OCR	oxygen consumption rate
OLETF rats	Otsuka Long-Evans Tokushima Fatty
Om3	omega-3 fatty acids
OxPhos	oxidative phosphorylation
p47phox/Ncf1	neutrophil cytosolic factor 1
PBA	4-phenylbutyrate
PCr	phosphocreatine
PDH	pyruvate dehydrogenase
PDK	pyruvate dehydrogenase kinase
PDX1/Pdx1	pancreatic and duodenal homeobox 1
PEPCK	phosphoenolpyruvate carboxylase
PERK	double-stranded RNA-dependent protein kinase (PKR)-like ER kinase
PFK	phosphofructokinase
PGC1/Pgc1	peroxisome proliferator-activated receptor gamma coactivator-1
PI3K	phosphoinositide 3-kinase
PINK1/Pink1	PTEN Induced Putative Kinase 1
PK	pyruvate kinase
PKC	protein kinase C
PLIN2/Plin2	perilipin
PNPLA3	patatin-like phospholipase domain-containing protein 3
POMC/Pomc	pro-opiomelanocortin
PP2A	protein phosphatase 2A
PPAR/Ppar	peroxisome proliferatior-activated receptor
PPI	protein-protein interaction (network)
Prdm16	PR Domain Containing 16
PUFA	polyunsaturated fatty-acids
PVN	paraventricular nuclei
RER	respiratory exchange ratio
RI	reversibility index
ROS	reactive oxygen species
RT	room temperature
RT-PCR	Real-time polymerase chain reaction
SAT	subcutaneous adipose tissue
SD	standard deviation

SDH/Sdh	succinate dehydrogenase (different subunits)
SEM	standard error of the mean
Ser	serine
SGLT2	sodium/glucose transporter 2
SIRT3/Sirt3	NAD-dependent deacetylase sirtuin-3
Slc2a	gene encoding GLUT protein
SOCS/Socs	suppression of cytokine signal
SODM	protein encoded by superoxide dismutase 2 (Sod2)
SREBP1/Srebp1	sterol regulatory element-binding protein 1
SS	subsarcolemal
STAT3	signal transducer and activator of transcription-3
sTNFR	soluble TNF receptor
SU	sulfonilureas
SUIT	substrate-uncoupler-inhibitor titration protocol
SVF	stromal vascular fraction
T	thymine
T2DM	type 2 diabetes mellitus
TA	tibialis anterior
TCA cycle	tricarboxylic acid cycle
TCF7L2/Tcf7l2	transcription factor 7-like 2
TFAM/Tfam	transcription factor A mitochondrial
TG	triglycerides
Thr	threonine
TLR4	toll-like receptor 4
TNFα/Tnfα	tumor necrosis factor α
TUDCA	tauroursodeoxycholate
Tyr	tyrosine
TZD	thiazolidinediones
UCP/Ucp	uncoupling protein
UI	units of insulin
UPR	unfolded protein response
UPR^{mt}	mitochondrial unfolded protein response
VAT	visceral adipose tissue
VEGF/Vegf	vascular endothelial growth factor
VMN	ventromedial nuclei
WAT	white adipose tissue
WB	western blot
WHO	World Health Organization
wks	weeks
XBP1/Xbp1	X-box binding protein 1
ZDF	Zucker Diabetic Fatty rats
ZF	Zucker-fatty rats

INTRODUCTION

Introduction

1. Obesity-related Type 2 Diabetes Mellitus (T2DM)

1.1. Epidemiology of obesity-related T2DM

Type 2 Diabetes Mellitus (T2DM) also known as a non-insulin-dependent diabetes mellitus (NIDDM) is the metabolic disorder that accounts for the presence of hyperglycemia within insulin resistance (IR). The International Diabetes Federation (IDF, www.idf.org) estimated in 2013 that 382 million people (8.3% of world society) had diabetes and that this number is set to rise beyond 592 million people in the next 22 years. It is worth mentioning that in 2013 IDF estimated that 175 million people were undiagnosed for diabetes, which is 46% of the total cases. Among the millions of people suffering from diabetes, T2DM accounts for 90% of people with diabetes, while the other 10% accounts for type 1, gestational diabetes (GDM) or monogenic diabetes (WHO 1999).

Obesity is considered a major risk factor for developing T2DM over time. The World Health Organization (WHO, www.who.int) stated in 2014 that more than 1.9 billion adults were overweight and, of these, over 600 million were obese (body mass index (BMI) > 30 kg/m^2). That is, 39% of adults aged 18 years and over were overweight and 13% were obese. These numbers have doubled since 1980 worldwide. Thus, the current epidemic of T2DM could be attributable to the increased incidence of overweight and obesity. Obesity is also a risk factor for cardiovascular disease (CVD) associated with T2DM.

Apart from the impact on society's health, it is important to stress other facts about both T2DM and obesity. On one hand, IDF stated that diabetes caused in 2013 5.1 million of deaths. On the other hand, both diabetes and obesity have become a huge healthcare cost that would be unsustainable in the future years. IDF estimated that America and Caribbean spent in 2013 around 263 billion US dollars, which was equivalent to the money spent by half of the world, and Europe spent 147 million US dollars. Worth mentioning is that although diabetes incidence is increasing in South-East Asia and Africa, these two zones spent less than 1% of the global healthcare diabetes. In fact, WHO estimated that in 2012 diabetes was the direct cause of 1.5 million deaths, 80% of them in low- and middle-income countries (WHO 2014). WHO projected that diabetes will be the 7th leading cause of death in 2030 (Mathers & Loncar 2006).

Once T2DM is diagnosed, the first therapeutic approach is by lifestyle counselling consisting of an increase in physical activity and changes in the patient dietary habits.

When these new measures are not able to lower the concentration of glucose in blood, medication is prescribed (Inzucchi et al. 2012). The most prescribed drug for T2DM especially in cases of overweight or obesity is *metformin*, an oral biguanide that acts by suppressing glucose production in the liver (Inzucchi et al. 2012).

1.2. Social main causes for obesity-related T2DM

Obesity-related T2DM is a complex disease that has been linked to many different and heterogeneous causes. On one hand, poor nutrition, and **over-nutrition** are without any doubt leading to obesity and overweight. Western countries often rely on calorie-dense diets that include refined foods and beverages. On the other hand, **physical inactivity** has been shown to increase the risk for diabetes after an obese or overweight state. Another social problem that increases the risk of suffering from T2DM are the **sleeping habits**: sleeping deprivation can affect the body's balance of insulin and glucose by reducing postprandial insulin secretion, suggesting impaired pancreatic β-cell function (Mesarwi et al. 2013), a situation that if it is prolonged can lead to T2DM. Also, studies show how persons with night shifts such as nurses or people that sleep less than five hours per night had an increased risk. However, same studies show that the risk was also increased for those sleeping more than nine hours per night (Gangwisch et al. 2007).

Last but not least, various **genetic mutations** have been linked to an increased risk to develop T2DM (Zeggini et al. 2008; Morris et al. 2012; Mahajan et al. 2014). Many different loci have been identified through genome-wide association studies (GWAS) to exert a disease risk upon mutations, among them: *TCF7L2* related to insulin secretion (Groves et al. 2006), the zinc transporter *SLC30A8* (exclusively expressed in insulin-producing β-cells), two genes involved in β-cell development or function (*IDE-KIF11-HHEX* and *EXT2-ALX4*) (Sladek et al. 2007), and many others that have recently been discovered. At the time of writing, around 88 published loci were linked to T2DM and 83 to one or more glycemic traits (Mohlke & Boehnke 2015). GWAS studies have been able to explain around 10% of disease heritability (Billings & Florez 2010). Unlike T2DM, other types of diabetes such as maturity onset diabetes of the young (MODY) have been totally attributed to genetic disturbances (Tattersall 1998).

Although one might be predisposed to develop T2DM partly due to a family inheritance, social behaviour and habits can be altered and modified by **lifestyle interventions (LI)** towards healthy eating and a more physically active life in order to prevent, delay or fight

the disease. Pathophysiological response to this predisposition and environmental stress will be further discussed later in this Thesis.

1.3. Insulin resistance and Type 2 Diabetes

Insulin resistance (IR) is the pathophysiological multi-organ condition in which living cells fail to respond to normal concentrations of released insulin to perform its action. In this *scenario*, insulin is properly secreted by the β-cells in the pancreas but the peripheral insulin-sensitive tissues such as skeletal muscle (DeFronzo et al. 1985), adipose tissue (Kashiwagi et al. 1983), liver (DeFronzo et al. 1989) and hypothalamus (Matsuda et al. 1999) are incapable to use it efficiently. Thus, hyperglycemia appears along with increased lipolysis and plasma triglycerides (TG) (Defronzo 2009). The origins of IR can be traced to their genetic background (DeFronzo 1997; Groop & Lyssenko 2008), but as aforementioned the epidemic of T2DM is driven by the obesity and physical inactivity epidemics (James 2008).

A compensatory effect of increasing insulin secretion by the β-cells exists to offset the decrease in insulin sensitivity. However, β-cells begin to fail over time and postprandial plasma glucose levels and subsequently the fasting plasma glucose concentrations start to rise, leading to the clinical onset of T2DM (DeFronzo 1988; Saad et al. 1989; Lillioja et al. 1988; Lillioja et al. 1993; DeFronzo 2004; Bergman et al. 2002). This phenomenon was first observed by Jallut and colleagues (Jallut et al. 1990) when individuals with normal glucose tolerance (NGT) progressed to impaired glucose tolerance (IGT) reducing 28% of their insulin sensitivity but without effects in plasma glucose due to the compensatory effect described above. Moreover, DeFronzo and others demonstrated that the onset of β-cell failure occurs much earlier and is more severe than previously thought (Gastaldelli et al. 2004; Ferrannini et al. 2005; Abdul-Ghani, Jenkinson, et al. 2006; Abdul-Ghani, Tripathy, et al. 2006). In their studies they showed that by the time diabetes was diagnosed, patients had lost over 80% of their β-cell function. Butler and colleagues showed similar results with a decrease in β-cell mass occurring long before T2DM was diagnosed (Butler et al. 2003).

The inverted U-shaped curve that shows the increase and consequent decrease in insulin secretion, known as the Starling's curve of the pancreas (Figure 1) (DeFronzo 1988), is characteristic in a situation of IR and hyperglycemia. At the end of the curve, when the β-cell is not capable of maintaining the high insulin secretion, hyperinsulinemia, along with a lack of insulin sensitivity (thus, IR) and hyperglycemia are present. In Figure 1, this point is represented with circles.

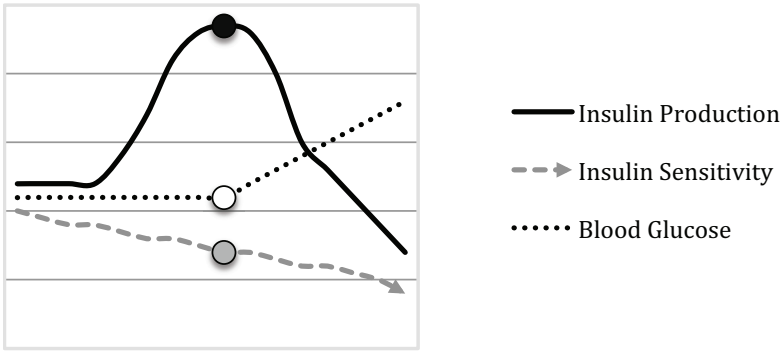

Figure 1. Starlings' curve of the pancreas.

Taken all these studies and considerations, diagnosis criteria should be reconsidered or an earlier intervention should be performed, at the stage of IGT or impaired fasting glucose (IFG), to avoid the β-cell failure that will ultimately lead to T2DM.

1.3.1 Tissue-specific IR

IR has a different impact on a variety of tissues. IR in adipose tissue fails to suppress lipolysis, leading to an **ectopic fatty acid (FA) accumulation** in insulin-sensitive tissues (ie. liver, skeletal muscle) while contributing to hyperlidipemia in insulin-resistant states (Boden 2011) and lipotoxicity. Next, intracellular FA accumulation might disrupt insulin signalling by increasing serine residues phosphorylation in IRS1, ultimately decreasing insulin-stimulated protein kinase B (AKT) activity and glucose transporter isoform 4 (GLUT4) translocation (in skeletal muscle) (Zierath et al. 1996); and in IRS2 ultimately increasing gluconeogenesis (in liver) (Morino et al. 2006). Thus, IR **impairs glucose uptake** into skeletal muscle, and in liver IR leads to impairment in the glucose input because of **disrupted suppression of gluconeogenesis,** and presence of glycogenolysis (Home & Pacini 2008), with a consequent increase in hepatic glucose production (HGP).

The mentioned defect in adipose lipolysis suppression is most detrimental in visceral adipose, and is also thought to disrupt the secreted adipokines profile leading to a **low-grade inflammatory state,** which can later affect numerous tissues (Suganami et al. 2012).

Other causes apart from disrupted insulin signalling have been proposed for impaired insulin-stimulated glucose uptake, such as palmitate or oxidative stress that can induce IR without a decrease in AKT phosphorylation (Hoehn et al. 2008). This oxidative stress can be

produced by intracellular accumulation of FA that contributes to production of reactive oxygen species (ROS) (Boden 2002).

The satiety centres of the hypothalamus such as the arcuate nucleus (ARC) can show reduced insulin sensitivity (Marino et al. 2011). In a healthy situation, insulin would reduce food intake and enhance energy expenditure. Thus, IR in the ARC leads to hyperphagia and a **reduction in energy expenditure**. Also, studies by Obici and colleagues showed evidence for cerebral IR leading to increased HGP and reduced skeletal muscle glucose uptake in rodents (Silvana Obici, Feng, et al. 2002; Obici et al. 2001).

Taken all this together, IR becomes the hallmark of T2DM in multiple tissues. In fact, IR-induced hyperlipidemia and hyperglycemia are thought to be responsible for many of the co-morbidities in T2DM (Brownlee 2005). Apart from the mentioned processes, numerous studies have described links between **impaired mitochondrial function** and the development of IR.

Further explanation of the link between ectopic FA accumulation and IR and/or T2DM is briefly discussed below (section 1.4) and detailed in sections 1.8. The relationship between mitochondria and IR and/or T2DM is briefly discussed in section 1.6.2 and sections 1.8. Regarding the concrete processes taking place in an IR and obese-related T2DM states in each tissue, these are further explained and detailed in sections 1.8, where causes of IR and T2DM are broken down by tissue.

1.3.2. Phenotype overview in a mouse model of obesity-related T2DM

Apart from the phenomena mentioned in the above section about the IR consequences in each of the tissues involved in T2DM, a brief definition of the diet-induced obesity (DIO) phenotype might be of interest. C57BL/6J mice, the strain used for this PhD thesis, can increase their body weight (BW) in a rate of 10g after 6 wks on a high-fat diet (HFD) (Cummins et al. 2014; Kim et al. 2008; Sansbury et al. 2012). A twofold increase in percentage of fat mass was observed with a concomitant decrease in the percentage of lean mass. HFD-fed mice showed glucose intolerance and IR, along with an increase in plasma insulin levels. Regarding metabolic parameters measurements through indirect calorimetry, the HFD-fed mice showed a decrease in VO_2 and VCO_2 values, a decrease in respiratory exchange ratio (RER), and no significant changes regarding ambulatory and fine movements (Cummins et al. 2014).

1.4. Intracellular Fatty Acids (FA) in T2DM

More than 50 years ago, Randle and colleagues demonstrated how FA caused IR *in vitro* in rat muscle preparations (Randle et al. 1963). Therefore, they hypothesized the substrate competition mechanism (Randle et al. 1963), lately named Randle or "glucose-fatty-acid" cycle. According to his hypothesis, the increase in muscle FA oxidation in the mitochondria would raise the ratios of intracellular acetyl Coenzyme A (CoA)/CoA and nicotinamide nucleotide ratio NADH/NAD^+, inhibiting pyruvate dehydrogenase (PDH), which in turn, would increase citrate levels. Increased citrate would inhibit phosphofructokinase (PFK) that would then increase glucose-6-phosphate (G6P), which in turn, would promote glycogen synthesis and inhibit hexokinase (HK), ultimately increasing intracellular glucose and thus decreasing glucose uptake. Hence, Rande cycle claimed that impaired glucose uptake was due to inhibition of key glycolytic enzymes.

Had Randle's hypothesis been correct, muscle glycogen was predicted to be high as a result of the accumulation of the intracellular glucose and G6P. However, more recent magnetic resonance spectroscopy (MRS) studies showed that glucose uptake, glycogen synthesis and G6P were decreased in T2DM patients and lean, normaglycemic, insulin-resistant first-degree relatives of T2DM patients (Rothman et al. 1995; Shulman et al. 1990; Rothman et al. 1992). Roden and colleagues also demonstrated a decrease in glucose uptake and G6P after 3h of lipid infusion in skeletal muscle (Roden et al. 1996). Moreover, intramyocellular glucose was lower than predicted in relation with raising plasma FA concentration (Dresner et al. 1999) in T2DM individuals, had HK been controlling the glucose uptake by muscle. Hence, Randle cycle's hypothesis was untenable in skeletal muscle (Roden et al. 1996). FA might directly inhibit insulin-stimulated glucose uptake at the glucose transport level itself and not through an impairment in glycolysis (Dresner et al. 1999).

Nowadays, the hypothesis pointing at intracellular FA accumulation as the cause of cellular IR is widely accepted, although Randle cycle was replaced. Intracellular accumulation of fatty-acyl CoA and diacylglycerol (DAG) activates critical signal transduction pathways leading to insulin signalling suppression. Thus, any perturbation promoting the accumulation of FA in insulin-sensitive tissues (ie. liver and/or skeletal muscle) and/or any defect in the ability to metabolize the FA might end up in IR (Shulman 2000). One example of accumulation of FA leading to IR without cofounding factors such as obesity is lipodystrophy disease, which occurs with defects in adipocyte metabolism (Petersen et al. 2002). Of note, there is a current hypothesis further extended in section

1.6.2, not yet demonstrated, which proposes that defects in FA oxidation due to mitochondrial dysfunction are responsible for causing IR (Morino et al. 2006).

1.5. Metabolic inflexibility in T2DM

Different sources to obtain energy, such as glucose and lipids, can be in competition while interacting to each other (Randle 1998). The capacity of healthy individuals to adjust and properly switch between the utilization of lipid or carbohydrate (CH) as an energy fuel according to the nutrient availability was named "metabolic flexibility" back in 2004 (Storlien et al. 2004; Kelley et al. 2002). T2DM and obese insulin-resistant individuals show an inability to do so, presenting the so-called "metabolic inflexibility", which does not allow these patients to increase the use of CH in a fed state (when it is plentiful) nor to increase FA oxidation during fasting. Metabolic inflexibility could play an important role during the early onset of T2DM when there is already evidence of IR, since T2DM individuals are not capable of switching to CH utilization when they are plentiful. It is then the consequence of a disruption in energy balance and glucose homeostasis that can hasten the appearance of IR and T2DM, and has also been proposed as the key dysfunction of the cluster of diseases included in the "metabolic syndrome" (Storlien et al. 2004). Metabolic inflexibility has also been reported to lead to ectopic lipid accumulation and mitochondrial dysfunction (Galgani, Moro, et al. 2008; Sugden et al. 2009). In summary, it has been related to obesity, T2DM, metabolic syndrome and also CVD.

1.6. Mitochondria in obesity-related T2DM

Mitochondria are cellular organelles engaged in a wide range of cellular processes and are therefore essential for cell viability. The primary role of mitochondria consists in generating adenosine triphosphate (ATP) through energy metabolism. However, other essential metabolic functions include generation of reactive oxygen species (ROS) and detoxification, with important signalling functions (Starkov 2010; Murphy 2009); the control of cytoplasmic calcium (Rimessi et al. 2008); and regulation of apoptosis and autophagy (Murgia et al. 2013).

1.6.1 Energy metabolism and oxidative phosphorylation

The major cellular organelle in charge to produce ATP is the mitochondrion, also called the cellular powerhouse. ATP production occurs mainly through oxidative phosphorylation (OxPhos) that takes place in the mitochondrion inner membrane, the membrane between the intermembrane space and the mitochondrial matrix. This membrane gives room to mitochondria cristae, that is, foldings that expand the surface

area of the membrane. OxPhos consists in the flux of electrons that are transferred from electron donors (electron carrier coenzymes) to electron acceptors such as oxygen, in a path with redox reactions, to form H_2O. The electrons that are produced by the oxidation of nutrients can be transferred to major electron carrier coenzymes: nicotinamide adenine dinucleotide (NAD^+) and flavin adenine dinucleotide (FADH). These coenzymes get reduced (NADH and $FADH_2$, respectively) during glycolysis and TCA cycle reactions.

The OxPhos takes place through the electron transport system (ETS), formed by the aligned complexes in the inner-membrane: NADH dehydrogenase or complex I (CI), succinate dehydrogenase or complex II (CII), cytochrome b or complex III (CIII), complex IV (CIV) and complex V or ATP synthase (CV). The electrons coming from NADH flow through NADH dehydrogenase (CI), cytochrome reductase (CIII), and cytochrome oxidase (CIV). In the same manner, $FADH_2$ electrons that come from the reactions of succinate dehydrogenase of the TCA cycle and acyl-CoA dehydrogenase of the FA oxidation pathway, go through CII, CIII and CIV. This way, NADH obtained during glycolysis and TCA cycle enters OxPhos through CI and $FADH_2$ enters through CII.

The ETS uses electrons from reduced NADH and $FADH_2$ that flow from one complex to the other and is associated with a proton pumping from the matrix to the intermembrane space. In 1961, Peter Michael proposed the chemiosmotic hypothesis where proton pumping generates a proton motive force that creates a pH gradient across the mitochondria inner-membrane and a membrane potential, that drives ATP synthesis (Mitchell 1961). The chemical gradient makes the protons flow back to the matrix. These protons can flow through ATP synthase (CV) synthetizing ATP from adenosine diphosphate (ADP) and inorganic phosphate. It is worth mentioning that these protons can also flow across the inner-membrane producing a proton leak or, in some tissues, flow through an uncoupler protein, releasing energy as heat, the so-called "non-shivering thermogenesis".

Of note, when ATP is obtained in glycolysis and TCA cycle pathways high-energy molecules provide organic phosphate groups and, in the OxPhos situation, ATP is produced by ADP phosphorylation with an inorganic phosphate.

1.6.2 Mitochondrial dynamics

Mitochondria have their own quality control consisting in mitophagy, and also mitochondrial fusion and fission. Mitochondria suffer remodelling in both situations: when being challenged with different energy (nutrients) availability (Molina et al. 2009) and because of their own life cycle (Twig, Elorza, et al. 2008).

On one hand, when cells are challenged with rich-nutrient media, their mitochondria are separated and fragmented (fission), and when cells are under starvation their mitochondria are more connected and elongated (fusion) (Gomes et al. 2011; Molina et al. 2009). On the other hand, during the mitochondria life cycle, fusion and fission events are constantly happening to reorganize mitochondrial components and release the damaged material, thereby keeping mitochondria functional. Mitochondrial dynamics, including movement and mitochondria tethering apart from fusion and fission processes, have been reported to have a role in cell viability and senescence, mitochondria health, bioenergetics function, quality control, and intracellular signalling (Liesa et al. 2009; Twig, Hyde, et al. 2008). Hence, mitochondrial dynamics have a role in the bioenergetics adaption and survival of the cell.

In fact, a reduction in mitochondrial fusion might be related to obesity and IR (Bach et al. 2003), while fusion activation and/or fission inhibition were found to counteract different disease phenotypes related to IR and T2DM (Civitarese & Ravussin 2008). In the same line, enhanced fission was reported in skeletal muscle of DIO mice (Jheng et al. 2012) and *db/db* mice livers (Holmström et al. 2012).

1.6.3 Mitochondrial dysfunction and IR, the causality controversy

As aforementioned, mitochondrial dysfunction has been linked to IR and T2DM. In fact, one of the most contentious issues in the T2DM field is whether or not impaired mitochondrial function plays a causal role in the disease.

On the one hand, many studies propose the hypothesis that IR arises from impaired mitochondrial FA oxidation, increasing intracellular FA metabolites such as DAG and fatty-acyl CoA, ultimately disrupting insulin signalling. Example of these studies using MRS technique is the work of Petersen and colleagues who reported that young insulin-resistant offspring of parents with T2DM had decreased skeletal muscle mitochondrial activity and increased intramyocellular FA (Petersen et al. 2004), as well as a lower ratio of type 1 fibers (oxidative) to type 2 (glycolytic). Conceivably, these individuals with less

type 1 fibers might have lower mitochondria number and less expression of mitochondrial biogenesis genes (Mootha, Lindgren, et al. 2003; Patti et al. 2003). In line with this, Petersen and her group also studied mitochondrial function in insulin-resistant elderly to assess the aging consequences. They found that healthy lean elderly had severe IR in skeletal muscle along with higher levels of TG in the same muscle and in liver, in comparison to young controls (Petersen et al. 2003). These effects were accompanied by a decrease in mitochondrial oxidative capacity and ATP synthesis. In keeping with this, different studies have reported a decrease in the expression of nuclear-encoded genes that regulate mitochondrial biogenesis such as *PGC1α*-responsive genes in obese Caucasians with IGT and T2DM (Mootha, Lindgren, et al. 2003), and *PGC1α* and -*β* in obese and overweight non-diabetic Mexican-Americans (Patti et al. 2003).

Almost 40 years ago, Vondra and colleagues studied isolated mitochondria from muscle biopsies observing lower mitochondrial activity in T2DM subjects (Vondra et al. 1977). Later, Kelley and colleagues reported 30-40% lower mitochondrial marker enzymes activity in T2DM patients (Kelley et al. 2002; Kelley et al. 1999; Simoneau et al. 1999; He et al. 2001). However, Kelley and colleagues did not assess strictly "mitochondrial function". Of note, the effects observed in the experiments with isolated mitochondria might be related to obesity rather than IR, given that the isolated mitochondria samples were from diabetic obese individuals, and obese individuals are known to have smaller mitochondria size, reduced mitochondrial content, and altered mitochondrial performance (Kelley et al. 2002).

On the other hand, there are other studies and proofs that mitochondria are not in causal relationship to IR. These studies did not hypothesize that IR might be the cause to mitochondrial dysfunction, but that if there is mitochondrial dysfunction, it might be concomitant. The 30% reduction in mitochondrial density in T2DM and insulin-resistant individuals (Morino et al. 2005) might suggest that it is itself the cause of IR, but it is also clear that correlation does not mean causality. It is problematic to study the causality between IR and mitochondrial function since, as explained in the section 1.3, T2DM and obese insulin-resistant individuals are insulin-resistant for many years before they are diagnosed. Therefore, evidence should be found in rodent studies that develop skeletal muscle IR after a few weeks on HFD. Among these studies, HFD was found to increase muscle levels of mitochondrial marker enzymes (β-hydroxybutyrate dehydrogenase and citrate synthase, CS) (Miller et al. 1984; McAinch et al. 2003); and HFD (Turner et al. 2007; Hancock et al. 2008) or intermittently elevating plasma FA (Garcia-Roves et al. 2007) induced an increase in muscle mitochondrial biogenesis, evidenced by increased mitochondrial

marker enzymes, FA oxidation and mitochondrial DNA (mtDNA) copy number, at the same time that showed clear evidence of IR. Moreover, in transgenic rodent studies with severe muscle mitochondria deficiency/dysfunction, the animals ended up with even increased glucose tolerance, insulin sensitivity and insulin-stimulated glucose uptake (Wredenberg et al. 2006; Pospisilik et al. 2007; Zechner et al. 2010; Han et al. 2004). The high severity of the mitochondrial deficiency/dysfunction caused, in fact, an extremely low substrate oxidative capacity, increasing adenosine monophosphate (AMP) and activating AMP-activated protein kinase (AMPK) which ultimately would stimulate glucose transport and increase GLUT4, improving insulin responsiveness (Wredenberg et al. 2006; Han et al. 2004; Han et al. 2011).

Important to mention is that, in humans, T2DM patients have a sufficiently high respiratory capacity to increase substrate oxidation 40-fold, in a way that the mentioned 30% lower mitochondria content (Mootha, Lindgren, et al. 2003; Patti et al. 2003; Morino et al. 2005; Befroy et al. 2007) would not limit the resting substrate oxidation in skeletal muscle (Larsen et al. 2009). In fact, other studies revealed normal mitochondrial function, although mitochondria were smaller or less in T2DM skeletal muscle (Boushel et al. 2007; Larsen et al. 2009; Ara et al. 2011).

Moreover, Toledo and colleagues demonstrated how diet-induced weight loss improved IR without increasing mitochondrial capacity (Toledo et al. 2008), while Nair and colleagues found that insulin-resistant Asian Indians with T2DM have a muscle mitochondrial capacity for oxidative metabolism similar to that of nondiabetic Indians and even higher than that of North Americans of Northern European ancestry (Nair et al. 2008).

Considering that studies aiming to define the cause-consequence between IR and mitochondrial dysfunction have differences in their methodology, sex, genetic background, and experimental design, the mechanism by which mitochondrial function might contribute to the development of IR and T2DM needs yet to be clarified. As mentioned before, the causes of IR and/or T2DM in each tissue will break down in sections 1.8.

1.6.4 Tissue-specific mitochondria

A diverse functional program determined by the translation of nuclear DNA exists for different tissues mitochondria and even within a tissue for different environmental or clinical conditions (Balaban 2010). In the last decade, mitochondrial proteome studies showed that depending on the functional needs of a given tissue, its mitochondrial

program was altered (Forner et al. 2006; Johnson et al. 2007; Mootha, Bunkenborg, et al. 2003). Apart from proteome, rodent studies provided evidence for tissue-specific differences in mitochondrial properties such as mtDNA copy number, cytochrome c oxidase activity and mitochondrial mass in liver, cardiac muscle, and glycolytic and oxidative skeletal muscle (Weibel et al. 1969; Eisenberg & Kuda 1975; Eisenberg & Kuda 1976; Gagnon et al. 1991; Wiesner et al. 1992; Holmström et al. 2012). Also, mitochondrial function can be also modulated by post-translational modifications in a disease- and tissue-specific manner (Balaban 2010). Hence, mitochondrial function varies from tissue to tissue and it will also be discussed in the sections 1.8 for each of them.

1.7. Current interventions and approaches - Overview

The current treatments for obesity-related T2DM encompass from LIs to pharmaceutical and surgical approaches.

1.7.1 Current algorithm of treatment of T2DM

The ADA and the European Association for the Study of Diabetes (EASD) described an algorithm for the treatment of T2DM that advocated a stepwise therapeutic approach based upon the reduction in plasma glucose concentration and not upon the already published pathophysiological derangements. During the last years, pathophysiological-based algorithms have been proposed (Defronzo 2009) to achieve better goals such as β-cell preservation and durability, aiming to avoid hypoglycaemia and weight gain.

Furthermore, ADA and EASD published a "Position Statement" (Inzucchi et al. 2012) describing joint guidelines for the T2DM treatment (Figure 2). As mentioned, this statement advocates for a control on hyperglycemia with general recommendations. As a first step, **lifestyle changes** are prescribed (healthy eating, weight control and increased physical activity) and metformin monotherapy is added at, or soon after, diagnosis (unless it is contradindicated for the patient). ADA's "Standard of Medical Care in Diabetes" defined in 2011 the goal of lowering glycated hemoglobin (HbA1c) to 7.0% in most patients to reduce microvascular disease incidence (American Diabetes Association (ADA) 2011). If the HbA1c at 7% is not achieved after 3 months, different new steps of combination therapy with two or three types of drugs are considered as indicated in the Figure 2.

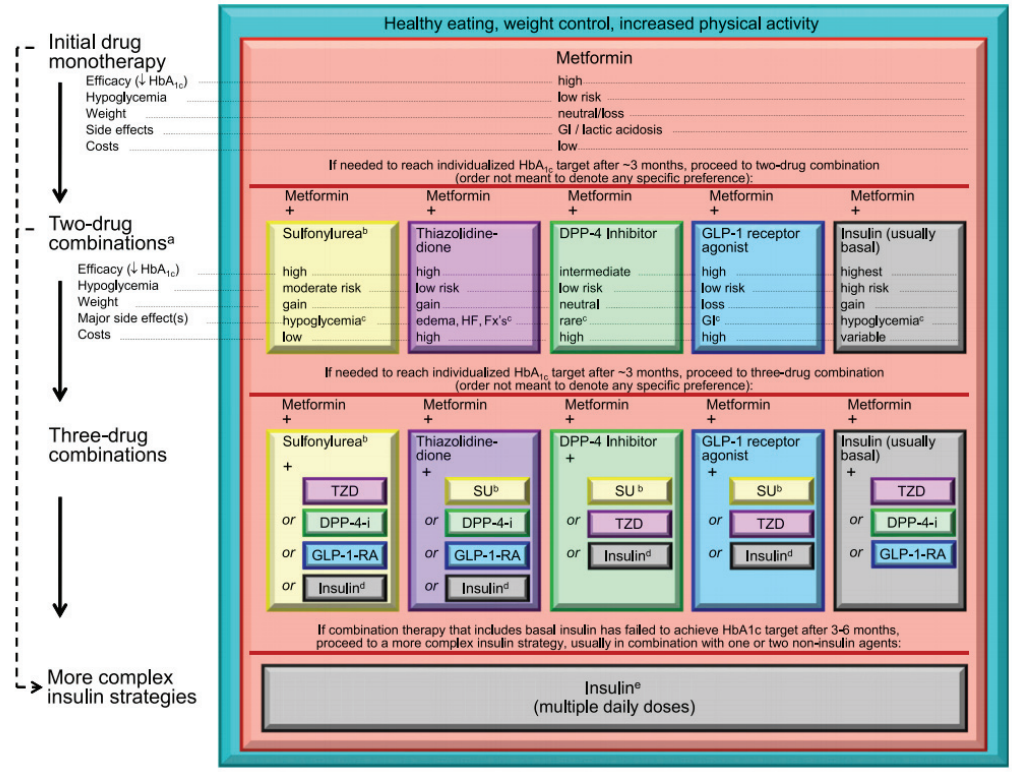

Figure 2. ADA-EASD algorithms for the treatment of T2DM.

1.7.2 Education and support

An important approach with people at high risk of developing T2DM, the so-called "pre-diabetes" state, is the education, counseling and support to the patients. These strategies aim to raise awareness of the risk of suffering T2DM and support the patients with their disease's self-management. Although the ADA established Diabetes Self-Management Education And Support (DSME and DSMS) for patients already diagnosed with T2DM, people with pre-diabetes might also be eligible. In this pre-diabetes case, though, the goal is defined as developing and maintaining behaviours and habits that delay or even prevent the onset of T2DM.

1.7.3 Pharmacological interventions

Nowadays, several drugs attempting to improve the health of T2DM patients are in the market. However, the ones approved for being successful in this purpose show limitations in curing or avoiding the major comorbidities associated with the disease. Thus, pharmacological targets are still being studied. The drugs used for obesity-related T2DM

such as metformin, TZD, and α-glucosidase inhibitors have shown a decrease in the incidence of diabetes at different degrees.

1.7.3.1 Current first-line therapy

Metformin is an oral biguanide that suppresses HGP, and has demonstrated long-term safety as a therapy for T2DM prevention with strong evidence (Bray et al. 2012). However, the molecular mechanism is yet poorly understood. Inhibition of mitochondrial redox shuttle enzyme glycerophosphate dehydrogenase has been proposed as mechanism, leading to alterations in redox state, reduction of convertion of lactate and glycerol to glucose and decrease in hepatic gluconeogenesis (Madiraju et al. 2014). Inhibition of mitochondrial CI by inhibiting ubiquinone reduction (but not competitively) while stimulating ROS production by CI flavin is also a mechanism described in the literature (Bridges et al. 2014). As a consequence of CI inhibition, mitochondrial respiration is decreased; diminishing energy availability that leads to activation of AMPK, inhibition of glucagon receptor-cAMP signal, and decrease of gluconeogenic enzyme activity (Rena et al. 2013).

Diabetes Prevention Program (DPP) and Diabetes Prevention Program Outcomes Study (DPPOS) studies showed that LI was more effective and cost-effective than metformin therapy after a 10-year follow-up study (Herman et al. 2012; Knowler et al. 2002). Metformin was as effective as LI in patients with BMI equal or above 35 kg/m^2, although it was not more effective compared with the placebo treatment in patients over 60 years of age (Knowler et al. 2002). In the DPP study, both metformin and LI also showed a 50% reduction in the risk of developing T2DM in women with a previous GDM (Ratner et al. 2008). In general, metformin is recommended for all those patients with a high-risk of suffering T2DM (i.e. the ones with history of GDM, who are very obese and/or suffer more severe or progressive hyperglycemia) but not prescribed with patients suffering from severe kidney or liver problems (Vijan 2010).

Apart from prevention, metformin is generally also used as a first line of treatment, after T2DM has been diagnosed. After 3 months, if metformin itself is not sufficient, other classes of oral drugs might be prescribed or insulin may be added to the pharmacological therapy (Inzucchi et al. 2015). Second oral drugs that can be added to the therapy according to the guidelines, which show no significant differences among them (Inzucchi et al. 2015) are: **TZD** that act by activating peroxisome proliferatior-activated receptors (PPARs), nuclear receptors that bind DNA and modify transcription of certain genes and that have

not shown to improve long-term outcomes (Richter et al. 2007) producing complications such as CVD and even death (Chen et al. 2012); **sulfonylureas** (SU) that act by increasing insulin secretion in the pancreatic β-cell but might then produce hypoglycaemia as a severe side effect; and newer and more promising ones such as glucagon-like peptide-1 (GLP-1) receptor agonists, DPP inhibitors and SGLT2 inhibitors.

1.7.3.2 GLP-1 receptor agonists or incretin mimetics

GLP-1 receptor agonists or incretin mimetics act by activating the GLP-1 receptor and performing hypoglycemic effects by inducing glucose-stimulated insulin secretion (GSIS) and suppressing glucagon secretion. Back in 2005, *exenatide* was approved as the first drug of this class. This class of drugs show a lower risk of hypoglycaemia in comparison with SU (American Diabetes Association (ADA) 2012).

1.7.3.3 DPP-4 inhibitors or gliptins

Inhibitors of dipeptidyl peptidase 4 (DPP-4 inhibitors) are oral hypoglycemic drugs that block DPP-4. The mechanism by which DPP-4 inhibitors reduce blood glucose levels and glucagon consists in increasing incretin levels (GLP-1 and gastic inhibitory polypeptide, GIP), which in turn blunts the release of glucagon that finally increases insulin secretion, and decreases the glycemia and the gastric emptying (McIntosh et al. 2005; Behme et al. 2003; Dupre et al. 1995). Back in 2006, the Food and Drug Administration (FDA) in the US approved the first drug of this class: *sitagliptin*. Many different gliptins have been approved after successful clinical trials.

1.7.3.4 SGLT2-inhibitors

Sodium/glucose transporter 2 (SGLT2)-inhibitors are the newest class of drug for T2DM patients. Its mechanism consists in increasing urinary glucose excretion and therefore reducing hyperglycemia, independently of insulin secretion and/or action. The clinical results of the use of this new class of drug have shown a decrease in HbA1c with no increase in hypoglycaemia, and a decrease in BW along with a reduction in systolic blood pressure (Cuypers et al. 2013). The European Medecine Agency (EMEA) approved back in 2012 *dapagliflozin* as the first highly selective SGLT2-inhibitor. In 2014, the FDA also approved it for T2DM patients: first for glycemic control with the concomitant prescription of diet and exercise LI, and later in combination with metformin-hydrochloride extended-release.

It is worth mentioning that prediabetes patients normally suffer from other comorbilities such as hypertension, dyslipidemia and obesity that lead to an increased risk for CVD. For

this purpose, it is important that the treatment takes these risk factors into account and increases the vigilance over the selected treatment.

1.7.4 Surgical interventions

For those patients suffering from a serious and severe obesity (i.e. morbid obesity), a gastric by-pass surgery can be performed in order to treat obesity itself and ameliorate other comorbid conditions such as T2DM, hypertension and sleep apnea. The long-term mortality after a gastric by-pass can be reduced up to 40% (Sjöström et al. 2007; Adams et al. 2007) although many patients have complications that can ultimately lead to death.

1.7.5. Lifestyle interventions, an overview

Sedentary habits along with an excess of macronutrients intake are spreading obesity-related T2DM, hence becoming an epidemic global problem. In light of the above, it is becoming clear nowadays that a LI that includes regular physical activity and a healthy diet to reduce or maintain a normal BW could prevent or delay the onset of T2DM (Knowler et al. 2002) and improve the detrimental effects of obesity (Unick et al. 2013).

Hence, LI becomes the first approach for insulin-resistant individuals. The first goal is the prevention of the onset of T2DM, although LI is also prescribed after the diagnosis to ameliorate the prognosis. Individuals at high risk for developing T2DM (those with IFG, IGT or both conditions at the same time) have shown to decrease the rate of diagnosed diabetes undergoing different LI (Knowler et al. 2002; Buchanan et al. 2002; Chiasson et al. 2002; Lin et al. 2014; Paulweber et al. 2010). These LI included programs that have shown high effectiveness in follow-up studies showing sustained reduction in the rate of conversion to T2DM: 43% of reduction after 7 years in the Finnish Prevention Study (Lindström et al. 2006), 43% of reduction after 20 years in the Da Qing study (Li et al. 2008), and a 34% of reduction after 10 years in the US DPPOS (Knowler et al. 2009).

Furthermore, the DPP reported that after an average follow-up of 2.8 years, the incidence of T2DM was 4.8% in the group undergoing LI (Knowler et al. 2002), in contrast to a 7.8% in the group treated with metformin or a 11% in the group treated with placebo. Thus, LI reduced the incidence by 58% after 3 years compared to placebo, while metformin decreased incidence by only 31%.

Among the different LIs, **exercise** has been able to prevent or delay T2DM in patients at risk (Eriksson & Lindgärde 1991; Pan 1997; Tuomilehto et al. 2001). Exercise has been known

to increase insulin sensitivity and improve impaired insulin action in insulin-resistant humans and animals (Perrini et al. 2004). Already years ago, different studies showed how specifically chronic exercise was able to improve insulin sensitivity and glucose tolerance, improving the glucose homeostasis process in general (Mikines et al. 1989; DeFronzo et al. 1987; Rogers et al. 1988). Mikines and coworkers observed a 2.7-fold increase in maximal insulin-stimulated glucose disposal rate (GDR) in insulin-resistant subjects after 6 wks of exercise training (Mikines et al. 1989). Olefsky and colleagues observed how 4 wks of exercise alone did not significantly decrease glycemia, although it decreased free FA (FFA) and improved insulin sensitivity by increasing GDR (Hevener et al. 2000). Moreover, the glycemia decreased along with other improvements when the exercise was prescribed in combination with thiazolidinediones (TZD) treatment. Exercise alone was able to reduce the risk of T2DM and CVD through the reduction of blood pressure, the improvement in the lipid profile and the increase in insulin sensitivity (Slentz, Houmard, et al. 2009).

Insulin signalling pathway has also been studied after exercise, to decipher if the beneficial effects of the physical activity had their mechanism through the signalling cascade. Protein kinase C β (PKCβ), a kinase involved in the insulin signalling cascade, has been suggested to be involved in the exercise-induced improvements in IR in skeletal muscle (Itani et al. 2000; Cooper et al. 1993; Itani et al. 2001). Therefore, and after reporting a decreased the expression of *Pkcβ* in liver and skeletal muscle after 8 wks of exercise, a rodent model *Pkcβ*-deficient (*Pkcβ*-/-) was created (Rao et al. 2013). WT and *Pkcβ*-deficient mice were fed on HFD for 12 wks, and divided then in exercised and sedentary groups. After the exercise, exercised WT and both exercised and sedentary *Pckβ*-deficient mice lowered BW in comparison to the sedentary WT mice. Also, sedentary WT showed more glucose intolerance, less insulin sensitivity and higher plasma insulin and leptin levels. Hence, *Pkcβ* deficiency enhanced insulin sensitivity regardless of exercise, suggesting that exercise-induced improvements may involve PKCβ mediated pathways. Of note, the four groups showed the same levels of adiponectin (Rao et al. 2013).

Regarding the type and/or dose of exercise, Rosenkilde and colleagues divided moderately overweight patients in sedentary, moderate and high-intensive exercise for 13 wks to discern the effects of different doses of exercise (Rosenkilde et al. 2012). They observed a similar body fat loss regardless of the exercise dose. However, Slentz and colleagues demonstrated how vigorous exercise decreased visceral fat and improved VO_{2peak} by increasing energy expenditure (Slentz, Tanner, et al. 2009). Moreover, pancreatic β-function

was improved in both moderate- and vigorous-intensity exercise but the former showed no reduction in insulin secretion (which happened in the vigorous-intensity group).

Furthermore, exercise has been observed in Zucker rats to lead to a **reduction of BW** and/or fat mass that improves insulin sensitivity and ultimately delays hyperglycemia (Gabriely et al. 2002). Kelley and colleagues showed how weight loss could improve partially the aforementioned metabolic inflexibility in obese individuals (Kelley et al. 1999). Other human studies showed how 5-7% of weight loss after modification of the diet had beneficial effects on circulating inflammatory markers in obese subjects (Christiansen, Paulsen, Bruun, Pedersen, et al. 2010). However, in this same study no effects on inflammatory markers appeared after 12 wks of aerobic exercise, although VO_{2max} increased. Thus, Christiansen and colleagues suggested that in order to affect systemic inflammation, more intensive exercise might be necessary (Christiansen, Paulsen, Bruun, Pedersen, et al. 2010).

Dietary LIs have also showed promising results. Polyunsaturated FA (PUFA) such as omega-3 (Om3) FA have shown to stimulate insulin sensitivity (Popp-Snijders et al. 1987; Gingras et al. 2007; González-Perín et al. 2009; Oh et al. 2010) and reduce inflammation (Oh et al. 2010; Rangel-Huerta et al. 2012; Hellmann et al. 2011; Reinders et al. 2012), both phenomena being beneficial for delaying or supressing the development and onset of T2DM. Thus, Om3 FA have been suggested to exert a protective effect against disease and/or metabolic dysfunction. In fact, patients with lower levels of Om3 FA revealed an increasing risk of T2DM while increasing also the non-sterified FA (NEFA) in the circulation (Steffen et al. 2015). Caloric restriction (CR) has also shown beneficial effects, such as improving insulin sensitivity and attenuating the development of hyperglycemia in Zucker rats (Ohneda et al. 1995). However, Holloszy and colleagues observed that a 30% CR for 14 wks in mice did not improve mitochondrial biogenesis in any of the following tissues: heart, brain, liver, adipose tissue, and skeletal muscle (Hancock et al. 2011).

It is worth mentioning the Look AHEAD (Action for Health in Diabetes) study focused on long-term weight loss effects. This study randomly assigned T2DM overweight/obese patients to intensive lifestyle intervention (ILI) (**diet** and **exercise** intervention, which provided comprehensive behavioural weight loss counseling with weekly group or individual treatment for the first year and less frequent the following ones) and DSE (diabetes support and education, with three group educational sessions during all study years). ILI beneficial results were shown already after the first year: T2DM patients

showed improvements in adipose tissue distribution (upper body fat, visceral fat, and deep abdominal subcutaneous adipose tissue decreased), insulin sensitivity, fasting glucose and circulating FFAs (Albu et al. 2010). Moreover, the most important metabolic improvements were the changes in overall BW, adipose mass, and hepatic fat. After the first year and due to the fact that the Look AHEAD study attempted to assess whether CV morbidity and mortality in T2DM patients could be reduced with long-term weight reduction, only weight loss and CV features were monitored. In year 4, ILI participants lost an average of 4.7% of initial BW, compared with 1.1% for DSE ($p<0.0001$) (Wadden et al. 2011). After 8 years, the study registered still a higher weight loss in the ILI group with an overall of at least 5% weight loss in 50% of T2DM patients (Wadden et al. 2014). One could expect these weight losses to be beneficial for the T2DM patients. However, after 9.6 years the Look AHEAD study was stopped for futility with no CV outcomes (Pi-Sunyer 2014).

Mitochondrial function has been assessed in different studies after performing LI. **Exercise** intervention increased skeletal muscle mitochondrial content and thereby oxidative capacity (TCA enzymes activity) (Toledo et al. 2007; Bruce et al. 2004; Hansen et al. 2009; Dubé et al. 2011), activity of the ETS (Toledo et al. 2007; Hansen et al. 2009), β-oxidation (Bruce et al. 2004; Dubé et al. 2011), and improved IR (Dubé et al. 2011). Also, T2DM patients recovered mitochondrial content and *in vivo* submaximal ADP-stimulated OxPhos after 12 wks of exercise (Meex et al. 2010; Phielix et al. 2010). Apart from exercise, **diet**-induced weight loss improved insulin sensitivity with no improvement in mitochondrial capacity (Toledo et al. 2008; Rabøl, Svendsen, et al. 2009). It is worth mentioning that in some cases, **genetic** inherited factors contribute to the mitochondrial response to a LI that is, mitochondrial plasticity. Such is the case of the carriers of the *NDUFB6* gene SNP rs540467 (G/G) that encodes part of the CI, who showed increased insulin sensitivity and mitochondrial activity after a 1-wk endurance exercise training. This also increases correlated with maximal whole-body oxygen consumption. None of these changes were observed in carriers of the A allele (Kacerovsky-Bielesz et al. 2009).

Another fact is that LI tend to be **cost-effective**, and the DPP and the DPPOS studies confirmed this fact (Herman et al. 2012). Nowadays, the ADA describes an increased risk for T2DM in people who has Hba1c 5.7-6.4%, IGT or IFG (American Diabetes Association (ADA) 2010). Given the increased risk of these individuals, they should be counseled on lifestyle changes attempting to achieve similar results as the DPP study, which showed a 7% weight loss after a moderate intensity exercise training of at least 150min/wk.

1.7.5.1. LI best approach

In keeping with this, some studies have suggested a combination of different types of interventions. It is the case of the study by Christiansen and colleagues (Christiansen, Paulsen, Bruun, Ploug, et al. 2010), where overweight subjects were randomized in undergoing different LI: diet-induced weight loss only (D), exercise only (EX), or the combination of both for 12 wks (DEX). EX and DEX group increased the VO_2max, while D and DEX showed the greatest weight loss (11% in contrast to the 3.5% in EX), and the greatest decrease in anthropometric parameters such as waist conference and a decrease in homeostatic model assessment (HOMA) (EX did not reduce HOMA). In this same study, D and DEX groups increased adiponectin by 20% while in EX group a reduction by 6% was observed. Taking all this together, DEX group appears to correct more disrupted features that appear in obese healthy subjects.

Other works include the study from Toledo and colleagues which reported that the combined intervention of exercise and diet improved skeletal muscle mitochondrial content (mitochondrial density and size, NADH oxidase activity, cardiolipin levels) in obese patients, significantly more than a LI with diet alone (Toledo et al. 2008); or the study from Suga and colleagues where they observed that combination of dietary and exercise LI normalized the decrease in mitochondrial function and inhibited the oxidative stress after HFD (Suga et al. 2014).

1.8. Multiorgan implication

T2DM is a multi-organic disease, meaning that many tissues play an important role in the early development of IR and the later onset of the disease. Consistent with this concept, DeFronzo stated back in 2009 (Defronzo 2009) that research for the treatment of T2DM should consider not only the so-called triumvirate including the pancreas, liver and skeletal muscle, but also new players that could form the new concept of the "octet" including adipose tissue, gastrointestinal tract, α-cells, kidney and brain. In keeping with this, DIAMAP (a program that attemps to find gaps and highlight strengths in European Diabetes research to guide future strategies in the field) proposed integrative physiology approaches in order to understand both tissue-specific and whole body metabolism in T2DM (Zierath et al. 2013). This way, new research strategies also stress the importance to decipher tissue-specific phenomena and inter-organ crosstalk (Zierath & Wallberg-Henriksson 2015). Hence, there is a demand to look at T2DM disease through integrative physiology, stressing the need to take advantage of systems-biology tools. Along these lines, new research guidelines confirm the importance of the approach presented in this PhD thesis consisting of an integrated understanding of the pathophysiology of T2DM.

The key players in T2DM studied in this PhD thesis are: pancreas, adipose tissue, liver, skeletal muscle, and hypothalamus. The interpretation of T2DM including other tissues besides the historical "pancreas-liver-muscle" also raises concerns about the implications for therapy. That is to say, a treatment algorithm should then achieve the reversal of known pathophysiological defects and not be based only upon the reduction of plasma glucose concentration, should require multiple drugs used in combination to correct the multiple pathophysiological defects and, if progressive β-cell failure is to be prevented, the therapy must start early in the natural history of T2DM (Defronzo 2009). Taken all stated above, lifestyle changes such as healthy eating and an increase in physical activity became an essential first front to prevent or delay the onset of T2DM.

1.8.1. Pancreas

The pancreas has an endocrine and an exocrine functions. As an endocrine gland, it is capable of producing several hormones such as insulin, glucagon, somatostatin and pancreatic polypeptide, which can circulate in the blood stream. It also has a role in the digestive system as an exocrine gland by secreting pancreatic juice that contains digestive enzyme that are responsible for helping in the digestion and absorption of nutrients in the small intestine. The endocrine cells are grouped in structures called islets of Langerhans that account approximately for the 1-2% of pancreas mass (Langerhans 1869). In a healthy adult human pancreas there could be around one million islets distributed through the organ and separated from the surrounding pancreatic tissue by connective tissue (Sleisenger et al. 2009). In islets of Langerhans in rodents, different cell subsets have been described producing different hormones: α-cells that produce glucagon (15-20% of total islet cells), β-cells that produce insulin and amylin (65-80%), δ-cells that produce somatostatin (3-10%), γ-cells that produce pancreatic polypeptide (3-5%) and ε-cells that produce ghrelin (less than 1% of total islet cells) (Elayat et al. 1995). Unlike rodent islets, human islets contain α- and β-cells in a similar proportion (Brissova et al. 2005; Cabrera et al. 2006).

1.8.1.1 Pancreatic β-cell dysfunction in IR and obesity-related T2DM

Pancreatic islets have one of the main roles in T2DM since, as aforementioned, β-cell function is not preserved and starts to fail prior to the onset of the disease. With the onset of IR, insulin secretion is increased due to the compensatory effect exerted by the pancreas which, at first, increases its β-cell mass and shows hypertrophy (Efrat 2001). During this compensatory effect in IR obese normoglycemic individuals there was an

increase of 150% in β-cell mass (Vinik et al. 1996), while at the time of T2DM diagnosis, these individuals showed a β-cell mass reduction by 80% (Butler et al. 2003). Therefore, T2DM does not occur in the absence of a progressive β-cell failure (Defronzo 2009). However, T2DM cannot be reproduced by simply reducing β-cell mass in animal models (D R Laybutt et al. 2002), since it involves different disruptions. In fact, hyperglycemia appears after a 85-95% pancreatectomy (Leahy et al. 1988) and not with a 40-60% reduction of β-cell mass (D. Ross Laybutt et al. 2002). Regarding the obese state, Butler and colleagues observed how obese individuals with IFG had a 40% reduction in β-cell mass while this percentage reached 63% when the obese individuals had T2DM. They also showed how lean T2DM individuals had a 41% in the β-cell mass loss (Butler et al. 2003). The β-cell mass expansion and involution (shrinkage) in order to compensate the loss of insulin sensitivity and maintain glucose levels is known as β-cell plasticity. Furthermore, they studied β-cell apoptosis and observed a 10-fold and a 3-fold increase in T2DM lean and T2DM obese individuals, respectively. The studies of Butler and colleagues suggest that obese individuals that have IFG rely on β-cell plasticity to meet the homeostatic demand for more insulin secretion. In addition, these findings indicate that the loss in β-cell mass in T2DM states is due to an increased β-cell apoptosis (Butler et al. 2003).

Moreover, there is an increase in β-cell proliferation prior to an increase in β-cell mass. This increase in β-cell proliferation in an obese state was proposed to be a consequence of IR, but studies from Mosser an colleagues with C57BL/6J male mice demonstrated that after only 3 days on HFD β-cell proliferation was present, and this happened weeks before an increase in β-cell mass or peripheral IR was detected (Mosser et al. 2015). They also performed *in vitro* studies with isolated islets from 1-week HFD-fed mice to confirm the increase in islet proliferative gene expression when compared to mice fed with chow diet.

Hence, the point when β-cell mass reaches its threshold to compensate IR without exerting any plasticity precedes the β-cell failure (Porte 2001). This way, it seems well established that IR is the earlier process during the onset of T2DM, and that the disease does not occur without progressive β-cell failure (Defronzo 2009).

Pathogenesis of β-cell failure

There are many factors that play a role in the pathogenesis of β-cell failure that instigate a ultimate loss in β-cell mass by apoptosis (Butler et al. 2003): some that could be ameliorated and/or reversed such as IR, glucotoxicity, lipotoxicity, incretins, islet amyloid

polypeptide (IAPP) deposition and oxidative stress and inflammation; and some others for which there are not feasible therapeutic options such as genetic predisposition and aging.

One of the theories for this failure consists of the β-cells wearing away and getting exhausted after the compensatory hypersecretion, although it has not yet been demonstrated. Moreover, it has been proposed that the fat deposition could be the cause for both: β-cell failure and IR itself. The ectopic FA accumulation that happens in insulin-sensitive tissues such as liver and skeletal muscle leading to peripheric IR, could also take place in β-cells impairing insulin secretion and leading to β-cell failure. This FA accumulation in the tissues is known as **lipotoxicity**. In keeping with this, different studies have described how lipotoxicity impairs insulin secretion. DeFronzo and colleagues described an impaired insulin secretion in genetically predisposed individuals after elevating their plasma FFA during 48h (Kashyap et al. 2003). In the same line, Higa and colleagues performed *in vitro* studies with human pancreatic islets and observed a reduction in insulin secretion during the acute insulin response when the islets were previously incubated for 48h with FFA. In this condition, the islets showed reduced insulin mRNA expression, islet insulin content and glucose-stimulated insulin release (Higa et al. 1999). Apart from impairing insulin secretion by diminishing β-cell function, long-term elevation of FFA has been shown to be cytotoxic (Lupi et al. 2004). In fact, FFA and in concrete ceramide formation within β-cells induced apoptosis by activating the caspase pathway (Lupi et al. 2002).

Conversely, when a hypolipidemic agent such as *acipimox* was used in nondiabetic patients with a family history of T2DM, a sustained reduction in plasma FFA along with an improved insulin secretion was observed (Kashyap et al. 2003). In the same line, TZD such as *rosiglitazone* and *pioglitazone*, that activate PPAR and specially PPAR-γ which acts by taking fat away from the β-cell, showed an ameliorated insulin secretion and IR in T2DM patients (Lupi et al. 2004; Gastaldelli et al. 2007), and directly protected β-cells (Unger & Zhou 2001).

Glucotoxicity, chronic hyperglycemia, has been proposed to occur independently of lipotoxicity, whereas the later seems to only occur with concomitant hyperglycemia (Poitout & Robertson 2002). In a similar trend, glucotoxicity also impairs β-cell function (Rossetti et al. 1990). Leahy and colleagues described an inhibition of GSIS in isolated perfused pancreas from rats under a treatment with a slight elevation during one day of the plasma glucose levels *in vivo* (Leahy et al. 1986). Studies of isolated human islets *in vitro*

also demonstrated that impaired insulin secretion appears after a chronic exposure to elevated glucose levels in plasma (Patanè et al. 2002; Andreozzi et al. 2004). Regarding the concrete pathways that might be affected, hyperglycemia leads to a reduction in insulin secretory genes expression as well as key transcriptions factors such as pancreatic and duodenal homeobox 1 (*Pdx*-1), the activator of glucose-regulated insulin gene *expression* (D Ross Laybutt et al. 2002; Laybutt et al. 2001; Leibowitz et al. 2001) and the main regulator of pancreas development and β-cell differentiation and function (Stoffers et al. 1997). In parallel, hyperglycemia increases the expression of genes involved in β-cell hypertrophy such as *cMyc*, a transcription factor related to β-cell growth and apoptosis (D Ross Laybutt et al. 2002). The same way hypolipidemic chemicals were able to improve IR, the use of *phlorizin*, an inhibitor of renal glucose transport, normalized the plasma glycemia in pancreatomized diabetic rats (Rossetti et al. 1987). Hyperglycemia should then be reverted to avoid β-cell glucotoxicity, and IR in liver and skeletal muscle. Of note, by reverting hyperglycemia many of its microvascular complications might also be prevented.

Regarding metabolic hormones, **incretins** have also been implicated in β-cell failure. Incretins decrease glycemia before it is increased after a meal, by increasing insulin released by pancreatic β-cells and decreasing glucagon secreted by α-cells. GLP-1 and GIP are the two main incretins that account for a 90% of the incretin effect (Drucker 2006; Drucker & Nauck 2006; Meier & Nauck 2006). In T2DM individuals, a deficiency in GLP-1 (Drucker 2006; Drucker & Nauck 2006; Meier & Nauck 2006) along with GLP-1 resistance was observed (Kjems et al. 2003; Holst & Gromada 2004) on the one hand; and on the other hand, GIP resistance was also observed (Nauck et al. 1986; Holst 2006; Nauck et al. 1993; Meier et al. 2001), although GIP plasma levels were increased without exerting its effect increasing insulin secretion (Jones et al. 1989). It is worth mentioning that GLP-1 replacement has been considered as an early treatment since its deficiency was shown to progressively appear with the transition from IGT to the onset of T2DM (Toft-Nielsen et al. 2001).

Another player in the β-failure hallmark is the **IAPP** hypersecretion and the consequent amyloid deposition in the pancreatic islets (Eriksson et al. 1992; Johnson et al. 1989). IAPP, or amylin, is co-localized with insulin in the secretory granules (Lukinius et al. 1989) and its deposition in the form of fibrils generates the amyloid, although the mechanism of amyloidogenesis remains unknown. The amyloid deposits seem to generate space-ocupying lesions that are responsible for the impairment in insulin secretion. In humans, some studies observed that up to 90% of individuals with T2DM have amyloid deposits (Finegood & Topp 2001) and the degree of amyloidosis is correlated with the duration and

severity of T2DM (Hayden & Tyagi 2002). Thus, human amyloid is toxic to pancreatic β-cells and might be a factor contributing to its β-cell mass loss (Janson et al. 1999; Lorenzo et al. 1994). Guardado-Mendoza and colleagues observed in baboons a progressive decline in the log of β-cell function (HOMA-β) when the relative amyloid area of the pancreatic islets increased (Guardado-Mendoza et al. 2009). In rodent studies, β-cell mass was progressively reduced as amyloid deposit increased (Wang et al. 2001). Butler and colleagues showed *in vitro* how IAPP deposition induced ER-stress-mediated β-cell apoptosis and impaired insulin secretion in isolated human islets (Huang et al. 2007; Ritzel et al. 2007). In general, as amyloid deposit increases, β-cell mass decreases leading to β-cell dysfunction and glucose intolerance. Since amylin is secreted in a 1:1 ratio with insulin (Hartter et al. 1991; Lukinius et al. 1989), interventions aiming to improve insulin sensitivity by reducing insulin secretion are believed to have an impact on amylin too, helping to preserve the β-cell function.

Oxidative stress also has a role within diabetic pancreas. Chronic hyperglycemia has been linked to oxidative stress in pancreatic β-cell (Kajimoto & Kaneto 2004; Robertson & Harmon 2007). In fact, clinical studies revealed chronic oxidative stress in T2DM subjects (Rehman et al. 1999; Gopaul et al. 1995) and in diabetic patients' pancreatic islets (Sakuraba et al. 2002). Moreover, pancreatic β-cell from a T2DM rat model revealed oxidative stress that might be due to chronic hyperglycemia (Ihara et al. 1999). Murakami and colleagues observed that glutathione (a primary intracellular antioxidant) was decreased in its reduced form in diabetic patients (Murakami et al. 1989), while Tanaka and colleagues showed how glutathione peroxidase (which oxidase reduced gluthatione) could protect pancreatic β-cell glucose-induced oxidative stress (Tanaka et al. 2002). Pancreatic β-cell might be then more sensitive to ROS when exposed to oxidative stress given their low expression of antioxidant enzymes such as catalase (*Cat*) and glutathione peroxidase (*Gpx*) (Tiedge et al. 1997). In fact, antioxidant treatment in C57BL-*db/db* mice diminished apoptosis in pancreatic β-cell with no alterations in β-cell proliferation, supporting that reduction of β-cell mass due to chronic hyperglycemia is caused by oxidative-stressed induced apoptosis (Kajimoto & Kaneto 2004).

A well-established observation that **advancing age** is related to the incidence of T2DM has been demonstrated with different studies (Muller et al. 1996; Rosenthal et al. 1982; Chang & Halter 2003) showing that age is an important factor that, when advancing, leads to a concomitant decline in the preservation of the β-cell function.

Regarding **gene predisposition**, a strong evidence for a gene-related β-cell failure has been demonstrated. Different studies have described genes in T2DM patients that could be related to the β-cell failure, such as *TCF7L2*. *TCF7L2* plays an important role in β-cell proliferation and insulin secretion (Welters & Kulkarni 2008) encoding for a transcription factor involved in Wnt signalling. Groop and colleagues observed that impaired insulin secretion *in vivo* and diminished response to GLP-1 are correlated with a T-allele single nucleotide polymorphism (SNP) rs7903146 of the *TCF7L2* gene (Lyssenko et al. 2007). The presence of the CT or TT genotypes can predict T2DM in different ethnic groups (Cauchi et al. 2006) as well as to lead to a diminished survival free from suffering T2DM (Lyssenko et al. 2007). Other studies apart from the aforementioned genes, described how Finnish families with T2DM and a susceptibility locus on chromosome 12, showed an inherited impaired insulin secretion (Watanabe et al. 1999).

Apart from the β-cell failure that appears in an IR hallmark, β-cell can also be affected after a unique condition of **obesity**. However, the functional analyses as well as morphological and genetic changes in pancreatic islets after a HFD challenge have been few. In different islet studies by Imai and colleagues, they observed that DIO C57BL/6J mice might compensate for IR by showing hyperinsulinemia, but only in a partial way since there was a blunted increase of insulin secretion upon a glucose load (Roat et al. 2014). In keeping with this, the group previously showed how isolated islets from mice on HFD increased insulin secretion *ex vivo* when being challenged with glucose (Imai et al. 2007). Also in this line, rodent studies showed that HFD feeding led to hyperinsulinemia by compensating the IR with the expansion of the islets (Flier et al. 2001; Sone & Kagawa 2005). Moreover, when HFD feeding took place during long-term periods, insulin release was insufficient reaching the maximum of the compensatory effect, and β-cell started to show senescence, and eventually induced T2DM (Sone & Kagawa 2005).

Unfolded protein response (UPR) provides the cell with the ability to adapt to new demand, which is beneficial, for exemple, in pancreatic β-cells in an insulin-resistant state. The increased demand in insulin production could overwhelm the capacity of the ER to properly secrete insulin, thus inhibition of UPR leads to a β-cell dysfunction, as seen in β-cell specific X-box binding protein 1 (*Xbp1)* KO mice (A.-H. Lee et al. 2011). Of note, in liver and adipose tissue, activated UPR is maladaptive.

Inflammation has been shown to play a role in the β-cell failure. T2DM individuals and HFD-fed rodents had increased number of macrophages in their pancreatic islets (Ehses et

al. 2007). T2DM individuals showed an increase in IL1β secretion by the islets (Maedler et al. 2002), which could impair insulin secretion and promote β-cell apoptosis (Bendtzen et al. 1986). All together, this suggests a role of an increased inflammatory response in pancreatic islets in the β-cell dysfunction in T2DM.

Regarding morphological analyses in DIO mice, an increase in total β-cell area with the presence of larger islets was observed, although their shape was not abnormal (Imai et al. 2007). Functional and gene expression studies revealed a blunted increase of islets oxygen consumption in the HFD-fed mice after titration of glucose or uncoupling with carbonyl cyanide-4-(trifluoromethoxy)phenylhydrazone (FCCP), a 1.7-fold increase in the expression of hypoxia up-regulated 1 (*Hyou1,* an endoplasmic reticulum (ER) stress chaperon) and 2.2-fold in *Pgc1α*, and a decrease in some genes implicated in the cellular architecture such as *Col1a1* (major component of type I collagen) and *Aspn* (asporin, an extracellular matrix protein) (Roat et al. 2014).

Finally, **mitochondrial function** might have a role in the pathogenesis of β-cell failure. Mitochondrial metabolism is central to GSIS in β-cells given that these organelles act as fuel sensors, coupling nutrient metabolism with the exocytosis of insulin vesicles. In fact, ATP generated in the mitochondria participates in increasing cytosolic Ca^{2+}, ultimately allowing the exocytosis of insulin vesicles (Maechler & Wollheim 2001). In keeping with this, specific mutations in the mitochondrial genome have reported hereditary disorders with β-cell dysfunction (Maechler & Wollheim 2001; Maassen et al. 2004). However, β-cell dysfunction has been related to mitochondrial function through other mechanisms. β-cell dysfunction has been reported to be secondary to lipo- and glucotoxicity (Unger 1995; Poitout & Robertson 2002; Prentki et al. 2002). One hypothesis to link this toxicity with β-cell dysfunction has been through the uncoupling protein 2 (UCP2) (Zhang et al. 2001; Chan et al. 2001; Joseph et al. 2002; Krauss et al. 2003). Activation of UCP2 uncouples OxPhos and decreases ATP, thus decreasing insulin secretion. Different studies support this hypothesis: overexpression of *Ucp2* in β-cells decreases (Chan et al. 2001) and targeted inactivation of *Ucp2* gene increases (Zhang et al. 2001) GSIS. Also, UCP2 can be stimulated *in vitro* and in rodent models by lipo- and glucotoxicity (Zhang et al. 2001; Joseph et al. 2002; Krauss et al. 2003; Winzell et al. 2003; D. Ross Laybutt et al. 2002; Poitout 2004; Kashyap et al. 2003). Obese and T2DM rodents with *Ucp2* deficiency have improved β-cell function (Prentki et al. 2002; Chan et al. 2001), and *in vitro* cultures with lipo- and glucotoxicity β-cell dysfunction is prevented when the β-cells had a *Ucp2* genetic deficiency (Krauss et al. 2003; Yamashita et al. 2004; Joseph et al. 2004). In humans, a polymorphism increasing UCP2 has

been linked to a reduction in insulin secretion and higher frequency of T2DM (Krempler et al. 2002; Sesti et al. 2003; Sasahara et al. 2004). UCP2 can also be activated by superoxide ROS. In fact, superoxide is increased in β-cells of T2DM rodents (Krauss et al. 2003; Bindokas et al. 2003) and its removal inhibits UCP2 activity and restores GSIS (Krauss et al. 2003). Taken all together, it is still not clear whether mitochondrial function leads directly to β-cell dysfunction and further T2DM.

1.8.1.2 LIs on pancreatic β-cell

Pancreatic β-cell has been little studied in different LI in obese and/or T2DM individuals. Although **exercise** effects have been largely studied, its effect on β-cell function has not drawn much attention. In humans, exercise has been shown in different studies to exert a protective effect on pancreatic β-cells increasing insulin sensitivity or action (Davis et al. 2012; Dubé et al. 2012; Magkos et al. 2008), by a diminished insulin demand, thus attenuating both β-cell exhaustion and the increase in β-cell apoptosis.

Different human studies show that GSIS is decreased after exercise training in young (King et al. 1990), some middle-aged individuals (Dela et al. 2004; Slentz, Tanner, et al. 2009) and old population (Bloem & Chang 2008; Kirwan et al. 1993). However, most of the mentioned studies focus on the first-phase pancreatic β-cell function, that is, the available pool of insulin released upon initial glucose stimulation; and not in the second-phase, which accounts for the synthesis of new insulin following fluctuations in postpandrial glucose. It is worth mentioning that the second-phase is clinically relevant for the maintenance of glycemic control (Kanat et al. 2011). For this purpose, Malin and colleagues studied the disposition index (DI), which is the product of GSIS and insulin sensitivity and is considered a better predictor of T2DM than insulin sensitivity alone. They observed that GSIS was decreased after exercise but the first- and second-phase DI resulted in an increase, suggesting an increase in β-cell function. In other words, exercise training with modest energy reduction (ie. **CR**) increased both first- and second-phase in pancreatic β-cell function when GSIS data was corrected for changes in insulin sensitivity (Malin et al. 2013). It is interesting to mention that the effect of training on β-cell function might depend on the residual secretory capacity of the individual, hence T2DM patients with a moderate secretory capacity revealed enhanced β-cell secretory capacity by improving GSIS after long-term exercise (Dela et al. 2004).

Regarding rodent studies, exercise increased insulin sensitivity and improved hyperglycemia in Zucker rats (Christ et al. 2002; Hevener et al. 2000; Pold et al. 2005) and in

ZDF rats (Király et al. 2008). Moreover, β-cell function was increased maintaining euglycemia in ZDF rats that were either running on a treadmill (Pold et al. 2005) or swimming (Király et al. 2007).

Regarding morphometry in rodents, in the study on ZDF rats mentioned (Király et al. 2007) the authors observed that the exercise itself increased the β-cell mass and specially the presence of small (<750um2) and large (>50000 um2) islets in comparison with non-trained rats. The authors stated that this increase in small islets might be due to an increase in β-cell neogenesis, since there is an increase in the number of β-cell clusters with less than 6 cells (Király et al. 2008). In line with the presence of small islets, a decrease in islet area was observed in exercised pancreatectomized OLETF rats with an overall increase in β-cell mass (Shima et al. 1997). However, another study showed that these small β-cell clusters might be due to neogenesis in pancreatectomized rats fed on HFD with a reduction in their number after the exercise load, suggesting that these β-cell clusters might be present already during the worsening with HFD (Park et al. 2007). Of note, in some cases β-cell mass expansion was partially maintained after exercise in OLETF (Shima et al. 1997) and ZDF rats by increasing β-cell proliferation in response to a worsening insulin sensitivity (Király et al. 2008; Pold et al. 2005).

In 13-wk swim trained ZDF rats, the β-cell compensatory adaptation of increased insulin secretion and sustained adaptive hyperinsulinemia was maintained for the duration of the study in contrast to sedentary controls. In this study, C-peptide, a more accurate measure of insulin secretion, was increased in exercided animals in comparison to sedentary controls (Király et al. 2008). Thus, GSIS was enhanced after exercise in rodents (Farrell et al. 1991); although some others observed that regular exercise can decrease insulin secretion by insulin secretagogues (Dela et al. 1990; King et al. 1990). Regarding insulin secretion signalling pathways, AKT/PKB staining was higher in these exercised ZDF rats in comparison with sedentary animals (Király et al. 2008). AKT signalling was also improved in other studies after exercise along with glucokinase (GK) activity (Delghingaro-Augusto et al. 2012; Király et al. 2008; Koranyi et al. 1991), an increase in glucose transporter 2 (GLUT2) (Király et al. 2008), and an icrease in mitochondrial respiration in pancreatic tissues (Delghingaro-Augusto et al. 2012).

In light of the above, exercise has a protective effect in pancreatic β-cell by increasing insulin sensitivity, β-cell mass and β-cell function, and by increasing and/or maintaining insulin secretion upon glucose stimulation.

1.8.2. Adipose tissue

During the last decades, fat has been shown to play a pivotal role in the pathogenesis of T2DM. In mammals, two types of adipose tissue are found: white adipose tissue (WAT) and brown adipose tissue (BAT). WAT accounts for approximately 10% of total BW in lean humans and can reach more than 50% of total BW in obese individuals (Wang et al. 2008). WAT is composed by adipocyte cells, which are rich in lipid droplets and have small cytoplasmatic volume. It is an important metabolic and endocrine tissue that secretes adipokines, including cytokines, chemokines, hormone-like factors and other mediators, which regulate appetite, inflammation, insulin action, and glucose and lipid metabolism (Rasouli & Kern 2008; Hotamisligil & Erbay 2008). Despite having low mitochondria density, WAT cells can sense nutritional and hormonal signals and coordinate a mitochondrial response either to oxidize FA or CH or to store them until there is energy demand (Sun et al. 2011). Furthermore, mitochondria have also a role in adipocyte maturation by regulating the initiation and promotion of adipocyte differentiation (Tormos et al. 2011).

WAT tissue is divided in mature adipocytes and the "stroma vascular fraction" (SVF) that contains pre-adipocytes, fibroblasts, endothelial cells and resident macrophages. As explained in the next section, chronic inflammation in WAT is crucial in the development of obesity-related IR and T2DM (Xu et al. 2003), and macrophages have a principal role in this process secreting inflammatory molecules and establishing the chronic "low grade" inflammation (Hotamisligil 2006).

Within WAT, there are two major types distributed differently throughout the body: visceral adipose tissue (VAT) and subcutaneous adipose tissue (SAT). These two types derive from different progenitor cells, ending up with a different gene expression pattern. This PhD thesis contemplates the epididymal VAT which, compared to SAT, secretes less adiponectin (Gil et al. 2011). Also, rat epididymal VAT adipocytes have more mitochondria than SAT; and in humans, obese individuals have a higher number of mitochondria per mg of tissue in VAT than SAT (Deveaud et al. 2004). In line with this, VAT have higher mitochondrial respiration and OxPhos in comparison to SAT (Kraunsøe et al. 2010), although this might be due to the higher number of mitochondria. Dela and colleagues studied the mitochondrial function in different types of WAT, observing that VAT was bioenergetically more active and responsive to substrates in the ETS than SAT, although mitochondrial respiratory flux per cell and per mitochondrial content was lower in VAT due to smaller cells (Kraunsøe et al. 2010). Moreover, VAT accumulates more macrophages

in obesity and secretes higher amounts of pro-inflammatory cytokines (O'Rourke et al. 2009), and is associated with IR and a higher risk of T2DM, dyslipidemia, progression of atherosclerosis and mortality (Carey et al. 1997; Wang et al. 2005; C. Zhang et al. 2008). Thus, suggesting VAT is the metabolically harmful fat. In keeping with this, it is worth mentioning that FFA produced from lipolysis in VAT are shuttled directly to the liver via the hepatic blood supply, whereas FFAs from SAT enter peripheral circulation. In the same line, some studies reported that SAT may actually be the "beneficial" type of fat (Tran et al. 2008).

1.8.2.1 WAT in IR and obesity-T2DM

Obesity-associated tissue inflammation is now recognized as a major cause of decreased insulin sensitivity (Heilbronn & Campbell 2008; Kanda et al. 2006; Oliver et al. 2010; Schenk et al. 2008). Approximately 25 years ago, the evidence that inflammation was an important mediator in the development of IR was reported: administration of the pro-inflammatory cytokine tumor necrosis factor α (TNFα) led to increased serum glucose concentrations suggesting that hyperglycemia was worsened by cytokine overproduction (Feingold et al. 1989; Grunfeld & Feingold 1991). However, the concept of **obesity-induced adipose inflammation** was not defined until Hotamisligil's studies (Hotamisligil et al. 1993). Therefore, some of the changes in adipose tissue that accompany obesity and IR include the development of a **chronic low-grade inflammatory state** that encompasses an increase in **infiltration of macrophages** named adipose tissue macrophages (ATMs), and circulating inflammatory markers such as TNFα, interleukin 6 (IL6), and also the monocyte chemotactic protein 1 (MCP1) (Weisberg et al. 2003; Xu et al. 2003; Kern et al. 2001; Hotamisligil 2006; Wellen & Hotamisligil 2005; Galic et al. 2010), among others.

The initial event in obesity-induced inflammation and IR is then the recruitment of macrophages into adipose tissue, on account of the chemokines secreted by adipocytes as a consequence of overnutrition (Olefsky & Glass 2010). Chemokines such as the MCP1 (also known as chemokine ligand CCL2) and leukotriene B4 (LTB4) create a chemotactic gradient (Olefsky & Glass 2010) that attracts monocytes into the adipose tissue, where they become ATMs. Of note, deletion of *Ccl2* has been shown to protect against HFD-induced IR and reduced hepatic lipid content (Kanda et al. 2006). These ATMs secrete in turn their own chemokines, thus attracting more macrophages and establishing the inflammatory process (Olefsky & Glass 2010).

Macrophages can polarize to two subpopulations: classically activated or M1, and alternatively activated or M2. Human adipocytes of obese and insulin-resistant subjects contain both M1 and M2 macrophages, with M1 predominating in crown-like structures (CLS), which are macrophages clusters surrounding a necrotic adipocyte (Kern et al. 2001). Increased number of M1 macrophages accounts for the majority of the increase in ATMs in obesity (Lumeng, DeYoung, Bodzin, et al. 2007; Nguyen et al. 2007), and more than 90% of the recruited macrophages end up expressing *Cd11c* (also known as *Itgax*, a M1 macrophage marker).

During weight gain macrophages undergo a "phenotypic switch" from an anti-inflammatory M2 phenotype to a pro-inflammatory M1 state (Lumeng, DeYoung & Saltiel 2007). Evidence was shown that ATMs increased the lipid metabolism suggesting that their number, rather than increasing the activation, might be in charge of the chronic low-grade inflammation (Xu et al. 2003). Hotamisligil and colleagues hypothesized that distinct pathways might promote macrophage inflammation in the context of obesity, in comparison with a context of infection (Calay & Hotamisligil 2013; Hotamisligil & Erbay 2008). This way, "metabolic activation" that is activating the macrophages using glucose, insulin and palmitate (elevated in T2DM subjects) failed to express cell surface markers used for diagnostic of classically activated macrophages M1 (Kratz et al. 2014). Indeed, palmitate alone might be the main driver of metabolic activation. Furthermore, palmitate levels at the lower limit in the T2DM patients (0.1mM) stimulated this metabolic activation (Reaven et al. 1988). In fact, in VAT and SAT from obese humans after bariatric surgery, cluster of differentiation 36 and ATP-binding cassette transporter (CD36 and ABCA1) that are metabolic activated macrophage (MMe) markers were detected, and a strong correlation was found between CD36 or ABCA1 levels and adiposity. It is interesting to mention the absence of M1 classically activated macrophages markers in these human samples. Moreover, in obese mice an increase in *Tnf*α and *Il1*β pro-inflammatory cytokines was observed along with the MMe markers (perilipin (*Plin2)* and *Abca1*). The same authors observed that p62 and PPARγ regulate the expression of *CD36*, *ABCA1* and *PLIN2* in humans and rodents, markers of these newly MMe. P62 and PPARγ attenuate pro-inflammatory cytokine production in this metabolic activation, suggesting that this could be the reason why inflammation associated with metabolic disease is often lower than the induced by bacterial infection (Kratz et al. 2014).

The increase in infiltration of ATMs in WAT also leads to an increase in ROS along with an increase in oxidative stress in visceral depots (Kotsias et al. 2013; Lee & Lee 2014; Weisberg et

al. 2003). ATMs infiltrations, which lead to adipocyte remodeling comprising up to 40% of the cells in obese adipose tissue (Weisberg et al. 2003), have been shown to have a key role in systemic T2DM (Olefsky & Glass 2010). Indeed, the pro-inflammatory pathways in ATMs are highly activated in obesity, leading to the secretion of various **cytokines**, such as TNFα and interleukin 1-β (IL1β) (Olefsky & Glass 2010). These cytokines can act locally in a paracrine manner or they can leak out causing actions in an endocrine manner, leading to IR in insulin sensitive cells (other adipocytes, hepatocytes and myocytes).

Cytokines secretion takes place after activation of the infiltrated ATMs (Wellen & Hotamisligil 2003), whose number is increased in the obese state (Xu et al. 2003; Weisberg et al. 2003). Among the **cytokines** playing a role in the inflammation pattern in an obesity-related T2DM, **IL6** studies have shown controversy whether IL6 correlates positively with obesity-related IR having pro-inflammatory effects (Pradhan et al. 2001) or IL6 can exert anti-inflammatory actions (Matthews et al. 2010; Frisdal et al. 2011; Tilg et al. 1994). IL6 has shown detrimental effects on insulin sensitivity in liver and adipose tissue. However, IL6 secreted by skeletal muscle revealed beneficial anti-inflammatory effects (Kristiansen & Mandrup-Poulsen 2005). IL6 can act stimulating JNK1 and IKKβ/NFκB pathways, leading to up-regulation of potential mediators of inflammation that can ultimately cause IR (Wellen & Hotamisligil 2005; Fain et al. 2004). Contrary, no discrepancies have been created regarding the pro-inflammatory effects of **IL1β** after being generated by inflammasome activation (Martinon et al. 2002). Inflammasome can be activated by HFD-induced elevation of FA resulting in IL1β production, and impaired insulin sensitivity and glucose tolerance (Wen et al. 2011). Deletion of NOD-like receptor family, pyrin domain containing 3 (*Nlrp3)* or apoptosis-associated speck-like protein containing CARD *(Asc)*, that form the inflammasome, have reported protection against HFD-induced IR and glucose tolerance (Stienstra et al. 2010). Also, the combination of saturated FA with pro-inflammatory cytokines showed up-regulation of the genes involved in ceramide biosynthesis (William L. Holland et al. 2011), consistent with a reported positive correlation between cytokine levels and plasma ceramides, and IR (Haus et al. 2009). In fact, ceramides impair insulin signalling and IR through dephoshorylation of AKT (Dobrowsky et al. 1993). Anti-inflammatory cytokines such as interleukin 10 (**IL10**), have been reported elevated in obesity (Ouchi et al. 2010). IL10 inhibits the effects of pro-inflammatory cytokines on insulin signalling (Schottelius et al. 1999), and administration of IL10 *in vivo* prevented the IL6- or lipid-induced IR (H. J. Kim et al. 2004). In the same line, whole-body insulin sensitivity was increased in a muscle-specific transgenic mice overexpressing *Il10* (Lumeng, Bodzin & Saltiel 2007; Hong et al. 2009). Adipose tissue from obese patients showed an increased ***TNFα***

expression along with IR, and a reduction in *TNFα* after weight loss (Hotamisligil et al. 1995; Kern et al. 1995). TNFα has also been shown to have effects in the disruption of insulin signalling (ie. in skeletal muscle), and it can also decrease the expression in adipocytes of *Slc2a4* (GLUT4) (Stephens & Pekala 1991) and *Pparγ* (Ye 2008). On the one hand, obese rodents showed increased *Tnfα* that, when neutralized, ameliorated IR. On the other hand, *Tnfα*-deficient mice improved insulin sensitivity in DIO (Uysal et al. 1997). Moreover, in IR and obesity, the signalling pathways leading to activation of inhibitor of κB kinase-β (IKKβ) and nuclear factor κ-B (NF-κB) were stimulated (Yin et al. 1998; Yuan et al. 2001). Heterogeneous deletion of IKKβ protected mice from IR during HFD (Yuan et al. 2001). Furthermore, the chronic low-grade inflammation induced by obesity can activate other protein kinases such JNKs. Indeed, TNFα might activate Jun-N terminal kinase (JNK1) which phosphorylates IRS1 at serine-307, a critical residue disrupting insulin signalling, and providing a plausible link between inflammation and IR (Aguirre et al. 2000; Hotamisligil et al. 1996). Moreover, ablation of *Jnk* in mice on HFD protected them from DIO and inflammation (Hirosumi et al. 2002; Tuncman et al. 2006; Solinas et al. 2007).

As aforementioned, the relationship between inflammation and IR seems to converge often in the JNK1 pathway. This way, *Jnk1* KO mice showed protection from diet-induced IR, gaining less weight than WT littermates and with higher temperature, suggesting an increase in energy expenditure (Hirosumi et al. 2002). Moreover, macrophages and acipocytes with *Jnk1* inactivation were also protected against DIO, hepatic steatosis and glucose intolerance, and had an increase energy expenditure (Tuncman et al. 2006); similarly to silenced *Jnk1* in *ob/ob* mice that showed increased energy expenditure, decreased BW gain, liver TG content, PKCε activation, and improved insulin sensitivity (Samuel & Shulman 2012). Thus, *Jnk1* deletion leads to an increase in energy expenditure, reduction of accumulation of ectopic lipids and protection against IR. Adipose-specific *Jnk1* KO mice showed similar weight gain and adiposity upon HFD, but they were protected against hepatic steatosis and hepatic IR (Sabio et al. 2008).

To demonstrate that inflammation alone can disrupt the signalling, Hellmann and colleagues (Hellmann et al. 2011), recovered decreased AKT-phosphorylation in *db/db* mice only by using a lipid mediator (resolving D1) that blunts the production of pro-inflammatory cytokines, while blocking leukocyte infiltration.

Genetically modified apoptosis inhibitor of macrophages (*Aim*) deficient mice ameliorated and reverted the glucose intolerance and insulin sensitivity and decreased all three

cytokines (*Tnfα*, *Il6* and *Il1β*) expression, all elevated in obese mice. Also, this *Aim* deficient mice recovered the loss of AKT-phoshorylation upon insulin after HFD in epididymal fat, liver and skeletal muscle (Kurokawa et al. 2011). In line with this, Lumeng and colleagues showed that lipopolysaccharide (LPS) could also activate inflammation in adipocytes by using a macrophages media (LPS-induced J774 macrophages media) in adipocytes, and decreasing deoxyglucose uptake upon insulin stimulation, decreasing GLUT4, IRS and its tyrosine (Tyr) phosphorylation, and AKT phosphorylation. The same authors showed how HFD increased TNFα (Lumeng, DeYoung & Saltiel 2007; Lumeng, DeYoung, Bodzin, et al. 2007).

Taken all together, inflammation has an important role in the pathogenesis of systemic IR, and activation of its pathways occurs in insulin sensitive tissues, including adipose tissue (Xu et al. 2003; Weisberg et al. 2003), liver (Cai et al. 2005) and skeletal muscle (Itani et al. 2002; Bandyopadhyay et al. 2005). This suggests that chronic low-grade inflammation situation is a hallmark of IR and later T2DM (Cildir et al. 2013; van den Borst et al. 2013; Fernández-Sánchez et al. 2011).

Along with the macrophage infiltration, there is also an **adipocytes expansion** given that during adipose IR insulin fails to suppress lipolysis in this tissue, defining an inverse correlation between lipolysis and glucose tolerance (Girousse et al. 2013). Regarding the relationship between inflammation and **adipose expandability**, numerous studies demonstrated that cytokines increase adipose lipolysis (Kawakami et al. 1987; Stone et al. 1969). In fact, IL6 infusion in healthy humans increased plasma FA and glycerol, indirect measures for lipolysis (Watt et al. 2005). Also, some studies suggested that cytokines might affect the lipid droplets stability by influencing structural proteins. For example, *Plin* expression was decreased by TNFα, enhancing the ability of lipases to access TG within the lipid droplets (Bézaire et al. 2009; Laurencikiene et al. 2007). In a similar way, TNFα and other cytokines decreased fat-specific protein 27 (*Fsp27*, also known as *Cidec*) expression (Ranjit et al. 2011), an homologous protein to PLIN. In fact, *Fsp27* silencing increased basal and TNFα-mediated lipolysis, whereas overexpression of *Fsp27* led to abrograted lipolysis. As seen, adipose tissue inflammation may increase lipolysis that could drive the FA re-esterification and ectopic lipid accumulation, ultimately leading to IR.

During the expandability, adipocyte size was found to increase threefold in rodents already after 6 wks on HFD without significant changes in macrophage infiltration or inflammation (Cummins et al. 2014). However, the authors in this study observed that after 12 wks on HFD, mice showed a fourfold increase in adipocyte size along with a higher

number of CLS, and an increased expression of *Emr1*, a marker of macrophages. Regarding the CLS, it has been shown that adipocyte necrosis is uncoupled from inflammation, since ATM accumulation preceeded adipocyte necrosis in the beginning of a HFD feeding (Li et al. 2010). The adipocyte expansion involves changes in the adipose vasculature, including a decrease in capillary density (Gealekman et al. 2011) and an increase in vascular endothelial growth factor *VEGFA* expression (Tinahones et al. 2012), leading to the hypothesis that adipocytes might suffer necrosis and inflammation due to the expansion in an **hypoxic situation** (Sun et al. 2011). In fact, obese individuals showed poorly oxygenated adipose tissue (Kabon et al. 2004). Hence, an hypothesis establishes that expandability limitation of the tissue leads to a situation of hypoxia secreting hypoxia inducible factor 1 α (HIF1α), necrosis of adipocytes and fibrosis (Pasarica et al. 2009; Trayhurn & Wood 2004; Rutkowski et al. 2009). *Hif1α* induced expression of pro-inflammatory cytokines (Jantsch et al. 2008) and, in macrophages, it was reported necessary for the energy generation needed for their migration. Also, adipocyte *Hif1α* deletion protected mice from HFD-induced obesity and IR (Jiang et al. 2011).

Lipotoxicity, the overload of lipid accumulation, could lead to the loss of WAT expandability that along with the impaired inhibition of adipose lipolysis, become the starting point from which FA are shuttled in a circulating FFA form to other peripheral tissues, such as liver and skeletal muscle, disrupting there the insulin signalling cascades and leading to spreaded peripheral IR.

Indeed, the primary mechanism by which this chronic low-grade inflammation and lipotoxicity worsens peripheral IR is explained by the **disruption of the signalling cascade** downstream the insulin receptor. For example, in skeletal muscle, tissue in charge of the majority of postpandrial glucose uptake, the disruption in the insulin signalling cascade starts when both inflammatory TNFα and/or elevated FFA activate serine kinase activity increasing the inhibitory phosphorylation of concrete serine residues (Ser302 in rodents, 307 in humans) in the insulin receptor substrate 1 (IRS1) (Aguirre et al. 2000; Aguirre et al. 2002), reducing then its Tyr phosphorylation and therefore inhibiting insulin action by disrupting the downstream signalling including Akt-phosphorylation (section 1.8.4.1) (Aguirre et al. 2002).

Interestingly and related to insulin signalling, fat-specific insulin receptor KO (FIRKO) showed protection against obesity promoted by age and hyperphagia, and also against

obesity-related glucose intolerance (Blüher et al. 2002). In fact, in comparison to controls, FIRKO mice highly expressed nuclear-encoded mitochondrial genes with functions in glycolysis, TCA cycle, β-oxidation and OxPhos, from 6 to 36 months of age (Katic et al. 2007).

Reduced mitochondrial function was observed in WAT suffering inflammation (Valerio et al. 2006). Thus, a decrease in mitochondrial activity would reduce the amount of FA that can be removed within adipocytes, redistributing FA to other tissues (Lowell & Shulman 2005), and participating in the so-called "ectopic FA accumulation". Hence, mitochondrial function has been suggested to be an early step in the pathogenesis of T2DM (Powelka et al. 2006). However different studies have reported reduced mitochondrial content in VAT after the development of hyperglycemia (Laye et al. 2009; Sutherland et al. 2008), thus suggesting that the mitochondrial derrangements due to HFD-induced obesity occur after the onset of impaired glucose homeostasis (Sutherland et al. 2008). Interestingly, a link between mitochondrial dysfunction and impaired glucose transport leading to IR has been deemed independent from FA accumulation. In adipocytes, insulin-stimulated translocation of GLUT4 is dependent on calcium/calmodulin kinase II (CaMKII) phosphorylation of myosin-1c (Myo1c) (Yip et al. 2008), a motor protein that is a part of the cytoskeleton. Since CaMKII activation depends on increases in cellular calcium and mitochondrial dysfunction might alter calcium-buffering capacity of mitochondria, mitochondria alterations might alter insulin-stimulated CaMKII activity and glucose uptake.

Independently of the cause of the decreased FA oxidation, an increase in ectopic lipid accumulation is present in several tissues, along with the impaired inhibition of lipolysis in WAT by insulin, both processes leading to the mentioned lipotoxicity.

Moreover, Kusminski and colleagues reported how after a nutritional overload, adipocytes moved towards lipid storage and reduced mitochondrial biogenesis along with an enhancement in glycolytic ATP synthesis (Kusminski & Scherer 2012). As aforementioned, these alterations in mitochondria might lead to lipid accumulation and potential progression to IR.

In human studies, T2DM patients showed **reduced mitochondrial content** in WAT biopsies (Bogacka, Xie, et al. 2005). Some studies showed a reduction in mitochondrial number in WAT of obese and T2DM individuals (Bogacka, Xie, et al. 2005), while others show a connection of this number and lipogenesis, although the decrease in mitochondrial

number was not correlated to BMI nor insulin sensitivity (Kaaman et al. 2007). In WAT from patients showing IR, T2DM and severe obesity, a **reduced expression of mitochondrial function key genes**, and reduced abundance of mitochondria were observed (Krishnan et al. 2012). In obese monozygotic cotwins, a significant reduction of expression of genes encoding elements of mitochondrial OxPhos in abdominal SAT was observed in the obese twin and associated with lower insulin sensitivity (Mustelin et al. 2008). Strikingly, Dahlman and colleagues showed how T2DM correlated with a major decreased expression in VAT of mitochondrial ETS genes independently of obesity in a study in non-obese, healthy obese and T2DM obese women (Dahlman et al. 2006).

T2DM patients showed decrease in mammalian target of rapamycin complex 1 (mTORC1) signalling, which has a role in IR, inhibiting autophagy and promoting mitochondrial biogenesis. Thus, mTORC1 decrease led to increased autophagic activity and **impaired mitochondrial function** (Ost et al. 2010). In fact, WAT from patients showing IR, T2DM and severe obesity reported decreased adipocyte oxygen consumption and ATP production (Bogacka, Ukropcova, et al. 2005). Other studies reported that the consumption of VAT in obese was of 66±30 pmol/s·mL/mg protein while non-obese subjects showed values of 118±56 pmol/s·mL/mg protein (Yin et al. 2014). Regarding SAT, a decrease in obese oxygen consumption was also observed (non-obese patients: 134±69 pmol/s·mL/mg protein; obese patients: 62±38 pmol/s·mL/mg protein).

In genetic rodent models of obesity (*ob/ob* mice) or rodent models fed on HFD there was also a down-regulation of genes involved in mitochondrial ATP production, energy uncoupling and other mitochondrial genes (Rong et al. 2007), suggesting an overall impairment of mitochondrial biogenesis. It is worth mentioning that in the two obesity models used in this later study, rosiglitazone induced mitochondrial biogenesis giving an important role of adipose mitochondria in obesity and T2DM. Moreover, *ob/ob* mice showed reduced mitochondrial dysfunction along with reduced FA oxidation (Choo et al. 2006), and a 50% lower mitochondrial levels in comparison to WT mice (Wilson-Fritch et al. 2004). In the VAT epididymal fat pad of *ob/ob* mice, markers of mitochondrial capacity, including gene expression, were reduced (Wilson-Fritch et al. 2004), as well as in the SAT inguinal fat pad of *db/db* mice (Choo et al. 2006; Rong et al. 2007). In the same line, obese HFD-fed (Keller & Attie 2010) and *db/db* mice (Devarakonda et al. 2011) reported a down-regulation of several genes important for mitochondrial function and OxPhos, in addition to *Pparα*, estrogen-related receptor α (*Errα)* and *Pgc1α*. Also, mitochondrial proteins were found decreased in the WAT of *db/db* mice in comparison to the liver and muscles which

showed similarities, along with a reduced number in mitochondria and mitochondrial dysfunction, and a decrease in mtDNA and ETS activity (Choo et al. 2006; Hammarstedt et al. 2003; Rong et al. 2007), all disruptions contributing to a worse OxPhos and β-oxidation. In another model of obesity, the OLEFT rats, the inability to increase WAT mitochondrial content was not a primary cause in IR, although it might play a role in worsening the disease state (Laye et al. 2009).

Regarding non-genetic models, and in line with everything stated above, mitochondrial dysfunction in 3T3-L1 adipocytes was stimulated in a T2DM-like condition by high levels of glucose and FFA (Gao et al. 2010). On the contrary, mitochondrial oxygen consumption in HFD-fed mice showed apparently no differences when normalized by protein content in comparison to low fat diet (LFD)-fed mice, although HFD-fed mice adipose tissue responded strongly to FCCP (Cummins et al. 2014). It has to be considered that the experiments were performed after 6 wks on HFD when obesity was evident but no inflammation in the adipose tissue was observed. However, expression of cytochrome C oxidase (*Cox7a1)* was increased in the HFD-fed mice while expression of *Pgc1a*, sirtuin (*Sirt3)* and pyruvate dehydrogenase kinase (*Pdk)* was diminished, globally indicating mitochondria remodeling despite preserved basal mitochondrial function. In the same study but after 12 wks on HFD, NADH dehydrogenase (NDUFB8), succinate dehydrogenase (SDHB) and COX4I1 protein levels were diminished significantly.

It has been proposed that improvements in WAT mitochondrial function might be linked to the improvements observed in whole-body insulin action. In fact, anti-diabetic *pioglitazone* in humans improved mitochondrial function and genes in SAT (Bogacka, Xie, et al. 2005), same way as physical activity in rodents with IR and T2DM normalized VAT mitochondrial content and improved glucose homeostasis (Laye et al. 2009). Also, TZD that increase insulin sensitivity, induced a coordinated stimulation of FA uptake, oxidation and OxPhos in WAT of T2DM patients (Guenther Boden et al. 2005) and *db/db* mice (Choo et al. 2006; Rong et al. 2007).

Besides the importance of mitochondria in mature functional adipocytes, mitochondrial function also becomes important in WAT during two stages of maduration: during **adipocyte differentiation and hypertrophy**. New small adipocytes are recruited during differentiation, with high metabolic activity, increased substrate consumption, and increased insulin sensitivity. Several studies reported increased mitochondrial biogenesis along with up-regulation of mitochondrial protein levels during adipocyte differentiation

(Lu et al. 2010; Gao et al. 2010; Krishnan et al. 2012; MacLaren et al. 2008). Among them, Corvera and colleagues revealed an initial 20- to 30-fold increase in mitochondrial content when preadipocytes embarked the adipogenic process, with a concomitant increase in β-oxidation (Gao et al. 2010; MacLaren et al. 2008), all regulated by PGC1α, PPARγ, ERRα, cAMP response element-binding (CREB), and CCAAT/enhancer binding proteins (C/EBPα and β) (Rieusset 2011; Lim et al. 2009). Certainly, mtDNA copy number also increased during differentiation (Muoio & Koves 2007), with induction of components of mitochondrial genome replication and transcriptional processes such as transcription factor A mitochondrial (*Tfam*) (Koves et al. 2008) and deoxynucleotide metabolism components required for mtDNA replication (William L Holland et al. 2011). Interestingly, *Tfam* (highly induced between 2-4 days of differentiation) knock-down in 3T3-L1 adipocytes caused reduced ETS capacity and disrupted GLUT4 translocation, although a paradoxically enhanced insulin-stimulated Akt phosphorylation was reported suggesting that mitochondrial dysfunction in adipose cells might impaire glucose transport by a mechanism downstream of AKT protein kinase (Shi et al. 2008). In line with the decrease in ETS in the knock-down model, inhibition of respiration or OxPhos disrupted adipocyte differentiation causing abnormal TG storage capacity of mature cells (Lu et al. 2010; Koves et al. 2008; Bikman & Summers 2011). Moreover, *Pgc1β*, *Pparγ* and *C/ebpα* and sterol regulatory element-binding protein 1 (*Srebp-1c*) expression was down-regulated (Lu et al. 2010) in the OxPhos inhibited model, while *Creb* was up-regulated (Wilson-Fritch et al. 2003).

Thus, an increase in mitochondrial biogenesis is observed during preadipocyte differentiation program during WAT expansion. On the contrary, adipocyte hypertrophy leads to reduced mitochondrial mass and loss of metabolic flexibility, a common trait for obesity. In fact, obesity, age and T2DM caused reduced mitochondrial content in mature adipocytes (Wernstedt Asterholm et al. 2012). Obesity-induced alterations in mitochondrial biogenesis impaired differentiation (Gao et al. 2010; Wernstedt Asterholm et al. 2012; MacLaren et al. 2008) while obesity-induced ROS caused detrimental inhibitory effects in preadipocyte proliferation and differentiation (Goldstein et al. 2005), synergistically worsening WAT during obesity.

Mitochondria also play a role in lipogenesis providing key intermediates for TG synthesis (Rosen & MacDougald 2006), and in lipolysis and re-esterification of FA. Lipolysis in the adipose tissue can be stimulated by fasting, exercise, and IL6 and TNFα, among others, inducing the hydrolysis of stored TG to FFA (Kaaman et al. 2007) while stimulating

mitochondrial β-oxidation (Shi et al. 2008). TNFα caused increased mitochondrial structure, OxPhos, β-oxidation and TCA cycle proteins expression (Shi et al. 2008).

A link between mitochondria and inflammation has been proposed since it is known that mitochondria can activate **inflammasome**, a multiprotein complex that initiates and controls inflammatory reactions in response to stress conditions, such as oxidative stress (Zhou et al. 2011). Mitochondrial ROS has been reported to be sufficient for the inflammasome activation (Lane et al. 2013). The inflammasome can also be activated by release of mtDNA (Shimada et al. 2012) and in response to elevation of lipids such as ceramides (Vandanmagsar et al. 2011). Of note, ceramides increase has been associated with impaired mitochondrial function (Yu et al. 2007).

Electron microscopy showed that after 12 wks on HFD autophagosomes localized next to mitochondria, which in turn appeared to be undergoing fission. Indeed, levels of PTEN induced putative kinase PINK1 –critical for identifying mitochondria that are destined for autophagy- were nearly 40% higher in the HFD; and levels of the E3 ubiquitin protein ligase PRKNK (Parkin) –which accumulates in mitochondria that are going to be degradated- were increased twofold (Cummins et al. 2014). Therefore, seems that adipocytes after 12 wks on HFD suffer a metabolic remodeling in the adipose tissue expansion that might be related to **autophagy**.

Other factors related to mitochondria are adiponectin and ROS. Adiponectin synthesis within adipocytes is linked to mitochondrial function, and indeed, adiponectin expression and mitochondrial content in WAT were reduced in obese *db/db* mice (Eun et al. 2007).

Oxidative stress was described clinically, and in WAT of different animal models such as DIO and *db/db* (Lee et al. 2010; Curtis et al. 2010; Chen et al. 2010). Enhanced **ROS** levels have been causally linked to an alteration in insulin sensitivity in different models (Loh et al. 2009; Brookheart et al. 2009; Curtis et al. 2010; Houstis et al. 2006). Studies in 3T3-L1 adipocytes showed how reactive species can carbonylate IRS1 and IRS2, reducing insulin-stimulated Tyr phosphorylation (De Pauw et al. 2012).

As seen, a link between ROS and IR was reported by Houstis and colleagues (Houstis et al. 2006) who showed how antioxidants prevented multiple, heterogeneous forms of cellular IR. Insulin-resistant *ob/ob* mice improved glucose tolerance and insulin sensitivity after the administration of these antioxidants. Also, obese and insulin-resistant rodents and

humans mitochondria released greated ROS in comparison with lean controls (Anderson et al. 2009). However, many opposing findings have also been reported, and the role of ROS in WAT and other tissues in insulin-resistant states remains elusive.

Looking into ROS concrete effects in adipocyte mitochondria, NEFA and TNFα reported an increase in ROS in 3T3-L1 experiments (Wang et al. 2010; Lin et al. 2005), along with reduced mitochondrial biogenesis, decreased insulin sensitivity (Brookheart et al. 2009; Curtis et al. 2010) and enhanced secretion of pro-inflammatory cytokines (Wang et al. 2010). ROS can inhibit oxygen consumption in adipocytes increasing lipid accumulation (Houstis et al. 2006), while ROS scavengers pyruvate or N-acetylcysteine can restore it. Moreover, a study showed how modifying ROS levels by mitochondrial activity (ie. by the action of UCP2) might lead to controlling the adiponectin gene expression (Chevillotte et al. 2007). Indeed, inhibition of *Ucp2* expression improved WAT insulin signalling transduction (De Souza et al. 2007).

As observed, the adipocyte has the particularity in comparison to other cell types that displays tolerance to high levels of ROS under basal conditions, without neither cell damage nor apoptosis (Houstis et al. 2006). Nonetheless, the appearance of obesity in the adipocyte promotes a scanvengers slack action, increasing ROS levels and leading to inhibition of oxygen consumption. Hence, TG are stored and accumulated because substrates cannot be properly oxidized.

ROS has also been reported to play a role in adipocyte differentiation (Tormos et al. 2011). In fact, antioxidant treatment blocked adipocyte differentiation and hydrogen peroxide treatment restored it. Therefore and as mentioned, although ROS might cause cellular damage at high levels, it is important to point out that at moderated levels, it might maintain cellular homeostasis creating a tolerable oxidative environtment that allows adipocyte differentiation (Tormos et al. 2011), phenomena known as hormesis. ROS also showed the ability to inhibit the proliferation of adipogenic progenitors (Goldstein et al. 2005) without inducing apoptosis (De Pauw et al. 2009), but leading to dysfunctional hypertrophic large adipocytes. Of note, antioxidant treatment also reverted these disruptions promoting adipogenesis (Goldstein et al. 2005).

ER stress has shown a role in the pathogenesis of obesity-related T2DM since it can activate inflammatory pathways (Hotamisligil 2005). ER stress is in charge of **UPR**,

protecting cells from producing aberrant proteins, and it has been reported activated in obesity models in rodents (Özcan et al. 2004) and humans (Boden et al. 2008).

Indeed, UPR is initiated with the accumulation of unfolded proteins within the ER lumen. The UPR consists of three different canonical arms: inositol-requiring protein-1 (IRE1), activating transcription factor-6 (ATF6) and double-stranded RNA-dependent protein kinase (PKR)-like ER kinase (PERK); which regulate the expression of various genes attempting to ameliorate ER stress (Ron & Walter 2007) such as ER chaperones (Okada et al. 2002). Of note, an intimate functional relationship exists between mitochondria and the ER, since their crosstalk might become disrupted during metabolic imbalance (Kusminski & Scherer 2012). In fact, the outer mitochondrial membrane and the ER are connected by specific tethers (Rieusset 2011). ER stress might lead to mitochondrial dysfunction (Rieusset 2011), and vice versa (Lim et al. 2009).

The UPR has also been reported to activate pro-inflammatory pathways. It is the case of JNK activation by IRE1, along with chaperone genes activation in response to ER stress (Urano et al. 2000), or by a PERK-homolog PKR (Nakamura et al. 2010). JNK activations increased serine phosphorylation of IRS1 and impaired insulin action. Furthermore, another evidence for the link between ER stress and IR was provided by the deletion of *Xbp1*, which is a UPR-promoter transcription factor, leading to IR (Özcan et al. 2004). In the same line, binding immunoglobulin protein (*Bip*) (a chaperone, also known as heat shock 70KDa Protein 5 Hspa5 or Grp78) deficient mice ($Grp78^{+/-}$) reported increased energy expenditure in comparison to HFD-fed WT mice, which can explain the protection against DIO, hepatic steatosis and IR (Ye et al. 2010). An increase in mitochondrial biogenesis consequent with an increased adipose expression of *Pgc1α* might be a likely mechanism. UPR activation after *Bip* loss might alter adipogenesis and energy balance, aiming to improve insulin sensitivity. In fact, studies in 3T3L1 adipocytes reported that IRE1-XBP1s pathway is critical for adipogenesis (Sha et al. 2009).

Hence, genetic or chemical modifications (chaperones) modulating ER stress ameliorate JNK activation and the development of IR in a mouse model of T2DM (Ozcan et al. 2006), while chemical inducers of UPR impaired insulin signalling (Özcan et al. 2004). Chaperones have also showed a leptin-sensitizing effect (Ozcan et al. 2009). Of note, ER stress markers have been reported to be reduced along with improvements in insulin sensitivity after substantial weight loss in patients after bariatric surgery (Gregor et al. 2009). It is interesting to point out that some studies showed how UPR did not reduce lipid content

(Kammoun et al. 2009), leading to a lipogenesis and lipid droplets stabilization, thus providing lipid accumulation (Samuel VT et al. 2012).

As seen above, adipose tissue can communicate with skeletal muscle and liver through cytokines, adipokines and lipids. Two concrete **adipokines** are important within the adipose tissue: leptin, produced in the adipose tissue and exerting negative feedback effects on energy intake, thus becoming the "satiety hormone" or appetite suppressant; and adiponectin, exclusively secreted by the adipose tissue.

Leptin receptors in the ARC in the hypothalamus are in charge of the regulation of appetite in order to regulate energy homeostasis. Resistance to this hormone appear in DIO individuals represented by elevated circulating leptin levels and decreased leptin sensitivity (Pan et al. 2014). The exact mechanism by which leptin resistance appears in obesity is still unclear, although many efforts from the scientific community have attempted to propose an explanation since the discovery of leptin in 1994 (Zhang et al. 1994).

Adiponectin levels inversely correlated with the body fat percentage of the individual (Ukkola & Santaniemi 2002), although a meta-analysis from 2011 demonstrated a lack of this association in healthy adults (Kuo & Halpern 2011). However, a recent different meta-analysis showed that the level of circulating adiponectin decreases before the onset of diabetes, since the levels in prediabetic patients were lower in comparison with healthy controls (Lai et al. 2015). In humans, plasma adiponectin levels are directly related to insulin sensitivity and inversely related to ectopic lipid accumulation (Lindsay et al. 2002; Weiss, Dufour, Groszmann, et al. 2003; Stefan et al. 2002) and fat mass (Berg et al. 2002; Kim et al. 2007). Mice overexpressing adiponectin displayed increased insulin sensitivity and increased adipocyte mitochondrial density along with up-regulation of lipid-storage and OxPhos components expression (Feldmann et al. 2009), and protective effects in the liver (Boström et al. 2012). Adiponectin acts as an insulin sensitizer, stimulating FA oxidation by an AMPK- and PGC1α-dependent manner (Scherer 2006; Kadowaki et al. 2006). This adipokine is a key player in the regulation of insulin sensitivity and has reported anti-atherosclerotic and anti-inflammatory effects (Ouchi et al. 2001; Lihn et al. 2005). Thus, it is involved in regulating glucose levels and FA breakdown (Díez & Iglesias 2003), and has been suggested to decrease IR by decreasing TG in skeletal muscle and liver in obese mice (Yamauchi et al. 2001). Concretely, adiponectin reversed IR in combination with leptin in lipoatrophic mice. It is important to mention that the ratio of the high molecular weight

adiponectin form to total adiponectin is more likely to be associated with T2DM and metabolic syndrome than total adiponectin itself (Basu et al. 2007; Lara-Castro et al. 2006). It is worth mentioning that the effects of the fibroblast growth factor 21 (FGF21) on improving whole-body metabolism and insulin sensitivity might be exerted through FGF21-stimulated adiponectin secretion, since these effects are almost abolished in adiponectin deficient mice (Holland et al. 2013; Lin et al. 2013). It is not clear whether cytokine FGF21 is contraction-regulated.

In obesity-related T2DM, a **change in the metabolomics profile** was reported. DIO mice showed an increase in lipid superfamily members, including the ones involved in glycerolipid and linoleic acid metabolism. Within the TCA intermediates, succinate and malate levels were higher while pantothenate, a precursor to CoA was decreased (Cummins et al. 2014).

The reason why the adipose tissue is considered the **master regulator of systemic IR**, relies on the fact that local changes in insulin sensitivity in liver (Arkan et al. 2005; Matsusue et al. 2003) or skeletal muscle (Sabio et al. 2010; Brüning et al. 1998) are maintained tissue autonomous and not extrapolated to other insulin sensitive tissues but, on the contrary, manipulations of adipocytes to increase its insulin sensitivity normally lead to enhanced insulin action in liver and muscle. Examples of this phenomenon are genetic modifications such as the adipocyte-specific ablation of *Jnk1* (Sabio et al. 2008; X. Zhang et al. 2011), overexpression of dominant-negative *Creb* (Qi et al. 2009) or consititutively active *Pparγ* (Sugii et al. 2009), that produced improvements in adipose insulin sensitivity and also, same effects in liver and skeletal muscle. To confirm this concept, adipocyte-specific *Slc2a4* (GLUT4) deletion (Abel et al. 2001) or overexpression of *Mcp1* (Kamei et al. 2006) resulted in systemic impaired insulin sensitivity.

1.8.2.2 Lifestyle interventions on WAT

Some beneficial effects from LI are ultimately due to **weight loss,** even small, which can return plasma glucose concentrations to normal in T2DM patients (Henry et al. 1985; Henry et al. 1986). However, some beneficial metabolic adaptations from **exercise** can happen also independently of significant changes in weight loss in rodents (Gollisch et al. 2009; Craig et al. 1981; Stanford, Middelbeek, Townsend, et al. 2015). Examples are the exercise-induced reduction in adipocyte size and lipid content (Gollisch et al. 2009; Craig et al. 1981), and increased expression of several key metabolic proteins such as GLUT4 and PGC1α (Gollisch et al. 2009; Craig et al. 1981; Stanford, Middelbeek, Townsend, et al. 2015; Stallknecht et al. 1991;

Sutherland et al. 2009). In any case, exercise LI have always shown beneficial effects on the metabolic disruptions present in the obesity-related T2DM state.

During the first year of a **diet** and **exercise** ILI in T2DM human patients, in the Look AHEAD study previously mentioned, the authors found changes in adipose tissue depots (section 1.7.1). BW decreased significantly in the ILI group in comparison to the DSE group, as well as the SAT and VAT in males and females (Gallagher et al. 2014). However, intramuscular adipose tissue (IMAT) was unchanged in ILI while increased in the DSE group. In turn, DSE subjects showed no changes in SAT and VAT. Altogether, reduction of specific adipose tissue depots was associated with improvement in metabolic variables such as cholesterol and TG.

Regarding studies with subjects that have a first-degree family history of T2DM, no differences were found in their SAT mRNA expression in comparison with subjects without a family history, neither at baseline or after the 6-month **exercise** intervention (Rönn et al. 2014). However, this study showed beneficial effects on clinic characteristics and influences in the mRNA expression pattern in adipose tissue samples from both groups (with and without T2DM family history). VO_2peak and oxygen consumption were increased although no changes in respiratory exchange ratio (RER) were observed. Also, waist circumference and waist/hip ratio, resting pulse, HDL cholesterol and LDL/HDL ratio were improved. This points to a decrease in abdominal obesity, suggesting a decreased risk of metabolic diseases (Slentz, Houmard, et al. 2009). Concerning mRNA patterns after exercise, KEGG pathways such as Ribosome and Proteasome were up-regulated suggesting high protein turnover. OxPhos pathway appeared as the second most enriched pathway (Rönn et al. 2014). Moreover, adherens junction and focal adhesion that have a role in cell communication, WNT and mitogen-activated protein kinases (MAPK) signalling, and apoptosis were down-regulated.

Different types and durations of exercise performance in humans have been associated with decreased inflammatory markers (King et al. 2003; Abramson & Vaccarino 2002; Geffken et al. 2001; Mattusch et al. 2000). Physical activity results in enhanced energy utilisation, leading to BW and VAT reduction, the later an important source of pro-inflammatory cytokines (Sell et al. 2012; Donges et al. 2009; Christiansen, Paulsen, Bruun, Pedersen, et al. 2010; Fischer et al. 2007; King et al. 2003; Geffken et al. 2001).

However, some studies assessed inflammation after a LI and showed how after 8 wks of **exercise** in diet-induced insulin-resistant rodents, no significant improve on adipose tissue inflammation was observed (Rao et al. 2013). Although exercise decreased macrophage numbers in epididymal SVF, it did not reach significant values. Similar levels of classical and alternative macrophage activation were observed in exercised and sedentary mice, along with comparable levels in cytokines IL6, IL10 and MCP1 (Rao et al. 2013). It is important to mention that in the study from Rao and colleagues, mice were run at 15m/min, way far from the speed to cause physical exhaustion. On the contrary, decreased VAT gene expression of inflammation (*Mcp1*), immune cell infiltration (*Cd68*, *Cd11c*, *F4/80*, *Cd11b/Cd18*), oxidative stress (*p47phox*, also known as neutrophil cytosolic factor 1 *Ncf1*) and ER stress (C/EBP homologous protein *Chop*, also known as DNA-Damage-Inducible Transcript 3 *Ddit3*) was reported in mice performing regular voluntary exercise (Wainright et al. 2015). Also, these mice showed a 24% reduction in VAT mass, and a trend toward improvement in glucose tolerance. In this last study, a group of mice with intermittent exercise performance (exercise intercalated with periods of inactivity) did not show all the metabolic improvements aforementioned, but the reduction in VAT mass, suggesting that intermittent exercise over prolonged period of time lead to adiposity reduction but retained the disrupted metabolic phenotype of a sedentary obese WAT.

A training of 8-week swimming period in rats showed exercise-induced increase in mitochondrial activity, measured by the increase in cytochrome c oxidase and TCA enzyme malate dehydrogenase in VAT (Stallknecht et al. 1991). Two weeks of swimming increased *Pgc1α* expression in SAT and VAT suggesting a final increase in mitochondrial biogenesis. Also, the mitochondrial content in OLEFT rats was normalized (preventing its reduction) along with improved glucose homeostasis after daily physical activity (Laye et al. 2009). Given that WAT is undervascularized, fibrotic and has few mitochondria during WAT expansion, adipocyte-specific up-regulation of *Vegfa* was performed. This improved vascularitzation of WAT along with massive up-regulation of *Ucp1* and *Pgc1α* levels (Kusminski & Scherer 2009), suggesting VEGF-A can induce mitochondrial biogenesis in WAT bringing benefits to mitochondrial metabolism and whole-body glucose and lipid homeostasis.

In a similar way, mice swim training increased mitochondrial biogenesis, mtDNA content and glucose uptake in SAT from WT mice, but not with mice deficient in endothelial nitric oxide synthase (eNOS), thus pointing to a crucial role of eNOS in the SAT metabolic adaptation. On the contrary, after a chronic treatment with NO donor (diethylenetrianine-

NO, DETA-NO), cultured murine and human adipocytes reported recovered promotion of mitochondrial biogenesis and elongation, glucose uptake and GLUT4 translocation (Trevellin et al. 2014).

Of note, **exercise** LI have been shown to produce a "browning" effect in SAT, moving to "beige" adipocytes, a newly described metabolic adipocyte type between WAT and BAT adipocytes. This way, rodents with 3-4 weeks of access to a running wheel increased the presence of beige cells in SAT which showed up-regulation of brown and beige adipocyte marker genes (*Ucp1*, PR Domain Containing 16 *Prdm16*) (Boström et al. 2012; Cao et al. 2011). *Prdm16* was also increased after 11 days of exercise training along with other browning genes like cell death-inducing DFFA-like effector A (*Cidea)* (Stanford, Middelbeek & Goodyear 2015). These 11-day LI increased UCP1 immunofluorescence, the number of blood vessels in SAT and marker genes of vascularization like *Vegfa*, and the basal rates of oxygen consumption rate (OCR) demonstrating an increase in mitochondrial activity (Stanford, Middelbeek, Townsend, et al. 2015; Vernochet et al. 2012). Moreover, the number of genes up-regulated by exercise training in SAT were of a greater number than the number reported in skeletal muscle (Stanford, Middelbeek & Goodyear 2015; Mahoney et al. 2005; Keller et al. 2011), indicating SAT might have an important role in the whole-body adaptations to exercise training. Among these up-regulation, gene-sets up-regulated included genes involved in metabolism, mitochondrial biogenesis, oxidative stress and signalling, membrane transport, cell stress, proteolysis, apoptosis, replication, glycoproteins, and genes involved in WNT signalling and PGC1α pathways. Contrary to VAT transplantations, SAT transplantation from trained mice into sedentary mice exhibited an improvement in glucose tolerance 9 days posttransplant, along with a decrease in fasting glucose, insulin and cholesterol, although some of these effects were not observed 4 weeks posttransplant (Stanford, Middelbeek & Goodyear 2015). A worsening in glucose tolerance appeared when the transplanted SAT had the same adipocyte size in trained and sedentary mice (Stanford, Middelbeek & Goodyear 2015), indicating that the improve in glucose tolerance comes from exercise-induced adaptations to SAT and not only transplantantion of smaller adipocytes. Finally, mice transplanted with SAT from trained mice exhibited increased rates of oxidative skeletal muscle glucose uptake.

Dietary LI with fish oils (FO) (Om3) to non-diabetic subjects with either IGT, IFG or at least three features of the metabolic syndrome, did not show changes in insulin sensitivity or first-phase insulin secretion (Spencer et al. 2013). As expected, all the subjects under the LI increased eicosapentaenoic acid (EPA) and docosahexaenoic acid (DHA). No changes

were observed after the LI in adiponectin, IL6, IL10, IL12, TNFα, resistin, plasminogen activator inhibitor-1 (PAI-1) and leptin levels. However, a significant decrease in blood MCP1 was observed, along with a significant decrease in ATMs. CLS were significantly decreased also after this dietary LI.

Om3 in rodents allowed a switch from M1 to M2 macrophages, coincident with increased insulin sensitivity (Oh et al. 2010). Although no changes in fibrosis, a small but consistent and significant increase in adipose capillaries was observed. mRNA expression studies in the adipose tissue confirmed a decrease of the previously mentioned *Mcp1* and also *Cd68* (a macrophages marker). In line with the studies with lack of an improvement in the glycemic control, other human studies with FO treatment showed a decrease in blood TG with no effects on glucose homeostasis (Friedberg et al. 1998).

Exercise training decreased adiposity along with a decrease in circulating leptin in both rodents and humans (Ellingsgaard et al. 2008; Ellingsgaard et al. 2011; Ueda et al. 2009; Martins et al. 2008; Shirazi et al. 2013; Henningsen et al. 2010). Because adiponectin is inversely correlated to fat mass and correlated with insulin sensitivity, it has been hypothesized that exercise increases circulating adiponectin levels. However, there is not yet a consensus about the effects of exercise in adiponectin concentrations.

Similarly, two recent studies with a **dietary** LI with FO treatment in insulin-resistant subjects found no changes on plasma adiponectin or IR (Vargas et al. 2011; Koh et al. 2012). Other studies showed changes in adiponectin: diet-induced only and diet-induced plus exercise LIs showed an increase in adiponectin by 20% while a non-significant decrease by 6% was observed in the only-exercise LI (Christiansen, Paulsen, Bruun, Ploug, et al. 2010).

Also, one study showed that a diet-induced **weight loss** of a given magnitude (≥10%) was needed to expect an increase in adiponectin in circulation, in contrast to the LI with the exercise alone (Madsen et al. 2008).

Summarizing the exercise effects: in human WAT decreased BW (decreasing VAT mass) (Gallagher et al. 2014; Christiansen, Paulsen, Bruun, Pedersen, et al. 2010), adipocyte size and lipid content (Gollisch et al. 2009; Craig et al. 1981), inflammatory markers (King et al. 2003; Abramson & Vaccarino 2002; Geffken et al. 2001; Mattusch et al. 2000) were observed; while GLUT4 and PGC1α protein expression (this later linked to increased mitochondrial biogenesis) were increased (Gollisch et al. 2009; Craig et al. 1981; Stanford, Middelbeek &

Goodyear 2015; Stallknecht et al. 1991; Sutherland et al. 2009). Also, OxPhos pathway appeared as the second most enriched pathway (Rönn et al. 2014). Regarding rodents, WAT inflammation, immune cell infiltration, oxidative and ER stress markers were decreased (Wainright et al. 2015); while mitochondrial activity (Stallknecht et al. 1991) and *Pgc1α* and *Ucp1* expression were increased (Kusminski & Scherer 2009), along with a feasible "browning" process (Boström et al. 2012; Cao et al. 2011; Stanford, Middelbeek & Goodyear 2015). Finally, exercise training decreased circulating leptin in both rodents and humans (Ellingsgaard et al. 2008; Ellingsgaard et al. 2011; Ueda et al. 2009; Martins et al. 2008; Shirazi et al. 2013; Henningsen et al. 2010).

Dietary intervention in humans including Om3 enrichment decreased plasma MCP1, ATMs and CLS (Spencer et al. 2013), although no changes in plasma cytokines were observed. Regarding rodents, a polarization towards M2 macrophaghes was observed along with a *Mcp1* and *Cd68* decreased mRNA expression (Oh et al. 2010).

1.8.3. Liver

The liver is a highly active metabolic organ, contributing about 2-3% of the total BW in humans. The liver is a key tissue for nutrient sensing and the maintenance of whole body energy metabolism. It exerts many functions, such as glycogen storage, synthesis of plasma proteins, hormone production and detoxification (Maton et al. 1993). Indeed, the liver participates in CH, fat and protein metabolism.

Regarding CH metabolism, the liver is important for maintaining normal blood glucose levels. Thus, the liver can both store glucose as glycogen (glycogenesis) and produce glucose by depolymerizing glycogen (glycogenolysis), converting galactose and fructose into glucose, and producing glucose from amino acids and glycerol from TG (gluconeogenesis) (Guyton & Hall 2006). In fact, the liver is the primary organ in charge of producing glucose in response to the glucose demand from the brain, which is responsible for about 50% of the glucose utilization under basal or fasting conditions (DeFronzo & Ferrannini 2015). In summary, the liver is the primary organ responsible for endogenous glucose production in fasting states and for storing glucose as glycogen after meal ingestion.

In a healthy state, the glucose transporter in liver GLUT2, suffers a translocation to the membrane for the glucose uptake. GLUT2 facilitates bidirectional glucose transport across

the hepatocyte plasma membrane under insulin regulation. In a healthy situation, insulin activates the insulin receptor kinase that phosphorylates IRS1 and IRS2, activating then phosphoinositide 3-kinase (PI3K) and ultimately AKT2 (Previs et al. 2000), which can ultimately promote glycogen synthesis, suppress gluconeogenesis and activate *de novo* lipogenesis (DNL).

The liver has an important role also in liver metabolism: it can both oxidize TG and convert the excess CH and proteins into fat, the mentioned DNL. 80% of the cholesterol synthetized in the liver is converted into bile acids, and the remainder is transported elsewhere as liproproteins. Lipoproteins are also carrying phospholipids synthetized in the liver (Guyton & Hall 2006).

Finally, the liver has a function in protein metabolism by deaminating amino acids too, synthetizing plasma proteins or formatting urea (Guyton & Hall 2006).

1.8.3.1 Liver in IR and obesity-related T2DM

IR is manifested by the presence of fasting hyperinsulinemia (DeFronzo et al. 1989) along with an impaired suppression of HGP in response to insulin (Groop et al. 1989). In fact, the increased HGP and fasting hyperglycemia are correlated in a strong manner ($R=0.847$, $p<0.001$(Defronzo 2009)). A T2DM patient who weights an average of 80kg, has 20-30g of glucose extra in the systemic circulation every night, since his/her liver is producing ≈2.5 instead of ≈2mg/kg/min (DeFronzo 1988; DeFronzo et al. 1989). As mentioned, these increases in HGP and fasting plasma glucose appear in a situation where the levels of fasting insulin are also increased by 2.5- to 3-fold (DeFronzo 1988; DeFronzo et al. 1989) showing how insulin is unable to suppress HGP, thus displaying hepatic IR. Although the raise in basal HGP can be explained by an increase in hepatic gluconeogenesis (DeFronzo & Ferrannini 1987; Magnusson et al. 1992; Consoli et al. 1990) and can be accelerated by the presence of hepatic IR, HGP can also have an accelerated rate due to increased glucotoxicity that leads to an increase in the glucose-6-phosphatase activity (Clore et al. 2000), thus avoiding the escape of glucose from the liver. Another phenomenon that can increase HGP is the increased sensitivity to glucagon, consequence of an increase of circulating glucagon (Matsuda et al. 2002; Unger et al. 1970; Baron et al. 1987).

In an obesity-related T2DM, the liver appears as a **fatty liver** due to steatosis, which is an abnormal retention of lipids within the hepatocytes. Slightly insulin-resistant humans at risk of T2DM reported higher hepatic lipid content in comparison to insulin-sensitive

individuals, even though both groups showed the content within the normal range (Prikoszovich et al. 2011). TG accumulated leading to **lipotoxicity** in large vacuoles within hepatic cells were believed mainly to have their origin in the already mentioned increase in adipose tissue lipolysis. When no alcoholic condition is known, the fatty liver disease is called Non-Alcoholic Fatty Liver Disease (**NAFLD**). NAFLD has been closely associated with obesity and IR, and believed to have a role in the pathogenesis of T2DM (Angulo 2002; Petersen, Dufour, Befroy, et al. 2005; Petersen et al. 2002; Fraser et al. 2009; Samuel et al. 2010).

This lipotoxicity supposes an **ectopic FA accumulation** and leads, as mentioned, to an increase in hepatocellular FA. These FA can induce HGP, increasing phosphoenolpyruvate carboxylase (PEPCK) and pyruvate kinase (PK), the rate-limiting enzymes of gluconeogenesis (Gastaldelli et al. 2000), and also disrupt the ability of insulin to inhibit HGP, worsening hepatic IR (Lam et al. 2003). Increased FA-induced HGP have been also related to a lack of inhibition of insulin-induced glycogenolysis (Boden et al. 2001; Boden et al. 2002). A role for ectopic lipid accumulation in hepatic IR was also confirmed with genetically modified rodent models: liver-specific lipoprotein lipase (*Lpl*, a key enzyme in lipid transport) overexpression lead to hepatic steatosis and IR (J K Kim et al. 2001; Merkel et al. 1998), and liver-specific *Cd36* (another protein involved in fat transport) overexpression in lean mice using adenovirus caused NAFLD (Koonen et al. 2007); while deletion of other proteins in charge of lipid transport such as FA transport proteins *Fatp5* (Doege et al. 2008) or *Fatp2* (Falcon et al. 2010) protected against hepatic steatosis and glucose intolerance. Regarding lipid transport, the liver actively exports lipids too. Some studies have shown that hepatic steatosis could be attributed to a **mismatch between the lipid liver uptake and export** after challenging situations such as HFD-feeding (H. Y. Lee et al. 2011). Overexpression of human apolipoprotein CIII (*Apoc3*) in HFD-fed mice caused hepatic steatosis with DAG accumulation, PKCε accumulation and hepatic IR (H. Y. Lee et al. 2011), with hepatic lipid content being unchanged in comparison to the WT when mice were fed chow-diet. In humans, lean individuals with an *APOC3* gene polymorphism showed an increase in fasting plasma APOC3 levels and fasting hypertriglyceridemia (Petersen et al. 2010) associated with a diminished plasma lipid clearance upon a lipid challenge and an increase in liver steatosis. Hence, both increased uptake and decreased export can lead to hepatic lipid accumulation, ultimately leading to hepatic IR.

Insulin action in the liver has similarities with skeletal muscle, hence a similar mechanism to the one in skeletal muscle explains how insulin signalling pathway is disrupted by lipotoxiticy leading to the suppression of the signalling cascade. In the literature, the most

accepted mechanism is via DAG molecules. Hepatic lipotoxicity leads to **disruption in insuling signalling cascade**: DAG increases PKCε (Crooke 2004) reducing insulin receptor kinase activity and decreasing the phosphorylation of IRS1- and IRS2-Tyr residues. As seen before, the mechanism by which PKCs inhibit IRS is through concrete serine phosphorylation (Schinner et al. 2005). Downstream, DAG has been shown to inhibit the IRS2-dependent phosphoinositide 3-kinase phosphorylation (Kim et al. 2000). PKCδ have been reported to be activated in livers of rats upon a 6h intralipid/heparin infusion, concomitant with hepatic IR (Lam et al. 2002). During this lipid infusion, IKKβ pathway was also activated, suggesting PKCδ might be activated also due to an inflammatory state (G. Boden et al. 2005). In fact, general or liver-specific loss of *Pkcδ* showed a diminishment of liver lipids and improved glucose tolerance, and *Pkcδ* overexpression leads to hepatic steatosis and worsens glucose tolerance (Bezy et al. 2011; Frangioudakis et al. 2009), suggesting PKCδ might have a role in lipid balance in rodents and humans. Moreover, apart from DAGs, ceramides can also disrupt some features in the obese-T2DM hallmark. Ceramides showed increased protein phosphatase 2A (PP2A) that sequestrates AKT2 by PKCζ, decreasing glycogen synthesis and also limiting forkhead box protein O1 (FOXO1) activation, ultimately increasing the expression of gluconeogenic genes (Samuel & Shulman 2012). Mechanistically, decreased FOXO1 phosphorylation (decreased activation) moves FOXO1 into the nucleus that activates gluconeogenic genes transcription such as *Pepck* and glucose-6-phosphate phosphatase (Morino et al. 2006).

In summary, all the signalling disruptions woud lead to **reduced stimulation of glycogen synthase** (GS) **activation** and decreased FOXO1 phosphorylation leading to an **increase in hepatic gluconeogenesis** (Morino et al. 2006). The increase in gluconeogenesis will ultimately **decrease the hepatic glucose uptake** through GLUT2, exacerbating hepatic IR.

In T2DM patients, the inability of the liver to regulate glycogen synthesis and glucose production has been reported in different studies (Krssak et al. 2004; Magnusson et al. 1992). Also implicated in this mechanism, oxidative stress is thought to contribute to the hepatic IR by activating PKCs (Schinner et al. 2005).

In line with the lipotoxicity, polyunsaturated FA (PUFA) have been shown to be potent ligands of PPARα, the main PPAR isoform expressed in liver (Delarue & Magnan 2007). Thus, gene expression of the gluconeogenic enzymes *Pepck* and glucose-6-phosphatase was activated by PUFA through PPAR recruitment, while FA inhibited *Pk* expression (Delarue &

Magnan 2007), suggesting an increase in gluconeogenesis and a limitation of the glucose degradation.

DAG molecules contributing to disrupting signalling could come either from the aforementioned increased lipolysis of the adipose tissue, or from the pathological increased ***de novo* lipogenesis** in the liver. This *de novo* lipogenesis was reported by Petersen and colleagues (Petersen et al. 2007) to have its origin in the CH redirection from skeletal muscle to the liver after a CH challenge. That is, IR in skeletal muscle would lead to an atherogenic dyslipidemia that increases in metabolic syndrome by altering postpandrial energy storage distribution. IR in skeletal muscle would then impair storage of CH as glycogen, redirecting them to the liver. Indeed, in insulin-resistant individuals a CH challenge increased plasma insulin but muscle glycogen was 61% lower than in the controls. Also, those individuals showed an increase in liver TG content that could origin in the almost twofold increase in hepatic *de novo* lipogenesis. VAT mass was identical in insulin-resistant and insulin-sensitive subjects, also confirming lipotoxicity to be independent of adipose tissue lipolysis. In keeping with this, other studies showed how the insulin-sensitive or resistant distinguishment was based in the lipid accumulation in the liver (Stefan et al. 2008; Fabbrini et al. 2009) and skeletal muscle (Stefan et al. 2008) and not in the visceral adiposity. All these studies demonstrate that the **lipotoxicity** effects in the liver can develop **independently of increased visceral adiposity**.

Hence, FA ectopic accumulation without peripheral and visceral adiposity can also lead to IR. This hypothesis was confirmed with studies using patients with lipodistrophy and mouse models of severe lipoatrophy, a phenotype consisting in hypertriglyceridemia, IR and ectopic fat deposition, including hepatic steatosis, but with a lack of adipose tissue. The animal model (Moitra et al. 1998) has no adipocytes and show FA accumulation in skeletal muscle and liver along with peripheral and hepatic IR (Kim et al. 2000), disruptions that were rescued after a fat pad transplantation from control WT mice. Also, leptin treatment corrected many of the lipodistrophy effects in mouse models (Shimomura et al. 1999) and in humans (Petersen et al. 2002; Oral et al. 2002). In one of the human studies, lipodistrophy patients showed higher HGP rates, lack of suppression of HGP, and lack of stimulation of glucose uptake in hyperinsulinemic conditions (Petersen et al. 2002). Leptin treatment decreased by about 90% the hepatic TG content and by 30% the content in skeletal muscle improving glucose uptake, leading to improvements in hepatic insulin responsiveness. In keeping with this, Fabbrini and colleagues removed VAT surgically without altering glucose homeostasis or insulin sensitivity, thus confirming that hepatic IR

might be related to intrahepatic lipids, instead of lipids from VAT non-suppressed lipolysis (Fabbrini et al. 2010).

Inflammation has an important role in the obesity-related T2DM hallmark. As in the adipose tissue, obesity leads to an increase in pro-inflammatory gene expression in the liver (Cai et al. 2005). Moreover, IR was also associated with an inflammatory response in the liver (Johnson & Olefsky 2013). Inflammation signals such as TNFα and IL6 can activate serine/threonine (Thr) kinases like IKKβ and JNK, both implicated in the increase in IRS1 concrete serine residues phosphorylation that, as aforementioned, ultimately disrupts insulin signalling. In the same line, liver-specific *Ikkβ* ablation blocked IKK signalling, protecting mice against hepatic IR and showing improved hepatic insulin signalling in HFD-fed and *ob/ob* mice, without any improvement in whole-body insulin-stimulated glucose metabolism (Arkan et al. 2005). In this context, hepatic IR after lipid infusions was associated with an increase in IKKβ-NFκB pathway (G. Boden et al. 2005). An animal model where this latter pathway was genetically activated in mice livers showed the potential of inflammation as a cause of IR (Cai et al. 2005). Indeed, anti-inflammatory drug salicylate ameliorated hepatic and peripheral IR, and protected against IR in rodents after acute lipid infusion (Jason K Kim et al. 2001) and in T2DM subjects (Hundal et al. 2002). The activation of *Ikkβ* led to enhanced ceramide synthesis, while JNK1 activation led to impaired lipogenesis (Samuel & Shulman 2012). Liver-specific *Jnk1* deletion promotes hepatic steatosis, increased expression of lipogenic key enzymes, impaired insulin signalling and hepatic IR with an unexpected increase in insulin clearance (X. Zhang et al. 2011). After adenoviral-mediated decrease in hepatic *Jnk1*, similar findings were observed: increase in liver lipid production and a decrease in fasting plasma insulin levels (Sabio et al. 2009). Studies that managed to increase JNK1 activation through mitogen-activated kinase phosphatase 1 (*Mkp1*) KO (*Mkp1*$^{-/-}$), a phosphatase that inactivates MAPKs such as JNK1, reported normal hepatic insulin sensitivity, increased lipid oxidation and decreased lipogenesis (Wu et al. 2006).

The liver contains its own resident **macrophages**, the Kupffer cells, and also suffers macrophage infiltration. Kupffer cells have their pro-inflammatory pathways activated in obesity with no increase in their number (Cai et al. 2005). They can express an alternative macrophage phenotype (M2) worsening obesity-related IR in response to, for example IL4 and under the direction of PPARγ (Odegaard et al. 2008). Apart from these resident macrophages, the liver can recruit circulating monocytes during obesity (Obstfeld et al. 2010), although the distinct function of Kupffer cells and the new recruited macrophages is

not known. In any case, liver macrophages can secrete inflammatory cytokines that can activate pathways such as the IKKβ, ultimately leading to IR (Cai et al. 2005).

Mitochondrial function in liver has been assessed in T2DM and steatotic patients, as well as in obese and diabetic animal models. Reduced expression of genes encoding OxPhos proteins was observed in obese T2DM, and the expression levels were directly correlated with reduction of *Pgc1α* expression and inversely correlated with hepatic lipid accumulation (Pihlajamäki et al. 2009). On the contrary, obese T2DM Japanese showed an increase in OxPhos complexes gene expression, in parallel with BMI and IR (Takamura et al. 2008). However, this disagreement could be due to the different degree of obesity and ethnic differents in the different cohorts.

Szendroedi and colleagues reported in T2DM patients reduced absolute hepatic ATP concentrations an inorganic phosphate levels, indicative of hepatic but not peripheral IR (Szendroedi et al. 2009). Later on, same T2DM patients showed reduced hepatic ATP turnover (indicative of mitocondrial activity) at rest, which was correlated with peripheral and hepatic IR (Schmid et al. 2011), but not with BMI and fasting glycemia. Having similar hepatic intracelular lipid content, age-matched non-diabetic persons showed no reduction in hepatic mitocondrial activity (Schmid et al. 2011).

Studies in NAFLD patients reported reduced (Schmid et al. 2011) or increased (Sunny et al. 2011) hepatic mitochondrial metabolism. Furthermore, obesity-related non-alcoholic steatohepatitis (NASH) patients, that is, patients with NAFLD who showed inflammation in their livers and jumped to the pathological stage of NASH, reported severe impairment of recovery from ATP depletion (Cortez-Pinto et al. 1999).

NAFLD and NASH have been associated with increased FA β-oxidation, IR, and hepatic oxidative stress, although only NASH showed defects in mitochondria structure (Sanyal et al. 2001). NASH patients showed increased mitochondrial β-oxidation (Miele et al. 2003; Sanyal et al. 2001; Chalasani et al. 2003), increasing NADH and $FADH_2$ and the delivery of electrons to ETS, along with a decreased in ETS complexes activity that blocked the electron flow. Thus, the accumulation of electrons in the CI and CIII might lead to ROS production. Moreover, NASH patients in another study reported a reduction in OxPhos complexes activities, which correlated with serum TNFα, IR and BMI (Pérez-Carreras et al. 2003). Other studies with NAFLD patients where, unfortunately, no hepatic insulin sensitivity was measured showed reduced submaximal ADP-stimulated OxPhos despite

increased FA oxidation (Sanyal et al. 2001; Miele et al. 2003). ADP-stimulated OxPhos was assessed by the rate of ATP resynthesis suggesting either reduced OxPhos capacity or mitocondrial plasticity (Cortez-Pinto et al. 1999).

Liver mitochondria from HFD-fed rats during 2 wks (Iossa et al. 2003), 7 wks (Raffaella et al. 2008) and mice for 16 wks (Mantena et al. 2009), showed DIO, IR, hepatic steatosis, and reduced respiratory capacity along with increased oxidative stress. In the same line, *db/db* mice showed a significant decrease in mitochondrial CI to CV activities in liver (Wang et al. 2007). Also, Holmström and colleagues reported decreased mitochondrial oxidative capacity in *db/db* and *ob/ob* mice (Holmström et al. 2012; Holmström et al. 2013). However, in genetically modified rodent studies, adult but not young *ob/ob* mice increased liver mitochondrial oxidative capacities (Brady et al. 1985) in the same way that obese insulin-resistant Zucker rats isolated liver mitochondria reported an increase in OxPhos efficiency in comparison to their lean controls (Ferreira et al. 1999), although the same mitochondrial function was observed when comparing obese with lean, both insulin-resistant (Flamment et al. 2008).

Genetic animals models have showed how genetic defects in hepatic mitocondrial FA oxidation can predispose to a hepatic steatosis an IR. It is the case of mice lacking long-chain acyl-CoA dehydrogenase (*Lcad*) (Zhang et al. 2007).

Liver from leptin deficient *ob/ob* mice showed UPR activation (Özcan et al. 2004) suggesting that **ER stress-UPR** might be involved in the IR pathogenesis in an obese state both in rodent and in humans (Gregor et al. 2009). In keeping with this, *ob/ob* mice overexpressing *Bip* chaperone (*Grp78*), resulted in suppression of UPR and reduction in liver lipid content (Kammoun et al. 2009) due to a reduced expression of two key transcriptional regulators of lipogenesis (*Srebp1* and carboxylate-responsive element-binding protein *Chrebp*).

Interestingly, liver-specific *Ire1* deficient mice ($Ire\alpha^{hepfe/-}$) showed a normal phenotype but when challenged with UPR chemical activators (*tunicamycin* or *bortezomid*) developed a greated hepatic steatosis (K. Zhang et al. 2011), similar to the mice lacking *Atf6* ($Atf6\alpha^{-/-}$) (Yamamoto et al. 2010). This suggests that UPR is tied to lipogenesis and that disruption of one of the UPR arms leads to a compensatory increase in other arms signalling. Of note, under hyperinsulinemic conditions in mice with liver-specific inhibition of *Perk*, insulin might activate the UPR increasing *Bip*, *Xpb1s* and *Chop* mRNA expression, while insulin-stimulated glucose uptake in skeletal muscle and adipose tissue were decreased

(Birkenfeld et al. 2011) without alterations in lipid concentrations in these tissues. Thus, a role for UPR in regulating peripheral insulin action by secreted factors in the liver might be feasible. A direct link between UPR and IR cannot be concluded, but one can think that activation of UPR leads first to an altered celular lipid balance and, via lipid accumulation, alters insulin signalling.

Oxidative stress from hyperglycemia and FFA can worsen IR impairing insulin secretion and leading to long-term complications of T2DM (Evans et al. 2003). ROS seem to play a direct role in the worsening effects of hyperglycemia and probably also of FFA by damaging DNA, protein and lipids and by activating stress-sensitive pathways that cause cellular damage such as the NF-κB inflammation pathway, which has a key role in immune and inflammatory responses, and apoptosis. Moreover, oxidative stress and ROS are known to activate serine kinases which, in turn, can phosphorylate IRS1 and IRS2 in skeletal muscle and liver, finally disrupting insulin signalling via PI3K and resulting in IR (Evans et al. 2003; Saltiel & Kahn 2001).

Additionally, ER membrane has lipogenic enzymes that give rise to lipid droplets, and proteins that can regulate these droplets (ie. adipose TG lipase ATGL or patatin-like phospholipase domain-containing protein 3 PNPLA3) might regulate lipid concentration in discrete hepatic cell compartments (Samuel & Shulman 2012). Hence, the ability of the UPR to cause hepatic IR may depend on whether UPR activation alters the balance of lipogenesis and lipid export to promote hepatic lipid accumulation (Samuel & Shulman 2012).

1.8.3.2 Lifestyle interventions on liver

Exercise LI in adolescents with risk of T2DM improved their cardiorespiratory fitness, improvement correlated to the changes in adiposity and hepatic TG. The adolescents with the highest improvement in **fitness** were significantly more likely to decrease their BW, BMI and hepatic TG in comparison with adolescents that had the lowest improvement (Sénéchal et al. 2015). In the same line, fitness might improve the resolution of NAFLD with weight loss according to human studies. Obese individuals with a high baseline cardiorespiratory fitness showed a greater reduction in liver TG with **diet**-induced weight loss (Kantartzis et al. 2009).

Exercise in rodents reported higher phosphorylation of liver AKT in the insulin signalling pathway, showing similar results in skeletal muscle samples (Rao et al. 2013). Other studies

assessing the effects of **voluntary exercise** showed that 20 wks with access to a voluntary exercise wheel reduced fasting glucose and HOMA-IR in OLEFT rats. In liver, reduced expression of *iNOS* and subsequent S-nitrosylation of key molecules implicated in insulin signalling were reported, supporting the hypothesis that voluntary exercise improves IR in part by supressing *iNOS* expression and subsequent AKT-S-nitrosylation (Tsuzuki et al. 2015).

Endurance training in rats of treadmill performance for 8 wks 5days/wk and 60min/day starting at 15m/min until 25m/min reported a decrease in serum TG, regardless of standard diet or HFD (Gonçalves et al. 2014). Gonçalves and colleagues also showed a decrease in FCCP respiration (ETS CI+II) in sedendary rats under HFD in comparison with sedentary rats with chow diet, which was increased and reverted after endurance training while maintained under HFD (Gonçalves et al. 2014). Surprisingly, the authors also assessed two groups with chow or HFD and voluntary wheel exercise, which showed the highest increase in FCCP respiration (Gonçalves et al. 2014).

Dietary LI including **weight loss** reversed NAFLD and IR: patients with poorly controlled T2DM who achieved a moderate weight loss of 8kg over 7 wks on LFD (**CR**) showed reductions in hepatic TG concentrations (from nearly 12% to 2%) (Petersen, Dufour, Befroy, et al. 2005), while the decrease in hepatocellular lipid levels was greater after 12 wks (approx. 81%). Although they only mobilized a small amount of hepatocellular lipids, concordant improvements in hepatic insulin sensivitiy reversing IR, decrease in HGP and correction of fasting hyperglycemia were reported, independently of changes in insulin-stimulated peripheral glucose metabolism and intramyocellular lipids (Petersen, Dufour, Befroy, et al. 2005).

In rodent studies, Om3 was reported to be beneficial by promoting hepatic FA oxidation through a PPARα-dependent mechanism (Neschen et al. 2006; Nakatani et al. 2003). Om3 also limited TG supply to WAT, thus preventing lipid accumulation in WAT (Nakatani et al. 2003; Ikemoto et al. 1996). In fact, PPARα activation in the liver has been suggested to exert PUFA-mediated anti-obesity and anti-steatotic effects (Nakatani et al. 2003). The beneficial effect of Om3 also included an increase in plasma adiponectin through PPARϒ activation (Neschen et al. 2006), ultimately preventing hepatic DAG accumulation and preserving insulin action even after a HFD (Neschen et al. 2002; Neschen et al. 2007; Storlien et al. 1991). Some monounsaturated FA (MUFA), like the palmitoleic acid, have been suggested to improve insulin action in liver and skeletal muscle in mice (Cao et al. 2008). Moreover,

higher concentrations of this endogenously-produced FA secreted from adipocytes have been associated with increased insulin sensitivity in humans (Stefan et al. 2010). Interestingly, Lionetti and colleagues, apart from observing also that FO (Om3) feeding led to less hepatic lipid accumulation through improved mitochondria FA oxidation in comparison to mice fed with lard, reported a concomitant shift to mitochondrial fusion processes in the Om3-fed group similar to that of the controls, thereby preventing oxidative stress (Lionetti et al. 2014).

In summary, human individuals performing exercise LIs with highest fitness reported a major decrease in BW, BMI and hepatic TG (Sénéchal et al. 2015). Rodents performing exercise showed higher liver AKT phosphorylation (Rao et al. 2013), and ameliorated IR through a iNOS-mediated mechanism in liver from obese rats (Tsuzuki et al. 2015). Exercise also ameliorated mitochondrial respiration in comparison to sedentary animals (Gonçalves et al. 2014).

In the same way patients with high fitness had greater effects from exercise, obese patients with a high baseline cardiorespiratory fitness reduced more liver TG after dietary weight loss (Kantartzis et al. 2009). This dietary CR-induced weight loss in human liver decreased hepatocellular lipids (reversing NAFLD), IR and HGP, as well as corrected fasting hyperglycemia (Petersen, Dufour, Befroy, et al. 2005). Of note, unsaturated FA such as palmitoleic improved insulin sensitivity in humans (Stefan et al. 2010).

Palmitoleic also improved insulin action in liver in rodents (Cao et al. 2008). Om3 in rodents promoted FA oxidation through a PPARα mechanisms (Neschen et al. 2006; Nakatani et al. 2003) (thought to have anti-obesity and anti-steatotic effects (Nakatani et al. 2003)); increased adiponectin preventing DAG accumulation and maintaining insulin action after a HFD (Neschen et al. 2002; Neschen et al. 2007); and shifted to mitochondrial fusion processes (Lionetti et al. 2014).

1.8.4. Skeletal muscle

Skeletal muscle is quantitatively the most important tissue in maintaining glucose homeostasis and is a major site of IR in T2DM patients (DeFronzo et al. 1985). In fact, skeletal muscle accounts for approx. 80% of post-pandrial glucose disposal in healthy individuals (Thiebaud et al. 1982). It is composed by different fiber types that differ in their metabolic and contractile properties, becoming a very heterogeneous tissue. Among the different muscle fiber types, *type I* fibers show a higher capacity for glucose and FA uptake

and have a higher content in mitochondria, fact that facilitates the production of energy by this fiber type through oxidative metabolism, while also showing high capillarity, leading to more oxygenation; *type IIb* fibers, on the contrary, have a limited oxidative capacity due to a low mitochondrial density, have less capillarity and are readily fatigable during periods of high activity (Schiaffino & Reggiani 2011); *type IIa* fibers are intermediate between the two previous types, showing similarities with *type I* fibers (higher mitochondrial density and myoglobin content than IIb hence showing also a higher oxidative capacity) and also with *type IIb* fibers (high glycogen content, less capillarized). *Type IIx* fibers have twitch properties similar to *IIa* and *IIb* and resistance to fatigue that is halfway between *IIa* and *IIb*. It is worth mentioning that *type IIb* fibers are not present in humans (Smerdu & Soukup 2008). In this PhD thesis, soleus has been used as an oxidative skeletal muscle sample; and tibialis anterior (TA), extensor digitorum longus (EDL) and gastrocnemius as glycolytic skeletal muscle samples.

Insulin signal transduction is, as aforementioned, the mechanism by which glucose is uptaken into the cell. At first, insulin binds and activates the insulin receptor by phosphorylating its Tyr residues in the β-chain (Bajaj & DeFronzo 2003; Saltiel & Kahn 2001; Taniguchi et al. 2006; Musi & Goodyear 2006). Through the signalling cascade, insulin receptor Tyr phosphorylation ultimately activates PI3K and AKT, resulting in the translocation of GLUT4 and the subsequent glucose uptake, and activation of nitric oxide synthase (NOS) with arterial vasodilation (Kashyap et al. 2005; Montagnani et al. 2001).

1.8.4.1. Skeletal muscle and IR and obesity-related T2DM

In skeletal muscle the IR is manifested by **impaired glucose uptake** upon a CH meal resulting in postpandrial hyperglycemia (Ferrannini et al. 1988). Many studies showed that T2DM individuals are more insulin-resistant compared with sex-, age-, weight-matched control subjects by measuring body glucose disposal using a hyperinsulinemic-euglycemic clamp and tritiated glucose (DeFronzo 1988; DeFronzo 2004; Groop et al. 1989; DeFronzo et al. 1985; Lillioja et al. 1993; Eriksson et al. 1989; Reaven et al. 1989; Henry et al. 1986; Ferrannini et al. 2005). Skeletal muscle IR accounts for over 85-90% of the impairment in total body glucose disposal in T2DM (Pendergrass et al. 2007; DeFronzo et al. 1985). A **defective insulin-stimulated glycogen synthesis** was reported due to defects in insulin-stimulated glucose transport/phosphorylation in young lean non-smoking insulin-resistant offspring of parents with T2DM, in order to avoid cofounding factors such as obesity or hyperglycemia (Perseghin et al. 1996; Rothman et al. 1995); along with a decrease in the rate of insulin-stimulated muscle glycogen synthesis by more than 50% in T2DM patients (Shulman et al.

1990). Hence, muscle becaming the major responsible for the IR under the hyperinsulinemic clamp conditions.

Besides impaired glucose uptake and phosphorylation (Pendergrass et al. 2007; Rothman et al. 1992; Cline et al. 1999; Vogt et al. 1998) and reduced glycogen synthesis (Shulman et al. 1985; Mandarino et al. 1987; Shulman et al. 1990), other intramyocellular defects in insulin action (DeFronzo 1997; Bajaj & DeFronzo 2003) such as decreased glucose oxidation (Groop et al. 1989; Groop et al. 1991) are reported in T2DM. Of note, in T2DM individuals, glucose utilization is maintained in the brain, adipose tissue and splanchnic tissue, but decreases notably in the skeletal muscle, becoming an insulin-sensitive tissue with an important role in the onset of the disease (DeFronzo 1988).

Impaired insulin signalling has been proposed as the molecular mechanism that explains IR and the decrease in glucose uptake. As aforementioned, for a proper insulin-stimulated glucose uptake, IRS1 Tyr residues need to be phosphorylated to recruit IRS1, which is not the case for T2DM patients where the ability of insulin and insulin receptor to phosphorylate IRS1 Tyr residues is impaired (Miyazaki et al. 2003; Bajaj & DeFronzo 2003; Cusi et al. 2000). This impaired insulin signalling was also observed in obese normal glucose-tolerant individuals (Cusi et al. 2000) and in normal glucose-tolerant, insulin-resistant offspring with two T2DM parents (Kashyap et al. 2004; Pratipanawatr et al. 2001). In fact, instead of Tyr residues, specific serine IRS1 residues (Ser307 in humans and Ser302 in rodents) are phosphorylated (Yu et al. 2002) by Ser/Thr kinases, in part activated by intramyocellular FA, ultimately leading to IR. This way, IRS1 cannot interact with the insulin receptor (Aguirre et al. 2002), reducing IRS1-associated PI3K activity. Indeed, phosphorylation of both IRS1 and PI3K was impaired in rodent models of IR (Folli et al. 1993). Reduced PI3K activity results in decreased insulin-stimulated AKT2 activity. Diminished AKT2 activity fails to activate GLUT4 translocation as well as AKT2-downstream signalling, ultimately reducing insulin-stimulated glucose uptake.

Ectopic FA accumulation in the skeletal muscle has been hypothesized for the mechanism disrupting insulin signalling, leading to IR and the impairment in glucose uptake. That is, FA shuttled from the WAT increase intramyocellular lipid content. Indeed, insulin activation of IRS1-associated PI3K activity in skeletal muscle was abolished in both rodents (Griffin et al. 1999; J. K. Kim, Fillmore, et al. 2004) and humans (Dresner et al. 1999) by raising plasma FA. Krssak and colleagues studied whether the IR was associated with circulating plasma FA or intramyocellular lipids, and found that IR did not develop until 3-

4h into the lipid infusion, concordant with accumulation of intracellular FA and impairment in glucose uptake (Krssak et al. 1999). Thus, intramyocellular lipids are a stronger predictor of skeletal muscle IR than circulating FA. Certainly, intramyocellular lipid content was reported to be a good predictor for IR in skeletal muscle in both adults (Krssak et al. 1999; Perseghin et al. 1999; Szczepaniak et al. 1999) and children (Weiss, Dufour, Taksali, et al. 2003).

Furthermore, evidence has been provided with genetic animal models for the role of ectopic lipid accumulation in IR: Kim and colleagues showed how muscle-specific overexpression of *Lpl* (key enzyme in lipid transport) promoted lipid uptake and IR in skeletal muscle (J K Kim et al. 2001); while other studies demonstrated that *Lpl* mice deletion (Wang et al. 2009) or deletion of other lipid transport proteins such as *Fatp1* (J. K. Kim, Gimeno, et al. 2004) and *Cd36* (Goudriaan et al. 2003; Hajri et al. 2002) protected mice from muscle lipid accumulation and IR when challenged with HFD.

However, some studies showed **IR independently of changes in TG** accumulation within skeletal muscle, dissociating intramyocellular TG concentrations and IR (Dresner et al. 1999; Yu et al. 2002). In fact, **DAGs** and not TG are the signalling intermediates that lead to disruption in insulin signalling, among all the FA forms. Studies in rodents overexpressing diglyceride acyltransferase *Dgat1* (DAG acyl transferase that transfers a fatty acyl CoA to DAG to form TG) showed an increase in TG in their muscles but were protected from fat-induced IR (Liu et al. 2007) since they had reduced DAG levels. These mice can be like the paradoxal elite endurance athletes who are insulin-sensitive, but have increased TG content in their muscles (Goodpaster et al. 2001; Krssak et al. 2000; Dela et al. 1992). Moreover, an inverse relationship between changes in DAGs content in the muscle and insulin sensitivity was reported (Dubé et al. 2011; Itani et al. 2002). DAG-induced IR in skeletal muscle and liver fits most forms of obesity, where the delivery of FA is increased and exceeds the capacity of the cells to oxidize fat or to convert DAG to TG. However, no relationship was found between DAG and insulin sensitivity in other studies (Coen et al. 2010; Vistisen et al. 2008; Amati et al. 2011).

Studies considering other lipids such as **ceramides** have reported controversial results. Intramyocellular ceramides content was not associated with IR in humans (Dubé et al. 2011; Helge et al. 2004; Vistisen et al. 2008; Itani et al. 2002; Skovbro et al. 2008), and their levels were similar between untrained subjects and athletes (Helge et al. 2004). However, some cross-sectional studies in athletes, in normal weight and obese sedentary humans (Amati et

al. 2011), and in obese humans (Coen et al. 2010; Adams II et al. 2004), linked ceramides and IR. Moreover, Holland and colleagues treated mice with *myirocin*, an inhibitor of serine palmitoyl transferase, which attenuated the increase in skeletal muscle of ceramide content in mice fed with HFD, without showing changes in long-chain acyl-CoAs, DAGs, or TG, and improved glucose tolerance (Holland et al. 2007). Since *myiricin* prevented acute skeletal muscle IR upon an infusion of palmitate (saturated) but not oleate (MUFA), the role of ceramides might be limited to saturated fats. Ceramides can also disrupt insulin signalling by increasing protein phosphatase 2A (PP2A) further sequestrating AKT2 by PKCζ, thus avoiding AKT2-induced GLUT4 translocaltion and decreasing insulin-stimulated glycogen synthesis (Samuel & Shulman 2012).

In any case, much research has been performed with **intramyocellular DAGs**, reporting results that support their role in skeletal muscle IR. DAGs act through activation of Ser/Thr kinases such as PKC, inhibitory IKKβ and NFκB, which are also activated by inflammatory molecules such as TNFα and IL6 (Schinner et al. 2005). Indeed, TNFα increased IRS1 serine phosphorylation through the stimulation of different serine kinases, such as the IKKβ and JNK, among others; while DAGs have been reported to activate PKC (Zick 2003). SOCS proteins showed enhanced expression by TNFα, and seemed to also bind the insulin receptor reducing its ability to phosphorylate IRS proteins (Kawazoe et al. 2001; Emanuelli et al. 2000; Ueki et al. 2004), through the same serine phosphorylation (Lebrun & Van Obberghen 2008). Itani and colleagues observed activation of both human muscle PKCβ and PKCδ after lipid or heparin infusions (Itani et al. 2002), and activation of PKCθ in T2DM subjects (Itani et al. 2001). Studies with rodents on HFD confirmed that increased concentrations of DAG due to the diet (or lipid infusion) activated novel PKCs isoforms (PKCθ, β and δ) in skeletal muscle (Schmitz-Peiffer et al. 1997; Griffin et al. 1999; Yu et al. 2002). Also, infusion of intralipid/heparin for 5h caused IR associated with an accumulation of intracellular DAG and specific activation of PCKθ (Griffin et al. 1999).

Regarding JNK pathway, muscle-specific *Jnk1* KO mice fed with HFD showed similar weight gain and glucose tolerance impairment in comparison with WT mice (Sabio et al. 2010). However, under hyperinsulinemic-euglycemic clamp conditions *Jnk1* KO reported an improvement in muscle-specific glucose uptake and insulin signalling, along with a surprising increase in adipose inflammation and in hepatic steatosis. Of note, no differences in adipose or hepatic insulin sensitivity were reported (Sabio et al. 2010). HFD-induced IR was reverted in rodent models where Ser/Thr kinases (JNK, IKKβ and PKCθ) were either knocked-down or pharmacologically inhibited (J. K. Kim, Fillmore, et al. 2004; Um et al. 2004; Furukawa et al. 2005; Hirosumi et al. 2002; Yuan et al. 2001). IKK and NFκB are the

two other main Ser/Thr kinases activated by lipid metabolites and inflammatory molecules. In fact, and as mentioned, anti-inflammatory salicylates inhibiting IKK serine-induced phosphorylation of insulin receptor in obese Zucker rats improved insulin sensitivity in skeletal muscle and liver (Savage et al. 2005).

Regarding the type of muscle, evidence has suggested that intramyocellular lipid content levels in soleus muscle but not TA are predictive of the IR degree in first-relatives of T2DM patients (Roden 2005). Similarly, oxidative capacity also differs between locomotor and structural muscle groups (Rabøl et al. 2010).

Besides the hypothesis that the increase in intramyocellular FA stems from an increased WAT lipolysis, another hypothesis has suggested that the cause for this FA increase is also a **reduced β-oxidation of FA**. Whether this decrease in β-oxidation is due to skeletal muscle mitochondrial dysfunction is still unclear.

Mitochondrial dysfunction in skeletal muscle has kept the focus when linking mitochondrial function, FA accumulation and IR-T2DM (Befroy et al. 2007; Kelley et al. 2002; Patti et al. 2003; Petersen et al. 2004; Ritov et al. 2005). In fact, impaired mitochondrial plasticity was observed in T2DM patients, in their first-degree relatives, and in healthy humans after a 6h lipid infusion (Szendroedi et al. 2007; Petersen, Dufour & Shulman 2005; Brehm et al. 2006). Insulin-resistant individuals cannot increase their mitochondrial activity or OxPhos capacity in hyperinsulinemic-euglycemic clamps. Moreover, mitochondrial defects themselves have been related to T2DM, in a way that physical inactivity in T2DM patients was reported a major contributor of the mitochondrial defects observed in their skeletal muscles (van Tienen et al. 2012).

To assess mitochondrial function during IR, Petersen and colleagues assessed ATP generation in skeletal muscle. Insulin-resistant offspring of T2DM parents revealed **decreased mitochondrial ATP synthesis** during insulin stimulation in comparison to controls (Petersen, Dufour & Shulman 2005). In the same line a reduction of 30% in the mitochondrial rates of ATP production in muscle was observed in another study (Petersen et al. 2004). In this last study, it is important to mention that one control subject showed more than 6 times a standard deviation increase in comparison to the control group mean, giving then room to difference between controls and insulin-resistant individuals. In any case, ATP generation at rest is used to maintain membrane potential while not being accumulated in skeletal muscle. Therefore, ATP is strickly adjusted to cell needs, and

seems difficult to imagine a decrease of 30% in insulin-resistant skeletal muscle (Dela & Helge 2013).

Moreover, **mitochondrial density was decreased** by 38% as measured by electron miscroscopy in skeletal muscle of the insulin-resistant offspring (Morino et al. 2005) suggesting that this reduction could account for the diminished rate in OxPhos in mitochondria. A decrease by 50% in mitochondrial cytochrome c oxidase I in these insulin-resistant offspring was also reported (Morino et al. 2005). Mitochondrial activity was also reduced in elderly, insulin-resistant individuals in comparison to controls (Szendroedi et al. 2007; Petersen et al. 2003). Of note, Chomentowski and colleagues reported that obese and insulin-resistant, but not T2DM patients, had reduced mitochondrial content (Chomentowski et al. 2011). Regarding mitochondrial genes and structure, skeletal muscle IR was correlated with reduced expression of OxPhos genes in humans (Roden 2005) and alterations in mitochondrial ultrastructure such as reduced mitochondrial size (Kelley et al. 2002; Toledo et al. 2007).

In keeping with this, T2DM patients showed *in vivo* lower submaximal ADP-stimulated OxPhos in skeletal muscle in comparison to non-diabetic humans matched for age, body mass and sex (Phielix et al. 2008; Schrauwen-Hinderling et al. 2007), suggesting that the current cellular energy demand was not achieved due to impaired mitochondrial plasticity, reduced OxPhos capacity or mitochondrial content. Indeed, T2DM compared to healthy individuals reported **lower OxPhos capacity** in muscle biopsies (Phielix et al. 2008; Kelley et al. 2002; Boushel et al. 2007; Ritov et al. 2010) that was then confirmed in isolated mitochondria (Mogensen et al. 2007) suggesting again compromised mitochondrial capacity in T2DM patients. Muscle biopsies showed a **lower activity of mitochondrial oxidative enzymes** in T2DM obese subjects (Kelley et al. 2002). Patients with T2DM (Morino et al. 2005; Chomentowski et al. 2011; Kelley et al. 2002; Ritov et al. 2005; Heilbronn et al. 2007) or IR (Morino et al. 2005; Heilbronn et al. 2007) frequently showed **reduced mitochondrial content**. Overweight and obese insulin-resistant T2DM patients also showed around 40% less intermyofibrillar mitochondria content in contrast to lean, insulin-sensitive individuals. In many of the studies presented and also as commented in section 1.6.3, the reduction in mitochondrial content might be related to obesity rather than IR. **Obesity might be a cofounding factor** in these studies since obese patients have shown smaller mitochondria, thus the mitochondrial abnormalities might be related to obesity rather than to IR.

Other studies showed **normal mitochondrial activity** without differences between **T2DM patients** and healthy humans (Szendroedi et al. 2007). Hence, reduced mitochondrial content might be compensated by an increase in mitochondrial activity. The fact that in these studies the mitochondrial content, oxidative capacity and mitochondrial activity in the fasting did not correlated with insulin sensitivity in insulin-resistant group, suggested a dissociation between insulin sensitivity (thus, IR) and muscle mitochondrial function (Karakelides et al. 2010; Lefort et al. 2010; Nair et al. 2008). This dissociation was confirmed by different studies where no differences in mitochondrial content were found in T2DM patients in comparison to controls matched for body mass (Phielix et al. 2008; Boushel et al. 2007; Mogensen et al. 2007). Phielix and coworkers studied skeletal muscle from T2DM patients *in vivo* and *ex vivo* and found ADP-stimulated respiration and maximal respiratory capacity reduced by 35% and 31% respectively, without any alteration in mitochondrial content (Phielix et al. 2008), but with a mitochondrial function *in vivo* reduction of 25%. Ritov and colleagues observed a reduction in ETS activity in the subsarcolemmal mitochondrial fraction of muscle biopsies from obese and T2DM patients (Ritov et al. 2005), along with a decrease in mtDNA, whilst the decrease in mitochondrial content did not account for the mitochondrial dysfunction. Boushel and colleagues reported decreased oxygen flux capacity in permeabilized fibres from T2DM that was lost after normalization by mtDNA content or CS activity (Boushel et al. 2007). Finally, similar ETS capacity in T2DM subjects in comparison to controls, also advocates against this hypothesis (Gnaiger 2009).

Therefore, in order to explain the concomitant presence of IR and mitochondrial dysfunction, some studies have demonstrated that reduced mitochondrial function might not be related to IR, but to a **lack of exercise** or physical performance. It was demonstrated that exercise is the most powerful stimulus for mitochondrial biogenesis in skeletal muscle (Hoppeler et al. 1985), same way as exercise training is capable to restore muscle oxidative capacity in T2DM patients (Hey-Mogensen et al. 2010; Phielix et al. 2010), along with improvement of insulin sensitivity and metabolic flexibility (Toledo et al. 2007). Different studies showed that skeletal muscle mitochondrial function is unlikely a primary consequence of IR. Toledo and colleagues reported improvements in IR that might occur without changes in mitochondrial capacity, as they showed in their studies where dietary LI and dietary+exercise LI decreased weight loss and improved insulin sensitivity, but only diet+exercise LI improved aerobic capacity (Toledo et al. 2008). Irving and colleagues found an improvement after nine days of intensive training in skeleltal muscle OxPhos capacity similar in offspring of mothers with T2DM and non-diabetic controls, although only controls improved insulin sensitivity (Irving et al. 2011). Hey-Mogensen and colleagues

observed in T2DM patients in comparison to matched controls after training, increased insulin sensitivity without differences in muscle mitochondrial respiration unless the groups were pooled (Hey-Mogensen et al. 2010). In the same line, Lefort and colleagues showed normal mitochondrial oxidative capacity in skeletal muscle from obese and insulin-resistant, associated with high rates of ROS production (Lefort et al. 2010). Moreover, skeletal muscle dysfunction was not related to an early stage of T2DM (De Feyter, van den Broek, et al. 2008).

In keeping with this, a study with Asian-Indians and Caucasians showed how Indians were more insulin resistant although they had similar muscle OxPhos capacity (Petersen et al. 2006). In fact, Indians had more OxPhos capacity than Northern European Americans regardless of the IR state, suggesting that IR or T2DM are not a cause for mitochondrial dysfunction and mitochondrial dysfunction cannot lead to IR in Asian Indians (Nair et al. 2008). With all, a probable explanation for the decrease in mitochondrial content in muscle may simply be that IR and T2DM are associated with an imbalance between caloric intake and exercise in genetically predisposed invididuals, which will facilitate IR and further T2DM if the β-cells are under failure. Hence, **dissociation between IR and mitochondrial respiratory function** is confirmed.

Besides the decrease in mitochondrial function to explain IR, it has also been suggested that IR individuals' mitochondria might have an **intrinsic defect in ETS** components, thus compromising the quality of the mitochondria in T2DM individuals. Ritov and colleagues showed a dysfunction of the NADH oxidase (CI) in skeletal muscle of T2DM patients in comparison to lean control (Ritov et al. 2010). Thus, $NADH/NAD^+$ ratio must have been increased inhibiting TCA cycle and the glycolysis pathway via the accumulation of toxic intermediary byproducts, which could lead to muscle IR. An intrinsic mitochondrial defect in T2DM was proposed after the study by Phielix and colleagues (Phielix et al. 2010) although it was not clear in their article figure. In the same way, Hey-Mogensen and coworkers firstly stated an intrinsic defect in T2DM (Mogensen et al. 2007), which was not observed in their next study, being the statement corrected (Hey-Mogensen et al. 2010). Even Kelley and colleagues proposed an intrinsic defect in T2DM patients that was not evident when they normalized the data by mitochondrial content (Kelley et al. 2002). Moreover, no intrinsic defects with IR were found in many studies (Boushel et al. 2007; Rabøl, Højberg, et al. 2009; Asmann et al. 2006; Larsen et al. 2009; Larsen et al. 2011; Nair et al. 2008).

In summary to the human studies, some *in vivo* evidence support (Kelley et al. 1999; Roden 2005) and other counteract (De Feyter, Lenaers, et al. 2008) the mentioned hypothesis that mitochondrial dysfunction plays a role in the pathogenesis of IR and T2DM.

Rodent models have been used to decipher the role of mitochondrial function in IR and T2DM state. In the genetically modified obese diabetic *db/db* model, enhanced respiratory capacity was observed in glycolytic skeletal muscle, while in oxidative muscle mitochondrial respiratory capacity through CI was reduced, in concordance with reductions in mitochondrial biogenesis key regulators and mtDNA content (Holmström et al. 2012). In leptin-deficient *ob/ob* mice, an increase was observed in glycolytic skeletal muscle, and unaltered mitochondrial respiration was observed in oxidative muscle (Holmström et al. 2013). Thus, IR might develop in an independent way of mitochondrial dysfunction, with even a mitochondrial function increase (Holmström et al. 2012). Also, enhanced mitochondrial function (Lenaers et al. 2010; Turner et al. 2007) and density (van den Broek et al. 2010) were reported in insulin-resistant monogenetic or DIO rodents, regardless of IR. Other evidence that IR develops without mitochondrial dysfunction has been reported: De Feyter and colleagues showed how skeletal muscle of ZDF rats had normal mitocondrial OxPhos capacity (De Feyter, Lenaers, et al. 2008); and Bonnard and coworkers fed mice on high-fat and high-sucrose diet for one month, and observed that glucose- and lipid-induced ROS, rather tan IR *per se*, were the cause for mitocondrial alterations in skeletal muscle cells *in vitro* (Bonnard et al. 2008). Moreover, antioxidant treatment blocked these alterations.

Inherited defects in dysfunctional ETS elements to justify IR were also assessed in rodents. Rats fed a diet low in iron (Han et al. 2011) showed decreased cytochrome C and cytochrome C oxidase subunits I and IV, although the insulin-stimulated glucose uptake and insulin sensitivity were unaffected. In the same study, rats fed on HFD revealed IR. Interestingly, rats fed HFD plus a low iron diet had normal insulin action. Hence, down regulated iron containing mitochondrial ETS proteins did not disrupted insulin sensitivity in these rats, arguing against the idea that intrinsic defects in ETS would lead to IR. Of note, the diet lasted only 9 wks (Han et al. 2011) and it cannot be excluded that a more chronic deficiency/defect in ETS might actually lead to IR with time.

As commented above and in section 1.6.3, one of the possibilities that have been reported to explain the link between increased intramyocellular FA and disrupted insulin signalling has been a **reduction in lipid oxidation due to mitochondrial dysfunction** or a lower

mitochondrial content (Kelley et al. 2002; Lowell & Shulman 2005; Morino et al. 2006). Moreover, the relationship between skeletal muscle IR and intramyocellular lipids in insulin-resistant offspring has been proposed to be due to an inherited defect in mitochondrial OxPhos activity (Befroy et al. 2007).

Had this hypothesis been correct, mitochondrial respiration should increase and intramyocellular lipids decrease along with insulin sensitivity improvement (Kelley et al. 2002; Lowell & Shulman 2005; Morino et al. 2006). As aforementioned, some studies have claimed these results: mitochondrial oxidative capacity was decreased by 40% in eldery subjects with severe IR, associated with an increase in intramyocellular and intrahepatic lipids in comparison to BMI activity-matched young control subjects (Petersen et al. 2003); skeletal muscles from lean, insulin-resistant offspring of parents with T2DM had 30% reduced the rate of ATP synthesis along with a 80% increase in intramyocellular lipid content in comparison to age- weight- and activity-matched insulin-sensitive controls (Petersen et al. 2004; Petersen, Dufour & Shulman 2005); and in a similar group of individuals, the flux of the TCA cycle was also reduced 30% (Befroy et al. 2007). In fact, Roden and colleagues demonstrated defects in insulin-stimulated ATP synthesis during a lipid infusion in healthy individuals (Brehm et al. 2006). Moreover, obese humans reported reduced mitochondrial gene expression and capacity for FA oxidation (Simoneau et al. 1999). Morino and colleagues (Morino et al. 2012) reported a role for LPL in reduced mitochondrial content in human IR, through decreased PPARδ activation by PUFA.

Contrary to the above studies, others showed **dissociation between mitochondrial dynsfunction and the increase in FA** that supposedly would lead to IR. Short-term elevation of FFA at fasting insulin levels induced IR in muscle without reducing mitochondrial activity (Brehm et al. 2010; Chavez et al. 2010). OxPhos capacity for FA is not reduced in obese and T2DM patients mitochondria (Holloway et al. 2007; Bandyopadhyay et al. 2006), but a "normal" oxidation capacity might not be sufficient to prevent further lipid accumulation. Lipid oxidation, which in control subjects is correlated to mitochondrial content, expression of FA translocase *CD36* and *PGC1α*, is not correlated in humans with obesity (Szendroedi et al. 2012). This might be because elevation of plasma FA might impair the lipid-induced PPAR-PGC1 interaction that regulates FA oxidation in healthy insulin-sensitive individuals (Holloway, Bonen, et al. 2009). Also, T2DM reported a reduction in insulin sensitivity and mitochondrial function in comparison to controls, independently of intramyocellular lipid content (van de Weijer et al. 2013). In the same line, short-term reduction of lipolysis (by *acipimox* administration) did not improve OxPhos capacity basal

or insulin-stimulated conditions despite increased insulin sensitivity and decreased ROS in skeletal muscle of T2DM patients (Phielix et al. 2014). In keeping with this, obese women who underwent a low-caloric weight loss program showed increased insulin sensitivity along with a decrease in muscle mitochondrial respiration, but without changes in intramyocellular TG content (Rabøl, Svendsen, et al. 2009).

Also, a study from Meex and coworkers with combined LI of strength training and endurance exercise showed improved mitochondrial function in T2DM patients and insulin sensitivity with no decrease in intramyocellular lipids, with in fact a tendency in them to increase (Meex et al. 2010). The exercise-induced increase in mitochondrial function (28 to 48%) was explained by the concomitant increase in mitochondrial content, showed with an increase of mitochondrial content markers from 72 to 172% (Meex et al. 2010). Also, CR-induced weight loss enhanced insulin action and reduced muscle intramyocellular lipids while reporting reduced mitochondria size, without alterations or changes in mitochondrial enzyme activites (Toledo et al. 2008). In fact, detectable alterations in mitochondrial morphology in some studies were reported after the onset of IR (Bonnard et al. 2008). Furthermore, many human studies have reported even an increase of fat oxidation in insulin-resistant obese individuals and T2DM patients (Ara et al. 2011; Goodpaster et al. 2002; Groop et al. 1991; Boon et al. 2007).

The dissociation of mitochondrial dysfunction, lipid accumulation and IR has also been observed in **animal studies**. Increased mitochondrial function in glycolytic muscle was correlated with acute elevations in circulating FFA levels, probably due to increased lipid availability (Garcia-Roves et al. 2007; Holloway, Benton, et al. 2009). De Feyter and colleagues showed how skeletal muscle of ZDF rats had normal mitocondrial OxPhos capacity, along with an increase in intramyocellular lipids (De Feyter, Lenaers, et al. 2008). Furthermore, in insulin-resistant skeletal muscle and in HFD-fed rats (Garcia-Roves et al. 2007; Hancock et al. 2008), increasing lipid availability increased mitochondrial OxPhos capacity and biogenesis. Had been true that intramyocellular lipids lead to mitochondrial dysfunction and IR as commented above, HFD feeding should not has increased mitochondrial content or fat oxidation capacity. Hence, a mechanism was proposed to explain why FA can induce mitochondrial content, and it considers an activation of PPARδ (Garcia-Roves et al. 2007).

Other animal models studies showed how DIO mice and rats increased the expression of mitochondrial genes and mitochondrial FA oxidation (Turner et al. 2007). Genetic animal models such as the muscle- and liver-specific apoptosis-inducing factor (*Aif*) –a

component of CI- deficient mice revealed OxPhos deficiency similar in the human IR state, and showed increased insulin sensitivity and protection to diabetes and obesity (Pospisilik et al. 2007). Other modificated models were protected against IR: ablation of cytochrome C oxidase subunit IV peptide 2a (*Cox6a2*) (Quintens et al. 2013), ablation of iron-containing enzymes of the ETS (Han et al. 2011), deficiency of *Tfam* –a regulator of mitochondrial biogenesis- (Wredenberg et al. 2006), and deficiency of *Pgc1* family of transcriptional coactivators (Zechner et al. 2010). Moreover, skeletal muscle overexpression of *Ucp1* caused a disruption of mitochondria structure and large increase in intramyocellular lipids, but again was protected showing large increases in basal and insulin stimulated muscle glucose transport (Han et al. 2004). Also, other genetic model studies in which shifting substrate selection toward fat oxidation also protected against diet-induced IR (Abu-Elheiga et al. 2003; Perdomo et al. 2004).

Suga and colleagues observed in mice how skeletal muscle ATP levels, TCA cycle and ETS enzyme activities and gene expression were decreased after 16 wks on HFD (Suga et al. 2014). In this state, intramyofibrillar (IMF) and subsarcolemal (SS) mitochondria showed a reduced size, along with a decrease in SS and IMF mitochondrial proteins. mtDNA and expression of mitochondrial biogenesis related genes (*Pgc1α*, *Pparα* and mitofusin 1 *Mfn1*) were decreased also after HFD. Skeletal muscle TG and number of lipids droplets were increased after 16 wks on HFD. Regarding substrate utilization, both enzyme activity of HK and β-hydroxyacyl coenzyme A dehydrogenase (HADH), a key enzyme in FA β-oxidation, were reported decreased after HFD (Suga et al. 2014). 16 wks on HFD also increased plasma H_2O_2 levels and skeletal muscle O_2^- production and NAD(P)H oxidase activity.

Whether this reduction in mitochondrial function is a cause or a consequence of the impaired lipid oxidation is unknown. What is clear is that impaired mitochondrial function along with disrupted capacity of FA oxidation predisposes the individual to skeletal muscle intracellular FA accumulation and IR.

As mentioned in section 1.5, T2DM subjects show an inability to switch to glucose oxidation in a post-pandrial state, and also a decrease in FA oxidation (Kelley & Mandarino 2000). Hence, Galgani and colleagues reported decreased glucose disposal rate to be the main determinant of **metabolic inflexibility** in these patients, suggesting that the inflexibility might be a reflection of IR in obesity-related T2DM (Galgani, Heilbronn, et al. 2008). Since muscle has an importat role in substrate selection, its mitochondrial function

might have a role in metabolic flexibility. Of note, the relationship between metabolic flexibility and IR might be confounded by elevated FA and subsequent intramyocellular lipid accumulation. Van de Weijer and coworkers showed a lower increase in RER from fasting upon insulin stimulation in T2DM patients, indicating decreased metabolic flexibility (van de Weijer et al. 2013). Also, impaired *in vivo* mitochondrial function, by means of prolongation of phosphocreatine halftime (PCr), was observed in T2DM in comparison to age- and BMI-matched controls. Indeed, this study revealed that metabolic flexibility had a positive significant correlation with whole-body glucose disposal, and an inverse correlation with *in vivo* PCr-recovery time, indicative of mitochondrial function (van de Weijer et al. 2013). Similar to Galgani studies, insulin-stimulated plasma NEFA levels and whole-body glucose disposal were the main factors predicting the metabolic inflexibility model. Although PCr-recovery half-time (mitochondrial function *in vivo*) was correlated to the inflexibility, it was not a predictor for it. Regarding RER predictors, only whole-body glucose disposal rate upon insulin stimulation was a significant predictor of insulin-stimulated RER. Thus, *in vivo* mitochondrial function was the single predictor of basal RER, while insulin-stimulated RER was determined by whole-body glucose disposal, all suggesting that reduced mitochondrial function might be a primarily responsible for basal substrate utilization, and it does not negatively impact on the capacity of skeletal muscle to switch between substrates (van de Weijer et al. 2013).

Mitochondrial specific antioxidants ameliorated skeletal muscle IR induced by HFD (Anderson et al. 2009) supporting the hypothesis that increased substrate delivery to the mitochondria under nutrient oversupply states might result in hyperreduction of ETS when ATP demand is increased, increasing mitochondrial membrane potential which contributes to the electrons leak from ETS in the form of ROS (Fisher-Wellman & Neufer 2012).

ROS production has also been proposed to play a role in mitochondrial dysfunction and IR. Anderson and colleagues demonstrated that elevated mitochondrial-mediated oxidative stress was linked to IR in obese rodents and humans (Anderson et al. 2009). Also, mitochondrial ROS release was higher in skeletal muscle of T2DM in comparison to obese patients, but similar to lean controls (Abdul-Ghani et al. 2009). Thus, ROS has been proposed to have a beneficial effect when the increase is transient and might be essential for a training-induced increased in insulin sensitivity in T2DM (Ristow et al. 2009) and for protection against HFD-induced IR in rodents (Loh et al. 2009)l. On the contrary, ROS might be harmful when the increased concentration is sustained being proposed as an

explanation to the lower intrinsic mitochondrial activity observed in T2DM in some studies (Phielix et al. 2008; Ritov et al. 2005; Mogensen et al. 2007).

Moreover, Lee and coworkers overexpressed antioxidant mitochondrial-targeted catalase and observed a reduction in DAGs and protection against aged-induced IR (Lee et al. 2010). In mice fet 16 wks on hypercaloric diet showed a decrease in CI activity in comparison to only 4 wks of diet (Bonnard et al. 2008). In the same mice, an increase in hydrogen peroxide plasma concentration appeared concomitantly; suggesting that oxidative stress might drive mitochondrial alterations in muscle, but also that mitochondrial defects might not precede IR. Although the mechanisms are still unclear, this study mimicked the excessive substrate supply in T2DM as being the cause of increased ROS production *in vivo*. Another study showed mitochondrial dysfunction and mitochondrial morphological abnormalities (Boudina et al. 2012) in skeletal muscle of T2DM animal models, along with increases in the ROS production (Boudina et al. 2012). In fact, in this study mice treated with an antioxidant normalized muscle mitochondrial function but did not normalize glucose tolerance and insulin sensitivity. On the contrary, studies in T2DM patients failed to show *ex vivo* increase in hydrogen peroxide from CI in skeletal muscle mitochondria (Abdul-Ghani et al. 2009; Hey-Mogensen et al. 2010).

ROS production is tighly dependent on the protonmotive force in the inner mitochondrial membrane (Korshunov et al. 1997), but the studies mentioned above did not assessed mitochondrial membrane potential (Abdul-Ghani et al. 2009; Hey-Mogensen et al. 2010; Bonnard et al. 2008). However, sensitivity for CI and CII substrates has been proposed to protect against ROS production by keeping the membrane potential low. In T2DM patients, this sensitivity was reported (Larsen et al. 2011), although they showed decreased antioxidant capacity by means of manganese superoxide dismutase (MnSOD) in skeletal muscle in comparison to healthy controls (Larsen et al. 2011).

Another explanation mentioned for the reduction in mitochondrial OxPhos would be the decrease in **mitochondrial biogenesis**. PGC1α and PCG1β regulate mitochondrial biogenesis. Increased *PGC1* protein expression would activate the expression of target genes including nuclear respiratory factor 1 (*NRF1*), a transcription factor regulating nuclear-encoded mitochondrial genes such as mitochondrial transcriptional factor for the mitochondrial genome (*TFAM*) which in turn, can increase transcription of mitochondrial genes and replication of mtDNA (Scarpulla 2006). Genes encoded by PGC1α in the skeletal muscle showed a coordinated reduction in expression in T2DM patients (Mootha, Lindgren,

et al. 2003; Patti et al. 2003) and in non-diabetic subjects with T2DM familiar history (Patti et al. 2003). Nonetheless, this reduction in expression was not found in lean, insulin-resistant offspring of parents with T2DM (Morino et al. 2005). Thus, some (Patti et al. 2003; Mootha, Lindgren, et al. 2003) but not all (Morino et al. 2005; Karlsson et al. 2006) studies showed reduced expression of *PGC1*α and *PCG1β* in T2DM patients as well as in their non-diabetic relatives.

Less is known about the **macrophage infiltration** in IMAT, the adipose tissue depots between muscle fibers. As in any other adipose tissue, macrophages can be recruited (Hong et al. 2009) and many cytokines, such as TNFα, IL1β and IL6 (Frost et al. 2002) can be secreted by macrophages or even myocytes, although it is not yet proven their role in muscle IR (Saghizadeh et al. 1996). Skeletal muscle has been recognised as an endocrine organ, and proteins expressed by and released from skeletal muscle are named myokines. Myokine IL6 is chronically increased in patients with IR, obesity and T2DM (Dandona et al. 2004; Duncan et al. 2003; Kern et al. 2001). Expanding VAT is an important source of circulating IL6 in obesity and, while the IL6 secretion by ATMs depends on NFκB signalling pathway, secretion of IL6 in the skeletal muscle is regulated by different signalling pathways involving calcium, nuclear factor of activated T cells (Im & Rao 2004), calcineurin (Banzet et al. 2007), p38 MAPK signalling (Chan et al. 2004), and JNK/AP1 (activator protein 1) pathway (Whitham et al. 2012). Myokine IL6 has been shown to have a role in FA metabolism: after IL6 infusion, an increase in systemic FA oxidation and lipolysis was observed (van Hall et al. 2003; Wolsk et al. 2010). However, and since no effect on adipose tissue lipolysis was observed (Wolsk et al. 2010), IL6 was suggested to act within skeletal muscle FA metabolim in a local manner and even with a fiber-type specificity (MacDonald et al. 2013).

Interesting studies have tried to sheed light in the **crosstalk** between exercise-induced myokines and β-cell function. Possible interactions between peripheral tissues and β-cells have been suggested (Christensen et al. 2015) and Bouzakri and colleagues demonstrated that conditioned media from human skeletal muscle cells treated with TNFα to induce IR, increased β-cell apoptosis (Bouzakri et al. 2011). Other studies implicated directly IL6 in β-cell adaptations to exercise and disruptions in insulin secretion (Paula et al. 2015). IL6 is not toxic for β-cells (Eizirik et al. 1994; Wadt et al. 1998) and may even improve β-cell function (Ellingsgaard et al. 2011; Krause et al. 2012), but in a inflammatory context such as the presence of IL1β, it can increase the inflammatory effect (Eizirik et al. 1994; Wadt et al.

1998; O'Neill et al. 2013). Indeed, in prediabetic *db/db* mice showing already systemic inflammation, combined infusion of IL6 and IL1β reported disrupted GSIS increasing β-cell death and isolated islets (O'Neill et al. 2013). Christensen and colleagues recently confirmed that exercise-induced IL6 secreted from skeletal muscle helps preventing β-cell apoptosis under normal conditions, but under pro-inflammatory conditions it may contribute to β-cell apotosis (Christensen et al. 2015).

Also related to **inflammation**, TNFα and the activation of the toll-like receptor 4 (TLR4) can activate IKK which leads to ceramide synthesis, ultimately leading to insulin signalling disruption (Samuel & Shulman 2012). It is worth mentioning that inflammatory pathways activation was observed as part of a normal physiological response, ie. response to acute aerobic exercise; and increase in cytokine expression (*MCP1* and *IL6*) along with NfκB activation in skeletal muscle of lean and obese nondiabetic subjects were reported (Tantiwong et al. 2010). Of note, T2DM patients had already a basal NFκB activity without an increment after exercise. Zhou and colleagues (Zhou et al. 2011) found that inhibition of mitochondrial ETS activity caused ROS production further activating NLRP3; and that mitochondria voltage-dependent anion channels were essential for inflammasome activation too.

Within the **ER stress** cascade, ATF6 can become activated under certain cirumstances, as well as PGC1α-mediated adaptative response. PGC1α might coactivate a group of genes with ATF6α to induce the adaptative changes to physical activity (Samuel & Shulman 2012). ER membranes also contain key lipogenic enzymes that lead to lipid droplets (Samuel & Shulman 2012). In the same line as in the liver, proteins that can regulate lipid droplets created by the lipogenic enzymes in the ER membrane (ie. ATGL or PNPLA3) might regulate lipid concentration (Samuel & Shulman 2012).

Many studies have shown a strong association between IR and **atherosclerotic CVD** which affect non-diabetics but also T2DM patients (Hanley et al. 2002; Rutter et al. 2005; Bonora et al. 2007; Bonora et al. 2002). This association can be explained by the insulin action itself in a signalling transduction cascade: the mitogen-activated protein (MAP) kinase pathway. MAPK pathway is responsive to insulin (Cusi et al. 2000) and when stimulated, it leads to the activation of a number of intracellular pathways related to cellular proliferation, inflammation and atherosclerosis (Wang et al. 2004; Draznin 2006; Hsueh & Law 1999). The explanation comes then from the fact that impaired IRS1 phosphorylation impairs glucose uptake leading to hyperglycemia that stimulates at the same time more

insulin secretion. Is then this extra bout of secreted insulin that will activate MAPK (Cusi et al. 2000; Hsueh & Law 1999; Krook et al. 2000) that will ultimately activate inflammation and atherogenesis pathways.

1.8.4.2 Lifestyle interventions on skeletal muscle

Physical inactivity leads to a decrease in insulin sensitivity and insulin-stimulated glucose uptake and GLUT4 protein content in human skeletal muscle (Thyfault & Booth 2011). Some individuals were studied after 9 years of bed-rest and a down-regulation of a total of 54% of genes related to OxPhos pathway, including *PGC1α*, was reported (Alibegovic et al. 2010). Thus, exercise has been the LI more promoted and studied in skeletal muscle, with or without a context of IR and/or T2DM.

50 years ago Holloszy and colleagues already observed an increase in glucose uptake after skeletal **muscle contraction** (Holloszy & Narahara 1965). Exercise was shown to increase insulin sensitivity (Richter et al. 1982), and GLUT4 and its translocation (Ren et al. 1994; Hansen et al. 1998). It was then demonstrated that contractile activity increased glucose uptake in diabetic rats without insulin needed (Wallberg-Henriksson & Holloszy 1985), finally discovering that contraction and insulin have a combined effect on GLUT4 translocation acting through different pathways (Lund et al. 1995). Indeed, it was reported that exercise did not affect IRS1 phosphorylation (insulin signalling pathway) (Hansen et al. 1998), and that AMPK was involved in the exercise-induced effects (Ojuka et al. 2000). PKCβ down-regulation also contributes to the exercise-induced improvements in IR in HFD-fed mice (Rao et al. 2013). Rao and colleagues observed that PKCβ was decreased in skeletal muscle and liver after exercise. Both exercise and PKCβ deficiency improved HFD-induced IR, lipid accumulation and mitochondrial dysfunction. Other improvements in the exercised mice included the AKT-activation, while PKCβ deficient mice showed no differences between sedentary and exercised ones (Rao et al. 2013).

In rodents, Olefsky and colleagues (Hevener et al. 2000) observed how **exercise** alone and in combination with TZD was able to normalize the GLUT4 protein content, after the untreated Zucker-fatty (ZF) rats showed a 37% decrease in comparison with lean littermates. In these ZF rats, insulin receptor protein was decreased along with a decrease in its Tyr phosphorylation, compared to lean controls. Also, IRS1 protein was decreased by 70% and insulin-stimulated AKT-phosphorylation was diminished. 6-week chronic exercise ameliorated the defect in Tyr phosphorylation and completely normalized it when used in combination with TZD. Exercise alone seemed to normalize the IRS1 protein

content, although it needed the combination therapy with TZD to normalize AKT-phosphorylation. Moreover, exercise alone and with combined therapy led to a potentiation of the ability of insulin to supress HGP, and improved or completely normalized insulin sensitivity (respectively) (Hevener et al. 2000). In human patients, IR in muscle was not totally reverted although it was improved after training intervention (Dela et al. 1995).

The effects of **exercise** in inflammation have also been assessed in different human studies, since exercise is believed to induce a direct anti-inflammatory response (Starkie et al. 2003). Myokines released by contracting activity might play a role in the exercise beneficial effects (Pedersen & Febbraio 2012). Indeed, IL6 is increased in the circulation after exercise (Pedersen et al. 2007), and IL6 released after skeletal muscle contraction triggers an anti-inflammatory effect inducing the secretion of anti-inflammatory cytokines (ie. IL10 and soluble TNF receptor, sTNFR) (Pedersen & Febbraio 2008). In turn, IL10 inhibits the production of pro-inflammatory cytokines (ie. IL1β, TNFα) and sTNFR is a natural inhibitor of TNFα (Petersen & Pedersen 2005).

Regarding rodents, Experiments in murine C2C12 myotubes showed how contraction-induced *Il6* expression seems to be mediated by activation of JNK and AP1 (Whitham et al. 2012). The effect of this myokine on skeletal muscle insulin sensitivity has been reported in mice to depend on the duration of the **exercise** (acute IL6 would increase glucose uptake while chronic exposure would lead to IR) (Nieto-Vazquez et al. 2008), while some others demonstrated that chronic elevated IL6 levels improved glucose tolerance and insulin sensitivity in rats and humans (Holmes et al. 2008; Sadagurski et al. 2010). However, T2DM patients' myotubes exerted resistance to the acute effect of IL6 on glucose metabolism (Jiang et al. 2013). Healthy volunteers received LPS endotoxin to induce low-grade inflammation similar than the one appearing in an obesity-related T2DM state 2.5h after being cycling for 3h or resting. TNFα was increased in the group that was resting, while this TNFα response to LPS was blunted in the exercised subjects (Starkie et al. 2003), confirming that exercise is driving an anti-inflammatory response.

It is important to mention that high intensive training can result in increased systemic inflammation post-exercise (3-24h) (Gleeson 2007). TNFα and IL1β increase in response to muscle damage after a very intensive exercise performance in humans (Pedersen et al. 2007; Ostrowski et al. 1999; Bernecker et al. 2013). In fact, after acute muscle injury, tissue remodelling occurs along with growth-promoting inflammation in order to regenerate the

wound. Although it involves remodelling and inflammation, this inflammatory response is needed to repair the muscle and provide a positive outcome (Paulsen et al. 2012).

Holloszy and colleagues demonstrated already many years ago that **exercise** training increased OxPhos capacity in skeletal muscle from rats (Holloszy 1967). Exercise also showed an effect in the mitochondria architecture: skeletal muscle mitochondrial from exercised increased in number, and had a more clearly defined internal membrane, including wider cristae, in comparison with the sedentary mice. Sedentary mice showed enlarged and disordered mitochondria inside the cells. There is evidence that T2DM patients have the ability to increase their amount of muscle mitochondria. Indeed, endurance training increased CS activity in T2DM patients (Hey-Mogensen et al. 2010; Dela et al. 1995), or increased cardiolipin (Toledo et al. 2007), both markers of mitochondrial content in muscle (Larsen et al. 2012). Also, endurance training showed an increase in protein content of mitochondrial complexes in skeletal muscle (Meex et al. 2010). On the contrary and different from control subjects, T2DM individuals showed no increase in mitochondrial-related proteins such as pyruvate dehydrogenase lipoamide kinase isoenzyme 4 (PDK4), COX1 and COX4. Of note, strength training might increase insulin sensitivity, but did not show an increase in mitochondrial content (Holten et al. 2004).

Exercise alone improves the impaired skeletal muscle mitochondrial function in patients with T2DM (Hey-Mogensen et al. 2010; Meex et al. 2010). In fact, aerobic exercise increases skeletal muscle oxidative capacity and mitochondrial respiration in untrained obese participants with or without T2DM, demonstrating that increased metabolic fitness might not directly affect training-induced changes in insulin sensitivity (Hey-Mogensen et al. 2010). Of note, the increase in oxidative capacity seems to be most pronounced in the mitochondrial ability to use CI-supporting substrates. Mitochondrial ROS tended to be higher in T2DM patients than in control, and tended to decrease with physical activity. Indeed, UCP3 that protects against mitochondrial ROS production (Nabben et al. 2008) was increased in skeleltal muscle in all individuals by 72% after exercise LI (Hey-Mogensen et al. 2010). Interestingly, when separated by controls and T2DM patients, the increase in UCP3 protein content was only significant in the control group.

Taken all together and as aforementioned, exercise LI provide evidence for dissociating mitochondrial content and insulin sensitivity. Moreover, skeletal muscle mitochondrial respiratory capacity and mitochondrial biogenesis were stimulated by aerobic endurance exercise (Sun et al. 2011). Mitochondrial biogenesis was stimulated through increased

expression of genes *Ppargc*, *Nrf1*, and *Tfam* (Hawley & Gibala 2012). PGC1α could stimulate pro-angiogenic factors such as VEGF in a ERRα-dependent manner, enhancing exercise-induced neovascularization (Scherer et al. 1995; Asterholm & Scherer 2010), linking regulation of oxygen consumption by the mitochondria and oxygen and nutrients distribution through vasculature.

To concretely assess the mitochondrial function in skeletal muscle during **dietary** and **exercise** LIs, Suga and colleagues performed a study covering different LI in rodents: diet, exercise, and a combination of both. After 8 wks on HFD, mice were randomized for a 4-week LI including: caloric restriction (D) group, exercise group (EX) and the combination of both (DEX) (Suga et al. 2014). Although the decrease in BW in the D group was greater than the one in the EX group, only in DEX the BW was completely normalized and similar to a control group that was fed with normal standard diet. In the same line, blood parameters such as the increase in fasting glucose, plasma insulin, TG, total cholesterol and NEFA were all normalized only in the DEX group to the same levels as in the control mice. EX alone was able to decrease blood glucose, and D also improved insulin levels, total cholesterol levels, and showed a tendency to improve TG and NEFA. Moreover, DEX mice reached normal control values in the IGTT and ITT tests, while D values were significantly higher than the control ones, and EX even higher than in the D group. In this study the authors reported an increase to normal control values in the DEX group of skeletal muscle ATP levels, enzyme activites of CS, malate dehydrogenase, CI, CIII and ATPsynthase, NADH histochemical reaction and gene expression related to mitochondrial function (Suga et al. 2014). Of note, complexes CI and CIII are the main source for ROS production in the mitochondrial ETS (Ide et al. 2001; Suematsu et al. 2003), and DEX decreased and normalized plasma H_2O_2 levels, O_2^- muscle production. After the LI, the DEX mice showed recovered increase in IMF and SS mitochondria size, and an increase in SS mitochondrial proteins, in mtDNA, and in the expression of mitochondrial biogenesis related genes (*Pgc1α*, *Pparα* and *Mfn1*). The increase in skeletal muscle TG and lipid droplets after the HFD-feeding, was reverted in the DEX group, as well as the enzyme activities of HK and HADH that were first increased (Suga et al. 2014).

Kelley and coworkers observed in humans that after **dietary CR**-induced weight loss, both insulin sensitivity and insulin-stimulated RER were increased to lean control values. However, muscle insulin-stimulated β-oxidation capacity when determining substrate utilization in obese individuals, was diminished after weight loss (Kelley et al. 1999). In another study achieving 10% weight loss of initial BW, basal RER decreased suggesting an

increase in FA oxidation along with a decrease in mitochondrial function (Rabøl, Svendsen, et al. 2009). Thus, mitochondrial function was not improved after weight loss and baseline RER was not reverted to control values, findings in line with the theory that basal RER is mainly dependent on mitochondrial function (van de Weijer et al. 2013). Moreover, in obese individuals that suffered a mean of 57kg of weight loss via CR, β-oxidation was significantly decreased in comparison to a weight-matched control, as determined with indirect calorimetry (Larson et al. 1995). Snel and colleagues (Snel et al. 2012) also performed a **dietary** and **exercise** LI: a group with very low caloric intake (CR) and a group perfoming physical activity instead (EX). EX group patients suffered a major weight loss than CR group. Although both groups of patients increased similarly insulin-stimulated glucose disposal and PI3K/AKT phosphorylation in the insulin signalling pathway, only the EX group (with a major weight loss) increased mtDNA content in the skeletal muscle along with an increase in the maximal aerobic capacity (Snel et al. 2012).

In summary, exercise in humans did not fully revert IR in skeletal muscle from patients with T2DM (Dela et al. 1995) although it exerted an anti-inflammatory response (Starkie et al. 2003): IL6 was released into the circulation after exercise (Pedersen et al. 2007) and induced secretion of other anti-inflammatory cytokines such as IL10 (Pedersen & Febbraio 2008), which in turn inhibited production of pro-inflammatory cytokines (IL1β, TNFα)(Petersen & Pedersen 2005). Also related to inflammation, exercised volunteers revealed a blunted increase of TNFα in response to LPS (Starkie et al. 2003). However, inflammation can increase and persist after high intensive training (Gleeson 2007; Pedersen et al. 2007; Ostrowski et al. 1999; Bernecker et al. 2013), and it is important to point out that after exercise skeletal muscle suffers remodelling in order to repare and provide a positive outcome (Paulsen et al. 2012). Exercise improved the impaired skeletal muscle mitochondrial function in T2DM patients (Hey-Mogensen et al. 2010; Meex et al. 2010), increased muscle CD activity (Hey-Mogensen et al. 2010; Dela et al. 1995) and cardiolipin (Toledo et al. 2007) (markers of mitochondrial content in muscle (Larsen et al. 2012)), and protein content of mitochondrial complexes (Meex et al. 2010). Strength training might improve insulin sensivitity without changes in mitochondrial content (Holten et al. 2004). Exercise also decreased mitochondrial ROS while UCP3, which protects against ROS, increased (Nabben et al. 2008; Hey-Mogensen et al. 2010).

Regarding rodents, exercise ameliorated Tyr phosphorylation normalizing IRS1 protein content, enhanced the ability of insulin to suppress HGP, and improved insulin sensitivity (Hevener et al. 2000); while it also improved GLUT4 and its translocation (Ren et al. 1994;

Hansen et al. 1998). Murine myotubes showed contraction-induced IL6 expression (Whitham et al. 2012), which can improve glucose tolerance in rats (Holmes et al. 2008). In rodents, exercise OxPhos capacity in rats and mitochondria number (Holloszy 1967). CR-induced weight loss in humans revealed improved insulin sensitivity (Kelley et al. 1999) and no improvement (van de Weijer et al. 2013) or even a decrease in mitochondrial function (Rabøl, Svendsen, et al. 2009).

When facing CR vs exercise interventions, both groups increased insulin-stimulated glucose disposal ad PI3K/AKT phosphorylation but only the exercise group, with a major BW loss, increased mtDNA and maximal aerobic capacity (Snel et al. 2012). LI including dietary and exercise intervention reported in rodents a reversion to control values of BW, IGTT and ITT values, fasting glucose, plasma insulin, TG, ROS, cholesterol, NEFA, ATP levels, mitochondrial enzymes and genes related to mitochondrial function and biogenesis (Suga et al. 2014).

1.8.5. Hypothalamus

The hypothalamus is a portion of the brain present in all vertebrates, located above the brainstem and below the thalamus, being part of the limbic system. As part of the central nervous system (CNS), the hypothalamus contains the central circuits in charge of regulating energy expenditure, and fat and glucose metabolism (Friedman 2009). Therefore, hypothalamic nuclei play an important role in obese epidemic, whereof incidence is escalating rapidly along with the T2DM epidemic. Among hypothalamic nuclei, arcuate nucleus (ARC) is located within the mediobasal hypothalamus, and contains different neuron populations that play fundamental roles in energy balance regulation by regulating energy intake and feeding behavior (Williams & Elmquist 2012). Concretely, there are neurons coexpressing orexigenic neuropeptides (agouti-related protein, AgRP; and neuropeptide Y, NPY) and neurons coexpressing anorexigenic neuropeptides (pro-opiomelanocortin, POMC; and cocaine and amphetamine-related transcript, CART) (Schneeberger et al. 2013). Not until the beginning of this decade, substantial progress has been made to define the neural pathways controlling food intake. Porte and colleagues were among the first to demonstrate that insulin was a powerful appetite suppressant in rodents (Plum et al. 2006; Brüning et al. 2000; Porte Jr 2006; Schwartz et al. 2000). Fully insulin action in the hypothalamus includes modulation of the food intake-involved neuropeptides expression (Plum et al. 2005) and via hypothalamic insulin signalling, includes regulation of HGP (Obici, Zhang, et al. 2002), glucose homeostasis (Gelling et al. 2006)

including glycogen synthesis in skeletal muscle (Perrin et al. 2004), and fat metabolism in adipose tissue (Koch et al. 2008). Concretely, in mice, central insulin action reported regulation of glucose concentrations by lowering hepatic gluconeogenesis and stimulating lipogenesis in WAT (Koch et al. 2008). Moreover, there is an effect of leptin in insulin signalling (Koch et al. 2010), which has been reported to be PI3K-dependent (Morton et al. 2005). Central insulin (De Souza et al. 2005) and leptin (Münzberg et al. 2004) signalling are crucial to the regulation of whole-body energy homeostasis exerted by the hypothalamus. Hence, both neuron populations have reported roles in appetite, BW and metabolism regulation (Diéguez et al. 2011; Williams & Elmquist 2012). In fact, in a healthy situation, insulin would increase *POMC* expression, whilst reducing *NPY* and *AGRP*, which via neuropeptide signalling to second order neurons would reduce food intake and enhance energy expenditure.

1.8.5.1 Hypothalamus in IR and obesity-related T2DM

DeFronzo and colleagues observed how in the lower posterior hypothalamus (containing the ventromedial nuclei, VMN) and the upper posterior hypothalamus (containing the paraventricular nuclei, PVN) the magnitude of appetite inhibitory response upon glucose ingestion was reduced in obese, insulin-resistant, and normal glucose-tolerant subjects (Defronzo 2009). These subjects also exerted a delayed maximal inhibitory response; even though in the obese group the plasma insulin response was increased. Thus, hypothalamic IR appears, and rodent studies showed evidence for its effects in increasing HGP and reducing skeletal muscle glucose uptake (Silvana Obici, Feng, et al. 2002; Obici et al. 2001). **Leptin resistance** in the brain, which makes obese individuals minimally response to leptin, and defects in the transport of leptin through the blood brain barrier (BBB) is another disruption that appears in the obese context (Elmquist et al. 1999; Flier 2004; Schwartz et al. 2000). Suppressor of cytokine signalling 3 (SOCS3) has been reported to block leptin signalling (Bjørbæk et al. 2000; Flier 2004), although most of the molecular mechanism is still unknown.

Hypotalamic **lipotoxicity** have also been reported. Hence, in normal conditions accumulation of lipids in the hypothalamus is sensed as energy surplus. In fact, intracerebroventricular (ICV) injection of oleic (long-chain FA, LCFA), but not octanoic (medium-chain FA, CFA) acid inhibited food intake (S Obici, Feng, et al. 2002; Morgan et al. 2004). Also, inhibition of hypothalamic carnitil palmitoyltransferase 1 (*Cpt1*) restored lipid sensing, normalising LCFA-CoA levels in hypothalamus, and inhibited feeding behaviours and hepatic glucose fluxes in overfed rats (Pocai et al. 2006). There might be a resistance to

saciety effects of LCFA and a desensitization of the AgRP and NPY responses to circulating FA that contributes to BW gain (Martínez de Morentin et al. 2010). Recent work has helped decipher which lipid entities participate in hypothalamic lipoxicity. Obese ZF rats reported increased hypothalamic ceramides levels along with increased ER stress (Contreras et al. 2014). Therefore, the study by Contreras and colleagues demonstrated that ceramides induced hypothalamic lipoxicity as well as ER stress, ultimately increasing BW (Contreras et al. 2014).

The CNS, including the hypothalamus, has shown obesity-induced **inflammatory** events (De Souza et al. 2005). As other tissues explained above, the CNS has its own resident **macrophages**, the microglia. Proinfammatory signals can activate the microglia which in turn, releases cytokines such as TNFα, IL1β and IL10, and also can carry out phagocytosis (Hanisch 2002). Once the cytokines are secreted, they can have different actions locally or in other CNS cell types. IR has been associated with an inflammatory response in the hypothalamus (Johnson & Olefsky 2013). The link proposed between central leptin resistance and hypothalamic inflammation consists of cytokine-mediated inhibition of the signal transducer and activator of transcription-3 (STAT3), a key component in leptin signalling pathway. In fact, leptin resistance has been reported to be mediated through activators of IKKβ and NFκB in the hypothalamus (X. Zhang et al. 2008).

One of the mechanism by which lipids can be toxic is by inducing **ER stress**. Hypothalamic inflammatory IKKβ/NFκB pathways were activated upon overnutrition through hypothalamic ER stress, ultimately impairing insulin and leptin signalling (X. Zhang et al. 2008). ER stress provides also inhibition of leptin-induced STAT3 phosphorylation leading to leptin resistance (Ozcan et al. 2009). In line with this, supression of IKKβ/NFκB protects against disrupted insulin and leptin signalling (X. Zhang et al. 2008). Also, treatment with chemical chaperones (4-phenylbutyrate PBA or tautoursodeoxycholate TUDCA) rescued ER stress in the CNS, reduced BW and improved insulin and leptin resistance; while treatment with UPR-induced impaired IR (Ozcan et al. 2006; Ozcan et al. 2009), thus confirming the link between ER stress and insulin and leptin resistance. Furthermore, and as aforementioned, ceramides have been directly related to induce hypothalamic ER stress (Contreras et al. 2014). Thus, experiments increasing *Bip* chaperone in the hypothalamus abolished the effect of ceramide in ER stress, while genetic inhibition of Bip induced the mentioned ceramides-ER stress-induced increased in BW (Contreras et al. 2014).

Regarding the mechanism by which hypothalamic IR induces HGP, Schneeberger and colleagues recently demonstrated that hypothalamic ER stress in mice is linked with disrupted glucose homeostasis due to increased hepatic gluconeogenesis, via defective α-melanocyte-stimulating hormone (α-MSH, a neuropeptide derived from POMC processing) (Schneeberger et al. 2015).

Mitochondrial function has been assessed in hypothalamus, although one of the main limitations is that ARC nucleus integrate both neuronal systems, the anorexic and the orexigenic, leading to likely cofounding results. No differences were observed in the respiratory control ratios between lean and obese Zucker rats in permeabilized hypothalamus (Benani et al. 2009), but when mitocondria were isolated, a higher mitocondrial respiratory capacity in the obese rats was reported in comparison to lean rats (Colombani et al. 2009).

ROS has a role in the acute central regulation of energy balance too. ROS was reported to be an acute activator of POMC firing, and supression of ROS inhibited POMC neuronal activity (Diano et al. 2012). However, in NPY/AgRP population, ROS effects did not show firing but buffering effects (Horvath et al. 2008). Hyperglycemia inactivated nicotinic acetylcholine receptors on autonomic neurons through ROS, indicating a critical role for ROS as a second messenger in impairing sympathetic synaptic transmission (Campanucci et al. 2010).

1.8.5.2. Lifestyle interventions on hypothalamus

Little is known about the effects of **exercise** in the hypothalamus. However, some studies have tried to sheed light on this topic. Kang and colleagues studied leptin sensitivity by assessing leptin resistance-induced leptin receptor (ObRb) and leptin-related SOCS3 mRNA levels. They observed in hypothalamus an increase in *Obrb* and *Socs3* mRNA expression as well as in plasma leptin levels in HFD-fed rats group, in comparison to the other LI groups involving HFD: HFD and exercise (8 wks training), HFD changed to control diet, and HFD changed to control diet plus exercise (8 wks training) (Kang et al. 2013). In fact, *Obrb* and *Socs3* gene expression was decreased in the HFD that changed to control diet group, in comparison to both trainining groups: HFD and exercise, and HFD changed to control diet plus exercise. Contrary, in liver and skeletal muscle *Obrb* and *Socs3* expressions were decreased in the HFD-fed group in comparison with the other LI groups including HFD (Kang et al. 2013). Moreover, after 13 wks on diet, BW increased in the HFD-fed group in comparison to the normal-diet group. Taken all the results, the changes in

leptin sensitivity might be due to a combination of diet and exercise rather than only due to dietary interventions (Kang et al. 2013).

Borg and colleagues reported that a LI of HFD and exercise, which showed reduced animal BW and improved glucose tolerance, did not show any effects on hypothalamic lipids (Borg et al. 2012), suggesting that lipids in the diet are regulating hypothalamic lipid profiles and they are not reversed by an exercise LI.

As aforementioned, an obesity state associated with chronic low-grade inflammation leads to activation of pro-inflammatory Ser/Thr kinases (Wellen & Hotamisligil 2005). In keeping with this, Borg's study observed a reduction in IκBα expression indicating an activation of the NFκB pathway in the hypothalamus of HFD mice. HFD plus exercise LI increased the IκBα expression suggesting that exercise attenuated partially the pro-inflammatory state generated by HFD (Borg et al. 2012). Contrary to NFκB pathway, JNK signalling pathway was not affected by HFD nor exercise training.

Later on, Borg and colleagues focused their studes in leptin and leptin signalling in sedentary and exercised animals under a normal chow diet or HFD (Borg, Andrews, et al. 2014). After chronic exercise, reduced BW, increased food intake and improved glucose tolerance were observed. However, exercise did not enhance the anorexigenic effects exerted by the reduction in food intake in lean and obese mice after intraperitoneal leptin administration. Also, exercise did not enhance the leptin-mediated activation of STAT3 phosphorylation in the ARC and VMN of the hypothalamus. In fact, no differences were observed between any of the treatment groups (control diet, control diet and exercise, HFD, and HFD and exercise) for enhancement of leptin effects or activated phosphorylated STAT3. Thus, Borg's studies suggested that the previous concept that exercise enhances the hypothalamic signalling sensitivity and food intake might be related to the concrete exercise bout, and limited to the period immediately after it, rather than resulting from changes in exercise training (Borg et al. 2012).

Later studies assessed hypothalamic neurogenesis after exercise training, and whether it contributes to the exercise-induced improvements in peripheral insulin action (Borg, Lemus, et al. 2014). As seen before, exercise (4 wks training) improved whole-body insulin sensitivity in comparison to the sedentary mice. Answering their questions, exercise increased neurogenesis but this neurogenesis was not required for the enhanced insulin action effects of physical training.

Mice performing exercise under HFD feeding reduced BW and improved glucose tolerance with no changes in hypothalamic lipids, implying that lipids from diet that regulate lipid profiles are not reversed by exercise (Borg et al. 2012); as well as attenuated partially the pro-inflammatory state generated in hypothalamus by HFD. Exercise did not enhance the anorexigenic effects exerted by intraperitoneal leptin administration, neither activated STAT3 phosphorylation (Borg, Andrews, et al. 2014). Of note, leptin effects and STAT3 phosphorylation was not improved in any of the groups regardless of the diet and exercise. However, leptin resistance induced ObRb receptor and leptin-related SOCS3 mRNA expression decreased when HFD-fed mice were changed to control diet with no changes in the groups including exercise apart from HFD or control diet (Kang et al. 2013). Exercise increased neurogenesis that was not essential for enhanced insulin action effects (Borg, Lemus, et al. 2014).

1.8.7. Multi-organ implication summary

An overview picture of obesity-related T2DM etiology is summarized below (Figure 3):

1. IR leads to an increase in insulin secretion by pancreatic β-cells (hyperinsulinemia).
2. Plasma glucose levels are also increased due to IR (hyperglycemia).
3. An obesity-related T2DM phenotype is characterized by a chronic low-grade WAT inflammation including cytokines and chemokines release, the later to attract macrophages. WAT expansion and IR are present along with increased lipolysis, shuttling FA to other tissues and leading to ectopic FA accumulation.
4. IR in liver leads to increased gluconeogenesis and decreased glycogen synthesis. Along with the ectopic FA accumulation with lipids from WAT, *de novo* lipogenesis in liver is also increased. Intrahepatocellular lipids increase disrupts insulin signalling pathway leading to the mentioned processes taking place in liver.
5. IR in skeletal muscle is also reported, leading to a decreased glucose uptake and glycogen synthesis. As in liver, intramyocellular lipids increase disrupts insulin signalling pathway, leading to the mentioned processes ocurring in skeletal muscle.
6. Hypothalamus is in charge of regulating food intake and energy expenditure. Alterations in hypothalamic control of energy balance are ultimately affecting processes taking place in other tissues.

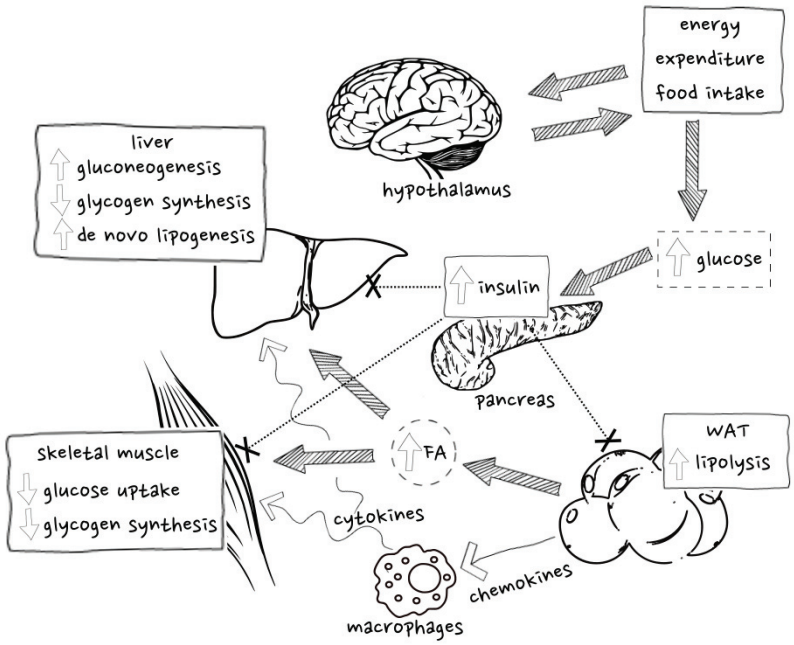

Figure 3. Overview summary of the main processes taking place in the tissues involved in obesity-related T2DM, as well as their cross-talk.

2. "See the forest for the trees", an integrative top-down approach

As stated above, T2DM (Defronzo 2009) and many other metabolic diseases should be treated and studied through systemic and multi-organic approaches (Figure 3). Nowadays, there is an urgent need to start looking at the diseases as a *sum mum* of different phenomena that take place in a variety of involved tissues. Current scientific projects are designed in a bottom-up approach that consists of the study of parts of a system such as a small part of metabolism, or even a unique gene or protein, to elaborate afterwards a more complex system that would resemble the whole disease. However, there is an aforementioned incoming trend that considers organ crosstalk (Zierath & Wallberg-Henriksson 2015; Zierath et al. 2013). Hence, the importance for deciphering the tissue-specific phenomena happening in T2DM as well as how these processes impact the inter-organ crosstalk and ultimately, the whole metabolism, is justified.

Considering that any metabolic disease has a number of key tissues that have a relevant role and none of them could be considered without the others, a **top-down approach** seems more feasible for this type of scientific research. This approach consists of an overview of the system that is broken down in order to gain insight into its subsystems.

This way, T2DM and metabolic disruptions are proposed in this PhD thesis as a whole system that can be decomposed in smaller systems such as each tissue or each molecular level of study.

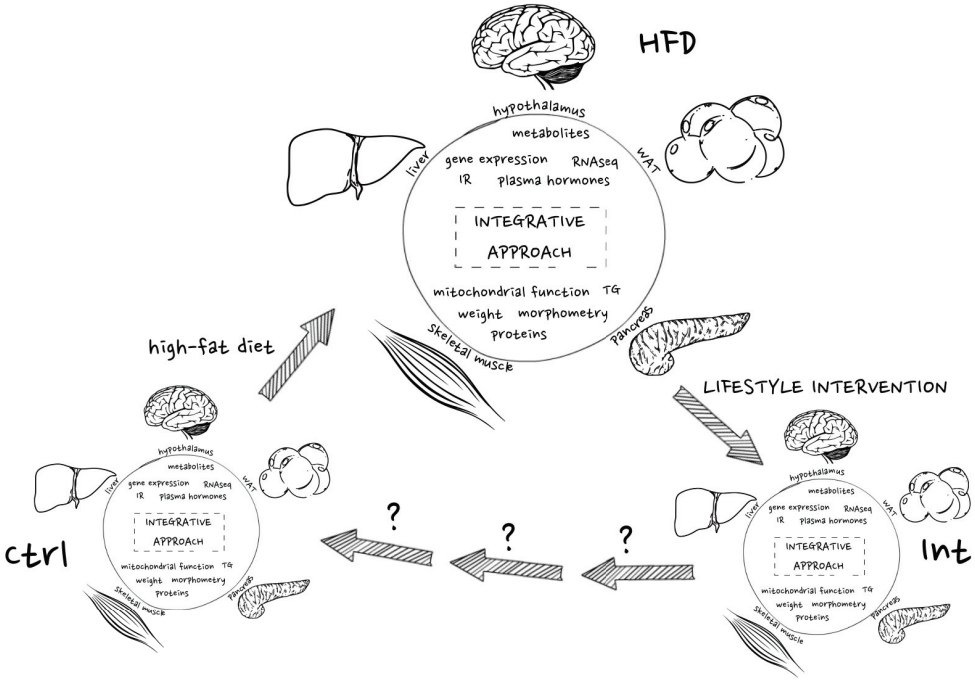

Figure 4. Integrative approach across the three experimental groups

2.1. Current trends in system-biology

Few precedents or current work are covering this new need of integrative physiology. Concretely, Mori and colleagues attempted to integrate metabolic, gene, protein and flow cytometry data in order to study the effect of inflammation markers in the onset of T2DM in two mouse strains with different disease susceptibility (Mori et al. 2010). Interestingly, their study covered data from adipose, skeletal muscle and liver tissue. However, instead of overlapping all the heterogenic data in one-layer data, they integrated gene expression data onto a protein-protein interaction (PPI) network (compiled from the Human Protein Reference Database Version 7), from which they performed gene network enrichment analysis. In fact, all the proteins in the created network were annotated by the z-score of the p-value of the given gene in the two compared strains. Later, over-representation of these genes (enrichment) was performed, and data was corrected for multiple hypotheses testing using the method of Benjamini-Hochberg. Taken all this together, and although their aims are in line with the system-biology new concept of integration of heterogenic

data, Mori and Colleagues used genetic data to identify different subnetworks that are represented in proteomic terms.

Regarding human studies including systems-biology approach it is worth mentioning the DIRECT (Diabetes REsearCh on patient straTification) study (Koivula et al. 2014) among the Innovative Medicine Initiatives (IMI) Diabetes Platform from the European Union. The DIRECT project was first presented in the 2012 EASD Annual Meeting in Berlin (www.direct-diabetes.org/news-events/flyer-screen.pdf). The main goal of DIRECT is to indetify novel markers in order to perform patient stratification according to glycaemic control and treatment response, leading to personalized medicine in T2DM patients. For this, the big project attemps to phenotype large cohorts in Europe creating a databank with phenotypical datasets and develop a systems-biolgy platform by integrating clinical and biological data, genomics, proteomics and metabolomics. Therefore, data mining tools and algorithms will be developed to stratificate biomarkers and identify the novel ones for diabetes prognosis and treatment. Finally, the project aims to validate the novel biomarkers in a intervention trial to delay or prevent T2DM, as well as studying the treatment response.

The Integrative Systems Biology group at Center for Biological Sequence Analysis (CBS) at the Technical University of Denmark is the main partner in charge of data integration and handling within the DIRECT project. Although many advances have been performed within the project, the final goal to integrate all the heterogenic mentioned data has not yet been achieved.

2.2. Data analysis approaches

During the development of this study, a variety of **heterogenic data** from **different tissues** has been collected. As in the DIRECT study, the challenge faced in this study relied on the fact that we were not aware of any way to combine all the data in one level of **integration**. For this purpose, collaboration with expert groups in this matter allowed us to perform both correlations analysis and integration analysis for all the available data.
It is worth mentioning that, beyond the challenge of having heterogenic data that needs to be integrated (Figure 3), three situations (three experimental groups, Figure 4) must be considered in our approach.

AIMS

Aims

This PhD Thesis is part of a bigger project that aims to identify the key metabolic pathways, metabolites and regulatory genes implicated in the re-establishment of whole body glucose homeostasis, as well as β-cell function. Moreover, the aim relies in determining the interplay of these molecules and pathways across multiple key tissues in T2DM aetiology: pancreatic islets, liver, oxidative and glycolytic skeletal muscle, white and brown adipose tissues and hypothalamus. In order to do so, systems biology analysis tools to integrate all the heterogenic data (phenotype data, functional data, signalling and omics data) from multiple tissues and multiple time points have been used, thus gaining broader knowledge in metabolic plasticity occurring in diet-induced obese mice upon a lifestyle intervention.

At this point, we have been able to collect all samples and performed most of the experiments, yet an integration strategy to obtain a holistic view of the disease has not been completed. However, this PhD Thesis covers most of the project as a first step into achieving the main goal, encompassing from storage of data, correlations with different parameters and definition of networks to identify important players in both pathological state and the metabolic situation after LI.

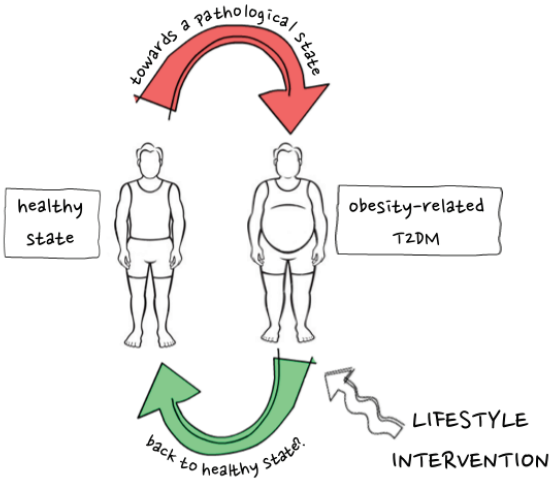

Taking this into account, the concrete aims of this PhD thesis are:

I. Define the phenotype in diet-induced obese mice, and after performing a lifestyle intervention consisting of caloric restriction, dietary changes and exercise training:

   - Assess body composition and energy homeostasis.
   - Assess glucose homeostasis, and define to which extent β-cell function is compromised in both states.
   - Determine tissue-specific metabolic adaptations in white adipose tissue, liver, pancreas, skeletal muscle and hypothalamus.

II. Design and implement systems biology approaches to integrate heterogenic data (phenotypical, functional, molecular and omics data) in order to obtain a holistic view of the metabolic plasticity during diet-induced obesity, and after the lifestyle intervention.

III. Analyse the collected data from the different experimental groups and mentioned tissues by using the designed approaches.

MATERIALS AND METHODS

Materials and Methods

1. Experimental design of the study

Mice were divided in three experimental groups: a control group (*Ctrl*), a pathological group (*HFD*) and an intervention group (*Int*) in which mice followed a LI after they had reached the pathological state (corresponding to *HFD* group) (Figure 5).

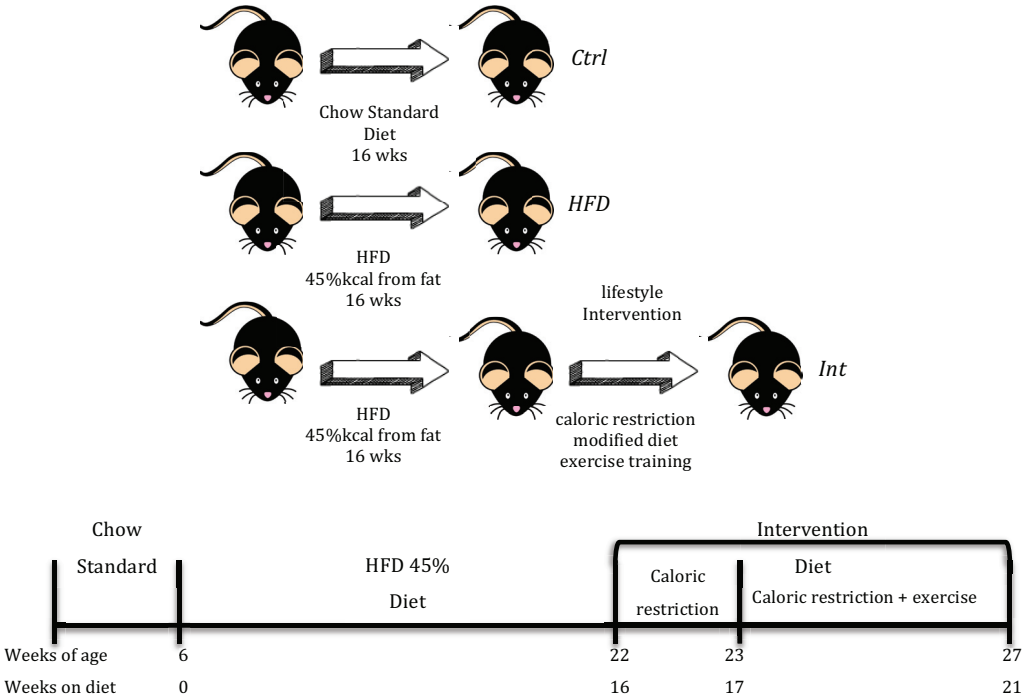

Figure 5. Experimental design.

2. Animals

All the animals used in this study were provided by Harlan Laboratories with 5 weeks of age. Males from the mouse strain C57BL6/J were selected for our research. C57BL/6J strain was used because when they are fed on a HFD they develop obesity, mild to moderate hyperglycemia, and hyperinsulinemia after an over night fasting, being one of the best animal models to resemble obesity-related T2DM condition. The development of obesity in the BL6J strain raises from diet and genetic susceptibility loci, mimicking human obesity (Surwit et al. 1988). Moreover, BL6J mice from Jackson Laboratories carry a naturally occurring deletion of functional protein nicotinamide nucleotide transhydrogenase (NNT), which is an antioxidant defense that catalyzes NADPH production which helps to detoxificate ROS through the regeneration of reduced

glutathione. This way, NNT knockdown increases the presente of ROS. Also, NNT mutation animals show a reduced insulin secretion in comparison with BL6 animals that are lacking the mutation (Freeman et al. 2006). This strain shows a compensatory hyperplasia of the β-cells, and hyperinsulinemia continues for its 18–20-month lifespan (http://jaxmice.jax.org/strain/000664.html). Animals were housed in an animal facilitiy room, at Facuty of Medicine at Universitat de Barcelona, under controlled condition on a 12-hour light/12-hour dark cycle. They were acclimatized for a period of 7 days before they were splitted in 4-mice cages and assigned to one of the groups previously defined. Within the project *per se*, consecutives cohorts of mice were used. Once they reached 16 weeks on the different diets, the decision was to assign them either to the group defining the pathological state phenotype (*HFD*) or to the group performing the LI (*Int*). It is worth mentioning that there were not differences between BW and insulin sensitivity (assessed by an insulin tolerance test, ITT). That is, before the ITT mice on HFD that afterwards were destined to HFD group had a BW of 42.92±0.53g (n=47) while mice that were destined to Int group weighted 42.84±0.67g (n=20) (p-value=0.935). Of note, it was due to the 4h fasting previous to the ITT test. Moreover, the p-values for different timepoints during the ITT were 0.253, 0.234, 0.799, 0.541 and 0.145 at 0, 15, 30, 60 and 120 minutes, respectively. In the same trend, glucose intolerance was also assessed showing no significant differences between the two last mentioned groups (*HFD* and the future *Int*).

All animal procedures were approved by the local ethics committee, Comitè Ètic d'Experimentació Animal at Universitat de Barcelona and the Departament d'Agricultura, Ramaderia, Pesca, Alimentació i Medi Natural at the Generalitat de Catalunya.

2.1. Animal experimental groups

***Ctrl* group** (control group): mice in this group were on Standard Chow diet (Teklad Global 14% Protein Rodent Maintenance Diet, Harlan Laboratories) for 16 weeks. **Inclusion criteria**: BW < 33g, fasting normoglycemia, fasting normal insulin, glucose tolerance and insulin sensitivity (assessed through an IGTT and ITT, respectively).

***HFD* group** (diet-induced pathological group): to achieve the pathological state the animals were on High-Fat diet (HFD) with 45% of energy content from fat D12451 (OpenSource Diets, Research Diets Inc; New Brunswick, NJ, USA) for 16 weeks. This decision was based on previous publications and our own data (unpublished). Inclusion criteria for the mice were set for them to be included in the so-called pathological group: overweight, mild to moderate hyperglycemia, and hyperinsulinemia (after an over night

fasting). **Inclusion criteria**: BW was at least 25% higher than final *Ctrl* BW (threshold at BW> 37g, fasting hyperglycemia, fasting hyperinsulinemia, glucose intolerance and IR (assessed through an IGTT and ITT, respectively).

***Int* group** (intervention group): mice performed a LI (after reaching the pathological state) that consisted of 5 weeks on intervention diet (D12451 and Preliminary Formula Rodent Diet with 45 kcal% Fat and Modification with Flaxseed and Olive Oil, OpenSource Diets, Research Diets Inc; New Brunswick, NJ, USA) combined with 4 weeks of exercise training, 5 days a week, one hour per day. The first week of the diet intervention, mice were fed with 80% in kcal of the daily energy intake determined for a *Ctrl* animal; the other 4 weeks of the diet intervention the mice were fed 100% in kcal of the daily energy intake determined for a *Ctrl* animal. **Inclusion criteria**: proper progression on exercise performance, achieving speed and inclination defined for each exercise session.

2.2. Diets

Three different diets were used in this study: a Standard Chow diet (Teklad Global 14% Protein Rodent Maintenance Diet, Harlan Laboratories); a High-Fat diet with 45% of enery content from fat D12451 (OpenSource Diets, Research Diets Inc; New Brunswick, NJ, USA) and the intervention diet (D12451 and Preliminary Formula Rodent Diet with 45 kcal% Fat and Modification with Flaxseed and Olive Oil, OpenSource Diets, Research Diets Inc; New Brunswick, NJ, USA). The newly designed intervention diet had several nutritional modifications such as the replacement of sucrose by cornstarch and the increase in mono- and polyunsaturated FA due to the change of their origin oil (flaxseed and olive oil were used instead of lard). Although the origin of the FA was modified, the energy content coming from fat was mantained at 45%.

2.3. Monitoring animals

Animals were weighed weekly using always the same weighing scale. Food intake per cage (4 mice/cage) was also monitored weekly and converted to energy intake per mice per day.

2.4. Lifestyle intervention

The physical exercise part of the intervention was performed in a Treadmill (Exer-6M Open Treadmill for Mice and Rats with Shocker and Software 2-102 M/m, Columbus Instruments; Columbus, OH, USA) with 6 lanes and a graduable electrical stimulus at the end of each of them. In order to encourage mice to run, mechanical stimulus (air blowing

from the back) was added when mice stopped running right before reaching the electrical stimulus. At the middle of the first week of intervention, when the animals were already under intervention diet, acclimatization started.

Acclimatization**:** lasted 3 days; the animals were on the intervention diet under a CR with the 80% in kcal of the daily energy intake for a *Ctrl* animal. The 3-day acclimatization occured as follows: day 1: the animals remained in the treadmill without forcing them to any speed neither inclination; day 2: the animals run 10min at the speed of 8m/min; day 3: the animals run 20min at the speed of 10m/min. No inclination was used during acclimatization.

The exercise training started when the mice had been already on the intervention diet for one week and also under CR (reason for which the animals lost weight and were more capable for an exercise performance).

Exercise Training (Figure 6): lasted 4 weeks; the mice were allowed to eat the 100% of kcal that a normal *Ctrl* mice would eat daily. The protocol was designed to rise gradually the speed until reaching a maximum speed of 24m/min with a second level inclination (10º) at the end of the exercise training.

This protocol was carried out as follows (only weekdays considered henceforth): **day 1**: 1h of perfomance at 10m/min; **day 2**: 1h of perfomance at 10m/min; **day 3**: 10min of perfomance at 10m/min + 50min at 12m/min; **day 4**: 10min of perfomance at 10m/min + 50min at 12m/min; from day 5 animals started running at 10m/min and gradually incremented the speed until the value indicated for the first 10 min each day: **day 5**: 10min of perfomance at 12m/min + 50min a 14m/min; **day 6**: 10min of perfomance at 12m/min + 50min a 14m/min; **day 7**: with a first level inclination (5º), 10min of perfomance at 12m/min + 50min at 14m/min; **day 8**: with a first level inclination (5º), 10min of perfomance at 12m/min + 50min at 14m/min; **day 9**: with a second level inclination (10º), 10min of perfomance at 12m/min + 50min at 14m/min; **day 10**: with a second level inclination (10º), 10min of perfomance at 12m/min + 50min at 14m/min; **day 11**: with a second level inclination (10º), 10min of perfomance at 14m/min + 50min at 16m/min; **day 12**: with a second level inclination (10º), 10min of perfomance at 14m/min + 50min at 16m/min; **day 13**: with a second level inclination (10º), 10min of perfomance at 16m/min + 50min at 18m/min; **day 14**: with a second level inclination (10º), 10min of perfomance at 16m/min + 50min at 18m/min; **day 15**: with a second level

inclination (10º), 10min of perfomance at 18m/min + 50min at 20m/min; **day 16**: with a second level inclination (10º), 10min of perfomance at 18m/min + 50min at 20m/min; **day 17**: with a second level inclination (10º), 10min of perfomance at 20m/min + 50min at 21m/min; **day 18**: with a second level inclination (10º), 10min of perfomance at 20m/min + 50min at 21m/min; **day 19**: with a second level inclination (10º), 10min of perfomance at 22m/min + 50min at 22m/min; **day 20**: with a second level inclination (10º), 10min of perfomance at 22m/min + 50min at 22m/min.

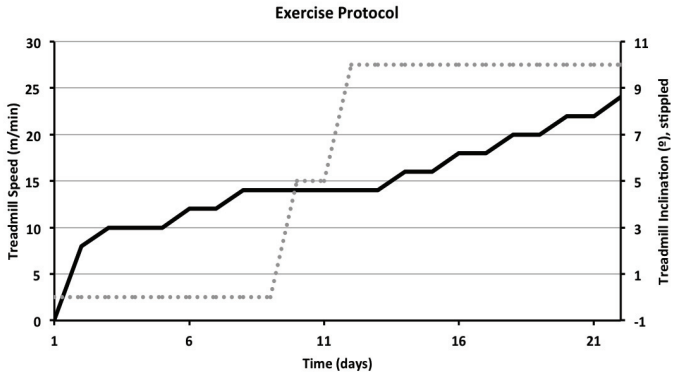

Figure 6. Lifestyle intervention protocol. Treadmill speed and inclination increase with time.

2.5. Anesthesia procedure

Avertin was used for anesthesia during the study. A stock at 100% was prepared with 10g 2,2,2-Tribromo ethanol (BR_2CH_2OH) 99+%(GC) and 10mL Tertiary amyl alcohol (2 Methlbutan-201, both from Sigma Aldrich). To dilute to 2.5%, 200uL of the 100% stock were added into 10mL of dH_2O. A warm water bath at 60ºC was used for 1h to facilitate dissolution. The ready-to-use mixture can be kept up to 1 week at RT although it is preferable to keep it at 4ºC. 0.015-0.017mL/g of mouse BW were used, that is 20 times their BW expressed in uL of intraperitoneal injection.

3. *In-vivo* metabolic studies

3.1. Body composition

A representative number of animals of each group (*Ctrl*, *HFD* and *Int*) were sent to the Magnetic Ressonance Imaging Services at the Hospital Clínic de Barcelona in collaboration with Dra. Guadalupe Soria's group. The animals were scanned in a 7.0 T BioSpec 70/30 horizontal (Bruker BioSpin, Ettlingen, Germany), equipped with an actively shielded gradient system (400 mT/m, 12 cm inner diameter). Animals were placed in a supine

position in a Plexiglas holder with a nose cone for administering anesthetic (1.5% isofluorane in a mixture of 30% O_2 and 70% N_2O). Animals were scanned from below the head to the beginning of the tail, in 15 um sections. A 3D reconstruction merging all the images was performed. Thus, fat volume was calculated merging the area values for each image, which is analysed given that fat is shown in white contrast.

Body composition was also assessed using NMR Imaging (Whole body Composition Analyzer; EchoMRI™, Houston, TX, USA) in collaboration with Dr. Rubén Nogueiras' group at Department of Physiology (CIMUS, University of Santiago de Compostela). EchoMRI instruments measure directly total body fat, lean mass, free water, and total body water. NMR discriminates the tissue by taking advantage of the differences in relaxation times of the hydrogen spins and/or hydrogen density in these tissues. Hydrogen nuclei generate radio frequency signals due to the precession of the spin axes, and this frequency has different properties (amplitude, duration and spatial distribution) that are related to the tissue. A contrast exists between fat, body free fluid, and muscle based on NMR amplitude and relaxation time, which can be enhanced by applicating certain radio frequency sequences.

3.2. Body temperature

Body temperature was assessed through rectal temperature and scapular temperature. Rectal temperature was recorded with a rectal probe connected to digital thermometer (BAT-12 Microprobe-Thermometer; Physitemp, Clifton, NJ). Scapular temperature was measure in the skin area surrounding BAT by using high-resolution infrared camera (FLIR Systems E60 Thermal Imaging Infrared Camera, FLIR; West Malling, Kent, UK) as previously described (Czyzyk et al. 2012). These two measuring techniques were performed in collaboration with Dr. Rubén Nogueiras' group at Department of Physiology (CIMUS, University of Santiago de Compostela).

3.3. Intraperitoneal Glucose Tolerance Test (IGTT)

This test studies how tolerant to a glucose bolus the animals are by administrating glucose and measuring how they are handling it. Overnight fasting was chosen in this test following the literature (Muniyappa et al. 2008). In mice a prolonged fast impairs insulin-stimulated glucose utilizations (Heijboer et al. 2005; Ayala et al. 2006). Thus, overnight fasting is reliable for focusing on glucose utilizations.

After an overnight fasting (16h) the animals were brought to the animal facility laboratory to perform the test. The test was performed with the mice conscious and properly identified for an easier performance. Blood glucose was measured at t=0min with a GlucocardG+ meter (A-Menarini Diagnostics) and blood was collected with Microvette® tubes. Right after, an intraperitoneal bolus of D-Glucose (2g/kg of mouse body weight) diluted in saline solution was administered. A 20% solution was prepared and used fresh the same day of the test, then it was injected intraperitoneally by means of 10 times the mouse BW. Blood was also collected again at t=15min and blood glucose was measured at each time point (15, 30, 60 and 120min post-injection). After the test, blood samples were centrifugated to obtain plasma (4ºC, 15', 3500g), which was then stored at -80ºC until use. Plasma samples were used to measure insulin, leptin and adiponectin at time 0; and to measure insulin also at time 15min to determine the *in vivo* insulin-stimulated glucose handling. These measures were performed with enzyme-linked immunosorbent assay (ELISA) (Section 4.1).

3.4. Insulin Tolerance Test (ITT)

This test allow us to observe the insulin sensitivity by administrating insulin and measuring how they are handling glucose levels. Contrary to IGTT, a 5-6h morning fasting is chosen for ITT given that it is sufficient to assess insulin action in a more physiological state while avoiding hyploglycemia during the insulin test. After a 4h fasting the animals were brought to the animal facility laboratory to perform the test. The test was performed with the mice conscious and properly identified for an easier performance. Blood glucose was measured at t=0min with a GlucocardG+ meter (A Menarini Diagnostics). Right after, an intraperitoneal solution of insulin (Humulin R 100UI/mL Regular by Eli Lilly and Company) (0.75UI/kg of mouse weight) was administered. A 0.185UI/mL (5 ul insulin 100 U/ml + 2698 ul saline buffer) solution was prepared and used fresh the same day of the test, then it was injected intraperitoneally by means of 4 times the mouse BW in uL. Blood glucose was measured at each time point (15, 30, 60 and 120min post-injection).

3.5. Indirect calorimetry

Animals were monitored in an indirect calorimetry, food intake, and locomotor activity monitoring System (TSE LabMaster; TSE Systems, Bad Homburg, Germany) as described previously (Pfluger et al. 2008; Czyzyk et al. 2010) in collaboration with Dr. Rubén Nogueiras' group at Department of Physiology (CIMUS, University of Santiago de Compostela). Mice were acclimated for 24h into test chambers and then monitored for an additional 48h. During these 48h data was collected to calculate different parameters: O_2 consumption

and CO_2 production were measured every 45min during 48h to determine energy expenditure with standard analysis software provided with the calorimeter system. Thus, VO_2 (mL/h/kg) and heat production (kcal/h/kg) were measured during the dark phase and light phase for 48h. Heat production was calculated by the Weir equation that describes the relationship between heat produced and oxygen consumption and is equivalent to the resting energy expenditure (REE). In the abbreviated Weir equation 24h urinary nitrogen is not needed. Thus, kcal per day are calculated as follows: $[3.94(VO_2) + 1.11(VCO_2)]$ 1.44 (Weir 1949). Food and water intake were determined continuously for 48h by scales integrated into the sealed cage environtment.

In parallel, locomotor activity was measured using a multidimensional infrared light beam system with installed beams on cage bottom and top levels. Thus, activity was expressed as beam breaks. The locomotor activity was assessed with the XF, XA and Z parameters defined by the LabMaster software. XA accounts for the X-beam breaks for ambulatory movement that are, breaks of any of two different X-beams of light. Beam breaks of movements in which light barrier in X_1 is first interrupted followed by an interruption to a different light barrier X_2 (being $X_1 \neq X_2$) are registered (Figure 7). On the contrary, XF accounts for fine movement where two breaks in succession of the same beam of light are registered at the X level (Figure 7). Concretely, when there is an interruption of a light barrier that has been interrupted for the second time in succession without different light barriers previously interrupted.

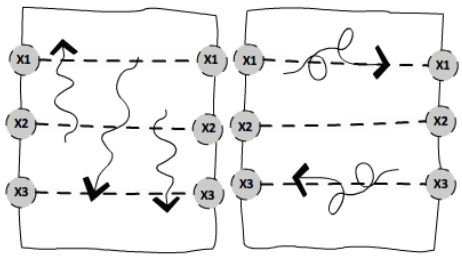

Figure 7. Representation of moviment types in the study. On the left cage, the mouse performs ambulatory movement by crossing different light barriers (X1 and X2, X2 and X3, X1 X2 and X3). On the right cage, the mouse performs fine moviment by repeatedly being detected in the same light barrier (X1 and X2, X3 and X3).

4. *In vitro* measurement of Glucose-Stimulated Insulin Secretion (GSIS)

In order to perform a GSIS assay, pancreatic islets need to be isolated from the pancreas and then incubated at different glucose concentrations in order to assess their insulin secretion when facing different glucose levels.

4.1. Mice islets isolation

4.1.1. Pancreas obtention

Once the animal was slept after the anesthesia, without showing any reflex, the peritoneal cavity was opened. The end of the bile duct inserted in the duodenum was clamped and 2-3mL of collagenase XI solution (Table 1) were injected in it. The pancreas was obtained and put in a 50mL tube with 2mL of collagenase XI solution and kept on ice. The collagenase XI solution was prepared fresh right before animals' dissection.

Collagenase XI solution	
Reagent	Concentration
Collagenase XI (Collagenase from Clostridium histolyticum, release of physiologically active rat pancreatic islets tested, Type XI, 2-5 FALGPA units/mg solid, >1200 CDU/mg solid; C7657, Sigma)	1000U/mL
Hank's Balanced Salt Solution (HBSS) without CaCl2 (HBSS 10X without MgCl2 and CaCl2; 14185-045, Gibco)	500mL

Table 1. Collagenase XI solution.

4.1.2. Pancreas digestion

The tubes containing the pancreas were incubated at 38ºC for 14min before manual agitation was performed. In order to stop the action of the collagenase two washes using ice-cold HBSS containing $CaCl_2$ (HBSS; H8264, Sigma) were performed as follows: 20mL ice-cold HBSS were added to the tube and then centrifugated (4ºC, 1100rpm, 1min) and the supernatant was discarded; 15mL HBSS were added and the centrifugation process was repeated. The final pellet was resuspended in 7mL of HBSS.

The resuspended pellet solution was filtered with a specific filter that keeps the islets (Cell Strainer 70um Nylon; Ref 352350, BD Falcon). The filtered liquid was discarded and the filter containing the islets was cleaned using HBSS two consecutive times. In order to avoid the filter getting dry it was mantained in a petri dish. After the two aforementioned washes, the filter was inverted and RPMI is added through to obtain the islets in a new and clean petri dish. It is worth mentioning the importance of having a petri dish for each animal so as not to mix islets from different animals, even they belong to the same experimental group.

4.1.3. Islets selection

Islets were handpicked with a 200uL pipette from the big petri dish and put in different, new and clean petri dishes (again, one petri dish for each animal). During all this process, the media used to pick the islets was RPMI (Table 2). About 70 islets per animal were picked for each animal and cultured overnight in RPMI media. Both the Hank's with glucose solution and the RPMI were prepared the day before the experiment.

RPMI	
Reagent	Amount
Glutamine (Hyclone L-Glutamine 200mM, 100x solution, Lot Aye 161445; Thermo Scientific)	5mL
Penicillin/Streptomycin (Hyclone 10.000 units/mL penicillin+ 10.000ug/mL streptomycin, Lot J140004; Thermo Scientific)	5mL
Serum (FBS inactivate, Lot 9312; Biosera), at 10%	50mL
RPMI (contains already 11mM Glucose)	500mL

Table 2. RMPI

The addition of glutamine, the antibiotics and the serum to RPMI was performed under a hood and both media were warmed up at 37ºC in a water bath.

4.2.Insulin secretion assay for isolated islets

The KRBH solution indicated below must be freshly prepared the same day or the day before the experiment. It has to be then warmed up in a water bath (37ºC, 1-2h) and pH adjusted at 7.4 accurately (Table 3). The secretion solution was splited in different tubes for the different glucose concentrations that will be assayed. Different amounts of glucose were then added to two different tubes to obtain 2.8mM and 16mM concentrations (Table 4).

Stock solution 10X		
Reagent	Amount for 500mL	Final concentration
$NaCl_2$	4.8g	140mM
KCl	1.676g	4.5mM
$MgCl_2 \cdot 6H_2O$	1.016g	1mM
HEPES	23g	20mM
Distilled H_2O	500mL	
$CaCl_2$ solution 10X		
Reagent	Amount for 500mL	

CaCl2	1.38g
Distilled H2O	500mL

Table 3. Stock solution 10X and CaCl2 solution 10X.

KRBH solution	
Reagent	Concentration
Stock solution 10X	10mL
$CaCl_2$ solution 10X	10mL
Bovine Serum Albumin, BSA	0.1% (0.1g/mL)
Distilled H_2O	80mL
KRBH 2.8mM glucose	
Reagent	
1M glucose	28uL
KRBH solution	10mL
KRBH 16.7mM glucose	
Reagent	
1M glucose	167uL
KRBH solution	10mL

Table 4. KRBH solution and KRBH solutions with different glucose concentrations. For the KRBH solution, the compounds need to be added in the indicated order to avoid precipitates.

KRBH solution as well as stock solutions 10X can be stored at 4ºC and need to be warmed up in case of following use.

Insulin secretion measurement:

For each animal, four 1.5mL-tubes containing 15 islets each were used for the insulin secretion assay. These islets were picked from the RPMI-containing petri dish that was incubated overnight. The use of magnifying lens was recommended henceforth in the protocol to assure that the islets were maintained in the tub after the different steps performed. For the insulin secretion assay, the following steps were performed:

1. Pre-incubation: 0.5mL of KRBH 2.8mM glucose was added to all the tubes. The tubes were placed in a water bath at 37ºC with agitation (30rpm) for 30min. The supernatant was discared and the magnifying lens allowed to chech that all the islets remained in the tube.

2. Insulin secretion at 2.8mM glucose: again, 0.5mL of KRBH 2.8mM glucose was added to all the tubes. The tubes were placed in a water bath at 37ºC with agitation (30rpm) for 1h.

The supernatant is collected in properly labelled tubes, to measure the insulin secretion of these islets in a media with 2.8mM of glucose (low glucose). The remaning islets in the bottom of the tubes were checked again with the lens.

3. Insulin secretion at 16.7mM glucose: 0.5mL of KRBH 16.7mM glucose was added to all the tubes. The tubes were placed in a water bath at 37ºC with agitation (30rpm) for 1h. The supernatant is collected in properly labelled tubes, to measure the insulin secretion of these islets in a media with 16.7mM of glucose (high glucose). The remaning islets in the bottom of the tubes were checked again with the lens.
Both supernatant were stored at -20ºC.

4. Insulin content: the insulin content of the islets was assessed by lysing the islets with an acetic-acid solution (Table 5).

Acetic-acid lysis buffer	
Reagent	Amount for 100mL
Glacial acetic acid	5.75mL
Bovine Serum Albumin, BSA	0.1% (0.1g/100mL)
Distilled H2O	94.25mL

Table 5. Acetic-acid lysis buffer.

The acetic-acid lysis buffer solution does not need to be prepared fresh. It is important to remember always to add the acid.

An amount of 150uL of acetic-acid lysis buffer solution was added into the tubes. The tubes were put in a -80ºC freezer and stayed overnight. The day after, tubes were defrozen as follows: vortexing the tubes, letting them stay at 95ºC for 10min in a thermo-block, vortexing the tubes vigorously and putting the tubes back on ice. The tubes were then centrifugated at 1200 rpm at 4ºC for 10min. The supernatant was stored at -20ºC to measure the insulin content of the islets.

The insulin levels were measured in the three supernatants to assess the insulin secretion of the islets in each tube by ELISA (Section 4.1.1). The insulin content was used to normalize the insulin secretion values at different glucose concentrations.

5. Analytical methods

5.1. Determination of plasma hormone levels

5.1.1. Insulin

Insulin was quantified at the different experiments (*in vivo* GSIS from IGTT and *in vitro* GSIS) using the Ultra Sensitive Mouse Insulin ELISA Kit (#90080, Crystal Chem Inc., Downers Grove, IL, USA) according to the manufacturer's instructions.

5.1.2. Leptin

Leptin was quantified using the Mouse Leptin ELISA Kit (#90030, Crystal Chem Inc., Downers Grove, IL, USA) according to the manufacturer's instructions. Plasma samples were collected after an overnight fasting (16h) from blood from the tail of the animal.

5.1.3. Adiponectin

Adiponectin was quantified using the Mouse Adiponectin ELISA (EZMADP-60K, Merck Millipore, Darmstadt, Germany) according to the manufacturer's instructions. Plasma samples were collected after an overnight fasting (16h) from blood from the tail of the animal.

5.2. Determination of triglyceride levels in tissues

5.2.1. Triglyceride extraction from tissue sample

For the triglyceride (TG) extraction, approx. 100mg of tissue homogenate were mixed with 500uL of SDS 0.1% in an eppendorf tube and then left shaking overnight (or at least 6h) at room temperature (RT). 400uL of the mixture were put into a 2mL eppendorf, where there were added 400uL of methanol before vortexing. The rest of the mixture was then used for protein quantification. 800uL of choloform were added to the 2mL tube and then vortexed and left to incubate on ice (30'). 48uL of KCL 0.5M were added and then vortexed and left again on ice (30') before centrigugation (4ºC, 10', 2000rpm). The upper phase (aqueous phase) and the interphase were discarded. A known volume (around 300uL) of the lower phase (organic phase) were transferred to a new eppendorf before letting overnight the chloroform to evaporate from the tubes. The pellet was resuspended with 100% ethanol (50uL or more, depending on the sample concentration) and a TG measuring kit was used. The results were expressed as TG/mg protein.

5.2.2. Triglyceride measurement

Triglyceride Reagent (T2449-10ML), Free Glycerol Reagent (F6428-40ML) and Glycerol Standard Solution (G7793-5ML) all from Sigma Aldrich were used for the triglyceride measurement. A 96-well microplate was used (96-well Microplate, NUNC, Denmark) with a modified protocol from the one provided by Sigma Aldrich. First, a glycerol standard curve (0mg/mL, 0.3125 mg/mL, 0.625 mg/mL, 1.25mg/mL and 2.5mg/mL) was prepared and 160uL of Free Glycerol Reagent were added to each well with 3uL of each sample or standard curve point tested. The plate was then incubated at 37ºC for 5min and then absorbance (initial absorbance) was readed at 540nm with the spectrophotometer (Synergy HT Multi-Mode Microplate Reader by BioTek®). 40uL of Triglyceride Reagent were added and the plate was again incubated at 37ºC for 5min. Absorbance (final absorbance) was read again at 540nm. The indications provided in the commercial protocol and the amounts we have used for triglyceride extraction, allowed us to perform the proper calculations.

6. Gene expression analysis

6.1. mRNA isolation

Sample preparation: samples were mixed with TRI Reagent® (T9424, Sigma Aldrich) by means of 1mL of reagent per 50-100mg of tissue (in any case the volume of tissue should exceed 10% of the TRI Reagent volume). The homogeneization was performed by adding a small quantity of magnetic beads (0.5mm diameter zirconium oxide ZrO_2 for BulletBlender ®, NextAdvance, NY, USA) and introducing the tubes in the Bullet Blender®. BulletBlender® was then used at 4ºC for a period of 3min at 8-9 speed level following manufacturer instructions (depending on the tissue). The homogenate was checked and another period of 3min was performed.

Note: in samples with high content of fat, a centrifugation (4ºC, 5', 16000g) was performed at this point and the layer of fatty material on the surface of the aqueous phase was removed. The supernatant was transferred to a fresh tube to proceed with the next step.

Phase separation: samples were left for 5min at RT and then 0.2mL of chloroform (ref) were added per mL of TRI Reagent used. The samples were covered and shaked vigorously for 15seconds before allowing them to stand for 5-15min at RT. The resulting mixture was centrifugated (4ºC, 15', 12000g) and three phases appeared: a red organic

phase (containing protein), an interphase (containing DNA), and a colorless upper aqueous phase (containing RNA).

RNA isolation: the aqueous phase was transferred to a fresh tube and 0.5mL of 2-propanol were added per mL of TRI Reagent used in sample preparation. Samples were mixed by shaking the same way as before and then allowed to stand for 5-10min at RT. The samples were centrifuged (4ºC, 10', 12000g) and the RNA precipitated forming a pellet. The supernatant was removed and the RNA pellet washed by adding 1mL of 75% Ethanol per mL of TRI Reagent used in sample preparation. Samples were vortexed and centrifugated (4ºC, 5', 7500g) and this washing step was repeated. The supernatant after the washing was discarded and the RNA pellets were dried by airdrying under a hood. Finally, RNA pellets were resuspended in 30-60 ul of RNAase free water. RNA was quantificated using a NanoDrop 1000 Spectrophotometer (Thermo Scientific).

6.2. cDNA obtention

cDNA obtention: once the RNA concentration was known, the reaction to obtain cDNA through the reverse transcriptase enzyme was performed. To do so, 1ug of RNA (or 2 ug if double reaction was performed) were added to a PCR tube that was filled with water and 2X RT Master Mix (Applied Biosystems, Table 6) until 20uL (or 40uL for double reaction) to perform the reaction. All the kit reagents and the Master Mix should be kept on ice.

2X RT Master Mix		
Reagents	Amount for 20uL (single reaction), uL	Amount for 40uL (double reaction), uL
10X RT Buffer	2	4
25X dNTP Mix	0.8	1.6
10X RT Rand Prim	2	4
MultiScribe™ RT	1	2
Nuclease-free H2O	4.2	8.4
Total	10	20

Table 6. 2X RT Master Mix.

10uL of 2X RT Master Mix were added to each tube with 10uL of RNA sample. Tubes were spinned and placed in the thermal cycler. The thermal cycler performed the following program: 10min at 25ºC, 120min at 37ºC, 5min at 85ºC and hold at 4ºC.

To optimize the dilution of the cDNA for each sample in the different tissues, different dilutions were checked using Real Time PCR (explained below) to elucidate which was the best dilution so as to dilute the rest of the samples to study gene expression. A cDNA pool was obtained by mixing 5uL of each sample into a tube and then the standard curve for the gene expression studies was performed by means of 1:8, 1:16, 1:32, 1:64, 1:128, 1:256, 1:512, 1:1024 dilutions.

6.3. Real Time PCR (RT-PCR):

RT-PCR were performed using a 384-well plate (G034-ABI, Attendbio) two different reagent kids: Premix Ex Taq™ (Perfect Real Time, by TaKaRa) and TaqMan® Master Mixes (Applied Biosystems).

Premix Ex Taq™ by TaKaRa: in each tube 5uL of the sample (diluted) were added with 5uL of the Mix (that is different for each Taqman® probe). The Mix is indicated in Table 7.

Mix per well	
Nuclease Free Water	0,5 uL
TaqMan Probe	0,5 uL
TaKaRa MasterMix	5 uL
ROX I	0,2 uL
Total per well	6,2 uL, but 5 uL real

Table 7. Mix per well for RT-PCR (using Premix Ex Taq™ by TaKaRa). Note: 6,2 uL were prepared per well although only 5 were needed, this way we already have an extra volume needed for avoiding the pipetting error.

Each Mix was prepared attending the number of wells in which the same Taqman® probe was tested. In each Mix tested, the number of samples were considered for the amount calculation as well as the standard curve points since a standard curve was assessed for each gene as a quantification method.

TaqMan® Master Mixes by Applied Biosystems: the process was the same but ROX I was already included in the commercial mix (Table 8).

Mix per well	
Nuclease Free Water	0,5 uL
TaqMan Probe	0,5 uL
Applied Byosystems Mix	5 uL
Total per well	6, but 5 uL real

Table 8. Mix per well for RT-PCR (using TaqMan® Master Mix)

Note: 6 uL were prepared per well although only 5 were needed, this way we already have an extra volume needed for avoiding the pipetting error.

Thermal cycler: the termal cycling program was the same for both kits (Table 9).

Stage 1	50ºC	2min
Stage 2	95ºC	10min
Stage 3 (40 repeats)	95ºC	15sec
	60ºC	1min
(Optional) Hold	4 °C only if products will be run out on a gel	

Table 9. Thermal cycling program.

Gene expression calculation: ABI Prism®7900 was used for reading the Ct for each probe and sample. An standard curve (detailed above) was used to determine the dilution of each sample so as to compare the expression in the different studied groups.

6.4. Taqman® probes

All Taqman® probes were obtained from Applied Biosystems (AB) (Table 10). Mouse Genome Informatics (www.informatics.jax.org) name consensus are described in the first column, and ID (given short name or synonym name) appears in the second column.

MGI	ID	Name	AB Reference
Acaca	Acaca	acetyl-Coenzyme A carboxylase alpha	Mm01304257_m1
Adgre1	Emr1	adhesion G protein-coupled receptor E1	Mm00802529_m1
Agrp	Agrp	agouti related neuropeptide	Mm00475829_g1
Atf4	Atf4	activating transcription factor 4	Mm00515324-m1
Atf6	Atf6	activating transcription factor 6	Mm01295317-m1
Atp5a1	Atp5a1	ATP synthase, H+ transporting, mitochondrial F1 complex, alpha subunit 1	Mm00431960-m1
Cartpt	Cart	CART prepropeptide	Mm04210469_m1
Cat	Cat	catalase	Mm00437992-m1
Ccl2	Ccl2	chemokine (C-C motif) ligand 2	Mm00441242_m1
Cd209e	Cd209e	CD209e antigen	Mm00459980_m1
Cd68	Cd68	CD68 antigen	Mm00839636_g1
Cidea	Cidea	cell death-inducing DNA fragmentation factor, alpha subunit-like effector A	Mm00432554_m1
Clpx	Clpx	caseinolytic mitochondrial matrix peptidase chaperone subunit	Mm00488586_m1
Cox4i1	Cox4i1	cytochrome c oxidase subunit IV isoform 1	Mm01250094-m1
Cpt1a	Cpt1a	carnitine palmitoyltransferase 1a, liver	Mm00550438-m1

Crh	Crh	corticotropin releasing hormone	Mm01293920_s1
Cs	Cs	citrate synthase	Mm00466043-m1
Ddit3	Chop	DNA-damage inducible transcript 3	Mm00492097_m1
Dgat2	Dgat2	diacylglycerol O-acyltransferase 2	Mm00499536_m1
Dnm1l	Drp1	dynamin 1-like	Mm01342903_m1
Esrra	Esrra	estrogen related receptor, alpha	Mm00433143-m1
Fasn	Fasn	fatty acid synthase	Mm00662319-m1
Fgf1	Fgf1	fibroblast growth factor 1	Mm00438906_m1
Fgf21	Fgf21	fibroblast growth factor 21	Mm00840165_g1
Fis1	Fis1	fission 1 (mitochondrial outer membrane)	Mm00481580_m1
Foxo1	Foxo1	forkhead box O1	Mm00490672_m1
Gabpa	Nrf2a	GA repeat binding protein, alpha	Mm00484598-m1
Gapdh	Gapdh	glyceraldehyde-3-phosphate dehydrogenase	Mm99999915_g1
Gpx1	Gpx1	glutathione peroxidase 1	Mm00656767-g1
Gys1	Gs1-skm	glycogen synthase 1, muscle	Mm01962575_s1
Gys2	Gs2	glycogen synthase 2	Mm00523953_m1
Hnf4a	Hnf4a	hepatic nuclear factor 4, alpha	Mm01247716_m1
Hspa5	Bip	heat shock protein 5	Mm00517691-m1
Hspa9	Hspa9	heat shock protein 9	Mm00477716_g1
Hspd1	Hsp60	heat shock protein 1 (chaperonin)	Mm00849835_g1
IL10	IL10	interleukin 10	Mm00439614_m1
IL1b	IL1b	interleukin 1 beta	Mm00434228_m1
IL6	IL6	interleukin 6	Mm00446190_m1
Itgax	Cd11c	integrin alpha X	Mm00498698_m1
Lepr	Lepr	leptin receptor	Mm00440181_m1
Lonp1	Lonp1	lon peptidase 1, mitochondrial	Mm01236887_m1
Lpl	Lpl	lipoprotein lipase	Mm00434764_m1
Mc3r	Mc3r	melanocortin 3 receptor	Mm00434876_s1
Mc4r	Mc4r	melanocortin 4 receptor	Mm00457483_s1
Mfn1	Mfn1	mitofusin 1	Mm00612599_m1
Mfn2	Mfn2	mitofusin 2	Mm00500120_m1
mt-Co1	CoxI	mitochondrially encoded cytochrome c oxidase I	Mm04225243_g1
mt-Cytb	Cytb	mitochondrially encoded cytochrome b	Mm04225271_g1
mt-Nd3	Nd3	mitochondrially encoded NADH dehydrogenase 3	Mm04225292_g1
Ndufa9	Ndufa9	NADH dehydrogenase (ubiquinone) 1 alpha subcomplex, 9	Mm00481216-m1
Nnmt	Nnmt	nicotinamide N-methyltransferase	Mm00447994_m1
Npy	Npy	neuropeptide Y	Mm00445771_m1
Nrf1	Nrf1	nuclear respiratory factor 1	Mm00447996_m1
Opa1	Opa1	optic atrophy 1	Mm00453879_m1
Pck1	Pck1-pepck	phosphoenolpyruvate carboxykinase 1, cytosolic	Mm00440636_m1
Pfkl	Pfk1-liv	phosphofructokinase, liver, B-type	Mm00435587_m1
Pfkm	Pfk1-skm	phosphofructokinase, muscle	Mm01309576_m1

Pomc	Pomc	pro-opiomelanocortin-alpha	Mm00435874_m1
Ppara	Ppara	peroxisome proliferator activated receptor alpha	Mm00440939_m1
Ppard	Ppard	peroxisome proliferator activator receptor delta	Mm00803184-m1
Pparg	Pparg	peroxisome proliferator activated receptor gamma	Mm00440945_m1
Ppargc 1a	Pgc1a	peroxisome proliferative activated receptor gamma coactivator 1 alpha	Mm01208835-m1
Ppargc 1b	Pgc1b	peroxisome proliferative activated recetor gamma coactivator 1 beta	Mm01258518_m1
Ppia	Ppia	peptidylprolyl isomerase A	Mm02342430_g1
Scd1	Scd1	stearoyl-Coenzyme A desaturase 1	Mm01197142-m1
Sdha	Sdha	succinate dehydrogenase complex, subunit A, flavoprotein (Fp)	Mm01352366-m1
Slc2a2	Glut2	solute carrier family 2 (facilitated glucose transporter), member 2	Mm00446224_m1
Slc2a4	Glut4	solute carrier family 2 (facilitated glucose transporter), member 4	Mm00436615_m1
Socs3	Socs3	suppressor of cytokine signalling 3	Mm00545913_s1
Sod2	Sod2	superoxide dismutase 2, mitochondrial	Mm01313000-m1
Srebf1	Srebf1	sterol regulatory element binding transcription factor 1	Mm00550338_m1
Tfam	Tfam	transcription factor A, mitochondrial	Mm00447485-m1
Tnf	Tnfa	tumor necrosis factor	Mm00443258_m1
Ubl5	Ubl5	ubiquitin-like 5	Mm01151181_m1
Ucp1	Ucp1	uncoupling protein 1 (mitochondrial, proton carrier)	Mm00494069_m1
Ucp2	Ucp2	uncoupling protein 2 (mitochondrial, proton carrier)	Mm00627599_m1
Ucp3	Ucp3	uncoupling protein 3 (mitochondrial, proton carrier)	Mm00494077_m1
Uqcrc2	Uqcrc2	ubiquinol cytochrome c reductase core protein 2	Mm00445961-m1
Xbp1sp	Xbp1sp	X-box binding protein 1 spliced	
Xbp1t	Xbp1t	X-box binding protein 1 total	Mm00457357_m1

Table 10. Taqman probes used for RT-PCR.

7. Transcriptome analysis

7.1. RNA sequencing analysis of WAT and liver

RNA obtained as in 5.1. from white adipose tissue and liver was sent to Centre Nacional d'Anàlisi Genòmica (CNAG, www.cnag.cat) for RNAseq analysis. Analysis was performed by the Dr. José I. Martín-Subero's group (Pathology, Pharmacology and Microbiology Department at UB and IDIBAPS).

RNA was extracted as explained in section 6.1. RNAseq libraries TruSeq mRNA were prepared, in order to perform sequencing. Quality of the cDNA libraries was checked and measured with the DNA-1000 kit (Agilent) on a 2100 Bioanalyzer. An Illumina HiSeq 2000

(v3) sequencer was used, obtaining 2x75bp paired-end reads and more than 20 million paired-end reads per sample.

The logarithm with base 2 was calculated for each read. To normalize the new value, the function rlog from the published Package "DESeq2"(Love et al. 2014) from Bioconductor was assessed.

8. Metabolomics

8.1. Metabolomics of WAT, liver and gastrocnemius

These experiments and the corresponding identification and analysis were perfomed by the Dr. Oscar Yanes' group (Metabolomics Platform, COS). Pulverised samples of WAT, liver, skeletal muscle gastrocnemius and hypothalamus were sent to Centre for Omic Sciences (COS, omicscentre.com) for metabolomics experiments based in NMR.

8.1.1. Sample preparation

The tissue processing and sample preparation was different attending the given tissue that was used, thus liver has a different processing than WAT, skeletal muscle and hypothalamus.

8.1.1.1. Liver sample preparation

From the pulverised tissue, 50-100mg were transferred to a 2mL eppendorf tube, in which 1mL of cold mixture of acetonitril:water (CH_3CN:H_2O 1:1 v/v T=0ºC) was added. The resulting suspension was vortexed and ultrasonicated. Then, a centrifugation (4ºC, 15', 4700g) of the tube content was performed and the supernatant was carefully transferred to a new tube. This step was repeated 3 times adding 500uL of cold acetonitril:water solution and the combined aqueous phases were frozen, lyophilized and stored at -80ºC until further analysis. The resultant pellet was dried and extracted with 1mL of mixture chloroform:metanol (2:1) by ultrasonication. Then, the mixture was centrifugated (4ºC, 30', 15000rpm, 22640g) and the supernatant (lipidic phase) was collected in a new tube. The lipidic phase was dried under nitrogen stream and stored at -80ºC. At this point, samples were stored at -80ºC until measurement experiments.

For the measurement experiment, an aqueous extract was dissolved in 600uL of D_2O (that contained 0.67mM trisilylpropionic acid, TSP), and the organic extract was reconstituted in 700uL of $CDCl_3$/CD_3OD (2:1) solution (that contained 1.18mM tetramethylsilane, TMS).

Then, both extracts were vortexed until homogenization and centrifugated (4ºC, 10', 4500rpm) and supernatant of both phases were transferred into 5mm NMR tubes.

8.1.1.2. WAT, skeletal muscle and hypothalamus sample preparation

An amount of the pulverized tissue (WAT: 30-70mg; skeletal muscle gastrocnemius: 20-40mg; hypothalamus: 10-25mg) was mixed with 400uL of methanol and then vortexed and ultrasonicated until homogenization. Then, 200uL of chloroform were also add and homogenated. This step was repeated. Finally, 200uL of water were added and again the mixing step was repeated. Afterwards, the biphasic mixture was centrifuged (4ºC, 20', 15000rpm, 22640g), and the upper aqueous phase (methanol/water) was introduced in a new eppendorf tube, while the lower organic phase was collected to another tube. At this point, samples were ready to be stored at -80ºC. For the NMR measurement experiments, steps were followed as in liver (section 8.1.1.1).

8.1.2. Nuclear Magnetic Ressonance (NMR) measurements

^{1}H-NMR spectra were recorded at 310K on a Bruker Avance III 600 spectrometer operating at a proton frequency of 600.20MHz using a 5mm CPTCI triple resonance (^{1}H, ^{13}C, ^{31}P). One-dimensional ^{1}H pulse experiments of aqueous samples were performed. In order to suppress the residual water peak the experiments were recorded using the *noesy presat* sequence, with the mixing time set at 100ms. A 75Hz-power irradiation was applied during recycling delay and mixing time to presaturate the solvent. A total of 256 transients were collected into 64k data points for each ^{1}H spectrum, being the spectral width set as 12kHz (20ppm). The exponential line broadening applied before Fourier transformation was of 0.3Hz. In order to remove the residual water moisture of deuterated methanol, lipidic samples were measured using a simple presaturation sequence. Thus, a 50Hz-power irradiation was used during recycling delay and mixing time to presaturate the solvent. Again, 256 transients were collected into 64k data points for each ^{1}H spectrum, being the spectral width set as 12kHz (20ppm). Also here, the exponential line broadening applied before Fourier transformation was of 0.3Hz. Of note, the frequency domain spectra were manually phased and baseline-corrected using TopSpin software (version 2.1, Bruker).

8.1.3. Data analysis

All the acquired ^{1}H NMR spectra were phased, baseline-corrected, and referenced to the chemical shift of TSP or TMS signal at 0 ppm. For metabolic identification, references of

pure compounds from the metabolic profiling AMIX spectra database (Bruker), human metabolome database (HMDB), and Chenomx databases were used. After baseline correction, specific ^{1}H NMR regions identified in the spectra were integrated for each extraction method entering the study using the AMIX 3.8 software package. Then, each integration region was normalized using the tissue weight used from each sample. Data (pre-) processing, data analysis, and statistical calculations were performed in RStudio (R version 3.0.2).

9. Immunoblot analysis (WesternBlot)

9.1. Tissue homogenization and lysis

Samples were smashed in a mortar with liquid nitrogen and the tissue amount of about 1-2 small spoons was added to an eppendorf tube. 300uL of Lysis Buffer (Table 11) were added along with the homogeneizating magnetic beads (0.5mm diameter zirconium oxide ZrO_2 for BulletBlender®, NextAdvance, NY, USA). BulletBlender® was then used at 4ºC for periods of 3min at 8-9 speed level (depending on the tissue). The homogenate was checked and another period of 3min was performed. Samples were placed in a mixing wheel (4ºC, 1h) and then placed at -80ºC until freezing. Samples were then placed again in the mixing wheel (4ºC, 1h) and then placed overnight at -80ºC. Samples were placed again in the mixing wheel (4ºC, 1h) and then placed again at -80º before the last step in the mixing wheel (4ºC, 1h).

Lysis buffer (LB)		
Reagents	Final Conc.	Amount for 100mL
Sodium Phosphate (Na_2HPO_4)	10mM	0.142g
Sodium Fluoride (NaF)	10mM	0.042g
Tris pH 7.5-8*	50mM	0.605g
EDTA	5mM	0.186g
NaCl	150mM	0.870g
Triton X-100	150mM/1%	1mL
H_2O		qsp 100mL**

Table 11. Lysis buffer. *For Tris: 4.03mL TRIS HCl 1M + 0.97mL Tris Base 1M (pH 7.5); ** half of the H2O was added and then the pH was adjusted with 10N HCl, water was then added until final volume. Right before use, protease inhibidor cocktail was added to the lysis buffer (1:10 dilution from stock (1 pill of cOmplete-Roche from Roche in 5mL → 10X)).

These freeze-thaw cycles intend to mechanically disrupt cellular membranes (including mitochondrial membranes) by formation of ice crystals and cell expansion upon thawing,

ultimately leading to rupture (Benov & Al-Ibraheem 2002). Samples were centrifugated (4ºC, 15', 10000rpm) and the supernatant was used for quantification of the protein.

9.2. Protein quantification

The Bradford method (Bradford 1976) was used for quantification of protein. An Standard curve from 0g/mL to 1.5-2g/mL of BSA was used and prepared fresh every time of quantification. Bradford reagent (Bradford, Bio-Rad Protein Assay Dye Reagent Concentrate, Bio-Rad) was diluted 1:5 (10mL Bradford + 40mL dH_2O) and stored at 4ºC after use. 10uL of the sample or Standard were added in the correspondent well (96-well Microplate, NUNC, Denmark) and 200uL of the Bradford working solution were added. The plate was shaked softly so as to release the bubbles in the wells. Then, 5min were waited before reading at 595nm in the spectrofotometer (Synergy HT Multi-Mode Microplate Reader by BioTek®).

9.3. Sample preparation

Once the protein was quantified, the volumes of supernatant, lysis buffer and Laemmli buffer (Table 12) were calculated in order to obtain the desired concentration of protein in the desired final volume.

Laemmli Sample Buffer (LSB)			
Reagens	Final Conc.	Amount for 8mL (4X)	Quantity for 50mL (4X)
Tris pH 6.8	250mM	2mL	12.5 mL
Glicerol	40%	3.2mL	20 mL
SDS	8% (w/v)	0.64g	4g
2-mercaptoethanol	20%	1.6mL	10mL
mQ-H_2O		1.2 mL	7.5 mL
Bromophenol Blue		q.s.p blue color	

Table 12. Laemmli buffer. Preparation: 1mL tubes were stored at RT.

9.4. Western Blotting (WB)

Criterion XT Bis-Tris Gel (#345-0124; 4–12% polyacrylamide gel, 18-well, 30 µl, 13.3W x 8.7L cm, BioRad) were used in a CriterionTM electrophoresis cells for protein quantification studies. The gel was run in XT MES Running Buffer (#161-0789, BioRad) at 90V during sample transition for the stacking gel and then increased to 120V.

Transference of the proteins to the membrane was performed using two techniques in this project: either using a Criterion Transfer Wet Tank or using the Trans-Blot® Turbo™ Transfer System (both from BioRad). Membranes were made of PVDF (Perkin Elmer, #NEF1002). Before the transfer, membranes were activated in methanol during 20s and then washed with distilled water. For the big-size gel WB, ice was used during the transfer to avoid overheating. The transfer was performed at 100V during 75min. Membranes were washed once with Tris-Buffered Saline Tween (TBST, Table 13) Buffer and blocked with 5% powder milk in TBST (RT, 1h). Afterwards, membranes were washed 3 times during 10min each, and submerged in primary antibody for an overnight period at 4ºC (or 1-2h if performed during the day). Then, membranes were again washed 3 times during 10min each, and submerged later in secondary antibody for 1h at RT. Membranes were then washed 3 times during 10min each and finally, Pierce™ ECL Western Blotting Substrate was added on the membranes before being scanned in an ImageQuant LAS 4000 (GE Healthcare). Membranes were being shaked during washings and blockings processes. Stripping was performed using the Restore Western Blot Stripping Buffer (Thermo Scientific), in a shaker at 60ºC for 20min and at RT for another 10min.

TBS-Tween (TBST)			
Reagents	Final Conc.	Amount for 2L	Source, product code
TBS (20x) (Table 14) Tris NaCl	1X 50mM 150mM	100mL	(below this table)
Tween®20 (Sigma Aldrich)	0.05%	1mL	Sigma Aldrich, P1379-500mL
mQ-H2O		q.s.p 2L	

Table 13. TBS-Tween (TBST)

Tris-Buffered Saline (TBS) 20X			
Reagents	Final Conc.	Amount for 2.5L	Source, product code
Tris Base	1M	120g	Serva, 371190.03
NaCl	3M	438.5g	EMD Millipore, 1.06404.5000
HCl (solution)		q.s.p pH 7.4	Panreac, 131020.1611
mQ-H2O		q.s.p 2.5L	

Table 14. Tris-Buffered Saline (TBS) 20X.

9.5. Development, image capturing and analysis

Pierce™ ECL Western Blotting Substrate (Thermo Scientific) was used as the enhanced chemilumescent (ECL) substrate for 1 min over the membrane to detect horseradish peroxidase (HRP). ImageQuant LAS 4000 (GE Healthcare) was used for the digital imaging of blots by chemiluminescence. ImageQuant TL Software (GE Healthcare) was used for the blot images quantification.

9.6. Antibodies

Different antibodies were used for Western Blotting (Table 15).

	Protein name	KDa	Dilution	Commercial provider (reference)
OxPhos	Total OXPHOS Rodent WB Antibody Cocktail. KDa: 20 (CI), 30 (CII), 47 (CIII), 39 (CIV), 53 (CV)	20-53	1:1000	MitoSciences (MS604), abcam (ab110413)
Actin	Monoclonal Anti-beta-Actin-Peroxidase antibody produced in mouse	42	1:25000	Sigma (A3854)
ANT1	Anti-Adenine Nucleotide Translocase 1 antibody	33	1:1000	MitoSciences (MSA02), abcam (110322)
CS	Anti-Citrate synthetase antibody	52	1:2000	abcam (96600)
DNM1L	Dynamin Like Protein-1	79-84	1:1000	BD Transduction Laboratories (611112)
MCAD	Anti-ACADM antibody	47	1:1000	MitoSciences (MS726), abcam (ab110296)
MFN2	Anti-Mitofusin 2 antibody	86	1:500	abcam (56889)
OPA1	Purified Mouse Anti-OPA1	80-100	1:1000	BD Transduction Laboratories (612606)
PGC1A	Anti-PGC1alpha Mouse mAb	113	1:1000	Merck Millipore (ST1202)
PPARA	Anti-PPARalpha Mouse mAb	52	1:1000	EMD Millipore (MAB3890)
SODM	Anti-SOD2 antibody	25	1:4000	abcam (13534)
UCP1	Anti-UCP1 antibody	32	1:1000	abcam (ab10983)

Table 15. Antibodies used for WB

10. Microscopy

10.1. Parafin blocs preparation

10.1.1. Parafin blocs preparation

Pancreas were included in an histology casette and fixed in formalin. The casettes stayed immersed in formalin at 4ºC over night, and then the dehydratation process was performed with the following immersion steps: PBS1X for 15min twice; ethanol 50% for 45min-1h (henceforth, all the steps were performed in the hood); ethanol 70% for 45min-1h or at 4ºC over night; ethanol 70% (different flask) for 45min-1h; ethanol 96% for 45min-1h; ethanol 96% (different flask) for 45min-1h; ethanol absolute for 45min-1h; ethanol absolute (different flask) for 45min-1h; xylene for 45min; xylene (different flask) for 45min; liquid parafin at 60ºC for 1h or over night (in the parafin oven) and finally, líquid parafin at 60ºC (different recipient) for 1h. The blocs were then prepared in a parafin embedding station (Embedding Center, Dispenser + hot Plate, EG1160 by Leica).

10.1.2. Histology cuts

Once the tissue was embedded in molten parafin, the blocs were cut with a microtome (Rotary Microtome, RM2135 by Leica). A bath at 40ºC (Bath, HI1220 by Leica) was used to ease the deposition of the section cuts in the Poly-L-Lisine treated microscope slides. For pancreas, 3 sections cuts of 4 um were taken separated by 150um between them.

10.2. Immunohistochemistry (IHC)

Once the cuts were placed in the microscope slides, the parafin needs to be removed. Thus, the immersion steps performed in the hood were as follows: xylene for 5min; xylene for 5min (different flask); ethanol absolute for 3min; ethanol 96% for 3min; ethanol 70% for 3min; ethanol 50% for 3min and destilled water for 3min. The steps for the staining were: washing step in PBS1X for 5min twice; permeabilization in PBS1X+1%Triton for 20min; washing step in PBS1X for 5min twice; selection of the tissue borders with the PapPen; blocking of unspecific bindings in PBS1X+3%BSA for 30min, washing step in PBS1X for 5min three times; incubation with the primary antibodies in PBS1X+0.1%BSA at 4ºC for an over night period and a washing step in PBS1X for 5min twice. Henceforth, no light exposure was allowed for the following steps: incubation with the secondary antibodies in PBS1X+0.1%BSA for 2h; washing step in PBS1X for 5min twice; incubation with Hoechst 1/500 in PBS1X to stain the nuclei; washing step in PBS1X for 5min and finally, preparation of the microscopy slides to be used in the microscope.

10.2.1. IHC antibodies

Insulin/Glucagon staining antibodies (Table 16).

Protein name	Staining	Dilution	Commercial provider (reference)
Glucagon (Polyclonal Rabbit anti-GCG Ab)	-	1:1000	Dako (A0565)
Insulin (Polyclonal Guinea Pig Anti-Insulin)	-	1:1000	Dako (A0564)
Donkey anti-Rabbit IgG secondary Ab, Alexa Fluor®488 conjugate	green	1:500	Life Technologies (A21206)
Goat anti-guinea pig IgG secondary Ab, Alexa Fluor®555 conjugate	red	1:500	Life Technologies (A21435)

Table 16. Antibodies used for insulin/glucagon staining.

10.2.2. Image obtention

An inverted-fluorescence microscope (DMI6000B, Leica) and a microscope camera (DFC360FX, Leica) were used in order to obtain the images from the different stainings.

10.2.3. Image quantification

ImageJ software was used to measure the area of positive cells and number of cells. Tolonium chloride, also known as toluidine blue, was used to stain the pancreas cut and by scanning the slide with a ruler, the area cut of each slide was measured in order to normalize the values obtained from ImageJ.

10.3. Optical microscopy

Optical microscopy was performed in collaboration to Dr. Laura Herrero (Department of Biochemistry and Molecular Biology, Faculty of Pharmacy, University of Barcelona) at the Pathology Department of the Hospital Clinic (Barcelona).

10.3.1. Histological examination (H&E)

Histological examination was done using 4 μm thick formalin-fixed, paraffin-embedded tissue sections stained with hematoxylin and eosin (H&E). This staining allowed to study the morphology of adipocytes. Hematoxilin (basic compound) stains the nucleus in blue, while eosin (acid compound) is used as counterstaining and it dyes eosinophilic structures in pink/red (ie. erythrocyte, cytoplasm).

10.3.2. Immunohistochemistry

Immunohistochemistry was performed using 4 μm thick formalin-fixed, paraffin-embedded tissue sections. Briefly, slides soaked in xylene were passed through graded

alcohols and into distilled water. Slides were then pretreated with 1 mM EDTA, pH 8.0 in a steam pressure cooker (Decloaking Chamber, Bio-Care Medical) followed by a distilled water wash as instructed by the supplier (Zymed). Subsequent steps were performed at RT in a hydrated chamber. Slides were pretreated with Peroxidase Block (DAKO) for 5 min to quench endogenous peroxidase activity. Each of the following steps were conducted in DAKO diluent for 1 h. Primary polyclonal rabbit anti-murine CD3 antibody (CMC363, Cell Marque) at 1:1.500 was used for T cells staining. Slides were washed in 50 mM Tris-Cl, pH 7.4, and detected with anti-rabbit Envision+ (DAKO). After further washing, brown immunoperoxidase staining was developed using a DAB chromogen (DAKO) and counterstained with hematoxylin (blue).

11. Mitochondrial respirometry

11.1. Substrate-Uncoupler-Inhibitor Titration (SUIT) protocol

Oroboros-2k respirometer (Oroboros® Instruments GmbH Corp, Austria) was used in the respirometry experiments to measure the oxygen consumption by the experimental biological sample. DatLab (Oxygraph-2k-associated software) was used to calculate the negative derivative of the oxygen concentration with respect to time, to provide the respiration values.

A substrate-uncoupler-inhibitor titration (SUIT) protocol (Cantó & Garcia-Roves 2015; Pesta & Gnaiger 2012) using Hamilton® siringes was performed and the titrations were as follows (with a minimum period of 4-5min between titrations to stabilize the slope signal): malate (final concentration 2mM) and pyruvate (20mM) for measuring the **LEAK** state of uncoupled respiration in the absence of ADP (due to proton leak, electron slip and cation cycling that do not depend on ATP synthase activity). **OXPHOS** state was then measured by adding ADP+$MgCl_2$ (5mM) and cytochrome C (10mM) (to check that the membrane was not damaged during sample preparation), followed by additions of glutamate (20mM) for measuring the complex I respiration NADH-dependent (where the proton pumping (CI, CIII, CIV) is partially used by the ATP synthase to drive phosphorylation in a coupled respiration and partially dissipated due to proton leaks in an uncoupled respiration); and later succinate (10mM) for measure the complex II respiration $FADH_2$-dependent along with the respiration of complex I in the **OXPHOS CI+II** state. FCCP added in followed titrations (0.5+0.5+0.25 uM) until reaching the maximal respiration for quantifying the maximal capacity of the electron transport System through the non-physiologic uncoupling of the mitochondrial internal membrane

(**ETS CI+II** State); rotenone (0.5mM) to inhibit complex I and study the maximal respiration of complex II (**ETS CII**); antimycin A (2.5uM) to inhibit complex III and then quantifying the residual oxygen consumption (**ROX** State) that shows any non-mitochondrial respiration and allow to substrat this value from the previous ones.

11.2. Tissue preparation for high-resolution respirometry studies

Fresh tissues were put into a tube containing Biopsy Preservation Solution (BIOPS) (Veksler et al. 1987; Letellier et al. 1992) in order to transfer them to the laboratory for performing the respirometry experiments. However, there was a different procedure to prepare the different samples.

Liver: Liver samples were weighted (8-12 mg) and homogenized using a PBI-Schredder SG3 (Pressure Biosciences Inc; South Easton, MA) so as to obtain a 1mg/mL homogenate with MiR05 medium. Gain of sensor was set at 1 and slope smoothing (number of data points) at N=40. The number of data points uses a polynomial fit to calculate the slope (high N shows highly smoothed curves, low N improves time resolution). All the medium in the O2k chambers (2mL) was exchanged by 2,1mL of this homogenate and all the experiment options in the software were set up.

White adipose tissue (WAT): WAT samples were weighted (120-160 mg) and homogenized using a PBI-Schredder SG3 (Pressure Biosciences Inc; South Easton, MA) so as to obtain a 40mg/mL homogenate with MiR05 medium. Gain of sensor was set at 2 and number of data points at 40. All the medium in the O2k chambers (2mL) was exchanged by 2,1mL of this homogenate and all the experiment options in the software were set up.

Hypothalamus: hypothalamus samples were introduced in a 1.5mL tube and homogenized in 200 uL of MiR05 with the help of a 1.5mL pestile (431-0094, VWR). Afterwards, to improve the homogeneization 100uL of MiR05 were added and five gentle strokes with a needle (25G) were performed. 40uL of this mixture were added to the 2mL chamber that contained MiR05 medium. Protein concentration of the mixture was quantified in order to normalize the respiration values for each sample.

Skeletal muscle: soleus and tibialis anterior (TA) skeletal muscle samples were introduced in two different fresh ice-cold BIOPS-containing 2mL wells. A pair of very sharp angular forceps was used to remove the connective tissue as well as to separate the fiber bundles mechanically. A magnifying lens was used to observe that fibers were teased apart and

stretched out. After the fibers were mechanically separated, the fiber bundles were transferred into 2mL freshly prepared saponin solution for a proper permeabilization (adding 20 ml saponin stock solution of 5 mg saponin/ml BIOPS into the 2mL BIOPS in a new well). The plate with the different wells containing different skeletal muscle samples was put on a shaker on ice with gentle agitation for 30min. Fiber bundles were then transferent to a new 2mL well containing MiR05 and the plate was still under agitation on ice. The connected fiber bundles were taken with the pair of forceps with rounded tip for half a minute on a filter paper to let them dry before placed onto a small plastic plate on a tared balance (Mettler Toledo XA105 DualRange. Max 41g/120g; d=0.01mg/0.1mg). 1-2mg of skeletal muscle sample were enough to be introduced in the O2k chamber, with the proper normalization by tissue weight.

11.3. Reagents and media used for high-resolution respirometry

11.3.1. Substrates

The details chemicals and media used in high-resolution mitochondrial respiratory have been adapted from (Gnaiger 2014). Different substrates were used (Table 17).

Substrates	FW	Stock soln. Conc [mM]	Stock soln. Amount	Comments	Source, product code and storage
G: L-Glutamic acid, sodium salt, C5H8NO4Na (contains 1 mol/mol H2O)	187.1 169.1 anhy-drous	2000	3.742 g/ 10 ml H2O	Neutralize with 5 N KOH, check pH. Divide into 0.5 ml portions. Store frozen at -20 °C.	Sigma, G 1626 RT
M: L-Malic acid, C4H6O5	134.1	400	536 mg/ 10 ml H2O	Neutralize with 10 N KOH, check pH. Divide into 0.5 ml portions. Store at -20°C.	Sigma, M 1000; RT
P: Pyruvic acid sodium salt, C3H3O3Na	110.0	2000	44 mg/ 0.2 ml H2O	Prepare everyday new.	Sigma, P 2256 4°C
S: Succinate disodium salt, hexahydrate, C4H4O4Na2. 6 H2O	270.1	1000	2.701 g/ 10 ml H2O	Adjust pH to 7.0 with 37% HCl. Divide into 0.5 ml portions. Store frozen at -20 °C.	Sigma, S 2378 (100 g); RT

As: Ascorbate sodium salt, C6H7O6Na	198.1	800	1.584 g/ 10 ml H2O	To prevent autooxidation, adjust pH to aprox. 6 with ascorbic acid (a 137.6 mg ml-1 solution of pH aprox. 2). Divide into 0.2 ml portions. Store frozen at -20 °C. Light sensitive.	Sigma, A 4034 (100 g); RT
Tm: TMPD *N,N,N',N'*-Tetramethyl-p-phenylenediamine dihydrochloride, C10H16N2.2 HCl	237.2	200	47.4 mg/ 1 ml H2O	To prevent autooxidation add 0.8 M ascorbate to a final concentration of 10 mM. Divide into 0.2 ml portions. Store frozen at -20 °C.	Sigma T 3134 (5 g); RT
c: Cytochrome c	12500	4.0	50 mg/ 1 ml H2O	Divide into 0.2 ml portions. Store frozen at -20 °C. Light sensitive.	Sigma, C 7752 (50 mg); -20 °C
D: ADP** (Adenosine 5'diphosphate, C10H15N5O10P2K , potassium salt, contains 1 mol/mol H2O)	501.3	500	0.501 g/ 2 ml H2O	Neutralize with 5 N KOH (approx.450 µl), check pH. Divide into 0.2 ml portions. Store frozen at -80 °C.	Sigma, A 5285 (1 g); -20 °C

Table 17. Substrates used for SUIT protocols. ** To keep [Mg2+] constant during respiration measurement mix ADP or ATP with MgCl2 (0.6 mol/mol ADP or 0.8 mol/mol ATP)

11.3.2. Uncoupler

FCCP was used as an uncoupler (Table 18).

Uncoupler	FW	Stock soln. Conc. [mM]	Stock soln. Amount	Comments	Source, product code and storage
F (FCCP): Carbonyl cyanide p-(trifluoro-methoxy) phenyl-hydrazone C10H5F3N4O	254.2	1.0	2.54 mg/ 10 ml ethanol	Divide into 0.5 ml portions. Store in glass vials at -20 °C.	Sigma C 2920 (10 mg); 4 °C

Table 18. FCCP uncoupler used for SUIT protocols.

11.3.3. Inhibitors

Different inhibitors were used (Table 19).

Inhibitors	FW	Stock soln. Conc. [mM]	Stock soln. Amount	Comments	Source, product code and storage
Ama: Antimycin A	540	5.0	11 mg/ 4 ml ethanol	Divide into 0.2 ml portions. Store at -20 °C. Very toxic.	Sigma A 8674 (25 mg); -20 °C
Omy: Oligomycin	800	4 mg/ml	4 mg/ 1 ml ethanol	Divide into 0.2 ml portions. Store at -20 °C. Very toxic.	Sigma O 4876 (5 mg); -20 °C
Rot: Rotenone, C23H22O6	394.4	1.0 *a*	3.94 mg/ 10 ml ethanol	Difficult to dissolve. Store at -20 °C. Light sensitive. Very toxic.	Sigma R 8875 (1 g); R.T.

Table 19. Inhibitors used for SUIT protocols.

11.3.4. Permeabilization agents

Different permeabilization agents were used (Table 20).

Permeabilization agents	FW	Stock sol. Conc.	Stock solution Amount	Comments	Source, product code and storage
Dig: Digitonin	1229.3	8.1 mM	10 mg/1 ml DMSO	Store frozen at -20 °C. Toxic.	Fluka 37008 (1 g); RT
Sap: Saponin	-	5 mg/ml	5 mg/1 ml H2O	Prepare everyday new.	Sigma S 2149 (25 g); RT

Table 20. Permeabilization agents used for mitochondrial respiratory assays.

11.3.5. Mitochondrial Respiration medium MiR05

MiR05 was used as a mitochondrial respiratory medium (Table 21). Given amounts of the listed compounds (Table 21) (except BSA and lactobionic acid) were introduced into a 1L

glass beaker. 800mL of H2O were added and the mixture was dissolved on a magnetic stirrer at 30ºC. 120mL of K-lactobionate stock solution were add and pH was adjusted to 7.1 with 5 N KOH (Sigma P 1767). Final volume was adjusted to 1L with H2O. BSA was dissolved separately to prevent foam building and transferred to the final solution while stirring continuously but gently. pH was checked again and 40mL MiR05 plastic tubes were stored frozen at -20ºC.

MiR05	Final conc.	FW	Addition to 1 litre final volume	Source, product code
EGTA	0.5 mM	380.4	0.190 g	Sigma, E 4378
MgCl2.6 H2O	3 mM	203.3	0.610 g	Scharlau, MA 0036
K-lactobionate	60 mM	358.3 free acid	120 ml of 0.5 M K-lactobionate stock*	Aldrich, 153516
Taurine	20 mM	125.1	2.502 g	Sigma, T 0625
KH2PO4	10 mM	136.1	1.361 g	Merck, 104873
HEPES	20 mM	238.3	4.77 g	Sigma, H 7523
Sucrose	110 mM	342.3	37.65 g	Roth, 4621.1
BSA, essentially fatty acid free	1 g/l	1 g		Sigma, A 6003 fraction V

Table 21. MiR05 respiratory medium. * Preparation of K-lactobionate stock solution: 35.83 g lactobionic acid were dissolved in 100 ml H2O, pH was adjusted to 7.0 with KOH and final volume was adjusted to 200mL with H2O.

11.3.6. Biopsy preservation solution BIOPS

BIOPS (Tables 22 and 23) was used to preserve the tissue samples before mitocondrial respiration (Veksler et al. 1987; Letellier et al. 1992). Given amounts of the listed compounds were introduced into a 1L glass beaker. pH was adjusted to 7.1 with 5 N KOH at 0ºC. 20mL BIOPS plastic tubes were stored frozen at -20ºC.

BIOPS	FW	Stock solution	Addition to 1 litre final	Source and product code
CaK_2EGTA*	2.77 mM	100 mM	27.7 ml	
K_2EGTA*	7.23 mM	100 mM	72.3 ml	
Na_2ATP	5.77 mM	551.1	3.141 g	Sigma, A 2383

$MgCl_2 \cdot 6\ H2O$	6.56 mM	203.3	1.334 g	Scharlau, MA 0036
Taurine	20 mM	125.1	2.502 g	Sigma, T 0625
Na_2Phosphocreatine	15 mM	273.1	4.097 g	Sigma, P 7936
Imidazole	20 mM	68.1	1.362 g	Fluka, 56750
Dithiothreitol (DTT)	0.5 mM	154.2	0.077 g	Sigma, D 0632,
MES	50 mM	195.2	9.76 g	Sigma, M8250

Table 22. BIOPS medium. * Preparation of stock solutions K_2EGTA and CaK_2EGTA:
K_2EGTA: mix 100 mM EGTA (Sigma, E 4378) and 200 mM KOH (Sigma, P 1767) (dissolve 7.608 g EGTA and 2.3 g KOH in 200 ml H2O, adjust the pH to c. 7.0 with KOH).
CaK_2EGTA: dissolve 2.002 g $CaCO_3$ (Sigma, C 4830) in 100 mM hot (80 °C) solution of EGTA (7.608 g / 200 ml) while stirring continuously, add 2.3 g KOH, adjust the pH to c. 7.0.

BIOPS contains the following ion concentrations:	
Ca2+ free	0.1 µM
Mg2+ free	1 mM
MgATP	5 mM
Ionic strength	160 mM

Table 23. BIOPS ion concentrations.

Saponin solution

Saponin solution for muscle permeabilization was prepared fresh everyday. 5mg of saponin (Sigma, S 2149; 25 g) were added to 1mL BIOPS to prepare the saponin stock solution. 21 µL of the saponin stock solution were added to 2mL BIOPS.

12. Statistical analyses

Results are expressed as Mean±SEM. The statistical significance among the three experimental groups was assessed using one-way ANOVA, and differences between means were subsequently tested by Tukey post-hoc test. Data curation involved the removal of values that were ±2 standard deviation (SD) in puntual situations. A p-value <0.05 was considered significant in all cases, meaning a confidence interval of 95% and setting significance level at α=0.05. Tendencies with p-value between 0.05 and 0.07 are also indicated. All statistical analyses were performed using GraphPad 6 (GraphPad Software, Inc; La Jolla, CA, USA).

The integrative analysis was performed in collaboration to Dr. Roger Guimerà and Dra. Marta Sales-Pardo in the SEES:lab (Universitat Rovira i Virgili, Tarragona). For these approaches, non-parametric Mann-Whitney U test was used instead of parametric t-test,

and non-parametric Krustal-Wallis one-way analysis of variance instead of parametric ANOVA One-way test.

13. Integrative approach

The approach in this PhD thesis pretends to be holistic in the data integration including pathway definitions and statistical analysis of all the data obtained in order to understand the T2DM disease process in an integrative and systemic manner. Hence, first steps in analyzing and integrating the heterogenic data through different computing approaches were performed.

13.1. Data Analysis – correlations and comparisons of multiple parameters

The first part of the data analysis was performed in collaboration with the SEES:lab at Department of Chemical Engineering, at Universitat Rovira i Virgili (Tarragona, Spain) under the supervision of Dr. Marta Sales-Pardo, Dr. Roger Guimerà, and Dr. Antoni Aguilar.

13.1.1. Data Base (DB) design and structure

A Content Management System (CMS) DB was used in order to dump all the data obtained in this study. A CMS is a computer application that allows dumping and editing data as well as modifying content and performing maintenance from a central interface. Thus, a CMS needs two elements: a front-end user interface or a content management application (CMA), that is a website (idibaps.seeslab.net), in which the user can dump the data; and the Content Delivery Application (CDA) that compiles all the information dumped through the CMA and updates the website. DB was designed to cover the needs of the consecutive data analysis and programmed and edited in collaboration with the SEES:lab researchers, at Department of Chemical Engineering, at Universitat Rovira i Virgili (Tarragona, Spain). It is worth mentioning that it is in fact a dynamic DB meaning that data can still be dumped or removed.

The DB includes a template for each mice where all the available information that follows is dumped (Figures 8 and 9):

- *Phenotypical information*: animal identification, group (Control, HFD or Intervention), inclusion or exclusion of the study, body weight (BW), IGTT and ITT glucose levels at different timepoints, weight of the collected tissues, triglyceryde levels in different tissues, etc.
- *Specific-tissue data* including mitochondrial respiratory values, gene expression data, protein content data, targeted metabolomics data, etc.

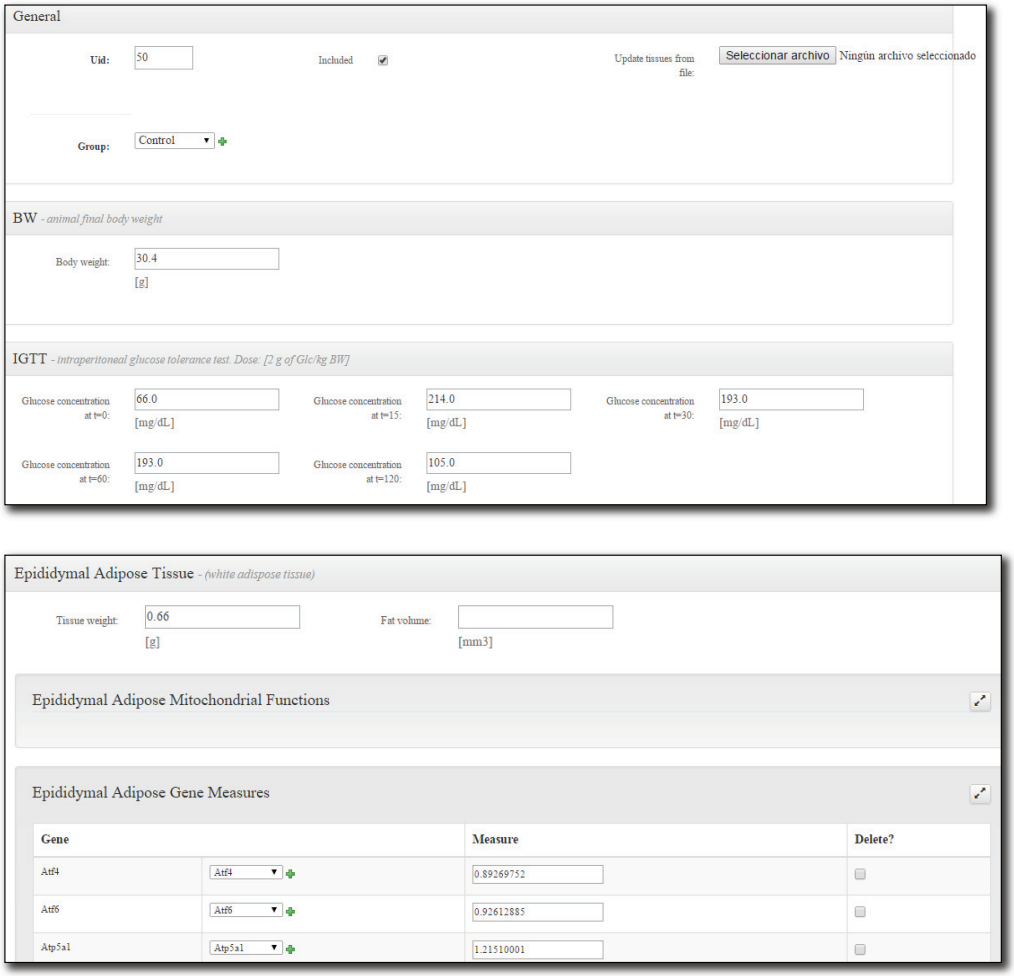

Figure 8. Partial representation of data fields of the DB.

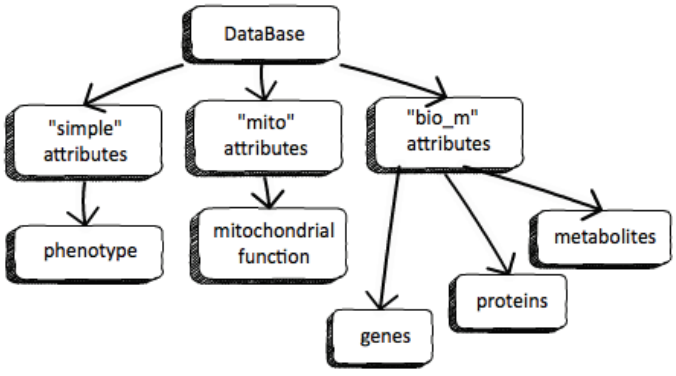

Figure 9. Data structure within the DB.

Where the "simple" attributes acccount for **phenotypical data**; the "mito" attributes for **mitochondrial funcional data**; and the "bio_m" attributes for **genes, protein and metabolites measurements**.

13.1.2 Data obtention from the DB

The first part of the data analysis was performed at the SEES:lab at Department of Chemical Engineering, at Universitat Rovira i Virgili (Tarragona, Spain).

Python, a high-level programming Language, was used for computing the codes for the correlations and comparisons analysis. The data from the DB was called from the code through a `pandas.DataFrame` data structure. Pandas (http://pandas.pydata.org/) is a software library for Python programming language which allows data manipulation and analysis. `pandas.DataFrame` creates a 2-dimensional labeled data structure with different columns and different rows. `pandas.DataFrame` can have different types of inputs, such as 1D `numpy.array`, lists, dics or Series; 2D `numpy.array`, another DataFrame, etc. The `pandas.DataFrame` accepts "index" (row labels) and "columns" (column labels) as arguments. An script **dfgenetator.py** was used to generate the DataFrame from the DB before the analysis.

i.e. we want to obtain the mitochondrial function data from de DB, so first we include only the included mice in the study `included=True`:

```
mControl = Mouse.objects.filter(included=True, group='Control')
mHFD = Mouse.objects.filter(included=True, group='HFD')
mIntervention = Mouse.objects.filter(included=True, group='Intervention')
```

then we generate the DataFrame only with these mice that include mitochondrial function data `mito=True`:

```
dfControl = get_mice_data(mControl, exclude_tissues=['gastrocnemius', 'pancreas', 'blood'], simple=False, mito=True, bio_m=[])
dfHFD = get_mice_data(mHFD, exclude_tissues=['gastrocnemius', 'pancreas', 'blood'], simple=False, mito=True, bio_m=[])
dfIntervention = get_mice_data(mIntervention, exclude_tissues=['gastrocnemius', 'pancreas', 'blood'], simple=False, mito=True, bio_m=[])
```

NumPy and SciPy were also used for working with multi-dimensional arrays and matrices as well as for calculating high-level mathematical functions. Matplotlib, a plotting library for the Python programming language, was used for graphical representations.

13.1.3 Data Analysis – correlations and comparisons

13.1.3.1. Inter-group correlations and comparisons

The approach atempted to compare the three experimental groups at the same time was achieved by defining a 3-point vector for each parameter/attribute in which the 3 points

correlated to the mean of this given parameter/attribute for 1) Control group 2) HFD-pathological group and 3) Intervention group. In this approach, given that each vector gave information about a certain parameter in a certain tissue for the 3 groups had no limitation regarding common assessed parameters and allowed to represent all the parameters in all the tissues. This approach allowed to build up different matrix to compare the phenotypical data, the mitochondrial function data in all the tissues, the gene expression data in all the tissues and the metabolites values in all the tissues. For the correlation and comparison analysis to compare these 3-point vectors *attribute=[Ctrl mean, HFD mean, Int mean]*, Cosine similarity was used.

13.1.3.2. Across-groups patterns definition

The across-groups approach atempted to visually show how much some parameters were reversed after the intervention was performed. For this purpose, the vectors aforementioned were used (ie. *attribute=[Ctrl mean, HFD mean, Int mean]*). Mann-Whitney comparisons were used to compare if the means among groups were significantly different or not (ie. Ctrl mean vs HFD mean for a given parameter). Once the significant differences were calculated, a pattern was defined taking them into account (Table 24). A pattern list is showed in the table below:

General patterns			HEX	RGB	Group: pattern
B	132		#c7e9c0	199/233/192	green: 132
D	231		#a1d99b	161/217/155	green: 231
L	121		#74c476	116/196/118	green: 121
C	213		#41ab5d	65/171/93	green: 213
E	312		#238b45	35/139/69	green: 312
M	212		#006d2c	0/109/44	green: 212
A	123		#4292c6	66/146/-	blue: 123
F	321		#08519c	8/81/156	blue: 321
H	122		#de2d26	222/45/38	red: 122
I	211		#a50f15	165/15/21	red: 221
J	112		#969696	150/150/150	grey: 112
K	221		#525252	82/82/82	grey: 221
G	111		#000000	0/0/0	black: 111

Table 24. Pattern list, indicating the pattern and the color associated.

The table shows all the different patterns that can appear depending on which means are significantly different after the Mann-Whitney test. *Ie. a reversion pattern like the one*

defined with the letter 'L' shows a 121 patterns meaning that a parameter was significanly increased in the HFD compared to the Ctrl group and in the HFD compared to the Int group, indicating that it was due to an increase of the parameter mean value.

A code of colours was established to define the different patterns, this way, **green** accounts for a reversion pattern where the HFD is significantly different from the Ctrl and Int and in which different options can appear (ie. the Int can still be significantly different from the Ctrl, leading to a 132 pattern); **blue** accounts for an *emphasis*, a tendency across the groups to increase or decrease (ie. the HFD group has an significantly increased value mean compared to the Ctrl group and the Int group has also a significant increase in comparison to the HFD group); **red** indicates no reversion regarding the intervention group, so the mean value in the HFD group, which is significantly different from the Ctrl group, is not different in comparison to the Int group; **grey** accounts for a difference in the Int group in comparison to the other two groups, between the ones there is no difference; and **black** indicates that there are no significant differences in any of the comparisons between groups.

Moreover, a crossing pattern was added in the cases when there was no transitivity property. This happened in 3 scenarios: when Ctrl vs HFD showed no statistical difference, Ctrl vs Int showed no statistical difference, but HFD vs Int showed a statistical difference (Ctrl≈HFD, Ctrl≈Int, HFD≠Int); when Ctrl≈HFD, Ctrl≠Int, HFD≈Int; and when Ctrl≠HFD, Ctrl≈Int, HFD≈Int. In these cases, the minus letter of the letter that followed a certain given pattern was used. *Ie. L" and minus "l" shared color although "l" was represented with a crossing pattern due to the lack of transitivity property.*

Once these patterns were defined for gene expression and metabolites parameters, a graphical representation of stacked bars allowed us to see which relative percentatge of all the genes showed each of the patterns, and the same graphical representation was performed for metabolomics and mitochondrial function data.

Henceforth, "non-reversion" terminology (also mentioned in this Thesis as "non-reverted") would account for a situation in which LI was not reverting and recovering a given parameter. Moreover, reversion would define a recovery and "half-reversion" a state halfway between *Ctrl* and *HFD* groups values.

13.2. Data Analysis - RNAseq data

13.2.1. Definition of reversion patterns and gene ontology enrichment analysis

RNAseq data from epididymal white adipose tissue (eWAT) was curated and genes were divided in the possible expression patterns. That is, pair comparisons (*Ctrl* vs *HFD*, *Ctrl* vs *Int*, and *HFD* vs *Int*) were performed between groups and fold change calculated. Afterwards, p-value was calculated and adjusted for each pair comparison and genes divided into the different possible patterns.

Thus, among all the variants detected (21761), 5147 (23.65%) were separated in expression patterns. The patterns were defined and named as in Materials and Methods part 13.1.3.2 section. All the genes detected in RNAseq experiments were separated attending the reversion pattern. For graphical representation, gene expression was re-scaled and translated into Z-scores, and a gene for each row represented in a color scale meaning that the reddish, the more expressed and the more blue, the less expressed.

Another representation included the use of GOrilla (Gene Ontology enRichment anaLysis and visuaLizAtion tool). Running mode was set up with two unranked lists of genes: target list consisted of the given pattern to study, and background list consisted of the 21761 genes detected during sequentiation. Different ontologies were used including process, function and component. Finally, p-value tresshold was set at 10^{-10} given that setting the tresshold in a p-value bigger than 10^{-10} led to too big representations.

13.2.2. Detection of *non-reverted* gene clusters by using a protein-protein interaction (PPI) network approach

After the correlations and comparison analysis, and the concurrently gene ontology analysis were performed, the objective to integrate heterogenic data in one layer was the reason for a PhD stay. Thus, the second part of the data analysis was performed under the supervision of Dr. Kirstine Belling at the Integrative Systems Biology Group at the Center for Biological Sequence Analysis (CBS) at the Department of Systems Biology at the Technical University of Denmark (DTU) in collaboration with the Disease Systems Biology group at The Novo Nordisk Foundation Center for Protein Research (CPR) at Faculty of Health and Medical Sciences at University of Copenhagen (KU). However, the tools for this analysis were not yet implemented in the host laboratory and a “network-like” analysis of the RNAseq data available was performed.

In this approach, Python and Perl programming languages were used. Although the starting point for the network analysis approach was the raw data from the RNAseq from liver and WAT samples from the three experimental groups (*Ctrl*, *HFD*, *Int*), this approach involves work with protein-protein interaction (PPIs) networks and protein complexes. Gene/variants were translated into IDs that allowed these entities to be used for PPIs studies. Henceforth, entities will be named as "genes" although they are outcomes from a PPIs network.

13.2.1. The reversibility index (RI) definition

The reversibility index consists of a a numeric value that could define how reversible was the Intervention (*Int*) group compared to the changes observed between the *Ctrl* and the *HFD* group. This value allows observing if a given gene was reverted after intervention or not, and if not, to what extent.

The RI is defined for each gene, and an average of the index is calculated for each protein complex. The RI is calculated based on the mean value for each experimental condition as follows:

$$RI=[(mean\_Int-mean\_Ctrl)/(mean\_HFD-mean\_Ctrl)]*100$$

Considering the RI, different scenarios are possible (Figure 10, Table 25).

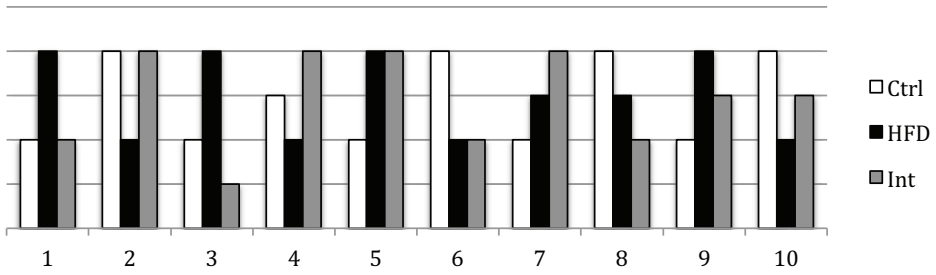

Figure 10. Possible cases across the three experimental groups..

Case	1	2	3	4	5	6	7	8	9	10
RI	0%	0%	-50%	-100%	100%	100%	200%	200%	50%	50%

Table 25. RI values for each of the possible cases.

Cases 1 and 2 would account for a reversion; cases 3 and 4 for an "over-reversion"; cases 5, 6, 7 and 8 for a *non-reversion* and cases 9 and 10 for a *half-reversion*.

Considerations: The closer RI is to 0% the more similar is the Int mean to the Ctrl mean that is, the more reverted the gene is.

13.2.2. Protein complex's RI approach

RI was used in the protein complexes approach, and steps performed were as follows:

1. Cleaning and translation of the raw data:

Raw RNAseq data was cleaned by means of removing gene/variants where no expression was detected. Only lines in which the sample values were equal or above zero, and lines were group means were above zero, were included for the consequent analysis. Hence, genes that were not detected were removed.

2. Group-pair comparisons:

Statistical analyses allowed calculating which genes/variants were significantly changed from one experimental group to another. For each tissue, the group-pair comparison: *Ctrl* vs *HFD* was performed.

The criteria used to consider that a given gene is significantly different between two experimental groups were:

- only variants with a difference with p-values<0.05 were considered (t-student tests were run between the two matrixes of values of the two groups for each pair comparison)
- a cut-off of reads=5.8 was established for the reads that is, at least there is one of the two means of the groups that are being compared with a value above 5.8 (Appendix 1)

P-value was considered significant below 0.05.

After this process, the genes/variants were translated from EntrezGene ID to Ensembl ID for mice (ENSMUSG) and afterwards to paralogous Ensembl ID for humans (ENSG). ENSG IDs are needed to run the code that defines the PPIs.

Another process performed in this step was to limit the duplicates in ENSG ID codes. That is, different EntrezGene ID were translated to the same ENSG ID meaning that they describe variants not contemplated in the ENSG annotation. The gene/variant with the highest expression value was considered for translation to ENSG ID.

The datasets to translate from EntrezGene ID to ENSMUSG ID and ENSG ID were downloaded through biomart (http://www.biomart.org/biomart/martview) from the Ensembl genes 80 database (Sanger, UK).

Glossary

nodes: elements of a network (proteins in the current case)

edges: binary relations between nodes. In this study observed physical protein-protein interactions that have been confidence scored based on network topology and experimental reproducibility.

neighbor: the nodes connected by an edge

protein complex: cluster of nodes (proteins) connected by edges

hubs: central nodes in a network connecting to multiple interacion *partners*

3. Definition of PPIs:

In order to run the code to extract the PPIs, the ENSG ID were translated to InWeb ID (protein ID) for the CH (*Ctrl-HFD*) comparison file that is, henceforth, only these genes/variants that changed significantly from the *Ctrl* to the *HFD* group were considered.

The PPIs were extracted using a Perl code. No neighbors were considered, thus, only first-order PPIs were present in the lists uploaded to run the script. The Perl code run in this step used the InWeb PPIs database, a file created and curated by researchers at CBS that has been previously used to work with PPI networks (Pers et al. 2011; Lage et al. 2010; Thomas et al. 2013).

4. Definition of hubs and protein complexes:

Among the PPIs detected in each of the two tissues studied, protein complexes were defined. Before defining them, the InWeb IDs were translated back to ENSG ID. Once the PPIs were represented with the ENSG IDs, these IDs were used to find the hubs among all the genes described in the PPIs list. Finally, only hubs having at least five interaction partners were considered for the subsequent analytical steps.

5. RI for each gene and complex:

The RI was calculated for each gene. After the complexes were defined, it was possible to calculate the Avg_RI for the complexes. Although the Avg_RI was calculated for all complexes, the standard deviation (SD) allowed performing a cut-off of the significant results.

For this purpose, the Avg_RI/SD ratio was calculated for each complex, studying the amount of variation or dispersion of all the RI values of the genes of the complex. Concretely, only Avg_RI/SD ratios above 1 were considered and the included ones were ranked according to this ratio. The ten complexes with highest Avg_RI/SD ratio were further studied.

6. Classification of complexes according to the Avg_RI

According to the possible scenarios described above in point 5 with the RI, the complexes were classificated in different groups (Table 26).

Physiological assumption	Avg_RI
Reverted	- ∞ to 25%
Half-reverted	25% to 75%
Non-reverted	75% to ∞

Table 26. Classification according to RI value.

7. Network and graphical representation

Cytoscape 3.2.0 (www.cytoscape.org) was used to graphically represent different networks. This software was used to represent the most relevant complexes. For network building, the data dumped to Cytoscape included the node information as well as the confidence score for each PPI. All this mentioned confidence score values come from the InWeb database. ENSG IDs were translated in this case to HUGO Gene Nomenclature Committee (HGNC) names from Ensembl Database. ENSG IDs are better to represent the genes but HGNC supposed an easier way to visually identify them in this analysis. Different colors, shapes and borders were used to discern the different types of nodes, and different line types were used to discern the different types of PPIs.

RESULTS

Results

Considering the cohorts used for this PhD thesis and following the inclusion criteria mentioned in the Materials and Methods part, the final sample size for each experimental group was, respectively: n=95 for *Ctrl* group, n=76 for *HFD* group, and n=54 for *Int* group (Figure 11). The non-included animals in each group due to application of the inclusion criteria were n=26 for *Ctrl* group, n=28 for *HFD* group, and n=1 for *Int* group. It is important to mention that the 55 mice that were destined to undergo LI were previously included as *HFD* mice. Thus, a total of 131 *HFD* mice followed the inclusion criteria, and 55 of them were destined to become *Int* group.

This way, 78.5% of the study animals in *Ctrl* (95/121), 82.4% in *HFD* (131/159), and 98.2% in *Int* group (54/55) followed inclusion criteria.

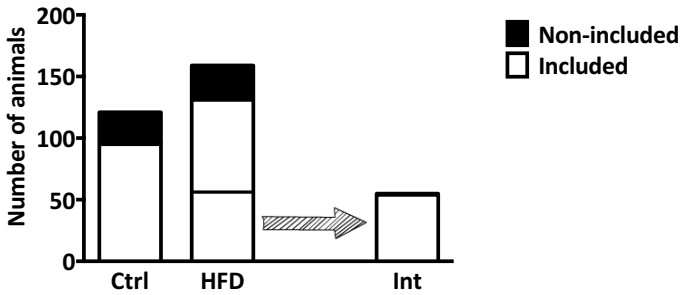

Figure 11. Number of animals included and non-included.

1. Phenotype overview

1.1. BW increased after HFD and reverted upon LI

By the time mice were sacrificed at the end of the experiments (*Ctrl* and *HFD* groups) or diet plus LI (*Int* group), mice were weighted (Figure 12A). Analyzing BW evolution (Figure 12B), and also final BW (Figure 12A), it can be appreciated how the animals that underwent LI ended up with BW values comparable with *Ctrl* group. Final BW were *Ctrl*: 29.33±0.24g; *HFD*: 43.21±0.42g; *Int*: 29.59±0.21g.

It is important to point out that animals from *HFD* group assigned to undergo the LI showed no BW differences with mice assigned to the *HFD* group itself (Materials and Methods, section 1.1).

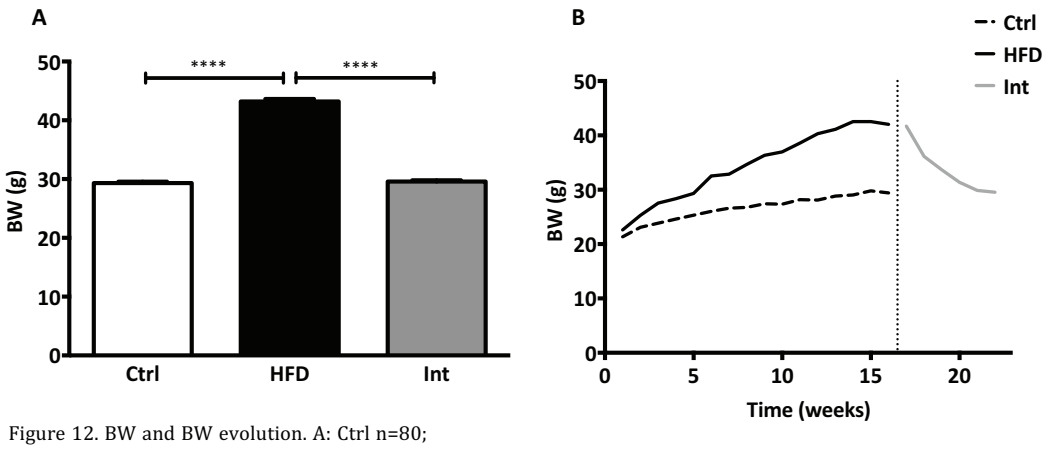

Figure 12. BW and BW evolution. A: Ctrl n=80; HFD n=70; Int n=46. B: Same animals used as in A. Mean±SEM, ANOVA One-way, Post-hoc Tukey; ****p<0.0001.

1.2. Fat content increased after HFD and reverted upon LI

The pathological *HFD* group had significantly higher fat volume compared to *Ctrl* and *Int* groups (Figure 13A and 13B). Values were *Ctrl*: 2035.00±498.94mm^3; *HFD*: 5413.85±964.74mm^3; *Int*: 2201.80±368.88mm^3. EchoMRI was used to discern between lean and fat mass content.Same significant pattern for the *HFD* mice to be increased in comparison to the other groups was observed in both types of mass (Figure 13C), *being the values for fat mass Ctrl: 3.60*±0.12g; *HFD*: 11.65±0.90g; *Int*: 5.35±0.88g; and for lean mass *Ctrl*: 23.06±0.58g; *HFD*: 25.85±0.59g; *Int*: 21.24±0.22g. However, regarding lean mass the *Int* group showed an almost significant decrease (p=0.0597) compared to *Ctrl* group.

1.3. The increase in tissue weights after HFD was reverted upon LI

The same way BW was annotated during the mice sacrifice, other tissue' weights were also measured. Of note, tissues were gently dried a little bit spreading and tapping them in dry absorbing paper before taking the measure. This way, a significant increase in pancreas, epididymal WAT (eWAT) and liver weight was observed in the *HFD* group. These increased values were significantly reverted in the *Int* group, reaching weight values not different from the *Ctrl* group (Figure 14A, Table 27). However, when the tissue' weights were normalized by the BW of each animal, the differences observed in the *HFD* and *Int* groups regarding liver weight disappeared (Figure 14B, Table 27). This means, the proportion of the increase in liver weight was similar to the proportion of the increase in the animal BW, different from pancreas and eWAT where the proportion of the increase in tissue weight was greater than the increase in animal BW.

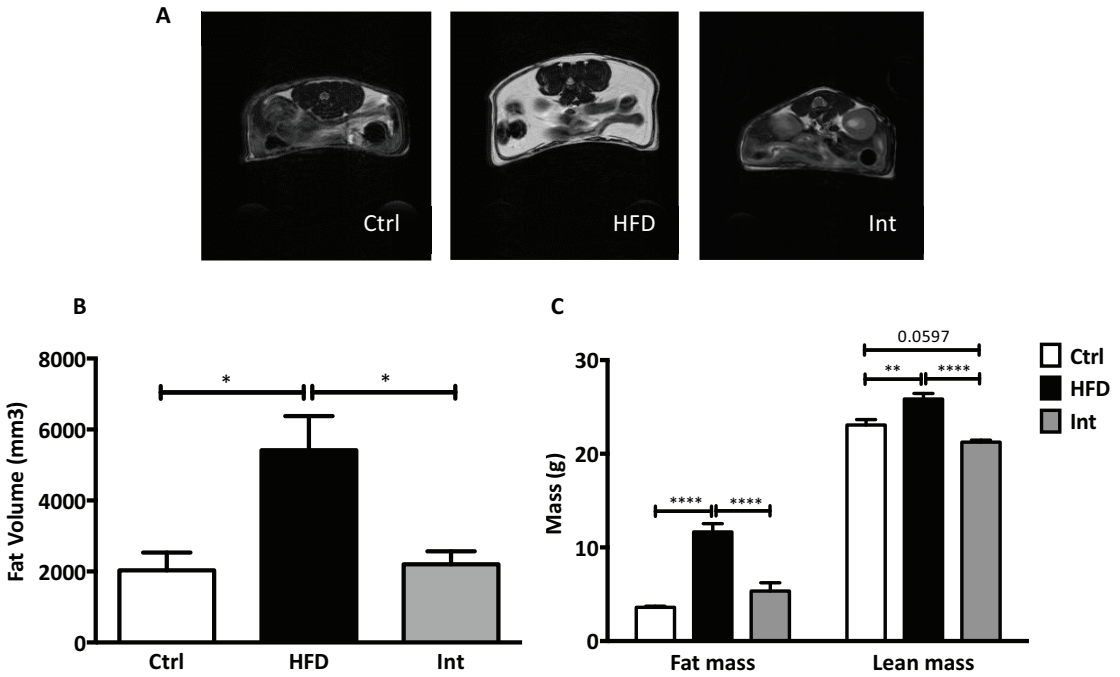

Figure 13. Body composition. A: 7Teslas scan representative images of the three experimental groups, where fat is indicated in white contrast, after 12 week on diet (Ctrl and HFD groups) and after the LI (Int). B: quantification of the fat volume observed in the previous figure. Ctrl n=4; HFD n=4; Int n=3. C: quantification of the fat and lean mass with the EchoMRI technique. Ctrl n=9; HFD n=6; Int n=6. Mean±SEM, ANOVA One-way, Post-hoc Tukey; *p<0.05, **p<0.01, ****p<0.0001.

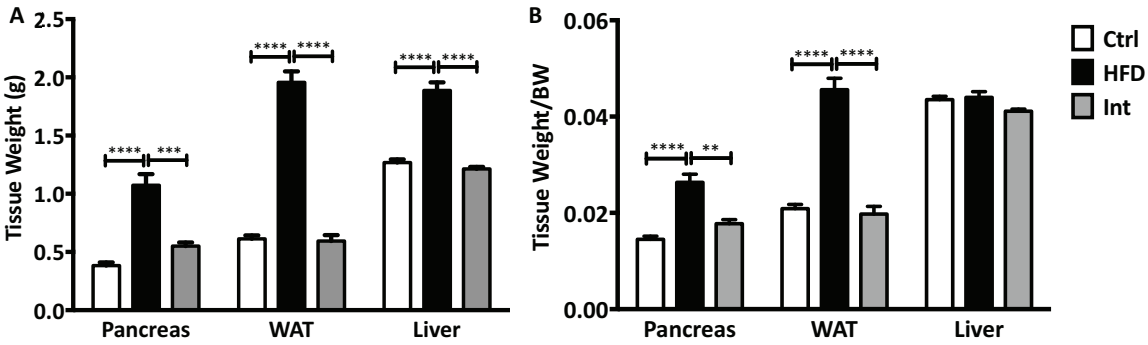

Figure 14. Tissue weights. A: pancreas, WAT and liver weights without normalization. Ctrl n=6/32/35 (pancreas/WAT/liver); HFD n=6/32/37; Int n=4/26/27. B: pancreas, WAT and liver weights normalized by BW. Same number of animals as in A. Mean±SEM, ANOVA One-way, Post-hoc Tukey; **p<0.01, ***p<0.001, ****p<0.0001.

Tissue weight no normalized (g)				Significance		
	Ctrl	HFD	Int	C - H	C - I	H - I
Pancreas	0.383±0.028	1.073±0.095	0.550±0.032	****	ns	***
eWAT	0.613±0.030	1.957±0.094	0.594±0.051	****	ns	****
Liver	1.268±0.027	1.888±0.069	1.213±0.018	****	ns	****
Tissue weight normalized by BW				Significance		
	Ctrl	HFD	Int	C - H	C - I	H - I
Pancreas	0.014±0.001	0.026±0.002	0.018±0.001	****	ns	**
eWAT	0.021±0.001	0.046±0.002	0.020±0.002	****	ns	****
Liver	0.044±0.001	0.044±0.001	0.041±0.0004	ns	ns	ns

Table 27. Tissue weight values. Mean±SEM. ANOVA One-way, Post-hoc Tukey; **p<0.01, ***p<0.001, ****p<0.0001, ns=no significant. C-H: comparison Ctrl and HFD groups; C-I: comparison Ctrl and Int groups; H-I: comparison HFD and Int groups.

Liver weight ranged from 1.02 to 1.50g in *Ctrl* group, from 1.29 to 3.00g in *HFD* group, and from 1.02 to 1.52g in *Int* group. 64.3% of *HFD mice* included mice showed a liver weight at least 35% higher than *Ctrl* mice.

1.4. TG were increased after HFD in insulin-sensitive tissues and reverted upon LI

Ectopic FA accumulation was studied by measuring TG levels in different insulin-sensitive tissues. In the case of the liver, the significant increase in TG levels in the *HFD* group was reverted in the *Int* group (Figure 15A, Table 28). The same pattern was observed in the oxidative skeletal muscle soleus (Figure 15B, Table 28) although in the glycolytic skeletal muscle tibialis anterior (TA), no differences were observed (Figure 15C, Table 28).

TG concentration (ug TG/ug of protein)				Significance		
	Ctrl	HFD	Int	C - H	C - I	H - I
Liver	193.00±39.91	1582.07±483.79	57.79±18.47	**	ns	**
Soleus	143.64±15.30	336.79±73.63	106.84±14.60	*	ns	**
TA	5.95±1.13	8.42±1.28	7.21±2.15	ns	ns	ns

Table 28. TG concentrations in insulin-sensitive tissues. Mean±SEM. ANOVA One-way, Post-hoc Tukey; *p<0.05, **p<0.01, ns=no significant. C-H: comparison Ctrl and HFD groups; C-I: comparison Ctrl and Int groups; H-I: comparison HFD and Int groups.

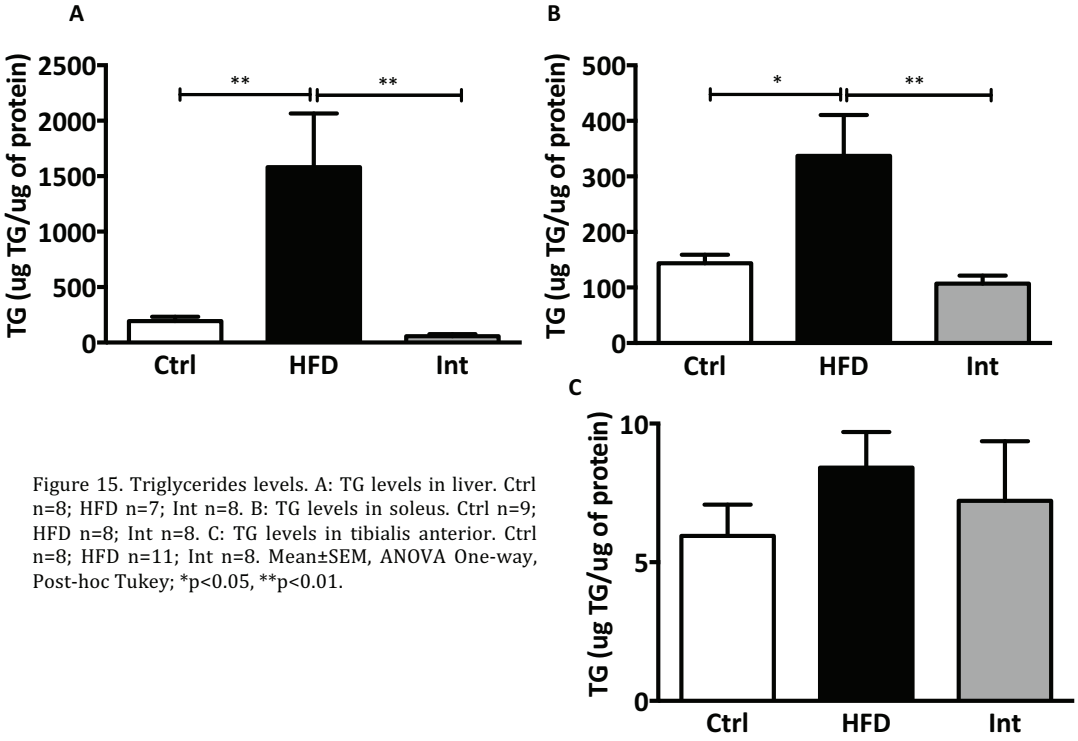

Figure 15. Triglycerides levels. A: TG levels in liver. Ctrl n=8; HFD n=7; Int n=8. B: TG levels in soleus. Ctrl n=9; HFD n=8; Int n=8. C: TG levels in tibialis anterior. Ctrl n=8; HFD n=11; Int n=8. Mean±SEM, ANOVA One-way, Post-hoc Tukey; *p<0.05, **p<0.01.

1.5. Glucose intolerance and IR after HFD were partially reverted upon LI

To assess glucose homeostasis on the different experimental groups an IGTT and an ITT were performed. These studies showed that *HFD* mice were more glucose intolerant (Figure 16A) and insulin resistant than *Ctrl* mice (Figure 16B). The glucose intolerance and insulin resistance present in *HFD* mice were reverted in *Int* mice after LI (Figure 16A and 16B). AUC values for the IGTT test were *Ctrl*: 15045±522; *HFD*: 33712±1011; *Int*: 6985±824 (*Ctrl* vs *HFD* p<0.0001, *Ctrl* vs *Int* p<0.0001, *HFD* vs *Int* p<0.0001). According to glucose homeostasis experiments, *HFD* mice showed glucose intolerance and insulin resistance, and on the contrary, *Int* mice showed glucose tolerance and insulin sensitivity suggesting the reversion of the pathological hyperglycemia. Insulin secretion *in vivo* was also assessed during the IGTT and, although the *Int* mice seemed recovered regarding glucose homeostasis, this assay showed how they were compensating the previous pathological state, in part, by over-secreting insulin (Figure 16C, Table 29). However, it is important to point out that while the *HFD* and the *Int* mica were secreting similar amounts of insulin after the glucose bolus, the *Int* mice were able to handle it and therefore showed increased glucose tolerance and insulin sensitivity.

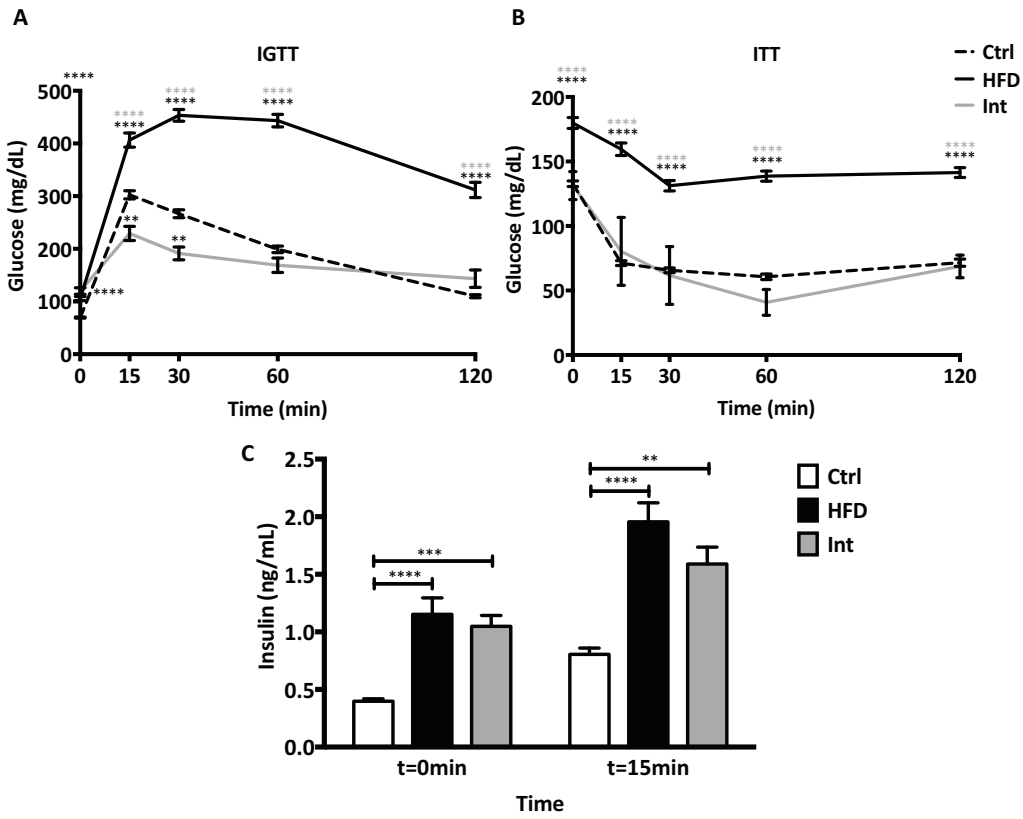

Figure 16. Glucose homeostasis. A: IGTT after overnight (16h) fasting. Ctrl n=54; HFD n=48; Int n=12. B: ITT after 4 hours fasting. Ctrl n=55; HFD n=47; Int n=6. C: In vivo insulin secretion. Ctrl n=15; HFD n=19; Int n=13. Mean±SEM, ANOVA One-way, Post-hoc Tukey; **p<0.01, ***p<0.001, ****p<0.0001. Black asterisks mean significance vs Ctrl, and grey asterisks mean significance vs Int.

Insulin concentration during IGTT (ng/mL)				Significance		
min	Ctrl	HFD	Int	C - H	C - I	H - I
t=0	0.397±0.021	1.152±0.143	1.048±0.094	****	***	ns
t=15	0.805±0.055	1.956±0.165	1.589±0.146	****	**	ns
Glucose concentration during IGTT (ng/mL)				Significance		
t=0	69.556±1.029	105.667±3.995	119.750±6.157	****	*****	ns
Glucose concentration during ITT (ng/mL)				Significance		
t=0	132.782±2.192	179.809±4.200	131.333±4.447	****	ns	****

Table 29. Insulin and glucose concentrations during IGTT and ITT *in vivo*. Glucose concentrations represent only mice for which insulin was measured. Mean±SEM. ANOVA One-way, Post-hoc Tukey; **p<0.01, ***p<0.001, ****p<0.0001, ns=no significant. C-H: comparison Ctrl and HFD groups; C-I: comparison Ctrl and Int groups; H-I: comparison HFD and Int groups.

1.6. Increased fasting leptin plasma levels after HFD were reverted upon LI

Fasting (16h) leptin and adiponectin levels were also assessed. The significant increase in leptin in *HFD* group indicating hyperleptinemia was reverted after LI was performed (Figure 17A). Leptin concentration values were *Ctrl*: 2.767±0.369ng/mL; *HFD*: 25.826±1.302ng/mL; *Int*: 8.042±1.005ng/mL. However, *Int* mice leptin levels were still increased significantly compared to the *Ctrl* group. No differences were observed in adiponectin levels through the three experimental groups (Figure 17B). Adiponectin concentration values were *Ctrl*: 12.404±0.348ng/mL; *HFD*: 13.266±0.387ng/mL; *Int*: 12.686±0.451ng/mL.

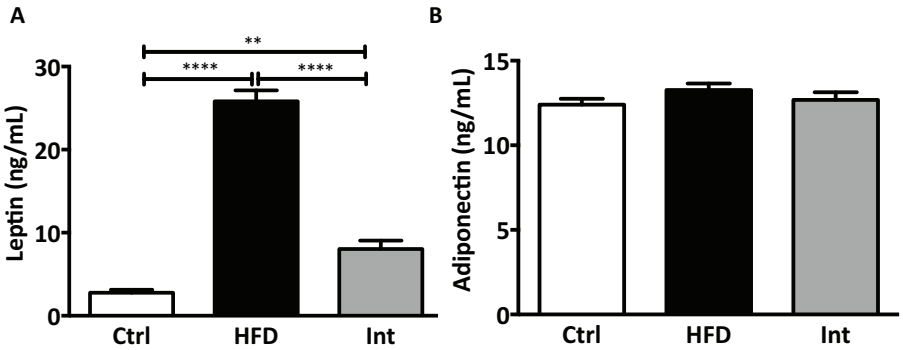

Figure 17. Leptin and adiponectin levels. A: leptin plasma concentration. Ctrl n=14; HFD n=20; Int n=14. B: adiponectin plasma concentration. Ctrl n=10; HFD n=11; Int n=11. Mean±SEM, ANOVA One-way, Post-hoc Tukey; **p<0.01, ****p<0.0001.

1.7. Decreased oxygen consumption after HFD was not reverted upon LI

Indirect calorimetry experiments allowed assessing whole body oxygen consumption for the three experimental animal groups. *HFD* mice showed a decrease in the oxygen consumption (VO_2) in comparison to *Ctrl* mice (Figure 18, Table 30). This decrease was not reverted after LI, although a tendency to recover *Ctrl* mice VO_2 values was observed in the *Int* group during the light phase.

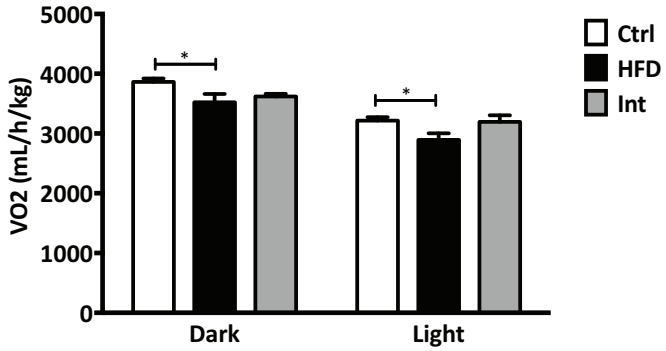

Figure 18. Oxygen consumption. Average VO_2 measurements normalized by the animal BW during the dark and light phase of the day. Ctrl n=9; HFD n=5; Int n=6. Mean±SEM, ANOVA One-way, Post-hoc Tukey; *p<0.05.

Indirect calorimetry parameters					Significance		
		Ctrl	HFD	Int	C - H	C - I	H - I
VO_2 (mL/h/kg)	Dark	3864±57	3522±140	3619±46	*	ns	ns
	Light	3217±56	2893±111	3195±109	*	ns	ns
Ambulatory movement (Cnts)	Dark	20982±2261	18698±1725	21645±3408	ns	ns	ns
	Light	7064±673	5979±892	13172±2865	ns	*	*
Fine movement (Cnts)	Dark	11003±731	10669±440	8125±425	ns	*	0.0563
	Light	5254±236	4965±356	5804±659	ns	ns	ns
Heat (kcal/h/kg)	Dark	18.627±0.290	16.616±0.666	17.211±0.223	**	*	ns
	Light	15.345±0.275	13.546±0.510	15.7040±0.523	*	ns	0.0692
Temperature (ºC)	Scapular	38.46±0.12	37.74±0.15	38.56±0.23	*	ns	**
	Rectal	37.72±0.23	37.48±0.27	37.70±0.15	ns	ns	ns

Table 30. Indirect calorimetry parameters and activity values in individual caged mice. Mean±SEM. ANOVA One-way, Post-hoc Tukey; *p<0.05, **p<0.01, ns=no significant. C-H: comparison Ctrl and HFD groups; C-I: comparison Ctrl and Int groups; H-I: comparison HFD and Int groups.

1.8. No relevant effects in locomotor activity

Individual housing of the mice in cages with a multidimensional infrared light beam system allowed studying locomotor activity of the animals. Locomotor activity is divided in ambulatory (active movement) and fine movement (grooming and *in-place* movement) (Matherials and Methods, section 2.5).

During the light phase, *Int* mice showed an increase in ambulatory movement (Figure 19A, Table 30) that could be due to the fact that they were under caloric restriction (CR) and therefore the mice where more active trying to find some food. Regarding the fine movement, a decrease in dark phase was observed in *Int* mice in comparison to the other groups (Figure 19B, Table 30). No differences were showed neither during the dark phase in the ambulatory movement nor during the light phase in the fine movement.

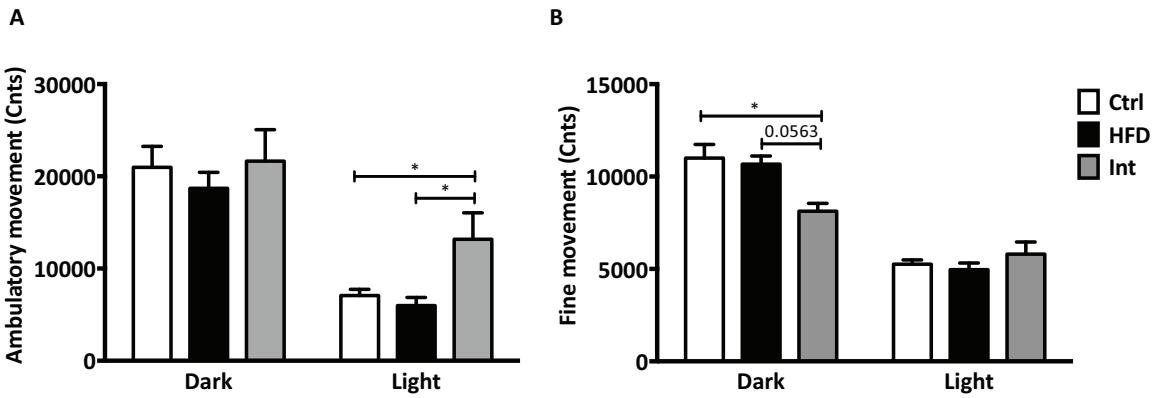

Figure 19. Activity. A: counts of ambulatory movement. Ctrl n=9; HFD n=5; Int n=6. B: counts of fine movement. Ctrl n=9; HFD n=5; Int n=6. Mean±SEM, ANOVA One-way, Post-hoc Tukey; *p<0.05, **p<0.01, ***p<0.001, ****p<0.0001.

1.9. Decreased heat production in HFD was partly reverted upon LI

Heat production was calculated by the Weir equation using the values of VO_2 consumed and VCO_2 produced obtained during the indirect calorimetry experiments, thus giving an idea of mice' energy expenditure. The energy expenditure includes the basal metabolic rate (BMR), the thermic effect of food (TEF) and the physical activity energy expenditure (PAEE). The calculations showed that there was a decrease in heat production in *HFD* mice compared to *Ctrl* mice (Figure 20, Table 30). However, this decrease was not reverted after LI although a tendency was observed during the light phase.

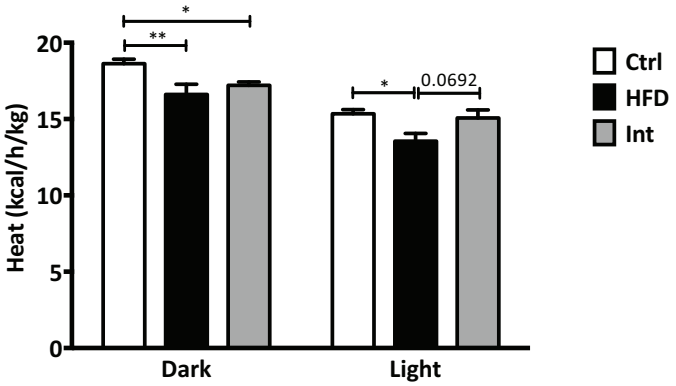

Figure 20. Heat production. Heat production during the dark and light phases, normalized by BW. Ctrl n=9; HFD n=5; Int n=6. Mean±SEM, ANOVA One-way, Post-hoc Tukey; *p<0.05, **p<0.01.

1.10. The decrease in scapular temperature after HFD was reverted upon LI

A significant decrease in *HFD* mice's scapular temperature compared to *Ctrl* mice was observed (Figure 21A and 21B, Table 30). Also, a recovery in scapular temperature was shown in the *Int* group. However, no differences were observed in the rectal temperature among groups (Figure 21B, Table 30).

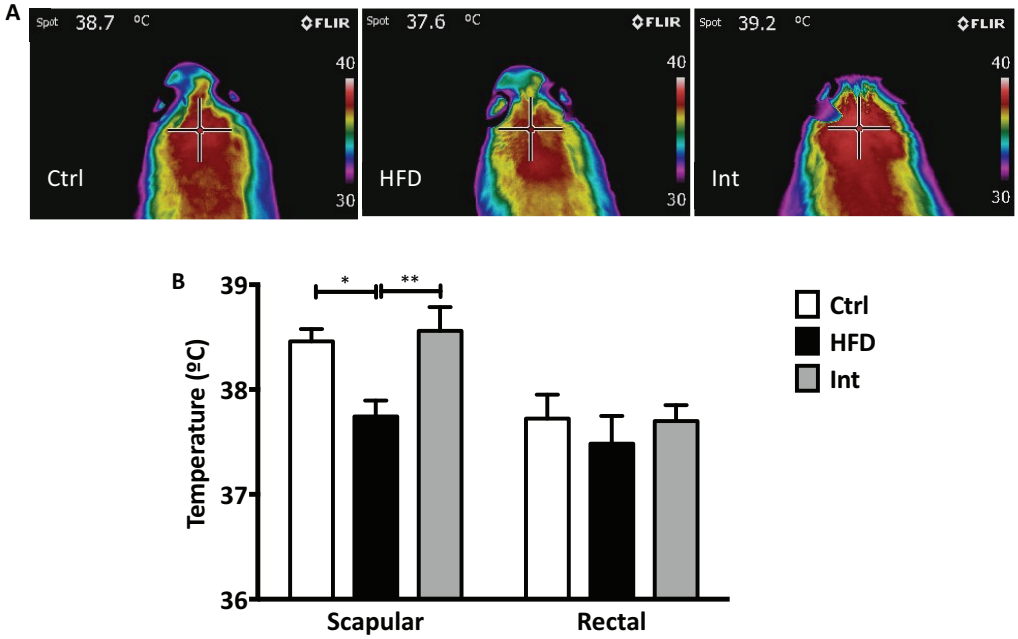

Figure 21. Body temperature. A: Representative images taken with a thermal imager of the three experimental groups, where scapular temperature can be measured with the color scale. B. Quantification of the scapular temperature observed in the previous figure. Ctrl n=9; HFD n=6; Int n=6; and measured rectal temperature. Ctrl n=9; HFD n=6; Int n=6. Mean±SEM, ANOVA One-way, Post-hoc Tukey; *p<0.05, **p<0.01.

2.1. Pancreatic islets

Apart from the pancreas' weight measurement, the morphometry of pancreatic islets as well as their insulin and glucagon content and *in vitro* insulin secretion capability were assessed.

2.1. The increase in pancreatic islets insulin area after HFD was maintained high upon LI

Insulin and glucagon areas were studied in different pancreas' sections from the three experimental animal groups. By immunohistochemistry assays, an increase in the *HFD* group in insulin and glucagon areas, when both were normalized by pancreas' area, were observed when compared to the *Ctrl* group (Figure 22A). After LI was performed, the insulin and glucagon area values were not reverted, thus maintaining similar values to the *HFD* group. Regarding the islet sizes, biggest islets (area greater than 10000mm^2) increased significantly in the *HFD* mice in comparison to the *Ctrl* group and again, the increase seemed not reverted after LI (Figure 22B and 22C). A similar pattern was

observed in the smallest islets with areas ranging from <1000 mm^2 to 2500 mm^2, although in these cases the increase in *HFD* group was not significant and the difference between *Ctrl* and *Int* groups was only a tendency (Figure 22C). Of note, a significant increase in *HFD* compared to *Ctrl* group was also revealed in islets with a size between 5001 and 7500 mm^2, suggesting a general pattern -statistically significant in some cases- of an increase in number of islets in *HFD* mice ranging different sizes without a decrease after LI.

In order to study further the presence of small area islets that seemed to increase in the *HFD* mice and to have the number maintained in the *Int* group, the islets with less than 6 cells were counted. This is an approach that suggests islet neogenesis based on previous scientific reports (Király et al. 2008). As expected, there was a tendency to increase in the number of the islets with less than 6 cells in *HFD* group that was again maintained in *Int* group (Figure 22D).

2.2. Disrupted GSIS after HFD was reverted upon LI

To complete the information obtained during the *in vivo* assessment of the insulin plasma levels after overnight fasting and during the IGTT 15 minutes after the glucose injection, an *in vitro* GSIS assay was performed. The GSIS allows the study of insulin secretion by isolated pancreatic islets under controlled conditions, hence focusing in β-cell insulin secretion.

Contrary to the insulin secretion assay during the IGTT *in vivo* (Figure 16C), in the *in vitro* assay with isolated pancreatic islets, the increase in insulin secretion observed -in this case, only after glucose stimulation, 16.7 mM- in the *HFD* group, was reverted in the *Int* group (Figure 23A, Table 31).

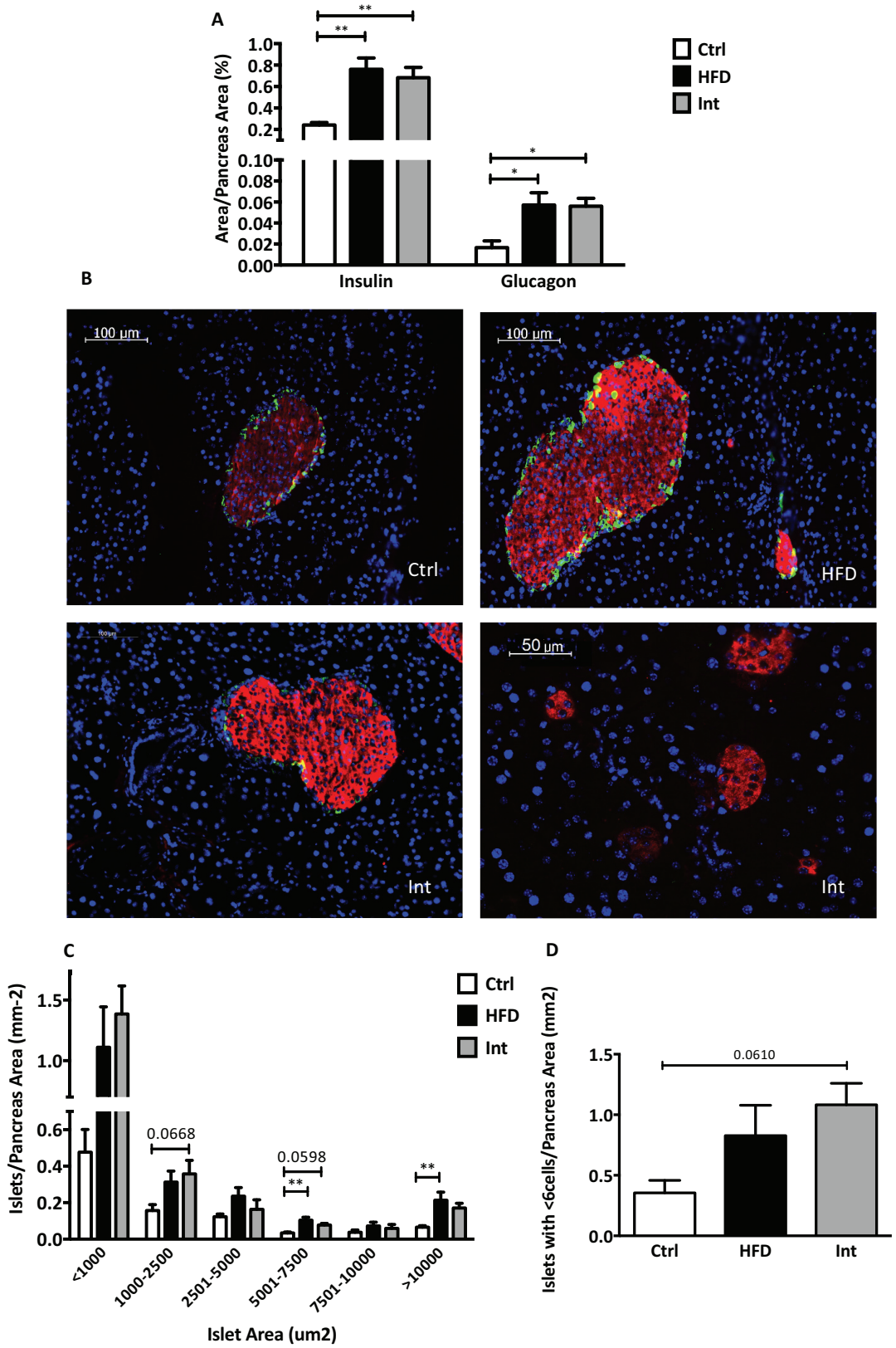
A
Area/Pancreas Area (%)
1.0
0.8
0.6
0.4
0.2
0.10
0.08
0.06
0.04
0.02
0.00
**
**
*
*
Insulin
Glucagon
Ctrl
HFD
Int
B
100 µm
Ctrl
100 µm
HFD
Int
50 µm
Int
C
Islets/Pancreas Area (mm-2)
1.5
1.0
0.6
0.4
0.2
0.0
0.0668
0.0598
**
**
<1000
1000-2500
2501-5000
5001-7500
7501-10000
>10000
Islet Area (um2)
Ctrl
HFD
Int
D
Islets with <6cells/Pancreas Area (mm2)
1.5
1.0
0.5
0.0
0.0610
Ctrl
HFD
Int

Figure 22. Insulin/Glucagon content. A: insulin and glucagon islet areas normalized by pancreas area. Ctrl n=5-6; HFD n=4; Int n=4. B: representative images of insulin (red) and glucagon (green) immunohistochemistry staining for the three experimental animal groups. C: histogram for the different islet size ranges. Ctrl n=6; HFD n=4; Int n=4. D: number of islets with less than 6 cells normalized by pancreas area (mm2). Ctrl n=6; HFD n=4; Int n=4. Mean±SEM, ANOVA One-way, Post-hoc Tukey; *p<0.05, **p<0.01.

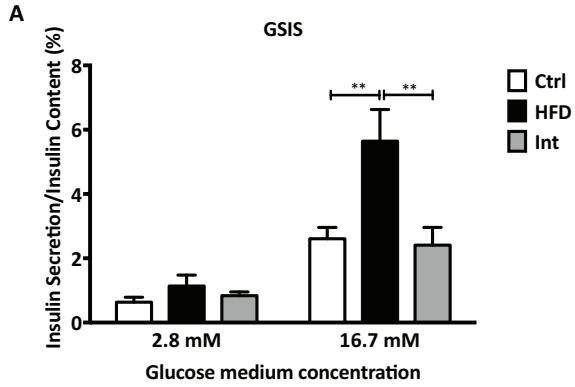

Figure 23. GSIS. A: insulin secretion normalized by insulin content at low and high glucose concentrations. Ctrl n=10-11; HFD n=7; Int n=6-7. Mean±SEM, ANOVA One-way, Post-hoc Tukey; *p<0.05, **p<0.01, ***p<0.001.

Insulin concentration in GSIS (%)				Significance		
glucose	Ctrl	HFD	Int	C – H	C - I	H - I
2.8mM	0.63±0.15	1.14±0.34	0.84±0.11	ns	ns	ns
16.7mM	2.61±0.35	5.64±0.99	2.41±0.55	**	ns	**

Table 31. Insulin concentration values during GSIS. Mean±SEM. ANOVA One-way, Post-hoc Tukey; **p<0.01, ns=no significant. C-H: comparison Ctrl and HFD groups; C-I: comparison Ctrl and Int groups; H-I: comparison HFD and Int groups.

3. Epididymal white adipose tissue

Epididymal white adipose tissue (eWAT) weight increased after HFD and reverted after LI. Moreover, histological cuts, mitochondrial function, gene and protein expression, metabolomics and RNA sequencing were assessed in eWAT.

3.1. Mitochondrial dysfunction in eWAT after HFD was not reverted upon LI

Mitochondrial function was assessed in eWAT. The results of high-resolution respirometry experiments with fresh eWAT tissue showed a decrease in mitochondrial respiration in almost all respiratory states under assessment in the *HFD* group, which were not reverted after LI (Figure 24A).

However, only FCR in Leak and CI respiration showed an increase in the *HFD* group when compared to the *Ctrl* group; however after LI FCR-CI showed a significant reversion (Figure 24B). It is important to mention that contrary to mitochondrial function, the eWAT weight was totally reverted after LI (Figure 14A and 14B).

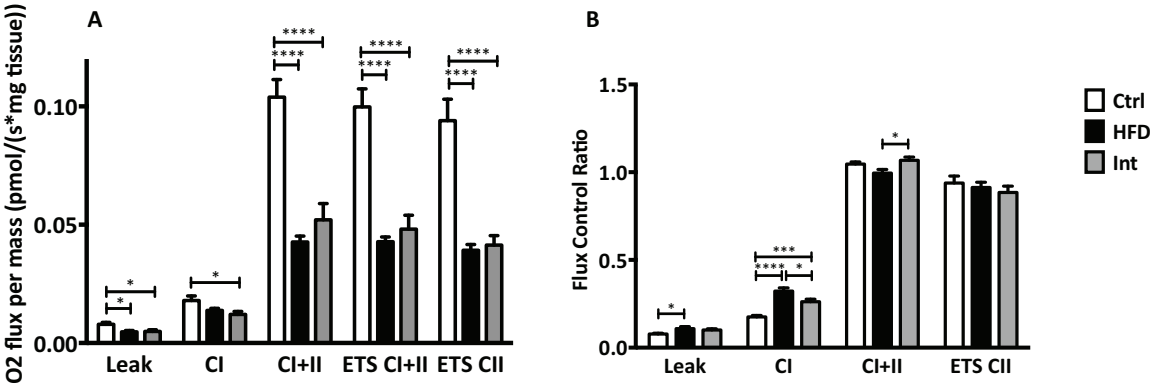

Figure 24. Mitochondrial function in eWAT. A: oxygen flux normalized by tissue weight. Ctrl n=10; HFD n=8; Int n=10. B: flux control ratio; oxygen flux in each respiratory state normalized by ETS CI+CII. Same number of animals as in A. Mean±SEM, ANOVA One-way, Post-hoc Tukey; *p<0.05, ***p<0.001, ****p<0.0001.

3.2. Disrupted adipocytes structure and inflammation after LI

Histological studies of eWAT tissue were carried out to observe the adipocytes architecture in all experimental animal groups. As expected, *HFD* group adipocytes showed the characterisitic architecture, greater adipocyte cell size and crown-like structures (CLS) (Figure 25A). Regarding the *Int* adipocytes, a massive increase of infiltrated immune cells was observed as well as more rounded and smaller adipocytes compared to *HFD* mice, all suggesting a worsening of the inflammatory eWAT state after LI.

Additional inmunohistological studies were perfomed to decipher the type of infiltrated immune cells. Macrophages are antigen-presenting cells (APC) involved in the immune response, which present antigen protein to Tcells (Raveney et al. 2010). Thus, macrophages interact with Tcells in order to activate Tcells in target organs, and are activated at the same time by cytokines produced by Tcells. Tcells were increased in HFD state and even more increased after LI (Figures 25B and 25C). Tcells detection was performed by using CD3 marker present in all stages of Tcell development.

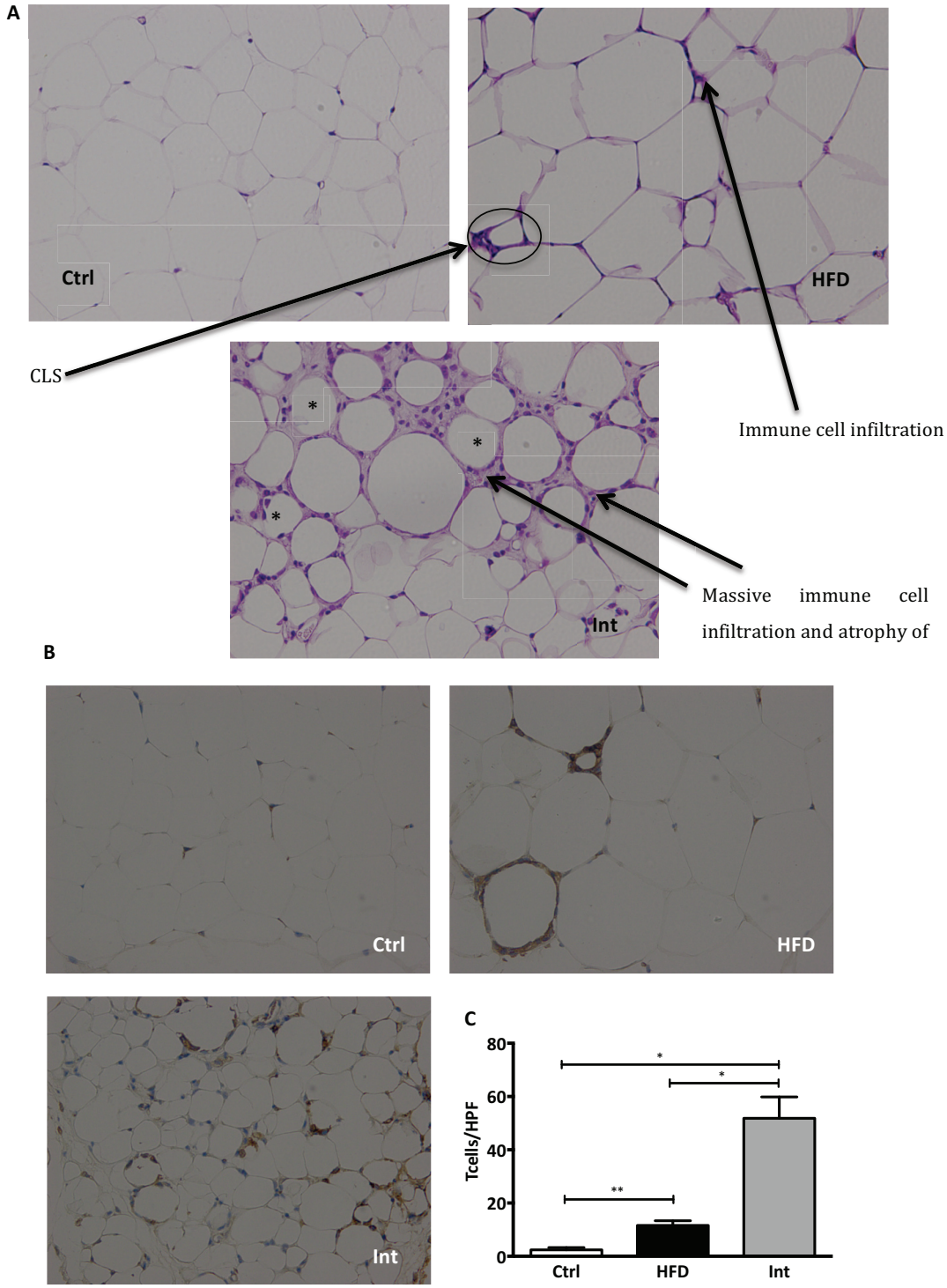

Figure 25. Immune cells infiltration and crown-like structures (CLS) in eWAT. A: Hematoxylin/eosin staining of eWAT tissue cuts from paraffin blocks of the three experimental groups, representative from 4 mice/group. B: CD3 staining (T cells) of eWAT cuts from paraffin blocks of the three experimental groups, representative from 4 mice/group. C: Quantifications for staining in B. Normalization is perform by normalizing by high-power field (HPF, number of fields studied, 10 in this case). Images are at 20X. (*) Dying adipocytes (lack of plasma membrane).

3.3. WAT gene expression studies

eWAT gene expression profile was also assessed in parallel with the findings of disrupted mitochondrial function and inflammation after HFD-feeding and after LI (Figure 26). All gene names can be found in Materials and Methods part, section 6.4.

First of all, we measured mRNA expression of the key co-activators, nuclear receptors and other transcription factors that control mitochondrial biogenesis: a decrease was observed in *HFD* group in the gene expression of main co-activators *Ppargc1a* and *Pparg1b* (Figure 26A), while neither the nuclear orphan receptor *Esrra*, and the transcription factors *Nrf1*, *Gabpa* and *Tfam* were affected after HFD (Figure 26B); after LI *Ppargc1a* and *Ppargc1b* reverted the decrease in expression (Figure 26A), while only *Gabpa* and *Tfam* increased their expression in *Int* mice (Figure 26B).

Genes related to lipid metabolism were also studied. Nuclear receptor *Ppara*, in charge of up-regulating genes involved in FA transport and mitochondrial FA β-oxidation among other functions, and nuclear receptor *Pparg* and gene *Foxo1*, these two laters key transcription factors regulating adipogenesis, all decreased their expression after HFD, and LI reverted the expression of the adipogenesis-related ones (Figures 26A and 26B). There was a decreased expression of genes related to lipid synthesis in *HFD* mice, given that FA synthase *Fasn* (transcription of which is regulated by FoxO1) and stearoyl-CoA desaturase 1 *Scd1* (in charge of the synthesis of unsaturated FA and regulated by PPARG) showed decreased expression; contrary to *Cpt1a* that showed increased expression indicating more transport of lipid into the mitochondria for its oxidation (Figure 26D). Given the ectopic FA accumulation that occurs in insulin-sensitive tissues such as liver and skeletal muscle due to increased WAT lipolysis after reaching its expandability limit in an obese state, of interest was to study lipoprotein lipase *Lpl* a gene encoding for a TG hydrolase. *Lpl* mRNA expression was decreased after HFD pointing at a decrease in lipolysis. After LI, *Fasn* and *Scd1* expression was increased suggesting a potential switch to lipid synthesis (Figure 26D). *Lpl* expression was still decreased, and lipid transport into mitochondria was maintained after LI, by still high *Cpt1a* expression (Figure 26D). *Ppard*, a nuclear receptor regulating the expression of different genes such as Plin2 (involved in metabolic activation of macrophages), reported no expression changes in any of the groups. In summary, *Lpl* expression was decreased and *Cpt1a* expression increased through the experimental groups *HFD* and *Int*, while *Fasn* and *Scd1* expression changed from being down-regulated in *HFD* mice to up-regulated after LI.

When glucose metabolism was assessed by studying mRNA expression of key proteins, potentially decreased glycolysis (by means of decreased *Gapdh* expression), decreased glucose uptake (decreased *Slc2a4* expression), and decreased gluconeogenesis (decreased *Pck1* expression) (Figure 26C) were observed. Also, *HFD* mice revealed an increase in glycogen synthase *Gys2* mRNA expression, potentially indicating that glucose metabolism was switch to glycogen storage. After LI, glucose uptake and gluconeogenesis seemed reverted, along with a decrease in glycogen formation (*Gys2* expression was decreased back to *Ctrl* mice values) (Figure 26C). However, glycolytic gene *Gapdh* expression was not increased in *Int* mice.

Mitochondrial OxPhos genes mostly showed decreased expression after HFD-feeding (CI: *Ndufa9*, CII: *Sdha*, CIII: *mt-Cytb* and *Uqcrc2*, and CV: *Atp5a1*) (Figure 26E). This generalized decreased expression might match the mitochondrial dysfunction in *HFD* mice. However, after LI mitochondrial dysfunction was not recovered and the decreased gene expression was reverted, meaning that *Ndufa9*, *Sdha*, *mt-Cytb* and *Uqcrc2* showed expression values similar or even higher than *Ctrl* mice. In contrast *Cox4i1* and *Atp5a1* mRNA expression was still decreased. mRNA expression of mitochondrial dynamic related genes was also measured (Figure 26F). Thus, *Mfn2* and *Opa1,* main players in mitochondrial fusion, the former also related to mitochondria-ER tethering and the later linked to cristae formation, decreased their expression in *HFD* mice, also in line with the reported mitochondrial dysfunction. After LI, both markers increased their expression reaching similar values when compared to the *Ctrl* mice. Of note, *Mfn1*, also implicated in mitochondrial fusion of the outer mitochondrial membrane, only showed an increase in expression after LI. Regarding fission genes the pattern of expression was similar in *Ctrl* and *HFD* mice. However, mRNA expression of *Dnm1l* increased and *Fis1* decreased in *Int* mice.

Other group of interest are the genes related to mitochondrial stress, leading to mitochondrial unfolded response (UPR^{mt}) that is a mitochondrial quality control machinery composed of proteases (i.e. LON and CLPX) and chaperones (HSP). Mitochondrial stress genes assess did not show a uniform expression pattern (Figure 26H), thus *Clpx* and *Hspd1* expression decreased after HFD, and only *Clpx* expression was reverted in *Int* mice while *Hspd1* expression decreased even more after LI. On the other hand, *Ubl5* and *Hspa9* expression was increased after LI, and *Lonp1* expression did not show any expression change across the experimental groups.

Endoplasmic reticulum (ER) stress genes that control the unfolded protein response (UPR) for misfolded proteins were also assessed, showing fewer changes in expression (Figure 26G). ER stress response starts with the chaperone Hspa5 (Bip, or Grp78) binding ER sensors (IRE1, PERK and ATF6) and allowing their release. Then different branches are activated downstream finally initiating the transcription of target genes: 1) IRE1 and XBP1s, 2) PERK, ATF4 and downstream CHOP, and 3) ATF6. *Hspa5* expression increased after HFD, while *Atf6* and *Xbp1(s/tot)* expression increased after LI. Of note, in *Int* mice *Hspa5* expression was maintained higher than *Ctrl* mice expression. Thus, the Int mice revealed an increase in both mitochondrial and ER stress gene expression.

Inflammation and macrophage markers in eWAT were also measured (Figures 26I and 26J). The cytokine *Ccl2* (also known as monocyte chemoatractant protein 1, *Mcp1*), reported increased expression after HFD, along with the macrophage marker *Adgre1* (also known as *Emr1*). In *Int* mice, expression of these genes was reverted (similar to *Ctrl* group) and decreased. Of note, another macrophage marker *Cd68* expression was not changed across the experimental groups. The polarization of macrophages was assessed by studying the expression of M1 marker *Itgax* (also known as *Cd11c*) and M2 marker *Cd209e*. *Itgax* expression was increased in *HFD* mice and after LI, while *Cd209e* expression was decreased in *HFD* and *Int* groups, thus showing an inverted pattern in comparison to M1, and suggesting a switch to M1 polarization after HFD that is maintained after LI. Inflammation markers *Tnf* (*Tnfa*) and pro-inflammatory cytokine *Il6* increased their expression after HFD, and it is reverted in *Int* mice. The same expression pattern was observed in *Il10* expression, although *Il10* is an anti-inflammatory cytokine. Other inflammation marker under study was *Il1b*, which did not show significant expression changes.

Oxidative stress seemed to be increased in *HFD* mice based on the increased mRNA expression of antioxidant genes, such as *Sod2* and *Gpx1* (Figure 26K). On the contrary, *Cat* expression showed a tendency to decrease. LI did not induce any significant changes in antioxidant genes expression. Thus, LI might have solved oxidative stress that appeared after HFD.

Among the other genes assessed that did not belong to the previous classified groups (Figure 26L): *Cs*, the first enzyme in the TCA cycle, revealed an increased expression in *Int*; while *Nnmt* showed the contrary, a decrease in expression after LI. NNMT methylates nicotinamide and its knockdown has showed protection against DIO (Kraus et al. 2014),

which correlates with a decreased expression in *Int* mice. mRNA expression of uncoupled proteins (*Ucp1* and *Ucp2*) was higher in *HFD* mice and persisted high after LI, suggesting also an uncoupling situation in OxPhos that might contribute to mitochondrial dysfunction. *Fgf21* expression increased only in *HFD* group, while no changes were revealed in *Socs3* expression and the browning marker *Cidea*. FGF21 has been shown to stimulate adiponectin secretion and decrease ceramides accumulation in obese rodents (Holland et al. 2013), thus the increased expression in *HFD* mice might be a defense mechanism against the high content in fat. SOCS3 was reported to inhibit leptin signalling (Bjørbæk et al. 2000), but no changes were detected in its expression.

As reported in previous scientific works, it is important to mention that mRNA expression of a gene might not correlate with the levels of protein that encodes (Wu et al. 2014). However, in order to assure that a protein is exerting a given function, post-translational changes might be also assessed ultimately.

3.4. Epididymal white adipose tissue metabolomics

Metabolomics, using NMR technology, were assessed for several tissues: eWAT, liver, skeletal muscle gastrocnemius and hypothalamus.

Regarding eWAT, an increase in succinate (Figure 27A) was detected in *HFD* mice, this is in relation with the also increased levels of branch-chain amino acids (BCAA) valine and leucine that could in fact synthetize succinate (Figure 27B). In general amino acids detected were either increased in *HFD* mice or not changed, and increased or not changed after LI. In *Int* group, the increase in glycerol could reflect an increase in eWAT lipolysis. Choline, a metabolite needed for neurotransmitter synthesis (acetylcholine), cell-membrane signalling (phospholipids), lipid transport (lipoproteins), and methyl-group metabolism (homocysteine reduction) (Zeisel & da Costa 2009) was increased (Figure 27A).

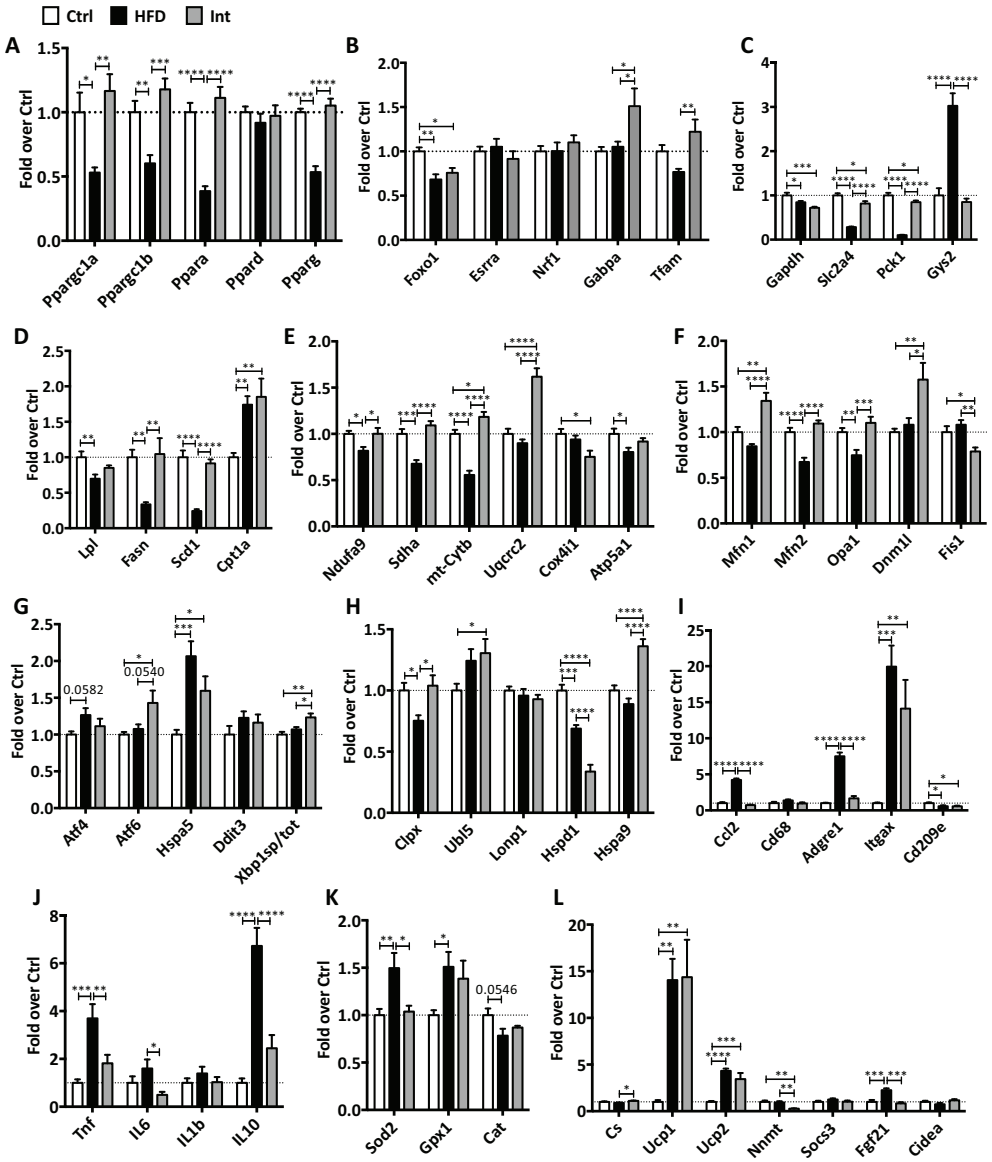

Figure 26. Gene expression in eWAT. A,B: Nuclear receptors, transcription factors and co-activators genes. C: glucose metabolism related genes. D: lipid metabolism related genes. E: mitochondrial oxidative phosphorylation system(OxPhos) genes. F: mitochondrial dynamics genes. G: endoplasmic reticulum (ER) stress genes. H: mitochondrial stress genes. I: macrophages markers genes. J: inflammation markers genes. K: antioxidant genes. L: different genes unclassified in previous categorized groups.. Complete name for each gene described in Materials and Methods section 5.4. Ctrl n=7-10; HFD n=6-8; Int n=6-8. Mean±SEM, ANOVA One-way, Post-hoc Tukey; *p<0.05, **p<0.01, ***p<0.001, ****p<0.0001.

In regard to lipid-soluble metabolites (Figure 27C), an increase was observed in *HFD* in free cholesterol, diglycerides (DAG) and phosphatidylcholine (a phospholipid incorporated in biological membranes), which was maintained after LI. Om3 FA were notably increased in the *Int* group in comparison to the other experimental groups (Om3 and α-linolenic fatty acids); while omega-6+Om3 fatty acids were decreased both after HFD and after LI (arachidonic - ARA and eicosapentaenoic – EPA fatty acids); omega-6 linoleic was also decreased in *HFD* and *Int* groups; and omega-9 oleic acid was increased only in *Int* mice. A full list of eWAT detected metabolites is described in Appendix 2.

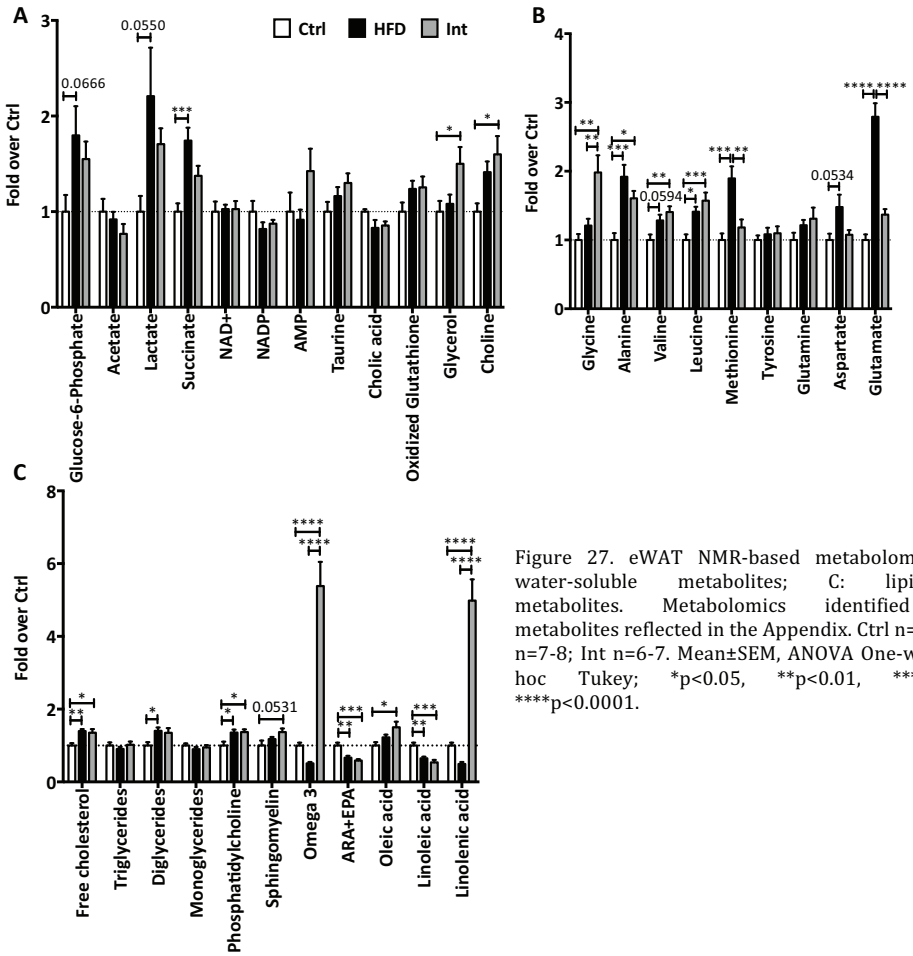

Figure 27. eWAT NMR-based metabolomics. A-B: water-soluble metabolites; C: lipid-soluble metabolites. Metabolomics identified other metabolites reflected in the Appendix. Ctrl n=6-7; HFD n=7-8; Int n=6-7. Mean±SEM, ANOVA One-way, Post-hoc Tukey; *p<0.05, **p<0.01, ***p<0.001, ****p<0.0001.

3.5. Epididymal white adipose tissue protein content assays

Besides gene expression studies, several related proteins were also studied in eWAT. Similarly to gene expression (*Ndufa9*) (Figure 26E), CI (NDUFB8) was decreased in *HFD* and then reverted (Figure 28A and 28C). This same pattern was observed in gene expression of subunits of the CII (*Sdha*) (Figure 26E), but not reproduced in protein content studies (SDHB) (Figure 28A and 28C). Regarding CIII subunit *Uqcrc2* increased after LI in gene expression and protein content (Figure 26E, 28A and 28C). Protein from CIV (MTCO1) showed the same behavior as CI protein subunit (Figure 28A and 28C), although CIV (*Cox4i1*) was decreased after LI in gene expression studies (Figure 26E). Despite *Atp5a1* gene expression decreased in *HFD* mice (Figure 26E), no changes were observed at protein level (Figure 28A and 28C). OPA1 fusion protein has different isoforms: long functional isoforms, and short isoforms product of a proteolytic cleavage by OMA1 and YME1L. Thus, a ratio between long-isoforms and short-isoforms gives an idea of the fusion activity of this protein. The only change observed for other mitochondrial-related proteins such as mitochondrial dynamics, β-oxidation or transport proteins, was a decreased in OPA1 in *HFD* and *Int* groups (Figure 28A and 28D). *Opa1* gene expression showed a decrease-increase pattern (Figure 26F). Thus, the increase in *Dnm1l* expression after LI (Figure 26F) was not reproduced at protein level (Figure 28A and 28D), same way the decrease-increase pattern for *Mfn2* gene expression was blunted at protein level.

Among other proteins assessed, there was a significant increase after LI in protein content of the co-activator PRGC1, the nuclear receptor PPARA and the uncoupling protein UCP1 (Figure 28B and 28E). At gene expression level, the increase after LI in *Ppargc1a* and *Ppara* reverted the decrease after HFD (Figure 26A), a different case than protein content behavior. Regarding uncoupling proteins, UCP1 was increased only after LI (Figure 28B and 28E), while it was already increased in *HFD* mice in gene expression studies (Figure 26L). While *Sod2* at gene expression raised after HFD and was reverted in *Int* group (Figure 26K), at protein level this increase was blunted (Figure 28A and 28E). Similarly, the increase in *Int* mice in citrate synthase gene expression (*Cs*) (Figure 26L) was not correlated to protein levels (Figure 28A and 28E).

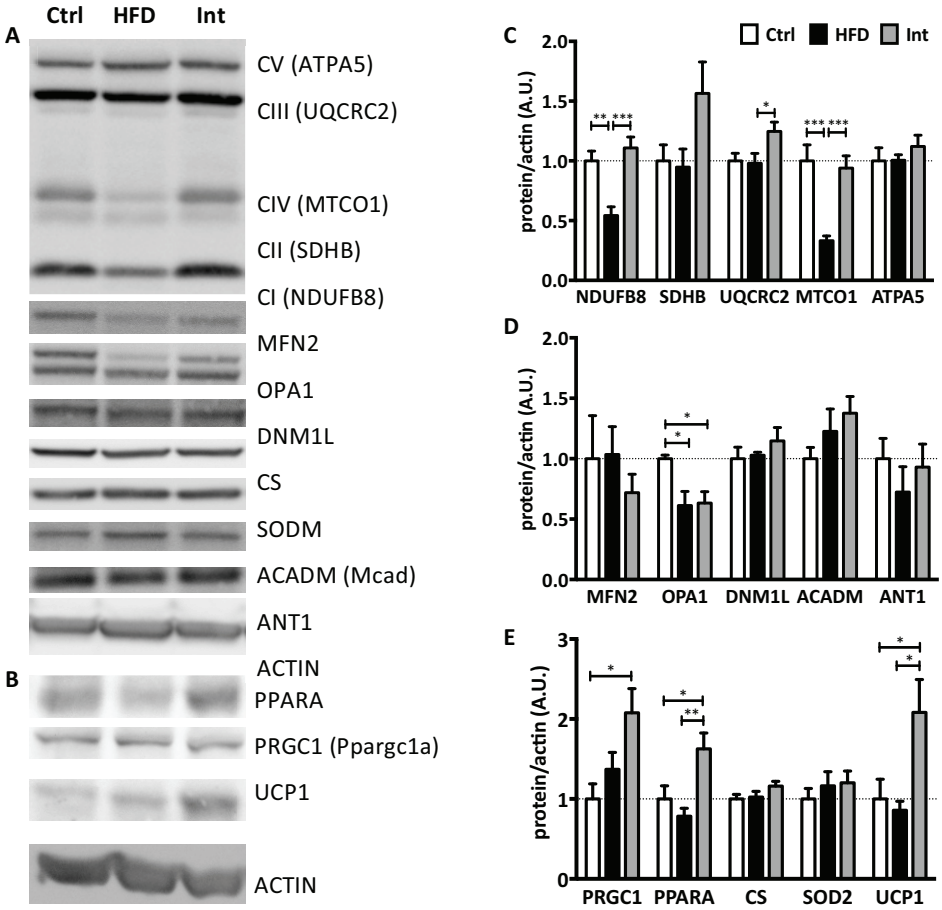

Figure 28. Protein content in eWAT. A-B: Western Blotting results. C-E: Analysis and normalization of protein content results. Values extracted by ImageQuant TL Software (GE Healthcare Life Sciences). Ctrl n=6-7; HFD n=7-9; Int n=8-9. Mean±SEM, ANOVA One-way, Post-hoc Tukey; *p<0.05, **p<0.01, ***p<0.001.

3.6. Epididymal adipose tissue transcriptome

Among all the results revealed by RNAseq arrays performed in eWAT, *Cd163* (macrophage M2 marker) expression was decreased after HFD and not reverted in *Int* mice; while other M2 markers such as *Tgfb1* and *Tgfbi* increased their expression after HFD, the former also significantly decreasing and reverting its expression in *Int* mice (Figure 29). Moreover, Tgfb2 showed no changes across the experimental groups (Figure 29). Interestingly, an increase in *Plin2* expression (a macrophage "metabolic" activator marker (Kratz et al. 2014)) was reported in *HFD* group and reverted after LI, although the levels were still higher than *Ctrl* values (Figure 29).

The integrative analysis (Results part, section 8.3.2) performed using RNAseq data through a protein-protein interaction (PPI) network in order to define clusters of genes, helped to identify a complex with OxPhos-related genes that showed *non-reversion* or *half-reversion* patterns among its genes.

Moreover, one of the hubs identified was COX7A2, a protein in charge of OxPhos complexes superassembly (Lapuente-Brun et al. 2013). Interestingly, although *Cox7a2l* expression did not show any changes, *Cox7a2* reported a decrease in expression after HFD and after LI. *Cox7a2l* is in charge of ETS complexes superassembly.

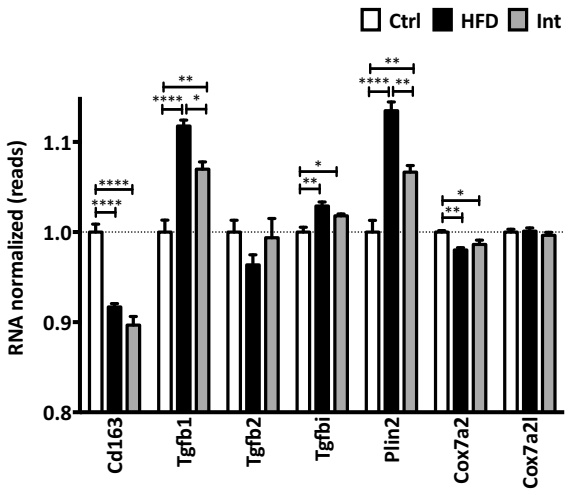

Figure 29. eWAT transcriptome. Reads from normalized RNA for different genes. Ctrl n=4; HFD n=4; Int n=4. Mean±SEM, ANOVA One-way, Post-hoc Tukey; *p<0.05, **p<0.01, ****p<0.0001.

4. Liver

Besides the increase in liver weight and TG in *HFD* and the decrease of both parameters after LI, mitochondrial function in liver was also assessed, along with gene expression studies, metabolomics and RNA sequencing.

4.1. Liver mitochondrial function

Regarding mitochondrial function studies, no differences were observed in any of the respiratory states (Figure 30A). However, FCR showed an increase in spare capacity in the CI+CII state in *Int* mice (Figure 30B).

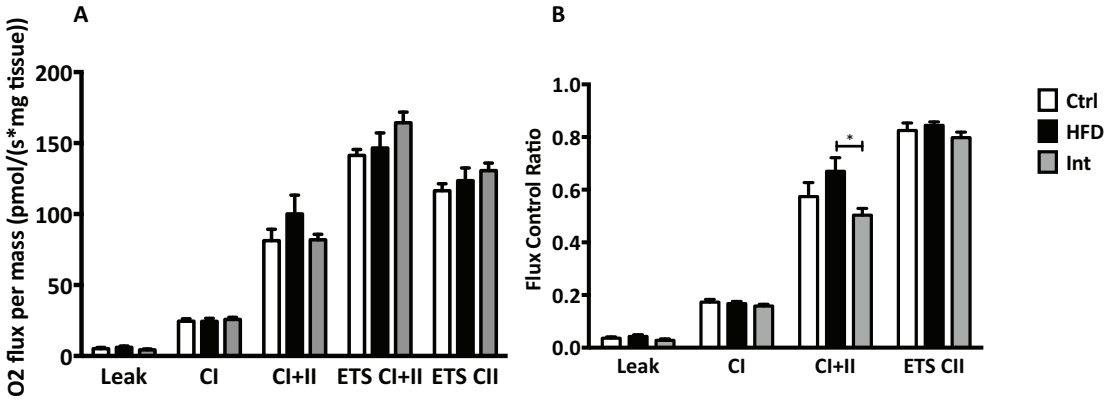

Figure 30. Mitochondrial function in liver. A: oxygen flux normalized by tissue weight. Ctrl n=8; HFD n=7; Int n=9. B: flux control ratio; oxygen flux in each respiratory state normalized by the maximum oxygen flux (ETS CI+CII). Same number of animals as in A. Mean±SEM, ANOVA One-way, Post-hoc Tukey; *p<0.05.

4.2. Liver gene expression studies

Mitochondrial biogenesis regulatory genes reported no changes in mRNA expression in *HFD* mice but their expression increased mainly after LI (*Ppargc1a*, *Ppargc1b*, *Esrra* and *Tfam*), although no expression changes were detected in *Nrf1* or *Gabpa* (Figures 31A and 31B). *HFD* mice livers, meaning that the expression of lipid metabolism regulators *Pparg* and *Ppara* was increased after HFD (Figure 31A), along with *Fasn* and *Scd1* expression (Figure 31D) suggested accumulation and synthesis of lipids. These results are in concordance with the increased liver TG content in the *HFD* group. After LI, the profile of lipid metabolism genes was completely changed suggesting a switch to oxidative metabolism meaning liver copes with increased lipids in the diet by metabolizing them. This was observed by the decrease in expression in *Pparg*, *Fasn* and *Scd1* genes (Figures 31A and 31D). In line with this, *Cpt1a* expression was increased (Figure 31D) suggesting more lipids might be transported into mitochondria for its oxidation, and *Ppara* and *Srebf1* (Figures 31A and 31B) expression was also increased, regulating FA and lipid metabolism and production in the liver.

Regarding glucose metabolism (Figure 31C), PEPCK, a key enzyme in gluconeogenesis regulation, showed not changes at the level of mRNA expression (*Pck1*). In *HFD* mice *Gapdh* reported increased expression that was reverted after LI, revealing a feasible increase in glycolysis after HFD. However, changes in *Pfkl* expression, gene encoding for another glycolytic enzyme, were not observed. In *Int* mice, the glucose transporter GLUT2 reported increased mRNA expression (*Slc2a2)* when compared to the *Ctrl* mice.

Mitochondrial OxPhos genes showed a different pattern of mRNA expression than the one observed in eWAT (Figure 31E). CI (*Ndufa9*) and CIV (*Cox4a1*) increased their expression after HFD, while CII (*Sdha*), CIII (*Uqcrc2*), CIV (*Cox4a1*) and CV (*Atp5a1*) increased their expression in *Int* mice (*Ndufa9* showed also a tendency to increased expression). Although the general increase after LI in mitochondrial OxPhos genes was not reflected in mitochondrial function studies. An increase in mitochondrial fusion genes expression (*Mfn1* and *Mfn2*) was observed only after LI (Figure 31F), in line with the fact that fission processes are related to obesity and T2DM (Gómez-Valadés et al. 2015).

ER stress markers (Figure 31G) such as *Hspa5* and *Ddit3* reported increased expression after HFD that was reverted in *Int* mice, although the other markers did not show any changes in expression. Neither major change in mitochondrial stress genes expression (Figure 31H) was observed. Thus, only a tendency to increased *Ubl5* expression was detected in *HFD* mice, and an increase in *Hspa9* expression was reported after LI.

Inflammation markers (Figure 31I) in liver were not increased after HFD, suggesting that the liver steatosis (with the liver actively synthetizing lipids, based on TG concentrations in the *HFD* group) did not develop into NASH state given that lack of up-regulation in different markers of inflammation. In fact, interleukines *Il1b* and *Il10* showed a tendency to decreased expression after LI.

Antioxidants markers expression in the liver (Figure 31J) was increased after HFD (*Gpx1*) and also after LI (*Gpx1* and a tendency to increase in *Sod2*). No changes were observed in *Cat* expression. No significant differences were present in the last group of genes (Figure 31K) despite an increased in *HFD* and *Int* groups in *Ucp2* expression, and an increase in *Nnmt* expression in the *HFD* mice in comparison to the *Ctrl* and *Int* groups.

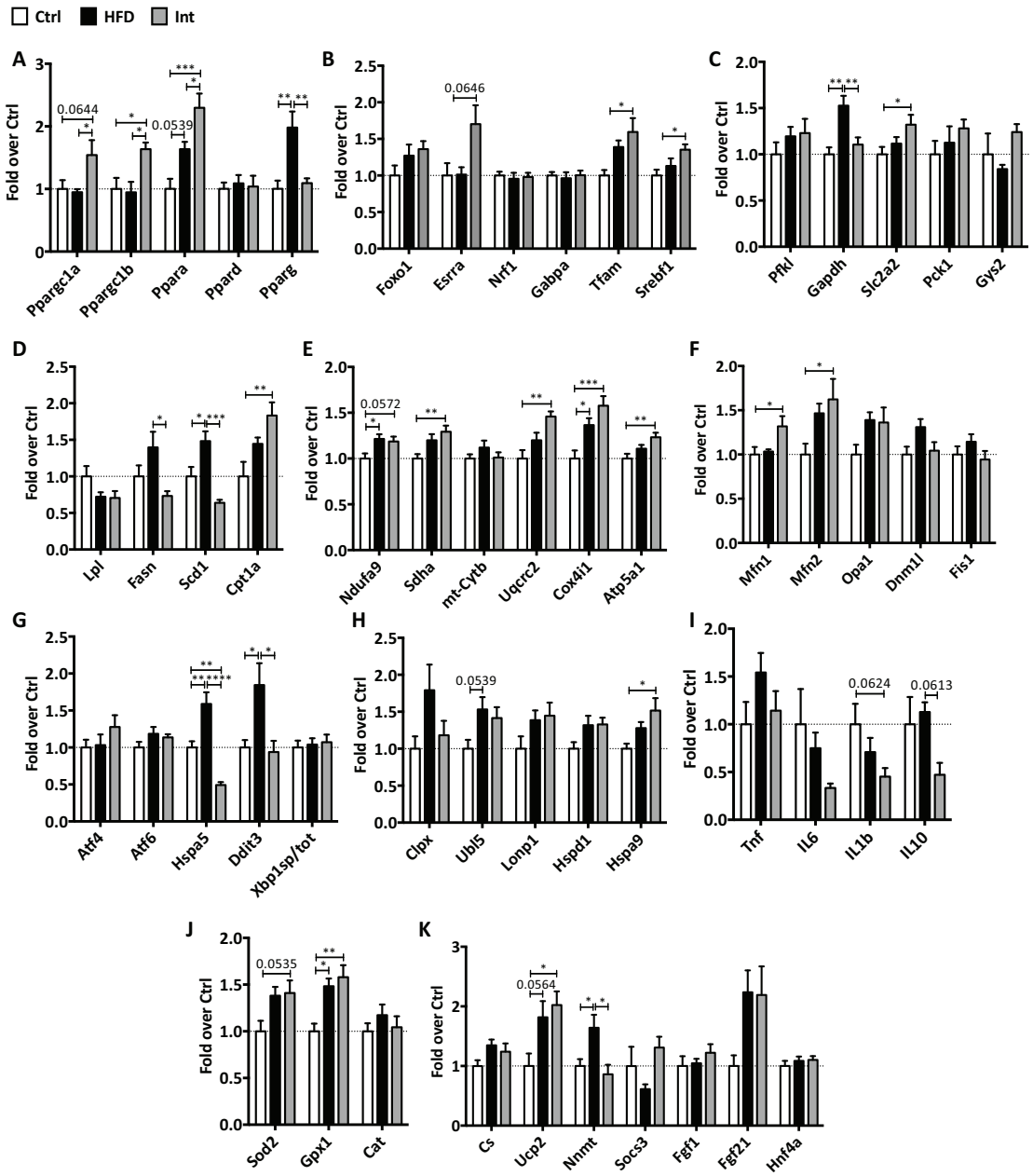

Figure 31. Gene expression in liver. A, B: transcription factors genes. C: glucose metabolism related genes. D: lipid metabolism related genes. E: mitochondrial electron transport system (ETS) genes. F: mitochondrial dynamics genes. G: endoplasmic reticulum (ER) stress genes. H: mitochondrial stress genes. I: inflammation markers genes. J: antioxidant genes. K: different genes unclassified in previous categorized groups. Complete name for each gene described in Materials and Methods section 5.4. Ctrl n=6-8; HFD n=6-8; Int n=5-8. Mean±SEM, ANOVA One-way, Post-hoc Tukey; *p<0.05, **p<0.01, ***p<0.001, ****p<0.0001.

4.3. Liver metabolomics

Metabolomics were also performed in liver. In line with mRNA expression studies that suggested an increase in lipid synthesis in the *HFD* mice, higher levels of esterified cholesterol, TG, DAG, and the increase in MUFAs and PUFAs (Om3, ARA+EPA, oleic acid, DHA and linoleic acid) were observed (Figure 32D). Indeed, after LI all these metabolites were decreased to *Ctrl* mice values, reverting the anabolic situation and coping with the oxidation of FA from the diet, feasible explanation for the decrease in all MUFAs and PUFAs.

In line with the tendency to increase mRNA expression in *Gys2*, glycogen was increased in *Int* mice in comparison to the other groups (Figure 32A). The reversion of *Gapdh* expression might be then in line with the tendency to decreased glucose-6-phosphate. Lactate was decreased in *Int* group, while $NADP^+$ and NAD^+ were increased only in *Int* mice or in *HFD* and *Int* mice, respectively. Amino acids were in general decreased in *HFD* and *Int* groups (Figure 32B), with a great decrease in BCAA (valine, leucine and isoleucine). Taurine, known to lessen oxidative-stress induced liver injury and hepatic fibrosis (Miyazaki et al. 2009), was decreased after LI (Figure 32C). Creatinine, a breakdown product of creatine, is synthesized within the liver and shuttled to skeletal muscle, where it is phosphorylated into phosphocreatine PCr allowing rapid ATP synthesis in times of increased energy demands. Creatinine was decreased after HFD and LI. Moreover, phosphatidylethanolamine, which seems to play a role in hepatic lipoprotein secretion by the liver (Vance 2008), decreased in *HFD* mice and reverted after LI. A full list of liver detected metabolites is described in Appendix 2.

5. Skeletal muscle

As mentioned, different skeletal muscles have been used for this PhD thesis. Until now, soleus showed an increase in TG in *HFD* mice with a decrease after LI, while TA did not show any differences. Soleus has been used as the skeletal muscle predominantly enriched in oxidative muscle fibers in the experiments below, while for predominantly enriched in glycolytic skeletal fibers extensor digitorum longus (EDL), TA and gastrocnemius muscles have been used.

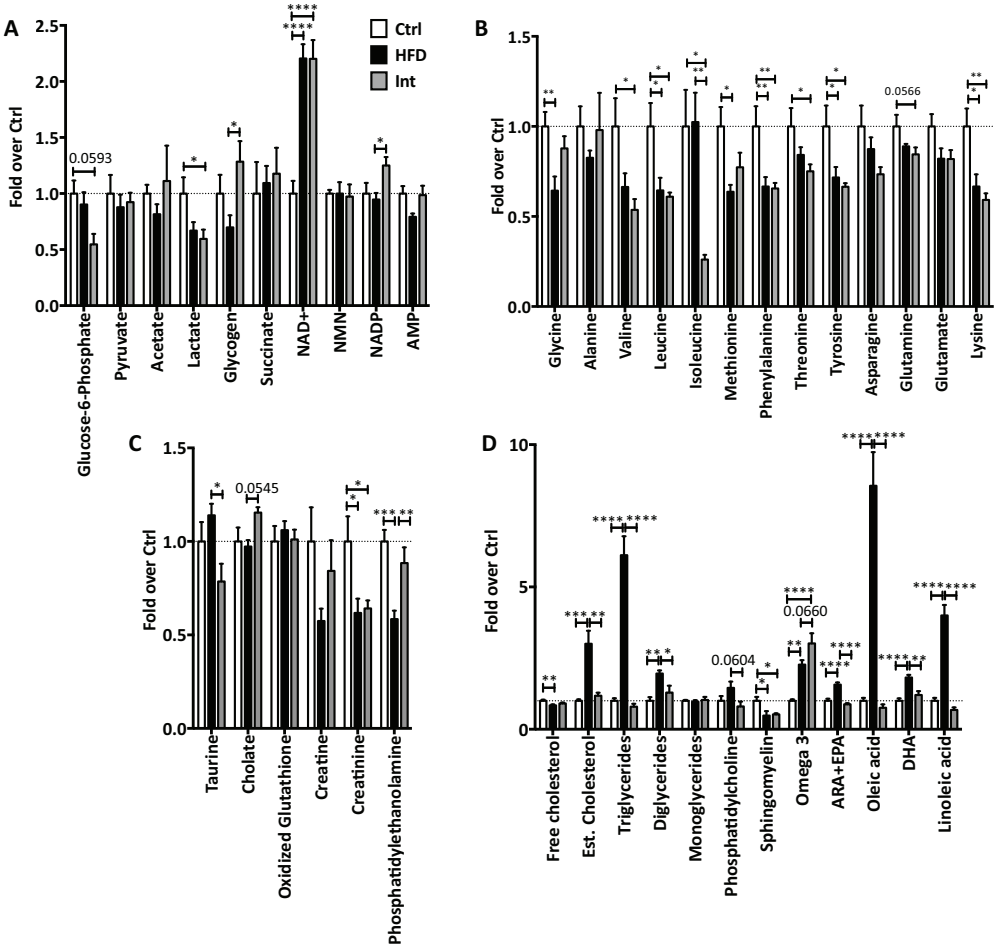

Figure 32. Liver NMR-based metabolomics. A-C: water-soluble metabolites; D: lipid-soluble metabolites. Metabolomics identified other metabolites reflected in the Appendix. Ctrl n=6-7; HFD n=7-8; Int n=6-7. Mean±SEM, ANOVA One-way, Post-hoc Tukey; *p<0.05, **p<0.01, ***p<0.001, ****p<0.0001.

5.1. Skeletal muscle mitochondrial function

5.1.1. Oxidative skeletal muscle (soleus)

No big significant changes were observed in soleus mitochondrial respiration studies apart from an increase in *HFD* mice in Leak state (also in FCR-Leak) and a reversion after LI (Figure 33A and 33B). Of note, an increase in FCR-CI+II was also observed in *Int* group mice, suggesting a loss of spare capacity that might be present in the other two experimental groups.

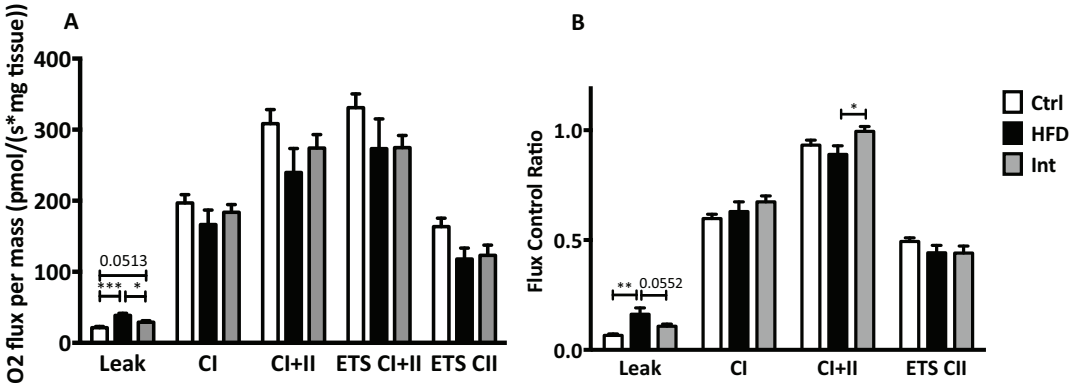

Figure 33. Mitochondrial function in soleus. A: oxygen flux normalized by tissue weight. Ctrl n=8; HFD n=6; Int n=9. B: flux control ratio; oxygen flux in each respiratory state normalized by the maximum oxygen flux (ETS CI+CII). Same number of animals as in A. Mean±SEM, ANOVA One-way, Post-hoc Tukey; *p<0.05, **p<0.01, ***p<0.001.

5.1.2. Glycolytic skeletal muscle (EDL)

Mitochondrial respiration in EDL showed no differences among the three experimental groups, neither in the respiratory states nor in the FCR (Figure 34A and 34B).

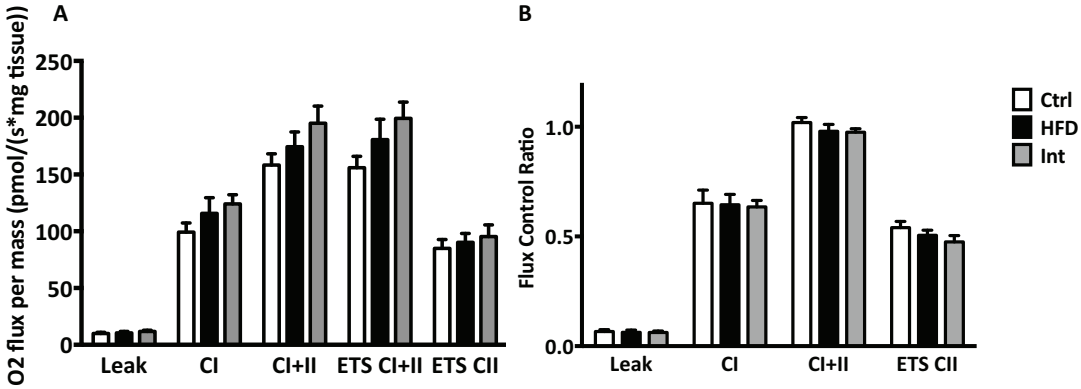

Figure 34. Mitochondrial function in EDL. A: oxygen flux normalized by tissue weight. Ctrl n=9; HFD n=7; Int n=11. B: flux control ratio; oxygen flux in each respiratory state normalized by the maximum oxygen flux (ETS CI+CII). Same number of animals as in A. Mean±SEM, ANOVA One-way, Post-hoc Tukey.

5.2. Skeletal muscle gene expression studies

5.2.1. Oxidative skeletal muscle (soleus)

At gene expression levels, several changes were observed in soleus among the experimental groups. A global pattern of mRNA expression was observed in soleus meaning that most of the genes showed an increased expression in *HFD* mice and reverted with a decreased expression in *Int* group.

Mitochondrial biogenesis regulatory markers (*Ppargc1a*, *Ppargc1b*, *Nrf1*, *Gabpa* and *Tfam*) showed increased expression after HFD that was reverted in *Int* mice (Figures 35A and 35B), suggesting an increase in biogenesis in the pathological state although only Leak changes in mitochondrial respiration correlated with these changes in expression. Transcription factors related to lipid metabolism (*Ppara*, *Ppard*, *Pparg* and *Foxo1*) showed also an increased expression in *HFD* mice with a posterior decrease in *Int* group (Figures 35A and 35B). *Lpl* and *Cpt1a* (lipolytic enzyme and lipid transporter into mitochondria) expression was also increased in *HFD* mice and decreased after LI (Figure 35D); these results were correlated with the expression patterns of transcription factors pointing that *HFD* mice might activate lipid metabolism in oxidative skeletal muscle. Of note, *Fasn* expression was decreased in *Int* mice suggesting a down-regulation of lipid synthesis in muscle after LI (Figure 35D). Regarding glucose metabolism (Figure 35C), markers of the glycolysis pathway (*Pfkm*) and glucose uptake (*Slc2a4*) showed increased expression in *HFD* group, which was decreased after LI.

Some of the mitochondrial OxPhos genes (*Sdha*, *mt-Cytb* and *Atp5a1*) expression was increased in *HFD* mice (Figure 35E), in line with the increase in mitochondrial biogenesis. Also in line with the decrease in expression after LI in mitochondrial biogenesis related genes, expression of *Ndufa9*, *Sdha*, *mt-Cyb*, *Uqcrc2* and *Atp5a1* was reduced. Of note, no changes were reported in CIV (*Cox4i1*) expression in any of the groups (Figure 35E). *Ucp2* followed the same global pattern with increased expression in *HFD* mice, later reverted, while *Ucp3* only reported a tendency (Figure 35J). The overall pattern of increased expression in *HFD* mice and reversion after LI was also reported in most of mitochondrial dynamic related genes (*Mfn1*, *Mfn2*, *Opa1* and *Dnm1l*), with the exception of *Fis1* (Figure 35F).

ER and mitochondrial stress also repeated the same pattern of expression (*Atf4*, *Atf6*, *Hspa5*, *Clpx*, *Lonp1* and *Hspa9*) (Figures 35G and 35H) meaning that stress markers showed increased expression in the pathological state and reverted after LI. Other ER stress markers (*Ddit3* and *Xbp1(s/tot)*) did not show any change in expression (Figure 35G), while *Ubl5* expression was decreased in *Int* mice in line with the above mentioned stress genes (Figure 35H).

Two antioxidant genes (*Sod2* and *Cat*) showed an increased expression in *HFD* mice that was decreased after LI, while *Gpx1* showed no changes in expression in oxidative skeletal muscle (Figure 35I). *Cs* expression, the first enzyme in the TCA was also increased in

pathological state with later reduction (Figure 35J). Of note, *Nnmt* expression showed no changes, while *Socs3* expression (known to inhibit leptin signalling) revealed a significant decrease after LI (Figure 35J).

5.2.2. Glycolytic skeletal muscle (TA)

Gene expression studies in TA showed different patterns from the ones observed in soleus. That is, instead of the common pattern of increased-reverted expression observed previously in soleus, TA revealed as a common pattern a decreased expression after the *Int* (Figure 36).

Mitochondrial biogenesis markers (*Ppargc1a*, *Esrra*, *Nrf1*, *Tfam*) expression was decreased after the LI, being *Ppargc1a* the only marker with already decreased expression in *HFD* mice (Figures 36A and 36B). No changes were observed in *Gabpa* gene expression (Figure 36B).

Lipid metabolism related transcription factor *Ppara* reported a decreased expression in *Int* mice, while no changes were reported in *Pparg* or *Ppard* expression (Figure 36A). *Lpl* mRNA expression was decreased after LI, when *Scd1* expression showed a tendency to increase (Figure 36D). No other changes were detected, pointing to a potential diminishment in TA lipid metabolism in *Int* mice. Glycolysis (*Pfkm* expression), glucose uptake (*Slc2a4* expression) and glycogen synthesis (*Gys1* expression) were decreased after LI, overall suggesting that glucose metabolism was also diminished in *Int* mice (Figure 36C).

As aforementioned, mitochondrial respiration was not changed significantly after LI, although a tendency towards an increase was observed (Figure 34). However, mitochondrial ETS genes (*Ndufa9*, *Sdha*, *Uqcrc2* and *Cox4i1*) reported a significant decreased expression or a tendency after LI (Figure 36E). *mt-Cytb*, on the contrary, revealed increased mRNA expression (Figure 36E). The same decrease in expression in *Int* mice was significant in mitochondrial dynamics fusion (*Mfn1* and *Mfn2*) and fission gene *Dnm1l*, and was a tendency in *Opa1* and *Fis1* (Figure 36F).

ER and mitochondrial stress genes (Figures 36G and 36H) did not report increased expression after HFD, but again a decreased expression after LI (*Atf6*, *Hspa5*, *Lonp1*, *Hspd1* and *Hspa9*). Of note, *Ddit3* expression was reduced already in *HFD* group (Figure 36G).

Regarding antioxidant genes, only *Sod2* expression was decreased after LI, and *Cat* expression revealed a tendency to increase in *HFD* and *Int* mice (Figure 36I). Among the other genes assessed, *Cs* expression was also decreased after LI, while *Nnmt* showed an increase in expression (Figure 36J).

5.3. Skeletal muscle metabolomics (gastrocnemius)

NMR based metabolomics was also performed in gastrocnemius muscle samples. Water-soluble metabolites that were not amino acids showed a general decrease in *HFD* and *Int* groups (Figure 37A). Lactate that can be converted into pyruvate to enter TCA, and succinate that is a TCA substrate, were decreased after LI (Figure 37A), probably pointing to a diminished general metabolism, in line with mRNA gene expression. In general, amino acids also showed a tendency to decrease in *HFD* and *Int* groups (Figure 37B). Concretely, glycine and glutamine were the two metabolites with greater decrease.

Regarding lipid-soluble metabolites, gastrocnemius muscle reported a profile similar to liver (Figure 37C) meaning that lipids were overall increased in *HFD* mice (TG, oleic and linoleic acid) due to ectopic lipid accumulation or increased liver lipid synthesis. The mentioned lipid metabolites were reverted and decreased after LI. However, Om3 FA increased levels after LI that correlated with the FA composition of the intervention diet, contrary to ARA+EPA that were decreased. A full list of gastrocnemius detected metabolites is described in Appendix 2.

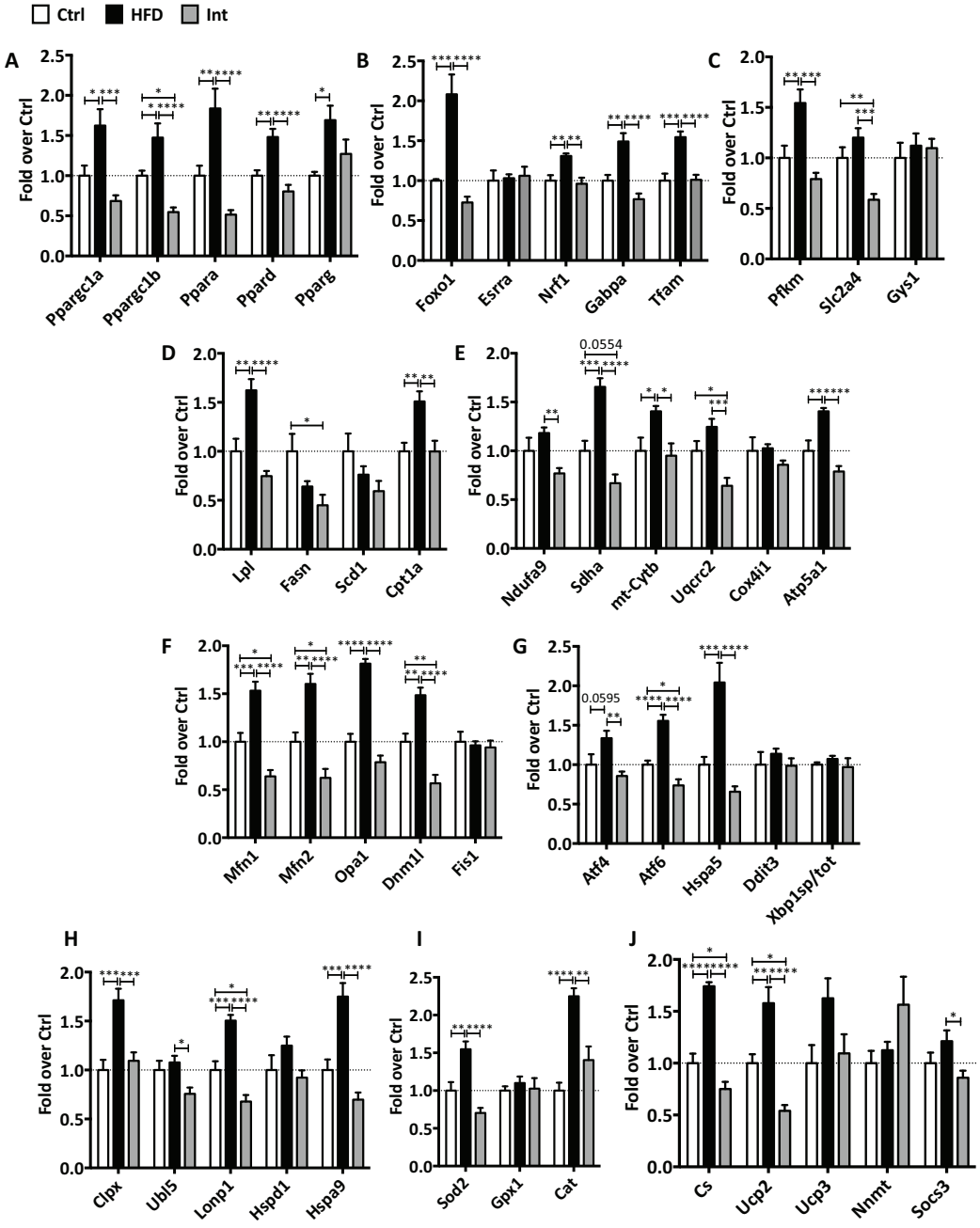

Figure 35. Gene expression in oxidative skeletal muscle (soleus). A,B: transcription factors genes. C: glucose metabolism related genes. D: lipid metabolism related genes. E: mitochondrial electron transport system (ETS) genes. F: mitochondrial dynamics genes. G: endoplasmic reticulum (ER) stress genes. H: mitochondrial stress genes. I: antioxidant genes. J: different genes unclassified in previous categorized groups. Complete name for each gene described in Materials and Methods section 5.4. Ctrl n=7; HFD n=6-8; Int n=6-8. Mean±SEM, ANOVA One-way, Post-hoc Tukey; *p<0.05, **p<0.01, ***p<0.001, ****p<0.0001.

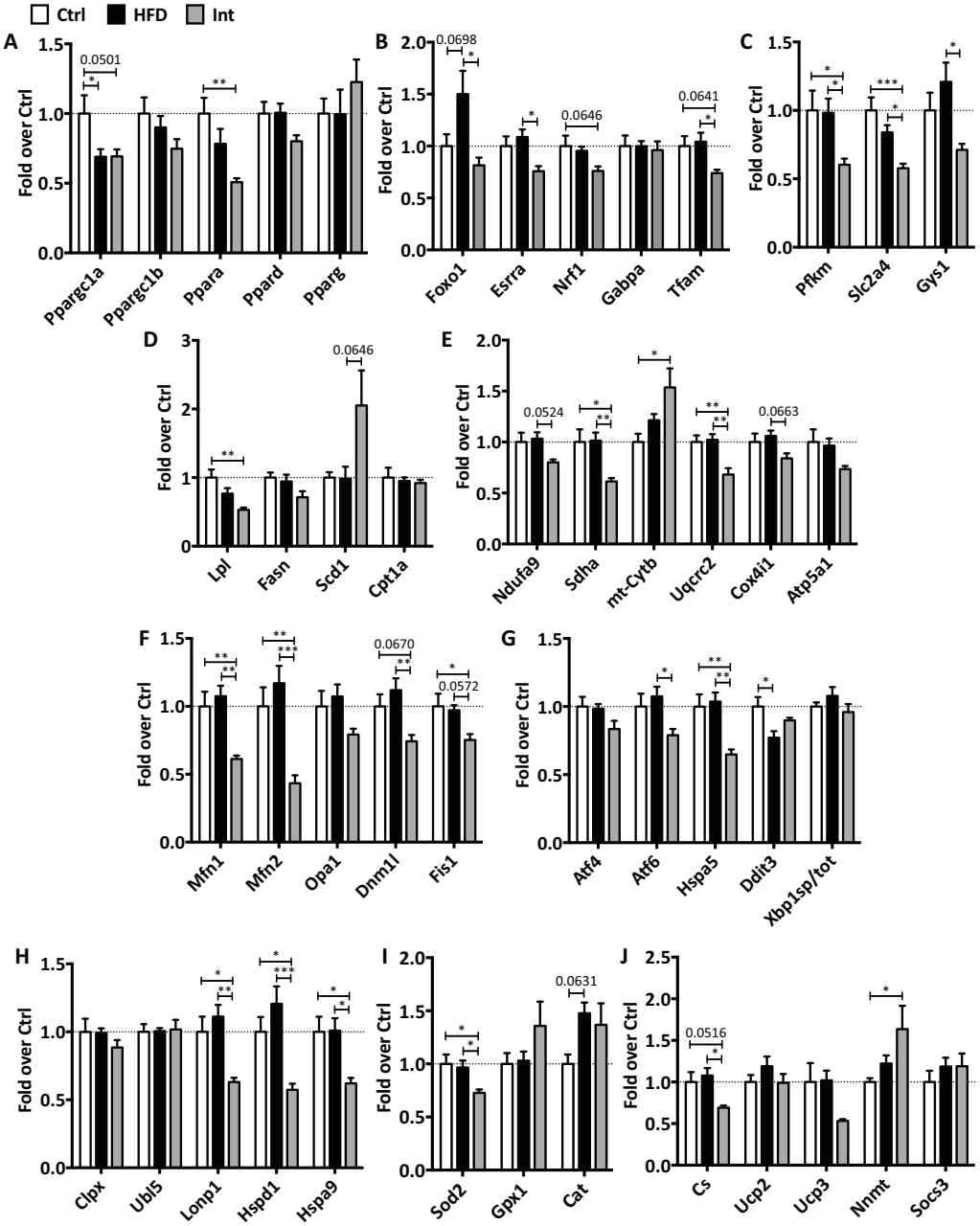

Figure 36. Gene expression in glycolytic skeletal muscle (TA). A,B: transcription factors genes. C: glucose metabolism related genes. D: lipid metabolism related genes. E: mitochondrial electron transport system (ETS) genes. F: mitochondrial dynamics genes. G: endoplasmic reticulum (ER) stress genes. H: mitochondrial stress genes. I: antioxidant genes. J: different genes unclassified in previous categorized groups. Complete name for each gene described in Materials and Methods section 5.4. Ctrl n=7-8; HFD n=7-9; Int n=7-9. Mean±SEM, ANOVA One-way, Post-hoc Tukey; *p<0.05, **p<0.01, ***p<0.001, ****p<0.0001.

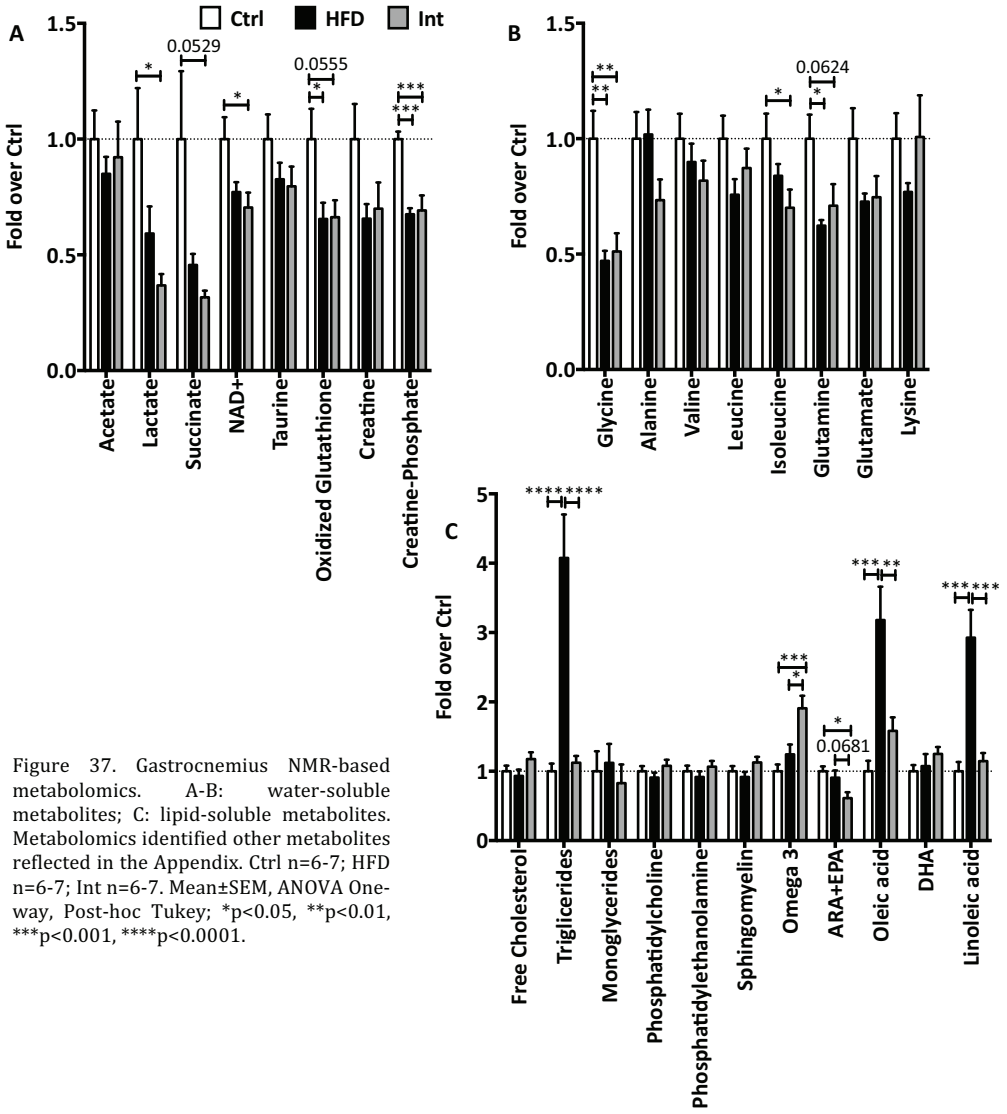

Figure 37. Gastrocnemius NMR-based metabolomics. A-B: water-soluble metabolites; C: lipid-soluble metabolites. Metabolomics identified other metabolites reflected in the Appendix. Ctrl n=6-7; HFD n=6-7; Int n=6-7. Mean±SEM, ANOVA One-way, Post-hoc Tukey; *p<0.05, **p<0.01, ***p<0.001, ****p<0.0001.

6. Hypothalamus

6.1. Hypothalamus mitochondrial function

No differences were observed in mitochondrial respiration in the hypothalamus across the three experimental groups, despite a decrease in Leak respiration in the Int group (Figure 38).

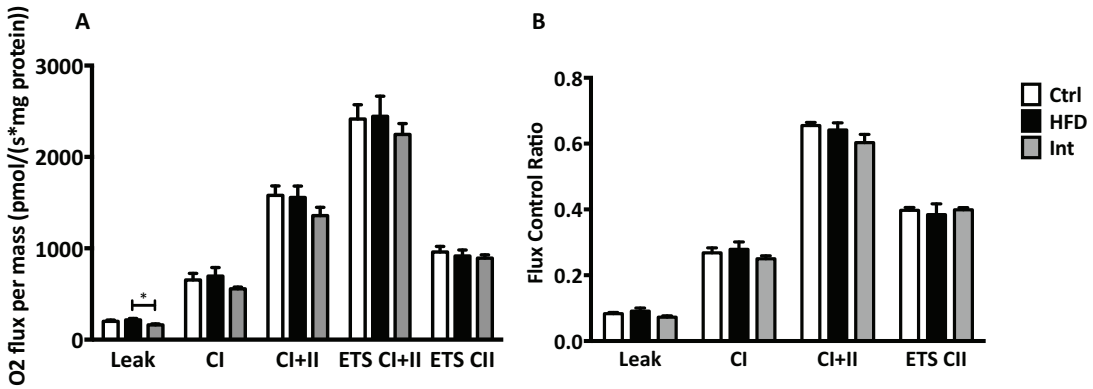

Figure 38. Mitochondrial function in hypothalamus. A: oxygen flux normalized by tissue weight. Ctrl n=7; HFD n=6; Int n=8. B: flux control ratio; oxygen flux in each respiratory state normalized by the maximum oxygen flux (ETS CI+CII). Same number of animals as in A. Mean±SEM, ANOVA One-way, Post-hoc Tukey; *p<0.05.

6.2. Hypothalamus gene expression studies

Regarding gene expression studies in hypothalamus, among all the genes assessed (Figure 39) few significant differences were observed in expression. The only transcription factor showing changes was *Pparg* with an increase in *HFD* mice expression and a reversion after LI (Figure 39A). In fact, *Pparg* is expressed in ARC neurons that control energy homeostasis and glucose metabolism (Sarruf et al. 2009). Related to the central control of metabolism, the orexigenic neuropeptides *Agrp* and *Npy* reported a decrease in expression in *HFD* mice and a reverted increase in *Int* mice (Figure 39H), while anorexigenic *Cartpt* showed the inversed pattern; all of these changes pointing to a decrease in appetite after HFD and an increase in appetite after LI that can be linked to the dietary CR situation. Of note, no changes in anorexigenic neuropeptide *Pomc* expression were observed (Figure 39H). Interestingly, *Hspa5* and *Ddit3* expression was increased in *HFD* mice and reverted in *Int* mice (Figure 39F). Moreover, *Socs3* that inhibits leptin signalling showed increased expression in *HFD*, reverted after LI (Figure 39I). No differences were revealed in the rest of transcription factor, lipid metabolism, mitochondrial OxPhos and dynamics,

mitochondrial stress, antioxidants and other unclassified genes expression (Figures 39B-E, 39G, and 39J-K).

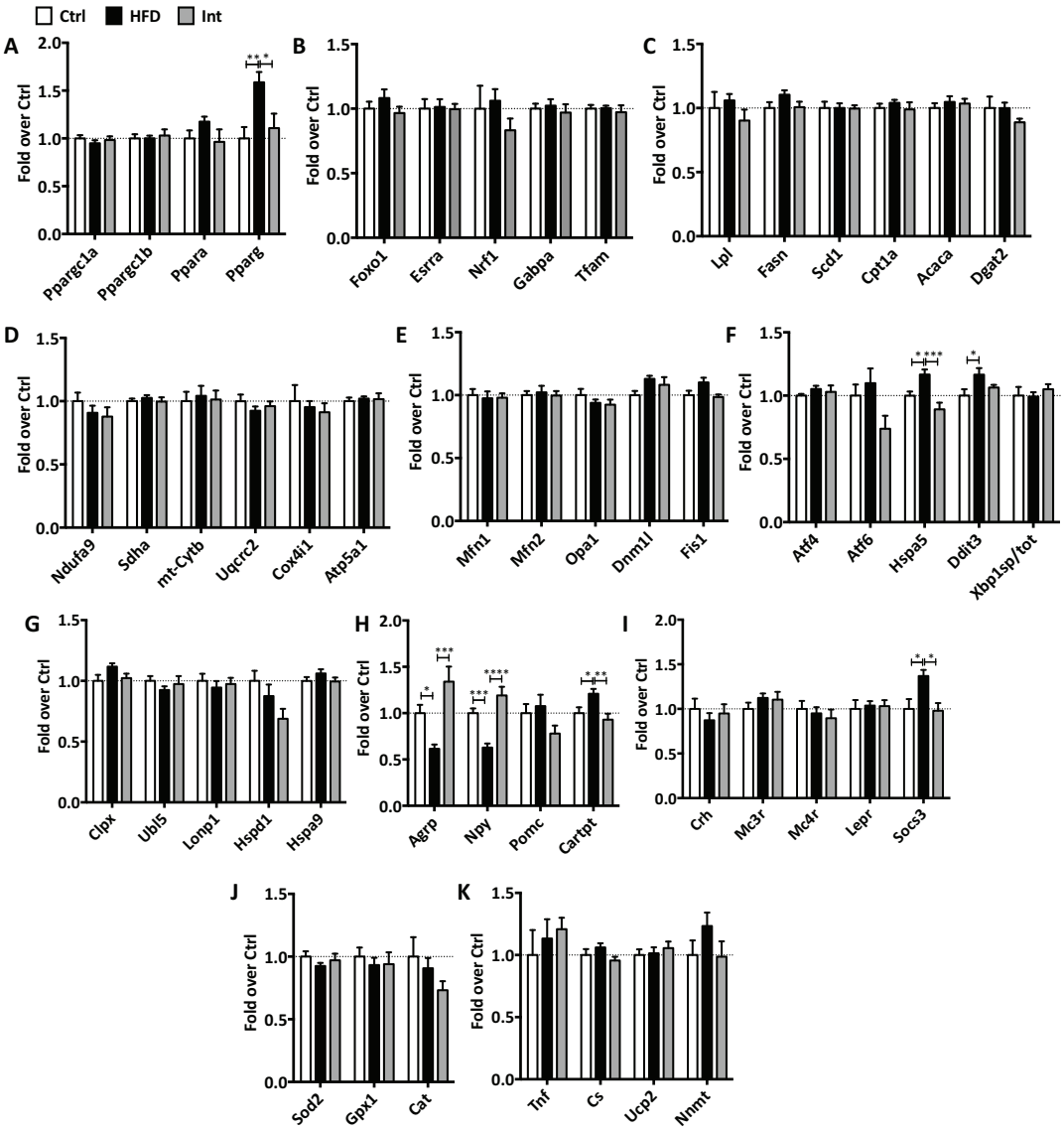

Figure 39. Gene expression in hypothalamus. A,B: transcription factors genes. C: lipid metabolism related genes. D: mitochondrial OxPhos genes. E: mitochondrial dynamics genes. F: endoplasmic reticulum (ER) stress genes. G: mitochondrial stress genes. H: antioxidant genes. I: neuropeptides genes. J: neuropeptides processing and receptor related genes. K: different genes unclassified in previous categorized groups. Complete name for each gene described in Materials and Methods section 5.4. Ctrl n=5-8; HFD n=7-9; Int n=5-6. Mean±SEM, ANOVA One-way, Post-hoc Tukey; *p<0.05, **p<0.01, ***p<0.001, ****p<0.0001.

6.3. Hypothalamus metabolomics

Similarly to the gene expression studies, fewer changes were observed in metabolomics experiments in hypothalamus (Figure 40). Among the water-soluble metabolites that were not amino acids, *HFD* mice showed decreased NAD^+ and increased choline (Figure 40A), while succinate and NAD^+ were increased after LI, along with the decrease and reversion of choline. No differences across the experimental groups were observed regarding amino acids (Figure 40B) or lipid-soluble metabolites (Figure 40C). A full list of hypothalamus detected metabolites is described in Appendix 2.

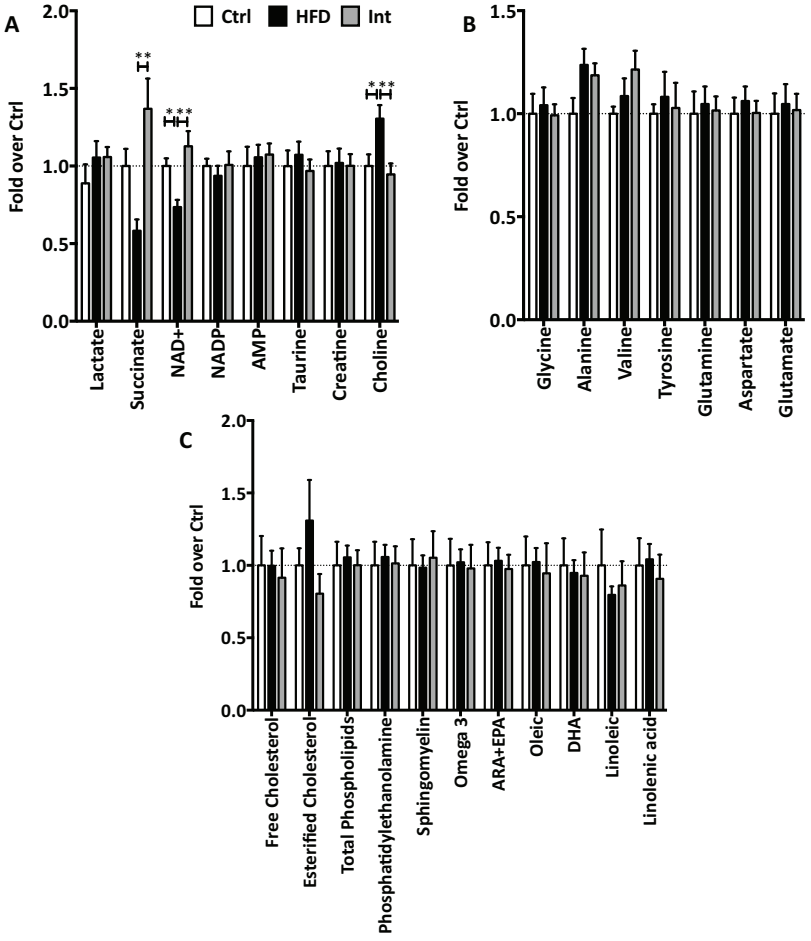

Figure 40. Hypothalamus NMR-based metabolomics. A-B: water-soluble metabolites; C: lipid-soluble metabolites. Metabolomics identified other metabolites reflected in the Appendix. Ctrl n=8-9; HFD n=7-8; Int n=7-8. Mean±SEM, ANOVA One-way, Post-hoc Tukey; *p<0.05, **p<0.01, ***p<0.001, ****p<0.0001.

7. Mitonuclear imbalance

Auwerx and colleagues suggested in 2013 that the stoichiometric imbalance between nuclear and mitochondrial encoded OxPhos subunits proteins, termed mitonuclear imbalance, which reduces mitochondrial respiration and activates mitochondrial UPR (Houtkooper et al. 2013). Hence, of interest was to assess this parameter in our experimental groups. Of note, Houtkooper and colleagues measures the imbalance by calculating the ratio between protein levels, and the current preliminary approach presented in this thesis considered mRNA expression. As a general overview, the patterns of the mitonuclear imbalance for CI and CIV seem mostly similar (Figure 41).

In eWAT mitonuclear imbalance decreased in both complexes CI and CIV in *HFD* mice and was reverted after LI. In liver, only a decrease in the imbalance in *Int* mice was observed. Oxidative skeletal muscle soleus reported an increase after HFD and return to *Ctrl* reported values in *Int* mice. As in liver, glycolytic skeletal muscle showed changes only in CIV, reporting an increase after LI of the ratio. Finally, hypothalamus only showed an increase in mitonuclear imbalance in CI after HFD. However, any of these results must be validated by protein content assays in the different ETS complexes.

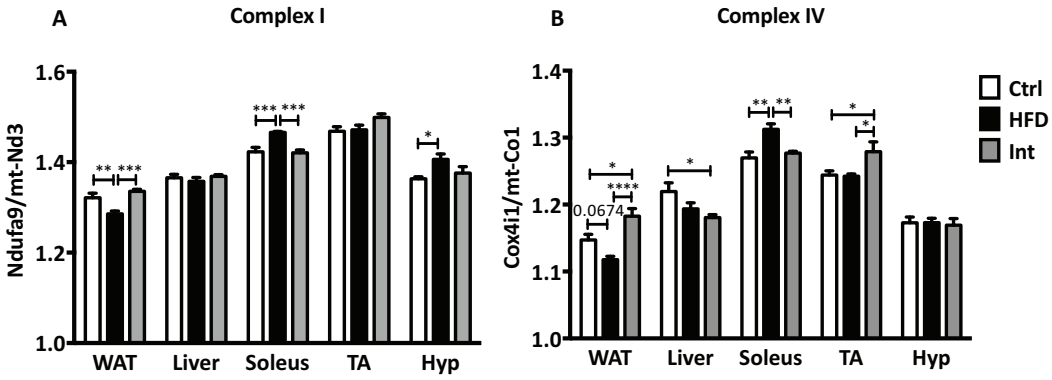

Figure 41. Mitonuclear imbalance across the studied tissues. For Complex I, Ndufa9 nuclear- and mt-Nd3 mitochondrial-encoded genes. For Complex IV, Cox4i1 nuclear- and mt-Co1 mitochondrial-encoded genes.

8. Integrative approach

8.1. Reversion level for different parameters

As explained in the Materials and Methods section 12.1.3.4, an across-groups approach analysis attempted to visually show parameters modulation due to each of the experimental conditions. The 3-point vectors explained in the section 12.1.3.3 were used in this approach in order to define a reversion or *non-reversion* pattern. Different possible scenarios were assigned to a color, hence: **green** accounts for a reversion pattern; **blue** accounts for an emphasis, a tendency across groups to increase or decrease; **red** indicates no reversion regarding the intervention group; **grey** accounts for a difference in the *Int* group in comparison to the other two groups, between the ones there was no significant difference; and **black** indicates that there were no significant differences in any of the comparisons between groups (more detailed in Materials and Methods 12.1.3.4).

8.1.1. Variation of gene expression profile among groups in the tissues under study

After the mentioned targeted analysis in gene expression data, the biggest percentage of genes showing *non-reversion* was observed in liver, while eWAT also showed a significant number of genes with a *non-reversion* profile (Figure 42). However, eWAT showed also many of the genes reverted. Regarding the skeletal muscle, the oxidative skeletal muscle (soleus) showed an almost fully reversion after intervention of gene expression that were changed from *Ctrl* to *HFD* mice, while in the glycolytic skeletal muscle (TA) most of the genes showed a difference in the *Int* group in comparison to *Ctrl* and *HFD* groups. Few changes were revealed in hypothalamus.

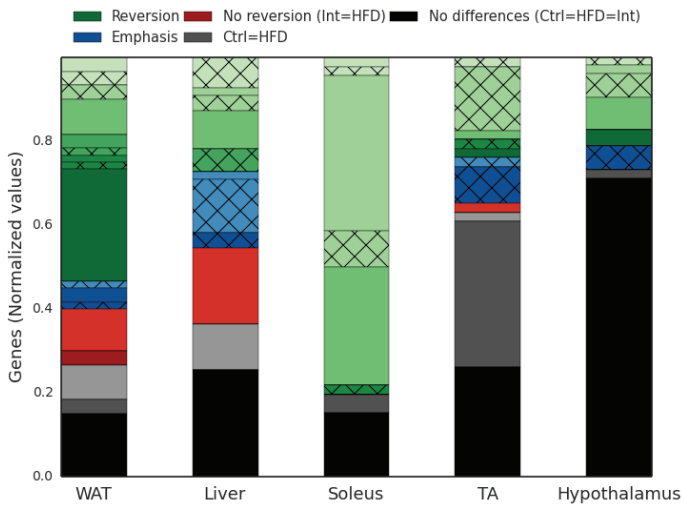

Figure 42. Gene expression patterns. Each stacked bar indicates which proportion of all the genes studied for each tissue followed a given pattern. Mann-Whitney test was used for the comparison between the 3-point vector points in order to define one of the following patterns: green (reversion), blue (emphasis), red (no reversion), grey (difference in the Int), black (no differences). For the crossed patterns, no transitivity property was observed.

8.1.2. Variation of metabolite levels among groups in the tissues under study

This approach was also used to study the reversion within metabolomics data (Figure 43). In this case, the greatest *non-reversion* appeared in eWAT and liver. In eWAT, the green pattern represents basically amino acids; the blue pattern represents unsaturated FA that are altered after LI; and the red pattern mostly represent water-soluble metabolites (ie. glucose-6-phosphate, lactate, succinate, free cholesterol, diglycerides, phosphatidylcholine, and some amino acids). Moreover, more liver metabolites were reverted in comparison to eWAT. In liver, the green pattern represents in general the lipid-soluble metabolites (ie. free cholesterol, TG, DAG, and unsaturated FA) as well as water-soluble phosphatidylethanolamine; the blue pattern might represent different water-soluble metabolites (ie. glucose-6-phosphate, lactate and some amino acids); and the red pattern accounts for amino acids, NAD^+, sphingomyelin and creatinine. Regarding skeletal muscle (gastrocnemius), most of metabolites were not affected across the three experimental groups, although there were some *non-reverted* metabolites. In this tissue, the green pattern accounts for lipid-soluble metabolites (ie. TG, oleic and linoleic acid); the blue pattern encompasses Om3, ARA and EPA; and the red pattern represents water-soluble metabolites in general. Finally, a similar pattern as in hypothalamus gene expression was observed in hypothalamus metabolites. In hypothalamus, green pattern represents NAD^+ and choline while blue pattern accounts for succinate.

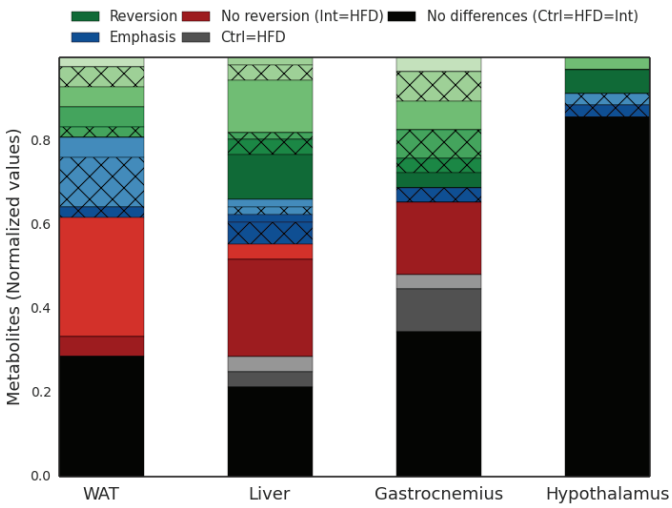

Figure 43. Metabolites patterns. Each stacked bar indicates which proportion of all the metabolites studied for each tissue followed a given pattern. Mann-Whitney test was used for the comparison between the 3-point vector points in order to define one of the following patterns: green (reversion), blue (emphasis), red (no reversion), grey (difference in the Int), black (no differences). For the crossed patterns, no transitivity property was observed.

8.1.3. Variation of mitochondrial respiratory states among groups in the tissues under study

When this analytical approach was used to assess the pattern of the mitochondrial respiratory states along with FCR among the different experimental groups, the greatest *non-reversion* was observed in eWAT samples, followed by soleus (Figure 44). This was a more comfortable way to visualize all the changes in the mitochondrial respiratory states. Oxidative skeletal muscle (soleus) showed a variety of different patterns, while glycolytic skeletal muscle (EDL) revealed almost no changes across the experimental groups. As in the metabolites case, hypothalamus showed mostly no changes across the three experimental animal groups.

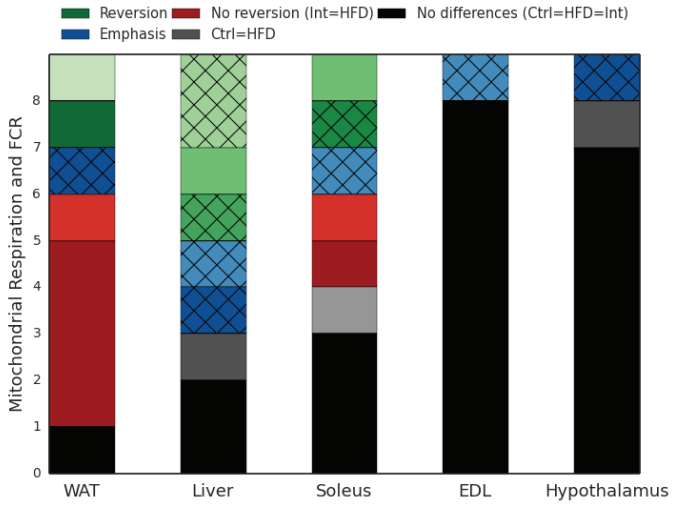

Figure 44. Mitochondrial function patterns. Each stacked bar indicates how many of the mitochondrial respiration states and flux control ratios followed a given pattern. Mann-Whitney test was used for the comparison between the 3-point vector points in order to define one of the following patterns: green (reversion), blue (emphasis), red (no reversion), grey (difference in the Int), black (no differences). For the crossed patterns, no transitivity property was observed.

8.2. Mitochondrial function (cosine similarity matrix)

Mitochondrial respiration in WAT was decreased in the *HFD* and maintained low in the *Int* group (Figure 24). These results, which were visualized in the previous approach (Results section 7.1.3), were confirmed after defining a cosine similarity matrix (Figure 45) with all the respiratory states in all tissues studied. That is, and as explained in Materials and Methods section 12.1.3.3, cosine similarity correlation was studied comparing pairs of the 3-point vectors defined in the aforementioned Materials and Methods part. Although cosine similarity values range from 0 to 1, the graphical representation started at 0.80 to ease the visual identification of the differences, and given that re-scaling the axis did not mean missing any relevant information. The decreased cosine similarity when comparing

WAT respiratory state parameters (CI+CII, ETS CI+CII and ETS CII) correlated with WAT mitochondrial function shown in Results section 3.2 (Figure 24).

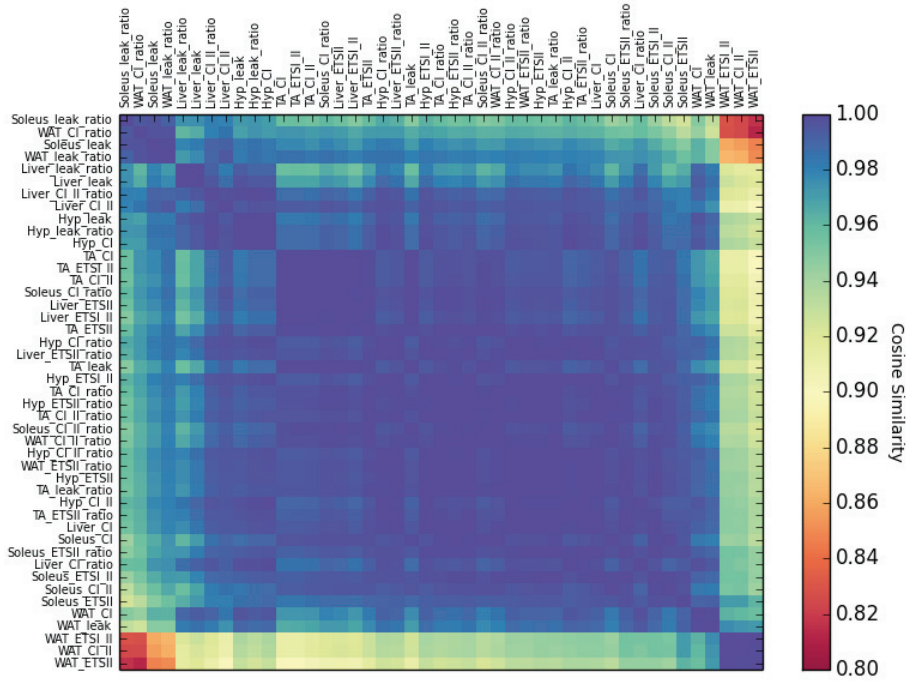

Figure 45. Mitochondrial respiratory states matrix. Cosine similarity was calculated for each pair comparison of 3-point vectors of mitochondrial function WAT data.

8.3. RNAseq data analysis reported no reversion in OxPhos and inflammation genes in eWAT

8.3.1. Gene enrichment analysis

As explained in Materials and Methods part 13.2.1 section, 5147 out of 21761 genes (23.65%) have mRNA expression value significantly different at least in one of the pair comparisons (*Ctrl* vs *HFD*, *Ctrl* vs *Int*, *HFD* vs *Int*). Subsequently, this subset of genes was separated in expression patterns (same as described in Materials and Methods part 13.1.3.2 section, or in Results part 8.1 section). The visualization of the different patterns by Z-score was translated into a color scale, meaning that the reddish the more expressed, and the more bluish, the less expressed (Figure 46). Among the genes separated in these patterns, 66.33% showed reversion (green pattern, Figures 46A-F), 0.64% showed emphasis (blue, Figures 46G-H), and 33.03% reported *non-reversion* (red, Figures 46I-J).

Of interest were the patterns showing *non-reversion* (Figure 46J and 46I), as well as *half-reversion* (meaning that Int values were between Ctrl and HFD values) (Figures 46C and 46D).

Some of the genes revealed a pattern of *non-reversion* with decreased expression after HFD and after LI (Figure 46J). Among these genes: *Opa1* and several OxPhos subunits: 15 genes encoding for CI subunits (*Ndufa2*, *Ndufa4*, *Ndufa7*, *Ndufa9*, *Ndufa10*, *Ndufa12*, *Ndufb8*, *Ndufb9*, *Ndufb10*, *Ndufs1*, *Ndufs2*, *Ndufs3*, *Ndufs7*, *Ndufv1*, and *Ndufv3*), 2 genes encoding for CI (*Sdha* and *Sdhd*), 6 genes encoding for CIII (*Cyb5a*, *Uqcrc1*, *Uqcrc2*, *Uqcrc11*, *Uqcrfs1*, and *Uqcc1*), 4 genes encoding for CIV (*Cox4i1*, *Cox8a*, *Cox14*, and *Cox18*), and 6 genes encoding for CV (*Atp2b4*, *Atp4b*, *Atp5a1*, *Atp5b*, *Atp5c1*, and *Atp5k*).

This pattern was of interest, given that followed the same pattern as mitochondrial dysfunction. A total of 963 genes followed this pattern. Thus, a gene ontology enrichment analysis was performed for this subset of genes as explained in Materials and Methods part 13.2.1 section. Defining the ontology for biological processes, respiratory electron transport chain, tricarboxylic acid cycle and mitochondrion organization appeared among enriched processes (Table 32, Figure 47).

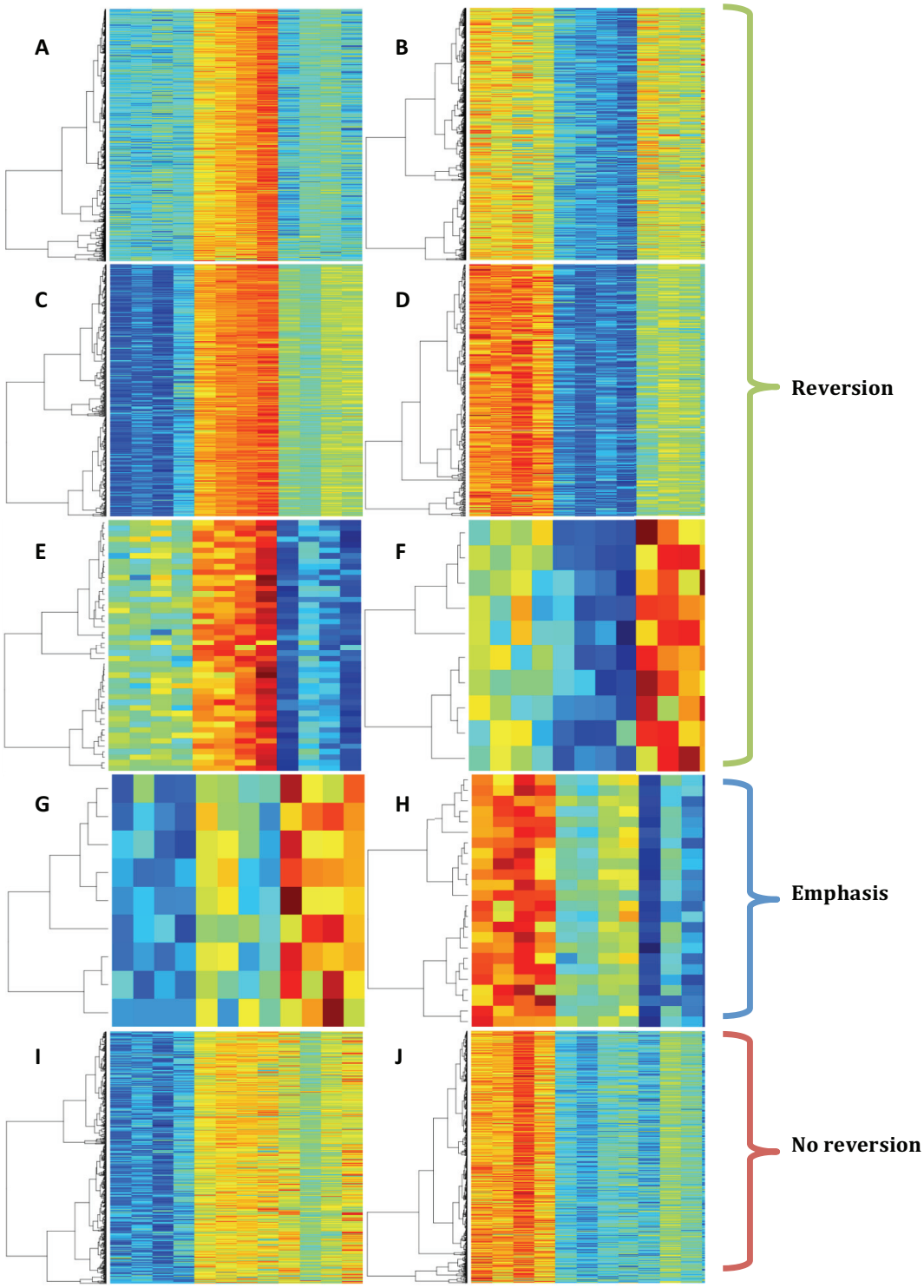

Figure 46. Heatmaps indicating the pattern of gene expression from RNAseq data in eWAT. Z-scores are represented (-2 accounts for dark blue, +2 accounts for dark red). Each row indicates a different gene.

GO Term	Description	P-value	FDR q-value	Enrichment
GO:0044710	single-organism metabolic process	5.72E-39	7.71E-35	2.07
GO:0008152	metabolic process	1.32E-33	8.91E-30	1.52
GO:0055114	oxidation-reduction process	7.36E-33	3.31E-29	3.38
GO:0044281	small molecule metabolic process	9.17E-28	3.09E-24	2.55
GO:0044237	cellular metabolic process	8.22E-25	2.22E-21	1.51
GO:0071704	organic substance metabolic process	5.06E-21	1.14E-17	1.43
GO:0019752	carboxylic acid metabolic process	3.39E-19	6.53E-16	2.83
GO:0044238	primary metabolic process	4.85E-19	8.17E-16	1.42
GO:0043436	oxoacid metabolic process	8.06E-19	1.21E-15	2.71
GO:0006082	organic acid metabolic process	3.18E-18	4.28E-15	2.66
GO:0006101	citrate metabolic process	5.75E-17	7.05E-14	12.71
GO:0006732	coenzyme metabolic process	1.80E-16	2.02E-13	4.36
GO:0072350	tricarboxylic acid metabolic process	2.87E-16	2.97E-13	11.92
GO:0051186	cofactor metabolic process	3.09E-15	2.98E-12	3.82
GO:1901564	organonitrogen compound metabolic process	3.84E-15	3.45E-12	2.17
GO:0006099	tricarboxylic acid cycle	4.24E-15	3.57E-12	12.55
GO:0006793	phosphorus metabolic process	2.17E-13	1.72E-10	1.94
GO:0009987	cellular process	6.73E-13	5.03E-10	1.21
GO:0044711	single-organism biosynthetic process	1.68E-12	1.19E-09	2.25
GO:0006796	phosphate-containing compound metabolic process	3.27E-12	2.20E-09	1.9
GO:0043648	dicarboxylic acid metabolic process	8.77E-12	5.62E-09	6.18
GO:0007005	mitochondrion organization	7.77E-11	4.76E-08	2.9
GO:0022904	respiratory electron transport chain	9.90E-11	5.80E-08	8.15

Table 32. GOrilla results for biological process gene ontology in eWAT in genes for a given pattern (Figure 46J). p-value tresshold at 10^{-10}.

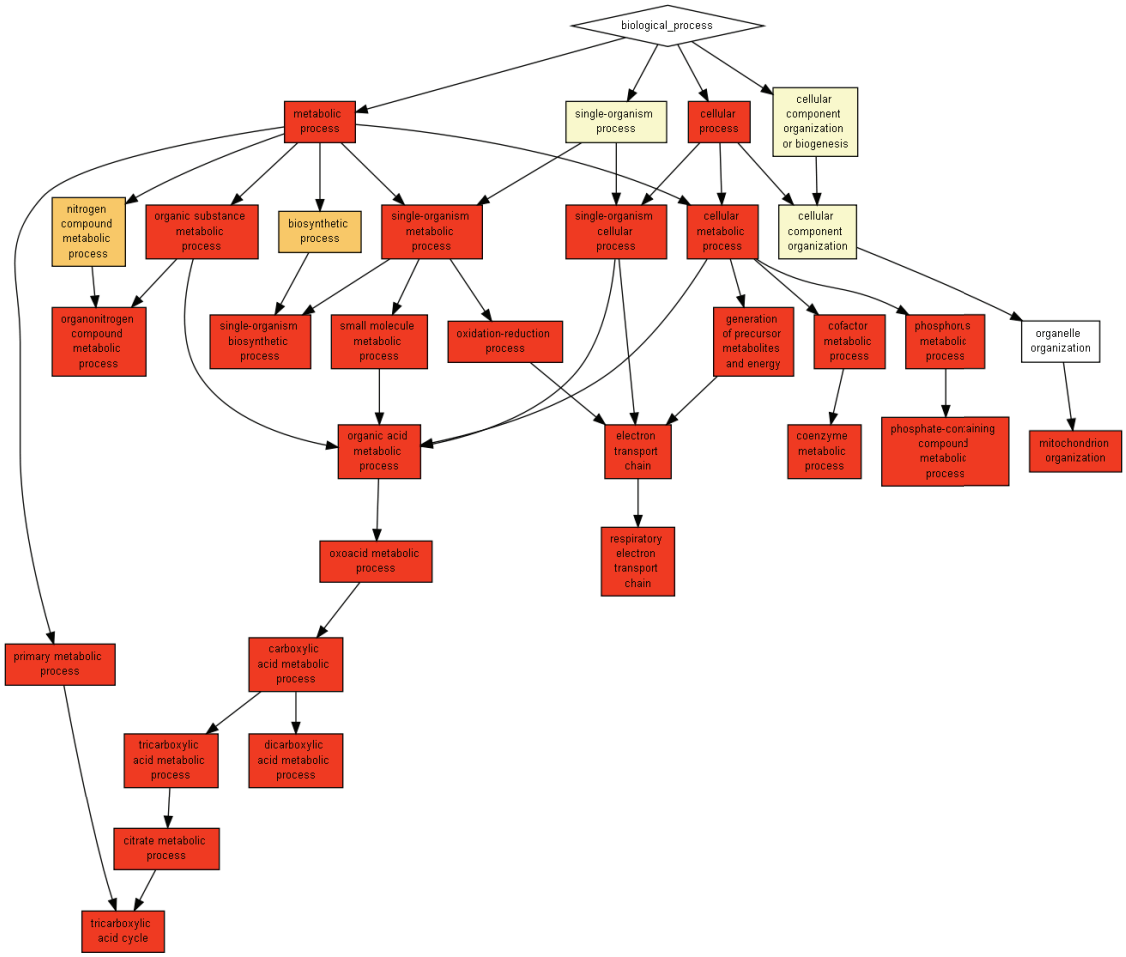

Figure 47. GOrilla results for biological process gene ontology in eWAT in genes for a given pattern (Figure 46J). p-value tresshold at 10^{-10}.

GOrilla enrichment analysis allowed the classification of the genes with a cellular component ontology. Results from this analysis are indicated in Table 33 and Figure 48. In this case, specifically CI (NADH dehydrogenase complex, respiratory chain complex I, and mitochondrial respiratory chain complex I) was enriched.

GO Term	Description	P-value	FDR q-value	Enrichment
GO:0005739	mitochondrion	3.22E-79	5.15E-76	3.66
GO:0044429	mitochondrial part	4.86E-49	3.89E-46	4.41
GO:0044444	cytoplasmic part	6.39E-43	3.40E-40	1.69
GO:0005743	mitochondrial inner membrane	1.29E-38	5.15E-36	5.48
GO:0019866	organelle inner membrane	8.53E-38	2.73E-35	5.22
GO:0031966	mitochondrial membrane	2.87E-33	7.65E-31	4.34
GO:0043227	membrane-bounded organelle	2.51E-28	5.74E-26	1.36
GO:0043231	intracellular membrane-bounded organelle	2.55E-26	5.09E-24	1.39
GO:0044424	intracellular part	3.02E-26	5.36E-24	1.27
GO:0043226	organelle	1.59E-24	2.55E-22	1.3
GO:0098798	mitochondrial protein complex	1.84E-24	2.68E-22	7.37
GO:0043229	intracellular organelle	2.57E-23	3.42E-21	1.33
GO:1990204	oxidoreductase complex	3.30E-22	4.06E-20	8.58
GO:0098800	inner mitochondrial membrane protein complex	2.03E-21	2.32E-19	8.17
GO:0044455	mitochondrial membrane part	2.60E-20	2.78E-18	6.03
GO:0031090	organelle membrane	7.73E-20	7.72E-18	2.23
GO:0098803	respiratory chain complex	2.29E-19	2.15E-17	9.81
GO:0070469	respiratory chain	7.62E-18	6.77E-16	9.74
GO:0044446	intracellular organelle part	2.97E-14	2.50E-12	1.4
GO:0030964	NADH dehydrogenase complex	4.99E-14	3.99E-12	10.29
GO:0045271	respiratory chain complex I	4.99E-14	3.80E-12	10.29
GO:0005747	mitochondrial respiratory chain complex I	4.99E-14	3.63E-12	10.29
GO:0044422	organelle part	1.19E-13	8.29E-12	1.38
GO:0005759	mitochondrial matrix	1.25E-12	8.33E-11	6.09
GO:1902494	catalytic complex	3.30E-12	2.11E-10	2.23
GO:0042579	microbody	7.19E-12	4.42E-10	4.63
GO:0005777	peroxisome	4.16E-11	2.46E-09	4.63
GO:0043233	organelle lumen	5.66E-11	3.23E-09	4.02

Table 33. GOrilla results for cellular component gene ontology in eWAT in genes for a given pattern (Figure 46J). p-value tresshold at 10^{-10}.

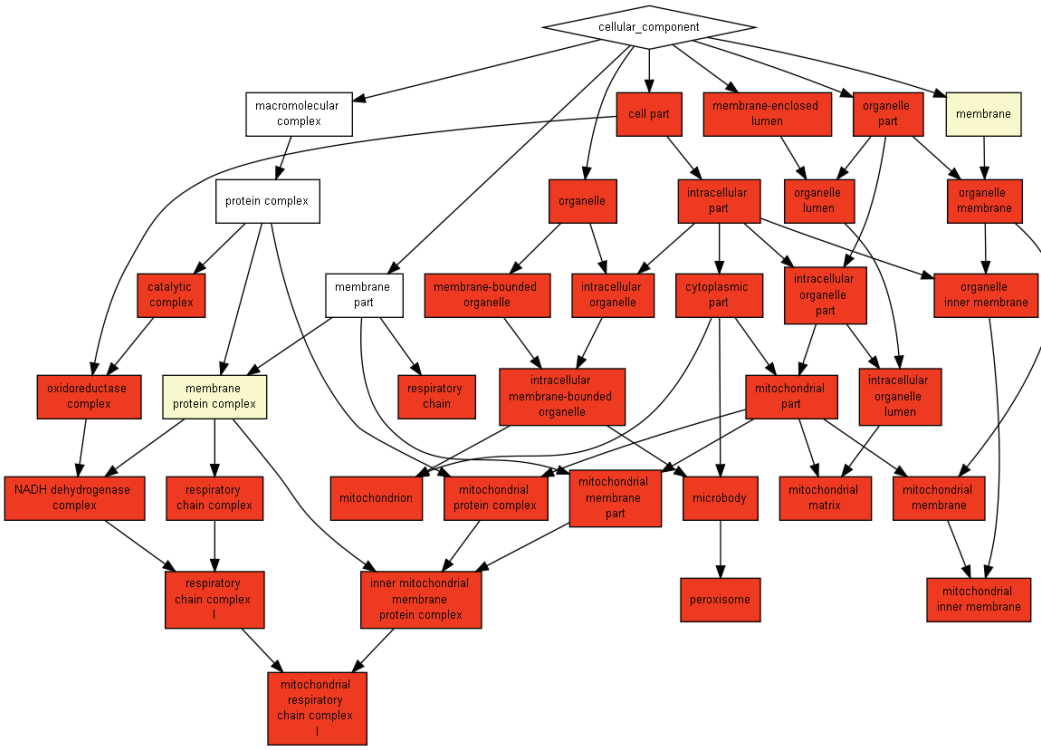

Figure 48. GOrilla results for cellular component gene ontology in eWAT in genes for a given pattern (Figure 46J). p-value tresshold at 10^{-10}.

The other *non-reversion* pattern (Figure 46I) included genes with increased expression after HFD and LI. In this case, this pattern seemed shared with the inflammatory and immune cell infiltration state. A total of 737 genes followed this pattern. Defining the ontology for biological processes, cell cycle and immune system processes were identified (Table 34, Figure 49).

GO Term	Description	P-value	FDR q-value	Enrichment
GO:1903047	mitotic cell cycle process	1.15E-15	1.55E-11	3.43
GO:0022402	cell cycle process	2.30E-14	1.55E-10	2.77
GO:0007059	chromosome segregation	8.85E-13	3.98E-09	6.7
GO:0098813	nuclear chromosome segregation	5.41E-12	1.82E-08	12.56
GO:0007067	mitotic nuclear division	1.48E-11	3.98E-08	3.95
GO:0007049	cell cycle	1.62E-11	3.63E-08	2.72
GO:0000280	nuclear division	4.44E-11	8.55E-08	3.54
GO:0000070	mitotic sister chromatid segregation	4.85E-11	8.16E-08	16.48
GO:0048285	organelle fission	9.43E-11	1.41E-07	3.38
GO:0044763	single-organism cellular process	1.37E-10	1.84E-07	1.29
GO:0000819	sister chromatid segregation	4.18E-10	5.12E-07	14.01

GO:0002376	immune system process	5.89E-10	6.62E-07	2.08
GO:0051301	cell division	3.24E-09	3.36E-06	2.98
GO:0048583	regulation of response to stimulus	9.81E-09	9.44E-06	1.56
GO:0051983	regulation of chromosome segregation	3.88E-08	3.48E-05	6.75
GO:0070269	pyroptosis	5.31E-08	4.47E-05	21.02

Table 34. GOrilla results for biological process gene ontology in eWAT in genes for a given pattern (Figure 46I). p-value tresshold at 10^{-7}.

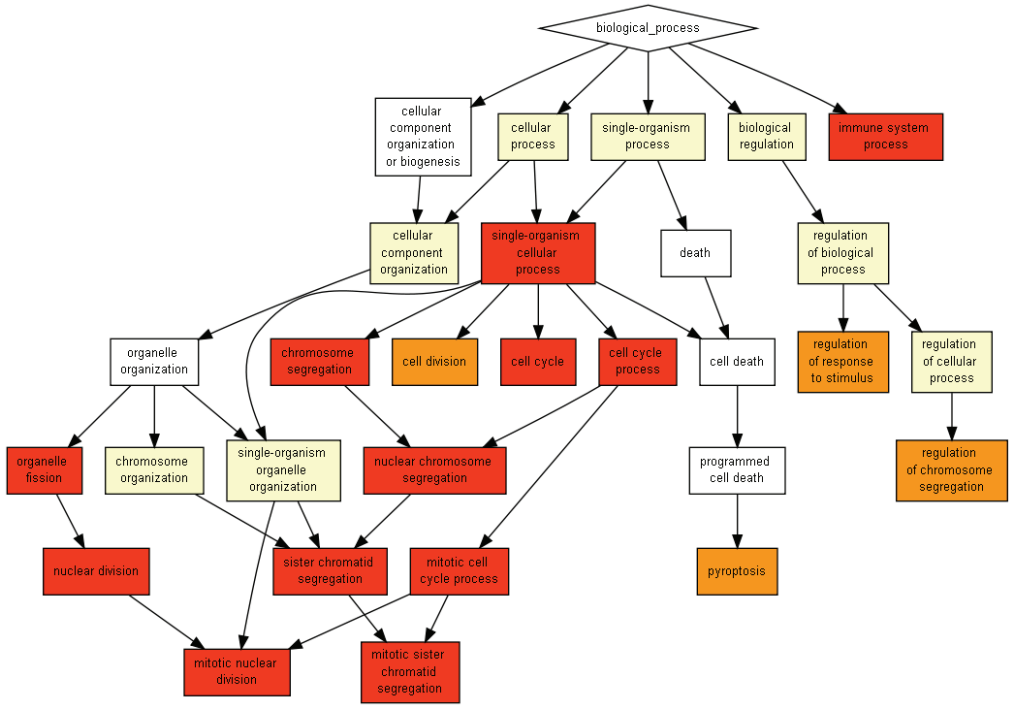

Figure 49. GOrilla results for biological process gene ontology in eWAT in genes for a given pattern (Figure 46I). p-value tresshold at 10^{-7}.

When a cellular component ontology was used, chromosome-related and inflammasome processes were identified (Table 35, Figure 50).

GO Term	Description	P-value	FDR q-value	Enrichment
GO:0000775	chromosome, centromeric region	1.07E-09	1.72E-06	4.99
GO:0061702	inflammasome complex	2.41E-09	1.93E-06	21.8
GO:0016020	membrane	2.45E-08	1.31E-05	1.27

Table 35. GOrilla results for cellular component gene ontology in eWAT in genes for a given pattern (Figure 46I). p-value tresshold at 10^{-7}.

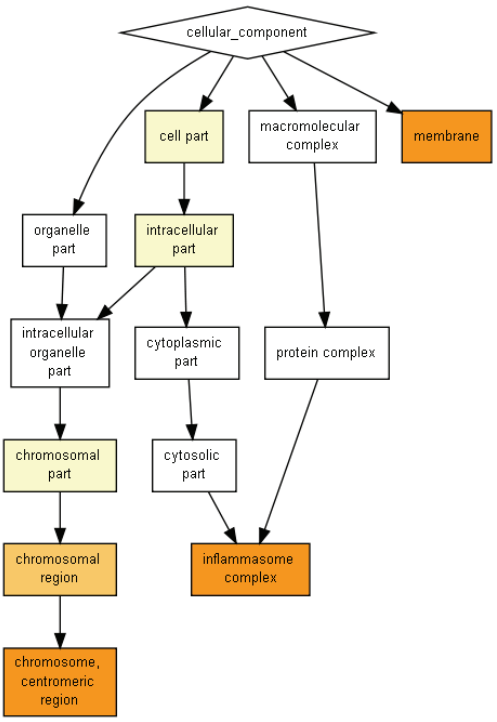

Figure 50. GOrilla results for cellular component gene ontology in eWAT in genes for a given pattern (Figure 46I). p-value tresshold at 10^{-7}.

Another interesting pattern consisted in the *half-reversion*, meaning expression was increased (or decreased) after HFD and partially decreased (or increased) back to *Ctrl* values after LI (Figures 46C and 46D).

In the case of an increase after HFD and a decrease after LI (Figure 46C), the pattern would be similar to the one above (which had a pattern similar to the inflammation state), although *Int* group values were significantly lower in comparison to *HFD* mice values. A subset of 556 genes followed this pattern. As observed in Table 36 and Figure 51, when gene ontology was performed by biological processes, immune system was enriched.

GO Term	Description	P-value	FDR q-value	Enrichment
GO:0048518	positive regulation of biological process	1.87E-16	2.51E-12	1.69
GO:0002376	immune system process	5.51E-13	3.71E-09	2.51
GO:0051128	regulation of cellular component organization	1.12E-12	5.02E-09	2.06
GO:0050776	regulation of immune response	1.21E-12	4.07E-09	3.68
GO:0002684	positive regulation of immune system process	1.24E-12	3.35E-09	3.14

GO:0032879	regulation of localization	1.35E-12	3.04E-09	1.98
GO:0048522	positive regulation of cellular process	1.92E-12	3.70E-09	1.63
GO:0002682	regulation of immune system process	3.11E-12	5.23E-09	2.53
GO:0048583	regulation of response to stimulus	8.19E-12	1.23E-08	1.79
GO:0044763	single-organism cellular process	1.30E-11	1.74E-08	1.36
GO:0032956	regulation of actin cytoskeleton organization	5.08E-11	6.22E-08	4.4
GO:0016043	cellular component organization	8.48E-11	9.52E-08	1.6

Table 36. GOrilla results for biological process gene ontology in eWAT in genes for a given pattern (Figure 46C). p-value tresshold at 10^{-10}.

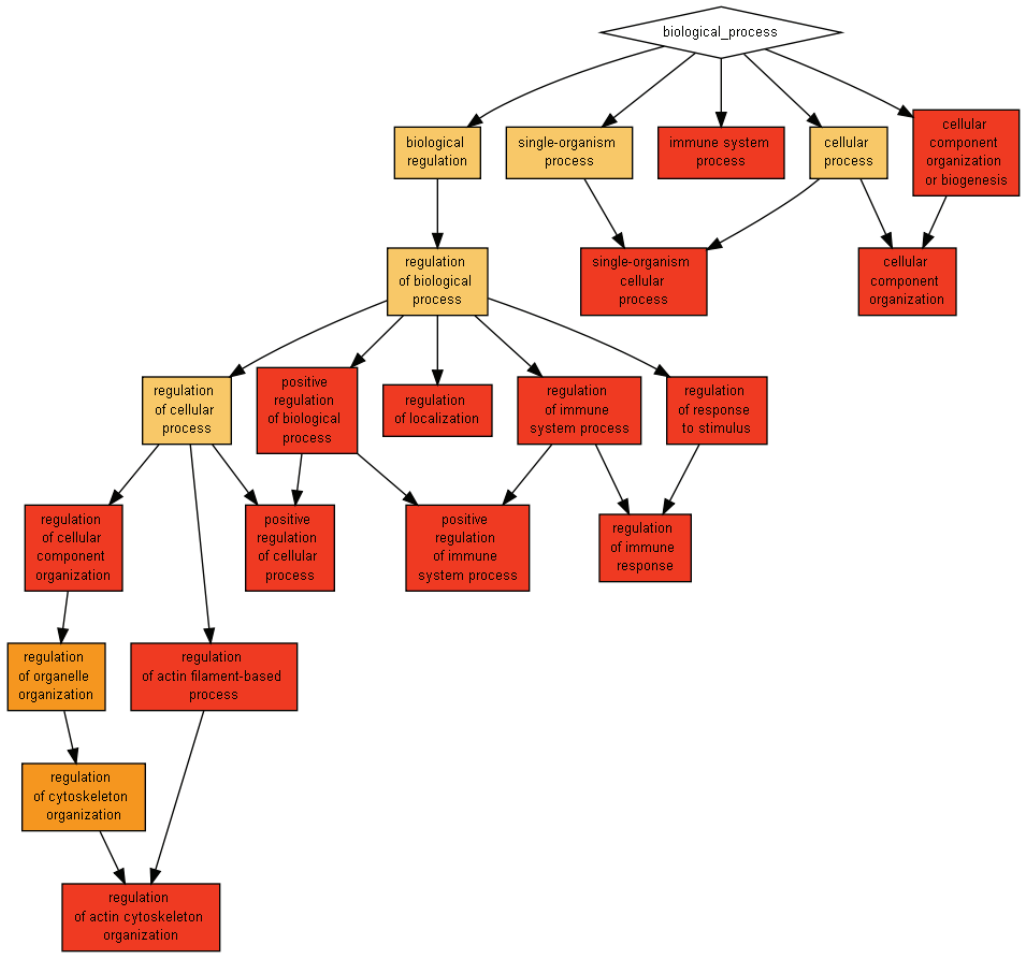

Figure 51. GOrilla results for biological process gene ontology in eWAT in genes for a given pattern (Figure 46C). p-value tresshold at 10^{-10}.

In the case of a decrease after HFD and an increase after LI (Figure 46D), the pattern would follow a similar trend to mitochondrial dysfunction, although *Int* group values were

significantly higher in comparison to *HFD* mice values. A subset of 342 genes followed this pattern. As observed in Table 37 and Figure 52, when gene ontology was performed by cellular components, mitochondrion was identified.

GO Term	Description	P-value	FDR q-value	Enrichment
GO:0005739	mitochondrion	6.50E-15	1.04E-11	2.87

Table 37. GOrilla results for cellular component gene ontology in eWAT in genes for a given pattern (Figure 46D). p-value tresshold at 10^{-10}.

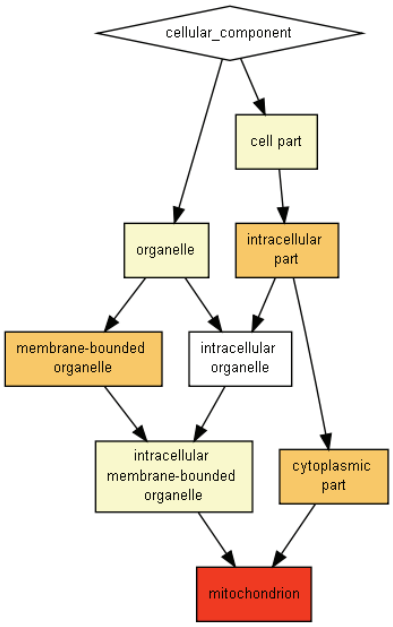

Figure 52. GOrilla results for cellular component gene ontology in eWAT in genes for a given pattern (Figure 46D). p-value tresshold at 10^{-10}.

8.3.2. Protein-Protein Interaction network approach confirmed OxPhos genes as *non-reverted*

A protein-protein interaction (PPI) network approach was performed among the different integrative data analysis approaches during this PhD thesis.

As explained in Materials and Methods 13.2.2 the approach consisted in identifying the genes/variants in the RNAseq data that changed significantly from *Ctrl* to *HFD* groups, with the idea to study which of the genes that changed were reverted and to which extent. Once these genes were identified, they were given a protein ID to be introduced in a PPI curated database. Once the interactions were defined among the genes of interest, hubs were identified to describe protein complexes (PC).

The reversibility index (RI) was calculated for each gene and, once the PCs were described, a mean of RI of all genes in the complex was calculated for each complex (average RI, Avg_RI) along with its standard deviation (SD). The Avg_RI/SD ratio was calculated for each complex, studying the amount of variation or dispersion of all the RI values of the genes of the complex. Concretely, only Avg_RI/SD ratios above 1 were considered and the included ones were ranked according to this ratio. The ten complexes with highest Avg_RI/SD ratio in eWAT were further studied (Appendix 3). In Appendix 3, hubs have their RI instead of labeled as "partner". Moreover, from these ten complexes five of them involved mitochondrial oxidative phosphorylation (OxPhos) genes (Figure 53, represented in a grid layout) from different complexes. Among these five complexes, complex 6 (Figure 55 is amplified and represented in an organic layout. Of note, protein complexes described in Appendix 3 and represented in Figures 53 and 55 contained genes, most of them not reverted (indicated by red/orange color). The legend for the network is explained in Figure 54.

The complex represented in Figure 55 included: NADH dehydrogenase (ubiquinone) known as complex I, that was the most represented with 28 subunits divided in the alpha subcomplex (NDUFA1, NDUFA2, NDUFA3, NDUFA4, NDUFA5, NDUFA6, NDUFA7, NDUFA9, NDUFA10, NDUFA12), the beta subcomplex (NDUFB4, NDUFB5, NDUFB6, NDUFB7, NDUFB9, NDUFB10, NDUFB11), an unknown subcomplex (NDUFC1), flavoprotein subunits (NDUFV1, NDUFV2, NDUFV3), and Fe-S proteins (NDUFS1, NDUFS2, NDUFS3, NDUFS5, NDUFS6, NDUFS7, NDUFS8). Complex I catalyzes the transfer of electrons from NADH to coenzyme Q10 and it is located in the inner mitochondrial membrane. The other represented complexes were cytochrome oxidase or complex IV (COX4I1, COX5B, COX6A1,

COX6C, COX7A2, and COX7C subunits), and ubiquinol cytochrome c reductase or complex III (UQCRFS1, UQCRB, UQCRQ, UQCRC1, UQCRC2, UQCR10, and CYC1). TRAF6 was also present in the protein complex, which was related to the TRAF2, an ubiquitin ligase that can also lead to the activation of NFκB and JUN and seems to play a role in signal transduction initiated via TNF receptor, IL-1 receptor and IL-17 receptor among other functions; and GOLGB1 which may participate in forming intercisternal cross-bridges of the Golgi complex.

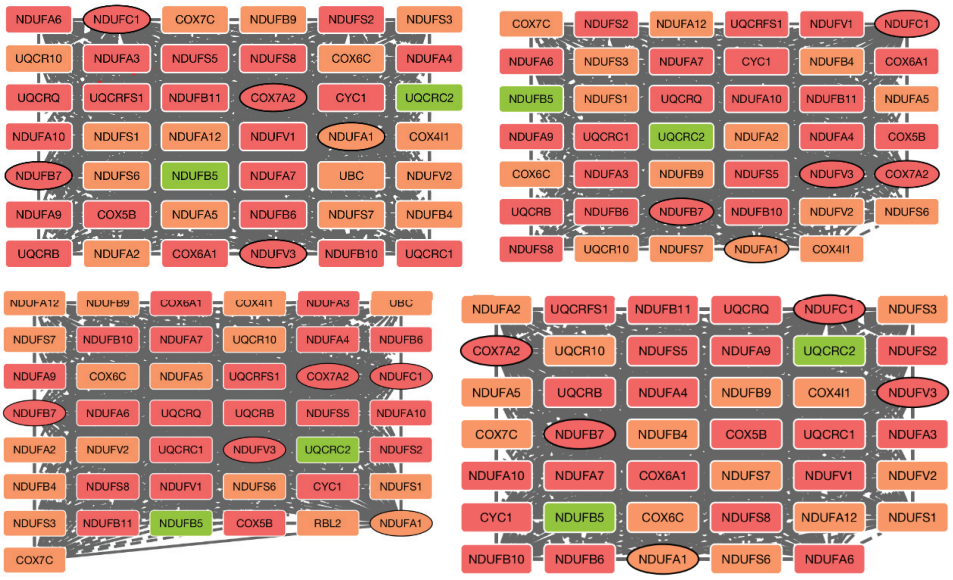

Figure 53. eWAT complexes 7,8,9 and 10 involving OxPhos subunits.

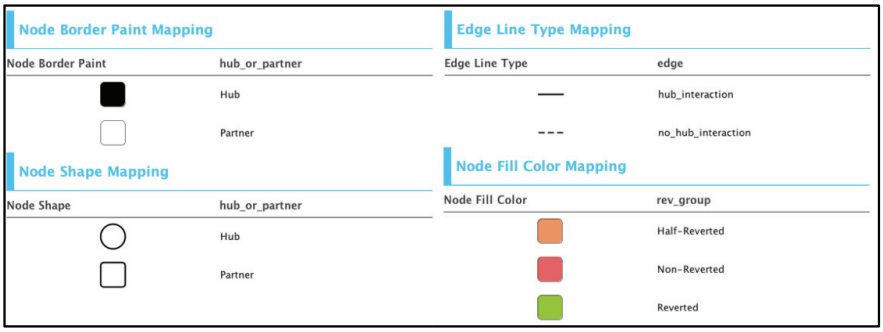

Figure 54. Legend for the network representations.

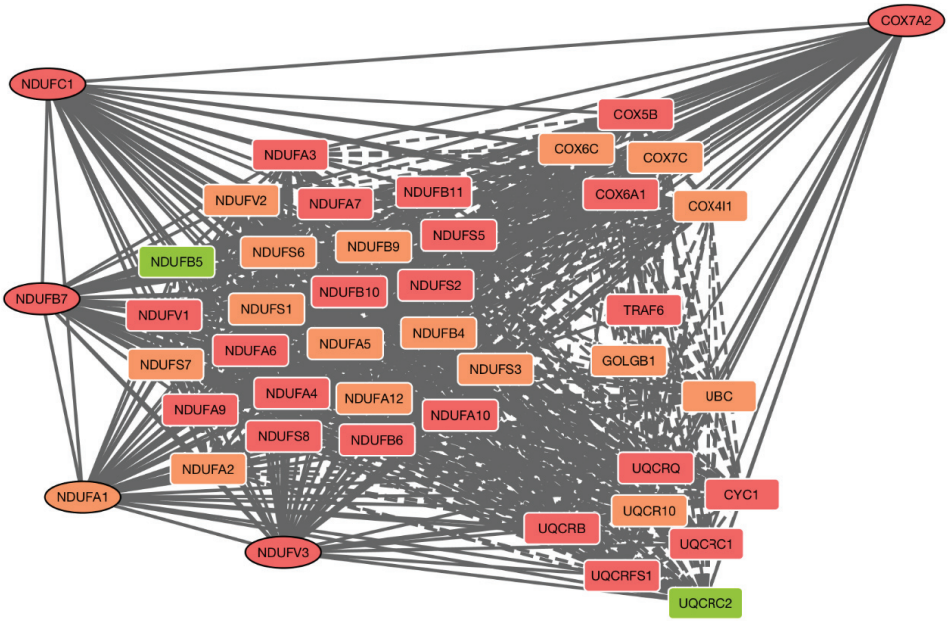

Figure 55. eWAT protein complex involving OxPhos subunits.

DISCUSSION

1. Animals phenotype

C57BL6/J mice after 16 wks on HFD reported overweight; increased fat mass and volume; increased epididymal white adipose tissue, pancreas and liver weight; glucose intolerance and insulin resistance; fasting hyperglycemia, hyperinsulinemia and hyperleptinemia; increased β-cell area, hypertrophic enlarged pancreatic islets and disrupted glucose-stimulated insulin secretion (GSIS) *in vivo* and *in vitro*; increased triglycerides (TG) accumulation in liver and oxidative skeletal muscle; and decreased oxygen consumption, heat production and scapular temperature. All these features in line with the literature about diet-induced obesity (DIO) (Buettner et al. 2007; Williams et al. 2014; Winzell & Ahrén 2004; Schneeberger et al. 2013; Hatori et al. 2012). After lifestyle intervention (LI), mice recovered BW; decreased fat mass and volume; decreased epididymal white adipose tissue, pancreas and liver weight; decreased TG accumulation in liver and oxidative skeletal muscle; and increased oxygen consumption, heat production and scapular temperature. Glucose homeostasis experiments revealed improved glucose tolerance and insulin sensitivity after LI despite impaired fasting glucose with hyperinsulinemia and hyperglycemia. It is worth mentioning that glucotoxicity has been seen to contribute to impairing β-cell function (Rossetti et al. 1990). Moreover, exercise intervention improved fasting hyperglycemia in ZDF rats (Király et al. 2007; Pold et al. 2005). An increase in insulin sensitivity was also achieved by physical LI, given that exercise in rodents showed higher phosphorylation of liver and skeletal muscle AKT in the insulin signaling pathway (Rao et al. 2013). Literature reported how caloric restriction (CR)-induced weight loss in humans improves insulin sensitivity and corrects fasting hyperglycemia (Petersen, Dufour, Befroy, et al. 2005), while CR in ZDF rats prevented the β-cells incompetence and the reduction of β-cell GLUT2, which coincide with hyperglycemia onset (Ohneda et al. 1995). In humans, unsaturated FA have been linked to improved insulin sensitivity (Summers et al. 2002; Riccardi et al. 2004). Moreover, a dietary intervention in mice assessing the effect of unsaturated FA in glucose homeostasis revealed that MUFAs like palmitoleic acid in mice reported an improvement of insulin action in liver and skeletal muscle (Cao et al. 2008). Also in rodents, activation of omega-3 (Om3) FA receptor mediated anti-inflammatory responses and insulin sensitizing effects (Oh et al. 2010). Thus, physical training, CR, and enrichment in MUFA and PUFA in the diet, three types of intervention included in our LI, showed improved insulin sensitivity in line with our findings.

Of note, *Int* group fasting glucose levels were similar after an overnight fasting (16h) and after a morning fasting (4h), this is explained by the fact that *Int* animals suffered the same type of fasting whether it was overnight or morning fasting for the test. Mice were under

CR and exercise training, and ate the given amount of daily food right after physical performance. Thus, they showed almost the same glycemia levels in both tests. However, if these values were compared to *Ctrl* values, *Int* mice showed hyperglycemia before the IGTT test (after 16h-fasting), but not before the ITT (4h-fasting). CR within the LI limits therefore the interpretation of the fasting glycemia levels across the experimental groups. Hence, overnight fasting glycemia is the more accurate state to assess this parameter among these experimental groups.

1.1. Fasting hyperinsulinemia after HFD and LI

Hyperinsulinemia after HFD might account for the compensatory insulin-secretion arising from IR to overcome hyperglycemia, in an attempt to maintain normoglycemia, in line with the literature (DeFronzo et al. 1989; DeFronzo 1988; Lillioja et al. 1993). β-cell area was increased after HFD, in line with the increase in β-cell mass and hypertrophy during this compensatory effect at IR states (Efrat 2001; Vinik et al. 1996). In fact, the number of all size-range islets (specially small and large islets) increased, being this a feasible cause of the increase in β-cell area (Imai et al. 2007). Our findings are in consonance with the results where HFD leads to β-cell proliferation even before IR was detected (Mosser et al. 2015). However, and contrary to our results, Butler studies reported a decrease in β-cell mass even before the onset of T2DM (Butler et al. 2003). After LI, β-cell area did not decrease nor revert, in line with maintained and even increased β-cell mass that has been observed in different studies performing exercise interventions in OLEFT or ZDF fatty rats (Shima et al. 1997; Király et al. 2008; Pold et al. 2005). Moreover, the presence of small and big islets persisted, as seen in Király studies with swimming rats (Király et al. 2007).

As mentioned, plasma insulin in *HFD* mice was already increased before glucose stimulation during the IGTT (after fasting). After glucose injection *in vivo*, GSIS increased in comparison to before the stimulation, to the same proportional extend as the *Ctrl* mice. Moreover, upon increase of glucose in the medium (16.7mM) during GSIS *in vitro*, *HFD* mice isolated islets showed a significantly higher GSIS in comparison to *Ctrl* mice islets, suggesting hypersecretion to compensate IR. An increase in insulin secretion both *in vivo* and *in vitro* has also been described in rodents after HFD-feeding (Flier et al. 2001; Sone & Kagawa 2005).

Fasting hyperinsulinemia was maintained after LI, suggesting a persistent compensatory effect, though glucose tolerance and insulin sensitivity were improved in comparison to *HFD* mice. Different studies showed a protective role in rodents for exercise by increasing

insulin sensitivity or action (Davis et al. 2012; Dubé et al. 2012; Magkos et al. 2008) that is observed in our results. However, our results counteract the work from Suga and colleagues where a diet+exercise intervention normalized fasting glucose and insulin, which were increased after 8 wks on HFD-feeding (Suga et al. 2014). In fact, *in vivo* IGTT in *Int* mice reported increased plasma insulin levels at fasting and after glucose injection in comparison to *Ctrl* mice, as it happened in the pathological *HFD* state. Differently, pancreatic islets insulin secretion *in vitro* at high glucose was reverted back to *Ctrl* values: islets responded by secreting insulin in a more similar mode to *Ctrl* values, meaning that isolated islets from *Int* mice performed better than *HFD* mice and similarly to *Ctrl* mice. A general enhancement in GSIS after exercise was observed in β-cell deficient rats (Farrell et al. 1991).

We conclude that *HFD* mice were glucose-intolerant, considering the results from the IGTT test, and also insulin-resistant, corroborated by the ITT test and the hyperinsulinemia *in vivo* in fasting and after glucose stimulation, which seems to exert a compensatory effect to reach normoglycemia with no success. Indeed, GSIS *in vitro* confirmed a hypersecretion of insulin that was concomitant with an increase in β-cell area. On the contrary, after LI mice reported glucose tolerance and insulin sensitivity attending the *in vivo* IGTT and ITT tests. Hyperinsulinemia was still present in fasting and after glucose injection, but this might be due to the persistent increased β-cell area. Even though the *Ctrl* and *Int* mice revealed similar glucose tolerance, the fact that pancreatic islets after LI showed overall increased insulin secretion might explain that IGTT-AUC in *Int* mice was significantly lower than *HFD* mice and half the size of *Ctrl* mice.

1.2. VO_2 and heat production

Regarding the parameters measured through indirect calorimetry, the decrease in VO_2 consumption after HFD has been observed also in IR and/or T2DM state in comparison to control insulin sensitive individuals (Cummins et al. 2014). Heat production is tightly related to energy expenditure, and in the pathological state a decrease in heat production after HFD was observed suggesting diminished energy expenditure, linked to an obese phenotype (Dauncey & Brown 1987). Scapular temperature is related to brown adipose tissue (BAT) activity; thus, less scapular temperature, as reported after HFD, would imply less non-shivering thermogenesis. LI allowed the recovery of scapular temperature as well as heat production, in line with the increase in BAT temperature induced by exercise (Ardévol et al. 1996). Of note, other BAT measurements and experiments are being performed at the time of writing, but not concluded to be part of this PhD thesis. After LI,

changes observed in ambulatory movement, such as an increase during the light phase for *Int* mice, could be attributed to the eating behaviour during CR. CR mice eat their food within few hours after food was supplied (17:00-18:00). Thus, by morning of the following day mice would feel hungry and be actively searching for food.

2. Epididymal white adipose tissue (eWAT)

The increase in eWAT tissue weight after HFD was reverted to *Ctrl* values after LI. Different studies have reported a decrease in visceral adipose tissue (VAT) mass after physical activity due to enhanced energy utilization; decreasing the secretion of pro-inflammatory cytokines as a result (Sell et al. 2012; Donges et al. 2009; Christiansen, Paulsen, Bruun, Pedersen, et al. 2010; Fischer et al. 2007; King et al. 2003; Geffken et al. 2001), and revealing a trend toward improvement in glucose tolerance (Wainright et al. 2015), which is in line with our findings.

In order to achieve a holistic view of metabolic plasticity during DIO and after LI, this project studies and aims to integrate the metabolic responses that regulate glucose homeostasis in different tissues related to T2DM. The most significant results accomplished to date among the different systems biology approaches performed during this research, are detailed next. Cosine similarity matrix presenting mitochondrial function parameters (Figure 45) showed a different behavior (decreased correlation) for eWAT respiratory state parameters (CI+CII, ETS CI+CII and ETS CII) from the respiratory states assessed in other tissues (liver, oxidative and glycolytic skeletal muscle, and hypothalamus). This loss in correlation in mitochondrial respiratory states in eWAT was corroborated in the integrative approach showing a higher number of respiratory states with patterns of *non-reversion* after LI among the tissues assessed (Figure 44). Regarding the study defining patterns of metabolite levels (Figure 43), eWAT reported many metabolites with a *non-reversion* pattern. Contrary to the variation studies assessing mitochondrial function and metabolite levels, gene expression in eWAT (Figure 42) showed many patterns with reversion, although some genes reported *non-reversion*. Overall, when assessing metabolism at different levels (mitochondrial function, mRNA expression and metabolomics), eWAT was the most frequently *no-reverted* tissue.

From the statistical analysis of eWAT RNAseq data, 23.65% of all genes detected reported expression values significantly different in at least one of the pair comparisons (*Ctrl* vs *HFD*, *Ctrl* vs *Int*, *HFD* vs *Int*). Subsequently, this subset of genes was separated into expression patterns of reversion, *non-reversion* and *half-reversion*. **Gene ontology**

enrichment analysis (GOrilla) performed in the group of genes with a pattern of *non-reversion* (Figure 46J) described enriched biological processes related to ETS, and cellular components related to both **ETS and inner mitochondrial membrane** (Tables 32 and 33, Figures 47 and 48). A group of genes with a pattern of *half-reversion* (Figure 46C), meaning *Int* mice expression was between *Ctrl* and *HFD* mice values, was also studied. Several biological processes involving **immune system** were reported enriched (Table 36, Figure 51).

2.1. Mitochondrial dysfunction in eWAT

Key co-activators of **mitochondrial biogenesis,** *Ppargc1a* and *Ppargc1b*, decreased their gene expression after HFD feeding, and increased it after LI reaching similar values to those of the *Ctrl* group. Of note, PGRC1 protein levels were also increased after LI. In line with our results, several studies described the increase in *Ppargc1a* mRNA expression after exercise in rat adipose tissue (Stallknecht et al. 1991; Sutherland et al. 2009). Additionally, *Gapba* and *Tfam* revealed a significant increase in expression after LI, confirming a feasible increase in mitochondrial biogenesis in this experimental group.

Mitochondrial OxPhos genes from CI, CII, CIII and CV from ETS (*Ndufa9*, *Sdha*, *mt-Cytb* and *Atp5a1*) were down-regulated after HFD, being CI (NDUFB8) and CIV (MTCO1) also decreased at protein level. Previous research in adipose tissue is in line with our gene expression results: *db/db* mice or rodents models fed on HFD reported down-regulation of genes involved in mitochondrial ATP production, energy uncoupling and other mitochondrial genes (Rong et al. 2007), and *ob/ob* mice showed decreased markers of mitochondrial capacity, including gene expression (Wilson-Fritch et al. 2004). In line with this, HFD-fed mice for 12 wks showed diminished NADH dehydrogenase (NDUFB8, CI), succinate dehydrogenase (SDHB, CII) and COX4I1 (CIV) protein levels (Cummins et al. 2014). In human studies, a reduced expression of mitochondrial function key genes was also observed in patients with IR, T2DM and severe obesity (Krishnan et al. 2012).

In line with a general decrease in OxPhos-related mRNA expression, **mitochondrial respiration was decreased in eWAT after HFD**, significant in most of the respiratory states studied (Leak, CI+II, ETS CI+II and ETS CII); these results are in line with previously reported works: in rodents, oxygen consumption was decreased in DIO and *ob/ob* mice (Valerio et al. 2006; Wilson-Fritch et al. 2004) with 50% lower mitochondrial levels in comparison to WT mice (Wilson-Fritch et al. 2004); while *db/db* mice showed reduced number in mitochondria and mitochondrial dysfunction, along with a decrease in mtDNA

and ETS activity (Choo et al. 2006; Rong et al. 2007). Human studies also reported mitochondrial disruptions in an IR or T2DM state. Interestingly, reduced mitochondrial content in VAT appeared after hyperglycemia (Laye et al. 2009; Sutherland et al. 2008), thus ruling out mitochondrial dysfunction as a cause for IR and T2DM (Sutherland et al. 2008). Other studies showed how obesity, age and T2DM caused reduced mitochondrial content in mature adipocytes and mitochondrial number in gonadal and subcutaneous WAT (SAT) (Wernstedt Asterholm et al. 2012; Bogacka, Xie, et al. 2005). It is important to point out that our eWAT mitochondrial function studies were performed using tissue homogenate and not isolated adipocytes.

Within **ETS subunits after LI** an increased mRNA expression of *Ndufa9*, *Sdha*, *mt-Cytb* and *Uqrcr2* (CIII) was observed, reverting the decreased expression in *HFD*. Moreover, CI (NDUFB8), CIII (UQCRC) and CIV (MTCO1) protein levels increased after mice undergoing LI. The increase in CIII goes in line with an increase in CORE1 protein levels after training in epididymal adipose tissue in rats (Sutherland et al. 2009), same way our results match the increase in COXIV protein.

Mitochondrial dysfunction persisted after LI despite of increased OxPhos mRNA expression and protein levels after LI. Our results are in agreement with a study that demonstrated mitochondrial protein content was normalized along with improved glucose homeostasis in exercised OLETF rats (Laye et al. 2009).

Through the clustering reversibility index approach performed with a curated protein-protein interaction (PPI) network using RNAseq data from eWAT, an approach used in previous scientific reports (Mori et al. 2010), several complexes involving mainly mitochondrial proteins were reported as *no-reverted*. Within them, a clear hub was identified: **COX7A2** (Figure 55). COX7A2 is a protein that **takes part in supercomplexes formation within the inner mitochondrial membrane**, which was in fact proposed to be named supercomplex assembly factor I (SCAFI) (Lapuente-Brun et al. 2013). Our RNAseq data from eWAT showed how *Cox7a2* followed the same pattern as mitochondrial dysfunction. It is worth mentioning that *Cox7a2l*, the variant proposed in the study from Enríquez and colleagues (Lapuente-Brun et al. 2013), showed no changes in expression across the three experimental groups. ETS supercomplexes assembly might depend on the inner mitochondrial membrane functionality, thus linking supercomplexes with *cristae* formation. Of interest was then the study of *cristae*'s structure and formation, as we hypothesized that mitochondrial dysfunction might be linked to a problem in complexes

assembly within the inner membrane structure. OPA1 is a protein that mediates mitochondrial fusion along with MFN1 and MFN2, and *cristae* structure in the inner mitochondrial membrane, which might have a role in supercomplexes assembly and ETS proper organization. Once OPA1 precursor has entered the mitochondria, a long isoform of OPA1 (l-OPA1) remains embedded in the inner mitochondrial membrane. In normal conditions, only half of the OPA1 exists as l-OPA1 while the remainder suffers a cleavage at S1 and S2 sites leading to short OPA1 isoforms (s-OPA1), which are no longer attached to the inner membrane (Ishihara et al. 2006). Of note, proteases OMA1 and YME1L cleave differently l-OPA1 leading to S1 and S2 forms, respectively (Ehses et al. 2009; Head et al. 2009; Griparic et al. 2007; Song et al. 2007). It is worth mentioning that both isoforms (l-OPA1 and s-OPA1) act in combination to perform mitochondrial fusion activity. Thus, the ratio between l-OPA1 and s-short OPA1 isoforms increased with OPA1 fusion activity. Interestingly, **OPA1 protein ratio and *Opa1* gene expression decreased after HFD**. Moreover, all mitochondrial fusion markers assessed (*Mfn1*, *Mfn2* and *Opa1*) increased expression after LI along with *Dnm1l* fission gene. A switch to increased mitochondrial fission is related to T2DM phenotype (Gómez-Valadés et al. 2015), so a move to increased fusion would account for a recovery situation. However, and concurrently to mitochondrial dysfunction, **OPA1 protein was still decreased after LI**, suggesting that the decrease in eWAT mitochondrial respiration in both groups could account for a bad *cristae* formation leading to feasible derangements in ETS complexes assembly within the inner mitochondrial membrane.

Taken all together, the pathological state after HFD-feeding reported potential disruption in ETS supercomplexes assembly within the inner mitochondrial membrane (*cristae*), which persisted after LI. Further evidence is necessary to prove this hypothesis. At the time of writing, electronic microscopy images started to be studied regarding mitochondria ultrastructure in eWAT for further details in *cristae* and ETS supercomplexes formation. Moreover, supercomplex formation by blue-native page electrophoresis would also shed more light on this question.

2.2. Inflammation and immune cells infiltration in eWAT

Histological analysis of eWAT from *HFD* mice with hematoxilin-eosin staining reported enlarged adipocytes and increased infiltration of immune cells indicating **low-grade inflammation**, previously described in DIO (Hotamisligil et al. 1993; Shoelson et al. 2007). Careful examination of the immune cell infiltration revealed increased number of Tcells

after HFD, normally appearing as part of the crown-like structures (CLS) surrounding dead or dying adipocytes, as observed in the literature (Winer et al. 2009; Nishimura et al. 2009; Lumeng et al. 2009). Adipose tissue inflammation has been reported to be an important player in the pathogenesis of IR (Xu et al. 2003; Weisberg et al. 2003). eWAT gene expression studies confirmed an increase in inflammation with overexpression of *Tnf* and a compensatory increase of the anti-inflammatory marker *Il10* (Li et al. 2012; Bettini & Vignali 2009)(*Il6* and *Il1b* followed the same trend, but not significantly). *Tnf* gene expression is shown to be increased in obese humans (Hotamisligil et al. 1995; Kern et al. 1995) and rodents (Hofmann et al. 1994). Indeed, *Tnfα*-deficient mice improved insulin sensitivity in DIO (Uysal et al. 1997). Several studies have shown how TNFα and IL6 led to up-regulation of inflammatory mediators that ultimately caused IR by stimulating JNK1 and IKKβ/NFκB pathways (Wellen & Hotamisligil 2005; Fain et al. 2004).

Concerning **immune cell infiltration**, an increase in mRNA expression of monocyte chemoattractant protein *Ccl2* (also known as *Mcp1*) and macrophage marker *Adgre1* expression was reported, suggesting macrophage infiltration. Infiltration of macrophages and circulating inflammatory markers (TNFα, IL6, MCP1) participate in the low-grade chronic inflammatory state in adipose tissue in obesity and IR (Weisberg et al. 2003; Xu et al. 2003; Kern et al. 2001; Hotamisligil 2006; Wellen & Hotamisligil 2005; Galic et al. 2010). The increase in *Mcp1* (*Ccl2*) is in line with works describing that increased MCP1 creates a chemotactic gradient (Olefsky & Glass 2010), attracting more macrophages into the tissue, where they become ATMs. The secretory activity of these ATMs becomes then active, releasing more chemokines and recruiting more macrophages, thus participating in the inflammatory process (Olefsky & Glass 2010).

Regarding our results, M1 pro-inflammatory polarized macrophage marker *Itgax* (*Cd11c*) was increased after HFD while M2 anti-inflammatory polarization marker *Cd209e* was decreased, confirming a feasible infiltration of new macrophages producing inflammation with a release of resident M2 macrophages and a switch towards pro-inflammatory M1 macrophages. Besides mRNA gene expression, RNAseq data revealed a decrease in *Cd163* and *Tgfb1*, both markers for M2 macrophages. In keeping with our results, different works showed how ATMs in obesity are mainly M1-polarized and more than 90% end up expressing the *Itgax* marker up-regulated (Lumeng, DeYoung, Bodzin, et al. 2007; Nguyen et al. 2007). A current debate exists when describing macrophages regarding their activation. In fact, classically activated macrophages have always been divided between M1 macrophages with a pro-inflammatory profile and M2 with an anti-inflammatory one.

However, there is a newly defined type of macrophages that are metabolically activated (MMe), exerting a phenotype distinct from classical activation (Kratz et al. 2014). Metabolic activation of macrophages demonstrates the possibility of a metabolic-disease-specific phenotype of macrophages. PLIN2 is a protein involved in lipid metabolism known to be associated with M2 macrophages, and identified as a marker for this metabolic activation of macrophages (becoming MMe) (Kratz et al. 2014). Interestingly, RNAseq data showed an increased expression of *Plin2* in *HFD* mice, suggesting a MMe type of macrophages present in adipose tissue.

In general, different types and durations of exercise training in humans have been associated with decreased inflammation (King et al. 2003; Abramson & Vaccarino 2002; Geffken et al. 2001; Mattusch et al. 2000). Indeed, our results **after LI** reflect decreased mRNA expression of *Tnf*, *Il6* and *Il10*. However, after LI was performed, adipocyte morphometry was **worsened** being adipocytes smaller in comparison to *Ctrl* and *HFD* mice, and showing a massive increase of infiltrated immune cells. Thus, our results seem not to be in line with works showing exercise-induced reduction in adipocyte size (back to control size) and lipid content (Gollisch et al. 2009; Craig et al. 1981). Moreover, Tcells staining reported an increase in Tcells in comparison to *HFD* mice, confirming a persistent immune cell infiltration. Consistent with our results, insulin-resistant rodents did not show significant improvement in inflammation after 8 wks of exercise (Rao et al. 2013).

However, chemotaxis marker *Ccl2* as well as macrophage marker *Adgre1* revealed a totally reverted gene expression, decreased back to *Ctrl* values. A study showed how after deletion of *Ccl2*, animals were protected against HFD-induced IR (Kanda et al. 2006), suggesting a correlation with our results given that *Int* mice reveal improved insulin sensitivity. Other studies reported the same reversion from the pathological state in *Tnf*, *Il6* and *Il10* expression that we observed, along with a reduction in *TNFα* after weight loss (Hotamisligil et al. 1995; Kern et al. 1995). Furthermore, massive immune cell infiltration was reported, and could be linked to the persistently high mRNA expression of M1 marker (*Itgax*) and low mRNA expression of M2 marker (*Cd209e*). In line with this, *Cd163* showed a continual decreased expression. *Plin2* "metabolic" adaptation marker revealed decreased expression in comparison to *HFD* group, though it was still higher compared to *Ctrl* mice. The decrease in VAT of *Ccl2* (*Mcp1*) expression and other immune cell infiltration markers was decreased after voluntary exercise in one study, though *Itgax* (*Cd11c*) was also decreased, contrary to our results (Wainright et al. 2015). Also against our findings, a dietary intervention with Om3 in other studies revealed a switch from M1 to

M2 macrophages coincident with improved insulin sensitivity (Oh et al. 2010), and a significant decrease in ATMs and CLS (Spencer et al. 2013).

Different studies observed **oxidative stress** in WAT from DIO and *db/db* mice (Lee et al. 2010; Curtis et al. 2010; Chen et al. 2010), causally linked to disrupted insulin sensitivity in different models (Loh et al. 2009; Brookheart et al. 2009; Curtis et al. 2010; Houstis et al. 2006). In addition, oxidative stress increases after TNFα treatment (Schulze-Osthoff et al. 1992). Our eWAT mRNA expression data showed an increased expression of antioxidants genes (*Sod2* and *Gpx1*) after HFD, in line also with the increase in *Tnf* mRNA expression, suggesting an increase in oxidative stress. In the same way as *Tnf*, antioxidant *Sod2* reverted and decreased its expression after LI, pointing at a potentially recovered oxidative stress. However, in order to describe oxidative stress and make stronger conclusions, more experiments need to be performed to assess oxidative stress, such as measuring ROS with a spectrophotometer or protein carbonylation detection by colometric assay.

ER stress has been demonstrated to have an important role in the pathogenesis of obesity-induced T2DM in rodents (Özcan et al. 2004) and humans (Boden et al. 2008), as well as in activating inflammatory pathways (Hotamisligil 2005). In fact, *Hspa5* reported increased expression after HFD, while *Atf4* showed a tendency to increase, probably contributing to UPR responses. Regarding the remodelling in the eWAT, we hypothesized that the LI might be stressful for the animals due to significant weight loss in few weeks. In line with this, ER stress markers were increased after LI (*Atf6*, *Xbp1* spliced vs total) along with mitochondrial stress markers (*Clpx*, *Ubl5*, *Hspd1* and *Hspa9*).

In order to decipher whether the intensive LI, leading to significant weight loss, is the reason for the metabolic features described in the *Int* group, a new experimental group was established. This group underwent the same LI as *Int* mice (HFD-feeding for 16 wks and LI for 5 wks) followed by a more moderated intervention consisting in exercise (only 3 days/wk) and diet (same than in previous LI) with increased amount of food in order to maintain their BW stable. Thus, through studies with this group we intent to assess whether mitochondrial dysfunction and immune cell infiltration into the adipocyte are maintained when the intervention is not that much stressing for the animals. Indeed, preliminary results reported a recovered adipocyte shape and architecture without immune cell infiltration. Strikingly, although in this group the immune infiltration seemed recovered, eWAT mitochondrial respiration was still disrupted. Moreover, mRNA

expression analysis of ETS, inflammation markers and other genes, as well as histological studies to define the types of infiltrated cells, will be assessed to better define the new physiological situation.

It is worth mentioning the role of succinate, given that its accumulation has demonstrated to promote inflammatory signalling, and it has been shown to stabilize the transcription factor hypoxia inducible factor-1α (HIF-1α) in specific tumours and in activated macrophages (Mills & O'Neill 2014). A hypoxic environment has been described in WAT due to tissue expansion and new formation of vasculature (Corvera & Gealekman 2014) which could lead to a rise in succinate (Chouchani et al. 2014). In this regard, *HFD* mice showed increased succinate levels along with a potential increase in *Hif-α* gene expression (from RNAseq).

The cellular environment defined by increased macrophages polarized-populations and other immune cells in adipose tissue has been identified as an important player in communicating with adipocytes or preadipocytes for further **tissue remodelling** (Sorisky et al. 2013; Lee et al. 2013). In this process, crosstalk between different cellular components might determine adipocyte differentiation leading to tissue cells with different metabolic features. An increase in UCP1 protein levels might account for a "browning" process during this remodelling. Browning is defined as the enhancement of thermogenesis within WAT, such as the increased expression and activity of UCP1 in tissues that are considered WAT depots (Nedergaard & Cannon 2014). Uncoupling proteins have the ability to uncouple ETS in order to produce heat instead of synthetizing ATP. In line with this, uncoupling proteins (*Ucp1* and *Ucp2*) mRNA expression were up-regulated after HFD, in agreement with the study from García-Ruiz and colleagues who demonstrated that HFD might lead to the acquisition of brown adipocyte features in WAT depots in an attempt to counteract the increased adiposity due to the diet (García-Ruiz et al. 2015). This potential browning might be also enhanced after LI given that mRNA expression of these uncoupling proteins was maintained increased when compared to *Ctrl* mice; and when assessing protein content after LI, UCP1 protein levels appeared increased. RNAseq data from eWAT showed an increased expression of *Ucp1* and *Ucp2* after HFD and LI following the same pattern as in RT-PCR expression studies; while, more interestingly, *Fndc5* (a browning marker) increased its expression only in *Int* mice (data not shown). Moreover, increased expression of *Ucp1* in WAT through the overexpression of its gene promoter reported reduced obesity in mice (Kopecky et al. 1995). As aforementioned, UCP1 protein was clearly and significantly increased in the experimental group undergoing LI. Thus, it is not clear if

a potentially browning process might be occurring in eWAT. Moreover, epididymal adipose has been shown to be the less prone to browning in comparison to other white adipose tissue depots such as subcutaneous adipose tissue (Seale et al. 2011).

In order to better assess the browning phenomena after LI, if occurring, one must study browning markers (*Cidea* and also *Prdm16*) in subcutaneous adipose tissue, an adipose depots that has been shown to suffer browning (Spiegelman 2013; Seale et al. 2011).

3. Liver

3.1. Hepatic steatosis

Mice after HFD showed an increase in TG levels, known as non-alcoholic fatty liver (NAFLD). Thus, our results are in line with an study in insulin-resistant patients at risk of T2DM patients, which presented hepatic steatosis (Prikoszovich et al. 2011), and those showing that intrahepatocellular fat is linked with metabolic complications of obesity (Stefan et al. 2008; Fabbrini et al. 2009). The lipotoxicity present in the liver plays a role in hepatic IR, as different studies have previously suggested (J K Kim et al. 2001; Merkel et al. 1998; Koonen et al. 2007; Doege et al. 2008; Falcon et al. 2010). During DIO, WAT expands by storing fat while inappropriate angiogenesis creates an hypoxic environment within the adipocytes that limits their size and expandability (Corvera & Gealekman 2014; Hardy et al. 2012). Thus, WAT dysfunction and impaired expandability leads to shuttling of FA into the blood stream that will be arriving to the liver and skeletal muscle, known as ectopic FA accumulation (Suganami et al. 2012; Samuel & Shulman 2012). Hepatic steatosis has been suggested to be a consequence of increased WAT lipolysis, but also to *de novo* lipogenesis (DNL) (Petersen et al. 2007) or to a mismatch between the lipid liver uptake and export (H. Y. Lee et al. 2011) after a challenging situation such as HFD-feeding. *Pparg* expression, known to contribute to hepatic steatosis and TG clearance (Gavrilova et al. 2003), reported increased expression in liver from *HFD* mice. Different experiments in mice with lipodystrophy and FA accumulation in liver and skeletal muscle (Moitra et al. 1998; Kim et al. 2000), and humans with lipodystrophy or surgically removal of VAT (Petersen et al. 2002; Fabbrini et al. 2010) confirmed hepatic IR related to intrahepatic lipids, instead of lipids coming from VAT non-suppressed lipolysis. **Liver steatosis** is corroborated in our study by a great increase in TG and DAG metabolites after HFD. Moreover, liver from HFD mice seemed to have **increased lipid synthesis**. This could be supported by the overall increase in lipid-soluble metabolites (TG, DAG, Om3, ARA+EPA, DHA and oleic and linoleic

acid). In fact, the increase in lipids and also unsaturated lipids could be explained by the increase in FA synthase (*Fasn*) mRNA expression, involved in FA synthesis (Kohjima et al. 2007). Moreover, our findings also showed an increase in mRNA expression of *Scd1*, involved in the unsaturation of FA. This result is not in agreement with studies showing down-regulation of hepatic *Scd1* in HFD-fed rats developing NAFLD (Gianotti et al. 2013). In contrast to our results, NAFLD and NASH patients reported increased FA β-oxidation (Miele et al. 2003; Sanyal et al. 2001; Chalasani et al. 2003).

After LI, evidence for **steatosis** (liver TG, and TG and DAG metabolites) was **reverted**, suggesting the disappearance of hepatic lipid accumulation. Our results might be in line with human studies with weight loss-induced reversion of NAFLD and IR after a dietary LI (Petersen, Dufour, Befroy, et al. 2005). Moreover, LI increased *Ppara* mRNA expression, and PPARα activation in the liver has been suggested to exert PUFA-mediated anti-obesity and anti-steatotic effects in rodents (Nakatani et al. 2003), by promoting hepatic FA oxidation. **Increased FA oxidation** leading to decreased lipid accumulation in the liver was reported in other studies where diet was supplemented with Om3 PUFA (Willumsen et al. 1993), along with an inhibition of DNL secondary to decreased *Fasn* gene expression (Clarke & Jump 1994). In line with these studies, *Fasn* and *Scd1* expression after LI was decreased, suggesting a reduction in lipid synthesis and a switch to oxidation of FA supported by an increased expression of *Cpt1a,* the main lipid transporter into the mitochondria. Lionetti and colleagues observed that fish oil Om3-feeding decreased hepatic lipid accumulation by improving mitochondria FA oxidation, and shifted to mitochondrial fusion processes in the Om3-fed group similar to that of the controls (Lionetti et al. 2014). In line with this, liver TG content decreased to *Ctrl* group values, and *Mfn1* and *Mfn2,* mitochondrial fusion markers, showed increased mRNA expression after LI. The study of histological sections stained with oil red might supply additional information to decipher NAFLD existence and reversion.

Steatohepatitis, the inflammation in liver secondary to steatosis, has been previously demonstrated and involved in the development of IR, T2DM and the metabolic syndrome (Cai et al. 2005; Johnson & Olefsky 2013). This inflammation state seemed absent in our mice after HFD, attending no overexpression of inflammation markers, thus limiting the liver disease to an steatotic state or NAFLD in an obesity-induced T2DM context (Angulo 2002; Petersen, Dufour, Befroy, et al. 2005; Petersen et al. 2002; Fraser et al. 2009; Samuel et al. 2010).

As in eWAT, mRNA expression of antioxidant markers after HFD (*Gpx1*, and *Sod2*) might suggest an increase in **oxidative stress**. ROS and oxidative stress have shown to disrupt insulin signalling and to lead to IR by activating serine kinases, which, in turn, can phosphorylate and inhibit IRS1 and IRS2 in skeletal muscle and liver (Evans et al. 2003; Saltiel & Kahn 2001). FA oxidation, a potentially up-regulated pathway in this tissue after LI, might lead to an increase of ROS through increased OxPhos. Hence, antioxidants mRNA expression (*Sod2* and *Gpx1*) was maintained up-regulated after LI contrary to what happened in eWAT, suggesting a potential oxidative stress in liver in *Int* mice.

ER stress in liver could be increased in *HFD* mice based on *Bip* (*Hspa5*) and *Chop* (*Ddit3*) up-regulated mRNA expression, results in keeping with the activated UPR in *ob/ob* mice liver (Özcan et al. 2004). After LI, *Hspa5* and *Ddit3* mRNA expression was decreased and reverted meaning that LI was able to reduce ER stress in the hepatocytes.

3.2. Potential increased hepatic glucose production (HGP) in liver after LI

As discussed before mice after LI presented impaired fasting glucose handling. It could be of interest to evaluate the role of **HGP** on overall glucose metabolism. Even with hyperinsulinemia, in a IR state insulin cannot properly suppress HGP (Groop et al. 1989), thus increased HGP due to elevated hepatic gluconeogenesis has been observed in previous studies (DeFronzo & Ferrannini 1987; Magnusson et al. 1992; Consoli et al. 1990). Moreover, the increase in intrahepatocellular lipids can induce HGP by increasing gluconeogenic PEPCK and PK enzymes activity (Gastaldelli et al. 2000). However, *Pckl* encoding for PEPCK in the liver revealed no increase in mRNA expression after HFD. Even though gluconeogenic gene expression was not increased, there was an increase in unsaturated FA after HFD, and other studies demonstrated how specifically PUFA were able to activate *Pepck* and *G6p* expression, leading to increased gluconeogenesis (Delarue & Magnan 2007). Taken all this together, we cannot conclude much about this pathway, and assessment of gluconeogenic enzyme levels and a pyruvate tolerance test (PTT) are needed to further decipher this pathway and its potential role in the fasting hyperglycemia present in *Int* mice.

Also related to glucose metabolism, reduced stimulation of **glycogen** synthase and decreased in hepatic glucose uptake have been observed in an insulin-resistant state in previous scientific reports (Morino et al. 2006). However, no changes were observed after HFD in glucose transporter in liver *Glut2* (*Slc2a2*) nor glycogen synthase (*Gys2*), though glycolysis gene *Gapdh* increased after HFD. After LI, there was a tendency to an increased

expression of *Gys2*. Thus, glycogenesis could be taking place after the LI was performed. Also, an increased expression of *Glut2* (*Slc2a2*) allows the entry of glucose into the cell. In line with the aforementioned, glycogen in liver showed a tendency to decrease after HFD and increased significantly after LI. In fact, the tendency to decrease in glycogen in *HFD* mice could account for an increase in glycogenolysis and a decrease in glycogenesis, leading to increased HGP. In line with the results mentioned in the previous section, Gaíva and colleagues described a decrease in liver tissue lipid content after a dietary LI (increasing FO, soybean oil or both combined in the diet) (Gaíva et al. 2003), though the same study showed a decrease in hepatic glycogen too, being this finding opposed to our observed increase in glycogen after LI.

4. Skeletal muscle

4.1. Insulin resistance is not caused by mitochondrial dysfunction in skeletal muscle

As mentioned before, a current debate exists about the causality role of mitochondrial dysfunction in IR. Different authors claimed mitochondrial dysfunction as a cause of IR in T2DM subjects (Phielix et al. 2008; Kelley et al. 2002; Boushel et al. 2007; Ritov et al. 2010), observing also a reduced mitochondrial content in T2DM (Morino et al. 2005; Chomentowski et al. 2011; Kelley et al. 2002; Ritov et al. 2005; Heilbronn et al. 2007) or insulin-resistant patients (Morino et al. 2005; Heilbronn et al. 2007). However, and as discussed in the Introduction, the patients from these studies were mostly obese, being obesity a cofounding factor for the reduced mitochondrial content leading to mitochondrial dysfunction in muscle.

Contrary to this hypothesis, other authors claimed a **dissociation between IR and mitochondrial dysfunction** (Karakelides et al. 2010; Lefort et al. 2010; Nair et al. 2008) also in T2DM subjects compared to matched controls (Gnaiger 2009). Other studies in T2DM humans reported normal mitochondrial activity (Szendroedi et al. 2007). This dissociation was also reported in rodents, such as the work showing normal mitochondrial OxPhos capacity in TA from ZDF rats (De Feyter, Lenaers, et al. 2008). Similarly, Holmström and colleagues demonstrated how IR might develop independently of mitochondrial dysfunction in oxidative and glycolytic skeletal muscle from *db/db* mice (Holmström et al. 2012). In keeping with the dissociation mentioned between IR and mitochondrial dysfunction, even increased mitochondrial function (Lenaers et al. 2010; Turner et al. 2007) and density (van den Broek et al. 2010) were reported in insulin-resistant monogenetic or

DIO rodents, regardless of IR. In fact, lack of exercise or physical inactivity in T2DM patients was reported as a major contributor to the mitochondrial defects observed in their skeletal muscles (van Tienen et al. 2012), justifying the concomitant presence of IR and mitochondrial dysfunction. Exercise is capable in muscle to increase oxidative activity in T2DM patients (Hey-Mogensen et al. 2010; Phielix et al. 2010), along with insulin sensitivity and metabolic flexibility (Toledo et al. 2007). Our findings reported an up-regulation in most of ETS complexes genes (*Sdha*, *mt-Cytb*, *Uqcrc2* and *Atp5a1*) after HFD in soleus, along with no changes in OxPhos subunits in TA. Moreover, **no mitochondrial dysfunction** was observed in any of the skeletal muscles studied. In fact, a tendency to an increased respiration in *HFD* mice in comparison to *Ctrl* mice in EDL was observed, in line with two studies where glycolytic skeletal muscle respiration was mainly increased in *db/db* and *ob/ob* mice (Holmström et al. 2012; Holmström et al. 2013). Given that *HFD* mice phenotype exerts clear IR and glucose intolerance, our study claims against a causality role of mitochondrial dysfunction in IR.

4.2. Potential metabolic adaptations in glycolytic skeletal muscle after LI

Different studies have described a metabolic switch to enhanced oxidative capacity in glycolytic skeletal muscle after physical training (Holloszy & Coyle 1984). Regarding gene expression after LI (Figure 42), almost all genes in soleus that had an increased mRNA expression after HFD were reverted (mitochondria ETS, mitochondrial dynamics, mitochondrial biogenesis, mitochondrial stress, ER stress, lipid and glucose metabolism, and antioxidants related genes). On the contrary, TA glycolytic skeletal muscle showed a considerable amount of genes that only changed after LI, suggesting a metabolic **adaptation or remodelling of the glycolytic skeletal muscle**. Strikingly, our findings did not show an increase in mRNA expression of mitochondrial oxidative related genes that would point to an enhanced oxidative performance. Thus, the effect in TA of LI reflected a decrease from baseline in mitochondrial ETS (*Ndufa9*, *Sdha*, *Uqcrc2* and *Cox4i1*); mitochondrial dynamics (*Mfn1*, *Mfn2*, *Dnm1l* and *Fis1*), and mitochondrial biogenesis (*Ppargc1a*, *Esrra*, *Nrf1* and *Tfam*). However, this potential metabolic adaptation was observed with a tendency to increased mitochondrial respiration from *Ctrl* mice to *Int* mice. It is worth mentioning that ANOVA One-way was used for statistical analysis, due to the presence of three experimental groups. Thus, although no significant changes were detected in glycolytic skeletal muscle EDL after LI through ANOVA One-way test, if we perform a t-student test between *Ctrl* and *Int* mice data for respiration in CI, CI+II and ETS CI+II, statistical differences or a tendency are reported (CI p=0.043, CI+II p=0.066, ETS CI+II p=0.029).

Thus, the potential increase of mitochondrial function after LI in comparison to Ctrl mice is not supported by the reported decrease in mRNA and protein expression of mitochondrial biogenesis markers. Several works have reported an increase in mitochondrial gene transcripts after CR (Baker et al. 2006; Civitarese et al. 2007; Sreekumar et al. 2002). However, Lanza and colleagues suggested that CR improved mitochondrial function despite no changes in mRNA and protein expression (Lanza et al. 2012). These authors suggested that functional improvements after CR might be due to potential post-transcriptional modifications. In this regard, we have found in TA muscle an increase in SIRT3 protein levels after LI (only significant in comparison to *Ctrl* group, data not shown). SIRT3 is a member of the sirtuin family of NAD^+-dependent deacetylase placed within the mitochondria known to respond to exercise and nutritional signals in skeletal muscle in order to coordinate downstream molecular responses that lead to an improvement in mitochondrial function (Palacios et al. 2009). Glycolytic skeletal muscle metabolic responses after LI are of interest but definitely requires a deeper analysis before being able to withdraw any conclusion about the potential mechanism regulating such responses.

4.3. Ectopic FA accumulation in skeletal muscle

An ectopic FA accumulation in skeletal muscle was also observed in the *HFD* group. TG were increased in soleus and gastrocnemius muscles. The fact that no changes were observed in TG levels in TA is in line with evidence suggesting that intramyocellular lipid content levels in soleus muscle but not TA are predictive of the IR degree in first-relatives of T2DM patients (Roden 2005). After LI, our results are in agreement with studies from Suga and colleagues who showed that CR+exercise intervention reverted the HFD-induced increase in muscle TG (Suga et al. 2014).

FA accumulation within skeletal muscle has been suggested to disrupt insulin signalling leading to IR, exerting an ultimate impairment in glucose uptake (Lowell & Shulman 2005). In fact, and contrary to our hypothesis, different studies hypothesized that FA accumulation is due to decreased FA oxidation as a consequence of mitochondrial dysfunction or lower mitochondrial content (Lowell & Shulman 2005; Morino et al. 2006; Kelley et al. 2002). Whether FA accumulation is a consequence to the alleged reduction in FA oxidation, or just a consequence to the increase of fat in the diet and the increased lipolysis of the adipose tissue, is yet unknown.

In any case, insulin signalling in skeletal muscle was impaired in both humans (Dresner et al. 1999) and rodents (Griffin et al. 1999; J. K. Kim, Fillmore, et al. 2004) by raising plasma FA. Indeed, T2DM patients showed 80% increase in intramyocellular lipid content (Petersen et al. 2004; Petersen, Dufour & Shulman 2005). Elevation of FFA induced IR in muscle without reducing mitochondrial activity (Brehm et al. 2010; Chavez et al. 2010), experiments strictly in line with our results. Also, T2DM reduced insulin sensitivity and mitochondrial function without alterations in intramyocellular lipid content (van de Weijer et al. 2013); and the inhibition of lipolysis did not improve OxPhos capacity but increased insulin sensitivity (Phielix et al. 2014). Thus, different studies aimed to **dissociated IR and mitochondrial function from intramyocellular lipid content** (Rabøl, Svendsen, et al. 2009; Meex et al. 2010).

Given that not major changes were observed in skeletal muscle as a consequence of LI, we aimed to **confirm that our physical performance intervention was enough to exert the effect of an exercise intervention**. Thus, a group fed for 16 wks with chow standard diet as the control group performed exercise training identical to the one for LI (during 5 wks, 5days/wk, 1h/day). The analysis of samples from mice in this new experimental group will shed light on some of the questions that remain unsolved.

5. Hypothalamus

5.1. ER stress in hypothalamus

Of all tissues presented in this PhD thesis, hypothalamus was the less affected by the experimental conditions under assessment in our research. The integrative approaches aiming to visualize the reversion in mitochondrial respiratory states, gene expression and metabolites levels did not report relevant changes in hypothalamus across the experimental groups (Figures 43, 44 and 45).

mRNA expression of genes related to **ER stress** increased after HFD in this tissue (*Hspa5* and *Ddit3*) along with *Socs3*, an inhibitor of leptin signalling (Bjørbaek et al. 2001; Flier 2004); and correlated with the increase in fasting plasma leptin already demonstrated in obesity (Elmquist et al. 1999; Flier 2004; Schwartz et al. 2000). In fact, ER stress is known to lead to leptin resistance (Ozcan et al. 2009). After LI, ER stress genes and *Socs3* expression levels were reverted, pointing towards a recovered leptin sensitivity. Of note, the

reversion of *Socs3* after switching from HFD to control diet regardless of exercise has been demonstrated (Kang et al. 2013).

5.2. Central regulation of appetite

In relation to appetite central regulation, of interest was to study fasting leptin levels, which were increased after HFD to achieve a reduction in appetite. However, mice seemed to keep eating. This, along with an increase in *Socs3* mRNA expression suggests a potential leptin resistance. Previous studies reported the decrease of leptin levels after exercise (Ellingsgaard et al. 2008; Ellingsgaard et al. 2011; Ueda et al. 2009; Martins et al. 2008; Shirazi et al. 2013; Henningsen et al. 2010). Our findings showed that fasting hyperleptinemia was recovered and decreased after LI when compared to *HFD* group, although more interesting was the fact that fasting leptin levels were still significantly higher than *Ctrl* values. This result might account for a persistent degree of leptin resistance.

Interestingly, neuropeptides mRNA expression showed different responses. HFD-feeding led to decreased orexigenic genes expression in the hypothalamus (Agrp and Npy), in concordance with different studies in DIO mice (Camargo et al. 2015; Levin & Dunn-Meynell 2002) in which the authors claimed that this decrease in expression of orexigenic neuropeptides genes attempts to decrease food intake and obesity progression. Moreover, an increase in anorexigenic gene expression (*Cartpt*) was observed, in line with the study from Camargo and colleagues, although our results did not show an increase in *Pomc* (Camargo et al. 2015).

After LI, expression patterns were inverted: *Agrp* and *Npy* showed increased expression, contrary to *Cartpt*, an expression that might be due to increased appetite as a consequence of the CR situation. Taken all this together, central regulation of food intake seems not to be compromised in any of the experimental conditions. Moreover, leptin fasting levels were decreased and partially reverted in line with the mRNA expression of the aforementioned neuropeptides.

However, we are aware that only mRNA expression data and metabolomics are shown, and that a deeper analysis, including re-fed functional studies and leptin resistance assessment, would be needed to shed light on this topic,

CONCLUSIONS

C57BL6/J mice fed with a HFD for 16wks showed: overweight; fasting hyperglycemia and hyperinsulinemia; increased fat mass and volume; increased epididymal white adipose tissue, pancreas and liver weight; increased triglyceride accumulation in insulin-sensitive tissues; glucose intolerance and insulin resistance; increased beta-cell mass, hypertrophic enlarged pancreatic islets and disrupted glucose-stimulated insulin secretion in vivo and in vitro; leptin resistance; and decreased oxygen consumption, heat production and scapular temperature. Thus, we conclude that:

1. Our diet-induced obese mice reached the pathological phenotype described in the literature, that we were aiming for in order to perform a lifestyle intervention afterwards.

2. Considering our mitochondrial function studies in liver and skeletal muscles from diet-induced obese mice, our results claim that mitochondrial dysfunction might not be a cause of insulin resistance.

A subgroup of the included animals revealing the diet-induced obese phenotype underwent a lifestyle intervention consisting of the combination of exercise training, caloric restriction and modification of the diet towards unsaturated fatty acids and corn starch. The comparison of the phenotype after the lifestyle intervention with the control and diet-induced obese mice take us to conclude that:

3. Lifestyle intervention reverted body weight, fat mass and volume, epididymal white adipose tissue, pancreas, and liver weight, triglyceride levels in insulin-sensitive tissues, glucose-stimulated insulin-secretion *in vitro*, leptin plasma levels, heat production, and scapular temperature.

4. However, glucose homeostasis was not fully recovered after lifestyle intervention. Those animals showed impaired fasting glucose, with hyperglycemia and hyperinsulinemia after overnight fasting, increased β-cell area, increased hypertrophic enlarged pancreatic islets and maintained high glucose-stimulated insulin-secretion *in vivo*.

5. In epididymal white adipose tissue, lifestyle intervention did not revert the mitochondrial dysfunction observed in diet-induced obese mice. These data are supported by gene ontology enrichment analysis that identified as *no-reverted*

biological processes "respiratory electron transport chain" and "mitochondrial organization"; and as *no-reverted* cellular components "mitochondrial inner membrane" and "respiratory chain complex".

6. After lifestyle intervention, epididymal white adipose tissue gene ontology enrichment analysis identified as *no-reverted* biological processes "immune system"; and as *no-reverted* cellular components "inflammasome". These results are supported by histological analysis where a remarkable immune cell infiltration could be observed.

7. In liver, lifestyle intervention reverted the ectopic lipid accumulation and increased the expression of genes related to mitochondrial biogenesis and mitochondrial dynamics, in comparison to control mice.

8. In oxidative skeletal muscle, lifestyle intervention reverted the ectopic lipid accumulation and recovered the gene expression profile of genes related to mitochondrial function, and lipid and glucose metabolism, which were increased in diet-induced obese mice. On the contrary, glycolytic skeletal muscle showed a different gene expression profile characterized by a decrease in comparison to control and/or diet-induced obese mice.

9. In hypothalamus, lifestyle intervention restored the gene expression levels of the food intake regulatory neuropeptides and endoplasmic-stress.

Regarding the integrative analysis, the database creation along with the computing work depicts the first pillar for the global aim of the project, involving more tissues than the ones contemplated in this PhD Thesis. However, considering the integrative approaches performed and their results, we concluded that:

10. Systems biology approaches points at epididymal white adipose tissue as the major player contributing to the loss of metabolic plasticity after lifestyle intervention on diet-induced obese mice.

REFERENCES

Abdul-Ghani, M.A., Jenkinson, C.P., et al., 2006. Insulin secretion and action in subjects with impaired fasting glucose and impaired glucose tolerance: Results from the veterans administration genetic epidemiology study. *Diabetes*, 55(5), pp.1430–1435.

Abdul-Ghani, M.A. et al., 2009. Mitochondrial reactive oxygen species generation in obese non-diabetic and type 2 diabetic participants. *Diabetologia*, 52(4), pp.574–582.

Abdul-Ghani, M.A., Tripathy, D. & DeFronzo, R.A., 2006. Contributions of beta-cell dysfunction and insulin resistance to the pathogenesis of impaired glucose tolerance and impaired fasting glucose. *Diabetes Care*, 29(5), pp.1130–1139.

Abel, E.D. et al., 2001. Adipose-selective targeting of the GLUT4 gene impairs insulin action in muscle and liver. *Nature*, 409(6821), pp.729–733.

Abramson, J.L. & Vaccarino, V., 2002. Relationship between physical activity and inflammation among apparently healthy middle-aged and older US adults. *Arch Intern Med*, 162(11), pp.1286–1292.

Abu-Elheiga, L. et al., 2003. Acetyl-CoA carboxylase 2 mutant mice are protected against obesity and diabetes induced by high-fat/high-carbohydrate diets. *P Natl Acad Sci USA*, 100(18), pp.10207–10212.

Adams II, J.M. et al., 2004. Ceramide Content Is Increased in Skeletal Muscle from Obese Insulin-Resistant Humans. *Diabetes*, 53(1), pp.25–31.

Adams, T.D. et al., 2007. Long-Term Mortality after Gastric Bypass Surgery. *N Engl J Med*, 357(8), pp.753–761.

Aguirre, V. et al., 2002. Phosphorylation of Ser307 in insulin receptor substrate-1 blocks interactions with the insulin receptor and inhibits insulin action. *J Biol Chem*, 277(2), pp.1531–1537.

Aguirre, V. et al., 2000. The c-Jun NH(2)-terminal kinase promotes insulin resistance during association with insulin receptor substrate-1 and phosphorylation of Ser(307). *J Biol Chem*, 275(12), pp.9047–9054.

Albu, J.B. et al., 2010. Metabolic Changes Following a 1-Year Diet and Exercise Intervention in Patients With Type 2 Diabetes. *Diabetes*, 59(3), pp.627–633.

Alibegovic, A.C. et al., 2010. Insulin resistance induced by physical inactivity is associated with multiple transcriptional changes in skeletal muscle in young men. *Am J Physiol Endocrinol Metab*, 299, pp.E752–E763.

Amati, F. et al., 2011. Skeletal muscle triglycerides, diacylglycerols, and ceramides in insulin resistance: Another paradox in endurance-trained athletes? *Diabetes*, 60(10), pp.2588–2597.

American Diabetes Association (ADA), 2010. Diagnosis and Classification of Diabetes Mellitus. *Diabetes Care*, 33(Supplement_1), pp.S62–S69. Available at: http://care.diabetesjournals.org/cgi/doi/10.2337/dc10-S062.

American Diabetes Association (ADA), 2012. Standards of medical care in diabetes - 2012. *Diabetes Care*, 35(Suppl.1), pp.S11–S63.

American Diabetes Association (ADA), 2011. Standards of Medical Care in Diabetes—2011. *Diabetes Care*, 34(Suppl.1), pp.S11–S61.

Anderson, E.J. et al., 2009. Mitochondrial H2O2 emission and cellular redox state link excess fat

intake to insulin resistance in both rodents and humans. *J Clin Invest*, 119(3), pp.573–581.

Andreozzi, F. et al., 2004. Activation of the hexosamine pathway leads to phosphorylation of insulin receptor substrate-1 on Ser307 and Ser612 and impairs the phosphatidylinositol 3-kinase/akt/mammalian target of rapamycin insulin biosynthetic pathway in RIN pancreatic beta-cells. *Endocrinology*, 145(6), pp.2845–2857.

Angulo, P., 2002. Nonalcoholic Fatty Liver Disease. *N Engl J Med*, 346(16), pp.1221–1231.

Ara, I. et al., 2011. Normal mitochondrial function and increased fat oxidation capacity in leg and arm muscles in obese humans. *Int J Obesity*, 35(1), pp.99–108.

Ardévol, A. et al., 1996. Brown adipose tissue temperature in lean and obese rats during exercise. *Int J Obes Relat Metab Disord*, 20(8), pp.733–7.

Arkan, M.C. et al., 2005. IKK-beta links inflammation to obesity-induced insulin resistance. *Nat Med*, 11(2), pp.191–198.

Asmann, Y.W. et al., 2006. Skeletal muscle mitochondrial functions, mitochondrial DNA copy numbers, and gene transcript profiles in type 2 diabetic and nondiabetic subjects at equal levels of low or high insulin and euglycemia. *Diabetes*, 55(12), pp.3309–3319.

Asterholm, I.W. & Scherer, P.E., 2010. Enhanced metabolic flexibility associated with elevated adiponectin levels. *Am J Pathol*, 176(3), pp.1364–1376.

Ayala, J.E. et al., 2006. Considerations in the Design of Hyperinsulinemic-Euglycemic Clamps in the Conscious Mouse. *Diabetes*, 55, pp.390–397.

Bach, D. et al., 2003. Mitofusin-2 determines mitochondrial network architecture and mitochondrial metabolism: A novel regulatory mechanism altered in obesity. *J Biol Chem*, 278(19), pp.17190–17197.

Bajaj, M. & DeFronzo, R.A., 2003. Metabolic and molecular basis of insulin resistance. *T Molec Biol*, 10(3), pp.311–323.

Baker, D.J. et al., 2006. No decline in skeletal muscle oxidative capacity with aging in long-term calorically restricted rats: effects are independent of mitochondrial DNA integrity. *J Gerontol*, 61(7), pp.675–684.

Balaban, R.S., 2010. The Mitochondrial Proteome: A Dynamic Functional Program in Tissues and Disease States. *Environ Mol Mutagen*, 51(5), pp.352–359.

Bandyopadhyay, G.K. et al., 2006. Increased malonyl-CoA levels in muscle from obese and type 2 diabetic subjects lead to decreased fatty acid oxidation and increased lipogenesis; thiazolidinedione treatment reverses these defects. *Diabetes*, 55(8), pp.2277–2285.

Bandyopadhyay, G.K. et al., 2005. Increased p85/55/50 Expression and Decreased Phosphotidylinositol 3-Kinase Activity in Insulin-Resistant Human Skeletal Muscle. *Diabetes*, 54, pp.2351–2359.

Banzet, S. et al., 2007. Contraction-Induced Interleukin-6 Transcription in Rat Slow-Type Muscle is Partly Dependent on Calcineurin Activation. *J Cell Physiol*, 210, pp.596–601.

Baron, A.D. et al., 1987. Role of hyperglucagonemia in maintenance of increased rates of hepatic glucose output in type II diabetics. *Diabetes*, 36, pp.274–283.

Basu, R. et al., 2007. Selective Downregulation of the High-Molecular Weight Form of Adiponectin in Hyperinsulinemia and in Type 2 Diabetes. Differential Regulation From Nondiabetic Subjects.

Diabetes, 56, pp.2174–2177.

Befroy, D.E. et al., 2007. Impaired Mitochondrial Substrate Oxidation in Muscle of Insulin-Resistant Offspring of Type 2 Diabetic Patients. *Diabetes*, 56, pp.1376–1381.

Behme, M.T., Dupré, J. & McDonald, T.J., 2003. Glucagon-like peptide 1 improved glycemic control in type 1 diabetes. *BMC Endocr Disord*, 3, p.3.

Benani, A. et al., 2009. Method for functional study of mitochondria in rat hypothalamus. *J Neurosci Meth*, 178(2), pp.301–307.

Bendtzen, K. et al., 1986. Cytotoxicity of human interleukin-1 for pancreatic islets of Langerhans. *Science*, 232(4757), pp.1545–7.

Benov, L. & Al-Ibraheem, J., 2002. Disrupting Escherichia coli: A Comparison of Methods. *J Biochem Mol Biol*, 35(4), pp.428–431.

Berg, A.H., Combs, T.P. & Scherer, P.E., 2002. ACRP30/adiponectin: An adipokine regulating glucose and lipid metabolism. *Trends Endocrin Met*, 13(2), pp.84–89.

Bergman, R.N., Finegood, D.T. & Kahn, S.E., 2002. The evolution of beta-cell dysfunction and insulin resistance in type 2 diabetes. *Eur J Clin Invest*, 32(S3), pp.35–45.

Bernecker, C. et al., 2013. Evidence for an exercise induced increase of TNF-alpha and IL-6 in marathon runners. *Scand J Med Sci Spor*, 23(2), pp.207–214.

Bettini, M. & Vignali, D.A.A., 2009. Regulatory T cells and inhibitory cytokines in autoimmunity. *Curr Opin Immunol*, 21(6), pp.612–8.

Bézaire, V. et al., 2009. Chronic TNFα and cAMP pre-treatment of human adipocytes alter HSL, ATGL and perilipin to regulate basal and stimulated lipolysis. *FEBS Lett*, 583(18), pp.3045–3049.

Bezy, O. et al., 2011. PKCδ regulates hepatic insulin sensitivity and hepatosteatosis in mice and humans. *J Clin Invest*, 121(6), pp.2504–2517.

Bikman, B.T. & Summers, S.A., 2011. Ceramides as modulators of cellular and whole-body metabolism. *J Clin Invest*, 121(11), pp.4222–4230.

Billings, L.K. & Florez, J., 2010. The genetics of type 2 diabetes: what have we learned from GWAS? *Ann N Y Acad Sci*, 1212, pp.59–77.

Bindokas, V.P. et al., 2003. Visualizing superoxide production in normal and diabetic rat islets of Langerhans. *J Biol Chem*, 278(11), pp.9796–9801.

Birkenfeld, A.L. et al., 2011. Influence of the Hepatic Eukaryotic Initiation Factor 2 (eIF2) Endoplasmic Reticulum (ER) Stress Response Pathway on Insulin-mediated ER Stress and Hepatic and Peripheral Glucose Metabolism. *J Biol Chem*, 286(42), pp.36163–36170.

Bjørbaek, C. et al., 2001. Divergent roles of SHP-2 in ERK activation by leptin receptors. *J Biol Chem*, 276(7), pp.4747–55. Available at: http://www.ncbi.nlm.nih.gov/pubmed/11085989.

Bjørbæk, C. et al., 2000. SOCS3 mediates feedback inhibition of the leptin receptor via Tyr985. *J Biol Chem*, 275(51), pp.40649–40657.

Bloem, C.J. & Chang, A.M., 2008. Short-term exercise improves beta-cell function and insulin resistance in older people with impaired glucose tolerance. *J Clin Endocrinol Metab*, 93(2), pp.387–392.

Blüher, M. et al., 2002. Adipose tissue selective insulin receptor knockout protects against obesity and obesity-related glucose intolerance. *Dev Cell*, 3(1), pp.25–38.

Boden, G. et al., 2001. Effects of free fatty acids on gluconeogenesis and autoregulation of glucose production in type 2 diabetes. *Diabetes*, 50(4), pp.810–816.

Boden, G. et al., 2002. FFA cause hepatic insulin resistance by inhibiting insulin suppression of glycogenolysis. *Am J Physiol Endocrinol Metab*, 283(1), pp.E12–E19.

Boden, G. et al., 2005. Free Fatty Acids Produce Insulin Resistance and Activate the Proinflammatory Nuclear Factor- B Pathway in Rat Liver. *Diabetes*, 54(12), pp.3458–3465.

Boden, G. et al., 2008. Increase in Endoplasmic Reticulum Stress-Related Proteins and Genes in Adipose Tissue of Obese, Insulin-Resistant Individuals. *Diabetes*, 57, pp.2438–2444.

Boden, G., 2002. Interaction between free fatty acids and glucose metabolism. *Curr Opin Clin Nutr*, 5(5), pp.545–9.

Boden, G., 2011. Obesity, insulin resistance and free fatty acids. *Curr Opin Endocrinol Diabetes Obes*, 18(2), pp.139–143.

Boden, G. et al., 2005. Thiazolidinediones upregulate fatty acid uptake and oxidation in adipose tissue of diabetic patients. *Diabetes*, 54(3), pp.880–885.

Bogacka, I., Xie, H., et al., 2005. Pioglitazone Induces Mitochondrial Biogenesis in Human Subcutaneous Adipose Tissue In Vivo. *Diabetes*, 54(5), pp.1392–1399.

Bogacka, I., Ukropcova, B., et al., 2005. Structural and functional consequences of mitochondrial biogenesis in human adipocytes in vitro. *J Clin Endocrinol Metab*, 90(12), pp.6650–6656.

Bonnard, C. et al., 2008. Mitochondrial dysfunction results from oxidative stress in the skeletal muscle of diet-induced insulin resistant mice. *J Clin Invest*, 118(2), pp.789–800.

Bonora, E. et al., 2002. HOMA-Estimated Insulin Resistance Is an Independent Predictor of Cardiovascular Disease in Type 2 Diabetic Subjects: Prospective data from the Verona Diabetes Complications Study. *Diabetes Care*, 25(7), pp.1135–1141.

Bonora, E. et al., 2007. Insulin resistance as estimated by homeostasis model assessment predicts incident symptomatic cardiovascular disease in caucasian subjects from the general population: The Bruneck study. *Diabetes Care*, 30(2), pp.318–324.

Boon, H. et al., 2007. Substrate source utilisation in long-term diagnosed type 2 diabetes patients at rest, and during exercise and subsequent recovery. *Diabetologia*, 50(1), pp.103–112.

Borg, M.L. et al., 2012. Consumption of a high-fat diet, but not regular endurance exercise training, regulates hypothalamic lipid accumulation in mice. *J Physiol*, 590, pp.4377–89.

Borg, M.L., Lemus, M., et al., 2014. Hypothalamic Neurogenesis Is Not Required for the Improved Insulin Sensitivity Following Exercise Training. *Diabetes*, 63, pp.3647–3658.

Borg, M.L., Andrews, Z.B. & Watt, M.J., 2014. Exercise training does not enhance hypothalamic responsiveness to leptin or ghrelin in male mice. *J Neuroendocrinol*, 26(2), pp.68–79.

van den Borst, B. et al., 2013. Characterization of the inflammatory and metabolic profile of adipose tissue in a mouse model of chronic hypoxia. *J Appl Physiol*, 114, pp.1619–28.

Boström, P. et al., 2012. A PGC1α-dependent myokine that drives browning of white fat and thermogenesis. *Nature*, 481(7382), pp.463–468.

Boudina, S. et al., 2012. Early mitochondrial adaptations in skeletal muscle to diet-induced obesity are strain dependent and determine oxidative stress and energy expenditure but not insulin sensitivity. *Endocrinology*, 153(6), pp.2677–2688.

Boushel, R. et al., 2007. Patients with type 2 diabetes have normal mitochondrial function in skeletal muscle. *Diabetologia*, 50(4), pp.790–796.

Bouzakri, K. et al., 2011. Bimodal effect on pancreatic beta-cells of secretory products from normal or insulin-resistant human skeletal muscle. *Diabetes*, 60(4), pp.1111–1121.

Bradford, M.M., 1976. A rapid and sensitive method for the quantitation of microgram quantities of protein utilizing the principle of protein-dye binding. *Anal Biochem*, 72, pp.248–54.

Brady, L.J. et al., 1985. Elevated hepatic mitochondrial and peroxisomal oxidative capacities in fed and starved adult obese (ob/ob) mice. *Biochem J*, 231(2), pp.439–444.

Bray, G.A. et al., 2012. Long-term safety, tolerability, and weight loss associated with metformin in the Diabetes Prevention Program Outcomes Study. *Diabetes Care*, 35, pp.731–737.

Brehm, A. et al., 2010. Acute elevation of plasma lipids does not affect ATP synthesis in human skeletal muscle. *Am J Physiol Endocrinol Metab*, 299, pp.E33–E38.

Brehm, A. et al., 2006. Increased lipid availability impairs insulin-stimulated ATP synthesis in human skeletal muscle. *Diabetes*, 55(1), pp.136–140.

Bridges, H.R. et al., 2014. Effects of metformin and other biguanides on oxidative phosphorylation in mitochondria. *Biochemical J*, 462(3), pp.475–487.

Brissova, M. et al., 2005. Assessment of human pancreatic islet architecture and composition by laser scanning confocal microscopy. *J Histochem Cytochem*, 53(9), pp.1087–1097.

van den Broek, N.M.A. et al., 2010. Increased mitochondrial content rescues in vivo muscle oxidative capacity in long-term high-fat-diet-fed rats. *FASEB J*, 24(5), pp.1354–1364.

Brookheart, R.T., Michel, C.I. & Schaffer, J.E., 2009. As A Matter of Fat. *Cell Metab*, 10(1), pp.9–12.

Brownlee, M., 2005. The pathobiology of diabetic complications: a unifying mechanism. *Diabetes*, 54(6), p.1615.

Bruce, C.R. et al., 2004. Disassociation of muscle triglyceride content and insulin sensitivity after exercise training in patients with Type 2 diabetes. *Diabetologia*, 47(1), pp.23–30.

Brüning, J.C. et al., 1998. A muscle-specific insulin receptor knockout exhibits features of the metabolic syndrome of NIDDM without altering glucose tolerance. *Mol Cell*, 2, pp.559–569.

Brüning, J.C. et al., 2000. Role of Brain Insulin Receptor in Control of Body Weight and Reproduction. *Science*, 289(5487), pp.2122–2125.

Buchanan, T.A. et al., 2002. Preservation of pancreatic beta-cell function and prevention of type 2 diabetes by pharmacological treatment of insulin resistance in high-risk hispanic women. *Diabetes*, 51(9), pp.2796–2803.

Buettner, R., Schölmerich, J. & Bollheimer, L.C., 2007. High-fat diets: modeling the metabolic disorders of human obesity in rodents. *Obesity*, 15(4), pp.798–808.

Butler, A.E. et al., 2003. Beta-Cell Deficit and Increased Beta-Cell Apoptosis in Humans With Type 2 Diabetes. *Diabetes*, 52, pp.102–110.

Cabrera, O. et al., 2006. The unique cytoarchitecture of human pancreatic islets has implications for

islet cell function. *P Natl Acad Sci USA*, 103, pp.2334–2339.

Cai, D. et al., 2005. Local and systemic insulin resistance resulting from hepatic activation of IKK-beta and NF-kappaB. *Nat Med*, 11(2), pp.183–190.

Calay, E.S. & Hotamisligil, G.S., 2013. Turning off the inflammatory, but not the metabolic, flames. *Nat Med*, 19, pp.265–267.

Camargo, R.L. et al., 2015. Taurine supplementation preserves hypothalamic leptin action in normal and protein-restricted mice fed on a high-fat diet. *Amino Acids*, 47(11), pp.2419–2435.

Campanucci, V., Krishnaswamy, A. & Cooper, E., 2010. Diabetes depresses synaptic transmission in sympathetic ganglia by inactivating nAChRs through a conserved intracellular cysteine residue. *Neuron*, 66(6), pp.827–34.

Cantó, C. & Garcia-Roves, P.M., 2015. High-Resolution Respirometry for Mitochondrial Characterization of Ex Vivo Mouse Tissues. *Curr Protoc Mouse Biol*, 5(2), pp.135–53.

Cao, H. et al., 2008. Identification of a Lipokine, a Lipid Hormone Linking Adipose Tissue to Systemic Metabolism. *Cell*, 134(6), pp.933–944.

Cao, L. et al., 2011. White to brown fat phenotypic switch induced by genetic and environmental activation of a hypothalamic-adipocyte axis. *Cell Metab*, 14(3), pp.324–338.

Carey, V.J. et al., 1997. Body Fat Distribution and Risk of Non-lnsulin-dependent Diabetes Mellitus in Women. *A J Epidemiol*, 145(7), pp.614–619.

Cauchi, S. et al., 2006. Transcription factor TCF7L2 genetic study in the French population: expression in human beta-cells and adipose tissue and strong association with type 2 diabetes. *Diabetes*, 55, pp.2903–2908.

Chalasani, N. et al., 2003. Hepatic cytochrome P450 2E1 activity in nondiabetic patients with nonalcoholic steatohepatitis. *Hepatology*, 37(3), pp.544–550.

Chan, C.B. et al., 2001. Increased uncoupling protein-2 levels in beta-cells are associated with impaired glucose-stimulated insulin secretion: mechanism of action. *Diabetes*, 50(6), pp.1302–1310.

Chan, M.H.S. et al., 2004. Altering dietary nutrient intake that reduces glycogen content leads to phosphorylation of nuclear p38 MAP kinase in human skeletal muscle: association with IL-6 gene transcription during contraction. *FASEB J*, 18(14), pp.1785–1787.

Chang, A.M. & Halter, J.B., 2003. Aging and insulin secretion. *Am J Physiol Endocrinol Metab*, 284, pp.E7–12.

Chavez, A.O. et al., 2010. Effect of short-term free fatty acids elevation on mitochondrial function in skeletal muscle of healthy individuals. *J Clin Endocrinol Metab*, 95(1), pp.422–429.

Chen, X., Yang, L. & Zhai, S.D., 2012. Risk of cardiovascular disease and all-cause mortality among diabetic patients prescribed rosiglitazone or pioglitazone: a meta-analysis of retrospective cohort studies. *Chin Med J (Eng)*, 125(23), pp.4301–6.

Chen, X.-H. et al., 2010. TNF-alpha induces mitochondrial dysfunction in 3T3-L1 adipocytes. *Mol Cell Endocrinol*, 328(1-2), pp.63–69.

Chevillotte, E. et al., 2007. Uncoupling protein-2 controls adiponectin gene expression in adipose tissue through the modulation of reactive oxygen species production. *Diabetes*, 56(4), pp.1042–1050.

Chiasson, J.-L. et al., 2002. Acarbose for prevention of type 2 diabetes mellitus: the STOP-NIDDM randomised trial. *Lancet*, 359, pp.2072–2077.

Chomentowski, P. et al., 2011. Skeletal muscle mitochondria in insulin resistance: Differences in intermyofibrillar versus subsarcolemmal subpopulations and relationship to metabolic flexibility. *J Clin Endocrinol Metab*, 96(2), pp.494–503.

Choo, H.J. et al., 2006. Mitochondria are impaired in the adipocytes of type 2 diabetic mice. *Diabetologia*, 49(4), pp.784–791.

Chouchani, E.T. et al., 2014. Ischaemic accumulation of succinate controls reperfusion injury through mitochondrial ROS. *Nature*, 515(7527), pp.431–435.

Christ, C.Y. et al., 2002. Exercise training improves muscle insulin resistance but not insulin receptor signaling in obese Zucker rats. *J Appl Physiol*, 92(2), pp.736–744.

Christensen, C.S. et al., 2015. Skeletal muscle to pancreatic β-cell cross-talk: the effect of humoral mediators liberated by muscle contraction and acute exercise on β-cell apoptosis. *J Clin Endocrinol Metab*, pp.1–11.

Christiansen, T., Paulsen, S.K., Bruun, J.M., Ploug, T., et al., 2010. Diet-induced weight loss and exercise alone and in combination enhance the expression of adiponectin receptors in adipose tissue and skeletal muscle, but only diet-induced weight loss enhanced circulating adiponectin. *J Clin Endocrinol Metab*, 95(2), pp.911–9.

Christiansen, T., Paulsen, S.K., Bruun, J.M., Pedersen, S.B., et al., 2010. Exercise training versus diet-induced weight-loss on metabolic risk factors and inflammatory markers in obese subjects : a 12-week randomized intervention study. *Am J Physiol Endocrinol Metab*, 298, pp.824–831.

Cildir, G., Akincilar, S.C. & Tergaonkar, V., 2013. Chronic adipose tissue inflammation: All immune cells on the stage. *Trends Mol Med*, 19(8), pp.487–500.

Civitarese, A.E. et al., 2007. Calorie Restriction Increases Muscle Mitochondrial Biogenesis in Healthy Humans. *PLoS Medicine*, 4(3), p.e76.

Civitarese, A.E. & Ravussin, E., 2008. Minireview: Mitochondrial Energetics and Insulin Resistance. *Endocrinology*, 149(3), pp.950–954.

Clarke, S.D. & Jump, D.B., 1994. Dietary polyunsaturated fatty acid regulation of gene transcription. *Annu Rev Nutr*, 14, pp.83–98.

Cline, G.W. et al., 1999. Impaired glucose transport as a cause of decreased insulin-stimulated muscle glycogen synthesis in type 2 diabetes. *N Engl J Med*.

Clore, J.N., Stillman, J. & Sugerman, H., 2000. Glucose-6-Phosphatase Flux In Vitro Is Increased in Type 2 Diabetes. *Diabetes*, 49, pp.969–974.

Coen, P.M. et al., 2010. Insulin Resitance is Associated With Higher Intramyocellular Triglycerides in Type I but Not Type II Myocytes Concomitant With Higher Ceramide Content. *Diabetes*, 59, pp.80–88.

Colombani, A.L. et al., 2009. Enhanced hypothalamic glucose sensing in obesity: Alteration of redox signaling. *Diabetes*, 58(10), pp.2189–2197.

Consoli, A. et al., 1990. Mechanism of increased gluconeogenesis in noninsulin-dependent diabetes mellitus: Role of alterations in systemic, hepatic, and muscle lactate and alanine metabolism. *J Clin Invest*, 86(6), pp.2038–2045.

Contreras, C. et al., 2014. Central Ceramide-Induced Hypothalamic Lipotoxicity and ER Stress Regulate Energy Balance. *Cell Reports*, 9(1), pp.366–377.

Cooper, D.R., Watson, J.E. & Dao, M.L., 1993. Decreased expression of protein kinase-C alpha, beta, and epsilon in soleus muscle of Zucker obese (fa/fa) rats. *Endocrinology*, 133(5), pp.2241–7.

Cortez-Pinto, H. et al., 1999. Alterations in liver ATP homeostasis in human nonalcoholic steatohepatitis: a pilot study. *JAMA*, 282(17), pp.1659–1664.

Corvera, S. & Gealekman, O., 2014. Adipose tissue angiogenesis: impact on obesity and type-2 diabetes. *Biochim Biophys Acta*, 1842(3), pp.463–72.

Craig, B.W. et al., 1981. Adaptation of fat cells to exercise: response of glucose uptake and oxidation to insulin. *J Appl Physiol Respir Environ Exerc Physiol*, 51(6), pp.1500–6.

Crooke, S.T., 2004. Progress in antisense technology. *Annu Rev Med*, 55, pp.61–95.

Cummins, T.D. et al., 2014. Metabolic remodeling of white adipose tissue in obesity. *Am J Physiol Endocrinol Metab*, 307(3), pp.E262–E277.

Curtis, J.M. et al., 2010. Downregulation of adipose glutathione S-transferase A4 leads to increased protein carbonylation, oxidative stress, and mitochondrial dysfunction. *Diabetes*, 59(5), pp.1132–1142.

Cusi, K. et al., 2000. Insulin resistance differentially affects the PI 3-kinase- and MAP kinase-mediated signaling in human muscle. *J Clin Invest*, 105(3), pp.311–320.

Cuypers, J., Mathieu, C. & Benhalima, K., 2013. SGLT2-inhibitors: A novel class for the treatment of type 2 diabetes introduction of SGLT2-inhibitors in clinical practice. *Acta Clin Belg*, 68(4), pp.287–293.

Czyzyk, T.A. et al., 2010. kappa-Opioid receptors control the metabolic response to a high-energy diet in mice. *FASEB J*, 24, pp.1151–1159.

Czyzyk, T.A. et al., 2012. Mice lacking delta-opioid receptors resist the development of diet-induced obesity. *FASEB J*, 26(8), pp.3483–3492.

Dahlman, I. et al., 2006. Downregulation of electron transport chain genes in visceral adipose tissue in type 2 diabetes independent of obesity and possibly involving tumor necrosis factor-alpha. *Diabetes*, 55(6), pp.1792–1799.

Dandona, P., Aljada, A. & Bandyopadhyay, A., 2004. Inflammation: the link between insulin resistance, obesity and diabetes. *Trends Immunol*, 25(1), pp.4–7.

Dauncey, M.J. & Brown, D., 1987. Role of Activity-Induced Thermogenesis in Twenty-Four Hour Energy Expenditure of Lean and Genetically Obese (Ob/Ob) Mice. *Q J Exp Psychol*, 72(4), pp.549 –559.

Davis, C.L. et al., 2012. Exercise dose and diabetes risk in overweight and obese children: a randomized controlled trial. *JAMA*, 308(11), pp.1103–12.

Defronzo, R.A., 2009. Banting Lecture. From the triumvirate to the ominous octet: a new paradigm for the treatment of type 2 diabetes mellitus. *Diabetes*, 58(4), pp.773–95.

DeFronzo, R.A. et al., 1985. Effects of Insulin on Peripheral and Splanchnic Glucose Metabolism in Noninsulin-dependent (Type II) Diabetes Mellitus. *J Clin Invest*, 76, pp.149–155.

DeFronzo, R.A., 2004. Pathogenesis of type 2 diabetes mellitus. *Med Clin N Am*, 88(4), pp.787–835.

DeFronzo, R.A., 1997. Pathogenesis of type 2 diabetes: metabolic and molecular implications for identifying diabetes genes. *Diabetes Rev*, 5, pp.177–269.

DeFronzo, R.A., 1988. The triumvirate: beta-cell, muscle, or liver. A collusion responsible for NIDDM. *Diabetes*, 37, pp.667–687.

DeFronzo, R.A. & Ferrannini, E., 1987. Regulation of hepatic glucose metabolism in humans. *Diabetes Metab Rev*, 3(2), pp.415–59.

DeFronzo, R.A. & Ferrannini, E., 2015. Regulation of intermediary metabolism during fasting and refeeding. In J. J. DeGroot LJ, ed. *Endocrinology*. Philadelphia, PA: Saunders Elsevier, pp. 673–698.

DeFronzo, R.A., Ferrannini, E. & Simonson, D.C., 1989. Fasting hyperglycemia in non-insulin-dependent diabetes mellitus: contributions of excessive hepatic glucose production and impaired tissue glucose uptake. *Metabolism*, 38(4), pp.387–95.

DeFronzo, R.A., Sherwin, R.S. & Kraemer, N., 1987. The effect of physical training on insulin production in obesity. *Diabetes*, 36, pp.1379–85.

Dela, F. et al., 1990. Diminished arginine-stimulated insulin secretion in trained men. *J Appl Physiol*, 69(1), pp.261–267.

Dela, F. et al., 1992. Effect of training on insulin-mediated glucose uptake in human muscle. *Am J Physiol*, 263(6), pp.E1134–43.

Dela, F. et al., 1995. Insulin-stimulated muscle glucose clearance in patients with NIDDM. Effects of one-legged physical training. *Diabetes*, 44(9), pp.1010–20.

Dela, F. et al., 2004. Physical training may enhance beta-cell function in type 2 diabetes. *Am J Physiol Endocrinol Metab*, 287, pp.1024–1031.

Dela, F. & Helge, J.W., 2013. Insulin resistance and mitochondrial function in skeletal muscle. *Int J Biochem Cell Biol*, 45(1), pp.11–5.

Delarue, J. & Magnan, C., 2007. Free fatty acids and insulin resistance. *Curr Opin Clin Nutr*, 10, pp.142–148.

Delghingaro-Augusto, V. et al., 2012. Voluntary running exercise prevents beta-cell failure in susceptible islets of the Zucker diabetic fatty rat. *Am J Physiol Endocrinol Metab*, 302(2), pp.E254–E264.

Devarakonda, S. et al., 2011. Disorder-to-order transition underlies the structural basis for the assembly of a transcriptionally active PGC-1alpha/ERRgamma complex. *P Natl Acad Sci USA*, 108(46), pp.18678–18683.

Deveaud, C. et al., 2004. Regional differences in oxidative capacity of rat white adipose tissue are linked to the mitochondrial content of mature adipocytes. *Mol Cell Biochem*, 267, pp.157–66.

Diano, S. et al., 2012. Peroxisome proliferation-related ROS control sets melanocortin tone and feeding in diet-induced obesity. *Nat Med*, 17(9), pp.1121–1127.

Diéguez, C. et al., 2011. Hypothalamic control of lipid metabolism: Focus on leptin, ghrelin and melanocortins. *Neuroendocrinology*, 94(1), pp.1–11.

Díez, J.J. & Iglesias, P., 2003. The role of the novel adipocyte-derived hormone adiponectin in human disease. *Eur J Endocrinol*, 148(3), pp.293–300.

Dobrowsky, R.T. et al., 1993. Ceramide activates heterotrimeric protein phosphatase 2A. *J Biol Chem*, 268(21), pp.15523–15530.

Doege, H. et al., 2008. Silencing of hepatic fatty acid transporter protein 5 in vivo reverses diet-induced non-alcoholic fatty liver disease and improves hyperglycemia. *J Biol Chem*, 283(32), pp.22186–22192.

Donges, C.E., Duffield, R. & Drinkwater, E.J., 2009. Effects of Resistance or Aerobic Exercise Training on Interleukin-6, C-Reactive Protein, and Body Composition. *Med Sci Sport Exer*, (28), pp.304–313.

Draznin, B., 2006. Molecular mechanisms of insulin resistance: Serine phosphorylation of insulin receptor substrate-1 and increased expression of p85alpha: The two sides of a coin. *Diabetes*, 55(8), pp.2392–2397.

Dresner, A. et al., 1999. Effects of free fatty acids on glucose transport and IRS-1-associated phosphatidylinositol 3-kinase activity. *J Clin Invest*, 103, pp.253–259.

Drucker, D.J., 2006. The biology of incretin hormones. *Cell Metab*, 3, pp.153–165.

Drucker, D.J. & Nauck, M.A., 2006. The incretin system: glucagon-like peptide-1 receptor agonists and dipeptidyl peptidase-4 inhibitors in type 2 diabetes. *Lancet*, 368(9548), pp.1696–1705.

Dubé, J.J. et al., 2011. Effects of weight loss and exercise on insulin resistance, and intramyocellular triacylglycerol, diacylglycerol and ceramide. *Diabetologia*, 54, pp.1147–1156.

Dubé, J.J. et al., 2012. Exercise Dose and Insulin Sensitivity: Relevance for Diabetes Prevention. *Med Sci Sport Exer*, 44(5), pp.793–799.

Duncan, B.B. et al., 2003. Low-Grade Systemic Inflammation and the Development of Type 2 Diabetes: The Atherosclerosis Risk in Communities Study. *Diabetes*, 52(7), pp.1799–1805.

Dupre, J. et al., 1995. Glucagon-like peptide I reduces postprandial glycemic excursions in IDDM. *Diabetes*, 44, pp.626–630.

Efrat, S., 2001. Prospects for Treatment of Type 2 Diabetes by Expansion of the beta-Cell Mass. *Diabetes*, 50(Suppl.1), pp.189–190.

Ehses, J.A. et al., 2007. Increased Number of Islet-Associated Macrophages in Type 2 Diabetes. *Diabetes*, 56, pp.2356–2370.

Ehses, S. et al., 2009. Regulation of OPA1 processing and mitochondrial fusion by m-AAA protease isoenzymes and OMA1. *The Journal of Cell Biology*, 187(7), pp.1023–1036.

Eisenberg, B.R. & Kuda, A.M., 1976. Discrimination between fiber populations in mammalian skeletal muscle by using ultrastructural parameters. *J Ultra Res*, 54(1), pp.76–88.

Eisenberg, B.R. & Kuda, A.M., 1975. Stereological analysis of mammalian skeletal muscle. II. White vastus muscle of the adult guinea pig. *J Ultra Res*, 51(2), pp.176–87.

Eizirik, D.L. et al., 1994. Cytokines suppress human islet function irrespective of their effects on nitric oxide generation. *J Clin Invest*, 93(5), pp.1968–1974.

Elayat, A.A., El-Naggar, M.M. & Tahir, M., 1995. An immunocytochemical and morphometric study of the rat pancreatic islets. *J Anat*, 186, pp.629–637.

Ellingsgaard, H. et al., 2011. Interleukin-6 enhances insulin secretion by increasing glucagon-like peptide-1 secretion from L cells and alpha cells. *Nat Med*, 17(11), pp.1481–1489.

Ellingsgaard, H. et al., 2008. Interleukin-6 regulates pancreatic alpha-cell mass expansion. *P Natl Acad Sci USA*, 105(35), pp.13163–13168.

Elmquist, J.K., Elias, C.F. & Saper, C.B., 1999. From Lesions to Leptin : Hypothalamic Control of Food Intake and Body Weight. *Neuron*, 22, pp.221–232.

Emanuelli, B. et al., 2000. SOCS-3 is an insulin-induced negative regulator of insulin signaling. *J Biol Chem*, 275(21), pp.15985–15991.

Eriksson, J. et al., 1989. Early-metabolic defects in persons at increased risk for non-insulin-dependent diabetes mellitus. *N Engl J Med*, 321, pp.337–343.

Eriksson, J. et al., 1992. Islet amyloid polypeptide plasma concentrations in individuals at increased risk of developing Type 2 (non-insulin-dependent) diabetes mellitus. *Diabetologia*, 35, pp.291–293.

Eriksson, K.F. & Lindgärde, F., 1991. Prevention of type 2 (non-insulin-dependent) diabetes mellitus by diet and physical exercise: The 6-year Malmö feasibility study. *Diabetologia*, 34, pp.891–898.

Eun, H.K. et al., 2007. Essential role of mitochondrial function in adiponectin synthesis in adipocytes. *Diabetes*, 56(12), pp.2973–2981.

Evans, J.L. et al., 2003. Are Oxidative Stress - Activated Signaling Pathways Mediators of Insulin Resistance and Beta-Cell Dysfunction? *Diabetes*, 52(1), pp.1–8.

Fabbrini, E. et al., 2009. Intrahepatic fat, not visceral fat, is linked with metabolic complications of obesity. *P Natl Acad Sci USA*, 106(36), pp.15430–15435.

Fabbrini, E. et al., 2010. Surgical removal of omental fat does not improve insulin sensitivity and cardiovascular risk factors in obese adults. *Gastroenterology*, 139, pp.448–455.

Fain, J.N. et al., 2004. Comparison of the release of adipokines by adipose tissue, adipose tissue matrix, and adipocytes from visceral and subcutaneous abdominal adipose tissues of obese humans. *Endocrinology*, 145(5), pp.2273–2282.

Falcon, A. et al., 2010. FATP2 is a hepatic fatty acid transporter and peroxisomal very long-chain acyl-CoA synthetase. *Am J Physiol Endocrinol Metab*, 299, pp.E384–E393.

Farrell, P.A., Caston, A.L. & Rodd, D., 1991. Changes in insulin response to glucose after exercise training in partially pancreatectomized rats. *J Appl Physiol*, 70(4), pp.1563–1568.

Feingold, K.R. et al., 1989. Effect of tumor necrosis factor (TNF) on lipid metabolism in the diabetic rat. Evidence that inhibition of adipose tissue lipoprotein lipase activity is not required for TNF-induced hyperlipidemia. *J Clin Invest*, 83(4), pp.1116–1121.

Feldmann, H.M. et al., 2009. UCP1 Ablation Induces Obesity and Abolishes Diet-Induced Thermogenesis in Mice Exempt from Thermal Stress by Living at Thermoneutrality. *Cell Metab*, 9(2), pp.203–209.

Fernández-Sánchez, A. et al., 2011. Inflammation, oxidative stress, and obesity. *Int J Mol Sci*, 12, pp.3117–3132.

Ferrannini, E. et al., 2005. Beta-cell function in subjects spanning the range from normal glucose tolerance to overt diabetes: A new analysis. *J Clin Endocrinol Metab*, 90(1), pp.493–500.

Ferrannini, E. et al., 1988. The disposal of an oral glucose load in patients with non-insulin-dependent diabetes. *Metabolism*, 37(1), pp.79–85.

Ferreira, F.M.L. et al., 1999. Alterations of liver mitochondrial bioenergetics in diabetic Goto-Kakizaki rats. *Metabolism*, 48(9), pp.1115–1119.

De Feyter, H.M., van den Broek, N.M.A., et al., 2008. Early or advanced stage type 2 diabetes is not accompanied by in vivo skeletal muscle mitochondrial dysfunction. *Eur J Endocrinol*, 158(5), pp.643–653.

De Feyter, H.M., Lenaers, E., et al., 2008. Increased intramyocellular lipid content but normal skeletal muscle mitochondrial oxidative capacity throughout the pathogenesis of type 2 diabetes. *FASEB J*, 22(11), pp.3947–3955.

Finegood, D.T. & Topp, B.G., 2001. B-Cell Deterioration - Prospects for Reversal or Prevention. *Diabetes Obes Metab*, 3(Suppl.1), pp.20–27.

Fischer, C.P. et al., 2007. Plasma levels of interleukin-6 and C-reactive protein are associated with physical inactivity independent of obesity. *Scand J Med Sci Spor*, 17(5), pp.580–587.

Fisher-Wellman, K.H. & Neufer, P.D., 2012. Linking mitochondrial bioenergetics to insulin resistance via redox biology. *Trends Endocrin Met*, 23(3), pp.142–153.

Flamment, M. et al., 2008. Fatty liver and insulin resistance in obese Zucker rats: No role for mitochondrial dysfunction. *Biochimie*, 90(9), pp.1407–1413.

Flier, J.S., 2004. Obesity Wars: Molecular Progress Confronts an Expanding Epidemic. *Cell*, 116(2), pp.337–350.

Flier, S.N., Kulkarni, R.N. & Kahn, C.R., 2001. Evidence for a circulating islet cell growth factor in insulin-resistant states. *P Natl Acad Sci USA*, 98(13), pp.7475–7480.

Folli, F. et al., 1993. Regulation of phosphatidylinositol 3-kinase activity in liver and muscle of animal models of insulin-resistant and insulin-deficient diabetes mellitus. *J Clin Invest*, 92(4), pp.1787–1794.

Forner, F. et al., 2006. Quantitative proteomic comparison of rat mitochondria from muscle, heart, and liver. *Mol Cell Proteomics*, 5(4), pp.608–619.

Frangioudakis, G. et al., 2009. Diverse roles for protein kinase C delta and protein kinase C epsilon in the generation of high-fat-diet-induced glucose intolerance in mice: Regulation of lipogenesis by protein kinase C delta. *Diabetologia*, 52(12), pp.2616–2620.

Fraser, A. et al., 2009. Alanine Aminotransferase, gamma-Glutamyltransferase, and Incident Diabetes. *Diabetes Care*, 32(4), pp.741–750.

Freeman, H.C. et al., 2006. Deletion of nicotinamide nucleotide transhydrogenase: A new quantitive trait locus accounting for glucose intolerance in C57BL/6J mice. *Diabetes*, 55(7), pp.2153–2156.

Friedberg, C.E. et al., 1998. Fish oil and glycemic control in diabetes. A meta-analysis. *Diabetes Care*, 21(4), pp.494–500.

Friedman, J.M., 2009. Obesity: Causes and control of excess body fat. *Nature*, 459(7245), pp.340–342.

Frisdal, E. et al., 2011. Interleukin-6 protects human macrophages from cellular cholesterol accumulation and attenuates the proinflammatory response. *J Biol Chem*, 286(35), pp.30926–30936.

Frost, R.A., Nystrom, G.J. & Lang, C.H., 2002. Lipopolysaccharide regulates proinflammatory

cytokine expression in mouse myoblasts and skeletal muscle. *Am J Physiol Regul Integr Comp Physiol*, 283(3), pp.R698–R709.

Furukawa, N. et al., 2005. Role of Rho-kinase in regulation of insulin action and glucose homeostasis. *Cell Metab*, 2(2), pp.119–129.

Gabriely, I. et al., 2002. Removal of visceral fat prevents insuling resistance and glucose intolerance of aging: an adipokine-mediated process? *Diabetes*, 51, pp.2951–2958.

Gagnon, J. et al., 1991. Correlations between a nuclear and a mitochondrial mRNA of cytochrome c oxidase subunits, enzymatic activity and total mRNA content, in rat tissues. *Mol Cell Biochem*, 107(1), pp.21–9.

Gaíva, M.H. et al., 2003. Diets rich in polyunsaturated fatty acids: effect on hepatic metabolism in rats. *Nutrition*, 19(2), pp.144–9.

Galgani, J.E., Heilbronn, L.K., et al., 2008. Metabolic flexibility in response to glucose is not impaired in people with type 2 diabetes after controlling for glucose disposal rate. *Diabetes*, 57(4), pp.841–845.

Galgani, J.E., Moro, C. & Ravussin, E., 2008. Metabolic flexibility and insulin resistance. *Am J Physiol Endocrinol Metab*, 295, pp.1009–1017.

Galic, S., Oakhill, J.S. & Steinberg, G.R., 2010. Adipose tissue as an endocrine organ. *Mol Cell Endocrinol*, 316, pp.129–139.

Gallagher, D. et al., 2014. Changes in Adipose Tissue Depots and Metabolic Markers Following a 1-Year Diet and Exercise Intervention in Overweight and Obese Patients With Type 2 Diabetes. *Diabetes Care*, 37(12), pp.3325–3332.

Gangwisch, J.E. et al., 2007. Sleep duration as a risk factor for diabetes incidence in a large U.S. sample. *Sleep*, 30(12), pp.1667–1673.

Gao, C.L. et al., 2010. Mitochondrial dysfunction is induced by high levels of glucose and free fatty acids in 3T3-L1 adipocytes. *Mol Cell Endocrinol*, 320(1-2), pp.25–33.

Garcia-Roves, P. et al., 2007. Raising plasma fatty acid concentration induces increased biogenesis of mitochondria in skeletal muscle. *P Natl Acad Sci USA*, 104(25), pp.10709–10713.

Garcia-Roves, P.M., 2011. Mitochondrial pathophysiology and type 2 diabetes mellitus. *Arch Physiol Biochem*, 117(3), pp.177–187.

García-Ruiz, E. et al., 2015. The intake of high fat diets induces the acquisition of brown adipocyte gene expression features in white adipose tissue. *Int J Obesity*, 39, pp.1619–1629.

Gastaldelli, A. et al., 2004. Beta-cell dysfunction and glucose intolerance: Results from the San Antonio metabolism (SAM) study. *Diabetologia*, 47(1), pp.31–39.

Gastaldelli, A. et al., 2000. Infuence of Obesity and Type 2 Diabetes on Gluconeogenesis and Glucose Output in Humans. A Quantitative Study. *Diabetes*, 49, pp.1367–1373.

Gastaldelli, A. et al., 2007. Thiazolidinediones improve beta-cell function in type 2 diabetic patients. *Am J Physiol Endocrinol Metab*, 292, pp.871–883.

Gavrilova, O. et al., 2003. Liver Peroxisome Proliferator-activated Receptor Contributes to Hepatic Steatosis, Triglyceride Clearance, and Regulation of Body Fat Mass. *J Biol Chem*, 278(36), pp.34268–34276. Available at: http://www.jbc.org/cgi/doi/10.1074/jbc.M300043200.

Gealekman, O. et al., 2011. Depot-specific differences and insufficient subcutaneous adipose tissue angiogenesis in human obesity. *Circulation*, 123, pp.186–194.

Geffken, D.F. et al., 2001. Association between physical activity and markers of inflammation in a healthy elderly population. *A J Epidemiol*, 153(3), pp.242–250.

Gelling, R.W. et al., 2006. Insulin action in the brain contributes to glucose lowering during insulin treatment of diabetes. *Cell Metab*, 3(1), pp.67–73.

Gianotti, T.F. et al., 2013. Fatty Liver Is Associated with Transcriptional Downregulation of Stearoyl-CoA Desaturase and Impaired Protein Dimerization. *PLoS ONE*, 8(9), p.e76912.

Gil, A. et al., 2011. Is adipose tissue metabolically different at different sites? *Int J Pediatr Obes*, 6(S1), pp.13–20.

Gingras, A.-A. et al., 2007. Long-chain omega-3 fatty acids regulate bovine whole-body protein metabolism by promoting muscle insulin signalling to the Akt-mTOR-S6K1 pathway and insulin sensitivity. *J Physiol*, 579(1), pp.269–284.

Girousse, A. et al., 2013. Partial Inhibition of Adipose Tissue Lipolysis Improves Glucose Metabolism and Insulin Sensitivity Without Alteration of Fat Mass. *PLoS Biol*, 11(2), p.e1001485.

Gleeson, M., 2007. Immune function in sport and exercise. *J Appl Physiol*, 103(2), pp.693–699.

Gnaiger, E., 2009. Capacity of oxidative phosphorylation in human skeletal muscle: new perspectives of mitochondrial physiology. *Int J Biochem Cell Biol*, 41(10), pp.1837–45.

Gnaiger, E., 2014. *Mitochondrial Pathways and Respiratory Control. An Introduction to OXPHOS Analysis.* 4th ed., OROBOROS MiPNet Publications 2014.

Goldstein, B.J. et al., 2005. Role of Insulin-Induced Reactive Oxygen Species in the Insulin Signaling Pathway. *Antioxid Redox Sign*, 7(7-8), pp.1021–1031.

Gollisch, K.S.C. et al., 2009. Effects of exercise training on subcutaneous and visceral adipose tissue in normal- and high-fat diet-fed rats. *Am J Physiol Endocrinol Metab*, 297, pp.E495–E504.

Gomes, L.C., Di Benedetto, G. & Scorrano, L., 2011. During autophagy mitochondria elongate, are spared from degradation and sustain cell viability. *Nat Cell Biol*, 13(5), pp.589–598.

Gómez-Valadés, A.G. et al., 2015. Emerging concepts in Diabetes: mitochondrial dynamics and glucose homeostasis. *Curr Diabetes Rev*.

Gonçalves, I.O. et al., 2014. Exercise alters liver mitochondria phospholipidomic profile and mitochondrial activity in non-alcoholic steatohepatitis. *Int J Biochem Cell B*, 54, pp.163–173.

González-Perín, A. et al., 2009. Obesity-induced insulin resistance and hepatic steatosis are alleviated by ω-3 fatty acids: a role for resolvins and protectins. *FASEB J*, 23(6), pp.1946–57.

Goodpaster, B.H. et al., 2001. Skeletal muscle lipid content and insulin resistance: evidence for a paradox in endurance-trained athletes. *J Clin Endocrinol Metab*, 86(12), pp.5755–61.

Goodpaster, B.H., Wolfe, R.R. & Kelley, D.E., 2002. Effects of obesity on substrate utilization during exercise. *Obes Res*, 10(7), pp.575–584.

Gopaul, N.K. et al., 1995. Plasma 8-epi-PGF2 alpha levels are elevated in individuals with non-insulin dependent diabetes mellitus. *FEBS Lett*, 368(2), pp.225–229.

Goudriaan, J.R. et al., 2003. CD36 deficiency increases insulin sensitivity in muscle, but induces insulin resistance in the liver in mice. *J Lipid Res*, 44(12), pp.2270–2277.

Gregor, M.F. et al., 2009. Endoplasmic Reticulum Stress Is Reduced in Tissues of Obese Subjects After Weight Loss. *Diabetes*, 58, pp.693–700.

Griffin, M.E. et al., 1999. Free fatty acid-induced insulin resistance is associated with activation of protein kinase C theta and alterations in the insulin signaling cascade. *Diabetes*, 48(6), pp.1270–4.

Griparic, L., Kanazawa, T. & van der Bliek, A.M., 2007. Regulation of the mitochondrial dynamin-like protein Opa1 by proteolytic cleavage. *The Journal of Cell Biology*, 178(5), pp.757–764.

Groop, L. & Lyssenko, V., 2008. Genes and type 2 diabetes mellitus. *Curr Diabetes Rep*, 8(3), pp.192–7.

Groop, L.C. et al., 1989. Glucose and free fatty acid metabolism in non-insulin-dependent diabetes mellitus. Evidence for multiple sites of insulin resistance. *J Clin Invest*, 84(1), pp.205–213.

Groop, L.C. et al., 1991. The role of free fatty acid metabolism in the pathogenesis of insulin resistance in obesity and noninsulin-dependent diabetes mellitus. *J Clin Endocrinol Metab*, 72(1), pp.96–107.

Groves, C.J. et al., 2006. Association analysis of 6,736 U.K. subjects provides replication and confirms TCF7L2 as a type 2 diabetes susceptibility gene with a substantial effect on individual risk. *Diabetes*, 55, pp.2640–2644.

Grunfeld, C. & Feingold, K.R., 1991. The metabolic effects of tumor necrosis factor and other cytokines. *Biotherapy*, 3(2), pp.143–58.

Guardado-Mendoza, R. et al., 2009. Pancreatic islet amyloidosis, beta-cell apoptosis, and alpha-cell proliferation are determinants of islet remodeling in type-2 diabetic baboons. *P Natl Acad Sci USA*, 106(33), pp.13992–13997.

Guyton, A.C. & Hall, J.E., 2006. *Textbook of Medical Physiology* 11th ed., Elsevier Saunders.

Hajri, T. et al., 2002. Defective fatty acid uptake modulates insulin responsiveness and metabolic responses to diet in CD36-null mice. *J Clin Invest*, 109(10), pp.1381–1389.

van Hall, G. et al., 2003. Interleukin-6 stimulates lipolysis and fat oxidation in humans. *J Clin Endocrinol Metab*, 88(7), pp.3005–3010.

Hammarstedt, A. et al., 2003. Reduced expression of PGC-1 and insulin-signaling molecules in adipose tissue is associated with insulin resistance. *Biochem Bioph Res Co*, 301(2), pp.578–582.

Han, D.-H. et al., 2011. Deficiency of the mitochondrial electron transport chain in muscle does not cause insulin resistance. *PLoS ONE*, 6(5), p.e19739.

Han, D.-H. et al., 2004. UCP-mediated energy depletion in skeletal muscle increases glucose transport despite lipid accumulation and mitochondrial dysfunction. *Am J Physiol Endocrinol Metab*, 286(3), pp.E347–E353.

Hancock, C.R. et al., 2011. Does calorie restriction induce mitochondrial biogenesis? A reevaluation. *FASEB J*, 25, pp.785–91.

Hancock, C.R. et al., 2008. High-fat diets cause insulin resistance despite an increase in muscle mitochondria. *P Natl Acad Sci USA*, 105(22), pp.7815–7820.

Hanisch, U.-K., 2002. Microglia as a source and target of cytokines. *Glia*, 40(2), pp.140–155.

Hanley, A.J.G. et al., 2002. Homeostasis model assessment of insulin resistance in relation to the incidence of cardiovascular disease. The San Antonio Heart Study. *Diabetes Care*, 25(7), pp.1177–1184.

Hansen, D. et al., 2009. Continuous low- to moderate-intensity exercise training is as effective as moderate- to high-intensity exercise training at lowering blood HbA1c in obese type 2 diabetes patients. *Diabetologia*, 52, pp.1789–1797.

Hansen, P.A. et al., 1998. Increased GLUT-4 translocation mediates enhanced insulin sensitivity of muscle glucose transport after exercise. *J Appl Physiol*, 85(4), pp.1218–22.

Hardy, O.T., Czech, M.P. & Corvera, S., 2012. What causes the insulin resistance underlying obesity? *Curr Opin Endocrinol Diabetes Obes*, 19, pp.81–7.

Hartter, E. et al., 1991. Basal and stimulated plasma levels of pancreatic amylin indicate its co-secretion with insulin in humans. *Diabetologia*, 34, pp.52–54.

Hatori, M. et al., 2012. Time-Restricted Feeding without Reducing Caloric Intake Prevents Metabolic Diseases in Mice Fed a High-Fat Diet. *Cell Metab*, 15(6), pp.848–860.

Haus, J.M. et al., 2009. Plasma Ceramides Are Elevated in Obese Subjects With Type 2 Diabetes and Correlate With the Severity of Insulin Resistance. *Diabetes*, 58, pp.337–343.

Hawley, J.A. & Gibala, M.J., 2012. What's new since Hippocrates? Preventing type 2 diabetes by physical exercise and diet. *Diabetologia*, 55(3), pp.535–9.

Hayden, M.R. & Tyagi, S.C., 2002. Islet redox stress: The manifold toxicities of insulin resistance, metabolic syndrome and amylin derived islet amyloid in type 2 diabetes mellitus. *J Pancreas*, 3(4), pp.86–108.

He, J., Watkins, S. & Kelley, D.E., 2001. Skeletal muscle lipid content and oxidative enzyme activity in relation to muscle fiber type in type 2 diabetes and obesity. *Diabetes*, 50(4), pp.817–823.

Head, B. et al., 2009. Inducible proteolytic inactivation of OPA1 mediated by the OMA1 protease in mammalian cells. *J Cell Biol*, 187(7), pp.959–966.

Heijboer, A.C. et al., 2005. Sixteen hours of fasting differentially affects hepatic and muscle insulin sensitivity in mice. *J Lipid Res*, 46(3), pp.582–588.

Heilbronn, L.K. et al., 2007. Markers of mitochondrial biogenesis and metabolism are lower in overweight and obese insulin-resistant subjects. *J Clin Endocrinol Metab*, 92(4), pp.1467–1473.

Heilbronn, L.K. & Campbell, L. V, 2008. Adipose Tissue Macrophages, Low Grade Inflammation and Insulin Resistance in Human Obesity. *Curr Pharm Design*, 14, pp.1225–1230.

Helge, J.W. et al., 2004. Exercise and training effects on ceramide metabolism in human skeletal muscle. *Exp Physiol*, 89(1), pp.119–127.

Hellmann, J. et al., 2011. Resolvin D1 decreases adipose tissue macrophage accumulation and improves insulin sensitivity in obese-diabetic mice. *FASEB J*, 25(7), pp.2399–407.

Henningsen, J. et al., 2010. Dynamics of the skeletal muscle secretome during myoblast differentiation. *Mol Cell Proteomics*, 9(11), pp.2482–2496.

Henry, R.R., Scheaffer, L. & Olefsky, J.M., 1985. Glycemic effects of intensive caloric restriction and isocaloric refeeding in noninsulin-dependent diabetes mellitus. *J Clin Endocrinol Metab*, 61(5), pp.917–25.

Henry, R.R., Wallace, P. & Olefksy, J.M., 1986. Effects of weight loss on mechanisms of hyperglycemia in obese non-insulin-dependent diabetes mellitus. *Diabetes*, 35(9), pp.990–8.

Herman, W.H. et al., 2012. The 10-Year Cost-Effectiveness of Lifestyle Intervention or Metformin for Diabetes Prevention. An intent-to-treat analysis of the DPP/DPPOS. *Diabetes care*, 35, pp.723–730.

Hevener, A.L., Reichart, D. & Olefsky, J., 2000. Exercise and thiazolidinedione therapy normalize insulin action in the obese Zucker fatty rat. *Diabetes*, 49(12), pp.2154–2159.

Hey-Mogensen, M. et al., 2010. Effect of physical training on mitochondrial respiration and reactive oxygen species release in skeletal muscle in patients with obesity and type 2 diabetes. *Diabetologia*, 53, pp.1976–1985.

Higa, M. et al., 1999. Troglitazone prevents mitochondrial alterations, beta cell destruction, and diabetes in obese prediabetic rats. *P Natl Acad Sci USA*, 96(20), pp.11513–11518.

Hirosumi, J. et al., 2002. A central role for JNK in obesity and insulin resistance. *Nature*, 420, pp.333–336.

Hoehn, K.L. et al., 2008. IRS1-Independent Defects Define Major Nodes of Insulin Resistance. *Cell Metab*, 7(5), pp.421–433.

Hofmann, C. et al., 1994. Altered gene expression for tumor necrosis factor-alpha and its receptors during drug and dietary modulation of insulin resistance. *Endocrinology*, 134(1), pp.264–70.

Holland, W.L. et al., 2013. An FGF21-adiponectin-ceramide axis controls energy expenditure and insulin action in mice. *Cell Metab*, 17(5), pp.790–797.

Holland, W.L. et al., 2007. Inhibition of Ceramide Synthesis Ameliorates Glucocorticoid-, Saturated-Fat-, and Obesity-Induced Insulin Resistance. *Cell Metab*, 5(3), pp.167–179.

Holland, W.L. et al., 2011. Lipid-induced insulin resistance mediated by the proinflammatory receptor TLR4 requires saturated fatty acid-induced ceramide biosynthesis in mice. *J Clin Invest*, 121(5), pp.1858–1870.

Holland, W.L. et al., 2011. The Pleiotropic Actions of Adiponectin are Initiated via Receptor-Mediated Activation of Ceramidase Activity. *Nat Med*, 17(1), pp.55–63.

Holloszy, J.O., 1967. Biochemical Adaptations in Muscle. Effects of exercise on mitochondrial oxygen update and respiratory enzyme activity in skeletal muscle. *J Biol Chem*, 242(9), pp.2278–2282.

Holloszy, J.O. & Coyle, E.F., 1984. Adaptations of skeletal muscle to endurance exercise and their metabolic consequences. *J Appl Physiol*, 56, pp.831–838.

Holloszy, J.O. & Narahara, H.T., 1965. Studies of Tissue Permeability. *J Biol Chem*, 240(9), pp.3493–3500.

Holloway, G.P., Benton, C.R., et al., 2009. In obese rat muscle transport of palmitate is increased and is channeled to triacylglycerol storage despite an increase in mitochondrial palmitate oxidation. *Am J Physiol Endocrinol Metab*, 296(4), pp.738–747.

Holloway, G.P. et al., 2007. Skeletal muscle mitochondrial FAT/CD36 content and palmitate oxidation are not decreased in obese women. *Am J Physiol Endocrinol Metab*, 292(6), pp.E1782–E1789.

Holloway, G.P., Bonen, A. & Spriet, L.L., 2009. Regulation of skeletal muscle mitochondrial fatty acid metabolism in lean and obese individuals. *Am J Clin Nutr*, 89(Suppl.), p.455S–62S.

Holmes, A.G. et al., 2008. Prolonged interleukin-6 administration enhances glucose tolerance and increases skeletal muscle PPARα and UCP2 expression in rats. *J Endocrinol*, 198(2), pp.367–374.

Holmström, M.H. et al., 2013. Effect of leptin treatment on mitochondrial function in obese leptin-deficient ob/ob mice. *Metabolism*, 62, pp.1258–1267.

Holmström, M.H. et al., 2012. Tissue-specific control of mitochondrial respiration in obesity-related insulin resistance and diabetes. *Am J Physiol Endocrinol Metab*, 302(6), pp.E731–9.

Holst, J.J., 2006. Glucagon-like peptide-1: From extract to agent. The Claude Bernard Lecture, 2005. *Diabetologia*, 49(2), pp.253–260.

Holst, J.J. & Gromada, J., 2004. Role of incretin hormones in the regulation of insulin secretion in diabetic and nondiabetic humans. *Am J Physiol Endocrinol Metab*, 287(2), pp.E199–E206.

Holten, M.K. et al., 2004. Strength Training Increases Insulin-Mediated Glucose Uptake, GLUT4 Content, and Insulin Signaling in Skeletal Muscle in Patients With Type 2 Diabetes. *Diabetes*, 53(2), pp.294–305.

Home, P.D. & Pacini, G., 2008. Hepatic dysfunction and insulin insensitivity in type 2 diabetes mellitus: A critical target for insulin-sensitizing agents. *Diabetes Obes Metab*, 10(9), pp.699–718.

Hong, E.-G. et al., 2009. Interleukin-10 Prevents Diet-Induced Insulin Resistance by Attenuating Macrophage and Cytokine Response in Skeletal Muscle. *Diabetes*, 58, pp.2525–2535.

Hoppeler, H. et al., 1985. Endurance training in humans: aerobic capacity and structure of skeletal muscle. *J Appl Physiol*, 59(2), pp.320–7.

Horvath, T.L., Andrews, Z.B. & Diano, S., 2008. Fuel utilization by hypothalamic neurons: roles for ROS. *Trends Endocrin Met*, 20(2), pp.78–87.

Hotamisligil, G.S. et al., 1995. Increased adipose tissue expression of tumor necrosis factor-alpha in human obesity and insulin resistance. *J Clin Invest*, 95(5), pp.2409–2415.

Hotamisligil, G.S., 2006. Inflammation and metabolic disorders. *Nature*, 444, pp.860–867.

Hotamisligil, G.S. et al., 1996. IRS-1-mediated inhibition of insulin receptor tyrosine kinase activity in TNF-alpha- and obesity-induced insulin resistance. *Science*, 271(5249), pp.665–8.

Hotamisligil, G.S., 2005. Role of Endoplasmic Reticulum Stress and c-Jun NH2-Terminal Kinase Pathways in Inflammation and Origin of Obesity and Diabetes. *Diabetes*, 54(Suppl.2), pp.S73–S78.

Hotamisligil, G.S. & Erbay, E., 2008. Nutrient sensing and inflammation in metabolic diseases Gökhan. *Nat Rev Immunol*, 8(12), pp.923–34.

Hotamisligil, G.S., Shargill, N.S. & Spiegelman, B.M., 1993. Adipose expression of tumor necrosis factor-alpha: Direct role in obesity-linked insulin resistance. *Science*, 259(5091), pp.87–91.

Houstis, N., Rosen, E.D. & Lander, E.S., 2006. Reactive oxygen species have a causal role in multiple forms of insulin resistance. *Nature*, 440(7086), pp.944–948.

Houtkooper, R.H. et al., 2013. Mitonuclear protein imbalance as a conserved longevity mechanism. *Nature*, 497, pp.451–7.

Hsueh, W.A. & Law, R.E., 1999. Insulin signaling in the arterial wall. *Am J Cardiol*, 84, p.21J–24J.

Huang, C. et al., 2007. High expression rates of human islet amyloid polypeptide induce endoplasmic reticulum stress–mediated β-cell apoptosis, a characteristic of humans with type 2 but not type 1 diabetes. *Diabetes*, 56, pp.2016–2027.

Hundal, R.S. et al., 2002. Mechanism by which high-dose aspirin improves glucose metabolism in type 2 diabetes. *J Clin Invest*, 109(10), pp.1321–1326.

Ide, T. et al., 2001. Mitochondrial DNA damage and dysfunction associated with oxidative stress in failing hearts after myocardial infarction. *Circ Res*, 88(5), pp.529–535.

Ihara, Y. et al., 1999. Hyperglycemia Causes Oxidative Stress in Pancreatic beta-Cells of GK Rats, a Model of Type 2 Diabetes. *Diabetes*, 48(4), pp.927–932.

Ikemoto, S. et al., 1996. High-fat diet-induced hyperglycemia and obesity in mice: differential effects of dietary oils. *Metabolism*, 45(12), pp.1539–46.

Im, S.-H. & Rao, A., 2004. Activation and deactivation of gene expression by Ca2+/calcineurin-NFAT-mediated signaling. *Mol Cells*, 18(1), pp.1–9.

Imai, Y. et al., 2007. Insulin secretion is increased in pancreatic islets of neuropeptide Y-deficient mice. *Endocrinology*, 148(12), pp.5716–5723.

Inzucchi, S.E. et al., 2015. Management of hyperglycemia in type 2 diabetes, 2015: a patient-centered approach. Update to a position statement of the American Diabetes Association (ADA) and the European Association for the Study of Diabetes (EASD). *Diabetes Care*, 38, pp.140–149.

Inzucchi, S.E. et al., 2012. Management of hyperglycemia in type 2 diabetes: a patient-centered approach. Position statement of the American Diabetes Association (ADA) and the European Association for the Study of Diabetes (EASD). *Diabetes care*, 35(6), pp.1364–1379.

Iossa, S. et al., 2003. Effect of high-fat feeding on metabolic efficiency and mitochondrial oxidative capacity in adult rats. *Br J Nutr*, 90(5), pp.953–960.

Irving, B.A. et al., 2011. Nine days of intensive exercise training improves mitochondrial function but not insulin action in adult offspring of mothers with type 2 diabetes. *J Clin Endocrinol Metab*, 96(7), pp.E1137–E1141.

Ishihara, N. et al., 2006. Regulation of mitochondrial morphology through proteolytic cleavage of OPA1. *The EMBO Journal*, 25(13), pp.2966–2977.

Itani, S.I. et al., 2001. Increased protein kinase C theta in skeletal muscle of diabetic patients. *Metabolism*, 50(5), pp.553–557.

Itani, S.I. et al., 2000. Involvement of protein kinase C in human skeletal muscle insulin resistance and obesity. *Diabetes*, 49(8), pp.1353–1358.

Itani, S.I. et al., 2002. Lipid-induced insulin resistance in human muscle is associated with changes in diacylglycerol, protein kinase C, and IkappaB-alpha. *Diabetes*, 51(7), pp.2005–2011.

Jallut, D. et al., 1990. Impaired glucose tolerance and diabetes in obesity: A 6-year follow-up study of glucose metabolism. *Metabolism*, 39(10), pp.1068–1075.

James, W.P.T., 2008. The fundamental drivers of the obesity epidemic. *Obes Rev*, 9(Suppl.1), pp.6–13.

Janson, J. et al., 1999. The mechanism of islet amyloid polypeptide toxicity is membrane disruption by intermediate-sized toxic amyloid particles. *Diabetes*, 48(3), pp.491–498.

Jantsch, J. et al., 2008. Hypoxia and Hypoxia-Inducible Factor-1 Modulate Lipopolysaccharide-Induced Dendritic Cell Activation and Function. *J Immunol*, 180(7), pp.4697–4705.

Jheng, H.-F. et al., 2012. Mitochondrial Fission Contributes to Mitochondrial Dysfunction and Insulin Resistance in Skeletal Muscle. *Mol Cell Biol*, 32(2), pp.309–319.

Jiang, C. et al., 2011. Disruption of hypoxia-inducible factor 1 in adipocytes improves insulin sensitivity and decreases adiposity in high-fat diet-fed mice. *Diabetes*, 60(10), pp.2484–2495.

Jiang, L.Q. et al., 2013. Altered response of skeletal muscle to IL-6 in type 2 diabetic patients. *Diabetes*, 62(2), pp.355–361.

Johnson, A.M.F. & Olefsky, J.M., 2013. The origins and drivers of insulin resistance. *Cell*, 152, pp.673–684.

Johnson, D.T. et al., 2007. Tissue heterogeneity of the mammalian mitochondrial proteome. *Am J Physiol Endocrinol Metab*, 292, pp.C689–C697.

Johnson, K.H. et al., 1989. Islet amyloid, islet-amyloid polypeptide, and diabetes mellitus. *N Engl J Med*, 321(8), pp.513–8.

Jones, I.R. et al., 1989. The glucose dependent insulinotropic polypeptide response to oral glucose and mixed meals is increased in patients with Type 2 (non-insulin-dependent) diabetes mellitus. *Diabetologia*, 32, pp.668–677.

Joseph, J.W. et al., 2004. Free fatty acid-induced beta-cell defects are dependent on uncoupling protein 2 expression. *J Biol Chem*, 279(49), pp.51049–51056.

Joseph, J.W. et al., 2002. Uncoupling protein 2 knockout mice have enhanced insulin secretory capacity after a high-fat diet. *Diabetes*, 51(11), pp.3211–3219.

Kaaman, M. et al., 2007. Strong association between mitochondrial DNA copy number and lipogenesis in human white adipose tissue. *Diabetologia*, 50(12), pp.2526–2533.

Kabon, B. et al., 2004. Obesity decreases perioperative tissue oxygenation. *Anesthesiology*, 100(2), pp.274–80.

Kacerovsky-Bielesz, G. et al., 2009. Short-term exercise training does not stimulate skeletal muscle ATP synthesis in relatives of humans with type 2 diabetes. *Diabetes*, 58(6), pp.1333–1341.

Kadowaki, T. et al., 2006. Adiponectin and adiponectin receptors in insulin resistance, diabetes, and the metabolic syndrome. *J Clin Invest*, 116(7), pp.1784–1792.

Kajimoto, Y. & Kaneto, H., 2004. Role of Oxidative Stress in Pancreatic β-Cell Dysfunction. *Ann N Y Acad Sci*, 1011(1), pp.168–176.

Kamei, N. et al., 2006. Overexpression of monocyte chemoattractant protein-1 in adipose tissues causes macrophage recruitment and insulin resistance. *J Biol Chem*, 281(36), pp.26602–26614.

Kammoun, H.L. et al., 2009. GRP78 expression inhibits insulin and ER stress-induced SREBP-1c activation and reduces hepatic steatosis in mice. *J Clin Invest*, 119(5), pp.1201–1215.

Kanat, M. et al., 2011. Impaired early- but not late-phase insulin secretion in subjects with impaired fasting glucose. *Acta Diabetol*, 48, pp.209–217.

Kanda, H. et al., 2006. MCP-1 contributes to macrophage infiltration into adipose tissue, insulin resistance, and hepatic steatosis in obesity. *J Clin Invest*, 116(6), pp.1494–1505.

Kang, S., Kim, K.B. & Shin, K.O., 2013. Exercise training improves leptin sensitivity in peripheral tissue of obese rats. *Biochem Bioph Res Co*, 435, pp.454–9.

Kantartzis, K. et al., 2009. High cardiorespiratory fitness is an independent predictor of the reduction in liver fat during a lifestyle intervention in non-alcoholic fatty liver disease. *Gut*, 58(9), pp.1281–1288.

Karakelides, H. et al., 2010. Age, Obesity, and Sex Effects on Insulin Sensitivity and Skeletal Muscle Mitochondrial Function. *Diabetes*, 59, pp.89–97.

Karlsson, H.K.R. et al., 2006. Insulin signaling and glucose transport in skeletal muscle from first-degree relatives of type 2 diabetic patients. *Diabetes*, 55(5), pp.1283–1288.

Kashiwagi, A. et al., 1983. In vitro insulin resistance of human adipocytes isolated from subjects with noninsulin-dependent diabetes mellitus. *J Clin Invest*, 72, pp.1246–1254.

Kashyap, S. et al., 2003. A sustained increase in plasma free fatty acids impairs insulin secretion in nondiabetic subjects genetically predisposed to develop type 2 diabetes. *Diabetes*, 52(10), pp.2461–2474.

Kashyap, S.R. et al., 2004. Discordant effects of a chronic physiological increase in plasma FFA on insulin signaling in healthy subjects with or without a family history of type 2 diabetes. *Am J Physiol Endocrinol Metab*, 287(3), pp.E537–E546.

Kashyap, S.R. et al., 2005. Insulin resistance is associated with impaired nitric oxide synthase activity in skeletal muscle of type 2 diabetic subjects. *J Clin Endocrinol Metab*, 90(2), pp.1100–1105.

Katic, M. et al., 2007. Mitochondrial gene expression and increased oxidative metabolism: Role in increased lifespan of fat-specific insulin receptor knock-out mice. *Aging Cell*, 6, pp.827–839.

Kawakami, M. et al., 1987. Human recombinant TNF suppresses lipoprotein lipase activity and stimulates lipolysis in 3T3-L1 cells. *J Biochem*, 101(2), pp.331–338.

Kawazoe, B.Y. et al., 2001. Signal Transducer and Activator of Transcription (STAT)-induced STAT Inhibitor 1 (SSI-1)/Suppressor of Cytokine Signaling 1 (SOCS1) Inhibits Insulin Signal Transduction Pathway through Modulating Insulin Receptor Substrate 1 (IRS-1) Phosphorylation. *J Exp Med*, 193(2), pp.263–269.

Keller, M.P. & Attie, A.D., 2010. Physiological insights gained from gene expression analysis in obesity and diabetes. *Annu Rev Nutr*, 30, pp.341–64.

Keller, P. et al., 2011. A transcriptional map of the impact of endurance exercise training on skeletal muscle phenotype. *J Appl Physiol*, 110(1), pp.46–59.

Kelley, D.E. et al., 2002. Dysfunction of mitochondria in human skeletal muscle in type 2 diabetes. *Diabetes*, 51(10), pp.2944–50.

Kelley, D.E. et al., 1999. Skeletal muscle fatty acid metabolism in association with insulin resistance, obesity, and weight loss. *Am J Physiol*, 277, pp.E1130–41.

Kelley, D.E. & Mandarino, L.J., 2000. Fuel selection in human skeletal muscle in insulin resistance. A reexamination. *Diabetes*, 49(5), pp.677–683.

Kern, P.A. et al., 2001. Adipose tissue tumor necrosis factor and interleukin-6 expression in human obesity and insulin resistance. *Am J Physiol Endocrinol Metab*, 280, pp.745–751.

Kern, P.A. et al., 1995. The expression of tumor necrosis factor in human adipose tissue. Regulation

by obesity, weight loss, and relationship to lipoprotein lipase. *J Clin Invest*, 95(5), pp.2111–2119.

Kim, F. et al., 2008. Vascular inflammation, insulin resistance, and reduced nitric oxide production precede the onset of peripheral insulin resistance. *Arterioscler Thromb Vasc Biol*, 28(11), pp.1982–1988.

Kim, H.J. et al., 2004. Differential effects of interleukin-6 and-10 on skeletal muscle and liver insulin action in vivo. *Diabetes*, 53(4), pp.1060–1067.

Kim, J.-Y. et al., 2007. Obesity-associated improvements in metabolic profile through expansion of adipose tissue. *J Clin Invest*, 117(9), pp.2621–2637.

Kim, J.K., Gimeno, R.E., et al., 2004. Inactivation of fatty acid transport protein 1 prevents fat-induced insulin resistance in skeletal muscle. *J Clin Invest*, 113(5), pp.756–763.

Kim, J.K. et al., 2000. Mechanism of insulin resistance in A-ZIP/F-1 fatless mice. *J Biol Chem*, 275(12), pp.8456–8460.

Kim, J.K., Fillmore, J.J., et al., 2004. PKC-theta knockout mice are protected from fat-induced insulin resistance. *J Clin Invest*, 114(6), pp.823–827.

Kim, J.K. et al., 2001. Prevention of fat-induced insulin resistance by salicylate. *J Clin Invest*, 108(3), pp.437–446.

Kim, J.K. et al., 2001. Tissue-specific overexpression of lipoprotein lipase causes tissue-specific insulin resistance. *P Natl Acad Sci USA*, 98(13), pp.7522–7527.

King, D.E. et al., 2003. Inflammatory markers and exercise: Differences related to exercise type. *Med Sci Sport Exer*, 35(4), pp.575–581.

King, D.S. et al., 1990. Insulin secretory capacity in endurance-trained and untrained young men. *Am J Physiol*, 259, pp.E155–E161.

Király, M.A. et al., 2007. Attenuation of type 2 diabetes mellitus in the male Zucker diabetic fatty rat: the effects of stress and non-volitional exercise. *Metabolism*, 56(6), pp.732–744.

Király, M.A. et al., 2008. Swim training prevents hyperglycemia in ZDF rats : mechanisms involved in the partial maintenance of beta-cell function. *Am J Physiol Endocrinol Metab*, 294, pp.271–283.

Kirwan, J.P. et al., 1993. Endurance Exercise Training Reduces Glucose-Stimulated Insulin Levels in 60- to 70-Year-Old Men and Women. *J Gerontol*, 48(3), pp.M84–M90.

Kjems, L.L. et al., 2003. The Influence of GLP-1 on Glucose-Stimulated Insulin Secretion. Effects of Beta-Cell Sensitivity in Type 2 and Nondiabetic Subjects. *Diabetes*, 52, pp.380–386.

Knowler, W.C. et al., 2009. 10-year follow-up of diabetes incidence and weight loss in the Diabetes Prevention Program Outcomes Study. *Lancet*, 374, pp.1677–86.

Knowler, W.C. et al., 2002. Reduction in the incidence of type 2 diabetes with lifestyle intervention or metformin. *N Engl J Med*, 346(6), pp.393–403.

Koch, C. et al., 2010. Leptin rapidly improves glucose homeostasis in obese mice by increasing hypothalamic insulin sensitivity. *J Neurosci*, 30(48), pp.16180–16187.

Koch, L. et al., 2008. Central insulin action regulates peripheral glucose and fat metabolism in mice. *J Clin Invest*, 118(6), pp.2132–2147.

Koh, K.K. et al., 2012. Significant differential effects of omega-3 fatty acids and fenofibrate in patients with hypertriglyceridemia. *Atherosclerosis*, 220(2), pp.537–544.

Kohjima, M. et al., 2007. Re-evaluation of fatty acid metabolism-related gene expression in nonalcoholic fatty liver disease. *Int J Mol Med*, 20(3), pp.351–358.

Koivula, R.W. et al., 2014. Discovery of biomarkers for glycaemic deterioration before and after the onset of type 2 diabetes: rationale and design of the epidemiological studies within the IMI DIRECT Consortium. *Diabetologia*, 57(6), pp.1132–1142.

Koonen, D.P.Y. et al., 2007. Increased Hepatic CD36 Expression Contributes to Dyslipidemia Associated With Diet-Induced Obesity. *Diabetes*, 56, pp.2863–2871.

Kopecky, J. et al., 1995. Expression of the mitochondrial uncoupling protein gene from the aP2 gene promoter prevents genetic obesity. *J Clin Invest*, 96(6), pp.2914–23.

Koranyi, L.I. et al., 1991. Coordinate reduction of rat pancreatic islet glucokinase and proinsulin mRNA by exercise training. *Diabetes*, 40, pp.401–404.

Korshunov, S.S., Skulachev, V.P. & Starkov, A.A., 1997. High protonic potential actuates a mechanism of production of reactive oxygen species in mitochondria. *FEBS Lett*, 416(1), pp.15–18.

Kotsias, F. et al., 2013. Reactive Oxygen Species Production in the Phagosome: Impact on Antigen Presentation in Dendritic Cells. *Antioxid Redox Sign*, 18(6), pp.714–729.

Koves, T.R. et al., 2008. Mitochondrial overload and incomplete fatty acid oxidation contribute to skeletal muscle insulin resistance. *Cell Metab*, 7(1), pp.45–56.

Kratz, M. et al., 2014. Metabolic Dysfunction Drives a Mechanistically Distinct Proinflammatory Phenotype in Adipose Tissue Macrophages. *Cell Metab*, 20, pp.614–625.

Kraunsøe, R. et al., 2010. Mitochondrial respiration in subcutaneous and visceral adipose tissue from patients with morbid obesity. *J Physiol*, 588(12), pp.2023–2032.

Kraus, D. et al., 2014. Nicotinamide N-methyltransferase knockdown protects against diet-induced obesity. *Nature*, 508(7495), pp.258–262.

Krause, M. da S. et al., 2012. Physiological concentrations of interleukin-6 directly promote insulin secretion, signal transduction, nitric oxide release, and redox status in a clonal pancreatic beta-cell line and mouse islets. *J Endocrinol*, 214(3), pp.301–311.

Krauss, S. et al., 2003. Superoxide-mediated activation of uncoupling protein 2 causes pancreatic beta cell dysfunction. *J Clin Invest*, 112(12), pp.1831–1842.

Krempler, F. et al., 2002. A Functional Polymorphism in the Promoter of UCP2 Enhances Obesity Risk but Reduces Type 2 Diabetes Risk in Obese Middle-Aged Humans. *Diabetes*, 51(12), pp.3331–3335.

Krishnan, J. et al., 2012. Dietary obesity-associated Hif1α activation in adipocytes restricts fatty acid oxidation and energy expenditure via suppression of the Sirt2-NAD+ system. *Gene Dev*, 26(3), pp.259–270.

Kristiansen, O.P. & Mandrup-Poulsen, T., 2005. Interleukin-6 and Diabetes. The Good, the Bad, or the Indifferent? *Diabetes*, 54(Suppl.2), pp.114–124.

Krook, A. et al., 2000. Characterization of signal transduction and glucose transport in skeletal muscle from type 2 diabetic patients. *Diabetes*, 49(2), pp.284–292.

Krssak, M. et al., 2004. Alterations in Postprandial Hepatic Glycogen Metabolism in Type 2 Diabetes. *Diabetes*, 53(12), pp.3048–3056.

Krssak, M. et al., 2000. Intramuscular glycogen and intramyocellular lipid utilization during prolonged exercise and recovery in man: a C-13 and H-1 nuclear magnetic resonance spectroscopy study. *J Clin Endocrinol Metab*, 85(2), pp.748–754.

Krssak, M. et al., 1999. Intramyocellular lipid concentrations are correlated with insulin sensitivity in humans: a 1H NMR spectroscopy study. *Diabetologia*, 42(1), pp.113–116.

Kuo, S.-M. & Halpern, M.M., 2011. Lack of association between body mass index and plasma adiponectin levels in healthy adults. *Int J Obesity*, 35(12), pp.1487–1494.

Kurokawa, J. et al., 2011. Apoptosis inhibitor of macrophage (AIM) is required for obesity-associated recruitment of inflammatory macrophages into adipose tissue. *P Natl Acad Sci USA*, 108(29), pp.12072–7.

Kusminski, C.M. & Scherer, P.E., 2012. Mitochondrial Dysfunction in White Adipose Tissue. *Trends Endocrin Met*, 23(9), pp.435–443.

Kusminski, C.M. & Scherer, P.E., 2009. The road from discovery to clinic: adiponectin as a biomarker of metabolic status. *Clin Sci*, 86(6), pp.592–5.

Lage, K. et al., 2010. Dissecting spatio-temporal protein networks driving human heart development and related disorders. *Mol Syst Biol*, 6(381), pp.1–9.

Lai, H. et al., 2015. Association between the level of circulating adiponectin and prediabetes: A meta-analysis. *J Diabetes Invest*, 6(4), pp.416–429.

Lam, T.K. et al., 2003. Mechanisms of the free fatty acid-induced increase in hepatic glucose production. *Am J Physiol Endocrinol Metab*, 284(5), pp.E863–73.

Lam, T.K.T. et al., 2002. Free fatty acid-induced hepatic insulin resistance: a potential role for protein kinase C-delta. *Am J Physiol Endocrinol Metab*, 283, pp.E682–E691.

Lane, T. et al., 2013. TXNIP shuttling: missing link between oxidative stress and inflammasome activation. *Front Physiol*, 4, pp.1–3.

Langerhans, P., 1869. Beitrage zur mikroscopischen anatomie der bauchspeichel druse. Inaugural-Dissertation.

Lanza, I.R. et al., 2012. Chronic Caloric Restriction Preserves Mitochondrial Function in Senescence without Increasing Mitochondrial Biogenesis. *Cell Metab*, 16(6), pp.777–788.

Lapuente-Brun, E. et al., 2013. Supercomplex Assembly Determines Electron Flux in the Mitochondrial Electron Transport Chain. *Science*, 340, pp.1567–1570.

Lara-Castro, C. et al., 2006. Adiponectin Multimeric Complexes and the Metabolic Syndrome Trait Cluster. *Diabetes*, 55, pp.249–259.

Larsen, S. et al., 2009. Are substrate use during exercise and mitochondrial respiratory capacity decreased in arm and leg muscle in type 2 diabetes? *Diabetologia*, 52(7), pp.1400–1408.

Larsen, S. et al., 2012. Biomarkers of mitochondrial content in skeletal muscle of healthy young human subjects. *J Physiol*, 590(14), pp.3349–60.

Larsen, S. et al., 2011. Increased mitochondrial substrate sensitivity in skeletal muscle of patients with type 2 diabetes. *Diabetologia*, 54(6), pp.1427–1436.

Larson, D.E. et al., 1995. Energy metabolism in weight-stable and postobese individuals. *Am J Clin Nutr*, 62, pp.735–9.

Laurencikiene, J. et al., 2007. NF-kappaB is important for TNF-alpha-induced lipolysis in human adipocytes. *J Lipid Res*, 48(5), pp.1069–1077.

Laybutt, D.R. et al., 2002. Genetic regulation of metabolic pathways in beta-cells disrupted by hyperglycemia. *J Biol Chem*, 277(13), pp.10912–10921.

Laybutt, D.R. et al., 2002. Increased expression of antioxidant and antiapoptic genes in islets that may contribute to beta-cell survival during chronic hyperglycemia. *Diabetes*, 51, pp.413–423.

Laybutt, D.R. et al., 2002. Overexpression of c-Myc in Beta-Cells of Transgenic Mice Causes Proliferation and Apoptosis , Downregulation of Insulin Gene Expression, and Diabetes. *Diabetes*, 51(1), pp.1793–1804.

Laybutt, R. et al., 2001. B-Cell Adaptation To Hyperglycemia. *Diabetes*, 50(Suppl.1), pp.180–181.

Laye, M.J. et al., 2009. Changes in visceral adipose tissue mitochondrial content with type 2 diabetes and daily voluntary wheel running in OLETF rats. *J Physiol*, 587(14), pp.3729–3739.

Leahy, J.L. et al., 1986. Chronic hyperglycaemia is associated with impaired glucose influence on insulin secretion. A study in normal rats using chronic in vivo glucose infusions. *J Clin Invest*, 77, pp.908–915.

Leahy, J.L., Bonner-Weir, S. & Weir, G.C., 1988. Minimal chronic hyperglycemia is a critical determinant of impaired insulin secretion after an incomplete pancreatectomy. *J Clin Invest*, 81(5), pp.1407–1414.

Lebrun, P. & Van Obberghen, E., 2008. SOCS proteins causing trouble in insulin action. *Acta Physiol*, 192, pp.29–36.

Lee, A.-H. et al., 2011. Dual and opposing roles of the unfolded protein response regulated by IRE1alpha and XBP1 in proinsulin processing and insulin secretion. *P Natl Acad Sci USA*, 108(21), pp.8885–8890.

Lee, B.C. & Lee, J., 2014. Cellular and molecular players in adipose tissue inflammation in the development of obesity-induced insulin resistance. *Biochim Biophys Acta*, 1842(3), pp.446–462.

Lee, H.-Y. et al., 2010. Targeted expression of catalase to mitochondria prevents age-associated reductions in mitochondrial function and insulin resistance. *Cell Metab*, 12(6), pp.668–674.

Lee, H.Y. et al., 2011. Apolipoprotein CIII overexpressing mice are predisposed to diet-induced hepatic steatosis and hepatic insulin resistance. *Hepatology*, 54(5), pp.1650–1660.

Lee, Y.-H., Petkova, A.P. & Granneman, J.G., 2013. Identification of an adipogenic niche for adipose tissue remodeling and restoration. *Cell Metab*, 18(3), pp.355–67.

Lefort, N. et al., 2010. Increased Reactive Oxygen Species Production and Lower Abundance of Complex I Subunits and Carnitine Palmitoyltransferase 1B Protein Despite Normal Mitochondrial Respiration in Insulin-Resistant Human Skeletal Muscle. *Diabetes*, 59, pp.2444–2452.

Leibowitz, G. et al., 2001. Defective Glucose-Regulated Insulin Gene Expression Associated with PDX-1 Deficiencty in the Psammomys obesus Model of Type 2 Diabetes. *Diabetes*, 50(Suppl.1), pp.138–139.

Lenaers, E. et al., 2010. Adaptations in mitochondrial function parallel, but fail to rescue, the transition to severe hyperglycemia and hyperinsulinemia: a study in Zucker diabetic fatty rats. *Obesity*, 18(6), pp.1100–1107.

Letellier, T. et al., 1992. Mitochondrial myopathy studies on permeabilized muscle fibers. *Pediatr Res*, 32(1), pp.17–22.

Levin, B.E. & Dunn-Meynell, A.A., 2002. Reduced central leptin sensitivity in rats with diet-induced obesity. *Am J Physiol Regul Integr Comp Physiol*, 283(4), pp.R941–8.

Li, G. et al., 2008. The long-term effect of lifestyle interventions to prevent diabetes in the China Da Qing Diabetes Prevention Study: a 20-year follow-up study. *Lancet*, 371, pp.1783–1789.

Li, P. et al., 2010. Functional heterogeneity of CD11c-positive adipose tissue macrophages in diet-induced obese mice. *J Biol Chem*, 285(20), pp.15333–15345.

Li, X. et al., 2012. IL-35 is a novel responsive anti-inflammatory cytokine--a new system of categorizing anti-inflammatory cytokines. *PloS one*, 7(3), p.e33628.

Liesa, M., Palacín, M. & Zorzano, A., 2009. Mitochondrial dynamics in mammalian health and disease. *Physiol Rev*, 89(3), pp.799–845.

Lihn, A.S., Pedersen, S.B. & Richelsen, B., 2005. Adiponectin: action, regulation and association to insulin sensitivity. *Obes Rev*, 6(1), pp.13–21.

Lillioja, S. et al., 1988. Impaired glucose tolerance as a disorder of insulin action. Longitudinal and cross-sectional studies in Pima Indians. *N Engl J Med*, 318(19), pp.1217–25.

Lillioja, S. et al., 1993. Insulin resistance and insulin secretory dysfunction as precursors of non-insulin-dependent diabetes mellitus. *N Engl J Med*, 329(27), pp.1988–1992.

Lim, J.H. et al., 2009. Coupling mitochondrial dysfunction to endoplasmic reticulum stress response: A molecular mechanism leading to hepatic insulin resistance. *Cellular Signal*, 21(1), pp.169–177.

Lin, J.S. et al., 2014. Behavioral Counseling to Promote a Healthy Lifestyle in Persons With Cardiovascular Risk Factors: A Systematic Review for the U.S. Preventive Services Task Force. *Ann Intern Med*, 161(8), pp.568–579.

Lin, Y. et al., 2005. The hyperglycemia-induced inflammatory response in adipocytes: The role of reactive oxygen species. *J Biol Chem*, 280(6), pp.4617–4626.

Lin, Z. et al., 2013. Adiponectin mediates the metabolic effects of FGF21 on glucose homeostasis and insulin sensitivity in mice. *Cell Metab*, 17(5), pp.779–789.

Lindsay, R.S. et al., 2002. Adiponectin and development of type 2 diabetes in the Pima Indian population. *Lancet*, 360(9326), pp.57–58.

Lindström, J. et al., 2006. Sustained reduction in the incidence of type 2 diabetes by lifestyle intervention: followup of the Finnish Diabetes Prevention Study. *Lancet*, 368, pp.1673–79.

Lionetti, L. et al., 2014. High-lard and high-fish-oil diets differ in their effects on function and dynamic behaviour of rat hepatic mitochondria. *PLoS ONE*, 9(3), p.e92753.

Liu, L. et al., 2007. Upregulation of myocellular DGAT1 augments triglyceride synthesis in skeletal muscle and protects against fat-induced insulin resistance. *J Clin Invest*, 117(6), pp.1679–1689.

Loh, K. et al., 2009. Reactive Oxygen Species Enhance Insulin Sensitivity. *Cell Metab*, 10(4), pp.260–272.

Lorenzo, A. et al., 1994. Pancreatic islet cell toxicity of amylin associated with type-2 diabetes mellitus. *Nature*, 368, pp.756–760.

Love, M.I., Anders, S. & Huber, W., 2014. *Differential analysis of count data - the DESeq2 package*,

Lowell, B.B. & Shulman, G.I., 2005. Mitochondrial dysfunction and type 2 diabetes. *Science*, 307, pp.384–387.

Lu, R. et al., 2010. Mitochondrial development and the influence of its dysfunction during rat adipocyte differentiation. *Mol Biol Rep*, 37(5), pp.2173–2182.

Lukinius, A. et al., 1989. Co-localization of islet amyloid polypeptide and insulin in the B cell secretory granules of the human pancreatic islets. *Diabetologia*, 32(4), pp.240–244.

Lumeng, C.N., DeYoung, S.M., Bodzin, J.L., et al., 2007. Increased inflammatory properties of adipose tissue macrophages recruited during diet-induced obesity. *Diabetes*, 56(1), pp.16–23.

Lumeng, C.N., Bodzin, J.L. & Saltiel, A.R., 2007. Obesity induces a phenotypic switch in adipose tissue macrophage polarization. *J Clin Invest*, 117(1), pp.175–184.

Lumeng, C.N., DeYoung, S.M. & Saltiel, A.R., 2007. Macrophages block insulin action in adipocytes by altering expression of signaling and glucose transport proteins. *Am J Physiol Endocrinol Metab*, 292(1), pp.E166–E174.

Lumeng, C.N., Maillard, I. & Saltiel, A.R., 2009. T-ing up inflammation in fat. *Nat Med*, 15(8), pp.846–847.

Lund, S. et al., 1995. Contraction stimulates translocation of glucose transporter GLUT4 in skeletal muscle through a mechanism distinct from that of insulin. *P Natl Acad Sci USA*, 92, pp.5817–21.

Lupi, R. et al., 2002. Prolonged exposure to free fatty acids has cytostatic and pro-apoptotic effects on human pancreatic islets. Evidence that beta-cell death is caspase mediated, partially dependent on ceramide pathway, and Bcl-2 regulated. *Diabetes*, 51, pp.1437–1442.

Lupi, R. et al., 2004. Rosiglitazone prevents the impairment of human islet function induced by fatty acids: evidence for a role of PPARgamma2 in the modulation of insulin secretion. *Am J Physiol Endocrinol Metab*, 286(4), pp.E560–E567.

Lyssenko, V. et al., 2007. Mechanisms by which common variants in the TCF7L2 gene increase risk of type 2 diabetes. *J Clin Invest*, 117(8), pp.2155–2163.

Maassen, J.A. et al., 2004. Mitochondrial Diabetes: Molecular Mechanisms and Clinical Presentation. *Diabetes*, 53(Suppl.1), pp.S103–S109.

MacDonald, T.L. et al., 2013. IL-6 and epinephrine have divergent fiber type effects on intramuscular lipolysis. *J Appl Physiol*, 115(10), pp.1457–1463.

MacLaren, R. et al., 2008. Influence of obesity and insulin sensitivity on insulin signaling genes in human omental and subcutaneous adipose tissue. *J Lipid Res*, 49(2), pp.308–323.

Madiraju, A.K. et al., 2014. Metformin suppresses gluconeogenesis by inhibiting mitochondrial glycerophosphate dehydrogenase. *Nature*, 510(7506), pp.542–546.

Madsen, E.L. et al., 2008. Weight loss larger than 10% is needed for general improvement of levels

of circulating adiponectin and markers of inflammation in obese subjects: A 3-year weight loss study. *Eur J Endocrinol*, 158(2), pp.179–187.

Maechler, P. & Wollheim, C.B., 2001. Mitochondrial function in normal and diabetic beta-cells. *Nature*, 414(6865), pp.807–812.

Maedler, K. et al., 2002. Glucose-induced beta cell production of IL-1beta contributes to glucotoxicity in human pancreatic islets. *J Clin Invest*, 110, pp.851–860.

Magkos, F. et al., 2008. Improved insulin sensitivity after a single bout of exercise is curvilinearly related to exercise energy expenditure. *Clin Sci*, 114(1), pp.59–64.

Magnusson, I. et al., 1992. Increased rate of gluconeogenesis in type II diabetes mellitus. A 13C nuclear magnetic resonance study. *J Clin Invest*, 90, pp.1323–1327.

Mahajan, A. et al., 2014. Genome-wide trans-ancestry meta-analysis provides insight into the genetic architecture of type 2 diabetes susceptibility. *Nat Genet*, 46(3), pp.234–44.

Mahoney, D.J. et al., 2005. Analysis of global mRNA expression in human skeletal muscle during recovery from endurance exercise. *FASEB J*, 9(11), pp.1498–500.

Malin, S.K. et al., 2013. Pancreatic β-cell function increases in a linear dose-response manner following exercise training in adults with prediabetes. *Am J Physiol Endocrinol Metab*, 305, pp.E1248–54.

Mandarino, L.J. et al., 1987. Effects of insulin infusion on human skeletal muscle pyruvate dehydrogenase, phosphofructokinase, and glycogen synthase. Evidence for their role in oxidative and nonoxidative glucose metabolism. *J Clin Invest*, 80(3), pp.655–663.

Mantena, S.K. et al., 2009. High fat diet induces dysregulation of hepatic oxygen gradients and mitochondrial function in vivo. *Biochem J*, 417(1), pp.183–193.

Marino, J.S., Xu, Y. & Hill, J.W., 2011. Central insulin and leptin-mediated autonomic control of glucose homeostasis. *Trends Endocrin Met*, 22(7), pp.275–85.

Martínez de Morentin, P.B. et al., 2010. Hypothalamic lipotoxicity and the metabolic syndrome. *Biochim Biophys Acta*, 1801, pp.350–61.

Martinon, F., Burns, K. & Tschopp, J., 2002. The Inflammasome: A molecular platform triggering activation of inflammatory caspases and processing of proIL-beta. *Mol Cell*, 10(2), pp.417–426.

Martins, C., Robertson, M.D. & Morgan, L.M., 2008. Effects of exercise and restrained eating behaviour on appetite control. *P Nutr Soc*, 67(1), pp.28–41.

Mathers, C.D. & Loncar, D., 2006. Projections of global mortality and burden of disease from 2002 to 2030. *PLoS Med*, 3(11), p.e442.

Maton, A. et al., 1993. *Human Biology and Health*, Englewood Cliffs, New Jersey, USA: Prentice Hall.

Matsuda, M. et al., 1999. Altered hypothalamic function in response to glucose ingestion in obese humans. *Diabetes*, 48(9), pp.1801–1806.

Matsuda, M. et al., 2002. Glucagon dose-response curve for hepatic glucose production and glucose disposal in type 2 diabetic patients and normal individuals. *Metabolism*, 51(9), pp.1111–1119.

Matsusue, K. et al., 2003. Liver-specific disruption of PPARgamma in leptin-deficient mice improves fatty liver but aggravates diabetic phenotypes. *J Clin Invest*, 111(5), pp.737–747.

Matthews, V.B. et al., 2010. Interleukin-6-deficient mice develop hepatic inflammation and systemic insulin resistance. *Diabetologia*, 53(11), pp.2431–2441.

Mattusch, F. et al., 2000. Reduction of the plasma concentration of C-reactive protein following nine months of endurance training. *Int J Sports Med*, 21(1), pp.21–24.

McAinch, A.J. et al., 2003. Dietary regulation of fat oxidative gene expression in different skeletal muscle fiber types. *Obes Res*, 11(12), pp.1471–9.

McIntosh, C.H.S. et al., 2005. Dipeptidyl peptidase IV inhibitors: how do they work as new antidiabetic agents? *Regul Peptides*, 128(2), pp.159–165.

Meex, R.C.R. et al., 2010. Restoration of muscle mitochondrial function and metabolic flexibility in type 2 diabetes by exercise training is paralleled by increased myocellular fat storage and improved insulin sensitivity. *Diabetes*, 59, pp.572–579.

Meier, J.J. et al., 2001. Reduced insulinotropic effect of gastric inhibitory polypeptide in first-degree relatives of patients with type 2 diabetes. *Diabetes*, 50(11), pp.2497–2504.

Meier, J.J. & Nauck, M.A., 2006. Incretins and the development of type 2 diabetes. *Curr Diabetes Rep*, 6(3), pp.194–201.

Merkel, M. et al., 1998. Lipoprotein lipase expression exclusively in liver. A mouse model for metabolism in the neonatal period and during cachexia. *J Clin Invest*, 102, pp.893–901.

Mesarwi, O. et al., 2013. Sleep disorders and the development of insulin resistance and obesity. *Endocrin Metab Clin*, 42(3), pp.617–634.

Miele, L. et al., 2003. Hepatic Mitochondrial Beta-Oxidation in Patients With Nonalcoholic Steatohepatitis Assessed by 13C-Octanoate Breath Test. *Am J Gastroenterol*, 98(10), pp.2335–2336.

Mikines, K.J. et al., 1989. Effect of training on the dose-response relationship for insulin action in men. *J Appl Physiol*, 66(2), pp.695–703.

Miller, W.C., Bryce, G.R. & Conlee, R.K., 1984. Adaptations to a high-fat diet that increase exercise endurance in male rats. *J Appl Physiol Respir Environ Exerc Physiol*, 56(1), pp.78–83.

Mills, E. & O'Neill, L.A.J., 2014. Succinate: a metabolic signal in inflammation. *Trends Cell Biol*, 24(5), pp.313–320.

Mitchell, P., 1961. Coupling of phosphorylation to electron and hydrogen transfer by a chemi-osmotic type of mechanism. *Nature*, 191, pp.144–8.

Miyazaki, T. et al., 2009. The protective effect of taurine against hepatic damage in a model of liver disease and hepatic stellate cells. *Adv Exp Med Biol*, 643, pp.293–303.

Miyazaki, Y. et al., 2003. Rosiglitazone Improves Downstream Insulin Receptor Signaling in Type 2 Diabetic Patients. *Diabetes*, 52, pp.1943–1950.

Mogensen, M. et al., 2007. Mitochondrial respiration is decreased in skeletal muscle of patients with type 2 diabetes. *Diabetes*, 56, pp.1592–1599.

Mohlke, K.L. & Boehnke, M., 2015. Recent advances in understanding the genetic architecture of type 2 diabetes. *Hum Mol Genet*, 24(R1), pp.R85–92.

Moitra, J. et al., 1998. Life without white fat: A transgenic mouse. *Gene Dev*, 12(20), pp.3168–3181.

Molina, A.J.A. et al., 2009. Mitochondrial Networking Protects Beta Cells from Nutrient Induced

Apoptosis. *Diabetes*, 58, pp.2303–2315.

Montagnani, M. et al., 2001. Insulin-stimulated Activation of eNOS Is Independent of Ca2+ but Requires Phosphorylation by Akt at Ser1179. *J Biol Chem*, 276(32), pp.30392–30398.

Mootha, V.K., Bunkenborg, J., et al., 2003. Integrated analysis of protein composition, tissue diversity, and gene regulation in mouse mitochondria. *Cell*, 115(5), pp.629–40.

Mootha, V.K., Lindgren, C.M., et al., 2003. PGC-1alpha-responsive genes involved in oxidative phosphorylation are coordinately downregulated in human diabetes. *Nat Genet*, 34(3), pp.267–73.

Morgan, K., Obici, S. & Rossetti, L., 2004. Hypothalamic responses to long-chain fatty acids are nutritionally regulated. *J Biol Chem*, 279(30), pp.31139–31148.

Mori, M. a et al., 2010. A Systems Biology Approach Identifies Inflammatory Abnormalities Between Mouse Strains Prior to Development of Metabolic Disease. *Diabetes*, 59, pp.2960–2971.

Morino, K. et al., 2005. Reduced mitochondrial density and increased IRS-1 serine phosphorylation in muscle of insulin-resistant offspring of type 2 diabetic parents. *J Clin Invest*, 115(12), pp.3587–3593.

Morino, K. et al., 2012. Regulation of mitochondrial biogenesis by lipoprotein lipase in muscle of insulin-resistant offspring of parents with type 2 diabetes. *Diabetes*, 61(4), pp.877–887.

Morino, K., Petersen, K.F. & Shulman, G.I., 2006. Molecular mechanisms of insulin resistance in humans and their potential links with mitochondrial dysfunction. *Diabetes*, 55(Suppl.2), pp.S9–S15.

Morris, A.P. et al., 2012. Large-scale association analysis provides insights into the genetic architecture and pathophysiology of type 2 diabetes. *Nat Genet*, 44(9), pp.981–990.

Morton, G.J. et al., 2005. Leptin regulates insulin sensitivity via phosphatidylinositol-3-OH kinase signaling in mediobasal hypothalamic neurons. *Cell Metab*, 2(6), pp.411–420.

Mosser, R.E. et al., 2015. High Fat Diet-Induced Beta Cell Proliferation Occurs Prior to Insulin Resistance in C57Bl/6J Male Mice. *Am J Physiol Endocrinol Metab*, p.ajpendo.00460.2014.

Muller, D.C. et al., 1996. Insulin response during the oral glucose tolerance test: the role of age, sex, body fat and the pattern of fat distribution. *Aging (Milano)*, 8(1), pp.13–21.

Muniyappa, R. et al., 2008. Current approaches for assessing insulin sensitivity and resistance in vivo: advantages, limitations, and appropriate usage. *Am J Physiol Endocrinol Metab*, 294(1), pp.E15–E26.

Münzberg, H., Flier, J.S. & Bjørbæk, C., 2004. Region-specific leptin resistance within the hypothalamus of diet-induced obese mice. *Endocrinology*, 145(11), pp.4880–4889.

Muoio, D.M. & Koves, T.R., 2007. Lipid-induced metabolic dysfunction in skeletal muscle. *Novartis Found Symp*, 286, pp.24–38.

Murakami, K. et al., 1989. Impairment of glutathione metabolism in erythrocytes from patients with diabetes mellitus. *Metabolism*, 38(8), pp.753–8.

Murgia, M. et al., 2013. Controlling metabolism and cell death: at the heart of mitochondrial calcium signalling. *J Mol Cell Cardiol*, 18(9), pp.1199–1216.

Murphy, M.P., 2009. How mitochondria produce reactive oxygen species. *Biochem J*, 417(1), pp.1–

13.

Musi, N. & Goodyear, L.J., 2006. Insulin resistance and improvements in signal transduction. *Endocrine*, 29(1), pp.73–80.

Mustelin, L. et al., 2008. Acquired obesity and poor physical fitness impair expression of genes of mitochondrial oxidative phosphorylation in monozygotic twins discordant for obesity. *Am J Physiol Endocrinol Metab*, 295(1), pp.E148–E154.

Nabben, M. et al., 2008. The effect of UCP3 overexpression on mitochondrial ROS production in skeletal muscle of young versus aged mice. *FEBS Lett*, 582(30), pp.4147–4152.

Nair, K.S. et al., 2008. Asian indians have enhanced skeletal muscle mitochondrial capacity to produce ATP in association with severe insulin resistance. *Diabetes*, 57(5), pp.1166–1175.

Nakamura, T. et al., 2010. Double-Stranded RNA-Dependent Protein Kinase Links Pathogen Sensing with Stress and Metabolic Homeostasis. *Cell*, 140(3), pp.338–348.

Nakatani, T. et al., 2003. A low fish oil inhibits SREBP-1 proteolytic cascade, while a high-fish-oil feeding decreases SREBP-1 mRNA in mice liver: relationship to anti-obesity. *J Lipid Res*, 44(2), pp.369–379.

Nauck, M. et al., 1986. Reduced incretin effect in type 2 (non-insulin-dependent) diabetes. *Diabetologia*, 29(1), pp.46–52.

Nauck, M.A. et al., 1993. Preserved incretin activity of glucagon-like peptide 1 [7-36 amide] but not of synthetic human gastric inhibitory polypeptide in patients with type-2 diabetes mellitus. *J Clin Invest*, 91(1), pp.301–307.

Nedergaard, J. & Cannon, B., 2014. The Browning of White Adipose Tissue: Some Burning Issues. *Cell Metab*, 20(3), pp.396–407. Available at: http://dx.doi.org/10.1016/j.cmet.2014.07.005.

Neschen, S. et al., 2002. Contrasting effects of fish oil and safflower oil on hepatic peroxisomal and tissue lipid content. *Am J Physiol Endocrinol Metab*, 282(2), pp.E395–E401.

Neschen, S. et al., 2006. Fish Oil Regulates Adiponectin Secretion by a Peroxisome Proliferator-Activated Receptor-gamma-Dependent Mechanism in Mice. *Diabetes*, 55, pp.924–928.

Neschen, S. et al., 2007. n-3 Fatty Acids Preserve Insulin Sensitivity In Vivo in a Peroxisome Proliferator-Activated Receptor-alpha-Dependent Manner. *Diabetes*, 56, pp.1034–1041.

Nguyen, M.T.A. et al., 2007. A subpopulation of macrophages infiltrates hypertrophic adipose tissue and is activated by free fatty acids via toll-like receptors 2 and 4 and JNK-dependent pathways. *J Biol Chem*, 282(48), pp.35279–35292.

Nieto-Vazquez, I. et al., 2008. Dual role of interleukin-6 in regulating insulin sensitivity in murine skeletal muscle. *Diabetes*, 57(12), pp.3211–3221.

Nishimura, S. et al., 2009. CD8+ effector T cells contribute to macrophage recruitment and adipose tissue inflammation in obesity. *Nat Med*, 15(8), pp.914–920.

O'Neill, C.M. et al., 2013. Circulating levels of IL-1B+IL-6 cause ER stress and dysfunction in islets from prediabetic male mice. *Endocrinology*, 154(9), pp.3077–3088.

O'Rourke, R.W. et al., 2009. Depot-specific differences in inflammatory mediators and a role for NK cells and IFN-gamma in inflammation in human adipose tissue. *Int J Obesity*, 33(9), pp.978–990.

Obici, S., Feng, Z., et al., 2002. Central Administration of Oleic Acid Inhibits Glucose Production and Food Intake. *Diabetes*, 51(2), pp.271–275.

Obici, S. et al., 2001. Central melanocortin receptors regulate insulin action. *J Clin Invest*, 108(7), pp.1079–1085.

Obici, S., Feng, Z., et al., 2002. Decreasing hypothalamic insulin receptors causes hyperphagia and insulin resistance in rats. *Nat Neurosci*, 5(6), pp.566–572.

Obici, S., Zhang, B.B., et al., 2002. Hypothalamic insulin signaling is required for inhibition of glucose production. *Nat Med*, 8(12), pp.1376–1382.

Obstfeld, A.E. et al., 2010. C-C Chemokine Receptor 2 (CCR2) Regulates the Hepatic Recruitment of Myeloid Cells That Promote Obesity-Induced Hepatic Steatosis. *Diabetes*, 59, pp.916–925.

Odegaard, J.I. et al., 2008. Alternative M2 Activation of Kupffer Cells by PPARdelta Ameliorates Obesity-Induced Insulin Resistance. *Cell Metab*, 7(6), pp.496–507.

Oh, D.Y. et al., 2010. GPR120 is an Omega-3 Fatty Acid Receptor Mediating Potent Anti-Inflammatory and Insulin Sensitizing Effects. *Cell*, 142(5), pp.687–698.

Ohneda, M., Inman, L.R. & Unger, R.H., 1995. Caloric restriction in obese pre-diabetic rats prevents beta-cell depletion, loss of beta-cell GLUT 2 and glucose incompetence. *Diabetologia*, 38, pp.173–179.

Ojuka, E.O., Nolte, L.A. & Holloszy, J.O., 2000. Increased expression of GLUT-4 and hexokinase in rat epitrochlearis muscles exposed to AICAR in vitro. *J Appl Physiol*, 88(3), pp.1072–5.

Okada, T. et al., 2002. Distinct roles of activating transcription factor 6 (ATF6) and double-stranded RNA-activated protein kinase-like endoplasmic reticulum kinase (PERK) in transcription during the mammalian unfolded protein response. *Biochem J*, 366, pp.585–594.

Olefsky, J.M. & Glass, C.K., 2010. Macrophages, inflammation and insulin resistance. *Annu Rev Physiol*, 72, pp.219–46.

Oliver, E. et al., 2010. The role of inflammation and macrophage accumulation in the development of obesity-induced type 2 diabetes mellitus and the possible therapeutic effects of long-chain n-3 PUFA. *P Nutr Soc*, 69(2), pp.232–243.

Oral, E.A. et al., 2002. Leptin-replacement therapy for lipodystrophy. *N Engl J Med*, 346(8), pp.570–578.

Ost, A. et al., 2010. Attenuated mTOR signaling and enhanced autophagy in adipocytes from obese patients with type 2 diabetes. *Mol Med*, 16(7-8), pp.235–246.

Ostrowski, K. et al., 1999. Pro- and anti-inflammatory cytokine balance in strenuous exercise in humans. *J Physiol*, 515(1), pp.287–291.

Ouchi, N. et al., 2001. Adipocyte-Derived Plasma Protein, Adiponectin, Suppresses Lipid Accumulation and Class A Scavenger Receptor Expression in Human Monocyte-Derived Macrophages. *Circulation*, 103, pp.1057–1063.

Ouchi, N. et al., 2010. Sfrp5 Is an Anti-Inflammatory Adipokine That Modulates Metabolic Dysfunction in Obesity. *Science*, 329(5990), pp.454–457.

Ozcan, L. et al., 2009. Endoplasmic reticulum stress plays a central role in development of leptin resistance. *Cell Metab*, 9(1), pp.35–51.

Ozcan, U. et al., 2006. Chemical chaperones reduce ER stress and restore glucose homeostasis in a mouse model of type 2 diabetes. *Science*, 313(5790), pp.1137–1140.

Özcan, U. et al., 2004. Endoplasmatic Reticulum Stress Links Obesity, Insulin Action, and Type 2 Diabetes. *Science*, 306, pp.457–461.

Palacios, O.M. et al., 2009. Diet and exercise signals regulate SIRT3 and activate AMPK and PGC-1alpha in skeletal muscle. *Aging*, 1(9), pp.771–783.

Pan, H., Guo, J. & Su, Z., 2014. Advances in understanding the interrelations between leptin resistance and obesity. *Physiol Behav*, 130, pp.157–169.

Pan, X.-R. et al., 1997. Effects of Diet and Exercise in Preventing NIDDM in People With Impaired Glucose Tolerance. The Da Qing IGT and Diabetes Study. *Diabetes Care*, 20(4), pp.537–544.

Park, S. et al., 2007. Exercise improves glucose homeostasis that has been impaired by a high-fat diet by potentiating pancreatic beta-cell function and mass through IRS2 in diabetic rats. *J Appl Physiol*, 103, pp.1764–1771.

Pasarica, M. et al., 2009. Reduced Adipose Tissue Oxygenation in Human Obesity. Evidence for Rarefaction, Macrophage Chemotaxis, and Inflammation Without and Angiogenic Response. *Diabetes*, 58, pp.718–725.

Patanè, G. et al., 2002. Role of ATP production and uncoupling protein-2 in the insulin secretory defect induced by chronic exposure to high glucose or free fatty acids and effects of peroxisome proliferator-activated receptor-gamma inhibition. *Diabetes*, 51(9), pp.2749–2756.

Patti, M.E. et al., 2003. Coordinated reduction of genes of oxidative metabolism in humans with insulin resistance and diabetes: Potential role of PGC1 and NRF1. *P Natl Acad Sci USA*, 100(14), pp.8466–71.

Paula, F.M. et al., 2015. Exercise increases pancreatic beta-cell viability in a model of type 1 diabetes through IL-6 signaling. *FASEB J*, 29(5), pp.1805–1816.

Paulsen, G. et al., 2012. Leucocytes, cytokines and satellite cells: What role do they play in muscle damage and regeneration following eccentric exercise? *Exerc Immunol Rev*, 18, pp.42–97.

Paulweber, B. et al., 2010. A European Evidence-Based Guideline for the Prevention of Type 2 Diabetes. *Horm Metab Res*, 42(Suppl.1), pp.S3–36.

De Pauw, A. et al., 2012. Mild mitochondrial uncoupling does not affect mitochondrial biogenesis but downregulates pyruvate carboxylase in adipocytes: role for triglyceride content reduction. *Am J Physiol Endocrinol Metab*, 302(9), pp.E1123–E1141.

De Pauw, A. et al., 2009. Mitochondrial (dys)function in adipocyte (de)differentiation and systemic metabolic alterations. *Am J Pathol*, 175(3), pp.927–939.

Pedersen, B.K. et al., 2007. Role of myokines in exercise and metabolism. *J Appl Physiol*, 103(3), pp.1093–1098.

Pedersen, B.K. & Febbraio, M.A., 2008. Muscle as an Endocrine Organ : Focus on Muscle-Derived Interleukin-6. *Physiol Rev*, 88, pp.1379–1406.

Pedersen, B.K. & Febbraio, M.A., 2012. Muscles, exercise and obesity: skeletal muscle as a secretory organ. *Nat Rev Endocrinol*, 8(8), pp.457–465.

Pendergrass, M. et al., 2007. Muscle glucose transport and phosphorylation in type 2 diabetic, obese nondiabetic, and genetically predisposed individuals. *Am J Physiol Endocrinol Metab*, 292(1),

pp.E92–E100.

Perdomo, G. et al., 2004. Increased beta-oxidation in muscle cells enhances insulin-stimulated glucose metabolism and protects against fatty acid-induced insulin resistance despite intramyocellular lipid accumulation. *J Biol Chem*, 279(26), pp.27177–27186.

Pérez-Carreras, M. et al., 2003. Defective hepatic mitochondrial respiratory chain in patients with nonalcoholic steatohepatitis. *Hepatology*, 38(4), pp.999–1007.

Perrin, C., Knauf, C. & Burcelin, R., 2004. Intracerebroventricular infusion of glucose, insulin, and the adenosine monophosphate-activated kinase activator, 5-aminoimidazole-4-carboxamide-1-beta-D-ribofuranoside, controls muscle glycogen synthesis. *Endocrinology*, 145(9), pp.4025–4033.

Perrini, S. et al., 2004. Exercise-Induced Protein Kinase C Isoform-Specific Activation in Human Skeletal Muscle. *Diabetes*, 53, pp.21–24.

Pers, T.H. et al., 2011. Meta-analysis of heterogeneous data sources for genome-scale identification of risk genes in complex phenotypes. *Genet Epidemiol*, 35(5), pp.318–32.

Perseghin, G. et al., 1996. Increased glucose transport-phosphorylation and muscle glycogen synthesis after exercise training in insulin-resistant subjects. *N Engl J Med*, 335(18), pp.1357–1362.

Perseghin, G. et al., 1999. Intramyocellular triglyceride content is a determinant of in vivo insulin resistance in humans: a 1H-13C nuclear magnetic resonance spectroscopy assessment in offspring of type 2 diabetic parents. *Diabetes*, 48(8), pp.1600–6.

Pesta, D. & Gnaiger, E., 2012. High-Resolution Respirometry: OXPHOS Protocols for Human Cells and Permeabilized Fibers from Small Biopsies of Human Muscle. Mitochondrial Bioenergetics: Methods and Protocols. In C. M. Palmeira & A. J. Moreno, eds. *Methods Mol Biol*. Methods in Molecular Biology. Totowa, NJ: Humana Press.

Petersen, A.M.W. & Pedersen, B.K., 2005. The anti-inflammatory effect of exercise. *J Appl Physiol*, 98(4), pp.1154–1162.

Petersen, K.F. et al., 2010. Apolipoprotein C3 gene variants in nonalcoholic fatty liver disease. *N Engl J Med*, 362, pp.1082–9.

Petersen, K.F. et al., 2004. Impaired mitochondrial activity in the insulin-resistant offspring of patients with type 2 diabetes. *N Engl J Med*, 350, pp.664–71.

Petersen, K.F. et al., 2006. Increased prevalence of insulin resistance and nonalcoholic fatty liver disease in Asian-Indian men. *P Natl Acad Sci USA*, 103(48), pp.18273–18277.

Petersen, K.F. et al., 2002. Leptin reverses insulin resistance and hepatic steatosis in patients with severe lipodystrophy. *J Clin Invest*, 109(10), pp.1345–1350.

Petersen, K.F. et al., 2003. Mitochondrial Dysfunction in the Elderly: Possible Role in Insulin Resistance. *Science*, 300(5622), pp.1140–1142.

Petersen, K.F., Dufour, S., Befroy, D., et al., 2005. Reversal of Nonalcoholic Hepatic Steatosis, Hepatic Insulin Resistance, and Hyperglycemia by Moderate Weight Reduction in Patients With Type 2 Diabetes. *Diabetes*, 54(3), pp.603–608.

Petersen, K.F. et al., 2007. The role of skeletal muscle insulin resistance in the pathogenesis of the metabolic syndrome. *P Natl Acad Sci USA*, 104(31), pp.12587–12594.

Petersen, K.F., Dufour, S. & Shulman, G.I., 2005. Decreased insulin-stimulated ATP synthesis and phosphate transport in muscle of insulin-resistant offspring of type 2 diabetic parents. *PLoS Med*, 2(9), pp.0879–0884.

Pfluger, P.T. et al., 2008. Simultaneous deletion of ghrelin and its receptor increases motor activity and energy expenditure. *Am J Physiol Gastrointest Liver Physiol*, 294(3), pp.G610–8.

Phielix, E. et al., 2010. Exercise training increases mitochondrial content and ex vivo mitochondrial function similarly in patients with type 2 diabetes and in control individuals. *Diabetologia*, 53(8), pp.1714–1721.

Phielix, E. et al., 2008. Lower intrinsic ADP stimulated mitochondrial respirationin underlies in vivo mitochondrial dysfunction in muscle of male type 2 diabetic patients. *Diabetes*, 57, pp.2943–2949.

Phielix, E. et al., 2014. Reduction of non-esterified fatty acids improves insulin sensitivity and lowers oxidative stress, but fails to restore oxidative capacity in type 2 diabetes: a randomised clinical trial. *Diabetologia*, 57(3), pp.572–81.

Pi-Sunyer, X., 2014. The Look AHEAD Trial: A Review and Discussion of Its Outcomes. *Curr Nutr Rep*, 3(4), pp.387–391.

Pihlajamäki, J. et al., 2009. Thyroid hormone-related regulation of gene expression in human fatty liver. *J Clin Endocrinol Metab*, 94(9), pp.3521–3529.

Plum, L., Belgardt, B.F. & Brüning, J.C., 2006. Central insulin action in energy and glucose homeostasis. *J Clin Invest*, 116(7), pp.1761–1766.

Plum, L., Schubert, M. & Brüning, J.C., 2005. The role of insulin receptor signaling in the brain. *Trends Endocrin Met*, 16(2), pp.59–65.

Pocai, A. et al., 2006. Restoration of hypothalamic lipid sensing normalizes energy and glucose homeostasis in overfed rats. *J Clin Invest*, 116(4), pp.1081–1091.

Poitout, V., 2004. Beta-cell lipotoxicity: Burning fat into heat? *Endocrinology*, 145(8), pp.3563–3565.

Poitout, V. & Robertson, R.P., 2002. Minireview: Secondary beta-cell failure in type 2 diabetes--a convergence of glucotoxicity and lipotoxicity. *Endocrinology*, 143(2), pp.339–342.

Pold, R. et al., 2005. Long-term AICAR administration and exercise prevents diabetes in ZDF rats. *Diabetes*, 54(4), pp.928–934.

Popp-Snijders, C. et al., 1987. Dietary supplementation of omega-3 polyunsaturated fatty acids improves insulin sensitivity in non-insulin-dependent diabetes. *Diabetes Res*, 4(3), pp.141–7.

Porte, D., 2001. Clinical importance of insulin secretion and its interaction with insulin resistance in the treatment of type 2 diabetes mellitus and its complications. *Diabetes Metab Res*, 17(3), pp.181–8.

Porte Jr, D., 2006. Central regulation of energy homeostasis: The key role of insulin. *Diabetes*, 55(Suppl.2), pp.S155–S160.

Pospisilik, J.A. et al., 2007. Targeted Deletion of AIF Decreases Mitochondrial Oxidative Phosphorylation and Protects from Obesity and Diabetes. *Cell*, 131(3), pp.476–491.

Powelka, A.M. et al., 2006. Suppression of oxidative metabolism and mitochondrial biogenesis by the transcriptional corepressor RIP140 in mouse adipocytes. *J Clin Invest*, 116(1), pp.125–

136.

Pradhan, A.D. et al., 2001. C-reactive protein, interleukin 6, and risk of developing type 2 diabetes mellitus. *JAMA*, 286(3), pp.327–334.

Pratipanawatr, W. et al., 2001. Skeletal muscle insulin resistance in normoglycemic subjects with a strong family history of type 2 diabetes is associated with decreased insulin-stimulated insulin receptor substrate-1 tyrosine phosphorylation. *Diabetes*, 50(11), pp.2572–2578.

Prentki, M., Joly, E. & El-Assaad, W., 2002. Malonyl-CoA Signaling, Lipid Partitioning, and Glucolipotoxicity. Role in Beta-Cell Adaptation and Failure in the Etiology of Diabetes. *Diabetes*, 51(Suppl.3), pp.S405–S413.

Previs, S.F. et al., 2000. Contrasting effects of IRS-1 versus IRS-2 gene disruption on carbohydrate and lipid metabolism in vivo. *J Biol Chem*, 275(50), pp.38990–38994.

Prikoszovich, T. et al., 2011. Body and liver fat mass rather than muscle mitochondrial function determine glucose metabolism in women with a history of gestational diabetes mellitus. *Diabetes Care*, 34(2), pp.430–436.

Qi, L. et al., 2009. Adipocyte CREB Promotes Insulin Resistance in Obesity. *Cell Metab*, 9(3), pp.277–286.

Quintens, R. et al., 2013. Mice Deficient in the Respiratory Chain Gene Cox6a2 Are Protected against High-Fat Diet-Induced Obesity and Insulin Resistance. *PLoS ONE*, 8(2), p.e56719.

Rabøl, R., Højberg, P.M. V, et al., 2009. Effect of hyperglycemia on mitochondrial respiration in type 2 diabetes. *J Clin Endocrinol Metab*, 94(4), pp.1372–1378.

Rabøl, R., Svendsen, P.F., et al., 2009. Reduced skeletal muscle mitochondrial respiration and improved glucose metabolism in nondiabetic obese women during a very low calorie dietary intervention leading to rapid weight loss. *Metabolism*, 58(8), pp.1145–1152.

Rabøl, R. et al., 2010. Regional anatomic differences in skeletal muscle mitochondrial respiration in type 2 diabetes and obesity. *J Clin Endocrinol Metab*, 95(2), pp.857–863.

Raffaella, C. et al., 2008. Alterations in hepatic mitochondrial compartment in a model of obesity and insulin resistance. *Obesity*, 16(5), pp.958–964.

Randle, P.J., 1998. Regulatory interactions between lipids and carbohydrates: The glucose fatty acid cycle after 35 years. *Diabetes Metab Rev*, 14, pp.263–283.

Randle, P.J. et al., 1963. The Glucose Fatty-Acid Cycle. Its Role in Insulin Sensitivity and the Metabolic Disturbances of Diabetes Mellitus. *Lancet*, p.7285.

Rangel-Huerta, O.D. et al., 2012. Omega-3 long-chain polyunsaturated fatty acids supplementation on inflammatory biomakers: a systematic review of randomised clinical trials. *Brit J Nutr*, 107(S2), pp.S159–S170.

Ranjit, S. et al., 2011. Regulation of fat specific protein 27 by isoproterenol and TNF-alpha to control lipolysis in murine adipocytes. *J Lipid Res*, 52(2), pp.221–236.

Rao, X. et al., 2013. Exercise protects against diet-induced insulin resistance through downregulation of protein kinase Cbeta in mice. *PLoS ONE*, 8(12), p.e81364.

Rasouli, N. & Kern, P.A., 2008. Adipocytokines and the metabolic complications of obesity. *J Clin Endocrinol Metab*, 93(11), pp.64–73.

Ratner, R.E. et al., 2008. Prevention of diabetes in women with a history of gestational diabetes: effects of metformin and lifestyle interventions. *J Clin Endocrinol Metab*, 93(12), pp.4774–4779.

Raveney, B.J.E. et al., 2010. TNFR1 signalling is a critical checkpoint for developing macrophages that control of T-cell proliferation. *Immunology*, 131(3), pp.340–9. Available at: http://www.pubmedcentral.nih.gov/articlerender.fcgi?artid=2996554&tool=pmcentrez&rendertype=abstract.

Reaven, G.M. et al., 1988. Measurement of plasma glucose, free fatty acid, lactate, and insulin for 24 h in patients with NIDDM. *Diabetes*, 37(8), pp.1020–4.

Reaven, G.M., Hollenbeck, C.B. & Chen, Y.D., 1989. Relationship between glucose tolerance, insulin secretion, and insulin action in non-obese individuals with varying degrees of glucose tolerance. *Diabetologia*, 32(1), pp.52–5.

Rehman, A. et al., 1999. Increased oxidative damage to all DNA bases in patients with type II diabetes mellitus. *FEBS Lett*, 448(1), pp.120–122.

Reinders, I. et al., 2012. Association of serum n-3 polyunsaturated fatty acids with C-reactive protein in men. *Eur J Clin Nutr*, 66(6), pp.736–741.

Ren, J.-M. et al., 1994. Exercise induces rapid increases in GLUT4 expression, glucose transport capacity, and insulin-stimulated glycogen storage in muscle. *J Biol Chem*, 269(20), pp.14396–401.

Rena, G., Pearson, E.R. & Sakamoto, K., 2013. Molecular mechanism of action of metformin: old or new insights? *Diabetologia*, 56(9), pp.1898–906.

Riccardi, G., Giacco, R. & Rivellese, A., 2004. Dietary fat, insulin sensitivity and the metabolic syndrome. *Clin Nutr*, 23(4), pp.447–56.

Richter, B. et al., 2007. Rosiglitazone for type 2 diabetes mellitus. *Cochrane Db Syst Rev*, (3), p.CD006063.

Richter, E.A., Garetto, L.P. & Goodman, M.N., 1982. Muscle Glucose Metabolism following Exercise in the Rat. Increased sensitivity to insulin. *J Clin Invest*, 69, pp.785–793.

Rieusset, J., 2011. Mitochondria and endoplasmic reticulum: Mitochondria-endoplasmic reticulum interplay in type 2 diabetes pathophysiology. *Int J Biochem Cell B*, 43(9), pp.1257–1262.

Rimessi, A. et al., 2008. The versatility of mitochondrial calcium signals: from stimulation of cell metabolism to induction of cell death. *Biochim Biophys Acta*, 1777(7-8), pp.808–816.

Ristow, M. et al., 2009. Antioxidants prevent health-promoting effects of physical exercise in humans. *P Natl Acad Sci USA*, 106(21), pp.8665–8670.

Ritov, V.B. et al., 2010. Deficiency of electron transport chain in human skeletal muscle mitochondria in type 2 diabetes mellitus and obesity. *Am J Physiol Endocrinol Metab*, 298(1), pp.E49–E58.

Ritov, V.B. et al., 2005. Deficiency of subsarcolemmal mitochondria in obesity and type 2 diabetes. *Diabetes*, 54(1), pp.8–14.

Ritzel, R.A. et al., 2007. Human islet amyloid polypeptide oligomers disrupt cell coupling, induce apoptosis, and impair insulin secretion in isolated human islets. *Diabetes*, 56(1), pp.65–71.

Roat, R. et al., 2014. Alterations of pancreatic islet structure, metabolism and gene expression in

diet-induced obese C57BL/6J mice. *PLoS ONE*, 9(2), p.e86815.

Robertson, R.P. & Harmon, J.S., 2007. Pancreatic islet beta-cell and oxidative stress: The importance of glutathione peoxidase. *FEBS Lett*, pp.3743–3748.

Roden, M. et al., 1996. Mechanism of Free Fatty Acid – induced Insulin Resistance in Humans. *J Clin Invest*, 97(12), pp.2859–2865.

Roden, M., 2005. Muscle triglycerides and mitochondrial function: possible mechanisms for the development of type 2 diabetes. *Int J Obesity*, 29(Suppl.2), pp.S111–5.

Rogers, M.A. et al., 1988. Improvements in glucose tolerance after 1 week of exercise in patients with mild NIDDM. *Diabetes Care*, 11(8), pp.613–618.

Ron, D. & Walter, P., 2007. Signal integration in the endoplasmic reticulum unfolded protein response. *Nat Rev Mol Cell Bio*, 8(7), pp.519–529.

Rong, J.X. et al., 2007. Adipose Mitochondrial Biogenesis Is Suppressed in db/db and High-Fat Diet-Fed Mice and Improved by Rosiglitazone. *Diabetes*, 56, pp.1751–1760.

Rönn, T. et al., 2014. Extensive changes in the transcriptional profile of human adipose tissue including genes involved in oxidative phosphorylation after a 6-month exercise intervention. *Acta Physiol*, 211(1), pp.188–200.

Rosen, E.D. & MacDougald, O.A., 2006. Adipocyte differentiation from the inside out. *Nat Rev Mol Cell Bio*, 7(12), pp.885–896.

Rosenkilde, M. et al., 2012. Body fat loss and compensatory mechanisms in response to different doses of aerobic exercise--a randomized controlled trial in overweight sedentary males. *Am J Physiol Regul Integr Comp Physiol*, 303(6), pp.R571–9.

Rosenthal, M. et al., 1982. Effect of age on glucose tolerance, insulin secretion, and in vivo insulin action. *J Am Geriatr Soc*, 30(9), pp.562–7.

Rossetti, L. et al., 1987. Effect of chronic hyperglycemia on in vivo insulin secretion in partially pancreatectomized rats. *J Clin Invest*, 80(4), pp.1037–1044.

Rossetti, L., Giaccari, A. & DeFronzo, R.A., 1990. Glucose toxicity. *Diabetes Care*, 13(6), pp.610–630.

Rothman, D.L. et al., 1995. Decreased muscle glucose transport/phosphorylation is an early defect in the pathogenesis of non-insulin-dependent diabetes mellitus. *P Natl Acad Sci USA*, 92(4), pp.983–987.

Rothman, D.L., Shulman, R.G. & Shulman, G.I., 1992. 31P Nuclear Magnetic Resonance Measurements of Muscle Glucose-6-Phosphate. Evidence for Reduced Insulin-dependent Muscle Glucose Transport or Phosphorylation Activity in Non-Insulin-dependent Diabetes Mellitus. *J Clin Invest*, 89, pp.1069–1075.

Rutkowski, J.M., Davis, K.E. & Scherer, P.E., 2009. Mechanisms of obesity and related pathologies: The macro- and microcirculation of adipose tissue. *FEBS J*, 276, pp.5738–5746.

Rutter, M.K. et al., 2005. Insulin Resistance, the Metabolic Syndrome, and Incident Cardiovascular Events in the Framingham Offspring Study. *Diabetes*, 54(11), pp.3252–3257.

Saad, M.F. et al., 1989. Sequential Changes in Serum Insulin Concentration During Development of Non-Insulin-Dependent Diabetes. *Lancet*, pp.1356–1359.

Sabio, G. et al., 2008. A Stress Signaling Pathway in Adipose Tissue Regulates Hepatic Insulin

Resistance. *Science*, 322(5907), pp.1539–1543.

Sabio, G. et al., 2009. Prevention of Steatosis by Hepatic JNK1. *Cell Metab*, 10(6), pp.491–498.

Sabio, G. et al., 2010. Role of muscle c-Jun NH2-terminal kinase 1 in obesity-induced insulin resistance. *Mol Cell Biol*, 30(1), pp.106–115.

Sadagurski, M. et al., 2010. Human IL6 enhances leptin action in mice. *Diabetologia*, 53(3), pp.525–535.

Saghizadeh, M. et al., 1996. The expression of TNFalpha by human muscle. Relationship to insulin resistance. *J Clin Invest*, 97(4), pp.1111–1116.

Sakuraba, H. et al., 2002. Reduced beta-cell mass and expression of oxidative stress-related DNA damage in the islet of Japanese Type II diabetic patients. *Diabetologia*, 45(1), pp.85–96.

Saltiel, A.R. & Kahn, C.R., 2001. Insulin signalling and the regulation of glucose and lipid metabolism. *Nature*, 414, pp.799–806.

Samuel, V.T., Petersen, K.F. & Shulman, G.I., 2010. Lipid-induced insulin resistance: unravelling the mechanism. *Lancet*, 375(9733), pp.2267–2277.

Samuel, V.T. & Shulman, G.I., 2012. Mechanisms for insulin resistance: common threads and missing links. *Cell*, 148(5), pp.852–71.

Sansbury, B.E. et al., 2012. Overexpression of endothelial nitric oxide synthase prevents diet-induced obesity and regulates adipocyte phenotype. *Circ Res*, 111(9), pp.1176–1189.

Sanyal, A.J. et al., 2001. Nonalcoholic steatohepatitis: association of insulin resistance and mitochondrial abnormalities. *Gastroenterology*, 120(5), pp.1183–1192.

Sarruf, D.A. et al., 2009. Expression of peroxisome proliferator-activated receptor-γ in key neuronal subsets regulating glucose metabolism and energy homeostasis. *Endocrinology*, 150(2), pp.707–712.

Sasahara, M. et al., 2004. Uncoupling protein 2 promoter polymorphism-866G/A affects its expression in beta-cells and modulates clinical profiles of Japanese type 2 diabetic patients. *Diabetes*, 53(2), pp.482–485.

Savage, D.B., Petersen, K.F. & Shulman, G.I., 2005. Mechanisms of insulin resistance in humans and possible links with inflammation. *Hypertension*, 45(5), pp.828–833.

Scarpulla, R.C., 2006. Nuclear control of respiratory gene expression in mammalian cells. *J Cell Biochem*, 97(4), pp.673–683.

Schenk, S., Saberi, M. & Olefsky, J.M., 2008. Insulin sensitivity: Modulation by nutrients and inflammation. *J Clin Invest*, 118(9), pp.2992–3002.

Scherer, P.E. et al., 1995. A novel serum protein similar to C1q, produced exclusively in adipocytes. *J Biol Chem*, 270(45), pp.26746–26749.

Scherer, P.E., 2006. Adipose tissue: From lipid storage compartment to endocrine organ. *Diabetes*, 55(6), pp.1537–1545.

Schiaffino, S. & Reggiani, C., 2011. Fiber types in mammalian skeletal muscles. *Physiol Rev*, 91(4), pp.1447–531.

Schinner, S. et al., 2005. Molecular mechanisms of insulin resistance. *Diabetic Med*, 22(6), pp.674–682.

Schmid, A.I. et al., 2011. Liver ATP synthesis is lower and relates to insulin sensitivity in patients with type 2 diabetes. *Diabetes Care*, 34(2), pp.448–453.

Schmitz-Peiffer, C. et al., 1997. Alterations in the expression and cellular localization of protein kinase C isozymes epsilon and theta are associated with insulin resistance in skeletal muscle of the high-fat-fed rat. *Diabetes*, 46(2), pp.169–78.

Schneeberger, M. et al., 2013. Mitofusin 2 in POMC Neurons Connects ER Stress with Leptin Resistance and Energy Imbalance. *Cell*.

Schneeberger, M. et al., 2015. Reduced alpha-MSH Underlies Hypothalamic ER-Stress- Induced Hepatic Gluconeogenesis. *Cell Reports*, 12, pp.361–370.

Schottelius, A.J.G. et al., 1999. Interleukin-10 signaling blocks inhibitor of kappaB kinase activity and nuclear factor kappaB DNA binding. *J Biol Chem*, 274(45), pp.31868–31874.

Schrauwen-Hinderling, V.B. et al., 2007. Impaired in vivo mitochondrial function but similar intramyocellular lipid content in patients with type 2 diabetes mellitus and BMI-matched control subjects. *Diabetologia*, 50(1), pp.113–20.

Schulze-Osthoff, K. et al., 1992. Cytotoxic activity of tumor necrosis factor is mediated by early damage of mitochondrial functions. Evidence for the involvement of mitochondrial radical generation. *J Biol Chem*, 267(8), pp.5317–5323.

Schwartz, M.W. et al., 2000. Central nervous system control of food intake. *Nature*, 404, pp.661–671.

Seale, P. et al., 2011. Prdm16 determines the thermogenic program of subcutaneous white adipose tissue in mice. *J Clin Invest*, 121(1), pp.96–105.

Sell, H., Habich, C. & Eckel, J., 2012. Adaptive immunity in obesity and insulin resistance. *Nat Rev Endocrinol*, 8(12), pp.709–716.

Sénéchal, M. et al., 2015. Fitness is a determinant of the metabolic response to endurance training in adolescents at risk of type 2 diabetes mellitus. *Obesity*, 23(4), pp.823–32.

Sesti, G. et al., 2003. A Common Polymorphism in the Promoter of UCP2 Contributes to the Variation in Insulin Secretion in Glucose-Tolerant Subjects. *Diabetes*, 52, pp.1280–1283.

Sha, H. et al., 2009. The IRE1alpha-XBP1 Pathway of the Unfolded Protein Response Is Required for Adipogenesis. *Cell Metab*, 9(6), pp.556–564.

Shi, X. et al., 2008. Paradoxical effect of mitochondrial respiratory chain impairment on insulin signaling and glucose transport in adipose cells. *J Biol Chem*, 283(45), pp.30658–67.

Shima, K. et al., 1997. Exercise training in Otsuka Long-Evans Tokushima Fatty rat, a model of spontaneous non-insulin-dependent diabetes mellitus: Effects on the B-cell mass, insulin content and fibrosis in the pancreas. *Diabetes Res Clin Pr*, 35, pp.11–19.

Shimada, K. et al., 2012. Oxidized Mitochondrial DNA Activates the NLRP3 Inflammasome during Apoptosis. *Immunity*, 36(3), pp.401–414.

Shimomura, I. et al., 1999. Leptin reverses insulin resistance and diabetes mellitus in mice with congenital lipodystrophy. *Nature*, 401(6748), pp.73–76.

Shirazi, R. et al., 2013. Glucagon-like peptide 1 receptor induced suppression of food intake, and body weight is mediated by central IL-1 and IL-6. *P Natl Acad Sci USA*, 110(40), pp.16199–204.

Shoelson, S.E., Herrero, L. & Naaz, A., 2007. Obesity, Inflammation, and Insulin Resistance. *Gastroenterology*, 132(6), pp.2169–2180.

Shulman, G.I., 2000. Cellular mechanisms of insulin resistance. *J Clin Invest*, 106(2), pp.171–176.

Shulman, G.I. et al., 1985. Mechanism of liver glycogen repletion in vivo by nuclear magnetic resonance spectroscopy. *J Clin Invest*, 76(3), pp.1229–1236.

Shulman, G.I. et al., 1990. Quantitation of Muscle Glycogen Synthesis in Normal Subjects and Subjects with Non-Insulin-Dependent Diabetes by 12C Nuclear Magnetic Ressonance Spectroscopy. *N Engl J Med*.

Simoneau, J.-A. et al., 1999. Markers of capacity to utilize fatty acids in human skeletal muscle: relation to insulin resistance and obesity and effects of weight loss. *FASEB J*, 13, pp.2051–2060.

Sjöström, L. et al., 2007. Effects of Bariatric Surgery on Mortality in Swedish Obese Subjects. *N Engl J Med*, 357(8), pp.741–752.

Skovbro, M. et al., 2008. Human skeletal muscle ceramide content is not a major factor in muscle insulin sensitivity. *Diabetologia*, 51(7), pp.1253–1260.

Sladek, R. et al., 2007. A genome-wide association study identifies novel risk loci for type 2 diabetes. *Nature*, 445(7130), pp.881–885.

Sleisenger, M.H. et al., 2009. *Sleisenger and Fordtran's gastrointestinal and liver disease: pathophysiology, diagnosis, management* 9th ed. M. Feldman, L. S. Friedman, & L. J. Brandt, eds., Philadelphia : Saunders/Elsevier, c2010.

Slentz, C.A., Tanner, C.J., et al., 2009. Effects of Exercise Training Intensity on Pancreatic Beta-Cell Function. *Diabetes Care*, 32(10), pp.1807–1811.

Slentz, C.A., Houmard, J.A. & Kraus, W.E., 2009. Exercise, abdominal obesity, skeletal muscle, and metabolic risk: evidence for a dose response. *Obesity*, 17(Suppl.3), pp.S27–S33.

Smerdu, V. & Soukup, T., 2008. Demonstration of myosin heavy chain isoforms in rat and humans: the specificity of seven available monoclonal antibodies used in immunohistochemical and immunoblotting methods. *Eur J Histochem*, 52(3), pp.179–190.

Snel, M. et al., 2012. Effects of adding exercise to a 16-week very low-calorie diet in obese, insulin-dependent type 2 diabetes mellitus patients. *J Clin Endocrinol Metab*, 97(7), pp.2512–2520.

Solinas, G. et al., 2007. JNK1 in Hematopoietically Derived Cells Contributes to Diet-Induced Inflammation and Insulin Resistance without Affecting Obesity. *Cell Metab*, 6(5), pp.386–397.

Sone, H. & Kagawa, Y., 2005. Pancreatic beta cell senescence contributes to the pathogenesis of type 2 diabetes in high-fat diet-induced diabetic mice. *Diabetologia*, 48(1), pp.58–67.

Song, Z. et al., 2007. OPA1 processing controls mitochondrial fusion and is regulated by mRNA splicing, membrane potential, and Yme1L. *Journal of Cell Biology*, 178(5), pp.749–755.

Sorisky, A., Molgat, A.S.D. & Gagnon, A., 2013. Macrophage-induced adipose tissue dysfunction and the preadipocyte: should I stay (and differentiate) or should I go? *Adv Nutr*, 4(1), pp.67–75.

De Souza, C.T. et al., 2005. Consumption of a fat-rich diet activates a proinflammatory response and induces insulin resistance in the hypothalamus. *Endocrinology*, 146(10), pp.4192–4199.

De Souza, C.T. et al., 2007. Inhibition of UCP2 expression reverses diet-induced diabetes mellitus by

effects on both insulin secretion and action. *FASEB J*, 21(4), pp.1153–1163.

Spencer, M. et al., 2013. Omega-3 fatty acids reduce adipose tissue macrophages in human subjects with insulin resistance. *Diabetes*, 62(5), pp.1709–1717.

Spiegelman, B.M., 2013. Banting Lecture 2012: Regulation of adipogenesis: toward new therapeutics for metabolic disease. *Diabetes*, 62(6), pp.1774–82.

Sreekumar, R. et al., 2002. Effects of caloric restriction on mitochondrial function and gene transcripts in rat muscle. *Am J Physiol Endocrinol Metab*, 283, pp.E38–E43.

Stallknecht, B. et al., 1991. Increased activities of mitochondrial enzymes in white adipose tissue in trained rats. *Am J Physiol Endocrinol Metab*, 261(3), pp.E410–414.

Stanford, K.I., Middelbeek, R.J.W., Townsend, K.L., et al., 2015. A Novel Role for Subcutaneous Adipose Tissue in Exercise-Induced Improvements in Glucose Homeostasis. *Diabetes*, 64(January), pp.2002–2014.

Stanford, K.I., Middelbeek, R.J.W. & Goodyear, L.J., 2015. Exercise Effects on White Adipose Tissue: Beiging and Metabolic Adaptations. *Diabetes*, 64, pp.2361–8.

Starkie, R. et al., 2003. Exercise and IL-6 infusion inhibit endotoxin-induced TNF-alpha production in humans. *FASEB J*, 17(8), pp.884–6.

Starkov, A.A., 2010. The Role of Mitochondria in Reactive Oxygen Species Metabolism and Signaling. *Ann N Y Acad Sci*, 351(2), pp.37–52.

Stefan, N. et al., 2010. Circulating Palmitoleate Strongly and Independently Predicts Insulin Sensitivity in Humans. *Diabetes Care*, 33(2), pp.405–407.

Stefan, N. et al., 2008. Identification and characterization of metabolically benign obesity in humans. *Arch Intern Med*, 168(15), pp.1609–1616.

Stefan, N. et al., 2002. Plasma Adiponectin Concentration is Associated With Skeletal Muscle Insulin Receptor Tyrosine Phosphorylation, and Low Plasma Concentration Precedes a Decrease in Whole-Body Insulin Sensitivity in Humans. *Diabetes*, 50, pp.1884–1888.

Steffen, B.T. et al., 2015. n-3 Fatty Acids Attenuate the Risk of Diabetes Associated With Elevated Serum Nonesterified Fatty Acids: The Multi-Ethnic Study of Atherosclerosis. *Diabetes Care*, 38, pp.575–580.

Stephens, J.M. & Pekala, P.H., 1991. Transcriptional repression of the GLUT4 and C/EBP genes in 3T3-L1 adipocytes by tumor necrosis factor-alpha. *J Biol Chem*, 266(32), pp.21839–21845.

Stienstra, R. et al., 2010. The inflammasome-mediated caspase-1 activation controls adipocyte differentiation and insulin sensitivity. *Cell Metab*, 12(6), pp.593–605.

Stoffers, D.A., Thomas, M.K. & Habener, J.F., 1997. Homeodomain Protein IDX-1. A Master Regulator of Pancreas Development and Insulin Gene Expression. *Trends Endocrin Met*, 8(4), pp.145–151.

Stone, D.B., Brown, J.D. & Steele, A.A., 1969. Effect of sodium salicylate on induced lipolysis in isolated fat cells of the rat. *Metabolism*, 18(7), pp.620–4.

Storlien, L., Oakes, N.D. & Kelley, D.E., 2004. Metabolic flexibility. *P Nutr Soc*, 63(2), pp.363–368.

Storlien, L.H. et al., 1991. Influence of dietary fat composition on development of insulin resistance in rats. Relationship to muscle triglyceride and omega-3 fatty acids in muscle phospholipid.

Diabetes, 40(2), pp.280–9.

Suematsu, N. et al., 2003. Oxidative stress mediates tumor necrosis factor-alpha-induced mitochondrial DNA damage and dysfunction in cardiac myocytes. *Circulation*, 107(10), pp.1418–1423.

Suga, T. et al., 2014. Combination of exercise training and diet restriction normalizes limited exercise capacity and impaired skeletal muscle function in diet-induced diabetic mice. *Endocrinology*, 155(1), pp.68–80.

Suganami, T., Tanaka, M. & Ogawa, Y., 2012. Adipose tissue inflammation and ectopic lipid accumulation. *Endocr J*, 59(10), pp.849–57.

Sugden, M.C., Zariwala, M.G. & Holness, M.J., 2009. PPARs and the orchestration of metabolic fuel selection. *Pharmacol Res*, 60, pp.141–150.

Sugii, S. et al., 2009. PPARgamma activation in adipocytes is sufficient for systemic insulin sensitization. *P Natl Acad Sci USA*, 106(52), pp.22504–22509.

Summers, L.K.M. et al., 2002. Substituting dietary saturated fat with polyunsaturated fat changes abdominal fat distribution and improves insulin sensitivity. *Diabetologia*, 45(3), pp.369–377.

Sun, K., Kusminski, C.M. & Scherer, P.E., 2011. Adipose tissue remodeling and obesity. *J Clin Invest*, 121(6), pp.2094–2101.

Sunny, N.E. et al., 2011. Excessive hepatic mitochondrial TCA cycle and gluconeogenesis in humans with nonalcoholic fatty liver disease. *Cell Metab*, 14(6), pp.804–810.

Surwit, R.S. et al., 1988. Diet-induced type II diabetes in C57BL/6J mice. *Diabetes*, 37(9), pp.1163–7.

Sutherland, L.N. et al., 2009. Exercise and adrenaline increase PGC-1alpha mRNA expression in rat adipose tissue. *J Physiol*, 587(Pt.7), pp.1607–1617.

Sutherland, L.N. et al., 2008. Time course of high-fat diet-induced reductions in adipose tissue mitochondrial proteins: potential mechanisms and the relationship to glucose intolerance. *Am J Physiol Endocrinol Metab*, 295(5), pp.E1076–E1083.

Szczepaniak, L.S. et al., 1999. Measurement of intracellular triglyceride stores by 1H spectroscopy: validation in vivo. *Am J Physiol*, 276, pp.E977–E989.

Szendroedi, J. et al., 2009. Abnormal hepatic energy homeostasis in type 2 diabetes. *Hepatology*, 50(4), pp.1079–1086.

Szendroedi, J. et al., 2007. Muscle mitochondrial ATP synthesis and glucose transport/phosphorylation in type 2 diabetes. *PLoS Med*, 4(5), pp.0858–0867.

Szendroedi, J., Phielix, E. & Roden, M., 2012. The role of mitochondria in insulin resistance and type 2 diabetes mellitus. *Nat Rev Endocrinol*, 8(2), pp.92–103.

Takamura, T. et al., 2008. Obesity upregulates genes involved in oxidative phosphorylation in livers of diabetic patients. *Obesity*, 16(12), pp.2601–2609.

Tanaka, Y. et al., 2002. A role for glutathione peroxidase in protecting pancreatic beta cells against oxidative stress in a model of glucose toxicity. *P Natl Acad Sci USA*, 99(19), pp.12363–12368.

Taniguchi, C.M., Emanuelli, B. & Kahn, C.R., 2006. Critical nodes in signalling pathways: insights into insulin action. *Nat Rev Mol Cell Bio*, 7(2), pp.85–96.

Tantiwong, P. et al., 2010. NF-kappaB activity in muscle from obese and type 2 diabetic subjects

under basal and exercise-stimulated conditions. *Am J Physiol Endocrinol Metab*, 299, pp.E794–E801.

Tattersall, R., 1998. Maturity-onset diabetes of the young: a clinical history. *Diabetic Med*, 15(1), pp.11–14.

Thiebaud, D. et al., 1982. The effect of graded doses of insulin on total glucose uptake, glucose oxidation, and glucose storage in man. *Diabetes*, 31(11), pp.957–63.

Thomas, C.E. et al., 2013. MetaRanker 2 . 0 : a web server for prioritization of genetic variation data. *Nucleic Acids Res*, 41, pp.104–108.

Thyfault, J.P. & Booth, F.W., 2011. Lack of regular physical exercise or too much inactivity. *Curr Opin Clin Nutr*, 14(4), pp.374–378.

Tiedge, M. et al., 1997. Relation between antioxidant enzyme gene expression and antioxidative defense status of insulin-producing cells. *Diabetes*, 46(11), pp.1733–42.

van Tienen, F.H.J. et al., 2012. Physical activity is the key determinant of skeletal muscle mitochondrial function in type 2 diabetes. *J Clin Endocrinol Metab*, 97(9), pp.3261–9.

Tilg, H. et al., 1994. Interleukin-6 (IL-6) as an anti-inflammatory cytokine: induction of circulating IL-1 receptor antagonist and soluble tumor necrosis factor receptor p55. *Blood*, 83(1), pp.113–118.

Tinahones, F.J. et al., 2012. Obesity-associated insulin resistance is correlated to adipose tissue vascular endothelial growth factors and metalloproteinase levels. *BMC Physiology*, 12, p.4.

Toft-Nielsen, M.-B. et al., 2001. Determinants of the Impaired Secretion of Glucagon- Like Peptide-1 in Type 2 Diabetic Patients. *J Clin Endocrinol Metab*, 86(8), pp.3717–3723.

Toledo, F.G.S. et al., 2007. Effects of physical activity and weight loss on skeletal muscle mitochondria and relationship with glucose control in type 2 diabetes. *Diabetes*, 56, pp.2142–2147.

Toledo, F.G.S. et al., 2008. Mitochondrial capacity in skeletal muscle is not stimulated by weight loss despite increases in insulin action and decreases in intramyocellular lipid content. *Diabetes*, 57(4), pp.987–994.

Tormos, K. V. et al., 2011. Mitochondrial complex III ROS regulate adipocyte differentiation. *Cell Metab*, 14(4), pp.537–544.

Tran, T.T. et al., 2008. Beneficial Effects of Subcutaneous Fat Transplantation on Metabolism. *Cell Metab*, 7(5), pp.410–420.

Trayhurn, P. & Wood, I.S., 2004. Adipokines: inflammation and the pleiotropic role of white adipose tissue. *Br J Nutr*, 92, pp.347–355.

Trevellin, E. et al., 2014. Exercise training induces mitochondrial biogenesis and glucose uptake in subcutaneous adipose tissue through eNOS-dependent mechanisms. *Diabetes*, 63(8), pp.2800–2811.

Tsuzuki, T. et al., 2015. Voluntary Exercise Can Ameliorate Insulin Resistance by Reducing iNOS-Mediated S-Nitrosylation of Akt in the Liver in Obese Rats. *PLoS ONE*, 10(7), p.e0132029.

Tuncman, G. et al., 2006. Functional in vivo interactions between JNK1 and JNK2 isoforms in obesity and insulin resistance. *P Natl Acad Sci USA*, 103(28), pp.10741–6.

Tuomilehto, J. et al., 2001. Prevention of Type 2 Diabetes Mellitus By Changes in Lifestyle Among Subjects With Impaired Glucose Tolerance. *N Engl J Med*, 344(18), pp.1343–1350.

Turner, N. et al., 2007. Excess lipid availability increases mitochondrial fatty acid oxidative capacity in muscle: Evidence against a role for reduced fatty acid oxidation in lipid-induced insulin resistance in rodents. *Diabetes*, 56(8), pp.2085–2092.

Twig, G., Elorza, A., et al., 2008. Fission and selective fusion govern mitochondrial segregation and elimination by autophagy. *EMBO J*, 27(2), pp.433–446.

Twig, G., Hyde, B. & Shirihai, O.S., 2008. Mitochondrial fusion, fission and autophagy as a quality control axis: The bioenergetic view. *Biochim Biophys Acta*, 1777(9), pp.1092–1097.

Ueda, S. et al., 2009. Changes in gut hormone levels and negative energy balance during aerobic exercise in obese young males. *J Endocrinol*, 201(1), pp.151–159.

Ueki, K., Kondo, T. & Kahn, C.R., 2004. Suppressor of cytokine signaling 1 (SOCS-1) and SOCS-3 cause insulin resistance through inhibition of tyrosine phosphorylation of insulin receptor substrate proteins by discrete mechanisms. *Mol Cell Biol*, 24(12), pp.5434–5446.

Ukkola, O. & Santaniemi, M., 2002. Adiponectin: A link between excess adiposity and associated comorbidities? *J Mol Med*, 80(11), pp.696–702.

Um, S.H. et al., 2004. Absence of S6K1 protects against age- and diet-induced obesity while enhancing insulin sensitivity. *Nature*, 431(7005), pp.200–205.

Unger, R.H., 1995. Lipotoxicity in the pathogenesis of obesity-dependent NIDDM. Genetic and clinical implications. *Diabetes*, 44(8), pp.863–70.

Unger, R.H. et al., 1970. Studies of pancreatic alpha cell function in normal and diabetic subjects. *J Clin Invest*, 49, pp.837–848.

Unger, R.H. & Zhou, Y.-T., 2001. Lipotoxicity of beta-cells in obesity and in other causes of fatty acid spillover. *Diabetes*, 50(Suppl.1), pp.S118–S121.

Unick, J.L. et al., 2013. The long-term effectiveness of a lifestyle intervention in severely obese individuals. *Am J Med*, 126, pp.236–42.

Urano, F. et al., 2000. Coupling of stress in the ER to activation of JNK protein kinases by transmembrane protein kinase IRE1. *Science*, 287(5453), pp.664–666.

Uysal, K.T. et al., 1997. Protection from obesity-induced insulin resistance in mice lacking TNF-alpha function. *Nature*, 389(6651), pp.610–614.

Valerio, A. et al., 2006. TNF-alpha downregulates eNOS expression and mitochondrial biogenesis in fat and muscle of obese rodents. *J Clin Invest*, 116(10), pp.2791–2798.

Vance, J.E., 2008. Phosphatidylserine and phosphatidylethanolamine in mammalian cells: two metabolically related aminophospholipids. *J Lipid Res*, 49(7), pp.1377–87.

Vandanmagsar, B. et al., 2011. The NALP3/NLRP3 Inflammasome Instigates Obesity-Induced Autoinflammation and Insulin Resistance. *Nat Med*, 17(2), pp.179–188.

Vargas, M.L. et al., 2011. Metabolic and endocrine effects of long-chain versus essential omega-3 polyunsaturated fatty acids in polycystic ovary syndrome. *Metabolism*, 60(12), pp.1711–1718.

Veksler, V.I. et al., 1987. Mitochondrial respiratory parameters in cardiac tissue: a novel method of assessment by using saponin-skinned fibers. *Biochim Biophys Acta*, 892(2), pp.191–6.

Vernochet, C. et al., 2012. Adipose-Specific Deletion of TFAM Increases Mitochondrial Oxidation and Protects Mice against Obesity and Insulin Resistance. *Cell Metab*, 16(6), pp.765–776.

Vijan, S., 2010. Type 2 diabetes. *Ann Intern Med*, 152(5), pp.ITC31–15.

Vinik, A. et al., 1996. Determinants of pancreatic islet cell mass: a balance between neogenesis and senescence/apoptosis. *Diabetes Rev*, 4, pp.235–263.

Vistisen, B. et al., 2008. Effect of gender on lipid-induced insulin resistance in obese subjects. *Eur J Endocrinol*, 158(1), pp.61–68.

Vogt, C. et al., 1998. Effects of insulin on subcellular localization of hexokinase II in human skeletal muscle in vivo. *J Clin Endocrinol Metab*, 83(1), pp.230–234.

Vondra, K. et al., 1977. Enzyme activities in quadriceps femoris muscle of obese diabetic male patients. *Diabetologia*, 13, pp.527–529.

Wadden, T.A. et al., 2014. Eight-year weight losses with an intensive lifestyle intervention: The look AHEAD study. *Obesity*, 22(1), pp.5–13.

Wadden, T.A. et al., 2011. Four-year weight losses in the Look AHEAD study: factors associated with long-term success. *Obesity*, 19(10), pp.1987–98.

Wadt, K.A.W. et al., 1998. Ciliary neurotrophic factor potentiates the beta-cell inhibitory effect of IL-1beta rat pancreatic islets associated with increased nitric oxide synthesis and increased expression of inducible nitric oxide synthase. *Diabetes*, 47(10), pp.1602–08.

Wainright, K.S. et al., 2015. Retention of sedentary obese visceral white adipose tissue phenotype with intermittent physical activity despite reduced adiposity. *Am J Physiol Regul Integr Comp Physiol*, p.ajpregu.00042.2015.

Wallberg-Henriksson, H. & Holloszy, J.O., 1985. Activation of glucose transport in diabetic muscle: responses to contraction and insulin. *Am J Physiol*, 249(3), pp.C233–7.

Wang, C.C.L., Goalstone, M.L. & Draznin, B., 2004. Molecular Mechanisms of Insulin Resistance That Impact Cardiovascular Biology. *Diabetes*, 53, pp.2735–2740.

Wang, F. et al., 2001. Islet Amyloid Develops Diffusely Throughout the Pancreas before Becoming Severe and Replacing Endocrine Cells. *Diabetes*, 50, pp.2514–2520.

Wang, H. et al., 2009. Skeletal muscle-specific deletion of lipoprotein lipase enhances insulin signaling in skeletal muscle but causes insulin resistance in liver and other tissues. *Diabetes*, 58(1), pp.116–124.

Wang, P. et al., 2008. The secretory function of adipocytes in the physiology of white adipose tissue. *J Cell Physiol*, 216, pp.3–13.

Wang, T. et al., 2010. Respiration in adipocytes is inhibited by reactive oxygen species. *Obesity*, 18(8), pp.1493–1502.

Wang, Y. et al., 2005. Comparison of abdominal adiposity and overall obesity in predicting risk of type 2 diabetes among men. *Am J Clin Nutr*, 81, pp.555–63.

Wang, Y. et al., 2007. Overexpression of angiopoietin-like protein 4 alters mitochondria activities and modulates methionine metabolic cycle in the liver tissues of db/db diabetic mice. *Mol Endocrinol*, 21(4), pp.972–986.

Watanabe, R.M. et al., 1999. Familiarity of quantitative metabolic traits in Finnish families with non-

insulindependent diabetes mellitus: Finland-United States Investigation of NIDDM Genes (FUSION) Study. *Hum Hered*, 49, pp.159–168.

Watt, M.J. et al., 2005. Hormone-sensitive lipase is reduced in the adipose tissue of patients with type 2 diabetes mellitus: Influence of IL-6 infusion. *Diabetologia*, 48, pp.105–112.

Weibel, E.R. et al., 1969. Correlated Morphometric and Biochemical Studies on the Liver Cell. *J Cell Biol*, 42(1), pp.68–91.

van de Weijer, T. et al., 2013. Relationships between Mitochondrial Function and Metabolic Flexibility in Type 2 Diabetes Mellitus. *PLoS ONE*, 8(2), p.e51648.

Weir, J.B. de V, 1949. New methods for calculating metabolic rate with special reference to protein metabolism. *J Physiol*, 109(5), pp.1–9.

Weisberg, S.P. et al., 2003. Obesity is associated with macrophage accumulation in adipose tissue. *J Clin Invest*, 112(12), pp.1796–1808.

Weiss, R., Dufour, S., Groszmann, A., et al., 2003. Low adiponectin levels in adolescent obesity: A marker of increased intramyocellular lipid accumulation. *J Clin Endocrinol Metab*, 88(5), pp.2014–2018.

Weiss, R., Dufour, S., Taksali, S.E., et al., 2003. Prediabetes in obese youth: a syndrome of impaired glucose tolerance, severe insulin resistance, and altered myocellular and abdominal fat partitioning. *Lancet*, 362(9388), pp.951–957.

Wellen, K.E. & Hotamisligil, G.S., 2005. Inflammation, stress, and diabetes. *J Clin Invest*, 115(5), pp.1111–1119.

Wellen, K.E. & Hotamisligil, G.S., 2003. Obesity-induced inflammatory changes in adipose tissue. *J Clin Invest*, 112(12), pp.1785–1788.

Welters, H.J. & Kulkarni, R.N., 2008. Wnt signaling: relevance to beta-cell biology and diabetes. *Trends Endocrin Met*, 19(10), pp.349–355.

Wen, H. et al., 2011. Fatty acid-induced NLRP3-ASC inflammasome activation interferes with insulin signaling. *Nat Immunol*, 12(5), pp.408–415.

Wernstedt Asterholm, I. et al., 2012. Altered mitochondrial function and metabolic inflexibility associated with loss of caveolin-1. *Cell Metab*, 15(2), pp.171–185.

Whitham, M. et al., 2012. Contraction-induced interleukin-6 gene transcription in skeletal muscle is regulated by c-Jun terminal kinase/activator protein-1. *J Biol Chem*, 287(14), pp.10771–10779.

WHO, 1999. *Definition, diagnosis and classification of diabetes mellitus and its complications. Part 1: Diagnosis and classification of diabetes mellitus*, Geneva.

WHO, 2014. *Global Health Estimates: Deaths by Cause, Age, Sex and Country, 2000-2012*, Geneva.

Wiesner, R.J., Rüegg, J.C. & Morano, I., 1992. Counting target molecules by exponential polymerase chain reaction: copy number of mitochondrial DNA in rat tissues. *Biochem Bioph Res Co*, 183(2), pp.553–559.

Williams, K.W. & Elmquist, J.K., 2012. From neuroanatomy to behavior: central integration of peripheral signals regulating feeding behavior. *Nat Neurosci*, 15(10), pp.1350–1355.

Williams, L.M. et al., 2014. The Development of Diet-Induced Obesity and Glucose Intolerance in

C57Bl/6 Mice on a High-Fat Diet Consists of Distinct Phases. *PLoS ONE*, 9(8), p.e106159.

Willumsen, N. et al., 1993. Docosahexaenoic acid shows no triglyceride lowering effects but increases the peroxisomal fatty acid oxidation in liver of rats. *J Lipid Res*, 34, pp.13–22.

Wilson-Fritch, L. et al., 2003. Mitochondrial Biogenesis and Remodeling during Adipogenesis and in Response to the Insulin Sensitizer Rosiglitazone. *Mol Cell Biol*, 23(3), pp.1085–1094.

Wilson-Fritch, L. et al., 2004. Mitochondrial remodeling in adipose tissue associated with obesity and treatment with rosiglitazone. *J Clin Invest*, 114(9), pp.1281–1289.

Winer, S. et al., 2009. Normalization of obesity-associated insulin resistance through immunotherapy. *Nat Med*, 15(8), pp.921–929.

Winzell, M.S. et al., 2003. Pancreatic β-cell lipotoxicity induced by overexpression of hormone-sensitive lipase. *Diabetes*, 52(8), pp.2057–2065.

Winzell, M.S. & Ahrén, B., 2004. The High-Fat Diet–Fed Mouse. A Model for Studying Mechanisms and Treatment of Impaired Glucose Tolerance and Type 2 Diabetes. *Diabetes*, 53(S3), pp.215–219.

Wolsk, E. et al., 2010. IL-6 selectively stimulates fat metabolism in human skeletal muscle. *Am J Physiol Endocrinol Metab*, 299(5), pp.E832–E840.

Wredenberg, A. et al., 2006. Respiratory chain dysfunction in skeletal muscle does not cause insulin resistance. *Biochem Bioph Res Co*, 350, pp.202–207.

Wu, J.J. et al., 2006. Mice lacking MAP kinase phosphatase-1 have enhanced MAP kinase activity and resistance to diet-induced obesity. *Cell Metab*, 4(1), pp.61–73.

Wu, Y. et al., 2014. Multilayered Genetic and Omics Dissection of Mitochondrial Activity in a Mouse Reference Population. *Cell*, 158(6), pp.1415–1430.

Xu, H. et al., 2003. Chronic inflammation in fat plays a crucial role in the development of obesity-related insulin resistance. *J Clin Invest*, 112(12), pp.1821–1830.

Yamamoto, K. et al., 2010. Induction of Liver Steatosis and Lipid Droplet Formation in ATF6alpha-Knockout Mice Burdened with Pharmacological Endoplasmic Reticulum Stress. *Mol Biol Cell*, 21, pp.2975–2986.

Yamashita, T. et al., 2004. Role of uncoupling protein-2 up-regulation and triglyceride accumulation in impaired glucose-stimulated insulin secretion in a beta-cell lipotoxicity model overexpressing sterol regulatory element-binding protein-1c. *Endocrinology*, 145(8), pp.3566–3577.

Yamauchi, T. et al., 2001. The fat-derived hormone adiponectin reverses insulin resistance associated with both lipoatrophy and obesity. *Nat Med*, 7(8), pp.941–946.

Ye, J., 2008. Regulation of PPARgamma function by TNF-alpha. *Biochem Bioph Res Co*, 374(3), pp.405–408.

Ye, R. et al., 2010. Grp78 heterozygosity promotes adaptive unfolded protein response and attenuates diet-induced obesity and insulin resistance. *Diabetes*, 59(1), pp.6–16.

Yin, M.-J., Yamamoto, Y. & Gaynor, R.B., 1998. The anti-inflammatory agents aspirin and salicylate inhibit the activity of I(kappa)B kinase-beta. *Nature*, 396(6706), pp.77–80.

Yin, X. et al., 2014. Adipocyte mitochondrial function is reduced in human obesity independent of

fat cell size. *J Clin Endocrinol Metab*, 99(2), pp.E209–16.

Yip, M.F. et al., 2008. CaMKII-Mediated Phosphorylation of the Myosin Motor Myo1c Is Required for Insulin-Stimulated GLUT4 Translocation in Adipocytes. *Cell Metab*, 8(5), pp.384–398.

Yu, C. et al., 2002. Mechanism by which fatty acids inhibit insulin activation of insulin receptor substrate-1 (IRS-1)-associated phosphatidylinositol 3-kinase activity in muscle. *J Biol Chem*, 277(52), pp.50230–50236.

Yu, J. et al., 2007. JNK3 signaling pathway activates ceramide synthase leading to mitochondrial dysfunction. *J Biol Chem*, 282(35), pp.25940–25949.

Yuan, M. et al., 2001. Reversal of obesity- and diet-induced insulin resistance with salicylates or targeted disruption of Ikkbeta. *Science*, 293(5535), pp.1673–1677.

Zechner, C. et al., 2010. Total skeletal muscle PGC-1 deficiency uncouples mitochondrial derangements from fiber type determination and insulin sensitivity. *Cell Metab*, 12(6), pp.633–642.

Zeggini, E. et al., 2008. Meta-analysis of genome-wide association data and large-scale replication identifies additional susceptibility loci for type 2 diabetes. *Nat Genet*, 40(5), pp.638–645.

Zeisel, S.H. & da Costa, K.-A., 2009. Choline: an essential nutrient for public health. *Nutr Rev*, 67(11), pp.615–23.

Zhang, C. et al., 2008. Abdominal obesity and the risk of all-cause, cardiovascular, and cancer mortality: Sixteen years of follow-up in US women. *Circulation*, 117(13), pp.1658–1667.

Zhang, C.Y. et al., 2001. Uncoupling protein-2 negatively regulates insulin secretion and is a major link between obesity, beta cell dysfunction, and type 2 diabetes. *Cell*, 105(6), pp.745–755.

Zhang, D. et al., 2007. Mitochondrial dysfunction due to long-chain Acyl-CoA dehydrogenase deficiency causes hepatic steatosis and hepatic insulin resistance. *P Natl Acad Sci USA*, 104(43), pp.17075–17080.

Zhang, K. et al., 2011. The unfolded protein response transducer IRE1alpha prevents ER stress-induced hepatic steatosis. *EMBO J*, 30(7), pp.1357–1375.

Zhang, X. et al., 2008. Hypothalamic IKKbeta/NF-kappaB and ER stress link overnutrition to energy imbalance and obesity. *Cell*, 135(1), pp.61–73.

Zhang, X. et al., 2011. Selective inactivation of c-Jun NH2-terminal kinase in adipose tissue protects against diet-induced obesity and improves insulin sensitivity in both liver and skeletal muscle in mice. *Diabetes*, 60(2), pp.486–495.

Zhang, Y. et al., 1994. Positional cloning of the mouse obese gene and its human homologue. *Nature*, 372(6505), pp.425–32.

Zhou, R. et al., 2011. A role for mitochondria in NLRP3 inflammasome activation. *Nature*, 469(7329), pp.221–5.

Zick, Y., 2003. Role of Ser/Thr kinases in the uncoupling of insulin signaling. *Int J Obes Relat Metab Disord*, 27(Suppl.3), pp.S56–60.

Zierath, J. et al., 1996. Insulin action on glucose transport and plasma membrane GLUT4 content in skeletal muscle from patients with NIDDM. *Diabetologia*, 39(10), pp.1180–9.

Zierath, J.R. et al., 2013. Chapter 3 Pathophysiology / metabolism / integrative physiology. In

DIAMAP. Road Map for Diabetes Research in Europe. pp. 53–72.

Zierath, J.R. & Wallberg-Henriksson, H., 2015. Looking Ahead Perspective: Where Will the Future of Exercise Biology Take Us? *Cell Metab*, 22(1), pp.25–30.

APPENDICES

Appendix 1.

For 6 genes we compared the RNAseq data with the RT-PCR data.

We chose a pair of genes in each "range" of expression:

	Liver	WAT
Low expression	PGC1β, PPARδ	PGC1β, PGC1α
Medium expression	CPT1a, Fgf1	CPT1a, Fgf1
High expression	Fgf21, Catalase	Fgf21, SCD1

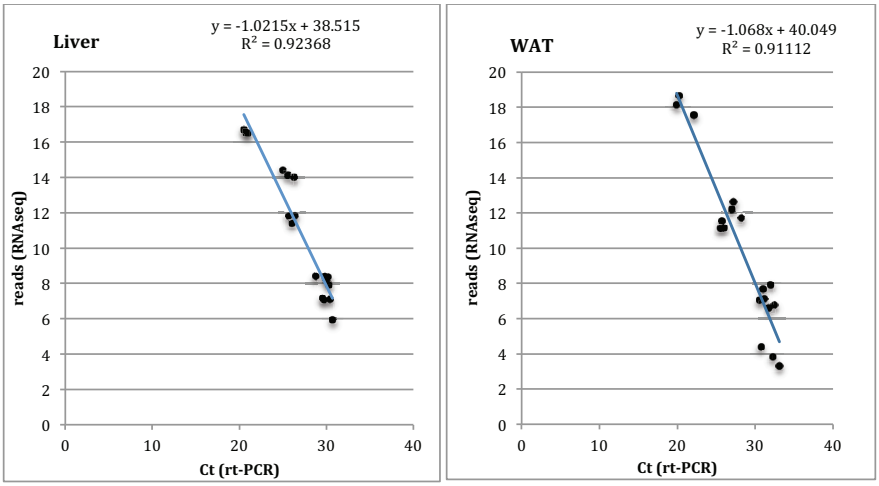

When performing RT-PCR analysis, the cut off we use is at Ct=32. If we are curring at Ct=32, that corresponds to:

WAT → y=5.873

Liver → y=5.827

Final decision in the cut off: 5.8

Appendix 2.

White Adipose Tissue (WAT) metabolomics

	Means			SEM			Significance		
	Ctrl	HFD	Int	Ctrl	HFD	Int	Ctrl vs HFD	Ctrl vs Int	HFD vs Int
Glucose-6-Phosphate	0.0005302	0.0009532	0.0008220	0.0000923	0.0001614	0.0000969	0.0666	ns	ns
3-Hydroxybutyric acid	0.0002180	0.0003529	0.0003156	0.0000266	0.0000333	0.0000154	**	0.0546	ns
Lactate	0.0048943	0.0108084	0.0083512	0.0008041	0.0024819	0.0008054	0.0550	ns	ns
Glycerol	0.0013546	0.0014649	0.0020324	0.0001516	0.0001315	0.0002376	ns	*	ns
NAD^+	0.0003038	0.0003121	0.0003118	0.0000319	0.0000136	0.0000257	ns	ns	ns
NADP	0.0002643	0.0002163	0.0002312	0.0000298	0.0000185	0.0000105	ns	ns	ns
AMP	0.0002642	0.0002418	0.0003762	0.0000526	0.0000277	0.0000618	ns	ns	ns
UDP-Glucoronate	0.0001989	0.0001831	0.0001714	0.0000164	0.0000151	0.0000056	ns	ns	ns
Choline	0.0004878	0.0006892	0.0007800	0.0000422	0.0000545	0.0000933	ns	*	ns
Acetate	0.0012820	0.0011782	0.0009840	0.0001710	0.0001007	0.0001317	ns	ns	ns
Glycine	0.0009856	0.0011925	0.0019540	0.0000853	0.0000969	0.0002448	ns	**	**
Alanine	0.0009605	0.0018444	0.0015424	0.0000961	0.0001648	0.0001023	***	*	ns
Valine	0.0002560	0.0003288	0.0003602	0.0000205	0.0000215	0.0000212	0.0594	**	ns
Leucine	0.0003323	0.0004689	0.0005223	0.0000271	0.0000235	0.0000389	*	***	ns
Methionine	0.0005180	0.0009820	0.0006125	0.0000490	0.0000908	0.0000598	***	ns	**
Tyrosine	0.0002836	0.0003073	0.0003113	0.0000189	0.0000265	0.0000287	ns	ns	ns
Glutamine	0.0008202	0.0009966	0.0010743	0.0000867	0.0000623	0.0001315	ns	ns	ns
Aspartate	0.0005416	0.0008014	0.0005833	0.0000494	0.0000971	0.0000363	0.0534	ns	ns
Glutamate	0.0006482	0.0018099	0.0008880	0.0000524	0.0001275	0.0000512	****	ns	****
Taurine	0.0084625	0.0098444	0.0110025	0.0008639	0.0007905	0.0008518	ns	ns	ns
Oxidized Glutathione	0.0008923	0.0011040	0.0011194	0.0000847	0.0000767	0.0001003	ns	ns	ns
2-Hydroxy-3-methylbutyric acid	0.0013441	0.0011108	0.0002130	0.0005233	0.0002527	0.0000102	ns	ns	ns
Succinate	0.0001945	0.0003391	0.0002674	0.0000168	0.0000260	0.0000202	***	ns	ns
Myo-inositol	0.0008672	0.0009477	0.0009507	0.0000757	0.0000556	0.0001025	ns	ns	ns
GTP	0.0001719	0.0002120	0.0001923	0.0000048	0.0000146	0.0000111	ns	ns	ns
Formate	0.0002119	0.0001729	0.0001841	0.0000177	0.0000146	0.0000143	ns	ns	ns
Cholic acid	0.0003647	0.0003026	0.0003118	0.0000096	0.0000303	0.0000156	ns	ns	ns
Propylene	0.0003542	0.0012167	0.0002020	0.0000665	0.0003427	0.0000244	*	ns	*

glycol									
2-Octenoate	0.0012694	0.0013660	0.0006985	0.0002716	0.0001295	0.0000592	ns	ns	*
Free cholesterol	0.0281989	0.0394246	0.0381187	0.0018584	0.0015322	0.0027690	**	*	ns
Triglycerides	3.4054836	3.0825657	3.4776831	0.2860653	0.1943367	0.3025805	ns	ns	ns
Diglycerides	0.0256762	0.0360156	0.0346375	0.0024131	0.0023390	0.0032993	*	ns	ns
Monoglycerides	0.0119833	0.0107750	0.0113872	0.0007199	0.0007180	0.0007218	ns	ns	ns
Phosphatidylcholine	0.0320055	0.0434071	0.0438037	0.0033869	0.0026233	0.0023839	*	*	ns
O-Phosphocholine	0.0008599	0.0010653	0.0016527	0.0000875	0.0000801	0.0003219	ns	*	ns
Glycerophosphocholine	0.0026585	0.0031952	0.0068010	0.0003201	0.0003380	0.0012854	ns	**	*
Sphingomyelin	0.0080268	0.0094590	0.0109871	0.0010916	0.0004472	0.0007934	ns	0.0531	ns
Omega 3	0.5588951	0.2845462	3.0087149	0.0446994	0.0211660	0.3713673	ns	****	****
ARA+EPA	0.1621723	0.1081340	0.0950565	0.0129239	0.0082226	0.0061969	**	***	ns
Oleic acid	14.3674050	17.6134331	21.5935120	1.3107816	1.0525896	2.1834700	ns	*	ns
Linoleic acid	7.7330501	5.0150943	4.1608707	0.6005528	0.3439124	0.5068978	**	***	ns
Linolenic acid	0.7844544	0.3858750	3.9099995	0.0630587	0.0432090	0.4568080	ns	****	****

Liver metabolomics

	Means			SEM			Significance		
	Ctrl	HFD	Int	Ctrl	HFD	Int	Ctrl vs HFD	Ctrl vs Int	HFD vs Int
Glucose-6-Phosphate	0.0447406	0.0403539	0.0285402	0.0051979	0.0049115	0.0009091	ns	0.0593	ns
Glycogen	0.0384904	0.0268710	0.0494337	0.0064341	0.0041405	0.0070331	ns	ns	*
Pyruvate	0.0001768	0.0001552	0.0001633	0.0000293	0.0000200	0.0000148	ns	ns	
3-Hydroxybutyric acid	0.0017163	0.0012775	0.0013519	0.0000629	0.0000959	0.0001035	**	*	ns
Lactate	0.1084946	0.0726377	0.0646378	0.0156743	0.0082013	0.0089672	ns	*	ns
Fumarate	0.0004233	0.0002735	0.0004215	0.0000400	0.0000233	0.0000321	**	ns	**
NAD	0.0006177	0.0013624	0.0013602	0.0000700	0.0000782	0.0001031	****	****	ns
NADP	0.0003418	0.0003235	0.0004276	0.0000326	0.0000200	0.0000255	ns	ns	*
AMP	0.0045162	0.0035774	0.0044538	0.0003011	0.0001350	0.0003765	ns	ns	ns
UDP-Glucose	0.0005169	0.0005075	0.0006326	0.0000765	0.0000275	0.0000275	ns	ns	ns
UDP-Glucoronate	0.0003462	0.0002737	0.0002888	0.0000409	0.0000127	0.0000144	ns	ns	ns
UDP-NAcGlu	0.0004661	0.0003100	0.0004616	0.0000424	0.0000121	0.0000287	**	ns	**
UDP-N-acetylglucosamine	0.0007854	0.0006143	0.0006163	0.0000226	0.0000259	0.0000273	***	***	ns
Acetate	0.0040984	0.0033432	0.0045569	0.0003200	0.0003623	0.0012942	ns	ns	ns
Glycine	0.0118247	0.0076064	0.0103841	0.0009448	0.0009313	0.0007966	**	ns	ns
Alanine	0.0227082	0.0187580	0.0222433	0.0025272	0.0009135	0.0046925	ns	ns	ns
Valine	0.0036342	0.0024127	0.0019516	0.0005696	0.0002756	0.0002170	ns	*	ns
Leucine	0.0070835	0.0045681	0.0043195	0.0009194	0.0004935	0.0001617	*	*	ns
Isoleucine	0.0033855	0.0034667	0.0008839	0.0006869	0.0005517	0.0000882	ns	*	**
Methionine	0.0024881	0.0015853	0.0019243	0.0002677	0.0000947	0.0002009	*	ns	ns
Phenylalanine	0.0025152	0.0016760	0.0016494	0.0002820	0.0001306	0.0000758	**	**	ns
Threonine	0.0021797	0.0018352	0.0016363	0.0002215	0.0000925	0.0000842	ns	*	ns
Tyrosine	0.0007429	0.0005322	0.0004939	0.0000860	0.0000433	0.0000149	*	*	ns
Asparagine	0.0002444	0.0002137	0.0001796	0.0000283	0.0000159	0.0000096	ns	ns	ns
Glutamine	0.0133860	0.0119104	0.0113090	0.0008636	0.0001785	0.0005165		0.0566	ns
Glutamate	0.0048530	0.0039832	0.0039743	0.0003306	0.0002788	0.0002393	ns	ns	ns
Lysine	0.0038849	0.0025882	0.0022996	0.0003861	0.0002634	0.0001417	*	**	ns
Taurine	0.1054462	0.1201513	0.0828407	0.0109017	0.0064832	0.0100189	ns	ns	*
Oxidized Glutathione	0.0242380	0.0256985	0.0245012	0.0019944	0.0011689	0.0012518	ns	ns	ns
Creatine	0.0025740	0.0014784	0.0021689	0.0004686	0.0001695	0.0004210	ns	ns	ns

Creatinine	0.0005040	0.0003112	0.0003236	0.0000675	0.0000384	0.0000212	*	*	ns
Uridine	0.0017230	0.0012119	0.0010650	0.0000873	0.0000473	0.0000335	****	****	ns
Nicotinamide mononucleotide	0.0002555	0.0002555	0.0002486	0.0000084	0.0000259	0.0000277	ns	ns	ns
Niacinamide	0.0008160	0.0006152	0.0007877	0.0000741	0.0000402	0.0000360	*	ns	ns
Succinate	0.0043004	0.0047047	0.0050641	0.0012115	0.0006562	0.0009917	ns	ns	ns
Glycerophosphocholine	0.0095606	0.0139926	0.0087315	0.0010334	0.0009209	0.0005786	**	ns	***
Guanosine	0.0006303	0.0004907	0.0005368	0.0000217	0.0000471	0.0000344	0.0523	ns	ns
Formate	0.0001891	0.0001795	0.0001718	0.0000103	0.0000137	0.0000128	ns	ns	ns
Cholate	0.0012612	0.0012264	0.0014555	0.0000936	0.0000435	0.0000367	ns	ns	0.0545
Propylene glycol	0.0040135	0.0051930	0.0002751	0.0012682	0.0012412	0.0000074	ns	ns	*
Myo-inositol	0.0017187	0.0009864	0.0011267	0.0002030	0.0001328	0.0000807	**	*	ns
Inosine	0.0008117	0.0009529	0.0010691	0.0000251	0.0000405	0.0000839	ns	*	ns
Free cholesterol	0.0500527	0.0420382	0.0455177	0.0018707	0.0018032	0.0013783	**	ns	ns
Est. Cholesterol	0.0136636	0.0410325	0.0161338	0.0007053	0.0062369	0.0014146	***	ns	**
Triglycerides	0.1932196	1.1813753	0.1536784	0.0174354	0.1287420	0.0194402	****	ns	****
Diglycerides	0.0112896	0.0220866	0.0145657	0.0014413	0.0012699	0.0026937	**	ns	*
Monoglycerides	0.0234851	0.0226946	0.0241805	0.0007044	0.0013236	0.0024769	ns	ns	ns
Phosphatidylcholine	0.0368866	0.0536645	0.0296641	0.0060974	0.0081139	0.0062038	ns	ns	0.0604
O-Phosphocholine	0.0054240	0.0039502	0.0034729	0.0006449	0.0003062	0.0002006	0.0529	*	ns
Phosphatidylethanolamine	0.0705970	0.0412774	0.0624469	0.0043520	0.0031818	0.0058863	***	ns	**
Sphingomyelin	0.0027242	0.0013045	0.0014299	0.0003735	0.0004301	0.0000955	*	*	ns
Omega 3	0.0624166	0.1417127	0.1882886	0.0033406	0.0098427	0.0222569	**	****	0.0660
ARA+EPA	0.0736181	0.1155555	0.0647071	0.0054272	0.0055103	0.0029077	****	ns	****
Oleic acid	0.3535378	3.0248645	0.2667819	0.0364056	0.4176522	0.0415667	****	ns	****
DHA	0.0572188	0.1040893	0.0689176	0.0050030	0.0053626	0.0076351	****	ns	**
Linoleic acid	0.1716507	0.6865951	0.1169382	0.0179458	0.0633056	0.0146528	****	ns	****

Gastrocnemius metabolomics

	Means			SEM			Significance		
	Ctrl	HFD	Int	Ctrl	HFD	Int	Ctrl vs HFD	Ctrl vs Int	HFD vs Int
Lactate	0.0204740	0.0121271	0.0075309	0.0045047	0.0023947	0.0010057	ns	*	ns
NAD^+	0.0005453	0.0004205	0.0003842	0.0000517	0.0000234	0.0000349	ns	*	ns
Acetate	0.0003126	0.0002656	0.0002882	0.0000386	0.0000230	0.0000479	ns	ns	ns
Glycine	0.0039449	0.0018575	0.0020189	0.0004746	0.0001711	0.0003108	**	**	ns
Alanine	0.0065089	0.0066288	0.0047746	0.0007532	0.0006996	0.0005858	ns	ns	ns
Valine	0.0005028	0.0004520	0.0004114	0.0000543	0.0000399	0.0000435	ns	ns	ns
Leucine	0.0008071	0.0006110	0.0007046	0.0000802	0.0000543	0.0000675	ns	ns	ns
Isoleucine	0.0002969	0.0002492	0.0002081	0.0000323	0.0000151	0.0000233	ns	*	ns
Glutamate	0.0015101	0.0010989	0.0011277	0.0001989	0.0000522	0.0001379	ns	ns	ns
Lysine	0.0015825	0.0012175	0.0015943	0.0001742	0.0000605	0.0002856	ns	ns	ns
Glutamine	0.0035974	0.0022426	0.0025537	0.0003732	0.0000864	0.0003351	*	0.0624	ns
Taurine	0.0631668	0.0522082	0.0502695	0.0067436	0.0044973	0.0053972	ns	ns	ns
Oxidized Glutathione	0.0022128	0.0014496	0.0014665	0.0002896	0.0001545	0.0001611	*	0.0555	ns
Creatine	0.0135853	0.0089124	0.0094993	0.0020591	0.0008566	0.0015394	ns	ns	ns
Creatine-Phosphate	0.0152993	0.0103286	0.0105809	0.0004971	0.0004073	0.0009945	***	***	ns
Propylene glycol	0.0015541	0.0016629	0.0001191	0.0004755	0.0003376	0.0000193	ns	*	*
Succinate	0.0010041	0.0004582	0.0003180	0.0002947	0.0000478	0.0000284	ns	0.0529	ns
Methylhistidine	0.0002152	0.0000952	0.0004084	0.0000256	0.0000391	0.0001888	ns	ns	ns
Free Cholesterol	0.0076284	0.0071073	0.0089641	0.0006111	0.0007009	0.0007554	ns	ns	ns
Triglicerides	0.0037493	0.0152812	0.0042127	0.0004148	0.0023478	0.0003641	****	ns	****
Monoglycerides	0.0018063	0.0020244	0.0014968	0.0005187	0.0004945	0.0004863	ns	ns	ns
Phosphatidylcholine	0.0222320	0.0202182	0.0239692	0.0016481	0.0015389	0.0019393	ns	ns	ns
Phosphatidylethanolamine	0.0109064	0.0100103	0.0116325	0.0008737	0.0008864	0.0009030	ns	ns	ns
Sphingomyelin	0.0008425	0.0007737	0.0009500	0.0000628	0.0000608	0.0000682	ns	ns	ns
Omega 3	0.0235953	0.0293372	0.0450203	0.0022875	0.0033347	0.0042537	ns	***	*
ARA+EPA	0.0082782	0.0075124	0.0050819	0.0005842	0.0008546	0.0006884	ns	*	0.0681
Oleic acid	0.0498210	0.1585048	0.0788312	0.0075067	0.0239113	0.0097330	***	ns	**
DHA	0.0166981	0.0179353	0.0208664	0.0014963	0.0029121	0.0016540	ns	ns	ns
Linoleic acid	0.0167439	0.0490177	0.0191798	0.0022433	0.0066739	0.0019762	***	ns	***

Hypothalamus metabolomics

	Means			SEM			Significance		
	Ctrl	**HFD**	**Int**	**Ctrl**	**HFD**	**Int**	**Ctrl vs HFD**	**Ctrl vs Int**	**HFD vs Int**
Lactate	0.0263519	0.0278020	0.0278880	0.0014766	0.0027672	0.0016951	ns	ns	ns
NAD^+	0.0007321	0.0005382	0.0008252	0.0000363	0.0000346	0.0000713	*	ns	**
NADP	0.0010732	0.0010054	0.0010812	0.0000501	0.0000691	0.0000931	ns	ns	ns
AMP	0.0043496	0.0045940	0.0046700	0.0005378	0.0003491	0.0003122	ns	ns	ns
Glycine	0.0069395	0.0072250	0.0068859	0.0006699	0.0006013	0.0003713	ns	ns	ns
Choline	0.0032572	0.0042523	0.0030826	0.0002447	0.0002834	0.0002289	*	ns	**
Alanine	0.0038232	0.0047289	0.0045365	0.0002904	0.0002980	0.0002221	ns	ns	ns
Valine	0.0010821	0.0011745	0.0013142	0.0000368	0.0000932	0.0000987	ns	ns	ns
Tyrosine	0.0010063	0.0010887	0.0010344	0.0000457	0.0001216	0.0001227	ns	ns	ns
Glutamate	0.0297115	0.0310981	0.0302440	0.0029147	0.0028698	0.0023250	ns	ns	ns
Glutamine	0.0305264	0.0319530	0.0310164	0.0032973	0.0026018	0.0020688	ns	ns	ns
Taurine	0.0303262	0.0325217	0.0293589	0.0030339	0.0025768	0.0022408	ns	ns	ns
Creatine	0.0415134	0.0423475	0.0415600	0.0039673	0.0038059	0.0031360	ns	ns	ns
N-Acetyl-Aspartate	0.0425314	0.0442544	0.0418190	0.0042346	0.0031362	0.0029111	ns	ns	ns
4-Aminobutyric acid	0.0316658	0.0323638	0.0307474	0.0025803	0.0024855	0.0016068	ns	ns	ns
Myo-inositol	0.0423695	0.0458625	0.0419305	0.0040184	0.0038306	0.0026726	ns	ns	ns
Niacinamide	0.0008199	0.0008792	0.0008543	0.0000374	0.0000572	0.0000997	ns	ns	ns
GTP Guanosine	0.0012702	0.0013279	0.0013263	0.0001077	0.0001033	0.0000973	ns	ns	ns
Inosine	0.0009187	0.0009793	0.0009728	0.0000833	0.0001003	0.0000983	ns	ns	ns
Succinate	0.0025539	0.0014895	0.0034964	0.0002822	0.0001863	0.0004973	ns	ns	**
Aspartate	0.0095781	0.0101669	0.0096135	0.0007479	0.0006768	0.0005624	ns	ns	ns
Propylene glycol	0.0040035	0.0033649	0.0017751	0.0007508	0.0008443	0.0002027	ns	ns	ns
Free Cholesterol	0.1762271	0.1756837	0.1612607	0.0356788	0.0183213	0.0355991	ns	ns	ns
Esterified Cholesterol	0.0018913	0.0024759	0.0015214	0.0002238	0.0005307	0.0002569	ns	ns	ns
Total Phospholipids	0.0891747	0.0941516	0.0893107	0.0144994	0.0072251	0.0091701	ns	ns	ns
Glycerophosphocholine	0.0344460	0.0384325	0.0334064	0.0037208	0.0032142	0.0022212	ns	ns	ns
O-Phosphocholine	0.0128136	0.0134154	0.0131253	0.0014167	0.0010223	0.0010404	ns	ns	ns
Phosphatidylet	0.1103586	0.1167579	0.1119015	0.0179564	0.0092802	0.0129853	ns	ns	ns

hanolamine									
Sphingomyelin	0.0193224	0.0190213	0.0203377	0.0034863	0.0016343	0.0035348	ns	ns	ns
Omega 3	0.1003102	0.1024807	0.0982221	0.0183682	0.0089057	0.0163163	ns	ns	ns
ARA+EPA	0.0295693	0.0305005	0.0288265	0.0047139	0.0026739	0.0029011	ns	ns	ns
Oleic	0.3137113	0.3210794	0.2965737	0.0626628	0.0303210	0.0650645	ns	ns	ns
DHA	0.0639536	0.0606216	0.0593867	0.0119173	0.0056418	0.0102888	ns	ns	ns
Linoleic	0.0032723	0.0026051	0.0028193	0.0008102	0.0001908	0.0005466	ns	ns	ns
Linolenic acid	0.0773034	0.0805259	0.0701373	0.0144911	0.0082045	0.0128773	ns	ns	ns

Appendix 3.

WAT 10 most relevant protein complexes (proteins describe

PC	AvgRI	ENSG	name	description
1	partner	ENSG00000198719	DLL1	delta-like 1 (Drosophila) [Source:HGNC Symbol;Acc:HGNC:2908]
1	partner	ENSG00000081692	JMJD4	jumonji domain containing 4 [Source:HGNC Symbol;Acc:HGNC:25724]
1	partner	ENSG00000221818	EBF2	early B-cell factor 2 [Source:HGNC Symbol;Acc:HGNC:19090]
1	38.4725011752	ENSG00000196323	ZBTB44	zinc finger and BTB domain containing 44 [Source:HGNC Symbol;Acc:HGNC:25001]
1	partner	ENSG00000161203	AP2M1	adaptor-related protein complex 2, mu 1 subunit [Source:HGNC Symbol;Acc:HGNC:564]
1	partner	ENSG00000196470	SIAH1	siah E3 ubiquitin protein ligase 1 [Source:HGNC Symbol;Acc:HGNC:10857]
2	partner	ENSG00000118007	STAG1	stromal antigen 1 [Source:HGNC Symbol;Acc:HGNC:11354]
2	partner	ENSG00000083642	PDS5B	PDS5 cohesin associated factor B [Source:HGNC Symbol;Acc:HGNC:20418]
2	67.2041469487	ENSG00000146670	CDCA5	cell division cycle associated 5 [Source:HGNC Symbol;Acc:HGNC:14626]
2	partner	ENSG00000105325	FZR1	fizzy/cell division cycle 20 related 1 (Drosophila) [Source:HGNC Symbol;Acc:HGNC:24824]
2	partner	ENSG00000163904	SENP2	SUMO1/sentrin/SMT3 specific peptidase 2 [Source:HGNC Symbol;Acc:HGNC:23116]
2	partner	ENSG00000164754	RAD21	RAD21 homolog (S. pombe) [Source:HGNC Symbol;Acc:HGNC:9811]
2	partner	ENSG00000090376	IRAK3	interleukin-1 receptor-associated kinase 3 [Source:HGNC Symbol;Acc:HGNC:17020]
3	82.9631564029	ENSG00000132768	DPH2	DPH2 homolog (S. cerevisiae) [Source:HGNC Symbol;Acc:HGNC:3004]
3	partner	ENSG00000150991	UBC	ubiquitin C [Source:HGNC Symbol;Acc:HGNC:12468]
3	partner	ENSG00000163931	TKT	transketolase [Source:HGNC Symbol;Acc:HGNC:11834]
3	partner	ENSG00000104808	DHDH	dihydrodiol dehydrogenase (dimeric) [Source:HGNC Symbol;Acc:HGNC:17887]
3	partner	ENSG00000144182	LIPT1	lipoyltransferase 1 [Source:HGNC Symbol;Acc:HGNC:29569]
3	partner	ENSG00000103479	RBL2	retinoblastoma-like 2 [Source:HGNC Symbol;Acc:HGNC:9894]
4	partner	ENSG00000150991	UBC	ubiquitin C [Source:HGNC Symbol;Acc:HGNC:12468]
4	partner	ENSG00000169372	CRADD	CASP2 and RIPK1 domain containing adaptor with death domain [Source:HGNC Symbol;Acc:HGNC:2340]
4	partner	ENSG00000197448	GSTK1	glutathione S-transferase kappa 1 [Source:HGNC Symbol;Acc:HGNC:16906]
4	91.5883153885	ENSG00000169738	DCXR	dicarbonyl/L-xylulose reductase [Source:HGNC Symbol;Acc:HGNC:18985]
4	partner	ENSG00000175104	TRAF6	TNF receptor-associated factor 6, E3 ubiquitin protein ligase [Source:HGNC Symbol;Acc:HGNC:12036]
4	partner	ENSG00000116918	TSNAX	translin-associated factor X [Source:HGNC Symbol;Acc:HGNC:12380]
5	partner	ENSG00000166851	PLK1	polo-like kinase 1 [Source:HGNC Symbol;Acc:HGNC:9077]
5	partner	ENSG00000150991	UBC	ubiquitin C [Source:HGNC Symbol;Acc:HGNC:12468]
5	partner	ENSG00000117399	CDC20	cell division cycle 20 [Source:HGNC Symbol;Acc:HGNC:1723]
5	partner	ENSG00000055130	CUL1	cullin 1 [Source:HGNC Symbol;Acc:HGNC:2551]
5	partner	ENSG00000110092	CCND1	cyclin D1 [Source:HGNC Symbol;Acc:HGNC:1582]
5	82.6771218131	ENSG00000112029	FBXO5	F-box protein 5 [Source:HGNC Symbol;Acc:HGNC:13584]
5	partner	ENSG00000134057	CCNB1	cyclin B1 [Source:HGNC Symbol;Acc:HGNC:1579]
5	partner	ENSG00000105325	FZR1	fizzy/cell division cycle 20 related 1 (Drosophila) [Source:HGNC Symbol;Acc:HGNC:24824]
5	partner	ENSG00000067208	EVI5	ecotropic viral integration site 5 [Source:HGNC Symbol;Acc:HGNC:3501]
5	partner	ENSG00000143947	RPS27A	ribosomal protein S27a [Source:HGNC Symbol;Acc:HGNC:10417]
6	partner	ENSG00000169021	UQCRFS1	ubiquinol-cytochrome c reductase, Rieske iron-sulfur polypeptide 1 [Source:HGNC Symbol;Acc:HGNC:12587]
6	partner	ENSG00000167792	NDUFV1	NADH dehydrogenase (ubiquinone) flavoprotein 1, 51kDa [Source:HGNC Symbol;Acc:HGNC:7716]
6	partner	ENSG00000164919	COX6C	cytochrome c oxidase subunit VIc [Source:HGNC Symbol;Acc:HGNC:2285]
6	partner	ENSG00000065518	NDUFB4	NADH dehydrogenase (ubiquinone) 1 beta subcomplex, 4, 15kDa [Source:HGNC Symbol;Acc:HGNC:7699]
6	partner	ENSG00000164405	UQCRQ	ubiquinol-cytochrome c reductase, complex III subunit VII, 9.5kDa [Source:HGNC Symbol;Acc:HGNC:29594]
6	partner	ENSG00000131495	NDUFA2	NADH dehydrogenase (ubiquinone) 1 alpha subcomplex, 2, 8kDa [Source:HGNC Symbol;Acc:HGNC:7685]
6	partner	ENSG00000175104	TRAF6	TNF receptor-associated factor 6, E3 ubiquitin protein ligase [Source:HGNC Symbol;Acc:HGNC:12036]
6	partner	ENSG00000213619	NDUFS3	NADH dehydrogenase (ubiquinone) Fe-S protein 3, 30kDa (NADH-coenzyme Q reductase) [Source:HGNC Symbol;Acc:HGNC:7710]
6	87.5061954344	ENSG00000168653	NDUFS5	NADH dehydrogenase (ubiquinone) Fe-S protein 5, 15kDa (NADH-coenzyme Q reductase) [Source:HGNC Symbol;Acc:HGNC:7712]

6	partner	ENSG00000128609	NDUFA5	NADH dehydrogenase (ubiquinone) 1 alpha subcomplex, 5 [Source:HGNC Symbol;Acc:HGNC:7688]
6	85.5999163474	ENSG00000160194	NDUFV3	NADH dehydrogenase (ubiquinone) flavoprotein 3, 10kDa [Source:HGNC Symbol;Acc:HGNC:7719]
6	partner	ENSG00000140740	UQCRC2	ubiquinol-cytochrome c reductase core protein II [Source:HGNC Symbol;Acc:HGNC:12586]
6	partner	ENSG00000184983	NDUFA6	NADH dehydrogenase (ubiquinone) 1 alpha subcomplex, 6, 14kDa [Source:HGNC Symbol;Acc:HGNC:7690]
6	partner	ENSG00000150991	UBC	ubiquitin C [Source:HGNC Symbol;Acc:HGNC:12468]
6	partner	ENSG00000023228	NDUFS1	NADH dehydrogenase (ubiquinone) Fe-S protein 1, 75kDa (NADH-coenzyme Q reductase) [Source:HGNC Symbol;Acc:HGNC:7707]
6	partner	ENSG00000147684	NDUFB9	NADH dehydrogenase (ubiquinone) 1 beta subcomplex, 9, 22kDa [Source:HGNC Symbol;Acc:HGNC:7704]
6	partner	ENSG00000179091	CYC1	cytochrome c-1 [Source:HGNC Symbol;Acc:HGNC:2579]
6	partner	ENSG00000184076	UQCR10	ubiquinol-cytochrome c reductase, complex III subunit X [Source:HGNC Symbol;Acc:HGNC:30863]
6	85.8292183301	ENSG00000099795	NDUFB7	NADH dehydrogenase (ubiquinone) 1 beta subcomplex, 7, 18kDa [Source:HGNC Symbol;Acc:HGNC:7702]
6	partner	ENSG00000145494	NDUFS6	NADH dehydrogenase (ubiquinone) Fe-S protein 6, 13kDa (NADH-coenzyme Q reductase) [Source:HGNC Symbol;Acc:HGNC:7713]
6	86.5837796245	ENSG00000125356	NDUFA1	NADH dehydrogenase (ubiquinone) 1 alpha subcomplex, 1, 7.5kDa [Source:HGNC Symbol;Acc:HGNC:7683]
6	partner	ENSG00000189043	NDUFA4	NDUFA4, mitochondrial complex associated [Source:HGNC Symbol;Acc:HGNC:7687]
6	86.3531071804	ENSG00000112695	COX7A2	cytochrome c oxidase subunit VIIa polypeptide 2 (liver) [Source:HGNC Symbol;Acc:HGNC:2288]
6	partner	ENSG00000139180	NDUFA9	NADH dehydrogenase (ubiquinone) 1 alpha subcomplex, 9, 39kDa [Source:HGNC Symbol;Acc:HGNC:7693]
6	partner	ENSG00000110717	NDUFS8	NADH dehydrogenase (ubiquinone) Fe-S protein 8, 23kDa (NADH-coenzyme Q reductase) [Source:HGNC Symbol;Acc:HGNC:7715]
6	partner	ENSG00000158864	NDUFS2	NADH dehydrogenase (ubiquinone) Fe-S protein 2, 49kDa (NADH-coenzyme Q reductase) [Source:HGNC Symbol;Acc:HGNC:7708]
6	partner	ENSG00000010256	UQCRC1	ubiquinol-cytochrome c reductase core protein I [Source:HGNC Symbol;Acc:HGNC:12585]
6	partner	ENSG00000178127	NDUFV2	NADH dehydrogenase (ubiquinone) flavoprotein 2, 24kDa [Source:HGNC Symbol;Acc:HGNC:7717]
6	partner	ENSG00000115286	NDUFS7	NADH dehydrogenase (ubiquinone) Fe-S protein 7, 20kDa (NADH-coenzyme Q reductase) [Source:HGNC Symbol;Acc:HGNC:7714]
6	partner	ENSG00000111775	COX6A1	cytochrome c oxidase subunit VIa polypeptide 1 [Source:HGNC Symbol;Acc:HGNC:2277]
6	partner	ENSG00000127184	COX7C	cytochrome c oxidase subunit VIIc [Source:HGNC Symbol;Acc:HGNC:2292]
6	partner	ENSG00000165264	NDUFB6	NADH dehydrogenase (ubiquinone) 1 beta subcomplex, 6, 17kDa [Source:HGNC Symbol;Acc:HGNC:7701]
6	partner	ENSG00000140990	NDUFB10	NADH dehydrogenase (ubiquinone) 1 beta subcomplex, 10, 22kDa [Source:HGNC Symbol;Acc:HGNC:7696]
6	partner	ENSG00000167774	NDUFA7	NADH dehydrogenase [ubiquinone] 1 alpha subcomplex subunit 7 [Source:UniProtKB/Swiss-Prot;Acc:O95182]
6	partner	ENSG00000136521	NDUFB5	NADH dehydrogenase (ubiquinone) 1 beta subcomplex, 5, 16kDa [Source:HGNC Symbol;Acc:HGNC:7700]
6	partner	ENSG00000130414	NDUFA10	NADH dehydrogenase (ubiquinone) 1 alpha subcomplex, 10, 42kDa [Source:HGNC Symbol;Acc:HGNC:7684]
6	partner	ENSG00000156467	UQCRB	ubiquinol-cytochrome c reductase binding protein [Source:HGNC Symbol;Acc:HGNC:12582]
6	partner	ENSG00000173230	GOLGB1	golgin B1 [Source:HGNC Symbol;Acc:HGNC:4429]
6	partner	ENSG00000170906	NDUFA3	NADH dehydrogenase (ubiquinone) 1 alpha subcomplex, 3, 9kDa [Source:HGNC Symbol;Acc:HGNC:7686]
6	partner	ENSG00000131143	COX4I1	cytochrome c oxidase subunit IV isoform 1 [Source:HGNC Symbol;Acc:HGNC:2265]
6	partner	ENSG00000135940	COX5B	cytochrome c oxidase subunit Vb [Source:HGNC Symbol;Acc:HGNC:2269]
6	partner	ENSG00000147123	NDUFB11	NADH dehydrogenase (ubiquinone) 1 beta subcomplex, 11, 17.3kDa [Source:HGNC Symbol;Acc:HGNC:20372]
6	85.5999163474	ENSG00000109390	NDUFC1	NADH dehydrogenase (ubiquinone) 1, subcomplex unknown, 1, 6kDa [Source:HGNC Symbol;Acc:HGNC:7705]
6	partner	ENSG00000184752	NDUFA12	NADH dehydrogenase (ubiquinone) 1 alpha subcomplex, 12 [Source:HGNC Symbol;Acc:HGNC:23987]
7	partner	ENSG00000169021	UQCRFS1	ubiquinol-cytochrome c reductase, Rieske iron-sulfur polypeptide 1 [Source:HGNC Symbol;Acc:HGNC:12587]
7	partner	ENSG00000167792	NDUFV1	NADH dehydrogenase (ubiquinone) flavoprotein 1, 51kDa [Source:HGNC Symbol;Acc:HGNC:7716]
7	partner	ENSG00000164919	COX6C	cytochrome c oxidase subunit VIc [Source:HGNC Symbol;Acc:HGNC:2285]
7	partner	ENSG00000065518	NDUFB4	NADH dehydrogenase (ubiquinone) 1 beta subcomplex, 4, 15kDa

				[Source:HGNC Symbol;Acc:HGNC:7699]
7	partner	ENSG00000164405	UQCRQ	ubiquinol-cytochrome c reductase, complex III subunit VII, 9.5kDa [Source:HGNC Symbol;Acc:HGNC:29594]
7	partner	ENSG00000131495	NDUFA2	NADH dehydrogenase (ubiquinone) 1 alpha subcomplex, 2, 8kDa [Source:HGNC Symbol;Acc:HGNC:7685]
7	partner	ENSG00000213619	NDUFS3	NADH dehydrogenase (ubiquinone) Fe-S protein 3, 30kDa (NADH-coenzyme Q reductase) [Source:HGNC Symbol;Acc:HGNC:7710]
7	87.5061954344	ENSG00000168653	NDUFS5	NADH dehydrogenase (ubiquinone) Fe-S protein 5, 15kDa (NADH-coenzyme Q reductase) [Source:HGNC Symbol;Acc:HGNC:7712]
7	partner	ENSG00000128609	NDUFA5	NADH dehydrogenase (ubiquinone) 1 alpha subcomplex, 5 [Source:HGNC Symbol;Acc:HGNC:7688]
7	85.5999163474	ENSG00000160194	NDUFV3	NADH dehydrogenase (ubiquinone) flavoprotein 3, 10kDa [Source:HGNC Symbol;Acc:HGNC:7719]
7	partner	ENSG00000140740	UQCRC2	ubiquinol-cytochrome c reductase core protein II [Source:HGNC Symbol;Acc:HGNC:12586]
7	partner	ENSG00000184983	NDUFA6	NADH dehydrogenase (ubiquinone) 1 alpha subcomplex, 6, 14kDa [Source:HGNC Symbol;Acc:HGNC:7690]
7	partner	ENSG00000150991	UBC	ubiquitin C [Source:HGNC Symbol;Acc:HGNC:12468]
7	partner	ENSG00000023228	NDUFS1	NADH dehydrogenase (ubiquinone) Fe-S protein 1, 75kDa (NADH-coenzyme Q reductase) [Source:HGNC Symbol;Acc:HGNC:7707]
7	partner	ENSG00000147684	NDUFB9	NADH dehydrogenase (ubiquinone) 1 beta subcomplex, 9, 22kDa [Source:HGNC Symbol;Acc:HGNC:7704]
7	partner	ENSG00000179091	CYC1	cytochrome c-1 [Source:HGNC Symbol;Acc:HGNC:2579]
7	partner	ENSG00000184076	UQCR10	ubiquinol-cytochrome c reductase, complex III subunit X [Source:HGNC Symbol;Acc:HGNC:30863]
7	85.8292183301	ENSG00000099795	NDUFB7	NADH dehydrogenase (ubiquinone) 1 beta subcomplex, 7, 18kDa [Source:HGNC Symbol;Acc:HGNC:7702]
7	partner	ENSG00000145494	NDUFS6	NADH dehydrogenase (ubiquinone) Fe-S protein 6, 13kDa (NADH-coenzyme Q reductase) [Source:HGNC Symbol;Acc:HGNC:7713]
7	86.5837796245	ENSG00000125356	NDUFA1	NADH dehydrogenase (ubiquinone) 1 alpha subcomplex, 1, 7.5kDa [Source:HGNC Symbol;Acc:HGNC:7683]
7	partner	ENSG00000189043	NDUFA4	NDUFA4, mitochondrial complex associated [Source:HGNC Symbol;Acc:HGNC:7687]
7	86.3531071804	ENSG00000112695	COX7A2	cytochrome c oxidase subunit VIIa polypeptide 2 (liver) [Source:HGNC Symbol;Acc:HGNC:2288]
7	partner	ENSG00000139180	NDUFA9	NADH dehydrogenase (ubiquinone) 1 alpha subcomplex, 9, 39kDa [Source:HGNC Symbol;Acc:HGNC:7693]
7	partner	ENSG00000110717	NDUFS8	NADH dehydrogenase (ubiquinone) Fe-S protein 8, 23kDa (NADH-coenzyme Q reductase) [Source:HGNC Symbol;Acc:HGNC:7715]
7	partner	ENSG00000158864	NDUFS2	NADH dehydrogenase (ubiquinone) Fe-S protein 2, 49kDa (NADH-coenzyme Q reductase) [Source:HGNC Symbol;Acc:HGNC:7708]
7	partner	ENSG00000010256	UQCRC1	ubiquinol-cytochrome c reductase core protein I [Source:HGNC Symbol;Acc:HGNC:12585]
7	partner	ENSG00000178127	NDUFV2	NADH dehydrogenase (ubiquinone) flavoprotein 2, 24kDa [Source:HGNC Symbol;Acc:HGNC:7717]
7	partner	ENSG00000115286	NDUFS7	NADH dehydrogenase (ubiquinone) Fe-S protein 7, 20kDa (NADH-coenzyme Q reductase) [Source:HGNC Symbol;Acc:HGNC:7714]
7	partner	ENSG00000111775	COX6A1	cytochrome c oxidase subunit VIa polypeptide 1 [Source:HGNC Symbol;Acc:HGNC:2277]
7	partner	ENSG00000127184	COX7C	cytochrome c oxidase subunit VIIc [Source:HGNC Symbol;Acc:HGNC:2292]
7	partner	ENSG00000165264	NDUFB6	NADH dehydrogenase (ubiquinone) 1 beta subcomplex, 6, 17kDa [Source:HGNC Symbol;Acc:HGNC:7701]
7	partner	ENSG00000140990	NDUFB10	NADH dehydrogenase (ubiquinone) 1 beta subcomplex, 10, 22kDa [Source:HGNC Symbol;Acc:HGNC:7696]
7	partner	ENSG00000167774	NDUFA7	NADH dehydrogenase [ubiquinone] 1 alpha subcomplex subunit 7 [Source:UniProtKB/Swiss-Prot;Acc:O95182]
7	partner	ENSG00000136521	NDUFB5	NADH dehydrogenase (ubiquinone) 1 beta subcomplex, 5, 16kDa [Source:HGNC Symbol;Acc:HGNC:7700]
7	partner	ENSG00000130414	NDUFA10	NADH dehydrogenase (ubiquinone) 1 alpha subcomplex, 10, 42kDa [Source:HGNC Symbol;Acc:HGNC:7684]
7	partner	ENSG00000156467	UQCRB	ubiquinol-cytochrome c reductase binding protein [Source:HGNC Symbol;Acc:HGNC:12582]
7	partner	ENSG00000170906	NDUFA3	NADH dehydrogenase (ubiquinone) 1 alpha subcomplex, 3, 9kDa [Source:HGNC Symbol;Acc:HGNC:7686]
7	partner	ENSG00000131143	COX4I1	cytochrome c oxidase subunit IV isoform 1 [Source:HGNC Symbol;Acc:HGNC:2265]
7	partner	ENSG00000135940	COX5B	cytochrome c oxidase subunit Vb [Source:HGNC Symbol;Acc:HGNC:2269]
7	partner	ENSG00000147123	NDUFB11	NADH dehydrogenase (ubiquinone) 1 beta subcomplex, 11, 17.3kDa [Source:HGNC Symbol;Acc:HGNC:20372]
7	85.5999163474	ENSG00000109390	NDUFC1	NADH dehydrogenase (ubiquinone) 1, subcomplex unknown, 1, 6kDa [Source:HGNC Symbol;Acc:HGNC:7705]
7	partner	ENSG00000184752	NDUFA12	NADH dehydrogenase (ubiquinone) 1 alpha subcomplex, 12

				[Source:HGNC Symbol;Acc:HGNC:23987]
8	partner	ENSG00000169021	UQCRFS1	ubiquinol-cytochrome c reductase, Rieske iron-sulfur polypeptide 1 [Source:HGNC Symbol;Acc:HGNC:12587]
8	partner	ENSG00000167792	NDUFV1	NADH dehydrogenase (ubiquinone) flavoprotein 1, 51kDa [Source:HGNC Symbol;Acc:HGNC:7716]
8	partner	ENSG00000164919	COX6C	cytochrome c oxidase subunit VIc [Source:HGNC Symbol;Acc:HGNC:2285]
8	partner	ENSG00000065518	NDUFB4	NADH dehydrogenase (ubiquinone) 1 beta subcomplex, 4, 15kDa [Source:HGNC Symbol;Acc:HGNC:7699]
8	partner	ENSG00000164405	UQCRQ	ubiquinol-cytochrome c reductase, complex III subunit VII, 9.5kDa [Source:HGNC Symbol;Acc:HGNC:29594]
8	partner	ENSG00000131495	NDUFA2	NADH dehydrogenase (ubiquinone) 1 alpha subcomplex, 2, 8kDa [Source:HGNC Symbol;Acc:HGNC:7685]
8	partner	ENSG00000213619	NDUFS3	NADH dehydrogenase (ubiquinone) Fe-S protein 3, 30kDa (NADH-coenzyme Q reductase) [Source:HGNC Symbol;Acc:HGNC:7710]
8	87.5061954344	ENSG00000168653	NDUFS5	NADH dehydrogenase (ubiquinone) Fe-S protein 5, 15kDa (NADH-coenzyme Q reductase) [Source:HGNC Symbol;Acc:HGNC:7712]
8	partner	ENSG00000128609	NDUFA5	NADH dehydrogenase (ubiquinone) 1 alpha subcomplex, 5 [Source:HGNC Symbol;Acc:HGNC:7688]
8	85.5999163474	ENSG00000160194	NDUFV3	NADH dehydrogenase (ubiquinone) flavoprotein 3, 10kDa [Source:HGNC Symbol;Acc:HGNC:7719]
8	partner	ENSG00000140740	UQCRC2	ubiquinol-cytochrome c reductase core protein II [Source:HGNC Symbol;Acc:HGNC:12586]
8	partner	ENSG00000184983	NDUFA6	NADH dehydrogenase (ubiquinone) 1 alpha subcomplex, 6, 14kDa [Source:HGNC Symbol;Acc:HGNC:7690]
8	partner	ENSG00000023228	NDUFS1	NADH dehydrogenase (ubiquinone) Fe-S protein 1, 75kDa (NADH-coenzyme Q reductase) [Source:HGNC Symbol;Acc:HGNC:7707]
8	partner	ENSG00000147684	NDUFB9	NADH dehydrogenase (ubiquinone) 1 beta subcomplex, 9, 22kDa [Source:HGNC Symbol;Acc:HGNC:7704]
8	partner	ENSG00000179091	CYC1	cytochrome c-1 [Source:HGNC Symbol;Acc:HGNC:2579]
8	partner	ENSG00000184076	UQCR10	ubiquinol-cytochrome c reductase, complex III subunit X [Source:HGNC Symbol;Acc:HGNC:30863]
8	85.8292183301	ENSG00000099795	NDUFB7	NADH dehydrogenase (ubiquinone) 1 beta subcomplex, 7, 18kDa [Source:HGNC Symbol;Acc:HGNC:7702]
8	partner	ENSG00000145494	NDUFS6	NADH dehydrogenase (ubiquinone) Fe-S protein 6, 13kDa (NADH-coenzyme Q reductase) [Source:HGNC Symbol;Acc:HGNC:7713]
8	86.5837796245	ENSG00000125356	NDUFA1	NADH dehydrogenase (ubiquinone) 1 alpha subcomplex, 1, 7.5kDa [Source:HGNC Symbol;Acc:HGNC:7683]
8	partner	ENSG00000189043	NDUFA4	NDUFA4, mitochondrial complex associated [Source:HGNC Symbol;Acc:HGNC:7687]
8	86.3531071804	ENSG00000112695	COX7A2	cytochrome c oxidase subunit VIIa polypeptide 2 (liver) [Source:HGNC Symbol;Acc:HGNC:2288]
8	partner	ENSG00000139180	NDUFA9	NADH dehydrogenase (ubiquinone) 1 alpha subcomplex, 9, 39kDa [Source:HGNC Symbol;Acc:HGNC:7693]
8	partner	ENSG00000110717	NDUFS8	NADH dehydrogenase (ubiquinone) Fe-S protein 8, 23kDa (NADH-coenzyme Q reductase) [Source:HGNC Symbol;Acc:HGNC:7715]
8	partner	ENSG00000136521	NDUFB5	NADH dehydrogenase (ubiquinone) 1 beta subcomplex, 5, 16kDa [Source:HGNC Symbol;Acc:HGNC:7700]
8	partner	ENSG00000010256	UQCRC1	ubiquinol-cytochrome c reductase core protein I [Source:HGNC Symbol;Acc:HGNC:12585]
8	partner	ENSG00000178127	NDUFV2	NADH dehydrogenase (ubiquinone) flavoprotein 2, 24kDa [Source:HGNC Symbol;Acc:HGNC:7717]
8	partner	ENSG00000115286	NDUFS7	NADH dehydrogenase (ubiquinone) Fe-S protein 7, 20kDa (NADH-coenzyme Q reductase) [Source:HGNC Symbol;Acc:HGNC:7714]
8	partner	ENSG00000111775	COX6A1	cytochrome c oxidase subunit VIa polypeptide 1 [Source:HGNC Symbol;Acc:HGNC:2277]
8	partner	ENSG00000127184	COX7C	cytochrome c oxidase subunit VIIc [Source:HGNC Symbol;Acc:HGNC:2292]
8	partner	ENSG00000165264	NDUFB6	NADH dehydrogenase (ubiquinone) 1 beta subcomplex, 6, 17kDa [Source:HGNC Symbol;Acc:HGNC:7701]
8	partner	ENSG00000140990	NDUFB10	NADH dehydrogenase (ubiquinone) 1 beta subcomplex, 10, 22kDa [Source:HGNC Symbol;Acc:HGNC:7696]
8	partner	ENSG00000167774	NDUFA7	NADH dehydrogenase [ubiquinone] 1 alpha subcomplex subunit 7 [Source:UniProtKB/Swiss-Prot;Acc:O95182]
8	partner	ENSG00000158864	NDUFS2	NADH dehydrogenase (ubiquinone) Fe-S protein 2, 49kDa (NADH-coenzyme Q reductase) [Source:HGNC Symbol;Acc:HGNC:7708]
8	partner	ENSG00000130414	NDUFA10	NADH dehydrogenase (ubiquinone) 1 alpha subcomplex, 10, 42kDa [Source:HGNC Symbol;Acc:HGNC:7684]
8	partner	ENSG00000156467	UQCRB	ubiquinol-cytochrome c reductase binding protein [Source:HGNC Symbol;Acc:HGNC:12582]
8	partner	ENSG00000170906	NDUFA3	NADH dehydrogenase (ubiquinone) 1 alpha subcomplex, 3, 9kDa [Source:HGNC Symbol;Acc:HGNC:7686]
8	partner	ENSG00000131143	COX4I1	cytochrome c oxidase subunit IV isoform 1 [Source:HGNC

				Symbol;Acc:HGNC:2265]
8	partner	ENSG00000135940	COX5B	cytochrome c oxidase subunit Vb [Source:HGNC Symbol;Acc:HGNC:2269]
8	partner	ENSG00000147123	NDUFB11	NADH dehydrogenase (ubiquinone) 1 beta subcomplex, 11, 17.3kDa [Source:HGNC Symbol;Acc:HGNC:20372]
8	85.5999163474	ENSG00000109390	NDUFC1	NADH dehydrogenase (ubiquinone) 1, subcomplex unknown, 1, 6kDa [Source:HGNC Symbol;Acc:HGNC:7705]
8	partner	ENSG00000184752	NDUFA12	NADH dehydrogenase (ubiquinone) 1 alpha subcomplex, 12 [Source:HGNC Symbol;Acc:HGNC:23987]
9	partner	ENSG00000169021	UQCRFS1	ubiquinol-cytochrome c reductase, Rieske iron-sulfur polypeptide 1 [Source:HGNC Symbol;Acc:HGNC:12587]
9	partner	ENSG00000167792	NDUFV1	NADH dehydrogenase (ubiquinone) flavoprotein 1, 51kDa [Source:HGNC Symbol;Acc:HGNC:7716]
9	partner	ENSG00000164919	COX6C	cytochrome c oxidase subunit VIc [Source:HGNC Symbol;Acc:HGNC:2285]
9	partner	ENSG00000065518	NDUFB4	NADH dehydrogenase (ubiquinone) 1 beta subcomplex, 4, 15kDa [Source:HGNC Symbol;Acc:HGNC:7699]
9	partner	ENSG00000164405	UQCRQ	ubiquinol-cytochrome c reductase, complex III subunit VII, 9.5kDa [Source:HGNC Symbol;Acc:HGNC:29594]
9	partner	ENSG00000131495	NDUFA2	NADH dehydrogenase (ubiquinone) 1 alpha subcomplex, 2, 8kDa [Source:HGNC Symbol;Acc:HGNC:7685]
9	partner	ENSG00000213619	NDUFS3	NADH dehydrogenase (ubiquinone) Fe-S protein 3, 30kDa (NADH-coenzyme Q reductase) [Source:HGNC Symbol;Acc:HGNC:7710]
9	87.5061954344	ENSG00000168653	NDUFS5	NADH dehydrogenase (ubiquinone) Fe-S protein 5, 15kDa (NADH-coenzyme Q reductase) [Source:HGNC Symbol;Acc:HGNC:7712]
9	partner	ENSG00000128609	NDUFA5	NADH dehydrogenase (ubiquinone) 1 alpha subcomplex, 5 [Source:HGNC Symbol;Acc:HGNC:7688]
9	85.5999163474	ENSG00000160194	NDUFV3	NADH dehydrogenase (ubiquinone) flavoprotein 3, 10kDa [Source:HGNC Symbol;Acc:HGNC:7719]
9	partner	ENSG00000140740	UQCRC2	ubiquinol-cytochrome c reductase core protein II [Source:HGNC Symbol;Acc:HGNC:12586]
9	partner	ENSG00000184983	NDUFA6	NADH dehydrogenase (ubiquinone) 1 alpha subcomplex, 6, 14kDa [Source:HGNC Symbol;Acc:HGNC:7690]
9	partner	ENSG00000023228	NDUFS1	NADH dehydrogenase (ubiquinone) Fe-S protein 1, 75kDa (NADH-coenzyme Q reductase) [Source:HGNC Symbol;Acc:HGNC:7707]
9	partner	ENSG00000147684	NDUFB9	NADH dehydrogenase (ubiquinone) 1 beta subcomplex, 9, 22kDa [Source:HGNC Symbol;Acc:HGNC:7704]
9	partner	ENSG00000179091	CYC1	cytochrome c-1 [Source:HGNC Symbol;Acc:HGNC:2579]
9	partner	ENSG00000184076	UQCR10	ubiquinol-cytochrome c reductase, complex III subunit X [Source:HGNC Symbol;Acc:HGNC:30863]
9	85.8292183301	ENSG00000099795	NDUFB7	NADH dehydrogenase (ubiquinone) 1 beta subcomplex, 7, 18kDa [Source:HGNC Symbol;Acc:HGNC:7702]
9	partner	ENSG00000145494	NDUFS6	NADH dehydrogenase (ubiquinone) Fe-S protein 6, 13kDa (NADH-coenzyme Q reductase) [Source:HGNC Symbol;Acc:HGNC:7713]
9	86.5837796245	ENSG00000125356	NDUFA1	NADH dehydrogenase (ubiquinone) 1 alpha subcomplex, 1, 7.5kDa [Source:HGNC Symbol;Acc:HGNC:7683]
9	partner	ENSG00000189043	NDUFA4	NDUFA4, mitochondrial complex associated [Source:HGNC Symbol;Acc:HGNC:7687]
9	86.3531071804	ENSG00000112695	COX7A2	cytochrome c oxidase subunit VIIa polypeptide 2 (liver) [Source:HGNC Symbol;Acc:HGNC:2288]
9	partner	ENSG00000139180	NDUFA9	NADH dehydrogenase (ubiquinone) 1 alpha subcomplex, 9, 39kDa [Source:HGNC Symbol;Acc:HGNC:7693]
9	partner	ENSG00000110717	NDUFS8	NADH dehydrogenase (ubiquinone) Fe-S protein 8, 23kDa (NADH-coenzyme Q reductase) [Source:HGNC Symbol;Acc:HGNC:7715]
9	partner	ENSG00000136521	NDUFB5	NADH dehydrogenase (ubiquinone) 1 beta subcomplex, 5, 16kDa [Source:HGNC Symbol;Acc:HGNC:7700]
9	partner	ENSG00000010256	UQCRC1	ubiquinol-cytochrome c reductase core protein I [Source:HGNC Symbol;Acc:HGNC:12585]
9	partner	ENSG00000178127	NDUFV2	NADH dehydrogenase (ubiquinone) flavoprotein 2, 24kDa [Source:HGNC Symbol;Acc:HGNC:7717]
9	partner	ENSG00000115286	NDUFS7	NADH dehydrogenase (ubiquinone) Fe-S protein 7, 20kDa (NADH-coenzyme Q reductase) [Source:HGNC Symbol;Acc:HGNC:7714]
9	partner	ENSG00000111775	COX6A1	cytochrome c oxidase subunit VIa polypeptide 1 [Source:HGNC Symbol;Acc:HGNC:2277]
9	partner	ENSG00000127184	COX7C	cytochrome c oxidase subunit VIIc [Source:HGNC Symbol;Acc:HGNC:2292]
9	partner	ENSG00000165264	NDUFB6	NADH dehydrogenase (ubiquinone) 1 beta subcomplex, 6, 17kDa [Source:HGNC Symbol;Acc:HGNC:7701]
9	partner	ENSG00000140990	NDUFB10	NADH dehydrogenase (ubiquinone) 1 beta subcomplex, 10, 22kDa [Source:HGNC Symbol;Acc:HGNC:7696]
9	partner	ENSG00000167774	NDUFA7	NADH dehydrogenase [ubiquinone] 1 alpha subcomplex subunit 7 [Source:UniProtKB/Swiss-Prot;Acc:O95182]
9	partner	ENSG00000158864	NDUFS2	NADH dehydrogenase (ubiquinone) Fe-S protein 2, 49kDa (NADH-coenzyme Q reductase) [Source:HGNC Symbol;Acc:HGNC:7708]

9	partner	ENSG00000130414	NDUFA10	NADH dehydrogenase (ubiquinone) 1 alpha subcomplex, 10, 42kDa [Source:HGNC Symbol;Acc:HGNC:7684]
9	partner	ENSG00000156467	UQCRB	ubiquinol-cytochrome c reductase binding protein [Source:HGNC Symbol;Acc:HGNC:12582]
9	partner	ENSG00000170906	NDUFA3	NADH dehydrogenase (ubiquinone) 1 alpha subcomplex, 3, 9kDa [Source:HGNC Symbol;Acc:HGNC:7686]
9	partner	ENSG00000131143	COX4I1	cytochrome c oxidase subunit IV isoform 1 [Source:HGNC Symbol;Acc:HGNC:2265]
9	partner	ENSG00000135940	COX5B	cytochrome c oxidase subunit Vb [Source:HGNC Symbol;Acc:HGNC:2269]
9	partner	ENSG00000147123	NDUFB11	NADH dehydrogenase (ubiquinone) 1 beta subcomplex, 11, 17.3kDa [Source:HGNC Symbol;Acc:HGNC:20372]
9	85.5999163474	ENSG00000109390	NDUFC1	NADH dehydrogenase (ubiquinone) 1, subcomplex unknown, 1, 6kDa [Source:HGNC Symbol;Acc:HGNC:7705]
9	partner	ENSG00000184752	NDUFA12	NADH dehydrogenase (ubiquinone) 1 alpha subcomplex, 12 [Source:HGNC Symbol;Acc:HGNC:23987]
10	partner	ENSG00000169021	UQCRFS1	ubiquinol-cytochrome c reductase, Rieske iron-sulfur polypeptide 1 [Source:HGNC Symbol;Acc:HGNC:12587]
10	partner	ENSG00000167792	NDUFV1	NADH dehydrogenase (ubiquinone) flavoprotein 1, 51kDa [Source:HGNC Symbol;Acc:HGNC:7716]
10	partner	ENSG00000164919	COX6C	cytochrome c oxidase subunit VIc [Source:HGNC Symbol;Acc:HGNC:2285]
10	partner	ENSG00000065518	NDUFB4	NADH dehydrogenase (ubiquinone) 1 beta subcomplex, 4, 15kDa [Source:HGNC Symbol;Acc:HGNC:7699]
10	partner	ENSG00000164405	UQCRQ	ubiquinol-cytochrome c reductase, complex III subunit VII, 9.5kDa [Source:HGNC Symbol;Acc:HGNC:29594]
10	partner	ENSG00000131495	NDUFA2	NADH dehydrogenase (ubiquinone) 1 alpha subcomplex, 2, 8kDa [Source:HGNC Symbol;Acc:HGNC:7685]
10	partner	ENSG00000213619	NDUFS3	NADH dehydrogenase (ubiquinone) Fe-S protein 3, 30kDa (NADH-coenzyme Q reductase) [Source:HGNC Symbol;Acc:HGNC:7710]
10	87.5061954344	ENSG00000168653	NDUFS5	NADH dehydrogenase (ubiquinone) Fe-S protein 5, 15kDa (NADH-coenzyme Q reductase) [Source:HGNC Symbol;Acc:HGNC:7712]
10	partner	ENSG00000128609	NDUFA5	NADH dehydrogenase (ubiquinone) 1 alpha subcomplex, 5 [Source:HGNC Symbol;Acc:HGNC:7688]
10	85.5999163474	ENSG00000160194	NDUFV3	NADH dehydrogenase (ubiquinone) flavoprotein 3, 10kDa [Source:HGNC Symbol;Acc:HGNC:7719]
10	partner	ENSG00000140740	UQCRC2	ubiquinol-cytochrome c reductase core protein II [Source:HGNC Symbol;Acc:HGNC:12586]
10	partner	ENSG00000184983	NDUFA6	NADH dehydrogenase (ubiquinone) 1 alpha subcomplex, 6, 14kDa [Source:HGNC Symbol;Acc:HGNC:7690]
10	partner	ENSG00000150991	UBC	ubiquitin C [Source:HGNC Symbol;Acc:HGNC:12468]
10	partner	ENSG00000023228	NDUFS1	NADH dehydrogenase (ubiquinone) Fe-S protein 1, 75kDa (NADH-coenzyme Q reductase) [Source:HGNC Symbol;Acc:HGNC:7707]
10	partner	ENSG00000147684	NDUFB9	NADH dehydrogenase (ubiquinone) 1 beta subcomplex, 9, 22kDa [Source:HGNC Symbol;Acc:HGNC:7704]
10	partner	ENSG00000179091	CYC1	cytochrome c-1 [Source:HGNC Symbol;Acc:HGNC:2579]
10	partner	ENSG00000184076	UQCR10	ubiquinol-cytochrome c reductase, complex III subunit X [Source:HGNC Symbol;Acc:HGNC:30863]
10	85.8292183301	ENSG00000099795	NDUFB7	NADH dehydrogenase (ubiquinone) 1 beta subcomplex, 7, 18kDa [Source:HGNC Symbol;Acc:HGNC:7702]
10	partner	ENSG00000103479	RBL2	retinoblastoma-like 2 [Source:HGNC Symbol;Acc:HGNC:9894]
10	partner	ENSG00000145494	NDUFS6	NADH dehydrogenase (ubiquinone) Fe-S protein 6, 13kDa (NADH-coenzyme Q reductase) [Source:HGNC Symbol;Acc:HGNC:7713]
10	86.5837796245	ENSG00000125356	NDUFA1	NADH dehydrogenase (ubiquinone) 1 alpha subcomplex, 1, 7.5kDa [Source:HGNC Symbol;Acc:HGNC:7683]
10	partner	ENSG00000189043	NDUFA4	NDUFA4, mitochondrial complex associated [Source:HGNC Symbol;Acc:HGNC:7687]
10	86.3531071804	ENSG00000112695	COX7A2	cytochrome c oxidase subunit VIIa polypeptide 2 (liver) [Source:HGNC Symbol;Acc:HGNC:2288]
10	partner	ENSG00000139180	NDUFA9	NADH dehydrogenase (ubiquinone) 1 alpha subcomplex, 9, 39kDa [Source:HGNC Symbol;Acc:HGNC:7693]
10	partner	ENSG00000110717	NDUFS8	NADH dehydrogenase (ubiquinone) Fe-S protein 8, 23kDa (NADH-coenzyme Q reductase) [Source:HGNC Symbol;Acc:HGNC:7715]
10	partner	ENSG00000136521	NDUFB5	NADH dehydrogenase (ubiquinone) 1 beta subcomplex, 5, 16kDa [Source:HGNC Symbol;Acc:HGNC:7700]
10	partner	ENSG00000010256	UQCRC1	ubiquinol-cytochrome c reductase core protein I [Source:HGNC Symbol;Acc:HGNC:12585]
10	partner	ENSG00000178127	NDUFV2	NADH dehydrogenase (ubiquinone) flavoprotein 2, 24kDa [Source:HGNC Symbol;Acc:HGNC:7717]
10	partner	ENSG00000115286	NDUFS7	NADH dehydrogenase (ubiquinone) Fe-S protein 7, 20kDa (NADH-coenzyme Q reductase) [Source:HGNC Symbol;Acc:HGNC:7714]
10	partner	ENSG00000111775	COX6A1	cytochrome c oxidase subunit VIa polypeptide 1 [Source:HGNC Symbol;Acc:HGNC:2277]
10	partner	ENSG00000127184	COX7C	cytochrome c oxidase subunit VIIc [Source:HGNC

				Symbol;Acc:HGNC:2292]
10	partner	ENSG00000165264	NDUFB6	NADH dehydrogenase (ubiquinone) 1 beta subcomplex, 6, 17kDa [Source:HGNC Symbol;Acc:HGNC:7701]
10	partner	ENSG00000140990	NDUFB10	NADH dehydrogenase (ubiquinone) 1 beta subcomplex, 10, 22kDa [Source:HGNC Symbol;Acc:HGNC:7696]
10	partner	ENSG00000167774	NDUFA7	NADH dehydrogenase [ubiquinone] 1 alpha subcomplex subunit 7 [Source:UniProtKB/Swiss-Prot;Acc:O95182]
10	partner	ENSG00000158864	NDUFS2	NADH dehydrogenase (ubiquinone) Fe-S protein 2, 49kDa (NADH-coenzyme Q reductase) [Source:HGNC Symbol;Acc:HGNC:7708]
10	partner	ENSG00000130414	NDUFA10	NADH dehydrogenase (ubiquinone) 1 alpha subcomplex, 10, 42kDa [Source:HGNC Symbol;Acc:HGNC:7684]
10	partner	ENSG00000156467	UQCRB	ubiquinol-cytochrome c reductase binding protein [Source:HGNC Symbol;Acc:HGNC:12582]
10	partner	ENSG00000170906	NDUFA3	NADH dehydrogenase (ubiquinone) 1 alpha subcomplex, 3, 9kDa [Source:HGNC Symbol;Acc:HGNC:7686]
10	partner	ENSG00000131143	COX4I1	cytochrome c oxidase subunit IV isoform 1 [Source:HGNC Symbol;Acc:HGNC:2265]
10	partner	ENSG00000135940	COX5B	cytochrome c oxidase subunit Vb [Source:HGNC Symbol;Acc:HGNC:2269]
10	partner	ENSG00000147123	NDUFB11	NADH dehydrogenase (ubiquinone) 1 beta subcomplex, 11, 17.3kDa [Source:HGNC Symbol;Acc:HGNC:20372]
10	85.5999163474	ENSG00000109390	NDUFC1	NADH dehydrogenase (ubiquinone) 1, subcomplex unknown, 1, 6kDa [Source:HGNC Symbol;Acc:HGNC:7705]
10	partner	ENSG00000184752	NDUFA12	NADH dehydrogenase (ubiquinone) 1 alpha subcomplex, 12 [Source:HGNC Symbol;Acc:HGNC:23987]